Flinders University

Sulfur-based polymers with long-wave infrared transparency for thermal imaging optics

By

Samuel Tonkin

Thesis
Submitted to Flinders University
for the degree of

Doctor of Philosophy
College of Science and Engineering
08 July 2025

Table of Contents

Abstract

Thermal imaging allows for the visualisation of heat and non-contact temperature measurements. It has long been used in high end applications like military, space exploration and medical thermography but has been prohibitively expensive for most consumer industries. Recent developments in microbolometer sensor technology has dramatically reduced the cost of long wave infrared thermal imaging, sparking interest in many low-cost, high-volume applications like home appliances or the mobile phone industry. However, thermal imaging systems require specialised and expensive optical materials for lenses. These materials have not seen the same decrease in cost, making them the largest obstacle preventing the realisation of the many applications of thermal imaging.

In this thesis, a range of new sulfur-based optical polymers were developed to be used as the lenses or other optics in thermal imaging systems. Novel and creative methods of synthesis were used to prepare polymers which had never been reported in literature. The raw materials used to prepare the sulfur-based polymers were several orders of magnitude cheaper than those commonly used for thermal imaging optics. These polymers were characterised, and a range of optimisation processes were used to prepare materials with some of the highest long wave infrared transmission, refractive index and glass transition temperature in literature.

A range of lenses were designed and fabricated using scalable and low-cost manufacturing methods like melt casting, compression moulding or injection moulding. These fabrication techniques were used to demonstrate how polymer lenses could be made in the quantities required for the emerging high-volume thermal imaging applications. The lenses were fully integrated into a prototype thermal imaging system and demonstrated excellent performance over a range of focal lengths and lens designs.

The research presented in this thesis has direct applications in the thermal imaging industry and could see rapid integration into a range of products. The integration of low-cost polymer optics into infrared imaging systems would make thermal imaging available to many new fields and industries that were not previously possible.

Declaration

I certify that this thesis:

1. does not incorporate without acknowledgment any material previously submitted for a degree or diploma in any university

2. and the research within will not be submitted for any other future degree or diploma without the permission of Flinders University; and

3. to the best of my knowledge and belief, does not contain any material previously published or written by another person except where due reference is made in the text.

Signed: Samuel Tonkin

Date: 08 July 2025

Acknowledgements

I would like to thank my supervisor Justin Chalker for all the guidance and support that he has provided me over the time in my PhD. This thesis would not have been possible without his hard work and passion. I see Justin as an excellent role model, and he has shaped me into the scientist that I am now.

I am grateful for all the members of the Chalker and wider chemical synthesis group. I thank you for making the lab an enjoyable place to work but I also appreciate the valuable conversations and support of all present and past members.

I thank my parents and brothers for the support and genuine interest in everything that I pursue. I am very grateful to have a loving family that I know will support me through anything.

To my beautiful girlfriend Phola, it was always you that I thought of when my motivation waivered. You have shown me love and support through every moment of my PhD. I never would have been able to do it without you and I'm glad that you could be by my side in this journey.

Finally, I would like to thank all the staff and students at Flinders University who have helped me with instrument training, expert advice and making Flinders a fantastic place to be.

This thesis was supported by an Australian Government Research Training Program Scholarship.

Publications and patents

Publications

1. Tonkin, S. J.; Pham, L. N.; Gascooke, J. R.; Johnston, M. R.; Coote, M. L.; Gibson, C. T.; Chalker, J. M. Thermal Imaging and Clandestine Surveillance using Low-Cost Polymers with Long-Wave Infrared Transparency. Advanced Optical Materials **2023**, 11 (16), 2300058. DOI: https://doi.org/10.1002/adom.202300058.

2. Yan, P.; Zhao, W.; Tonkin, S. J.; Chalker, J. M.; Schiller, T. L.; Hasell, T. Stretchable and Durable Inverse Vulcanized Polymers with Chemical and Thermal Recycling. Chemistry of Materials **2022**, 34 (3), 1167-1178. DOI: 10.1021/acs.chemmater.1c03662.

3. Lundquist, N. A.; Yin, Y.; Mann, M.; Tonkin, S. J.; Slattery, A. D.; Andersson, G. G.; Gibson, C. T.; Chalker, J. M. Magnetic responsive composites made from a sulfur-rich polymer. Polymer Chemistry **2022**, 13 (39), 5659-5665, 10.1039/D2PY00903J. DOI: 10.1039/D2PY00903J.

4. Patel, H; Tikoalu, A; Smith, J; Pei, Z; Shapter, R; Tonkin, S; Yan, P; Bloch, W; Johnston, M; Harmer, J; Gibson, C; Perkins, M; Hasell, T; Coote, M; Jia, Z; Chalker, J. Spontaneous Trisulfide Metathesis in Polar Aprotic Solvents. ChemRxiv. 2025; doi:10.26434/chemrxiv-**2025**-fnhdd. This content is a preprint and has not been peer-reviewed.

5. Mann, M.; Pauling, P. J.; Tonkin, S. J.; Campbell, J. A.; Chalker, J. M. Chemically Activated S-S Metathesis for Adhesive-Free Bonding of Polysulfide Surfaces. Macromolecular Chemistry and Physics **2022**, 223 (13), 2100333. DOI: https://doi.org/10.1002/macp.202100333.

6. Mann, A. K.; Tonkin, S. J.; Sharma, P.; Gibson, C. T.; Chalker, J. M. Probe-Based Mechanical Data Storage on Polymers Made by Inverse Vulcanization. Advanced Science **2025**, 12 (5), 2409438. DOI: https://doi.org/10.1002/advs.202409438.

7. Mann, A. K.; Lisboa, L. S.; Tonkin, S. J.; Gascooke, J. R.; Chalker, J. M.; Gibson, C. T. Modification of Polysulfide Surfaces with Low-Power Lasers. Angewandte Chemie **2024**, 136 (23), e202404802.

8. Mann, M.; Zhang, B.; Tonkin, S. J.; Gibson, C. T.; Jia, Z.; Hasell, T.; Chalker, J. M. Processes for coating surfaces with a copolymer made from sulfur and dicyclopentadiene. *Polymer Chemistry* **2022**, *13* (10), 1320-1327, 10.1039/D1PY01416A. DOI: 10.1039/D1PY01416A.

Patents

1. Chalker, J.; Tonkin, S. New polymers and uses thereof. Australian application number: 202316976, Filed 07 Feb **2023**.

2. Chalker, J.; Tonkin, S. Organic polysulfide polymers and uses thereof. Australian application number: 2024902135, Filed 10 July **2024**.

3. Chalker, J.; Tonkin, S.; Patel, H. Methods for making cyclic sulfide and polysulfide monomers, Australian application number: 2025900891, Filed 19 March **2025**.

Chapter 1 - Introduction to infrared imaging, long wave infrared optics and sulfur-based polymers

Thesis introduction

In this thesis, the development of new infrared transparent materials will be investigated and developed for the application of thermal imaging optics. Most of the materials that will be featured in this thesis were prepared for the application of low-cost lenses for long-wave infrared imaging. To gain a complete understanding of thermal imaging, the thesis will begin with a discussion of the background information required to understand the research presented in the later chapters. An overview of the different forms of thermal imaging, the applications and the technical challenges for each will be discussed.

After the overview of thermal imaging, a literature review will be presented. This literature review will be focussed on sulfur-based polymers and their use in thermal imaging applications. After giving a comprehensive review of the relevant literature, the areas of opportunity for future research will be discussed. This will lead into the main goals of the thesis and where they fit into the current literature.

Chapters 2 and 3 will investigate the development of several new sulfur-based polymers. These chapters will focus on polymers with high refractive index and transmission in the long-wave infrared region. Each chapter will discuss the synthesis and characterisation of each polymer as well as experiments to maximise their performance as an optical material for thermal imaging. The polymers prepared in these chapters also utilise unique methods of synthesis which allowed for the development of polymers which were deemed impossible with conventional methods. Note that the experimental details are provided inside the chapter rather than as an appendix.

Chapter 4 will utilise the polymers prepared in chapter 2 and 3 in a range of applications. The aim of this chapter will be to give a demonstration of how low-cost polymers can find use in thermal imaging applications. This chapter will show how the research presented in this thesis could be used in practice. Several of the applications that will be demonstrated are a long wave infrared transparent polymer window for concealment and protection of a thermal camera, injection moulding of complex Fresnel lenses and the development of stand-alone plano convex lenses designed to be used in a thermal imaging module. This chapter will detail the process of incorporating these lenses into a working camera to make a prototype thermal imaging system using only polymer lenses.

Finally, chapter 5 will conclude the thesis, discussing the most important findings of each chapter and detailing future experiments that could lead to commercialisation of this technology. The scale up of monomer synthesis and development of compression and injection moulding will be outlined as methods to accelerate manufacturing. This would allow for the realisation of the polymer materials as low-cost alternatives to the lenses used in thermal imaging.

Introduction to infrared imaging

Overview and blackbody radiation

The next sections will give the background information necessary to understand thermal imaging. The first principle that will be important to know is blackbody radiation. Black body radiation is the electromagnetic radiation given off by an object that absorbs all incident radiation, regardless of frequency or direction.[1] The wavelength and intensity of the emitted radiation is solely dependent on the temperature of the object.[2] At higher temperatures, the intensity of light emitted is increased and the wavelength decreases. The spectral radiance of a blackbody for a given temperature is given by Planck's law which can be seen below.[3] Where $B_\lambda(T)$ is the spectral radiance per unit solid angle ($Wm^{-2}m^{-1}sr^{-1}$), λ is the wavelength (m), T is the temperature (K), h is Planck's constant (6.626 x 10^{-34} Js), c is the speed of light in a vacuum (3 x 10^9 ms^{-1}) and k_b is the Boltzmann's constant (1.381 x 10^{-23} JK^{-1}).

$$B_\lambda(T) = \frac{2hc^2}{\lambda^5}\frac{1}{e^{\frac{hc}{\lambda k_B T}} - 1}$$

The wavelength of light that is emitted by a blackbody is dependent on temperature. As can be seen in the figure below, for a 5500 °C object, the maximum intensity falls within the visible region. The surface of the sun is approximately this temperature, resulting in a large amount of visible light hitting the earth's surface. For this reason, most cameras utilise reflected light in the visible region. Human and most animal eyes also use this wavelength range of light. For objects that are lower temperature, the maximum intensity is shifted to longer wavelengths, making their emitted light impossible to see with the human eye. Thermal imaging works by utilising sensors that can detect light at longer wavelengths.[4] This way, the emitted blackbody radiation can be visualised.

Infrared imaging has several different forms based on the wavelength of light detected. For this thesis, they will be defined as near infrared (NIR), short-wave infrared (SWIR), mid-wave infrared (MWIR), and long-wave infrared (LWIR). The exact wavelengths used depend on the sensor of the thermal camera but for this thesis they will be defined as 0.7 µm – 1.4 µm, 1.4 – 2.5 µm, 3 – 5 µm and 7 – 14 µm for NIR, SWIR, MWIR and LWIR respectively. The sensors and materials used for optics vary greatly between the different imaging types as do the applications. The following sections will give some background information about the different forms of infrared imaging and discuss the areas where the research in this thesis could be used.

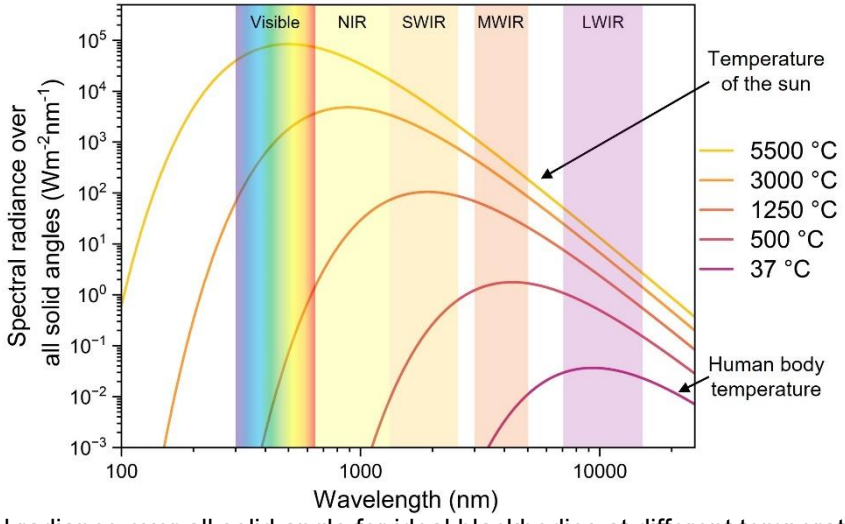

Figure 1.1: Spectral radiance over all solid angle for ideal blackbodies at different temperatures.

NIR and Short-wave infrared imaging

Near infrared and short-wave infrared both mostly utilise reflected light. Near infrared imaging usually uses light between 700 and 1000 nm but can extend up to 1.4 μm.[5] This light is just outside the visible region but in most ways, imaging in NIR is very similar to visible light. Similar complementary metal oxide-semiconductor (CMOS) or charge-coupled device (CCD) sensors can be used.[6] As these are used in visible light cameras, the technology is mature and relatively low cost. Near infrared systems can also use standard glasses for optical components, further reducing costs.

Near infrared imaging has many applications. The most obvious is night vision. As NIR light cannot be seen with the naked eye, many night vision systems actively illuminate a scene with NIR LEDs or lasers.[7] The reflected light from this active illumination can be detected with a NIR camera to grant night vision. NIR imaging also has many medical applications like near-infrared fluorescence which can be used in cancer treatment.[8] However, NIR is not truly thermal imaging as it still relies on reflected light. Furthermore, the materials used for the optics in these systems are well developed and understood so they will not be the focus of this thesis.

Short-wave infrared extends further into longer wavelengths than NIR. To achieve this, SWIR sensors utilise Indium Gallium Arsenide sensors.[9] These sensors employ a compound semiconductor to convert SWIR photons into an electrical signal.[9] This signal is converted into an image in the camera. This allows for these cameras to be sensitive to light between 0.9 μm and 2.5 μm. Standard glass loses its transmission to light in these wavelengths so specialised glass like fused silica or sapphire are typically used for lenses or optical components.[6] This can lead to an increased cost relative to NIR systems.

While still mostly using reflected light, the high sensitivity of SWIR sensors allows for passive night vision utilising the light from stars or ambient reflections.[10] Due to the longer wavelength of light used, SWIR imaging has other applications which are not possible with NIR. Silicon is opaque to visible or NIR light but is transparent to SWIR light.[11] Using SWIR light, silicon chips can be investigated for voids or imperfections. This is an extremely important application used in electronics manufacturing.[12] Likewise, SWIR or some NIR imaging systems can detect the accumulation of water in fruit, allowing for their quality control.[13,14]

While NIR and SWIR imaging technologies have many useful applications, they will not be the focus of this thesis as many of the polymers that will be developed in the following chapters were designed for mid or long-wave infrared imaging. The short-wave infrared transmission will still be characterised for all polymer systems to demonstrate their potential as SWIR optics.

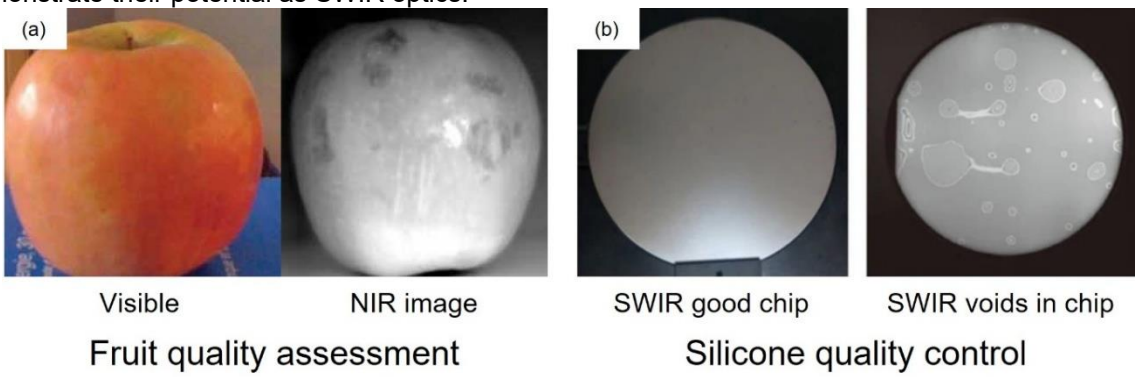

Figure 1.2: (a) Apple imaged with visible and NIR cameras. Modified with permission from.[14] (b) Silicon chips imaged with short wave infrared imaging to show voids or imperfections. Modified with permission from.[15]

Mid-wave infrared imaging

Mid-wave infrared imaging is different to NIR and SWIR as it utilises the emitted blackbody radiation from the objects that are being observed. MWIR imaging utilised wavelengths between 3 μm and 5 μm. As can be seen in figure 1.1 above, objects that are 500 °C will have their maximum intensity within the mid-wave infrared region. However, even objects at relatively lower temperatures like the human body release some mid-wave infrared radiation at this wavelength. This means that mid-wave infrared imaging does not rely only on reflected light but is the first true thermal imaging technique that has been described so far. Mid-wave infrared imaging can measure the intensity of blackbody radiation emitted from an object to enable non-contact temperature measurements while also allowing for imaging in complete darkness.[16]

Mid-wave infrared imaging requires specialised sensors which usually require cooling.[16] Several of the most common mid-wave infrared cooling systems include indium antimonide, mercury cadmium telluride or quantum well infrared photodetectors.[17] To reduce thermal noise and prevent saturation of the sensor, these sensors must be cooled to cryogenic temperatures (70 K – 100 K), requiring liquid nitrogen or Stirling coolers.[18] While there has been some research in recent years into higher operating temperature sensors for mid-wave infrared imaging, they suffer from reduced sensitivity and often still require cooling to 150 K – 200 K.[18] These cooling requirements mean that mid wave infrared imaging is usually much more expensive than uncooled long wave infrared imaging. However, the unmatched performance of MWIR imaging systems mean they find used in high-end industries like military,[17] medical[19] or manufacturing.[20]

The optical materials used in mid-wave infrared imaging are quite specialised as most polymers or standard glasses will be opaque to light at these wavelengths. Materials like germanium, zinc selenide or silicon are commonly used.[21] While high performance, these materials are expensive and difficult to manufacture. However, due to the high cost of the sensors and the nature of the applications that mid-wave infrared imaging is used for, the cost of the optical materials is usually of lower importance than performance. For this reason, low-cost polymeric lenses are less likely to be as useful in MWIR imaging as LWIR imaging as they are unlikely to match the performance of chalcogenide or semiconductors lenses. However, as lower cost, high temperature MWIR sensors are developed, lower cost optical materials would be required. Due to this, mid-wave infrared imaging will not be the focus of this thesis, but all polymers will be characterised for transmission and refractive index over the mid-wave infrared region. The effectiveness of each material as a MWIR transparent optical polymer will be discussed but all applications will be focussed on the LWIR region.

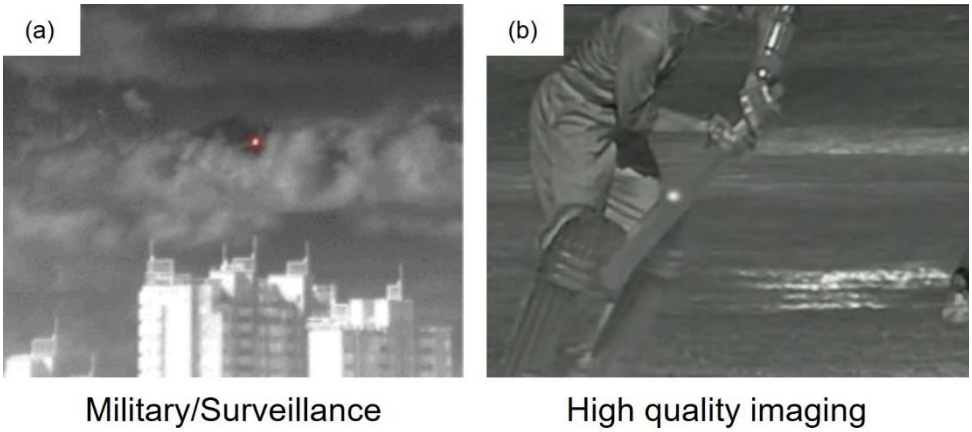

Figure 1.3: (a) MWIR imaging used to track a target. Modified with permission from.[17] (b) Hot spot technology using MWIR imaging. Modified with permission from.[22]

Long-wave infrared imaging

Long-wave infrared imaging utilises emitted blackbody radiation with a wavelength between 7 µm and 14 µm. As can be seen in the figure below, the maximum intensity of emitted radiation of a human body is in this region. This makes long-wave infrared imaging excellent for low temperature applications or detecting people or animals. Long-wave infrared imaging is often considered the lowest cost form of thermal imaging due to the relatively low-cost uncooled sensors.[23] While high sensitivity, cooled quantum sensors are available in the LWIR region,[24,25] most applications utilise microbolometers. These microbolometers contain materials which can absorb incident radiation to heat a thermal sensing array.[26] This change in temperature causes a change in resistance which can be measured and converted to an image. Much research has been conducted into the most effective materials to be used in microbolometers. The most common materials are amorphous Si and VO_x[26] but many others like ZnO, NiO, carbon nanotubes, poly-SiGe and Pt are being investigated.[27-29] Along with improvements in the process signalling, long wave infrared imaging has become much cheaper than other forms of thermal imaging.[30]

Due to the low cost of LWIR imaging, it has applications in a range of fields like home security,[31] agriculture,[32,33] construction[34] and medical thermography.[35,36] However, like with MWIR imaging, many of the more common optical materials are opaque to long wave infrared radiation.[21] For this reason, specialised and expensive materials like germanium or chalcogenide glasses must be used.[24] A more detailed explanation of the materials used in thermal imaging is presented in the “long wave infrared optics” section below. Due to the low-cost of LWIR sensors, the cost of the lens is a major factor in the overall cost of the system for LWIR imaging.

The main focus of this thesis is to provide alternatives to the expensive materials used for LWIR optics. With a decrease in the cost of the lenses, long wave infrared imaging could be brought into a new cost bracket which would make a range of previously inaccessible applications possible. High volume consumer markets like the mobile phone industry, self-driving vehicles or improved fire detection systems in houses could be reached. To achieve these goals, a material would need to be developed with a high refractive index, high transmission in the long wave infrared regions, good mechanical and thermal properties and low-cost raw materials and manufacturing methods. Developing a material that meets these criteria is the main goal of this thesis.

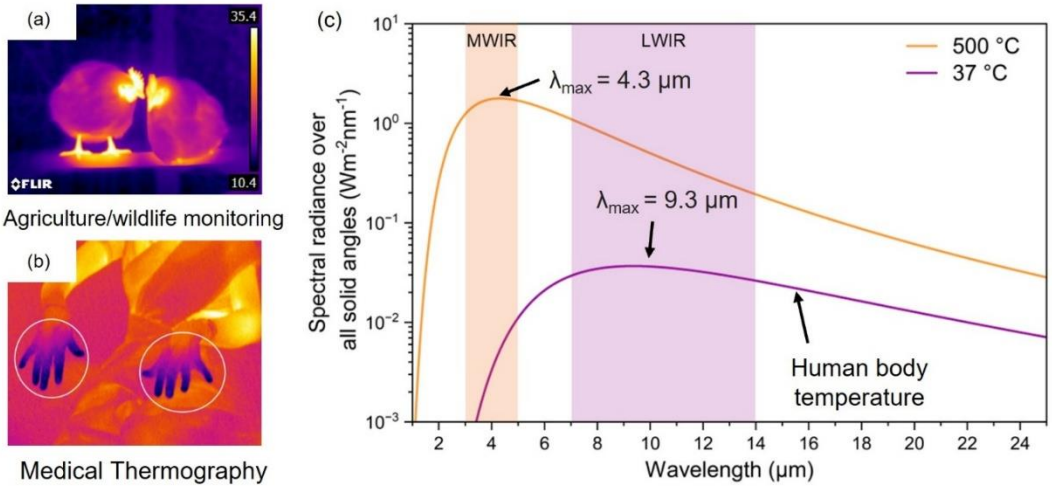

Figure 1.4: (a) Image of chickens taken with FLIR E6 thermal camera demonstrating agricultural monitoring. (b) Medical thermography image of a person with diabetes. Modified with permission from.[36] (c) Blackbody emission from two ideal objects with temperatures of 500 °C and 37 °C.

Long wave infrared optics

This section will discuss the commonly used materials for long wave infrared optics and discuss potential routes to find alternatives. Metal fluorides (LiF, BaF_2, CaF_2)[37, 38] and inorganic salts (NaCl, KCl, KBr)[21] show excellent transmission over all infrared regions. However, they suffer from high sensitivity to moisture, reducing their effectiveness over time and limiting their practical use. Semiconductors like germanium, silicon, zinc selenide and zinc sulfide show good transmission over the mid and long wave infrared regions and a high refractive index.[39, 40] However, these materials require expensive processes to grow crystals and must be milled from a bulk material to prepare lenses.[39, 40] This process is not only expensive but has difficulties in scaling to high production volumes, making low-cost applications impractical.

Chalcogenide glasses (GeAsSE, AsS, AsSe) also possess properties which would make them useful for infrared optics.[41-43] By varying the ratio of the chalcogenides present, glasses with a range of properties can be prepared. However, they often require complex manufacturing processes, specialised equipment and high raw material costs, preventing their use in high volume applications.[42]

The next category of materials are optical polymers. Most polymeric materials show very poor transmission in the LWIR region. This is due to the organic content of the polymers absorbing most of the light. [44] The long wave infrared region is often considered as the fingerprint region due to the many absorptions of organic functional groups. The only polymeric materials that see use as long wave infrared optics are those with simple aliphatic structures like ultrahigh molecular weight polyethylene or to a lesser degree cyclic olefin copolymers like Topas.[44-46] The transmission of ultrahigh molecular weight polyethylene in the long wave infrared region is due to the limited number of organic chemical environments in the material, leading to windows of low absorption. However, due to the low refractive index, thicker lenses are required which can decrease transmission.[44] Thin lenses have been prepared but usually require a second material like silicon to be functional.[47]

A material which could be produced at a low cost and with scalable manufacturing methods could provide an alternative to conventional long-wave infrared optics. In this thesis, the approach taken was to utilise high sulfur polymers. By replacing many of the highly absorbing organic portions with sulfur, a polymer could be prepared with high transmission in the LWIR region as well as a high refractive index. The following sections will describe the current literature on high sulfur polymers with an emphasis on optics applications.

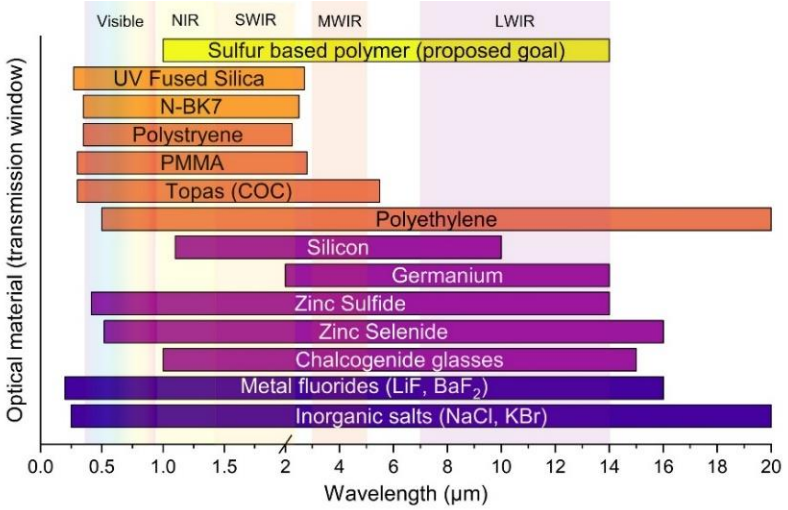

Figure 1.5: Approximate windows of transmission for a range of optical materials.

Sulfur based polymers overview

Inverse vulcanization overview

Sulfur is one of the most abundant elements on earth[48] and is isolated in vast quantities from the hydrodesulfurization of petroleum.[49, 50] While some applications for sulfur exist like the sulfuric acid production,[51, 52] or additives in asphalt[53] or concrete,[54] the production of sulfur far outweighs the applications. This leads to megatons of excess every year.[48] The storage of this excess sulfur can be expensive and has potential environmental implications.[55] Due to these factors, sulfur is extremely cheap and there is an economic and environmental incentive to develop high volume applications using sulfur.

In 2013, a new form of materials utilising elemental sulfur was developed by Jeffery Pyun in a process known as inverse vulcanization.[56] In this process, sulfur is heated to melt and initiate ring opening polymerisation. While initially thought to require temperatures over 160 °C,[56] many recent papers have successfully initiated reactions at temperatures as low as 110 °C using catalysts or highly reactive alkenes.[57-61] During the ring opening of sulfur, an S-S bond is broken to convert an octahedral sulfur ring into a linear polysulfide with thiyl radical end groups.[62] These linear polysulfides can react with sulfur to form long chain sulfur polymers. If left to cool, these polysulfides backbite and brake down over time, reforming the thermodynamically favoured eight membered sulfur ring.[63] Inverse vulcanization addresses this instability of the polysulfide backbone by incorporating organic stabilising monomers to the reaction. These stabilising monomers were usually dienes with reactive pi-bond and a high boiling point such that they are a liquid in molten sulfur. By adding these monomers to the reaction with sulfur, the thiyl radical would attack the pi-bonds in the organic monomer and initiate a radical chain polymerisation. The relative mass of the organic monomer usually ranges from 10 % to 50 % of the final material. The incorporation of organic stabilising groups also improves to processability and gives some flexibility in the thermal, mechanical, chemical and optical properties of the resulting polymer.[64, 65]

In the original paper by Jeffery Pyun published in nature chemistry, 1,3-diisopropenylbenzene was used as the stabilising organic monomer.[56] While it was originally considered to react in only a radical chain polymerisation, a later study was found that C-H abstraction would occur, creating a linear polymer rather than the initially proposed crosslinked structure with bis-sulfurated units per vinyl group in the monomer. [66] This demonstrates the potential for side reactions to occur during the high temperature reactions used in inverse vulcanization.

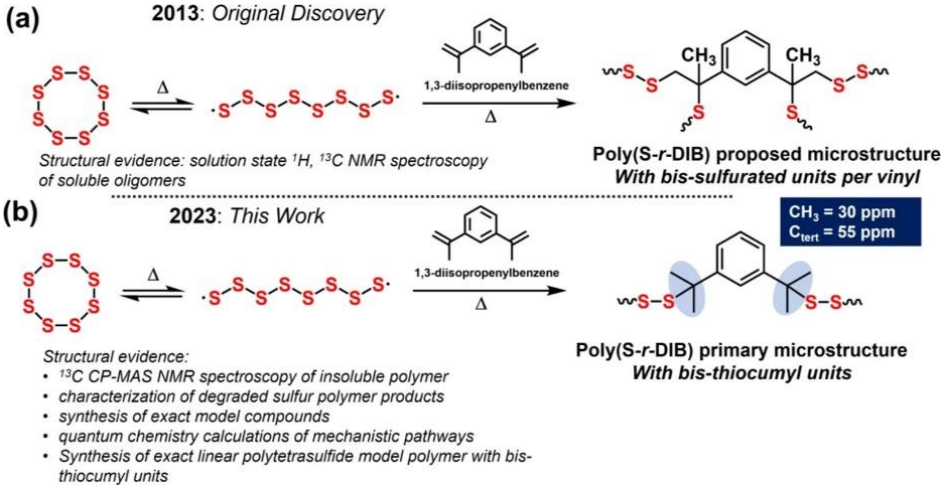

Figure 1.6: Figure showing the inverse vulcanization of 1,3-diisopropenylbenzene as well as the revised structure from 2023. Modified with permission from.[66]

In the last decade, polymers prepared by inverse vulcanization have proved versatile and have a range of applications. One of the original applications for these polymers was as a cathode in lithium sulfide batteries.[67-72] It was found that by replacing the sulfur cathode with an inverse vulcanized polymer, the diffusion of lithium polysulfides away from the cathode could be reduced.[73, 74] This would increase the lifespan of the battery and prevent reduction in efficiency. The use of inverse vulcanized polymers also prevented the formation of stable sulfur rings[75-78] and could incorporate conductive composites to aid in electron transfer and improve battery efficiency.[79-83]

Another highly researched application was the sorption and remediation of heavy metals and oils. The high sulfur content of the polymers aids them in capturing heavy metals to their surface.[84, 85] This allowed for the removal of hazardous environmental pollutants like mercury,[86-89] cadmium,[90] iron[91] or lead[92]. It was also found to be effective in binding to gold, allowing for applications in gold mining or electronic recycling.[93] In a similar application, it was found that the use of canola oil as a hydrophobic monomer allowed the synthesis of a polymer with high affinity for oil. This polymer was demonstrated to be useful in the removal of oil from water.[94]

The polymers prepared by inverse vulcanization also found applications in dynamic and self-healing materials,[95-99] adhesives,[97,100] composite materials,[101-103] slow-release fertilisers[104] and many more. Many of the applications of polymers prepared through inverse vulcanization utilise the properties obtained by the high sulfur content of the polymer while the variety of organic monomers gives a great flexibility in the physical and thermal properties of the materials.[64] While the field is becoming more mature, there are still many applications to be discovered and explored in detail.

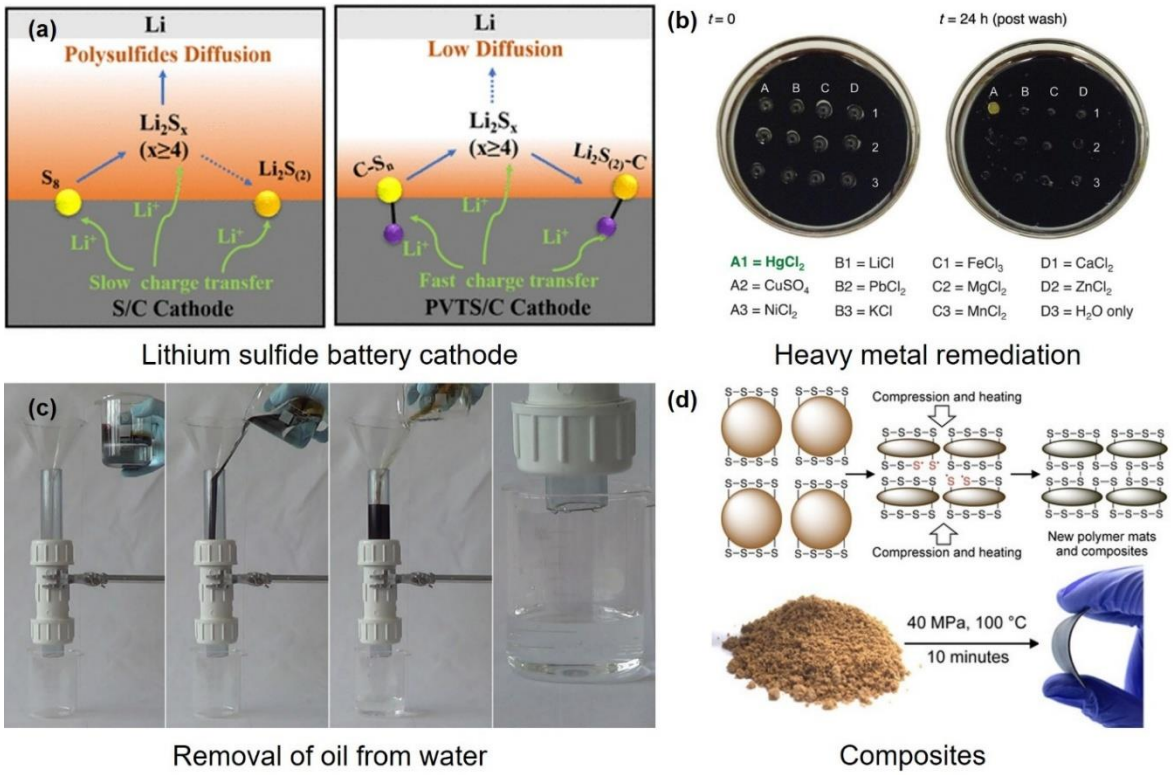

Figure 1.7: Applications of inverse vulcanization. (a) Use of polymer prepared through inverse vulcanization as the cathode in a lithium cathode battery. Modified with permission from.[69] (b) Heavy metal remediation using polymer prepared through inverse vulcanization. Modified with permission from.[86] (c) Removal of oil from water using polymer prepared through inverse vulcanization. Modified with permission from.[94] (d) Reactive compression moulding to form polymer mats and composites. Modified with permission from.[101]

Polymerisation of cyclic trisulfides

Another type of polymerisation that will be important for this thesis is the use of cyclic trisulfides as monomers in a polymerisation. In a publication by the Chalker group in 2023, a polymer could be prepared through the electrochemical polymerisation of the trisulfide of norbornene or dicyclopentadiene derivatives.[105] The method avoids many of the limitations of inverse vulcanization reactions. In particular, the reaction can be performed at room temperature, preventing many of the potential high temperature side reactions. Furthermore, inverse vulcanization does not give good control over sulfur rank or stereochemistry.[105] When using cyclic trisulfides as a monomer, the stereochemistry is set before the polymerisation reaction, giving greater control over the final structure of the polymer. The sulfur rank is also controlled as the reaction proceeds through a ring opening mechanism, resulting in almost every sulfur chain possessing exactly three sulfur atoms.

The cyclic sulfur monomers were prepared through a reaction between norbornene or dicyclopentadiene derivatives and sulfur in the presence of a nickel catalyst.[106] This reaction gives monomers with cis stereochemistry. Controlled synthesis of monomers would likely be very useful to prepare optical polymers as defined stereochemistry could limit vibrations which absorb radiation in the LWIR region. A similar procedure was used in chapter 3 to develop monomers for long wave infrared transparent polymers.

The norbornene based polymer was demonstrated to possess complete thermal depolymerisation and recycling. This was utilised to bind gold and remove it from water. Following this, the polymer could be thermally depolymerised to deposit the gold, leading to a waste free method to remove gold from water. When the dicyclopentadiene molecule was used, it could instead be thermally cured to prepare a crosslinked monomer by promoting a reaction at the second alkene. This demonstrates a potential method to prepare polymers with a high crosslinking density using this method.

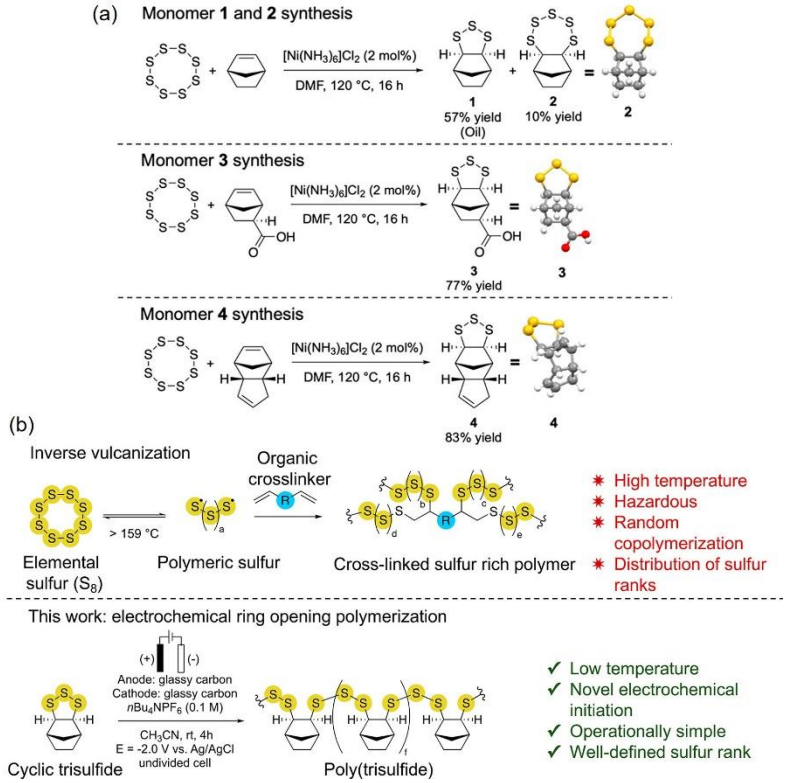

Figure 1.8: Electrochemical synthesis of polytrisulfides. (a) Synthesis of tri or pentasulfide monomers. (b) Comparison between inverse vulcanization and electrochemical ring opening polymerisation. Modified with permission from.[105]

High refractive index polymers

One of the most important features of an optical material is the refractive index. The refractive index is a measure of how the light slows down when passing through the material in relation to in a vacuum.[107] In a practical sense, the refractive index determines how much light will refract when entering a new medium and is described by Snell's law (see equation below). Higher refractive index materials can be used to preparate thinner and simpler lenses.[108] The preparation of thinner lenses is a significant advantage for LWIR infrared lenses as there is usually non-significant absorption of light. Therefore, any decrease in thickness results in an increase in transmission and subsequent signal in the imaging system.

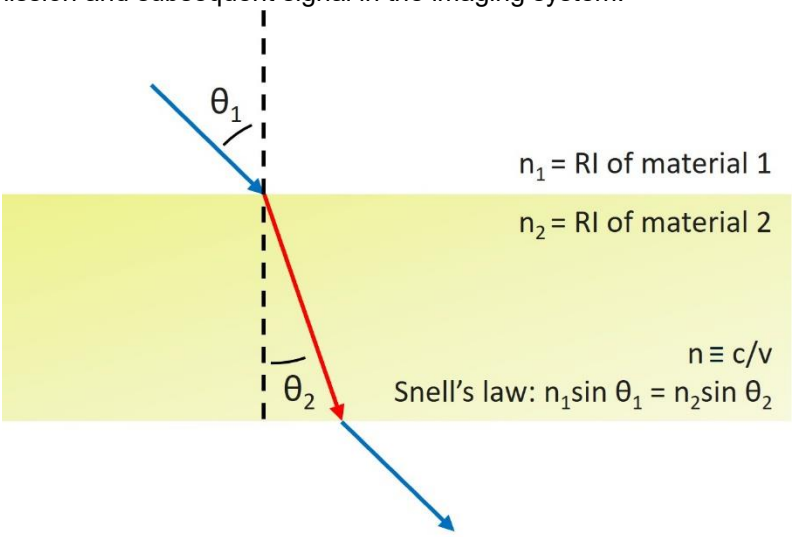

Figure 1.9: Refracted light based on Snell's law. Reflected rays have been ignored for simplicity.

The refractive index of a materials depends on many factors. Materials with heavy atoms and loosely bound electrons tend to have a high refractive index due as the electric field of light can polarise their loosely bound electrons.[109] Other factors that can influence refractive index are the optical density or dielectric constant.[109] Sulfur atoms are large and highly polarisable.[110] This means that the incorporation of sulfur into a material can increase the refractive index. Polymers made through inverse vulcanization show significantly improved refractive index than conventional carbon-based polymers, with refractive indices ranging from 1.7 to 2.1[110] while most polymers have a refractive index of only 1.4-1.6.[107]

There have been many publications on high refractive index polymers made through inverse vulcanization. The first publication to outline the high refractive index of these sulfur-based polymers was by Pyun and co-workers on a polymer made by diisopropenylbenzene (DIB).[111] They were able to prepare polymers with refractive indexes ranging from 1.7 to 1.85 by varying the sulfur content. This demonstrates that polymers prepared through inverse vulcanization have some flexibility in the refractive index by variations in sulfur loading, a property which is not common in polymers.[111] In a later publication, it was found that utilising divinylbenzene (DVB) could give polymers with a refractive index greater than 1.85.[112] This could potentially be explained by an increase in the crosslinking density of the polymer over those prepared from DIB. The polymers prepared from DIB have been shown to form a linear polymer[66] while those prepared from DVB form a dense network, likely leading to an increase in refractive index. In another publication, a polymer was again prepared using DVB but, in this case, it was prepared using a chemical vapour deposition method. [113] Using this method, they were able to prepare polymers with a refractive index of 1.97. This is likely to be one of the highest possible refractive indexes for a polymer made from sulfur and purely organic crosslinkers as the

refractive index of sulfur is 1.99 at the wavelength tested (600 nm).[113] The extremely high refractive index was likely due to the sulfur loading that could be achieved through this method. Polymers with over 87 % sulfur were prepared with the refractive index increasing with sulfur loading. Another factor that could have influenced the refractive index was the synthesis method. Synthesis of the polymer with a similar sulfur loading using a conventional inverse vulcanization reaction gave a refractive index on only 1.9. They proposed that greater packing and polymer density was responsible for the increase in refractive index. These publications demonstrate that increased sulfur loading, and polymer density could be a useful strategy to increase refractive index in polymers made by inverse vulcanization.

Another method to achieve high refractive index polymers is the incorporation of heavy atoms into the polymer backbone. The Boyd group prepared a polymer through inverse vulcanization using a tin atom in the crosslinking group.[114] In a well-designed project, tetravinyltin (TVSn) was used as a comonomer with sulfur. While there were issues with polymer stability, they were able to obtain an excellent refractive index of over 1.92.[114]

Another method of introducing heavy atoms into the polymer backbone is using selenium. Selenium and sulfur are both group 6 chalcogens, so they share some similar reactivity. Selenium is heavier than sulfur, leading to a higher refractive index ($n_{Se} \approx 2.7$, $n_S \approx 2.0$).[115] The integration of selenium therefore presents a promising method to improve the refractive index of polymers prepared through inverse vulcanization. In a publication in ACS Macro Letters by the Pyun group, selenium was used in inverse vulcanization reactions to prepare polymers with extremely high refractive indexes.[116] Despite grey selenium existing as a linear polymer, it was found that liquid sulfur could dissolve it, likely due to sulfur radicals reacting with the polymeric chains to prepare linear S-Se polymers. Diisopropenyl benzene (DIB) was then added to the sulfur/selenium liquid and was found to rapidly react to form a polymer. Similar reactions were reported around the same time by the Pyun[116] and Boyd[117] group. As expected, the incorporation of selenium was successful in increasing the refractive index of the polymer, leading to the Pyun group publishing the first inverse vulcanized polymer with a refractive index of over 2.[116] Since these publications, there have been two papers reporting polymers with selenium incorporated into their structure.[118, 119] While not explored in this thesis, the incorporation of selenium into the polymers prepared in this thesis could likely be performed to improve refractive index.

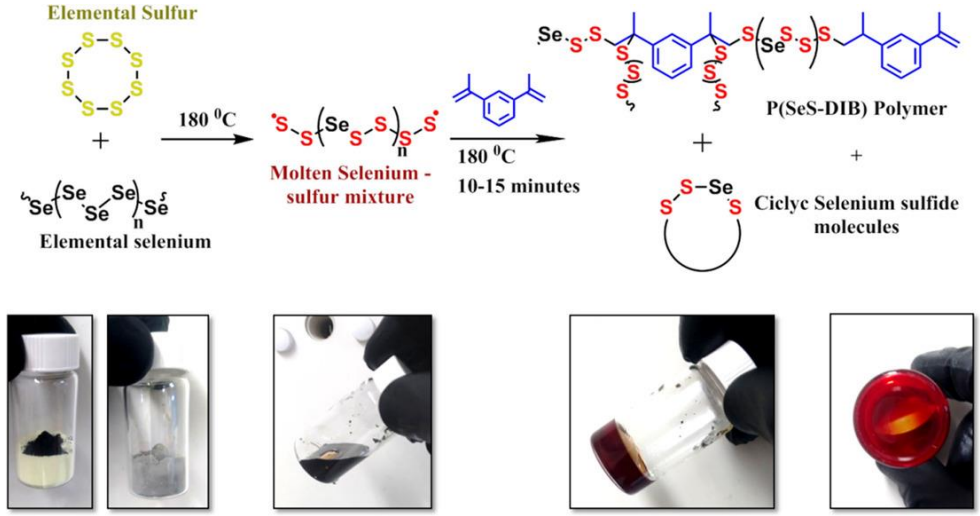

Figure 1.10: Process of incorporating selenium into polymers through inverse vulcanization to prepare high refractive index polymers. (structure likely incorrect due to corrected reaction mechanism). Reused with permission from.[117]

Infrared transparent polymers

While a high refractive index is important for optical materials, they must also be transparent to light in the desired wavelength range. While optical polymers are commonly used for visible and near infrared optics, it is rare for polymeric materials to be used as infrared optics. As explained in the LWIR optical materials section, this is mostly due to the range of absorptions from organic functional groups. The C-H stretching vibrational modes in most polymeric materials result in a large absorption in the middle of the MWIR region. The absorbance in the long wave infrared region is less simple. Many vibrational modes and complex overtones make most polymeric materials completely opaque to LWIR radiation. This presents a significant challenge to material scientists.

Polymers prepared through inverse vulcanization have a large sulfur content, often over 70 %. S-S and C-S bonds have minimal absorption in the mid or long-wave infrared regions.[120] By incorporating a significant amount of sulfur, the relative proportion of highly absorbing organic portion can be reduced. This gives a viable strategy for preparing polymeric materials with infrared transmission. However, there is more to the design of infrared transparent polymers than simply incorporating as much sulfur as possible. As most of the absorption of infrared radiation is from the organic portion, careful selection of the organic monomer is vital to the transmittance of the material.

Initial research on infrared transparent polymers focused on the mid-wave infrared region. Using the polymer prepared from sulfur and 1,3-diisopropenylbenzene (DIB), it was found that MWIR (3 μm – 5 μm) transparent windows could be produced.[120] It was shown that 1 mm thick windows could transmit enough light to image a person. This material also displayed one of the major advantages of polymeric materials over conventional semiconductors or chalcogenide glasses. The damaged windows prepared with inverse vulcanized polymers could be returned to a mould and exposed to relatively moderate heat (100 °C for 72). It was found that the polymeric windows could be completely repaired and returned to a similar level of optical transparency. This form of processing is not possible with semiconductors and the high melting point of chalcogenide glasses (400 °C-900 °C) makes this impractical without specialised equipment.

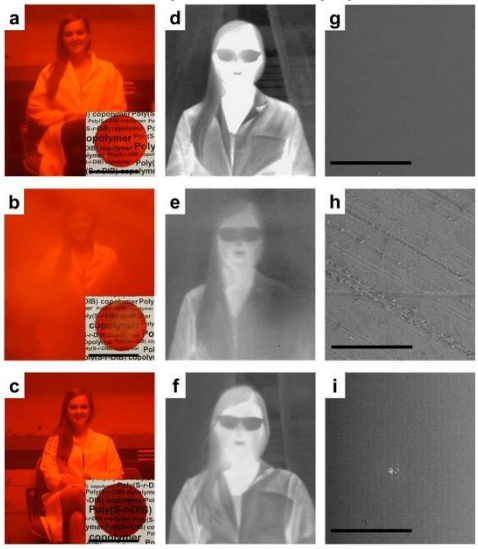

Figure 1.11: Imaging through poly(S-*r*-DIB$_{30}$) polymer. (a-c) visible images through (a) pristine, (b) sandpaper damaged, (c) repaired window. (d-g) MWIR images through (d) pristine, (e) sandpaper damaged, (c) repaired window. (g-j) Scanning electron microscope image of (g) pristine, (h) sandpaper damaged, (i) repaired window. Reused with permission from.[96]

While the polymer prepared using DIB demonstrated the advantages of inverse vulcanized polymers for use in mid-wave infrared imaging, it had several drawbacks. Namely, a low glass transition temperature and long-wave infrared transparency. A paper looked to address the low glass transition temperature by increasing the crosslinking of the polymer. This was achieved by using 1,3,5-triisopropenylbenzene as a comonomer with sulfur.[121] This monomer was prepared with a Suzuki cross-coupling reaction between 1,3,5-tribromobenzene and isopropenyl boronic acid. It was found that the increased crosslinking led to an improved glass transition temperature ranging from 68 °C to 130 °C based on sulfur loading while maintaining similar MWIR transmission.

These initial publications were important to demonstrate the use of high sulfur polymers as MWIR transparent materials. However, due to the high cost of MWIR imaging systems, there is a much greater need for low cost polymeric LWIR transparent materials. The LWIR transmission of both the DIB and TIB based polymers was very poor. This was explored in detail in chapter 2 where the DIB polymer was compared with the cyclopentadiene based polymer presented in that chapter.

To expand the use of inverse vulcanized polymers to include LWIR imaging, careful design of the polymer structure was required. One approach that was used was developed by the Boyd group to incorporate a metal atom into the monomer design.[114] By using tetravinyltin as a monomer in an inverse vulcanization reaction, they were able to prepare a polymer with a high refractive index but also high LWIR (7 µm – 14 µm) transparency. The high LWIR transparency was due to the metal atom shifting many of the vibrations outside of the long wave infrared region, leading to increased transmission. Furthermore, the tetravinyltin monomer was very simple had have very few vibration modes while also possessing some symmetry. This led to many windows of transmission to light in the long-wave infrared region. The long wave infrared transparency of the polymer was demonstrated to image a soldering iron through the polymer using a thermal camera. This was the first published long wave infrared image taken through an inverse vulcanized polymer and opened the door to further investigations into long wave infrared transparent materials made from high sulfur polymers. However, this polymer did suffer from stability issues and would degrade over several days, preventing its immediate use in optics applications.

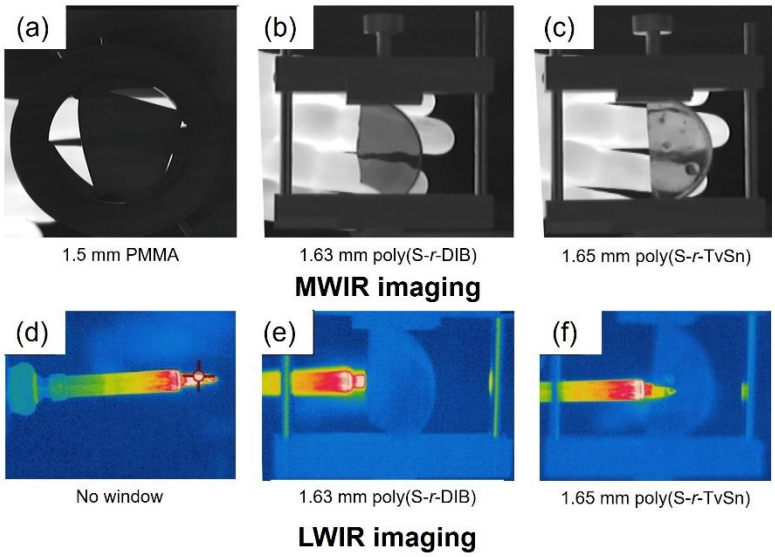

Figure 1.12: (a-c) MWIR (3 µm – 5 µm) imaging through (a) 1.5 mm thick PMMA, (b) 1.63 mm thick poly(S-r-DIB), (c) 1.65 mm thick poly(S-r-TvSn). (d-f) LWIR (7.5 µm – 14 µm) imaging through (d) no window, (e) 1.63 mm thick poly(S-r-DIB), (f) 1.65 mm thick poly(S-r-TvSn). Modified with permission from.[114]

The design of long wave infrared transparent polymers is much more difficult than mid-wave infrared transparent materials due to the many complex vibrations present. To help understand the design of long wave infrared transparent materials better, computational IR spectra were used. Initially performed by the Pyun group, many monomers were investigated for their long wave infrared transparency. This was done using dimers species connected with trisulfide linkages. This resulted in the discovery of norbornane based monomers showing very few absorbances in the long wave infrared region. It was then postulated that a sulfur-based polymer with a norbornane crosslinking organic unit would give excellent transmission in the long-wave infrared region. However, due to the low boiling point of the norbornadiene monomer, it was not possible to perform a conventional inverse vulcanization reaction. To overcome this limitation, they prepared a dimer of norbornadiene using a nickel-catalysed [2+2] cycloaddition reaction. This dimer molecule was then used in an inverse vulcanization reaction to prepare a high sulfur polymer.

The polymer prepared using the norbornadiene dimer known as NBD2 showed some transmission in the long-wave infrared region. This was used to prepare a LWIR image of a hotplate with a polymethylmethacrylate mask. While the transmission was still relatively low compared to conventional infrared optics, this paper demonstrated a stable polymer with high glass transition, low cost and scalable synthesis with enough transmission to prepare images.

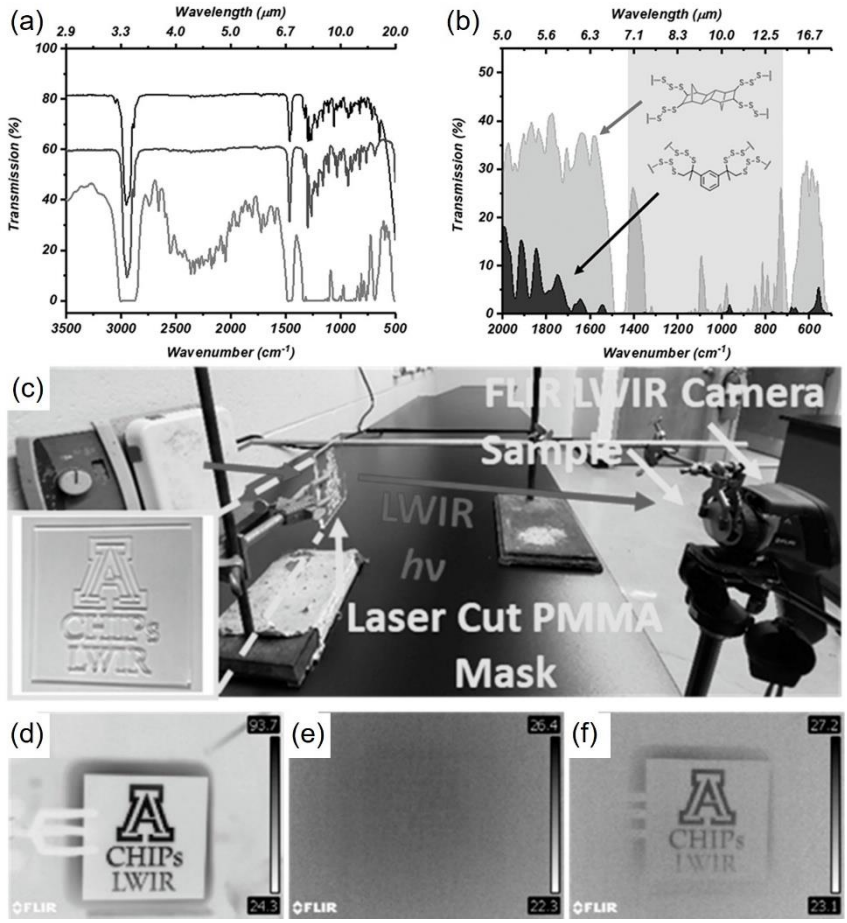

Figure 1.13: Poly(S-*r*-NBD2) optical characterisation. (a) FTIR spectra of 3 windows of poly(S_{70}-r-$NBD2_{30}$). Top spectrum (≈5 μm-30 μm) on NaCl plate, middle spectrum (60 μm) and bottom spectrum (1 mm) free standing windows. (c) imaging set up. (d) LWIR taken with FLIR LWIR camera of PMMA mask using "black hot" mode with no window. (e) Image taken through 1.3 mm thick poly(S_{70}-r-DIB_{30}) with no transmission. (f) Image taken through 1.3 mm thick poly(S_{70}-r-$NBD2_{30}$) showing transmission. Modified with permission from.[122]

After preparing and characterising the NBD2 based polymer, it was investigated as a lens in a thermal imaging system in a new publication in 2023.[123] In this publication, a Fresnel lens was designed and a master lens was prepared with diamond point turning of PMMA. Following this, a PDMS mould was fabricated which would allow for the preparation of polymer lenses. These lenses were designed to fit on a FLIR Lepton 2.5 imaging module which was used to prepare images. Two different types of lenses were prepared. The first were ultrathin polymer lenses on NaCl disks. NaCl is transparent to long-wave infrared radiation but does have some issues with sensitivity to water.[21] However, these dual material lenses were effective in focussing light onto the sensor of the FLIR lepton, allowing for the first optical system in which the focussing power was provided solely by an inverse vulcanized polymer.

Following the NaCl supported lenses, freestanding 0.7 mm thick lenses were prepared. While the transparency of the polymer at this thickness limited the imaging to higher temperatures (60 °C minimum) these were the first lenses prepared completely from an inverse vulcanized polymer to provide all the focusing for an optical system. Several important findings were made. The first is that the polymer could be made shape persistent and did not deform or warp over time which would lead to a decrease in the lens performance over time. It was also found that while the higher sulfur content composition had a greater transmittance to LWIR radiation, it would not always give the highest image contrast. It was proposed that this was due to unreacted S_8 in the polymer matrix, giving valuable information that sulfur crystals should be avoided for optical materials. This was a very important paper and showed the potential of high sulfur polymers to completely replace the lenses of long wave infrared imaging systems.

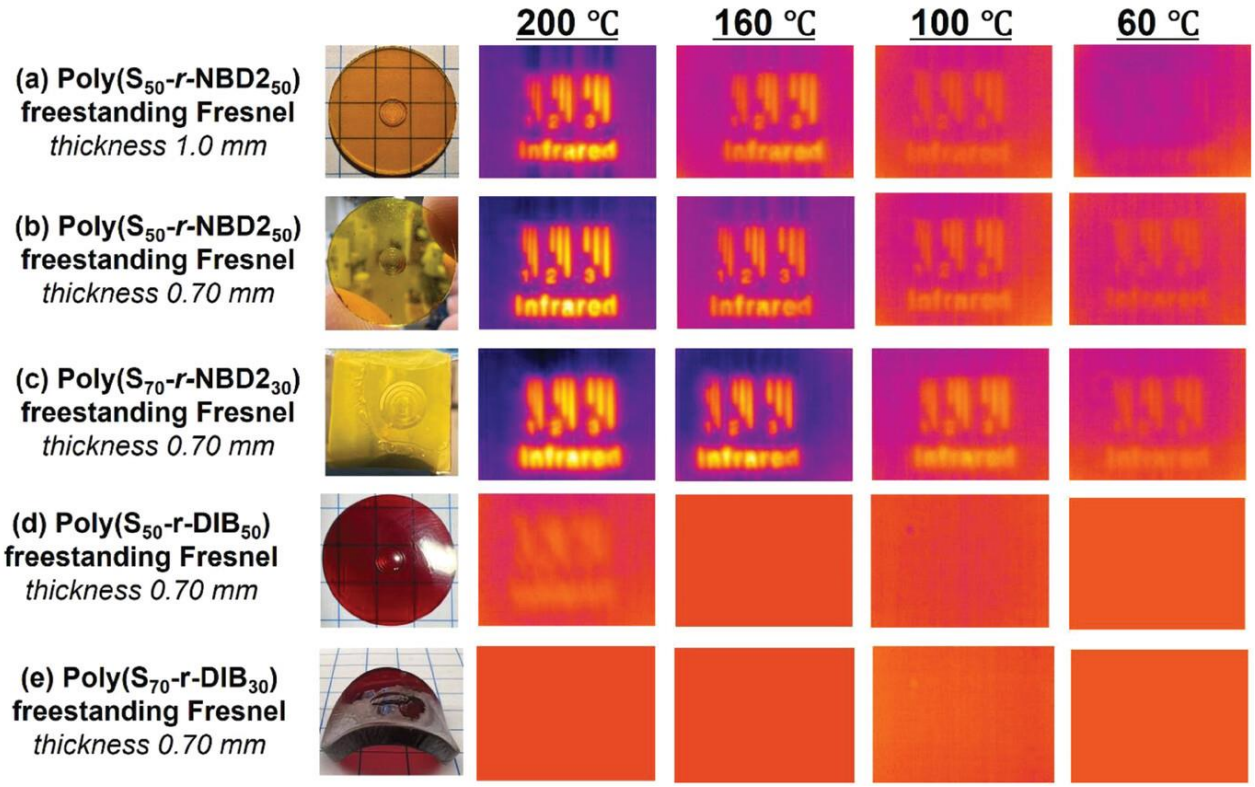

Figure 1.14: LWIR images through at different temperatures using lenses prepared from sulfur-based polymers. All images were taken on a FLIR Lepton 2.5. (a) 1 mm thick freestanding Fresnel lens prepared from poly(S_{50}-*r*-$NBD2_{50}$). (b) 0.7 mm thick freestanding Fresnel lens prepared from poly(S_{50}-*r*-$NBD2_{50}$). 0.7 mm thick freestanding Fresnel lens prepared from poly(S_{70}-*r*-$NBD2_{30}$). (d) 0.7 mm thick freestanding Fresnel lens prepared from poly(S_{50}-*r*-DIB_{50}). (e) 0.7 mm thick freestanding Fresnel lens prepared from poly(S_{70}-*r*-DID_{30}). Reused with permission from.[123]

While the polymer made with NBD2 was a significant improvement in the long wave infrared transparency and demonstrated lens manufacturing, it was not the polymer which was predicted computationally to have the greatest long-wave infrared transmission. Since then, there have been several attempts to prepare polymers with the norbornane organic core although most have used derivatives of norbornane. A paper in 2024 by Grimm *et al* synthesised a series of polymers based on norbornenyl esters.[124] While the paper was not focused on thermal imaging, they were successful in preparing a range of polymers where sulfur reacted with the norbornene double bond. The Pyun group followed up their research with the inverse vulcanization using a monomer derived from a reaction between cyclopentadiene and norbornadiene. This monomer was an endo-exo norbornadiene cyclopentadiene adduct known as stillene. The stillene monomer was reacted with sulfur in an inverse vulcanization reaction and showed similar long wave infrared transparency to polymers made with the NBD2 monomer.[125] Another norbornadiene derived monomer was prepared by Wuliu *et al*.[126] In this publication, they synthesised the monomer shown below which they called DMMD. While polymers made through a reaction of DMMD and sulfur showed an increase in glass transition temperature, they still had an average long wave infrared transmission of less than 6 %.

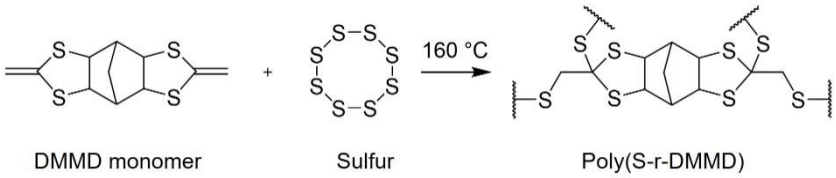

Figure 1.15: Reaction scheme for the synthesis of poly(S-r-DMMD). [126]

In the paper by Pyun focussing of stillene, the author also addressed the side products which can form from the direct reaction of norbornadiene with sulfur.[125] These side products contain cyclopropane groups which significantly reduce long wave infrared transparency. A paper claimed to have formed a norbornane based polymer through mechanochemical inverse vulcanization of norbornadiene and sulfur.[127] However, it is likely that this cyclopropane impurity is present in high quantities in their product. A greater explanation of this is presented in chapter 3 of this thesis where polymers with these cyclopropane groups were directly prepared and characterised to compare with the mechanochemically prepared polymers. This rearrangement and the low boiling point of norbornadiene are significant obstacles to the synthesis of the polymer predicted by Pyun. There is a significant gap in the literature which will require a unique approach to form the desired norbornane based polymer. This thesis will address this gap through a rigorous preparation of norbornane based sulfur polymers in chapter 3.

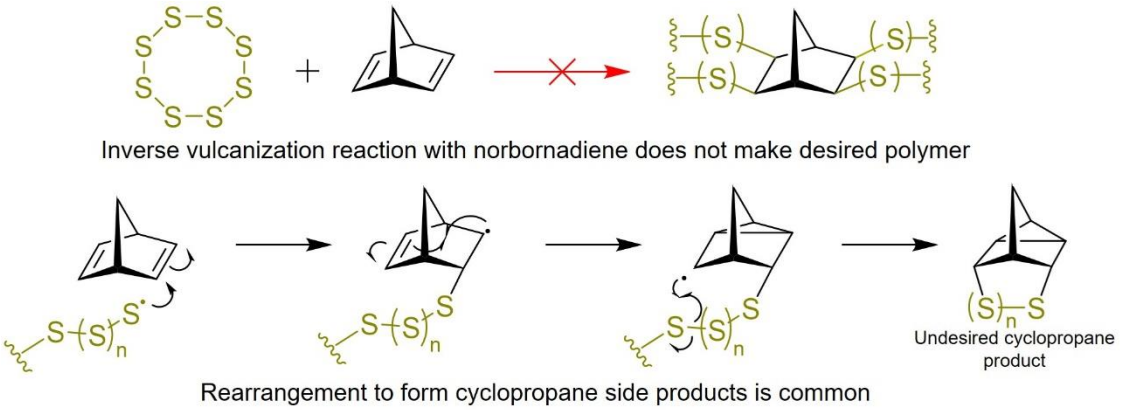

Figure 1.16: Reaction between sulfur and norbornadiene does not prepare the desired polymer as the major product but instead forms rearranged cyclopropane byproducts. (Experimental evidence in chapter 3).

Finally, there were two publications which demonstrated very high-performance materials based on reactions with thiols. The first was based on a benzene trithiol (BTT) monomer. This publication by Lee *et al* utilised a reaction between the thiols in BTT with sulfur to prepare a high sulfur polymer.[128] During this reaction, H_2S gas was eliminated and bubbled out of the reaction mixture, leaving sulfur chains at the 1,3 and 5 positions of the benzene ring. This polymer was very well designed and follows many of the principles for a high LWIR transparent material. First, the molecule is symmetric. This means that that there are limited unique chemical environments which would give absorptions in the long wave infrared regions. Secondly, the rigid benzene core and three attachment points for sulfur allowed for the incorporation of a very high sulfur loading without the formation of unreacted sulfur. They were able to incorporate 80 % sulfur without any issues of sulfur blooming. This allowed for an excellent refractive index of over 1.9 while also imparting a high transmission in the long wave infrared region. This paper presented some of the highest transmission of any published polymer with an average of over 18 %. This was an excellently designed polymer and had transmission great enough to be practically used in thermal imaging systems. However, it did show a relatively low glass transition temperature and released H_2S gas during the synthesis which may limit its scalability.

Another polymer by the same group was published in 2024 which utilised a dicyclopentadiene molecule with introduced thiol groups instead of the alkenes. [129] Dicyclopentadiene has been explored as a monomer for inverse vulcanization reactions in many publications,[91, 130] but shows relatively poor transmittance in the LWIR region.[131] However, when the alkenes were replaced with thiols and reacted with sulfur in a similar manner to BTT, it showed a significant improvement in the long wave infrared transmission. The polymer also had a yellow colour rather than black like most polymer prepared with dicyclopentadiene. The improvement in the long wave infrared transmittance was attributed to the prevention of side reactions and a more controlled polymerisation reaction. Using thiols would also prevent unreacted alkenes which are likely to add additional vibrational modes in the long-wave infrared region.

A quantitative analysis of the MWIR and LWIR transmittance of the polymers discussed here as well as several others can be found in the introduction to chapter 4. In this analysis, the transmission is compared to the polymers described in chapters 2 and 3 of this thesis.

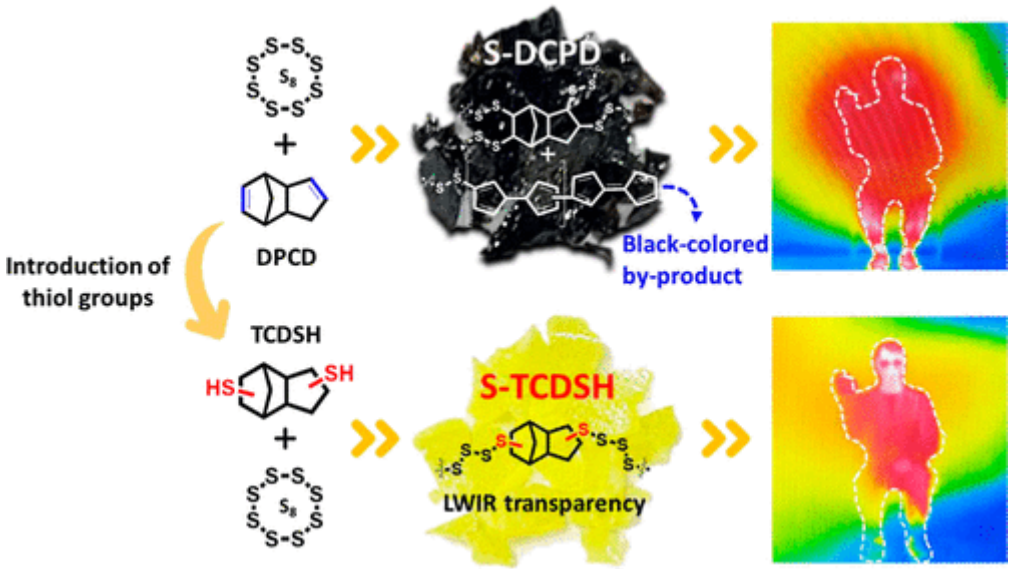

Figure 1.17: Introduction of thiol groups to dicyclopentadiene and inverse vulcanization to prepare long wave infrared transparent polymers. Reused with permission from.[129]

Chapter 1 references

(1) Prokhorov, A. V.; Hanssen, L. M.; Mekhontsev, S. N. Chapter 5 Calculation of the Radiation Characteristics of Blackbody Radiation Sources. In *Experimental Methods in the Physical Sciences*, Zhang, Z. M., Tsai, B. K., Machin, G. Eds.; Vol. 42; Academic Press, 2009; pp 181-240.
(2) Hartmann, J.; Hollandt, J.; Khlevnoy, B.; Morozova, S.; Ogarev, S.; Sakuma, F. Chapter 6 Blackbody and other Calibration Sources. In *Experimental Methods in the Physical Sciences*, Zhang, Z. M., Tsai, B. K., Machin, G. Eds.; Vol. 42; Academic Press, 2009; pp 241-295.
(3) Reiser, A.; Schächter, L. Geometric effects on blackbody radiation. *Physical Review A* **2013**, *87* (3), 033801. DOI: 10.1103/PhysRevA.87.033801.
(4) Stillwell, P. F. T. C. Thermal imaging. *Journal of Physics E: Scientific Instruments* **1981**, *14* (10), 1113. DOI: 10.1088/0022-3735/14/10/001.
(5) Altınoğlu, E. İ.; Adair, J. H. Near infrared imaging with nanoparticles. *WIREs Nanomedicine and Nanobiotechnology* **2010**, *2* (5), 461-477. DOI: https://doi.org/10.1002/wnan.77 (acccessed 2025/03/08).
(6) Kenry; Duan, Y.; Liu, B. Recent Advances of Optical Imaging in the Second Near-Infrared Window. *Advanced Materials* **2018**, *30* (47), 1802394. DOI: https://doi.org/10.1002/adma.201802394 (acccessed 2025/03/08).
(7) Luo, Y.; Remillard, J.; Hoetzer, D. Pedestrian detection in near-infrared night vision system. In *2010 IEEE Intelligent Vehicles Symposium*, 21-24 June 2010, 2010; pp 51-58. DOI: 10.1109/IVS.2010.5548089.
(8) Vahrmeijer, A. L.; Hutteman, M.; van der Vorst, J. R.; van de Velde, C. J. H.; Frangioni, J. V. Image-guided cancer surgery using near-infrared fluorescence. *Nature Reviews Clinical Oncology* **2013**, *10* (9), 507-518. DOI: 10.1038/nrclinonc.2013.123.
(9) Wen, M.; Wei, L.; Zhuang, X.; He, D.; Wang, S.; Wang, Y. High-sensitivity short-wave infrared technology for thermal imaging. *Infrared Physics & Technology* **2018**, *95*, 93-99. DOI: https://doi.org/10.1016/j.infrared.2018.10.020.
(10) Adomeit, U.; Krieg, J. Shortwave infrared for night vision applications: Illumination levels and sensor performance. In *Optics in Atmospheric Propagation and Adaptive Systems XVIII*, 2015; SPIE: Vol. 9641, pp 16-27.
(11) Becker, M.; Fan, H. Y. Optical Properties of Semiconductors. III. Infra-Red Transmission of Silicon. *Physical Review* **1949**, *76* (10), 1531-1532. DOI: 10.1103/PhysRev.76.1531.
(12) Hashagen, J. Seeing Beyond the Visible. *Optik & Photonik* **2015**, *10* (3), 34-37. DOI: https://doi.org/10.1002/opph.201500021.
(13) Bonifazi, G.; Gasbarrone, R.; Gattabria, D.; Lendaro, E.; Mosca, L.; Mattioli, R.; Serranti, S. Early Study on Visible (Vis) and Short-Wave Infrared (SWIR) Spectroscopy for Assessing Water Content in Olive Fruits: Towards Sustainable Land and Agricultural Practices. *Land* **2024**, *13* (12), 2231.
(14) Patel, K. K.; Pathare, P. B. Principle and applications of near-infrared imaging for fruit quality assessment—An overview. *International Journal of Food Science and Technology* **2023**, *59* (5), 3436-3450.
(15) R.J. Wilson, I. *SWIR Imaging 101: What Can it do for You?* 2025.
(16) Millikan, B.; Dutta, A.; Sun, Q.; Foroosh, H. Fast Detection of Compressively-Sensed IR Targets Using Stochastically Trained Least Squares and Compressed Quadratic Correlation Filters. *IEEE Transactions on Aerospace and Electronic Systems* **2017**, *PP*. DOI: 10.1109/TAES.2017.2700598.
(17) Deng, X.; Wang, Y.; He, D.; Han, G.; Xue, T.; Hao, Y.; Zhuang, X.; Liu, J.; Zhang, C.; Wang, S. A Compact Mid-Wave Infrared Imager System With Real-Time Target Detection and Tracking. *IEEE Journal of Selected Topics in Applied Earth Observations and Remote Sensing* **2022**, *15*, 6069-6085. DOI: 10.1109/JSTARS.2022.3192311.
(18) Razeghi, M.; Nguyen, B.-M. Advances in mid-infrared detection and imaging: a key issues review. *Reports on Progress in Physics* **2014**, *77* (8), 082401. DOI: 10.1088/0034-4885/77/8/082401.
(19) Faisal Abdulkareem, A.; Qusai Hashim, A. Infrared medical thermography, medical applications, and its basic principles: A review. In *BIO Web of Conferences*, 2024; EDP Sciences: Vol. 97, p 00140.
(20) Altenburg, S. J.; Straße, A.; Gumenyuk, A.; Maierhofer, C. In-situ monitoring of a laser metal deposition (LMD) process: Comparison of MWIR, SWIR and high-speed NIR thermography. *Quantitative InfraRed Thermography Journal* **2022**, *19* (2), 97-114.
(21) William, J. T.; Michael, E. T.; Paul, K. Infrared optical materials. In *Proc.SPIE*, 1996; Vol. 10286, p 102860A. DOI: 10.1117/12.245197.
(22) Shivakumar, R. What Technology Says About Decision-Making:Evidence From Cricket's Decision Review System (DRS). *Journal of Sports Economics* **2018**, *19* (3), 315-331. DOI: 10.1177/1527002516657218.
(23) Akin, T. Low-Cost LWIR-Band CMOS Infrared (CIR) Microbolometers for High Volume Applications. In *2020 IEEE 33rd International Conference on Micro Electro Mechanical Systems (MEMS)*, 18-22 Jan. 2020, 2020; pp 147-152. DOI: 10.1109/MEMS46641.2020.9056383.
(24) Argirusis, N.; Achilleos, A.; Alizadeh, N.; Argirusis, C.; Sourkouni, G. IR Sensors, Related Materials, and Applications. *Sensors* **2025**, *25* (3), 673.

(25) Alves, F. D. P.; Karunasiri, G.; Hanson, N.; Byloos, M.; Liu, H. C.; Bezinger, A.; Buchanan, M. NIR, MWIR and LWIR quantum well infrared photodetector using interband and intersubband transitions. *Infrared Physics & Technology* **2007**, *50* (2), 182-186. DOI: https://doi.org/10.1016/j.infrared.2006.10.021.
(26) Andrew, V.; Nibir, D.; Mukti, M. R. Materials for microbolometers: vanadium oxide or silicon derivatives. In *Proc.SPIE*, 2017; Vol. 10209, p 102090M. DOI: 10.1117/12.2263999.
(27) Yu, L.; Guo, Y.; Zhu, H.; Luo, M.; Han, P.; Ji, X. Low-Cost Microbolometer Type Infrared Detectors. In *Micromachines*, 2020; Vol. 11.
(28) Tankut, F.; Cologlu, M.; Ozturk, H.; Cilbir, G.; Akar, O.; Akin, T. *A 160x120 LWIR-band CMOS Infrared (CIR) microbolometer*; SPIE, 2019.
(29) Lenggenhager, R.; Baltes, H.; Elbel, T. Thermoelectric infrared sensors in CMOS technology. *Sensors and Actuators A: Physical* **1993**, *37-38*, 216-220. DOI: https://doi.org/10.1016/0924-4247(93)80037-H.
(30) Yadav, P. V. K.; Yadav, I.; Ajitha, B.; Rajasekar, A.; Gupta, S.; Ashok Kumar Reddy, Y. Advancements of uncooled infrared microbolometer materials: A review. *Sensors and Actuators A: Physical* **2022**, *342*, 113611. DOI: https://doi.org/10.1016/j.sna.2022.113611.
(31) Ismael, A. J.; Abdul Rahim, H.; Ghazali, R.; Mezher, K. N. Smart Home and Thermal Imaging Technology for COVID 19 Detection Using the Internet of Things (IoT). *ELEKTRIKA- Journal of Electrical Engineering* **2021**, *20* (2-2), 87-92. (acccessed 2025/03/14).
(32) Awais, M.; Li, W.; Cheema, M. J. M.; Zaman, Q. U.; Shaheen, A.; Aslam, B.; Zhu, W.; Ajmal, M.; Faheem, M.; Hussain, S.; et al. UAV-based remote sensing in plant stress imagine using high-resolution thermal sensor for digital agriculture practices: a meta-review. *International Journal of Environmental Science and Technology* **2023**, *20* (1), 1135-1152. DOI: 10.1007/s13762-021-03801-5.
(33) Vadivambal, R.; Jayas, D. S. Applications of Thermal Imaging in Agriculture and Food Industry—A Review. *Food and Bioprocess Technology* **2011**, *4* (2), 186-199. DOI: 10.1007/s11947-010-0333-5.
(34) Glowacz, A. Fault diagnosis of electric impact drills using thermal imaging. *Measurement* **2021**, *171*, 108815. DOI: https://doi.org/10.1016/j.measurement.2020.108815.
(35) Kumar, P.; Gaurav, A.; Rajnish, R. K.; Sharma, S.; Kumar, V.; Aggarwal, S.; Patel, S. Applications of thermal imaging with infrared thermography in Orthopaedics. *Journal of Clinical Orthopaedics and Trauma* **2022**, *24*, 101722. DOI: https://doi.org/10.1016/j.jcot.2021.101722.
(36) Bagavathiappan, S.; Philip, J.; Jayakumar, T.; Raj, B.; Rao, P. N. S.; Varalakshmi, M.; Mohan, V. Correlation between Plantar Foot Temperature and Diabetic Neuropathy: A Case Study by Using an Infrared Thermal Imaging Technique. *Journal of Diabetes Science and Technology* **2010**, *4* (6), 1386-1392. DOI: 10.1177/193229681000400613.
(37) Brekhovskikh, M. N.; Moiseeva, L. V.; Batygov, S. K.; Zhidkova, I. A.; Fedorov, V. A. Glasses on the basis of heavy metal fluorides. *Inorganic Materials* **2015**, *51* (13), 1348-1361. DOI: 10.1134/S0020168515130026.
(38) Tran, D.; Sigel, G.; Bendow, B. Heavy metal fluoride glasses and fibers: A review. *Journal of Lightwave Technology* **1984**, *2* (5), 566-586. DOI: 10.1109/JLT.1984.1073661.
(39) Depuydt, B.; Theuwis, A.; Romandic, I. Germanium: From the first application of Czochralski crystal growth to large diameter dislocation-free wafers. *Materials Science in Semiconductor Processing* **2006**, *9* (4), 437-443. DOI: https://doi.org/10.1016/j.mssp.2006.08.002.
(40) Venkatesh, V. C. Precision manufacture of spherical and aspheric surfaces on plastics, glass, silicon and germanium. *Current Science* **2003**, *84* (9), 1211-1219. (acccessed 2024/08/24/).JSTOR.
(41) Zakery, A.; Elliott, S. R. Optical properties and applications of chalcogenide glasses: a review. *Journal of Non-Crystalline Solids* **2003**, *330* (1), 1-12. DOI: https://doi.org/10.1016/j.jnoncrysol.2003.08.064.
(42) Sharma, P.; Sharma, N.; Sharda, S.; Katyal, S. C.; Sharma, V. Recent developments on the optical properties of thin films of chalcogenide glasses. *Progress in Solid State Chemistry* **2016**, *44* (4), 131-141. DOI: https://doi.org/10.1016/j.progsolidstchem.2016.11.002.
(43) Savage, J. A. Optical properties of chalcogenide glasses. *Journal of Non-Crystalline Solids* **1982**, *47* (1), 101-115. DOI: https://doi.org/10.1016/0022-3093(82)90349-0.
(44) D'Alessandro, G.; Paiella, A.; Coppolecchia, A.; Castellano, M. G.; Colantoni, I.; de Bernardis, P.; Lamagna, L.; Masi, S. Ultra high molecular weight polyethylene: Optical features at millimeter wavelengths. *Infrared Physics & Technology* **2018**, *90*, 59-65. DOI: https://doi.org/10.1016/j.infrared.2018.02.008.
(45) Liu, C.; Chen, Y.; Zhang, C.; Gui, Y.; Zhang, J.; Liu, Z.; Xu, T.; Shen, X. Obtaining ultra-high transmission of UHMWPE by hot uniaxial pressing for long-wave infrared imaging. *Infrared Physics & Technology* **2022**, *122*, 104102. DOI: https://doi.org/10.1016/j.infrared.2022.104102.
(46) Zhao, Y.; Zhang, Y.; Cui, L.; Jian, Z. Cyclic Olefin Terpolymers with High Refractive Index and High Optical Transparency. *ACS Macro Letters* **2023**, *12* (3), 395-400. DOI: 10.1021/acsmacrolett.3c00043.
(47) Manaf, A. R. A.; Sugiyama, T.; Yan, J. Design and fabrication of Si-HDPE hybrid Fresnel lenses for infrared imaging systems. *Opt. Express* **2017**, *25* (2), 1202-1220. DOI: 10.1364/OE.25.001202.
(48) Kutney, G. *Sulfur: history, technology, applications and industry*; Elsevier, 2023.
(49) Misra, P.; Badoga, S.; Dalai, A. K.; Adjaye, J. Enhancement of sulfur and nitrogen removal from heavy gas oil by using polymeric adsorbent followed by hydrotreatment. *Fuel* **2018**, *226*, 127-136. DOI: https://doi.org/10.1016/j.fuel.2018.04.014.

(50) Angelici, R. J. Heterogeneous catalysis of the hydrodesulfurization of thiophenes in petroleum: an organometallic perspective of the mechanism. *Accounts of Chemical Research* **1988**, *21* (11), 387-394.
(51) King, M.; Moats, M.; Davenport, W. G. *Sulfuric acid manufacture: analysis, control and optimization*; Newnes, 2013.
(52) Kiss, A. A.; Bildea, C. S.; Verheijen, P. J. T. Optimization studies in sulfuric acid production. In *Computer Aided Chemical Engineering*, Marquardt, W., Pantelides, C. Eds.; Vol. 21; Elsevier, 2006; pp 737-742.
(53) Nguyen, V. H.; Le, V. P. Performance evaluation of sulfur as alternative binder additive for asphalt mixtures. *International Journal of Pavement Research and Technology* **2019**, *12* (4), 380-387. DOI: 10.1007/s42947-019-0045-9.
(54) Amanova, N.; Turaev, K.; Shadhar, M. H.; Tadjixodjayeva, U.; Jumaeva, Z.; Berdimurodov, E.; Eliboev, I.; Hosseini-Bandegharaei, A. Sulfur-based concrete: Modifications, advancements, and future prospects. *Construction and Building Materials* **2024**, *435*, 136765. DOI: https://doi.org/10.1016/j.conbuildmat.2024.136765.
(55) Meyer, B. *Sulfur, energy, and environment*; Elsevier, 2013.
(56) Chung, W. J.; Griebel, J. J.; Kim, E. T.; Yoon, H.; Simmonds, A. G.; Ji, H. J.; Dirlam, P. T.; Glass, R. S.; Wie, J. J.; Nguyen, N. A.; et al. The use of elemental sulfur as an alternative feedstock for polymeric materials. *Nature Chemistry* **2013**, *5* (6), 518-524. DOI: 10.1038/nchem.1624.
(57) Zhang, B.; Gao, H.; Yan, P.; Petcher, S.; Hasell, T. Inverse vulcanization below the melting point of sulfur. *Materials Chemistry Frontiers* **2020**, *4* (2), 669-675, 10.1039/C9QM00606K. DOI: 10.1039/C9QM00606K.
(58) Hwang, J. H.; Lee, J. M.; Seo, J. H.; Noh, G. Y.; Byun, W.; Kim, S.; Lee, W.; Park, S.; Kim, D.-G.; Kim, Y. S. Inverse vulcanization of elemental sulfur catalyzed by trialkyl amines. *Green Chemistry* **2023**, *25* (12), 4641-4646, 10.1039/D3GC01102J. DOI: 10.1039/D3GC01102J.
(59) Dodd, L. J.; Omar, Ö.; Wu, X.; Hasell, T. Investigating the Role and Scope of Catalysts in Inverse Vulcanization. *ACS Catalysis* **2021**, *11* (8), 4441-4455. DOI: 10.1021/acscatal.0c05010.
(60) Wu, X.; Smith, J. A.; Petcher, S.; Zhang, B.; Parker, D. J.; Griffin, J. M.; Hasell, T. Catalytic inverse vulcanization. *Nature Communications* **2019**, *10* (1), 647. DOI: 10.1038/s41467-019-08430-8.
(61) Zhang, Y.; Pavlopoulos, N. G.; Kleine, T. S.; Karayilan, M.; Glass, R. S.; Char, K.; Pyun, J. Nucleophilic Activation of Elemental Sulfur for Inverse Vulcanization and Dynamic Covalent Polymerizations. *Journal of Polymer Science Part A: Polymer Chemistry* **2019**, *57* (1), 7-12. DOI: https://doi.org/10.1002/pola.29266.
(62) Shankarayya Wadi, V. K.; Jena, K. K.; Khawaja, S. Z.; Yannakopoulou, K.; Fardis, M.; Mitrikas, G.; Karagianni, M.; Papavassiliou, G.; Alhassan, S. M. NMR and EPR Structural Analysis and Stability Study of Inverse Vulcanized Sulfur Copolymers. *ACS Omega* **2018**, *3* (3), 3330-3339. DOI: 10.1021/acsomega.8b00031.
(63) Meyer, B. Elemental sulfur. *Chemical reviews* **1976**, *76* (3), 367-388.
(64) Smith, J. A.; Green, S. J.; Petcher, S.; Parker, D. J.; Zhang, B.; Worthington, M. J. H.; Wu, X.; Kelly, C. A.; Baker, T.; Gibson, C. T.; et al. Crosslinker Copolymerization for Property Control in Inverse Vulcanization. *Chemistry – A European Journal* **2019**, *25* (44), 10433-10440. DOI: https://doi.org/10.1002/chem.201901619.
(65) Yan, P.; Zhao, W.; Zhang, B.; Jiang, L.; Petcher, S.; Smith, J. A.; Parker, D. J.; Cooper, A. I.; Lei, J.; Hasell, T. Inverse Vulcanized Polymers with Shape Memory, Enhanced Mechanical Properties, and Vitrimer Behavior. *Angewandte Chemie International Edition* **2020**, *59* (32), 13371-13378. DOI: https://doi.org/10.1002/anie.202004311.
(66) Bao, J.; Martin, K. P.; Cho, E.; Kang, K.-S.; Glass, R. S.; Coropceanu, V.; Bredas, J.-L.; Parker, W. O. N., Jr.; Njardarson, J. T.; Pyun, J. On the Mechanism of the Inverse Vulcanization of Elemental Sulfur: Structural Characterization of Poly(sulfur-random-(1,3-diisopropenylbenzene)). *Journal of the American Chemical Society* **2023**, *145* (22), 12386-12397. DOI: 10.1021/jacs.3c03604.
(67) Alex, A.; Singha, N. K.; Choudhury, S. Exploring inverse vulcanization in lithium–sulfur batteries. *Current Opinion in Electrochemistry* **2023**, *39*, 101271. DOI: https://doi.org/10.1016/j.coelec.2023.101271.
(68) Grimm, A. P.; Deng, B.; Haridas, S. V.; Voll, D.; Schmitt, C. W.; von Delius, M.; Scheiba, F.; Théato, P. Inverse vulcanization of all-cis-fluorinated cyclohexylacrylate: Tailored polymers for Li-S battery cathode materials. *European Polymer Journal* **2025**, *228*, 113815. DOI: https://doi.org/10.1016/j.eurpolymj.2025.113815.
(69) Zhao, L.; Qiu, F.; Deng, X.; Huang, Y.; Li, Y.; Zhao, C.; Ren, W.; Zou, C.; Li, X.; Wang, M.; et al. Novel Sulfur-Containing Polymeric Cathode Material Prepared via an Inverse Vulcanization Method for Advanced Lithium–Sulfur Batteries. *ACS Applied Energy Materials* **2022**, *5* (6), 7617-7626. DOI: 10.1021/acsaem.2c00866.
(70) Yeşilot, S.; Küçükköylü, S.; Mutlu, T.; Demir-Cakan, R. Ethylene Glycol-Containing Acrylic Polyphosphazene Based Cathode Materials via Inverse Vulcanization of Sulfur for Li−S Batteries. *ChemElectroChem* **2024**, *11* (4), e202300461. DOI: https://doi.org/10.1002/celc.202300461.
(71) Deng, B.; Scheiba, F.; Zuo, A.; Indris, S.; Li, H.; Radinger, H.; Grimm, A.; Njel, C. Sulfur Distribution Analysis in Lithium−Sulfur Cathode via Confined Inverse Vulcanization in Carbon Frameworks. *Advanced Energy Materials* **2025**, *15* (9), 2402996. DOI: https://doi.org/10.1002/aenm.202402996.

(72) Yeşilot, S.; Küçükköylü, S.; Mutlu, T.; Demir, E.; Demir-Cakan, R. Highly sulfur-rich polymeric cathode materials via inverse vulcanization of sulfur for lithium–sulfur batteries. *Materials Chemistry and Physics* **2022**, *285*, 126168. DOI: https://doi.org/10.1016/j.matchemphys.2022.126168.
(73) Simmonds, A. G.; Griebel, J. J.; Park, J.; Kim, K. R.; Chung, W. J.; Oleshko, V. P.; Kim, J.; Kim, E. T.; Glass, R. S.; Soles, C. L.; et al. Inverse Vulcanization of Elemental Sulfur to Prepare Polymeric Electrode Materials for Li–S Batteries. *ACS Macro Letters* **2014**, *3* (3), 229-232. DOI: 10.1021/mz400649w.
(74) Hoefling, A.; Nguyen, D. T.; Partovi-Azar, P.; Sebastiani, D.; Theato, P.; Song, S.-W.; Lee, Y. J. Mechanism for the Stable Performance of Sulfur-Copolymer Cathode in Lithium–Sulfur Battery Studied by Solid-State NMR Spectroscopy. *Chemistry of Materials* **2018**, *30* (9), 2915-2923. DOI: 10.1021/acs.chemmater.7b05105.
(75) Ji, X.; Nazar, L. F. Advances in Li–S batteries. *Journal of Materials Chemistry* **2010**, *20* (44), 9821-9826, 10.1039/B925751A. DOI: 10.1039/B925751A.
(76) Marinescu, M.; O'Neill, L.; Zhang, T.; Walus, S.; Wilson, T. E.; Offer, G. J. Irreversible vs Reversible Capacity Fade of Lithium-Sulfur Batteries during Cycling: The Effects of Precipitation and Shuttle. *Journal of The Electrochemical Society* **2018**, *165* (1), A6107. DOI: 10.1149/2.0171801jes.
(77) Chang, A.; Wu, Q.; Du, X.; Chen, S.; Shen, J.; Song, Q.; Xie, J.; Wu, W. Immobilization of sulfur in microgels for lithium–sulfur battery. *Chemical Communications* **2016**, *52* (24), 4525-4528, 10.1039/C6CC00489J. DOI: 10.1039/C6CC00489J.
(78) Fu, C.; Li, G.; Zhang, J.; Cornejo, B.; Piao, S. S.; Bozhilov, K. N.; Haddon, R. C.; Guo, J. Electrochemical Lithiation of Covalently Bonded Sulfur in Vulcanized Polyisoprene. *ACS Energy Letters* **2016**, *1* (1), 115-120. DOI: 10.1021/acsenergylett.6b00073.
(79) Chang, C.-H.; Manthiram, A. Covalently Grafted Polysulfur–Graphene Nanocomposites for Ultrahigh Sulfur-Loading Lithium–Polysulfur Batteries. *ACS energy letters* **2018**, *3*, 72-77.
(80) Choudhury, S.; Srimuk, P.; Raju, K.; Tolosa, A.; Fleischmann, S.; Zeiger, M.; Ozoemena, K. I.; Borchardt, L.; Presser, V. Carbon onion/sulfur hybrid cathodes via inverse vulcanization for lithium–sulfur batteries. *Sustainable Energy & Fuels* **2018**, *2* (1), 133-146, 10.1039/C7SE00452D. DOI: 10.1039/C7SE00452D.
(81) Hu, G.; Sun, Z.; Shi, C.; Fang, R.; Chen, J.; Hou, P.; Liu, C.; Cheng, H.-M.; Li, F. A Sulfur-Rich Copolymer@CNT Hybrid Cathode with Dual-Confinement of Polysulfides for High-Performance Lithium–Sulfur Batteries. *Advanced Materials* **2017**, *29* (11), 1603835. DOI: https://doi.org/10.1002/adma.201603835.
(82) Li, B.; Li, S.; Xu, J.; Yang, S. A new configured lithiated silicon–sulfur battery built on 3D graphene with superior electrochemical performances. *Energy & Environmental Science* **2016**, *9* (6), 2025-2030, 10.1039/C6EE01019A. DOI: 10.1039/C6EE01019A.
(83) Shen, K.; Mei, H.; Li, B.; Ding, J.; Yang, S. 3D Printing Sulfur Copolymer-Graphene Architectures for Li-S Batteries. *Advanced Energy Materials* **2018**, *8* (4), 1701527. DOI: https://doi.org/10.1002/aenm.201701527.
(84) Ma, Y.; Shi, C.; Hong, Q.; Du, J.; Zhang, H.; Zheng, X.; Qu, Z.; Zhang, X.; Xu, H. Harnessing graft copolymerization and inverse vulcanization to engineer sulfur-enriched copolymers for the selective uptake of heavy metals. *Separation and Purification Technology* **2025**, *362*, 131902. DOI: https://doi.org/10.1016/j.seppur.2025.131902.
(85) Lyu, S.; Abidin, Z. Z.; Yaw, T. C. S.; Resul, M. F. M. G. Inverse vulcanization induced oxygen modified porous polysulfides for efficient sorption of heavy metals. *Environmental Science and Pollution Research* **2024**, *31* (11), 16940-16957. DOI: 10.1007/s11356-024-32323-z.
(86) Crockett, M. P.; Evans, A. M.; Worthington, M. J. H.; Albuquerque, I. S.; Slattery, A. D.; Gibson, C. T.; Campbell, J. A.; Lewis, D. A.; Bernardes, G. J. L.; Chalker, J. M. Sulfur-Limonene Polysulfide: A Material Synthesized Entirely from Industrial By-Products and Its Use in Removing Toxic Metals from Water and Soil. *Angewandte Chemie International Edition* **2016**, *55* (5), 1714-1718. DOI: https://doi.org/10.1002/anie.201508708.
(87) Worthington, M. J.; Mann, M.; Muhti, I. Y.; Tikoalu, A. D.; Gibson, C. T.; Jia, Z.; Miller, A. D.; Chalker, J. M. Modelling mercury sorption of a polysulfide coating made from sulfur and limonene. *Physical Chemistry Chemical Physics* **2022**, *24* (20), 12363-12373.
(88) Tikoalu, A. D.; Lundquist, N. A.; Chalker, J. M. Mercury sorbents made by inverse vulcanization of sustainable triglycerides: the plant oil structure influences the rate of mercury removal from water. *Advanced Sustainable Systems* **2020**, *4* (3), 1900111.
(89) Limjuco, L. A.; Nisola, G. M.; Parohinog, K. J.; Valdehuesa, K. N. G.; Lee, S.-P.; Kim, H.; Chung, W.-J. Water-insoluble hydrophilic polysulfides as microfibrous composites towards highly effective and practical Hg2+ capture. *Chemical Engineering Journal* **2019**, *378*, 122216.
(90) Cubero-Cardoso, J.; Cuadri, A. A.; Fermoso, F. G.; Martín-Alfonso, J. E.; Urbano, J. Promising chalcogenide hybrid copolymers for sustainable applications as bio-lubricants and metal adsorbents. *ACS Applied Polymer Materials* **2022**, *4* (5), 3667-3675.
(91) Chalker, J. M.; Mann, M.; Worthington, M. J.; Esdaile, L. J. Polymers made by inverse vulcanization for use as mercury sorbents. *Organic Materials* **2021**, *3* (02), 362-373.
(92) Eder, M. L.; Call, C. B.; Jenkins, C. L. Utilizing reclaimed petroleum waste to synthesize water-soluble polysulfides for selective heavy metal binding and detection. *ACS Applied Polymer Materials* **2022**, *4* (2), 1110-1116.

(93) Mann, M.; Nicholls, T.; Patel, H.; Lisboa, L.; Pople, J.; Le Nhan Pham, M. W., Matthew Smith, Yanting Yin, Gunther Andersson, Christopher Gibson, Louisa Esdaile, Claire Lenehan, Michelle Coote, Zhongfan Jia, Justin Chalker. Integrated methods for gold leaching and recovery from ore and electronic waste. *ChemRxiv* **2024**, *"[Online]" 10.26434*. DOI: doi:10.26434/chemrxiv-2024-1xd84.
(94) Worthington, M. J. H.; Shearer, C. J.; Esdaile, L. J.; Campbell, J. A.; Gibson, C. T.; Legg, S. K.; Yin, Y.; Lundquist, N. A.; Gascooke, J. R.; Albuquerque, I. S.; et al. Sustainable Polysulfides for Oil Spill Remediation: Repurposing Industrial Waste for Environmental Benefit. *Advanced Sustainable Systems* **2018**, *2* (6), 1800024. DOI: https://doi.org/10.1002/adsu.201800024.
(95) Griebel, J. J.; Nguyen, N. A.; Astashkin, A. V.; Glass, R. S.; Mackay, M. E.; Char, K.; Pyun, J. Preparation of dynamic covalent polymers via inverse vulcanization of elemental sulfur. *ACS Macro Letters* **2014**, *3* (12), 1258-1261.
(96) Griebel, J. J.; Nguyen, N. A.; Namnabat, S.; Anderson, L. E.; Glass, R. S.; Norwood, R. A.; Mackay, M. E.; Char, K.; Pyun, J. Dynamic Covalent Polymers via Inverse Vulcanization of Elemental Sulfur for Healable Infrared Optical Materials. *ACS Macro Letters* **2015**, *4* (9), 862-866. DOI: 10.1021/acsmacrolett.5b00502.
(97) Tonkin, S. J.; Gibson, C. T.; Campbell, J. A.; Lewis, D. A.; Karton, A.; Hasell, T.; Chalker, J. M. Chemically induced repair, adhesion, and recycling of polymers made by inverse vulcanization. *Chemical Science* **2020**, *11* (21), 5537-5546, 10.1039/D0SC00855A. DOI: 10.1039/D0SC00855A.
(98) Carothers, K.; Lee, K. M.; McConney, M. E.; Stevenson, P. R.; Godman, N. P. Inverse Vulcanization of Vinyl-polycyclic Aromatic Hydrocarbon Monomers and Dynamic Covalent Polymerization with Liquid Crystalline Monomers. *ACS Applied Polymer Materials* **2024**, *6* (18), 11118-11126.
(99) Hou, K. X.; Zhao, P. C.; Duan, L.; Fan, M.; Zheng, P.; Li, C. H. Bitumen-Like Polymers Prepared via Inverse Vulcanization with Shear Stiffening and Self-Healing Abilities for Multifunctional Applications. *Advanced Functional Materials* **2023**, *33* (51), 2306886.
(100) Fan, J.; Ju, C.; Fan, S.; Li, X.; Zhang, Z.; Hadjichristidis, N. Inverse Vulcanization of Aziridines: Enhancing Polysulfides for Superior Mechanical Strength and Adhesive Performance. *Angewandte Chemie International Edition* **2025**, *64* (6), e202418764. DOI: https://doi.org/10.1002/anie.202418764.
(101) Lundquist, N. A.; Tikoalu, A. D.; Worthington, M. J. H.; Shapter, R.; Tonkin, S. J.; Stojcevski, F.; Mann, M.; Gibson, C. T.; Gascooke, J. R.; Karton, A.; et al. Reactive Compression Molding Post-Inverse Vulcanization: A Method to Assemble, Recycle, and Repurpose Sulfur Polymers and Composites. *Chemistry – A European Journal* **2020**, *26* (44), 10035-10044. DOI: https://doi.org/10.1002/chem.202001841.
(102) Lundquist, N. A.; Chalker, J. M. Confining a spent lead sorbent in a polymer made by inverse vulcanization prevents leaching. *Sustainable Materials and Technologies* **2020**, *26*, e00222. DOI: https://doi.org/10.1016/j.susmat.2020.e00222.
(103) Hanna, V.; Yan, P.; Petcher, S.; Hasell, T. Incorporation of fillers to modify the mechanical performance of inverse vulcanised polymers. *Polymer Chemistry* **2022**, *13* (26), 3930-3937.
(104) Mann, M.; Kruger, J. E.; Andari, F.; McErlean, J.; Gascooke, J. R.; Smith, J. A.; Worthington, M. J. H.; McKinley, C. C. C.; Campbell, J. A.; Lewis, D. A.; et al. Sulfur polymer composites as controlled-release fertilisers. *Organic & Biomolecular Chemistry* **2019**, *17* (7), 1929-1936, 10.1039/C8OB02130A. DOI: 10.1039/C8OB02130A.
(105) Pople, J. M. M.; Nicholls, T. P.; Pham, L. N.; Bloch, W. M.; Lisboa, L. S.; Perkins, M. V.; Gibson, C. T.; Coote, M. L.; Jia, Z.; Chalker, J. M. Electrochemical Synthesis of Poly(trisulfides). *Journal of the American Chemical Society* **2023**, *145* (21), 11798-11810. DOI: 10.1021/jacs.3c03239.
(106) Poulain, S.; Julien, S.; Duñach, E. Conversion of norbornene derivatives into vicinal-dithioethers via S8 activation. *Tetrahedron Letters* **2005**, *46* (41), 7077-7079. DOI: https://doi.org/10.1016/j.tetlet.2005.07.161.
(107) Mazumder, K.; Voit, B.; Banerjee, S. Recent Progress in Sulfur-Containing High Refractive Index Polymers for Optical Applications. *ACS Omega* **2024**, *9* (6), 6253-6279. DOI: 10.1021/acsomega.3c08571.
(108) Lee, D.; Cho, H.; Yoon, I. Zirconia nanocomposites and their applications as transparent advanced optical materials with high refractive index. *Bulletin of the Korean Chemical Society* **2023**, *44* (4), 284-292. DOI: https://doi.org/10.1002/bkcs.12666 (acccessed 2025/03/16).
(109) Shahwar, D.; Yoon, H. H.; Akkanen, S.-T.; Li, D.; Muntaha, S. t.; Cherchi, M.; Aalto, T.; Sun, Z. Polarization management in silicon photonics. *npj Nanophotonics* **2024**, *1* (1), 35. DOI: 10.1038/s44310-024-00033-6.
(110) Pyun, J.; Norwood, R. A. Infrared plastic optics and photonic devices using chalcogenide hybrid inorganic/organic polymers via inverse vulcanization of elemental sulfur. *Progress in Polymer Science* **2024**, *156*, 101865. DOI: https://doi.org/10.1016/j.progpolymsci.2024.101865.
(111) Griebel, J. J.; Namnabat, S.; Kim, E. T.; Himmelhuber, R.; Moronta, D. H.; Chung, W. J.; Simmonds, A. G.; Kim, K. J.; Van Der Laan, J.; Nguyen, N. A. New infrared transmitting material via inverse vulcanization of elemental sulfur to prepare high refractive index polymers. *Adv. Mater* **2014**, *26* (19), 3014-3018.
(112) Park, S.; Lee, D.; Cho, H.; Lim, J.; Char, K. Inverse Vulcanization Polymers with Enhanced Thermal Properties via Divinylbenzene Homopolymerization-Assisted Cross-Linking. *ACS Macro Letters* **2019**, *8* (12), 1670-1675. DOI: 10.1021/acsmacrolett.9b00827.

(113) Jang, W.; Choi, K.; Choi, J. S.; Kim, D. H.; Char, K.; Lim, J.; Im, S. G. Transparent, Ultrahigh-Refractive Index Polymer Film (n ~1.97) with Minimal Birefringence (Δn <0.0010). *ACS Applied Materials & Interfaces* **2021**, *13* (51), 61629-61637. DOI: 10.1021/acsami.1c17398.
(114) Boyd, D. A.; Nguyen, V. Q.; McClain, C. C.; Kung, F. H.; Baker, C. C.; Myers, J. D.; Hunt, M. P.; Kim, W.; Sanghera, J. S. Optical Properties of a Sulfur-Rich Organically Modified Chalcogenide Polymer Synthesized via Inverse Vulcanization and Containing an Organometallic Comonomer. *ACS Macro Letters* **2019**, *8* (2), 113-116. DOI: 10.1021/acsmacrolett.8b00923.
(115) Sahoo, D.; Naik, R. A review on the linear/nonlinear optical properties of Se doped chalcogenide thin films as potential optoelectronic applications. *Journal of Non-Crystalline Solids* **2022**, *597*, 121934. DOI: https://doi.org/10.1016/j.jnoncrysol.2022.121934.
(116) Anderson, L. E.; Kleine, T. S.; Zhang, Y.; Phan, D. D.; Namnabat, S.; LaVilla, E. A.; Konopka, K. M.; Ruiz Diaz, L.; Manchester, M. S.; Schwiegerling, J.; et al. Chalcogenide Hybrid Inorganic/Organic Polymers: Ultrahigh Refractive Index Polymers for Infrared Imaging. *ACS Macro Letters* **2017**, *6* (5), 500-504. DOI: 10.1021/acsmacrolett.7b00225.
(117) Gomez, I.; Mantione, D.; Leonet, O.; Blazquez, J. A.; Mecerreyes, D. Hybrid Sulfur−Selenium Co-polymers as Cathodic Materials for Lithium Batteries. *ChemElectroChem* **2018**, *5* (2), 260-265. DOI: https://doi.org/10.1002/celc.201700882
(118) Jia, J.; Chai, Y.; Xun, X.; Gao, Y.; Qiao, T.; Wang, X.; Wang, X.-C.; Hasell, T.; Wu, X.; Quan, Z.-J. Dynamic Covalent Sulfur-Selenium Rich Polymers via Inverse Vulcanization for High Refractive Index, High Transmittance, and UV Shielding Materials. *Macromolecular Rapid Communications* **2025**, *n/a* (n/a), 2400998. DOI: https://doi.org/10.1002/marc.202400998
(119) Kleine, T. S.; Diaz, L. R.; Konopka, K. M.; Anderson, L. E.; Pavlopolous, N. G.; Lyons, N. P.; Kim, E. T.; Kim, Y.; Glass, R. S.; Char, K.; et al. One Dimensional Photonic Crystals Using Ultrahigh Refractive Index Chalcogenide Hybrid Inorganic/Organic Polymers. *ACS Macro Letters* **2018**, *7* (7), 875-880. DOI: 10.1021/acsmacrolett.8b00245.
(120) Griebel, J. J.; Namnabat, S.; Kim, E. T.; Himmelhuber, R.; Moronta, D. H.; Chung, W. J.; Simmonds, A. G.; Kim, K.-J.; van der Laan, J.; Nguyen, N. A.; et al. New Infrared Transmitting Material via Inverse Vulcanization of Elemental Sulfur to Prepare High Refractive Index Polymers. *Advanced Materials* **2014**, *26* (19), 3014-3018. DOI: https://doi.org/10.1002/adma.201305607.
(121) Kleine, T. S.; Nguyen, N. A.; Anderson, L. E.; Namnabat, S.; LaVilla, E. A.; Showghi, S. A.; Dirlam, P. T.; Arrington, C. B.; Manchester, M. S.; Schwiegerling, J.; et al. High Refractive Index Copolymers with Improved Thermomechanical Properties via the Inverse Vulcanization of Sulfur and 1,3,5-Triisopropenylbenzene. *ACS Macro Letters* **2016**, *5* (10), 1152-1156. DOI: 10.1021/acsmacrolett.6b00602.
(122) Kleine, T. S.; Lee, T.; Carothers, K. J.; Hamilton, M. O.; Anderson, L. E.; Ruiz Diaz, L.; Lyons, N. P.; Coasey, K. R.; Parker Jr., W. O.; Borghi, L.; et al. Infrared Fingerprint Engineering: A Molecular-Design Approach to Long-Wave Infrared Transparency with Polymeric Materials. *Angewandte Chemie International Edition* **2019**, *58* (49), 17656-17660. DOI: https://doi.org/10.1002/anie.201910856.
(123) Molineux, J.; Lee, T.; Kim, K. J.; Kang, K.-S.; Lyons, N. P.; Nishant, A.; Kleine, T. S.; Durfee, S. W.; Pyun, J.; Norwood, R. A. Fabrication of Plastic Optics from Chalcogenide Hybrid Inorganic/Organic Polymers for Infrared Thermal Imaging. *Advanced Optical Materials* **2024**, *12* (7), 2301971. DOI: https://doi.org/10.1002/adom.202301971.
(124) Grimm, A. P.; Plank, M.; Stihl, A.; Schmitt, C. W.; Voll, D.; Schacher, F. H.; Lahann, J.; Théato, P. Inverse Vulcanization of Activated Norbornenyl Esters—A Versatile Platform for Functional Sulfur Polymers. *Angewandte Chemie International Edition* **2024**, *63* (36), e202411010. DOI: https://doi.org/10.1002/anie.202411010.
(125) Marshall, C. M.; Molineux, J.; Kang, K.-S.; Kumirov, V.; Kim, K.-J.; Norwood, R. A.; Njardarson, J. T.; Pyun, J. Synthesis of Polycyclic Olefinic Monomers from Norbornadiene for Inverse Vulcanization: Structural and Mechanistic Consequences. *Journal of the American Chemical Society* **2024**, *146* (34), 24061-24074. DOI: 10.1021/jacs.4c08113.
(126) Wuliu, Y.; Dong, W.; Huang, G.; Xie, H.; Yao, P.; Tan, J.; Mu, K.; Zhang, Z.; Chen, Y.; Wang, M.; et al. Sulfur-Rich Norbornadiene-Derived Infrared Transparent Polymers by Inverse Vulcanization. *Angewandte Chemie International Edition* **2025**, *64* (7), e202419446. DOI: https://doi.org/10.1002/anie.202419446.
(127) He, L.; Yang, J.; Jiang, H.; Zhao, H.; Xia, H. Mechanochemistry Enabled Inverse Vulcanization of Norbornadiene for Optical Polymers and Elastomeric Materials. *Industrial & Engineering Chemistry Research* **2023**, *62* (25), 9587-9594. DOI: 10.1021/acs.iecr.3c00801.
(128) Lee, M.; Oh, Y.; Yu, J.; Jang, S. G.; Yeo, H.; Park, J.-J.; You, N.-H. Long-wave infrared transparent sulfur polymers enabled by symmetric thiol cross-linker. *Nature Communications* **2023**, *14* (1), 2866. DOI: 10.1038/s41467-023-38398-5.
(129) Lee, M.; Jang, S. G.; Yeo, H.; Park, J.-J.; Moon, B.; You, N.-H. Structural Effect of Cyclic Olefin Cross-Linkers on Long-Wave Infrared-Transmitting Sulfur Polymers. *Macromolecules* **2024**, *57* (6), 2905-2914. DOI: 10.1021/acs.macromol.4c00018.
(130) Smith, J. A. *Inverse Vulcanisation of Elemental Sulfur for functional materials*; The University of Liverpool (United Kingdom), 2020.

(131) Tonkin, S. J.; Pham, L. N.; Gascooke, J. R.; Johnston, M. R.; Coote, M. L.; Gibson, C. T.; Chalker, J. M. Thermal Imaging and Clandestine Surveillance using Low-Cost Polymers with Long-Wave Infrared Transparency. *Advanced Optical Materials* **2023**, *11* (16), 2300058. DOI: https://doi.org/10.1002/adom.202300058.

Chapter 2 – Long-wave infrared transparent polymers made from sulfur and cyclopentadiene

Publications and patents from this chapter

Tonkin, S. J.; Pham, L. N.; Gascooke, J. R.; Johnston, M. R.; Coote, M. L.; Gibson, C. T.; Chalker, J. M. Thermal Imaging and Clandestine Surveillance using Low-Cost Polymers with Long-Wave Infrared Transparency. Advanced Optical Materials 2023, 11 (16), 2300058. DOI: https://doi.org/10.1002/adom.202300058.[1]

Chalker, J.; Tonkin, S. New polymers and uses thereof. Australian application number: 202316976, Filed 07 Feb 2023.

Chapter introduction

The focus of this chapter is to develop a polymer with good properties for use in infrared imaging. As explained in the first chapter, the main properties that are important for infrared imaging are a high refractive index, high transmission in the long wave infrared region (7 µm – 14 µm) and preferably a high glass transition temperature to ensure shape persistent at higher operating temperatures. To achieve these goals, a polymer based on cyclopentadiene was developed.

In the long wave infrared region, there are a complex range of absorptions which originate from the vibrations in C-C, C-H and C-X heteroatom covalent bonds[2]. Larger atoms, like sulfur or selenium, shift these vibrations out of the mid and long wave infrared regions[3]. Furthermore, as these atoms are large and polarisable, they often increase the refractive index[3]. High sulfur polymers replace many of the highly absorbing carbon-carbon bonds of typical polymers with weakly absorbing carbon-sulfur bonds, while also increasing the refractive index of the polymer. This provides a theoretical basis for the use of polymer prepared through inverse vulcanization for infrared optics.

While sulfur-based polymers have several advantages over conventional polymers for infrared optics, the choice of monomers used in the reaction is still vitally important. This is because the absorptions from the bonds in the monomer would still be present in the polymer and highly absorbing groups would lead to low transmission in the mid and long wave infrared regions.[4] In this chapter, cyclopentadiene will be investigated as the organic portion of the polymer. Cyclopentadiene is relatively small and unsaturated, with two alkenes despite only having a mass of 66 g/mol. There is some theoretical precedent that monomers like this could result in polymers that are highly transparent in the mid and long wave infrared regions. The first piece of evidence comes from conventional polymers. The only carbon-based polymers that see use in infrared optics are those based on simple aliphatic structures.[5] This is because of these polymers have very few unique absorptions, resulting they have regions of transparency that are useful for infrared imaging.[5] The use of small, simple monomers has also been shown to hold true for polymers prepared through inverse vulcanization. In a well-designed paper by the Boyd group in 2019, tetravinyltin was used as a monomer to react with sulfur. This molecule contains only four vinyl groups bonded to a tin atom.[6] The large tin atom did not give many absorptions in the long wave infrared region while the simplicity of the vinyl groups only contributed a small

number of vibrations. These improvements resulted in excellent transmission in the long wave infrared region, particularly when compared to complex monomers like 1,3-diisopropenyl benzene (DIB).[6]

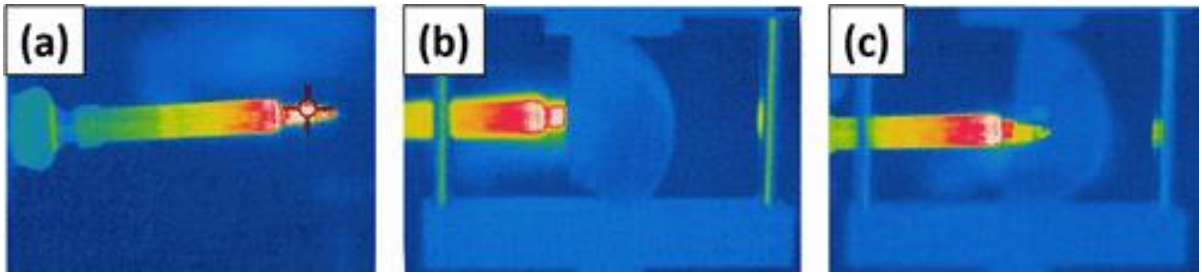

Figure 2.1: (a) LWIR image of a soldering iron. (b) LWIR image of a soldering iron through 1.63 mm this poly(S-*r*-DIB). (c) LWIR image of a soldering iron through 1.65 mm poly(S-*r*-TVSn). Reused with permission from.[6]

Many small and simple monomers which would give good transmission in the long wave infrared region are volatile, making them unsuitable for a conventional inverse vulcanization reaction. One of the major goals of this chapter was to address this issue, using cyclopentadiene as the volatile monomer. There are several methods in the literature which allow the use of lower boiling point monomers in reactions with sulfur. They are summarised here.

Researchers have looked to reduce the temperature of inverse vulcanization reactions using catalysts. In 2019, two groups developed different strategies to catalyse inverse vulcanization reactions. Zhang *et al*. found that nucleophilic amine activators could be used to increase the rate of reaction and molecular weight of the resulting polymer.[7] These catalysts worked by nucleophilic ring-opening of sulfur ring which would reduce the bond dispersion energy of the S-S bonds, leading to initiation of an inverse vulcanization reaction at lower temperature.[7] Furthermore, it was found that these activators could be used in a process known as dynamic covalent polymerization (DCP). In this process, a polymer made from sulfur and styrene was initially produced. It was then found that by using these activators, sulfur radicals could be produced in the polymer at temperatures as low as 60 °C which was used to insert additional monomers to the polymer.[7]

Wu *et al*. also found a catalyst system which could increase the rate of reaction and yield of the polymers made through inverse vulcanization. This catalyst system was based on metal diethyldithiocarbamates. They proved that this could be used to react monomers which were previously shown to be unreactive with sulfur like ethylene glycol dimethylacrylate.[8] In a future paper where they were able to reduce the required reaction temperature to below the melting point of sulfur, allowing for the first time an inverse vulcanization reaction with solid sulfur.[9] The authors then went on to perform a systematic analysis or a range of different classes of catalysts for inverse vulcanization reactions, showing that a range of metal diethyldithiocarbamates as well as some organic and organometallic species could act as catalyst for this reaction.[10] Below are the proposed mechanisms for the catalyst systems developed by the two groups.

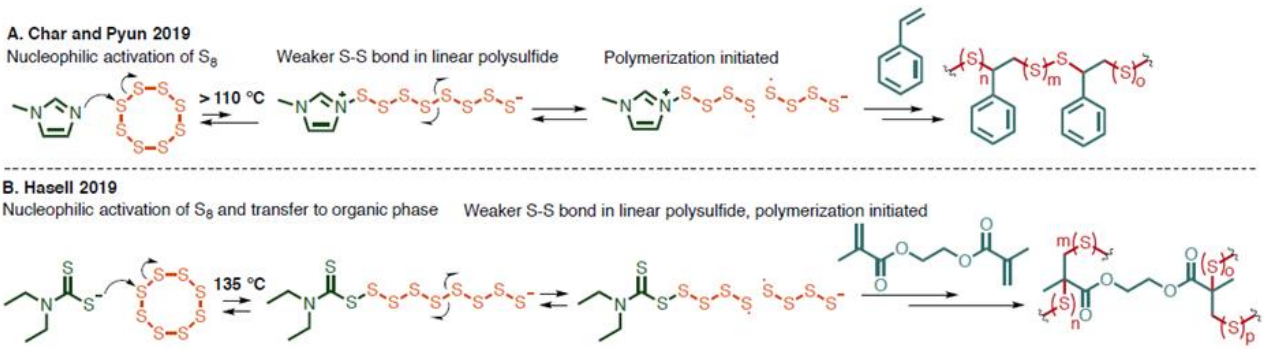

Figure 2.2: Mechanisms for the nucleophilic activation of S8 using catalyst systems developed by (a) the Pyun group[7] and (b) the Hasell group. Reused with permission from.[8]

While catalytic reactions are very promising and have already been used to react previously unsuitable monomers, they do have several drawbacks. The main one is that the catalysts are often not able to be removed from the polymer. This is particularly problematic for polymers designed for thermal imaging applications as the catalysts would introduce a range of additional absorbing groups into the polymers, reducing the long wave infrared transparency.

The Pyun group developed a method to react sulfur with monomers in the vapor phase. This allowed for several monomers to be used which were not able to be reacted in the liquid phase due to a lack of miscibility with molten sulfur. In this method, a hot filament was used to heated sulfur to above 350 °C to evaporate it. The sulfur could then react with a volatile monomer in the gas phase and deposit a polymer film on a substrate.[11] This is a useful technique for creating thin films or using monomers which are unreactive in conventional invers vulcanization reaction. However, preparing a bulk material using this technique would be impractical and the high temperature required means that only monomers with high thermal stability could be used.

To avoid the issues of high temperature reactions, several groups have looked to do inverse vulcanization reactions at room temperature using reactions that are initiated electrochemically,[12] photochemically[13] or mechanochemically.[14] These techniques can induce reactions at room temperature. Allowing for additional monomers to be used. While these methods are promising and allow for unique and useful polymers to be prepared, they do have some limitations. Electrochemical synthesis can produce high molecular weight polymers with a range of applications but does require cyclic trisulfides to first be prepared and isolated.[12] Photochemical and mechanochemically synthesis of polysulfides are very promising but have some issues with control of the reaction and scalability. Photo polymerisation reactions require the light to be able to penetrate the reactants to facilitate the reaction. This could limit the potential monomers that could be used or the scale of the reaction that could be performed. This issue could be solved by performing the reaction in flow but as of yet, this has not been published.

A method which could directly react molten sulfur with a gaseous monomer would be very useful. It would allow for gaseous monomers to be used without the drawbacks of the methods described above. Throughout this chapter, two methods will be developed to react gaseous cyclopentadiene with molten sulfur. Using these methods, a range of polymers will be prepared and fully characterised. Several side reactions will be investigated including the formation dicyclopentadiene through the Diels Alder reaction between two molecules of cyclopentadiene. After investigating these side reactions and determining a method to remove them from the reaction, the infrared properties of the polymers will be investigated. This will demonstrate the suitability of the polymers for use in thermal imaging applications.

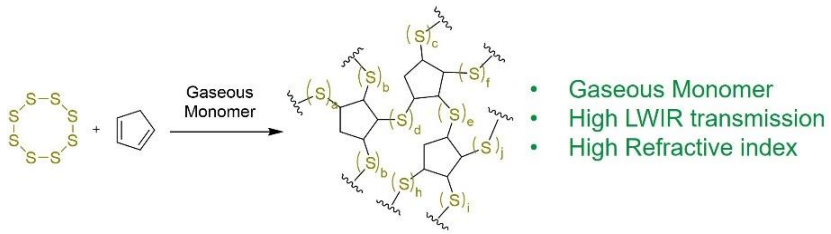

Figure 2.3: Polymerisation reaction between sulfur and cyclopentadiene.

Cyclopentadiene polymer synthesis

Retro Diels Alder reaction to prepare cyclopentadiene

To produce cyclopentadiene (CPD), dicyclopentadiene (DCPD) must be broken down in a retro Diels Alder reaction. To initiate this reaction, the DCPD must be heated to above 150 °C where the retro Diels Alder reaction becomes favoured to produce CPD. The CPD can then be separated by distillation due to its much lower boiling point. The specific conditions used to produce CPD can be seen below.

For all reactions, CPD was first prepared directly from DCPD by distillation using the following method. 20 g of DCPD was weighed and added to a 100 mL round bottomed flask with a magnetic stirrer. The round bottomed flask was added to a standard distillation set up with a water-cooled condenser and slowly heated to 180 °C. Another 100 mL round bottomed flask was used as an outlet to collect the CPD. The outlet round bottomed flask was cooled with an ice bath to reduce the rate of the Diels Alder conversion back to DCPD. The CPD was used immediately after distillation to reduce the chance that DCPD was reformed. The CPD would be keep in a freezer and tested by NMR before every use. If the proportion of DCPD was above 2 % by NMR, the CPD would be distilled again at 70 °C to separate it from DCPD.

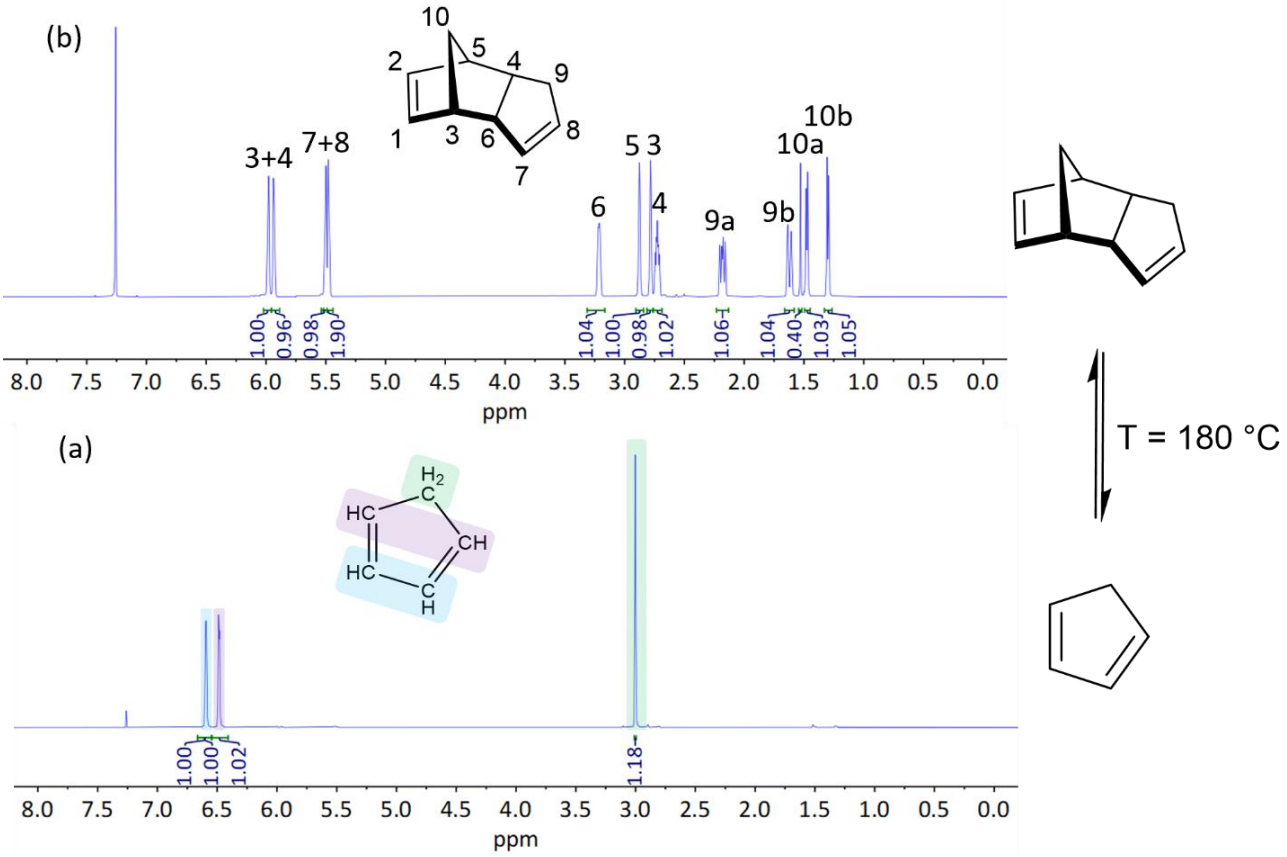

Figure 2.4: ^{1}H NMR spectra for the retro Diels Alder reaction of dicyclopentadiene to form cyclopentadiene. NMR reactions were obtained using a 600 MHz NMR spectrometer with deuterated chloroform as a solvent. Top: dicyclopentadiene. Bottom: cyclopentadiene after cracking and distillation.

Reflux method to prepare cyclopentadiene polymer

Inverse vulcanization is usually done at a high temperature, with most reactions being performed above 160 °C unless catalysed or utilising highly reactive monomers.[8, 9, 15] Likely due to the conjugated double bond in CPD, it was found that it could react at 140 °C. However, due to the high volatility of CPD, it could not be reacted with molten sulfur like most high boiling point monomers. There were several challenges that were faced when using a volatile monomer. The first was loss of the monomer. The effect of this was reduced by using a water-cooled condenser for the reaction, allowing cyclopentadiene to reflux on the molten sulfur.

The second issue was that as the CPD refluxed on the molten sulfur, it would cool the sulfur, often leading to crystallisation. Once crystallisation occurred, the sulfur would take some time to remelt and would often lead to poor polymerisation. To overcome this issue, it was found that the CPD could be added to the sulfur very slowly. When added slowly, it was found that the CPD would react with sulfur and remain in the sulfur layer rather than refluxing further. This meant that at any one time, there was only a small amount of CPD refluxing, reducing the cooling effect and preventing crystallisation of the sulfur. For the standard composition of 67 % sulfur, the CPD would be added in batches of 150 µL every three minutes. However, the rate the CPD could be added was found to depend on the composition, as reactions with more relative CPD would need to be added slower. The following method was used to prepare the polymers from CPD and sulfur.

Sulfur (3.00 g, 93.56 mmol S atoms) was added to a 21 mL vial with a magnetic stirrer. A threaded adapter was used to attach this vial to a water-cooled condenser. An oil bath and oven were preheated to 140 °C and the sulfur was lowered into the oil bath for three minutes. Over this time, the sulfur would melt to form a yellow liquid. CPD was added with a volumetric pipette down the reflux condenser. To adjust the composition of the polymer, the amount of sulfur would remain unchanged but the mass of CPD would change. The most optimized composition for infrared transmission was found to have 1.50 g (67 wt %) of CPD but stable polymers were produced with CPD masses ranging from 3.00 g (50 wt%) to 0.75 g (20 wt%). The composition was described by xx-poly(S-*r*-CPD), where xx indicates the mass percent of sulfur, the *r* indicates that this is a random polymerisation. As described earlier, the CPD was added in 150 µL additions every 3 minutes for the 67 % sulfur sample but would be added slower in samples with more relative CPD to prevent rapid cooling of the sulfur. For the standard composition of 3.00 g sulfur and 1.50 g CPD, the reaction would take a total time of 90 minutes from when the sulfur was first added. Over this time, the sample would slowly darken and increase in viscosity. The sample was then poured into a silicone mould and cured in an oven at 140 °C for 24 hours. After curing, the polymer was left at room temperature to cool before being removed from the silicone mould.

The polymer went through a liquid prepolymer stage, making it pourable but after curing would form a solid material. It was black, completely opaque to visible and were flexible, bending when force was applied. Samples with less sulfur were brittle, indicating a glass transition temperature above room temperature.

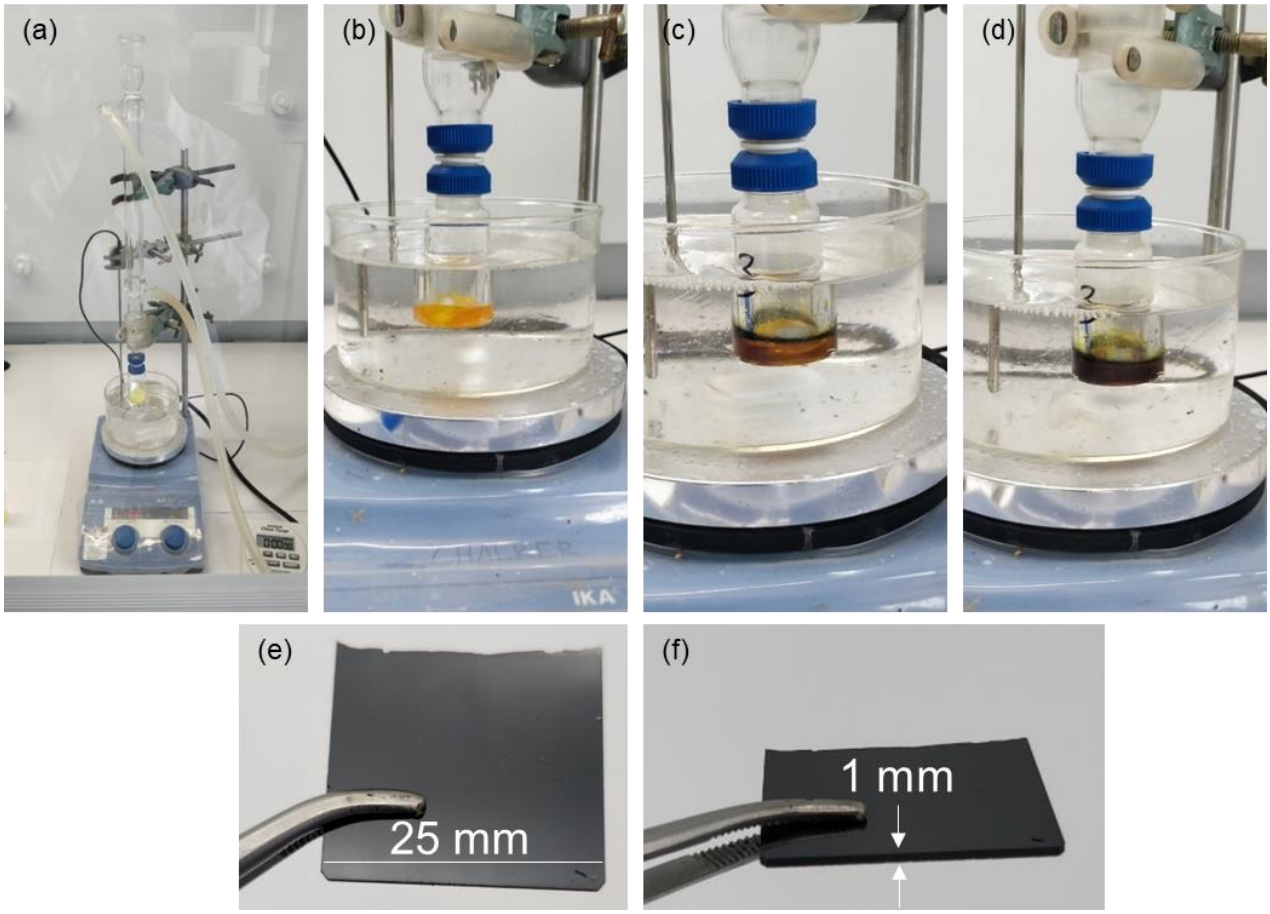

Figure 2.5: Images of reflux method for producing poly(S-r-CPD). (a) Image showing set up for reaction. (b) Image at 3 mins reaction time when sulfur has melted. (c) Image shortly after adding CPD to sulfur. (d) Image of prepolymer before being poured into silicone mould. (e) Polymer sample after cure. (f) Side view of polymer after cure.

Cyclopentadiene polymer characterisation

Compression testing at different cure times

When a new polymer system is developed that requires curing, one of the most important factors is the cure time. To test the cure time, changes in chemical, physical or thermal properties could be analysed. There should be a point where the properties no longer change, indicating a complete cure. The 67-poly(S-*r*-CPD) was tested for chemical changes using infrared analysis and physical changes using dynamic mechanical thermal analysis at eight different cure times. The polymer was prepared through the reflux method and poured into a silicone mould consisting of many 10 mm diameter cylinders. The samples were then left to cure at 140 °C for differing amounts of time. In triplicate, polymer samples were cured for 0.5 hr, 1 hr, 2, hr, 4 hr, 8 hr, 16 hr and 24 hr while another sample was left uncured. The samples were then tested using a TA Q800 dynamic mechanical analyzer in compression mode to investigate any changes in compression modulus over the time the sample was cured. The samples were compressed at room temperature (approximately 20 °C) with a ramp rate of 3 N/min to a maximum compression of 18 N. The uncured sample and the 30-minute cure samples were not shape persistent and acted like a highly viscous fluid. These samples formed a layer of sulfur over several days which is expected as the pre-polymer is likely unstable without adequate cure time. These samples were tested shortly after synthesis before sulfur layer formed. The viscous properties of these prepolymers were reflected in a significantly reduced Young's modulus. However, the compression modulus for these samples should not be considered accurate as they would flow when compressed while all other samples would maintain their shape. This prepolymer has a gel point between 30 and 60 minutes at 140 degrees and the compression modulus slowly increases with longer cure times, indicating an increase in crosslinking density. The sample was considered fully cured by 24 hours, at which point, it had a compression modulus of 1.45±0.2 MPa.

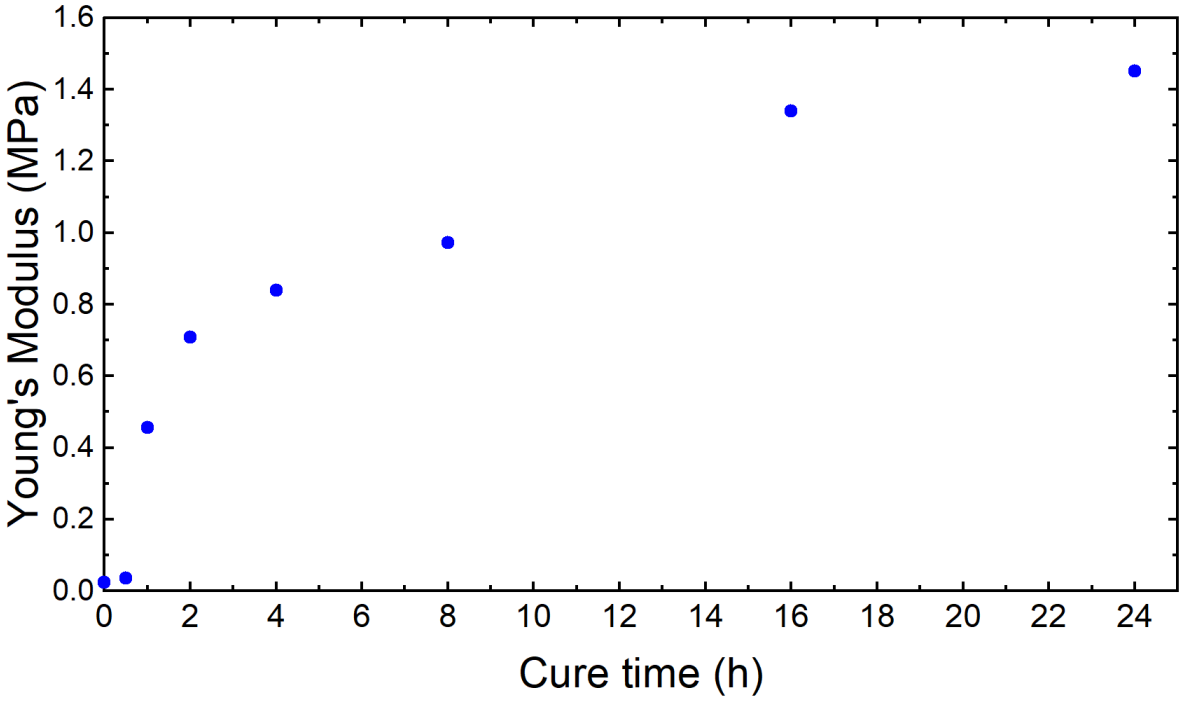

Figure 2.6: Plot showing Young's modulus of 67-poly(S-*r*-CPD) polymer samples at cure times tanging from 0 hours (uncured pre-polymer) to 24 hours. Each sample was analysed using a TA Q800 dynamic mechanical analyser in compression mode.

Infrared analysis of samples at different cure times

The study of the Young's modulus showed that the polymers cured over approximately 24 hours. To study any change in the chemical structure with cure time, the samples used for the compression study were analysed by infrared spectroscopy. The polymers were found to be largely insoluble in all common solvents so could not be analysed in solution. To overcome this issue, the samples were added to a heated press to prepare thin free-standing films to analyse by transmission FTIR analysis. Polyimide tape was used to create a 15 mm by 15 mm enclosure for the polymer and 50 mg of the polymer was ground into a powder and added to heated press. The polymer was then heated to 140 °C and compressed at 30 MPa for 10 minutes. This was repeated for one sample of each cure time. When removed, the polymer would have a thickness ranging from 180 to 220 µm. The samples were then tested using a Perkin Elmer Frontier FTIR. There was a clear reduction in the alkene stretching peak at 3050 cm^{-1} as well as a bending peak at 1350 cm^{-1}. This indicates that alkenes were consumed during the curing process. This would likely lead to an increase in crosslinking density which may explain the increased compression modulus with cure time. Note that the overall transmission of these samples shouldn't be considered as they have differing thicknesses and surface roughness, leading to changes in absorption and reflection.

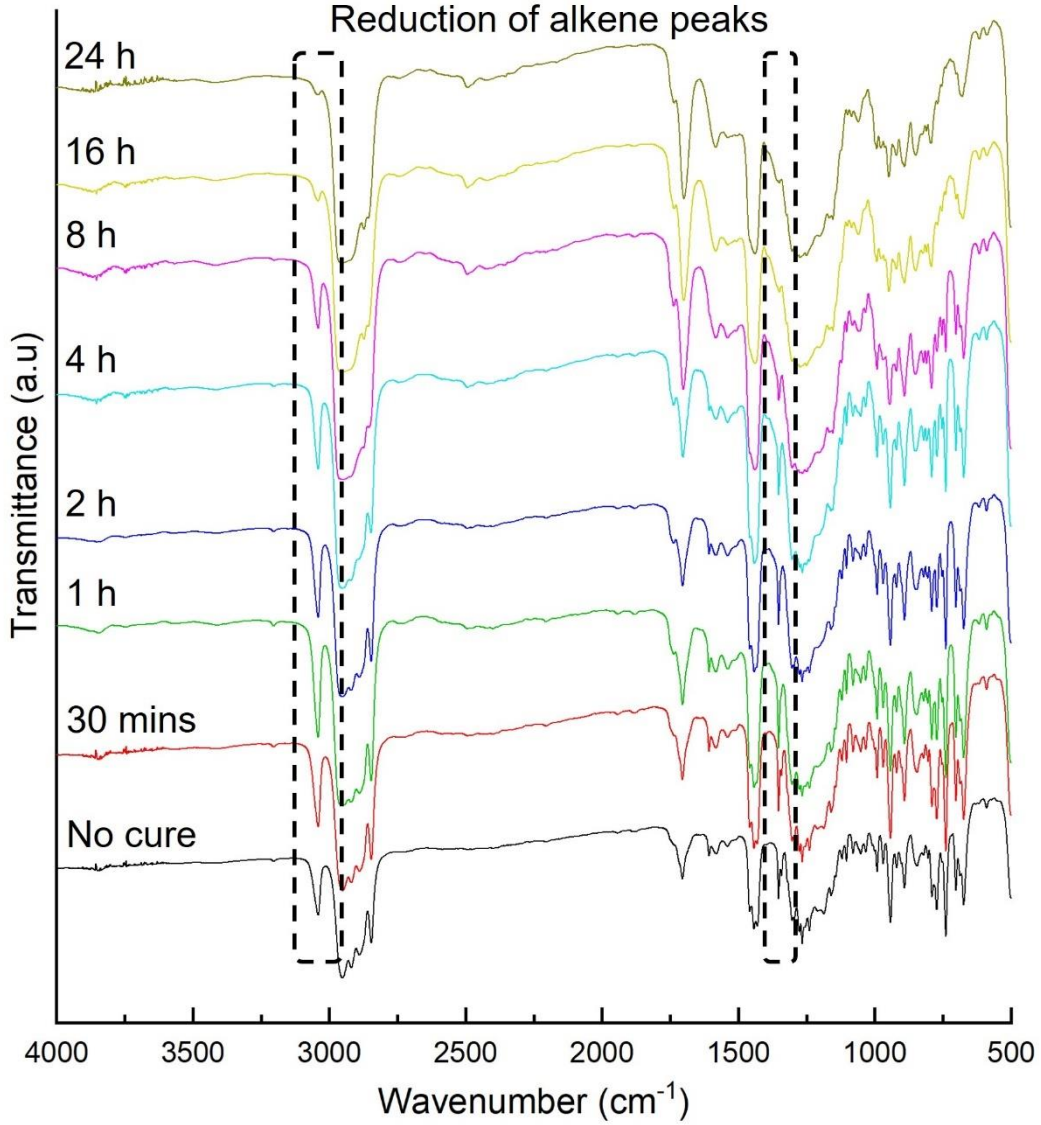

Figure 2.7: FTIR analysis of 67-poly(S-r-CPD) polymers prepared through the reflux method at different cure times ranging from no cure to 24 hours.

Laser desorption mass spectrometry (LD-MS) of polymer

LD-MS was performed on 67-poly(S-r-CPD) polymers with cure times ranging from 1 hour to 24 hours. This was done to determine if some polymeric or oligomeric material could be found, indicating a reaction. To prepare the samples for LD-MS, the polymer samples were ground into a powder and added to dichloromethane. The samples were mixed to form a suspension and drops were removed with a glass pipette and applied to the LD-MS sample tray. This was repeated multiple times until a thin layer of the sample covered the tray. Cure times of 1 hr, 2 hr, 4 hr, 8 hr, 16 hr and 24 hr were tested.

All samples showed a range of peaks between a 500 m/z and 1500 m/z. Only Oligomers were detected which is believed to be due to preferential ionisation of these species, leading to a larger signal. The samples with a greater cure time showed a reduced signal, this is likely due to an increase in crosslinking density, leading to a smaller proportion of the sample existing as oligomers. Every sample had many peaks which were separated by 32 m/z units. This shows that the samples consist of polymers with differences in mass by one sulfur atom. The mass of the peaks indicated that there was both CPD and sulfur in the polymers.

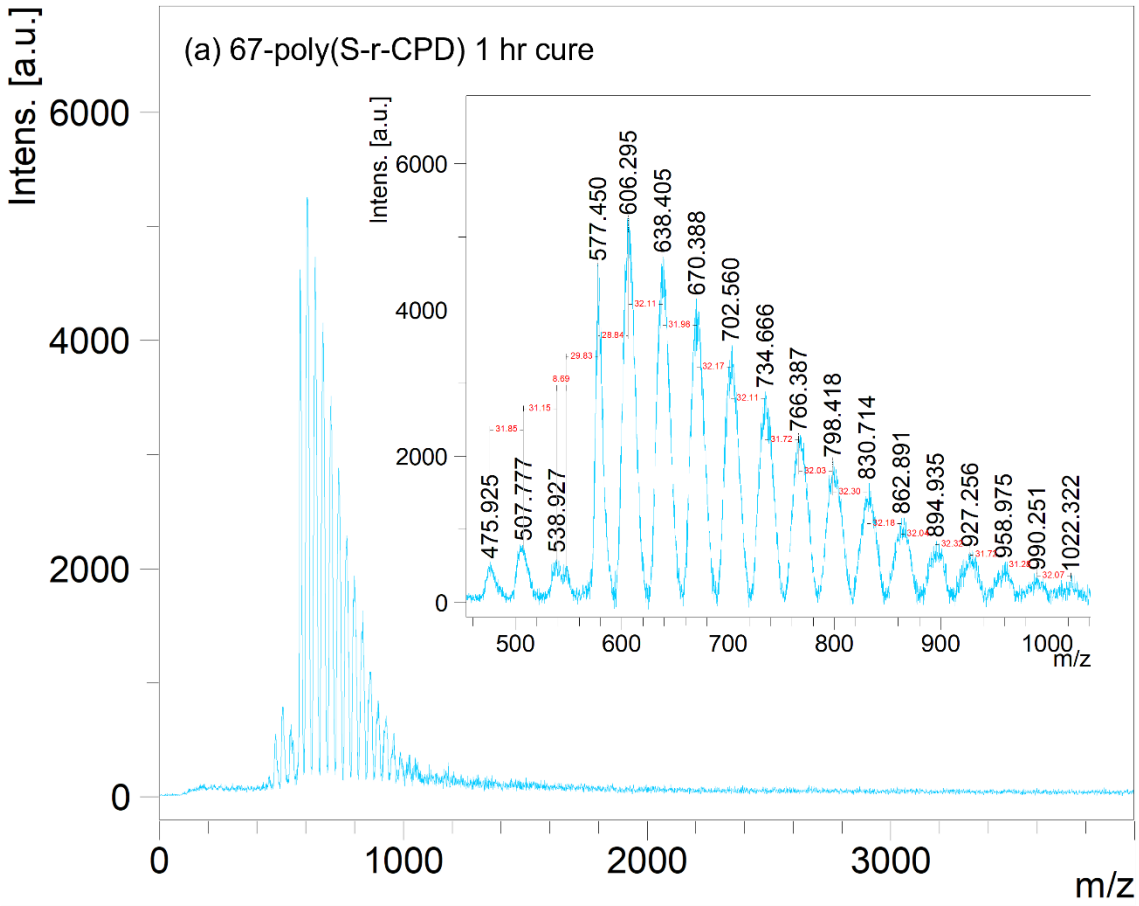

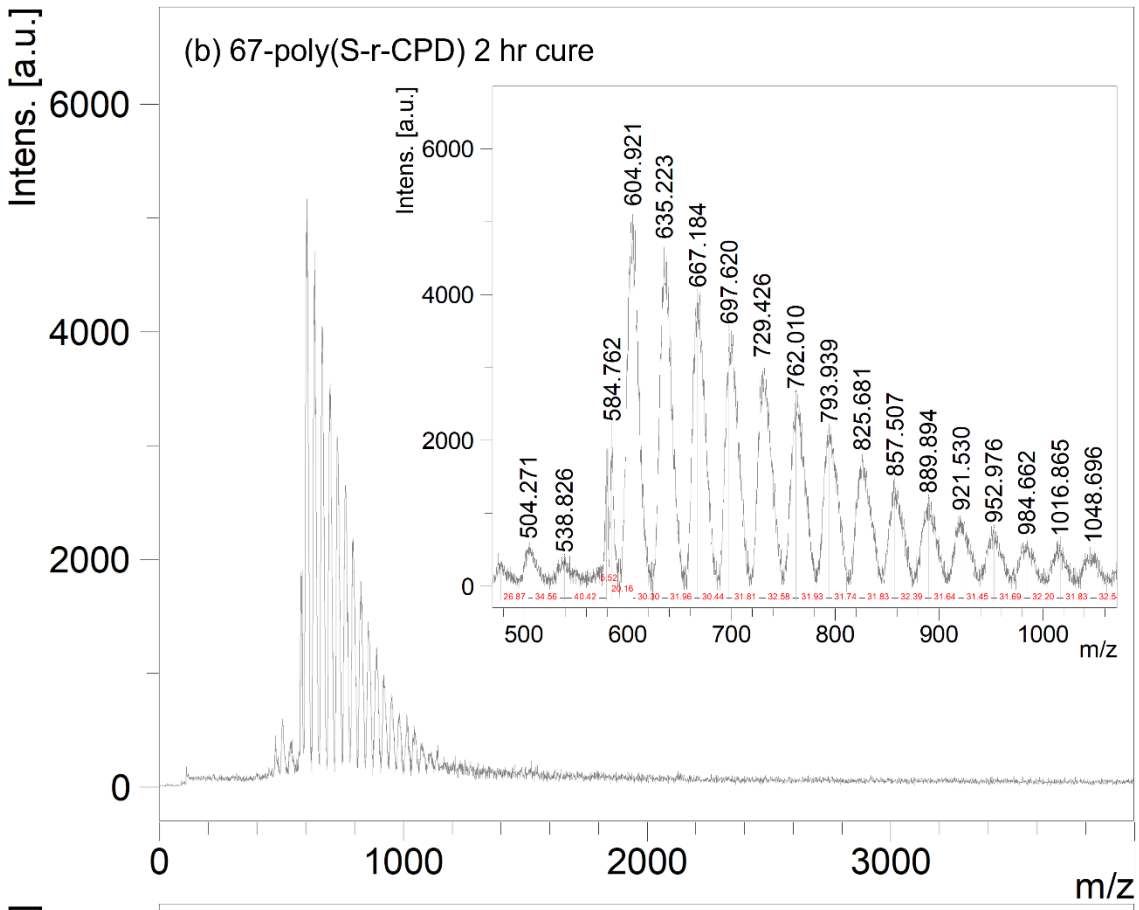
(b) 67-poly(S-r-CPD) 2 hr cure
Intens. [a.u.]
6000
4000
2000
0
0
1000
2000
3000
m/z
Intens. [a.u.]
6000
4000
2000
0
504.271
538.826
584.762
604.921
635.223
667.184
697.620
729.426
762.010
793.939
825.681
857.507
889.894
921.530
952.976
984.662
1016.865
1048.696
500
600
700
800
900
1000
m/z

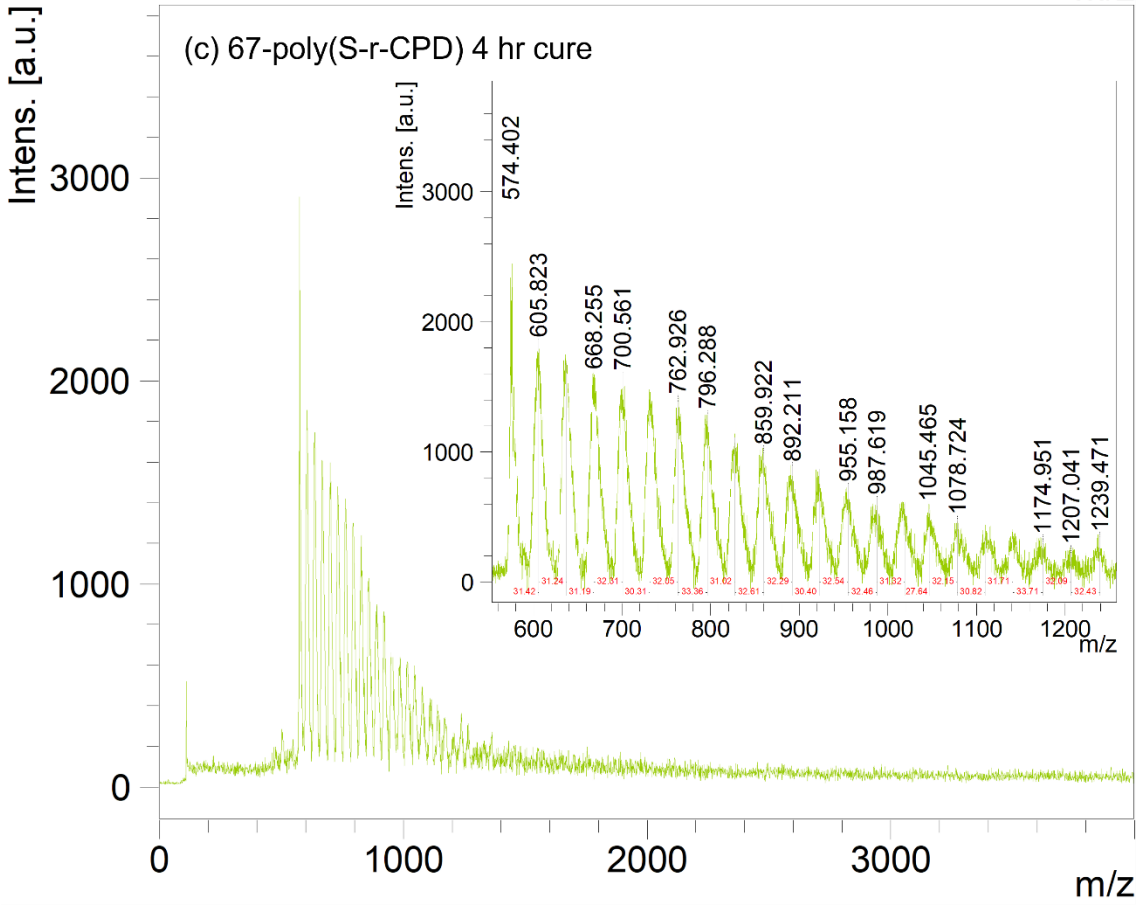
(c) 67-poly(S-r-CPD) 4 hr cure
Intens. [a.u.]
3000
2000
1000
0
0
1000
2000
3000
m/z
Intens. [a.u.]
3000
2000
1000
0
574.402
605.823
668.255
700.561
762.926
796.288
859.922
892.211
955.158
987.619
1045.465
1078.724
1174.951
1207.041
1239.471
600
700
800
900
1000
1100
1200
m/z

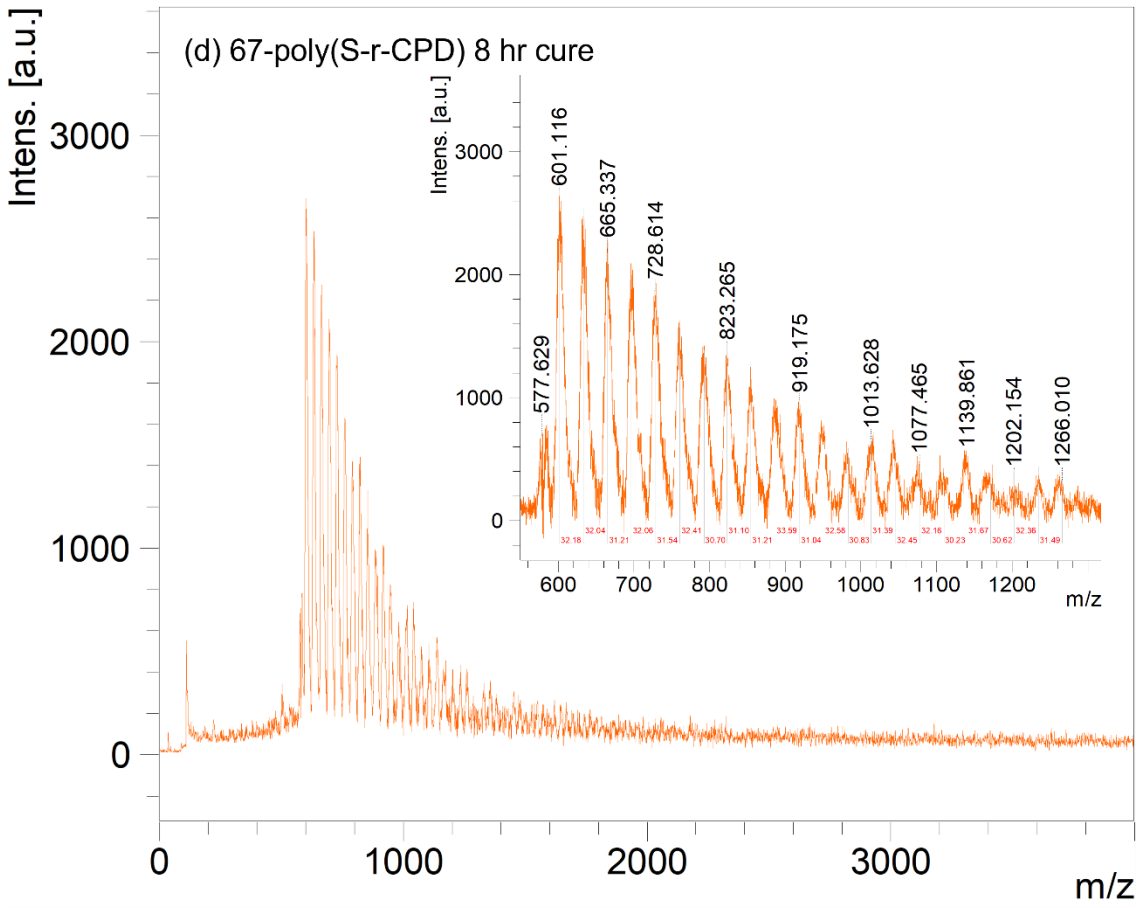
(d) 67-poly(S-r-CPD) 8 hr cure
Intens. [a.u.]
3000
2000
1000
0
0
1000
2000
3000
m/z
Intens. [a.u.]
3000
2000
1000
0
577.629
601.116
665.337
728.614
823.265
919.175
1013.628
1077.465
1139.861
1202.154
1266.010
600
700
800
900
1000
1100
1200
m/z

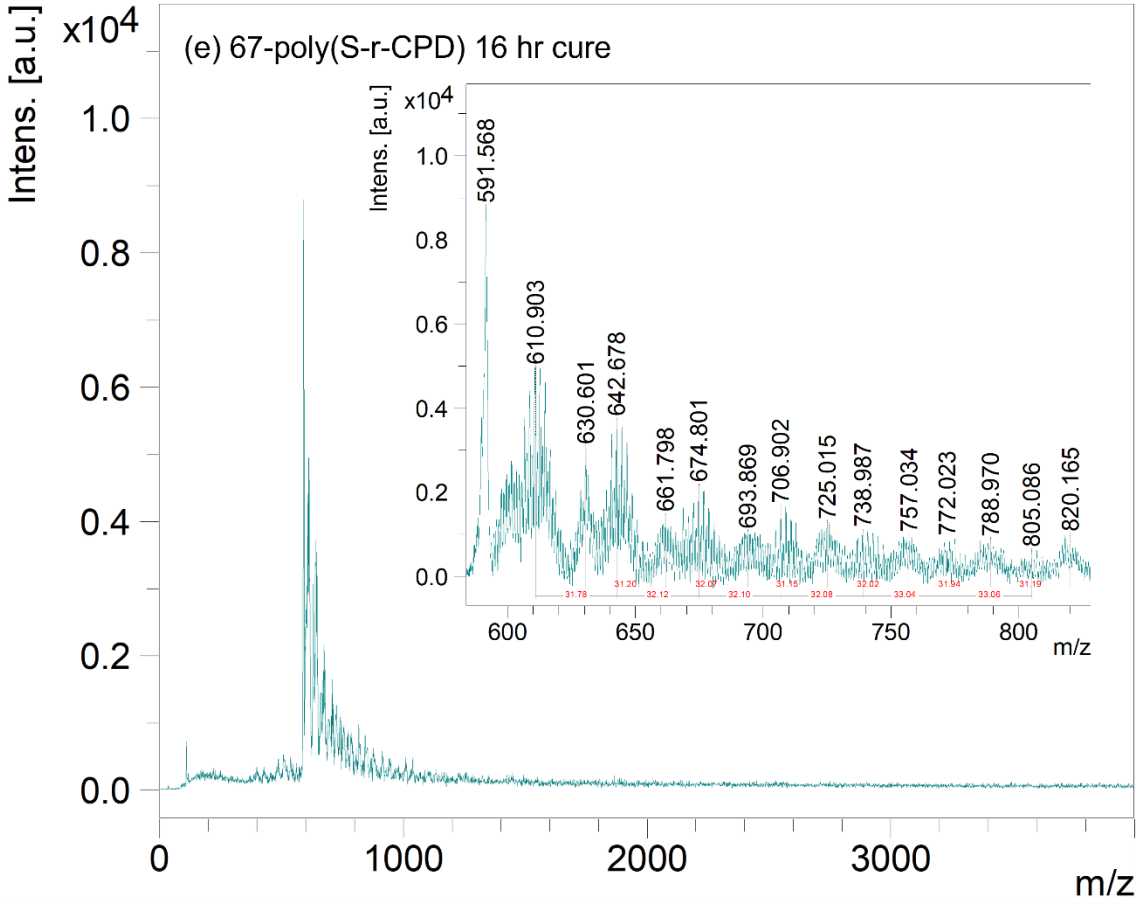
(e) 67-poly(S-r-CPD) 16 hr cure
Intens. [a.u.]
x10^4
1.0
0.8
0.6
0.4
0.2
0.0
0
1000
2000
3000
m/z
Intens. [a.u.]
x10^4
1.0
0.8
0.6
0.4
0.2
0.0
591.568
610.903
630.601
642.678
661.798
674.801
693.869
706.902
725.015
738.987
757.034
772.023
788.970
805.086
820.165
600
650
700
750
800
m/z

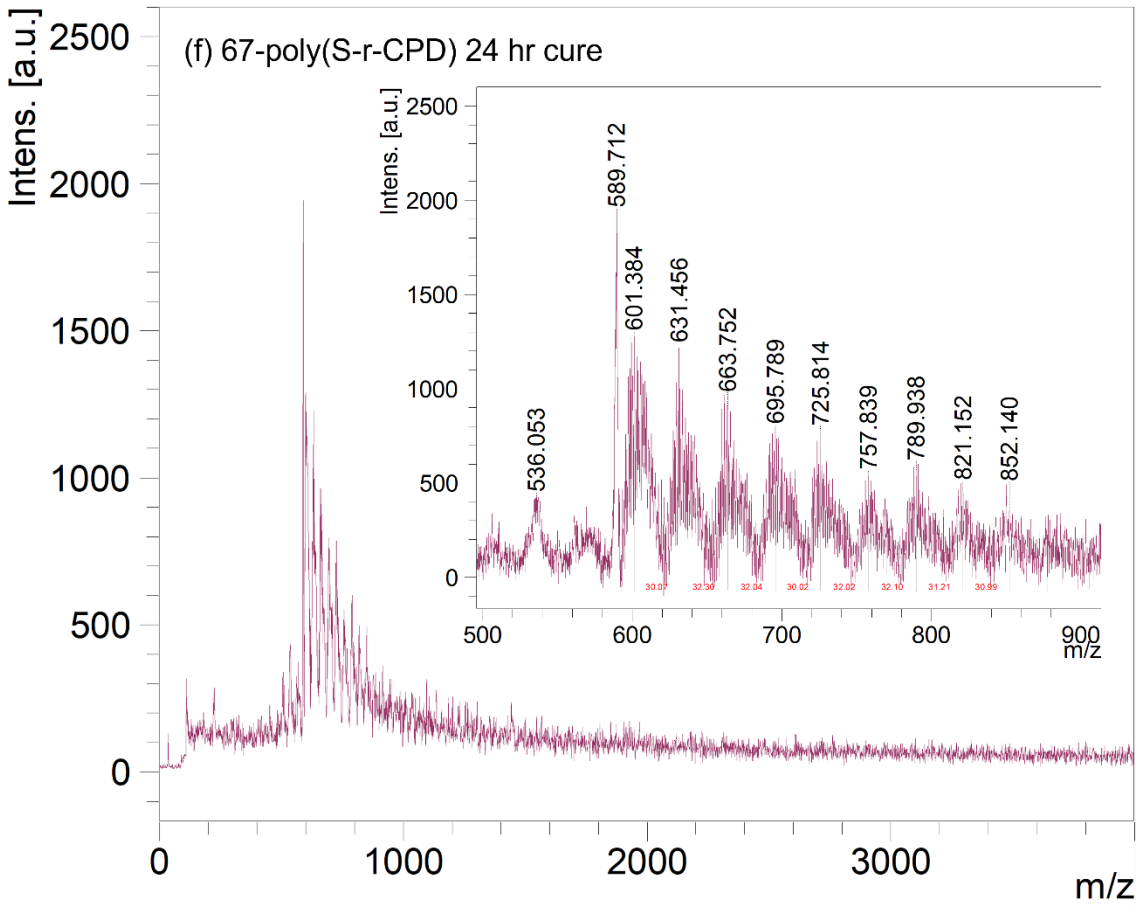

Figure 2.8: LD-MS spectra for 67-poly(S-*r*-CPD) sample with different cure times showing mass spectrum from 0 to 3000 m/z and an inset showing main peaks. (a) 1 hour cure time, (b) 2 hour cure time, (c) 4 hour cure time, (d) 8 hour cure time, (e) 16 hour cure time, (f) 24 hour cure time.

Raman analysis of surface

Acknowledgements: This section was completed in collaboration with Dr. Christopher Gibson.

When left for several months, it was found that the samples with 67 % sulfur or more would start to form sulfur crystals on the surface. This process was likely due to unreacted sulfur making its way to the surface of the polymer in a process known as sulfur blooming. This indicated that the polymers with 67 % or more sulfur may not be stable long term. The 50 % sulfur sample did not show any sulfur blooming. Therefore, the sulfur composition of the polymer should be selected carefully and the polymer should be used in the first month after synthesis if a higher sulfur content is required. There has been some research in the literature about sulfur blooming and the sulfur can usually be incorporated back into the polymer structure by recuring it at high temperature.[16] When analysed by Raman, the polymers show a lot of fluorescence but the sulfur peaks from crystalline sulfur can be observed in the samples with sulfur blooming.

The 50-poly(S-r-CPD) and 67-poly(S-r-CPD) polymers prepared through the reflux method were analysed by Raman Spectrometry. Raman spectra was collected using a Witec alpha300R Raman microscope at an excitation laser wavelength of 532 nm with a 100X and 40X objective (numerical apertures 0.9 and 0.6 respectively). 10 Raman images were collected on each surface with each image 80x80 microns in size with 1600 spectra in each image. The spacing between each Raman spectrum was 2 microns. The integration time for each spectrum was between 1 to 2 seconds. Raman images were acquired at distinct locations on each sample with each location separated by hundreds to thousands of microns.

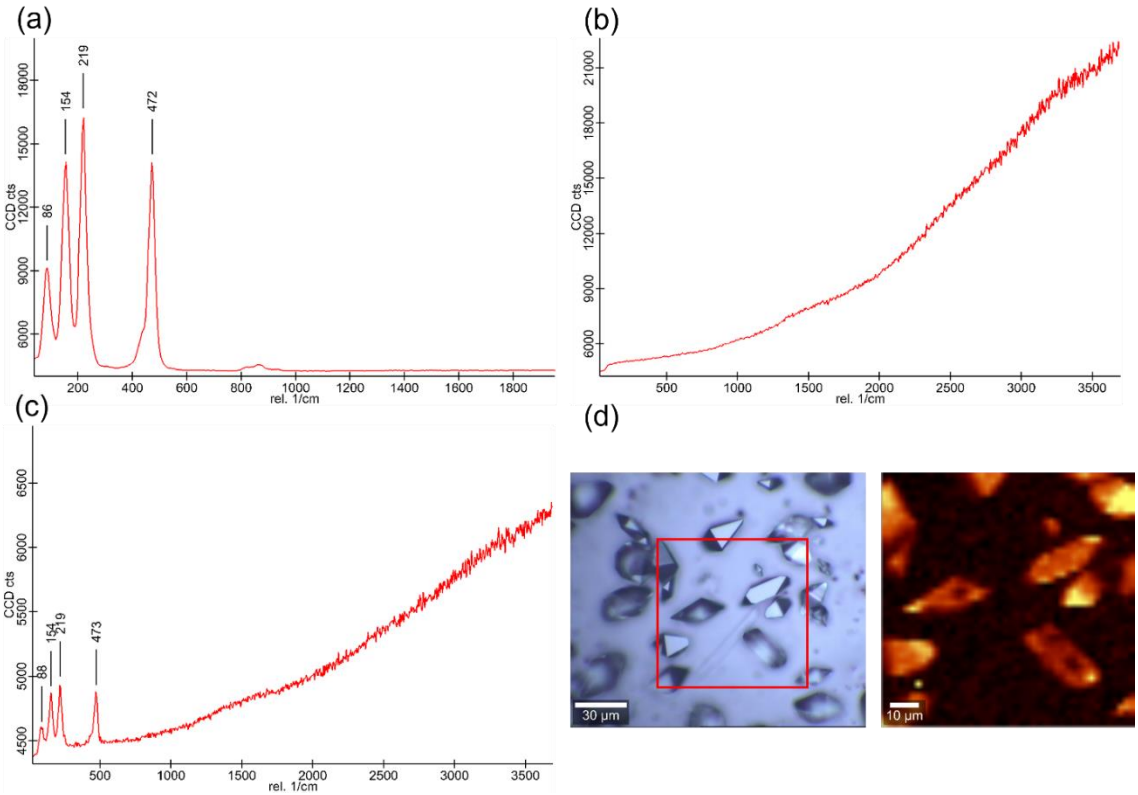

Figure 2.9: Raman spectra of polymers produced using Witec alpha300R Raman Microscope. (a) Raman spectrum of elemental sulfur. (b) Raman spectrum of 50-poly(S-r-CPD) polymer. (c) Raman spectrum of 67-poly(S-r-CPD) showing peaks for elemental Sulfur. (d) Optical and Raman image of 67-poly(S-r-CPD) polymer showing sulfur crystals.

AFM analysis of surface

Acknowledgements: This section was completed in collaboration with Dr Christopher Gibson.

The surface of an optical material is extremely important. If the surface roughness it too great, it can cause scattering and reduce the overall transmission of the material. Ideally, the surface roughness should be less than the wavelength of light which is being transmitted by the material. For the applications presented in this thesis. The shortest wavelength of interests is the 3 μm, which is the start of the mid-wave infrared region. The surface roughness should therefore be much less than 3 μm to ensure a good optical surface. The Ra of the polymers was below 4 nm so the possess the required smoothness for MWIR and LWIR imaging.

To analyse the surface roughness of the polymer samples along with the size of the sulfur crystals, atomic force microscopy was used. The 50-poly(S-*r*-CPD) and 67-poly(S-*r*-CPD) polymers were both analysed. The surface roughness was analysed using Ra and Rq. Ra and Rq roughness are standard analysis methods to report surface roughness using AFM. They differ in their mathematical description of roughness. Where Rq is the root mean square average of the height deviations taken from the mean image data line and Ra is the arithmetic average of the absolute values of the surface height deviations measured from the mean plane. It was found that the average roughness, Ra, and root mean square roughness, Rq, for each of the polymers was: 50-poly(S-r-CPD): Ra = 2.68 ± 0.47 nm, Rq = 4.18 ± 0.80 nm and 67-poly(S-r-CPD): Ra = 1.96 ± 0.79 nm, Rq = 3.50 ± 2.15 nm. The roughness for the polymers over the regions examined was comparable to other polymers studied using AFM (e.g. Ra = 8.84 nm Tonkin et al[17] and Ra = 1 to 4 nm Gibson et al[18]).

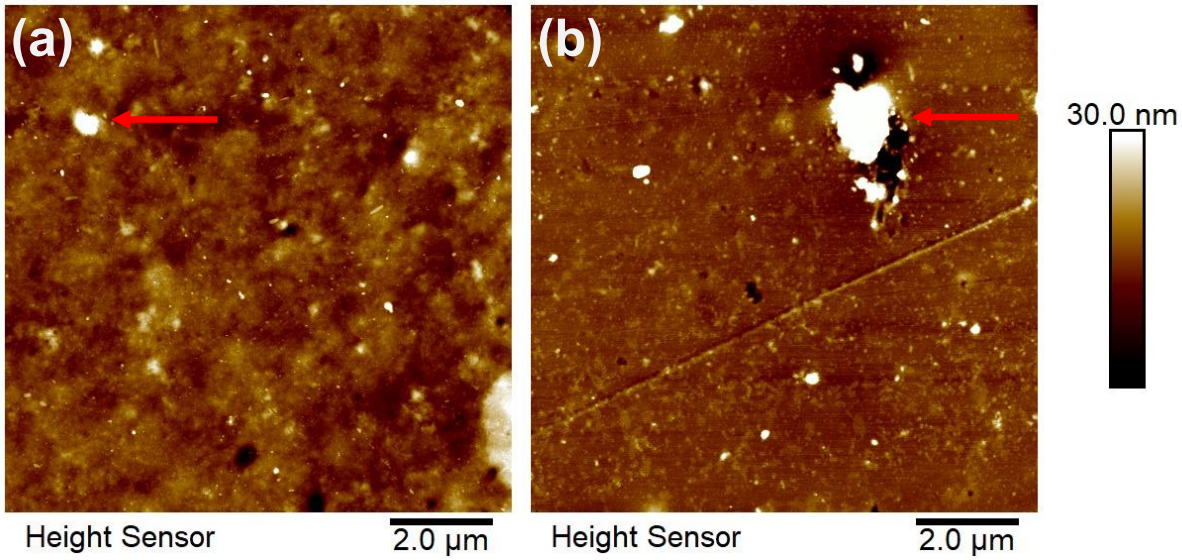

Figure 2.10: AFM images of (a) 50-poly(S-*r*-CPD) and (b) 67-poly(S-*r*-CPD).

Coefficient of thermal expansion testing

As the polymer was designed to be used as a lens or optic for thermal imaging, the coefficient of thermal expansion was very important. This is because as the temperature changes, any expansion in the material could change the power of any optic produced. To investigate this, the coefficient of thermal expansion of the 67-poly(S-*r*-CPD) polymer was investigated using a TA Q800 DMTA. In this test, the polymer was placed between two clamps of the DMTA. The sample was then slowly heated while any vertical displacement was measured by the DMTA. Most polymeric materials expand when heated below their glass transition temperature. The sample preparation, calibration and data analysis are described below.

For accurate testing of thermal expansion, the polymer had to be moulded into a circular disc with a known diameter and thickness. To achieve this, a silicone mould was prepared with 12 circular indents with a diameter of 10 mm and a depth of 5 mm. A 3D printed negative was used to fabricate the mould. The negative was designed on Autodesk fusion and printed on a Creality CR-10S Pro using PLA filament. A two-part silicone resin was mixed and poured into the 3D printed negative. The silicone was left for 2 hours at room temperature to cure before being removed from the negative to be used.

The samples were prepared using the standard method described earlier and cured for 24 hours using the cylinder mould. A total of 12 samples were prepared from two polymer batches. The samples ranged from 2 mm to 4 mm thick. After cure, the samples were left to cool to room temperature before removal from the silicone mould. The top surface of the polymer had a slight convex curve from the meniscus of the liquid prepolymer. The top surface was sanded flat using sandpaper ranging from 80 to 400 grit.

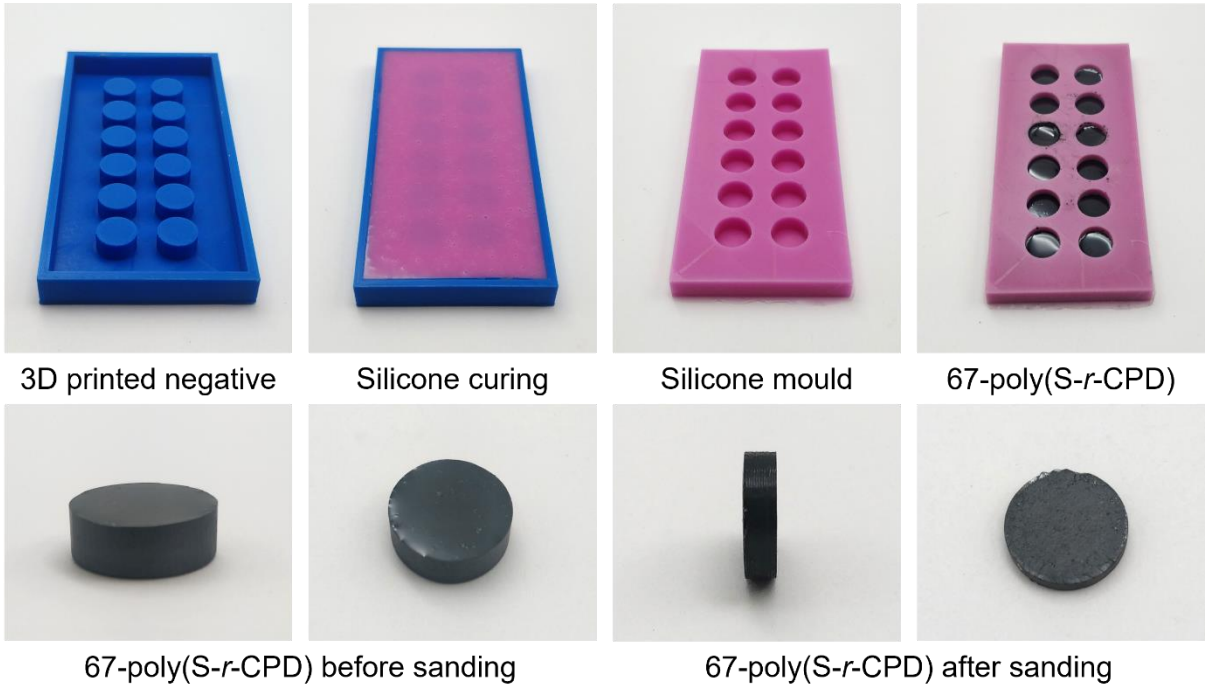

Figure 2.11: Images showing the mould fabrication and sample preparation to make 67-poly(S-*r*-CPD) for thermal expansion testing.

The clamp and instrument had to first be calibrated to account for expansion of the clamp or drive shaft, or any other change in displacement with temperature. A sapphire calibration sample with a diameter of 6.6 mm and thickness of 10 mm was used with the method described below. Using a coefficient of thermal expansion of 5.5 x 10^{-6} K^{-1} for sapphire, the expansion from the calibration sample could be removed to leave only the clamp and instrument. The instrument had a significant negative bias. The displacement plot for the instrument was then used to calibrate all samples by subtracting it from the displacement of the sample.

Six samples were tested for coefficient of thermal expansion. The samples were placed in the clamp and tested using the method described below. The calibration plot was used to remove any bias in the instrument. After this, the expansion of the polymer was calibrated for the thickness of the sample. The final units of the coefficient of thermal expansion was mm/mm K^{-1} or mm expansion per mm thickness per Kelvin. This unit is usually shortened to K^{-1} which is what was used below.

All samples followed a similar trend until 50 °C. After this point, the samples were above their glass transition temperature which dominated the displacement. The slope of the linear section of the plot between 5 °C and 35 °C was used to calculate the coefficient of thermal expansion. The average coefficient of thermal expansion was 12.6 ± 1.1 x 10^{-5} K^{-1}. This is within the standard range for polymer which would need to be considered when designing any optics that would be subject to changes in temperature.

A TA Q800 DMTA was used with a compression clamp. The frequency modulation was turned off and a controlled force method was used. A preload force of 0.01 N was applied over a temperature range of -20 °C to 100 °C. The displacement of the clamp was measured as the temperature was increased with a ramp rate of 2 °C/ min.

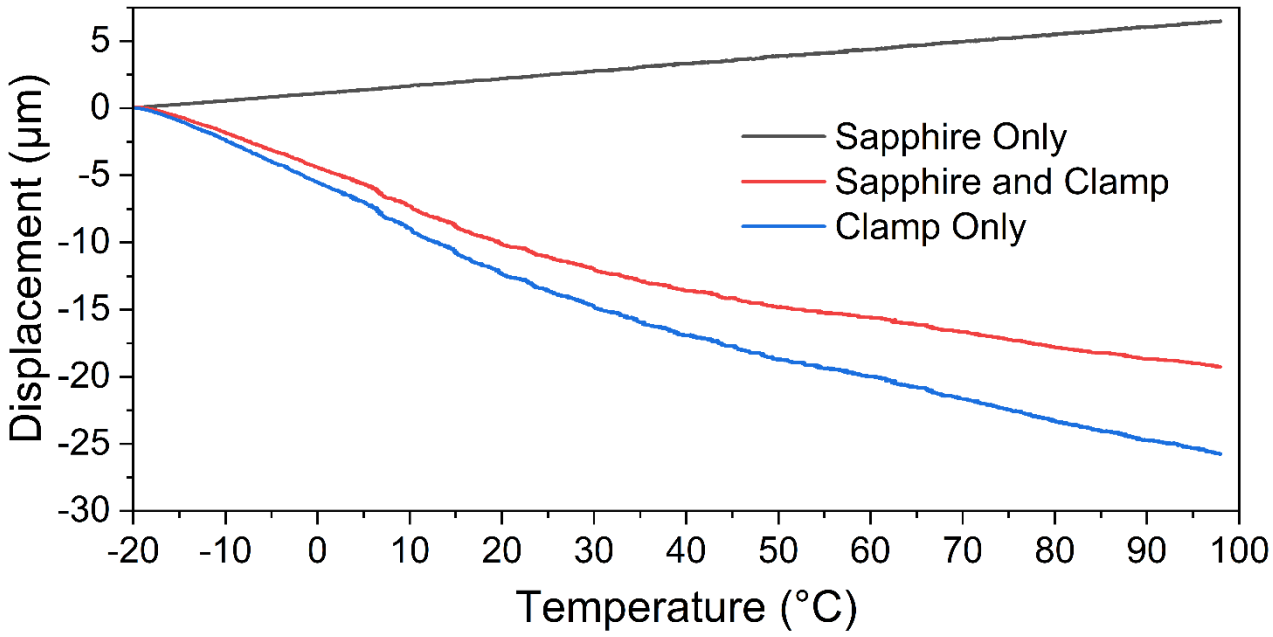

Figure 2.12: Plot of displacement against temperature for a sapphire calibration sample testing in a TA Q800 DMTA. The sample had a diameter of 6.6 mm, and a thickness of 10 mm. Top line is the expected expansion from the sapphire sample only using a coefficient of thermal expansion of 5.5x10^{-6} K^{-1}. The sapphire and clamp sample was the measured displacement of the DMTA clamp with the sapphire calibration sample when heated at a ramp rate of 2 °C. The clamp only line is a calibration curve found by subtracting the sapphire only plot from the sapphire and clamp plot.

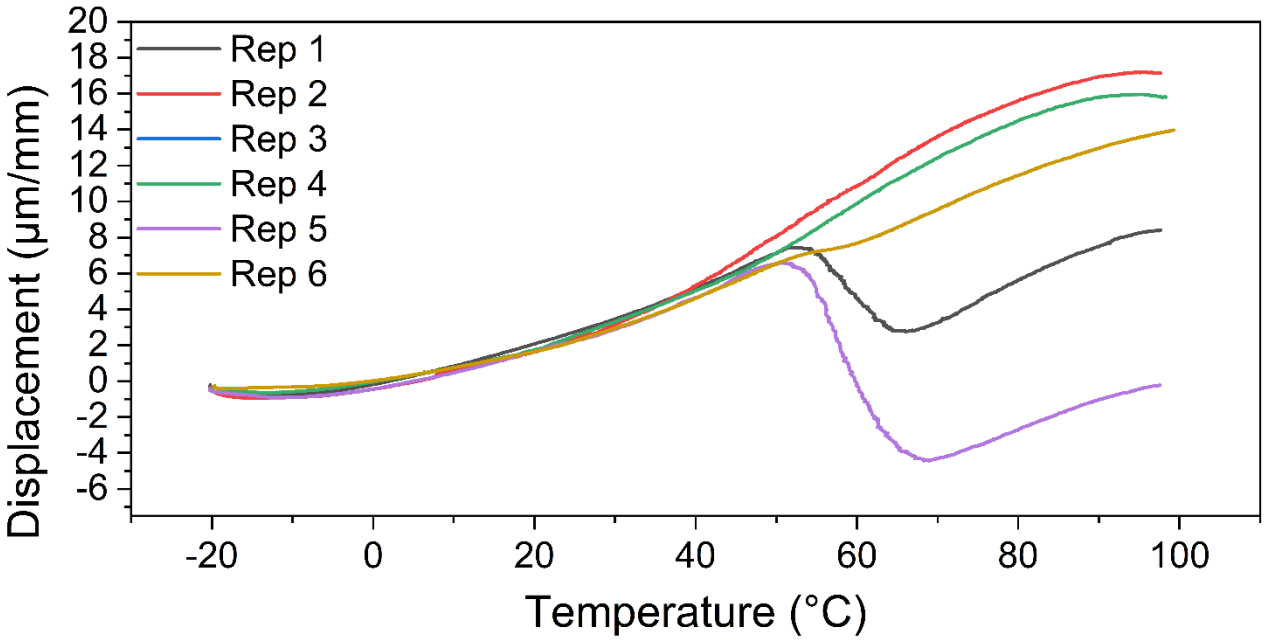

Figure 2.13: Plot showing the displacement against temperature for six samples of 67poly(S-*r*-CPD) tested on a TA Q800 DMTA. The samples were calibrated using the calibration curve on the previous page and accounts for thickness of the polymer samples.

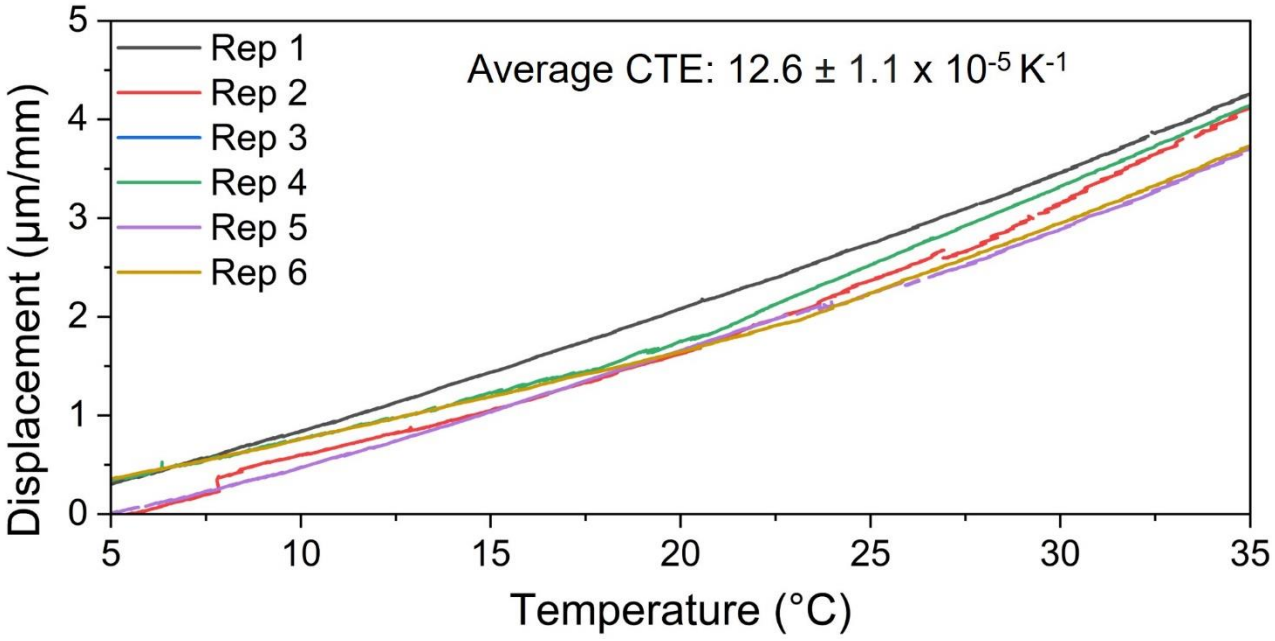

Figure 2.14:Plot from above between 5 °C and 35 °C. This slope of this part was used to calculate the coefficient of thermal expansion of the polymers. The average coefficient of thermal expansion of the six 67poly(S-*r*-CPD) was 12.6 ± 1.1 x 10 $^{-5}$ K^{-1}.

Investigating the effect of DCPD on polymer performance

Control experiment to see the conversion of CPD to DCPD

Cyclopentadiene is known to undergo a Diels Alder reaction at room temperature.[19] At the temperatures used in the reaction, it is possible that the conversion is accelerated. To determine the rate at which this conversion from CPD to DCPD occurs at different temperatures, a control experiment was conducted. In this experiment, 3 grams of cyclopentadiene was added to a two necked round bottom flask with an attached condenser. The cyclopentadiene was then heated with constant stirring. A range of temperatures were tested ranging from room temperature to 180 °C. Every 30 minutes, an aliquot was removed to analyse by NMR. Note that the CPD was not cooled before removal so it does not account for the CPD which would be in the gas phase. Therefore, this is likely an overestimation of DCPD and indicates the relative proportion in the liquid phase of the reaction. An improvement to this experiment would be to allow the CPD to cool before each aliquot is removed. This would cause any gaseous CPD to return to the liquid phase where it could be analysed.

The integration of the cyclopentadiene alkene peak at approximately 6.58 ppm (c) and the dicyclopentadiene alkene doublet at 5.97 ppm (a) was used for that analysis as they both correspond to 2 protons, and they are separated from any other peaks. Below are some example spectra from the 140 °C sample at 30 and 90 minutes.

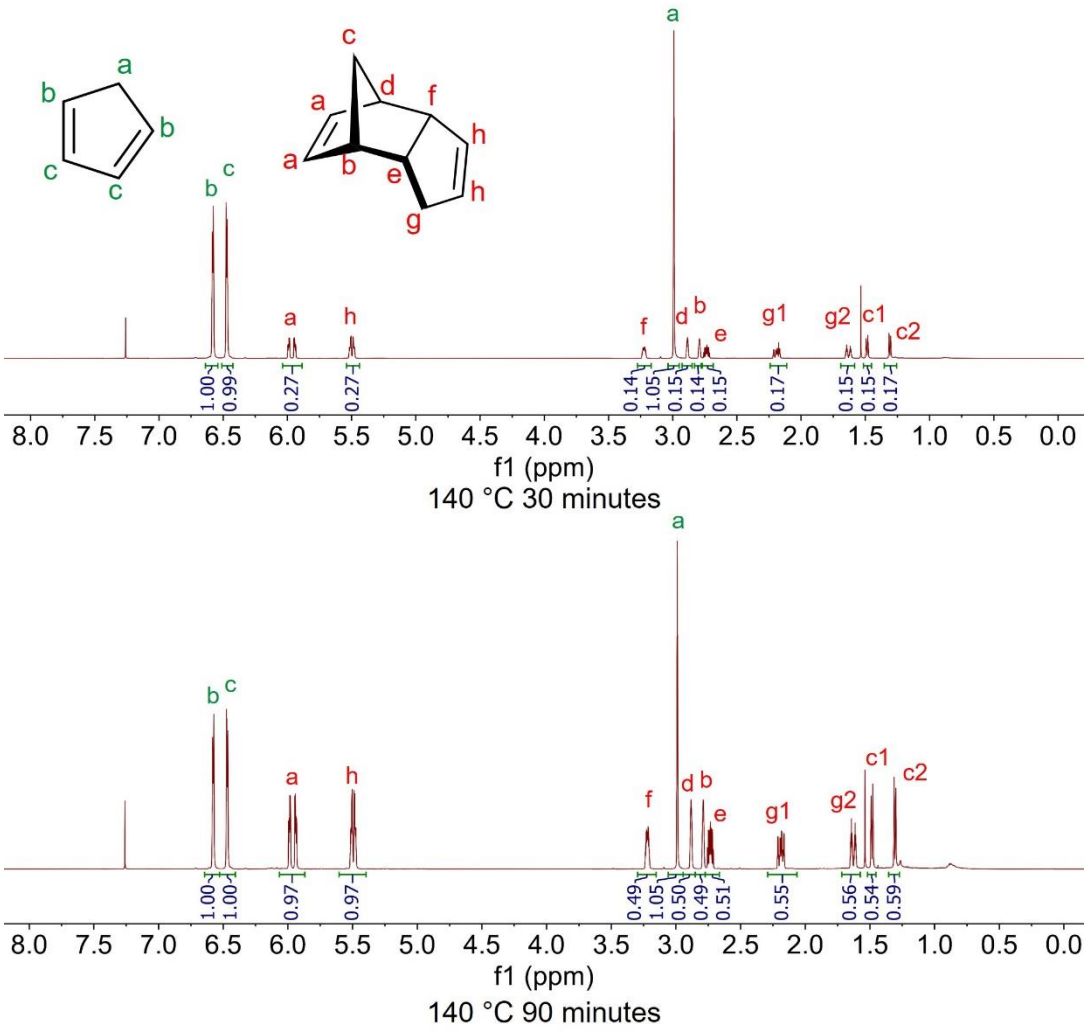

Figure 2.15: Example NMR of aliquots taken from cyclopentadiene that had been heated at 140 °C for 30 minutes or 90 minutes.

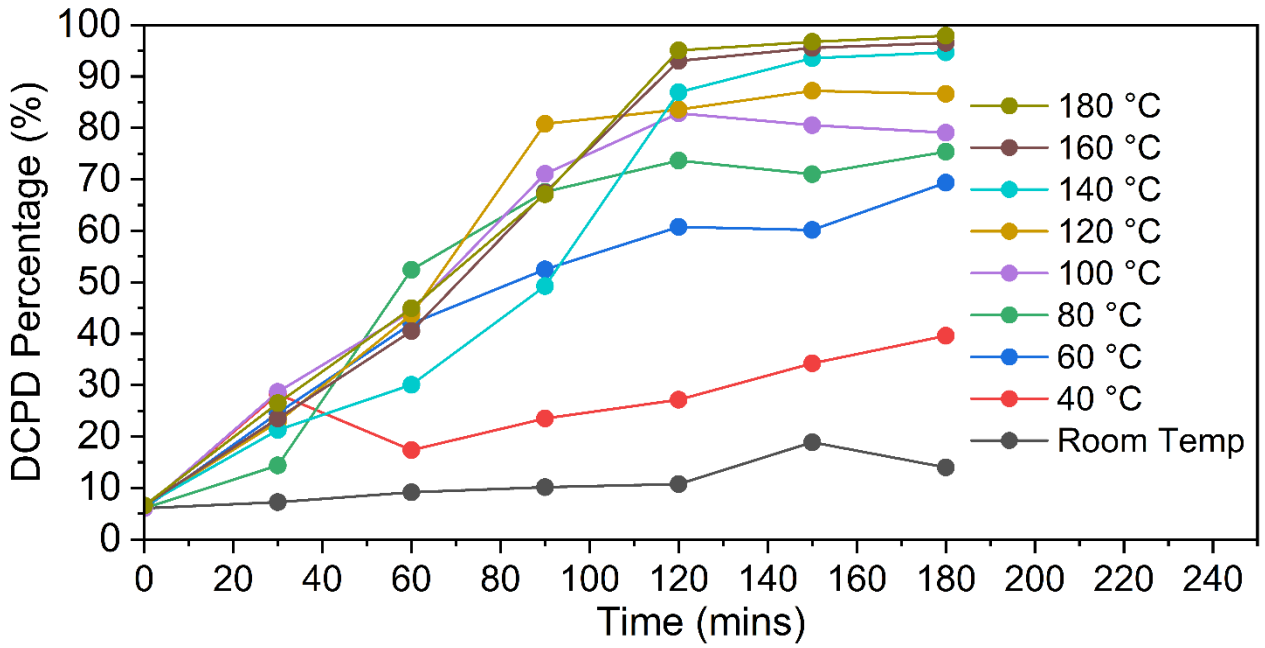

Figure 2.16: Percentage of DCPD in solutions of CPD at different temperatures. Conversion was determined from NMR analysis.

While this experiment was flawed in how the samples were collected, it did indicate that the liquid portion of the CPD solution was converted to DCPD quite quickly at higher temperatures. In the polymerisation reaction between CPD and sulfur, the CPD is added slowly so that it could react quickly with sulfur rather than reflux at high temperature. This would likely reduce the amount of DCPD which formed in the reaction. However, it would be very difficult to eliminate any DCPD from forming and reacting with sulfur. Therefore, it would be expected that some DCPD would be present in the polymer.

Once the CPD reacted at one alkene with sulfur, it could still act as a dienophile. By reacting with another molecule of CPD, it could still undergo a Diels Alder reaction to form DCPD. However, in this case, the less reactive alkene would not be present. This gives two ways in which DCPD could become incorporated into the polymer structure. Therefore, it is very important to determine how much DCPD is in the polymer and how that affects the chemical, physical or optical properties. It should be noted that the dimerization of CPD proceeds through a bis-pericyclic mechanism, making it very fast. Once one of the alkenes of CPD have reacted with sulfur, this mechanism is no longer possible, and the reaction would likely be slower than the dimerization of CPD.

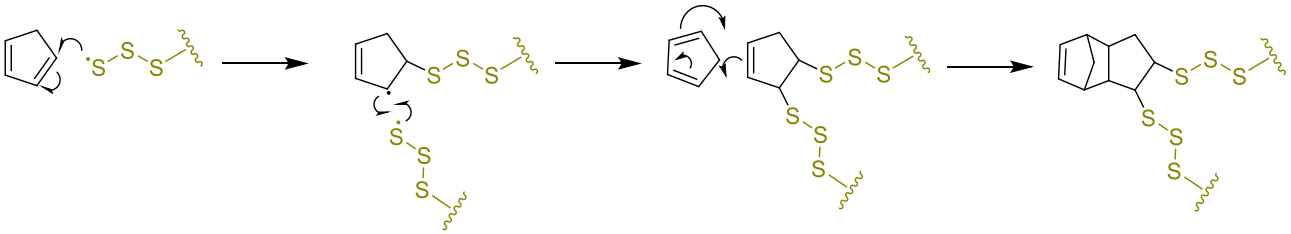

Figure 2.17: Mechanism for the reaction of CPD with sulfur and subsequent Diels Alder reaction with another CPD molecule.

Terpolymer synthesis using sulfur, CPD and DCPD

As explained in the previous section, it was expected that some DCPD would be present in the polymers when sulfur was reacted with CPD. Therefore, it was important to determine the effect that this would have on the properties of the polymer. It would also be useful to determine some characterisation techniques to investigate the proportion of DCPD to CPD in the polymer. To do this, a range of terpolymers were prepared. To prepare these polymers, a solution which contained a mixture of CPD and DCPD was used to react with sulfur. The method for the reaction can be seen below.

Solutions of dicyclopentadiene (DCPD) in cyclopentadiene (CPD) were produced by dissolving the DCPD in CPD. 3 grams of each solution was prepared with the ratio of DCPD varied from 0 % DCPD to 80 % DCPD. These solutions were reacted with sulfur in an inverse vulcanisation reaction using the same method as the CPD reactions. 3 g of sulfur was used for every sample, this gives an equal mass of sulfur to crosslinker in each reaction. Note that this is a greater relative proportion of crosslinker than what is typically used for the cyclopentadiene polymer. In every sample, the sulfur was heated at 165 °C with 500 rpm stirring for 3 mins. All samples had a water-cooled condenser attached. After 3 mins, 150 µL of the CPD/DCPD solution was added directly to the sulfur with a long needle. The main difference in the method for these polymers was that a long needle was used so that the solution could be applied directly to sulfur rather than at the top of the condenser. This prevented DCPD from getting stuck in the condenser. The CPD/DCPD solution was added at 150 µL every 3 minutes until it had all been added. The samples were removed from heat when viscosity increased, and the magnetic stirrer bar could no longer stir at 500 rpm. This would take between 45 and 60 mins depending on composition. Polymers with a greater amount of dicyclopentadiene would react quicker.

A polymer was also produced using 3 grams of DCPD as a crosslinker with no CPD. For this polymer, the method was modified as DCPD is a solid at room temperature. The 3 grams of DCPD was weighed into .294 g potions. These portions were added directly to sulfur using long tweezers at 3 minutes (after sulfur was first added at 165 °C) and every 3 minutes after that. Below is a table of all compositions of polymers that were produced.

Table 2.1: Mass of sulfur, cyclopentadiene and dicyclopentadiene used to prepare terpolymers via inverse vulcanization reaction.

Composition (S-CPD-DCPD)	Sulfur mass (g)	Cyclopentadiene mass (g)	Dicyclopentadiene mass (g)
50-50-0	3 g	3 g	0 g
50-45-5	3 g	2.7 g	0.3 g
50-40-10	3 g	2.4 g	0.6 g
50-30-20	3 g	1.8 g	1.2 g
50-25-25	3 g	1.5 g	1.5 g
50-20-30	3 g	1.2 g	1.8 g
50-10-40	3 g	0.6 g	2.4 g
50-0-50	3 g	0 g	3 g

Simultaneous thermal analysis of terpolymers

The thermal properties were first tested for all the terpolymers. Simultaneous Thermal analysis (STA) and differential scanning calorimetry (DSC) were used. STA gives the thermal stability of the material. Any changes in the thermal stability is important as it can indicate changes in the structure of the polymer. All terpolymers were analysed with a Perkin Elmer STA8000. The samples were heated from 60 °C to 800 °C at a temperature ramp rate of 20 °C/min under a flow of nitrogen. At 800 °C, the gas was switched to air for 10 mins to burn off any remaining polymer.

The STA did not show the characteristic sulfur melting peak at 119 °C for any of the samples, indicating that there was no unreacted sulfur after cure. There were subtle changes between the polymers. The samples with more CPD showed a larger overall mass loss. There are two explanations for this. The first is that they had more sulfur in the polymer. The high sulfur parts of the polymer are generally lost earlier. As can be seen in the sulfur control, all sulfur should be lost by around 350 °C- 400 °C. However, this is likely not the cause of the greater overall mass loss. The samples with more CPD showed a much greater loss at temperatures higher than 350 °C. This additional mass loss is likely due to the loss of carbon-based portions of the polymer. The mass loss results in an additional feature in the DSC between 600 °C and 700 °C. It is likely that this additional loss is due to the degradation products CPD portions of the polymer being more volatile than those of DCPD.

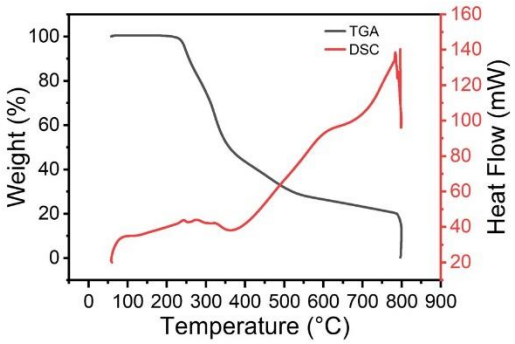

50-50-0 S-CPD-DCPD

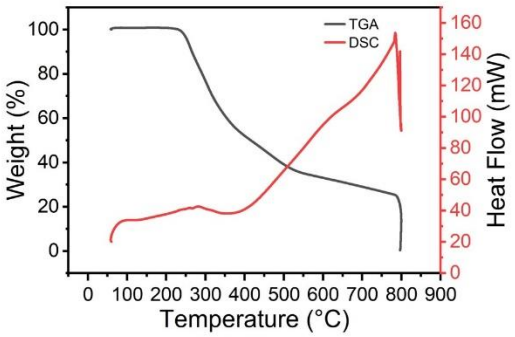

50-45-5 S-CPD-DCPD

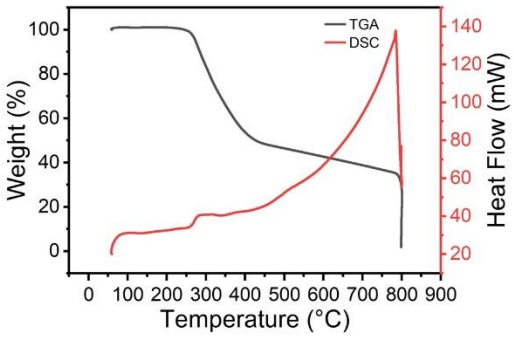

50-40-10 S-CPD-DCPD

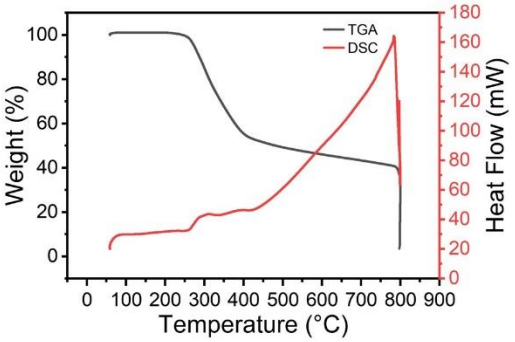

50-30-20 S-CPD-DCPD

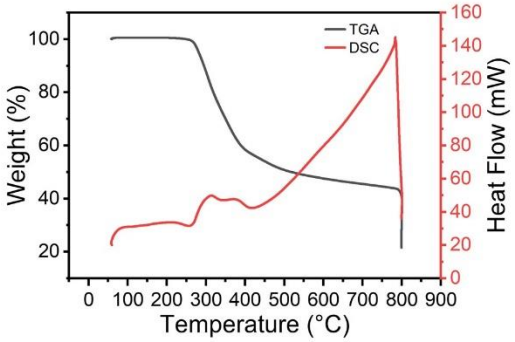

50-25-25 S-CPD-DCPD

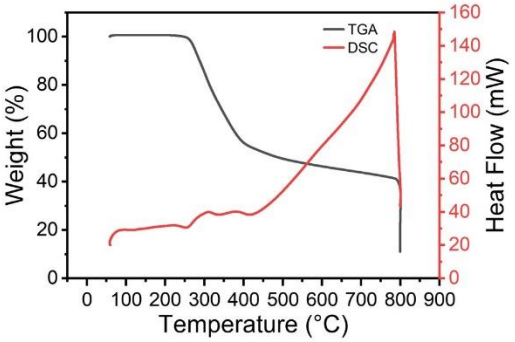

50-20-30 S-CPD-DCPD

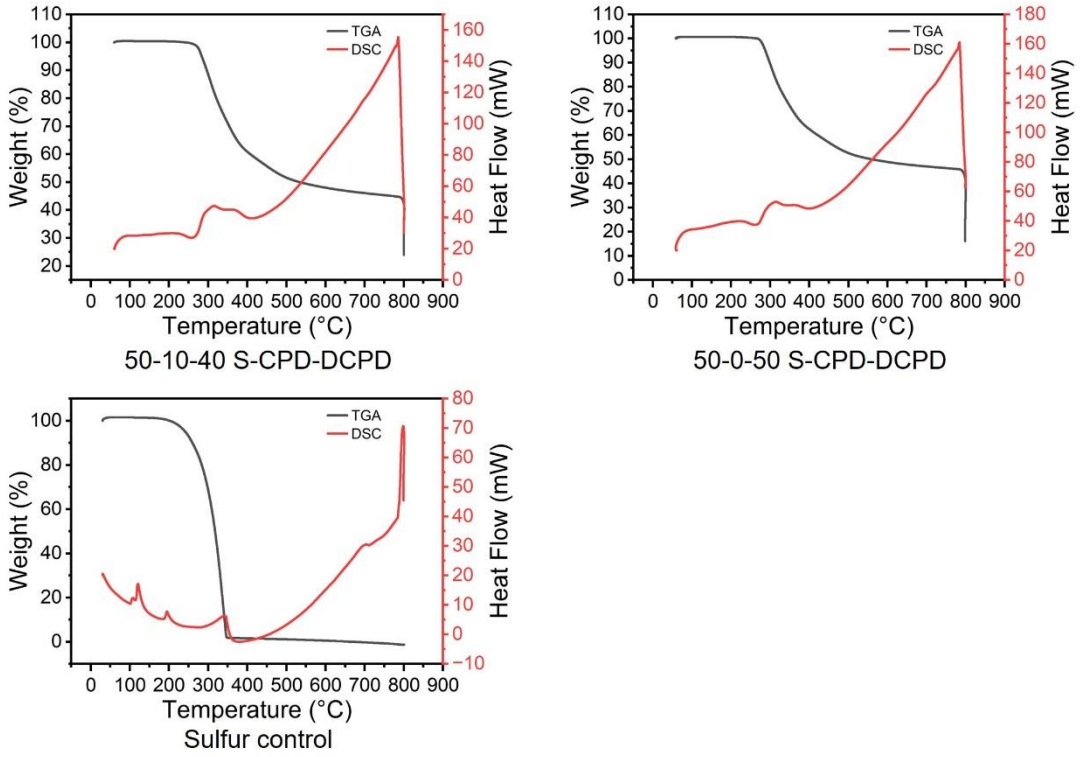

Figure 2.18: STA plots of all terpolymers made with sulfur, CPD and DCPD.

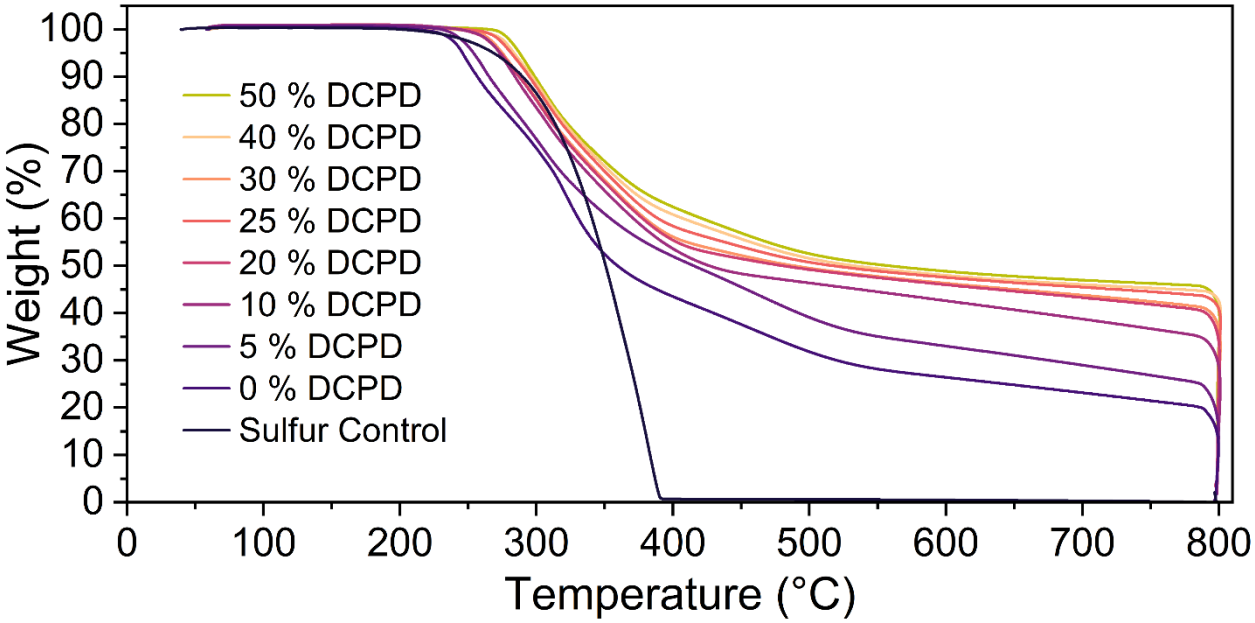

Figure 2.19: Plot of all TGA spectra for terpolymers made from sulfur, CPD and DCPD. The percentage of DCPD is labelled but all polymers had a feed ratio of 50 % sulfur. The feed ratio of CPD is equal to 50 % minus the percentage of DCPD.

Terpolymers analysis with DSC

All polymers were analysed by DSC using a Perkin Elmer DSC 8000 to find a glass transition temperature. Starting from 30 °C, the polymer samples were cooled to -80 °C at 5 °C/ min. The temperature was then cycled from -80 °C to 150 °C twice to find the Tg. All samples were analysed under nitrogen.

The glass transition temperature of the terpolymers increased rapidly with increased DCPD content. When only cyclopentadiene was used as a monomer, the Tg was around room temperature, but it quickly increased to over 100 °C as DCPD content is increased. This was likely because DCPD acts as a rigid crosslinker and reduced any movement of the polymer chains. None of the polymers showed the characteristic melting peaks of sulfur, indicating that there was no unreacted sulfur in the polymer. The results of the STA and DSC experiments indicate that additional DCPD in the reaction would lead to increased thermal stability and glass transition temperature.

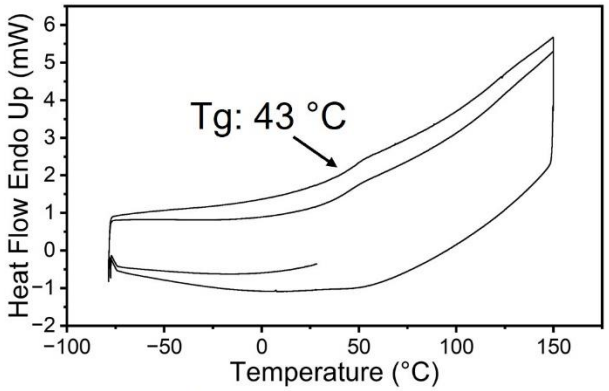

50-50-0 S-CPD-DCPD

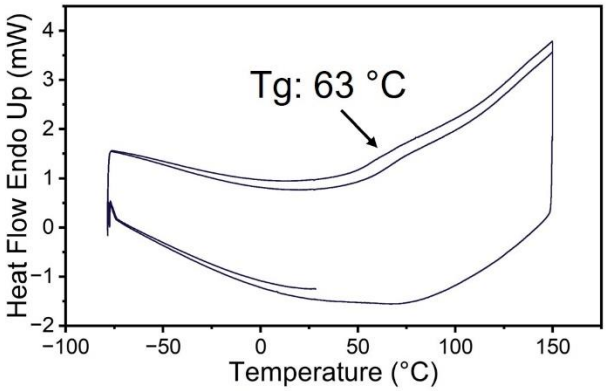

50-45-5 S-CPD-DCPD

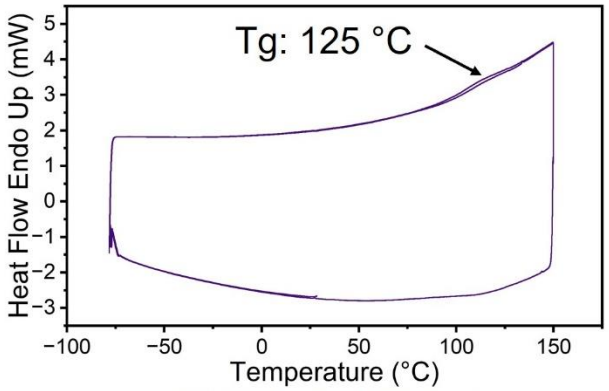

50-40-10 S-CPD-DCPD

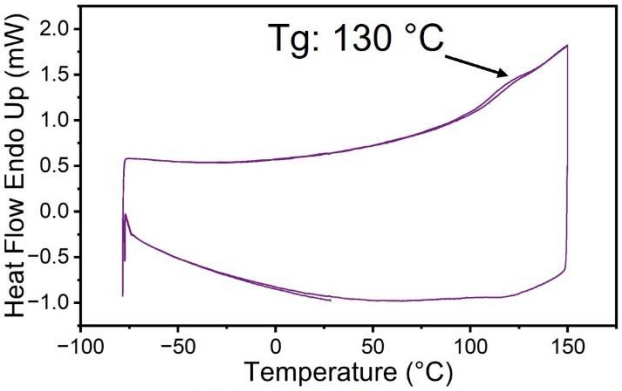

50-30-20 S-CPD-DCPD

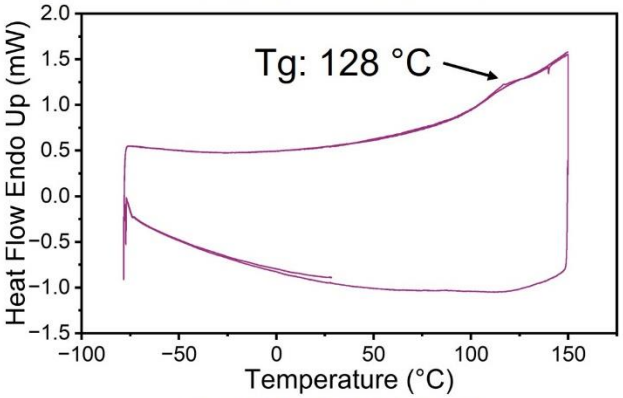

50-25-25 S-CPD-DCPD

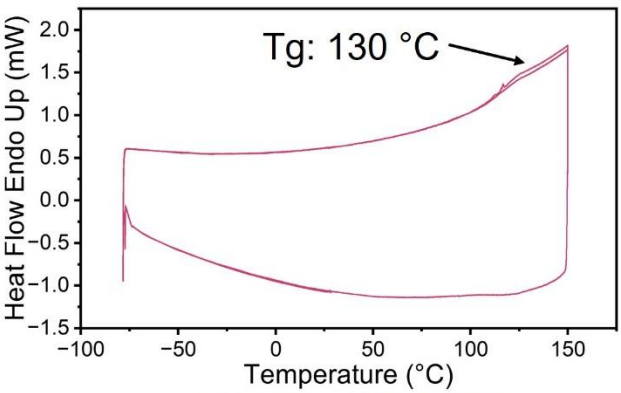

50-20-30 S-CPD-DCPD

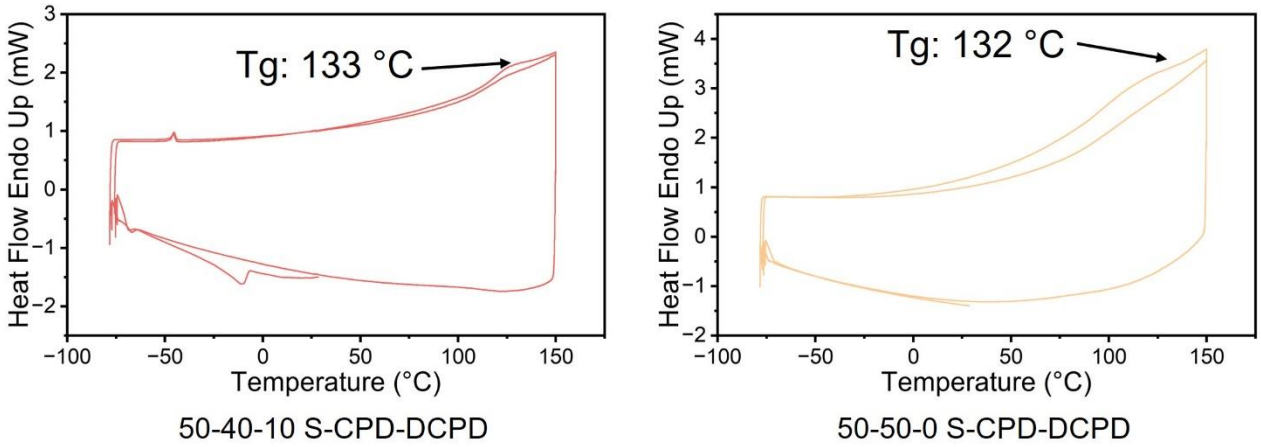

Figure 2.20: Differential scanning calorimetry plots of terpolymers made from sulfur, CPD and DCPD. The glass transition temperature at the inflection point is displayed.

When the glass transition temperature from DSC is plotted against the mass after the STA run, they appear to be linked. This likely indicates that DCPD increases the overall thermal stability of the polymer.

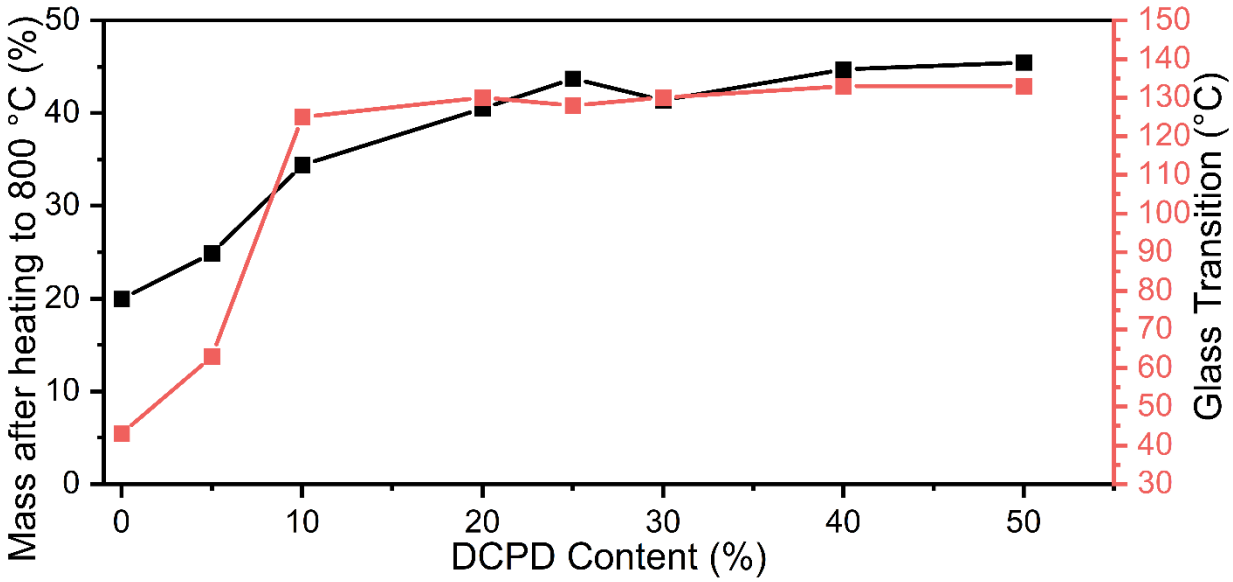

Figure 2.21: Plot showing the mass after heating to 800 °C in STA experiments and the glass transition temperature as measured by DSC of terpolymers made from sulfur, CPD and DCPD. All polymers have a sulfur content of 50 %. The other 50 % is made up of DCPD and CPD making the CPD content equal to 50 minus the displayed percentage of DCPD.

Reduction of terpolymers with $NaBH_4$ and analysis by GC-MS

With the thermal testing in hand, the next step was the characterise the chemical structure of the terpolymers. This would give a lot of information about the reaction between sulfur and CPD. As the polymers were not soluble in most common solvents, they were instead reduced with sodium borohydride. The sodium borohydride was used to reduce many of the sulfur-sulfur bonds to leave small molecules that could be analysed by GC-MS. All polymers were analysed so that the effect of feed ratio on the final polymer composition could be determined.

30 mg of each polymer was ground into a powder and weighed into a flame dried, 50 mL, 2-necked round bottom flask. 94 mg of sodium borohydride was weighed into the same round bottomed flask under a stream of nitrogen. The main neck of the round bottomed flask was added to an air condenser with a nitrogen line. The condenser and round bottomed flask were purged with nitrogen for 30 minutes to ensure all oxygen was removed from the reaction atmosphere. After purging, the outlet needle was removed but a constant flow of nitrogen was maintained. 2.5 mL of anhydrous THF was injected into the round bottomed flask and the mixture was stirred at 500 rpm. The round bottomed flask was then added to a 50 °C oil bath. While stirring was maintained, the mixture was heated at 50 °C for 24 hours. After 24 hours, the mixture was cooled to 0 °C using a salted ice bath and 5 mL of 1 M HCl was injected slowly. 5 mL of hexane was then injected into the round bottomed flask and stirred for an additional hour. After stirring, the organic layer was separated and analysed using GC-MS.

All polymer compositions were tested to analyse the change in the relative concentration of reduced products with the feedstock used in the polymerisation reaction. Several general trends were observed. As the amount of CPD in the polymer reduced, the relative height of the lower retention time (lower molecular weight) peaks decreased. As the amount of DCPD in the polymer increased, the chromatograms simplified and converged on only a few peaks. These peaks all belonged to the DCPD molecule in which the less reactive alkene remained intact. The peak at 12.58 minutes belonged to the dithiol peak with an alkene while the peak at 16.05 minutes corresponded to the trisulfide version of the same molecule. The second alkene did not appear to react when DCPD alone was reacted with sulfur but the tetrathiol of DCPD was observed when CPD was used. It is possible that this is due to the low reactivity of the second alkene in DCPD.

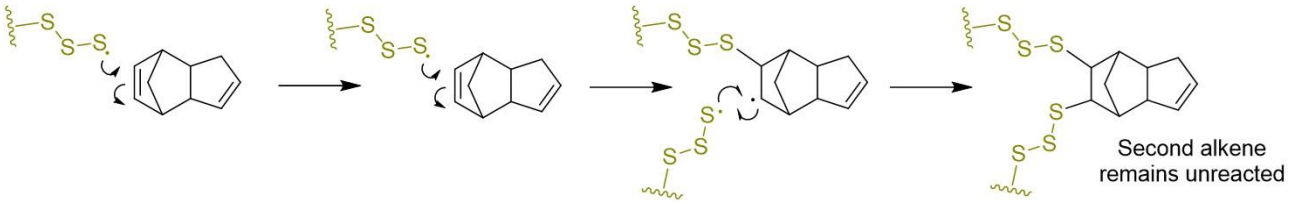

Figure 2.22: Mechanism for the reaction of sulfur and DCPD.

The chromatograms were quite complicated but will be separated into six groups to make it easier to explain. The chromatograms for each terpolymer composition are shown on the next two pages. After that, an overlay of the polymer with only CPD and only DCPD will be used to assign and explain each of the peaks.

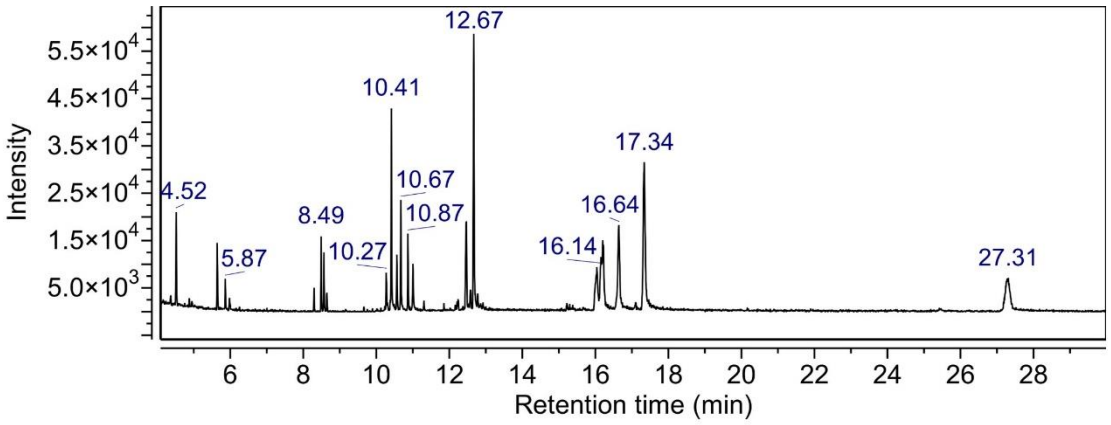

Reduced terpolymer made from 50-50-0 S-CPD-DCPD

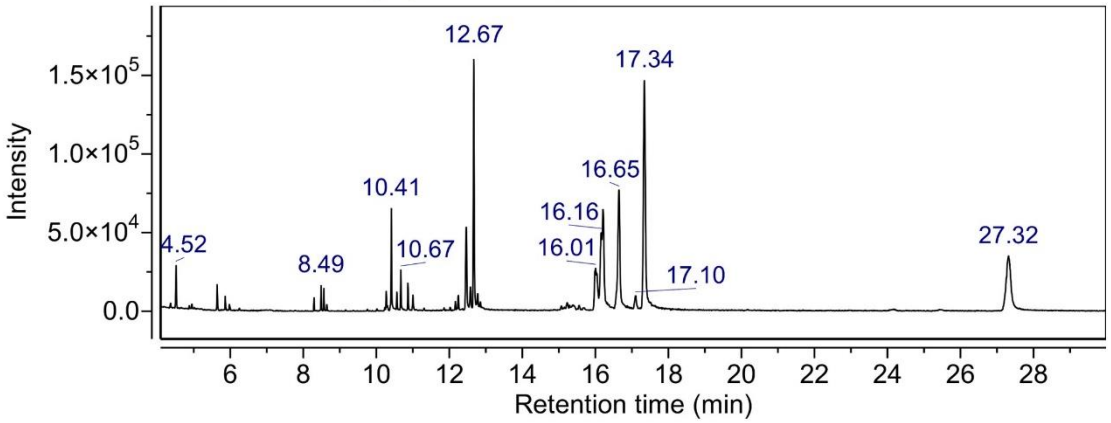

Reduced terpolymer made from 50-45-5 S-CPD-DCPD

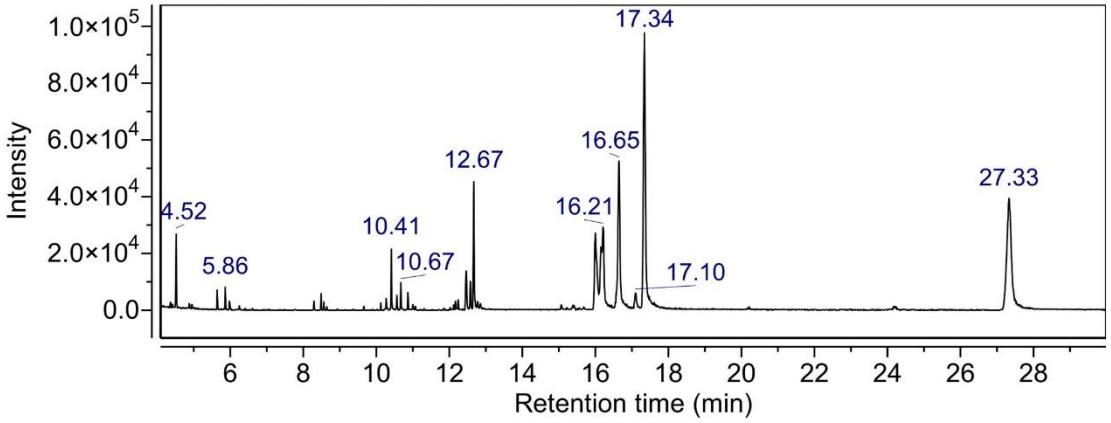

Reduced terpolymer made from 50-40-10 S-CPD-DCPD

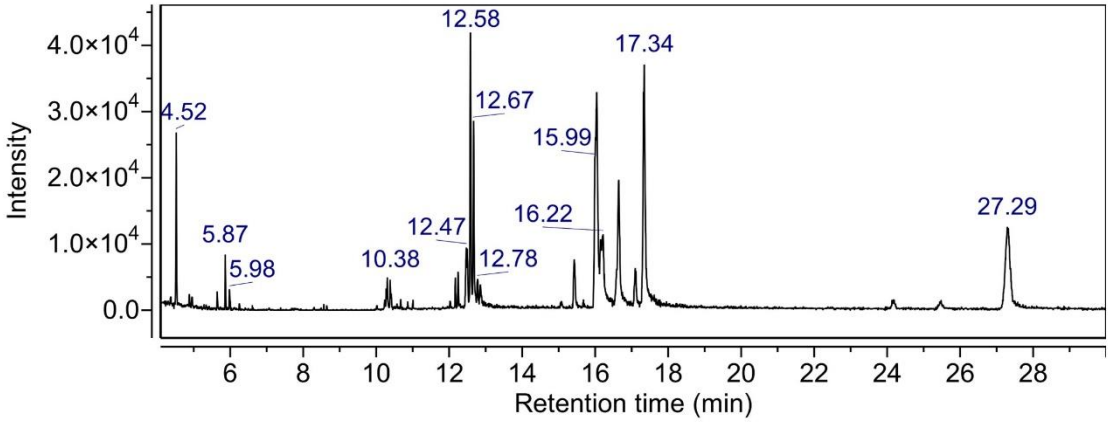

Reduced terpolymer made from 50-30-20 S-CPD-DCPD

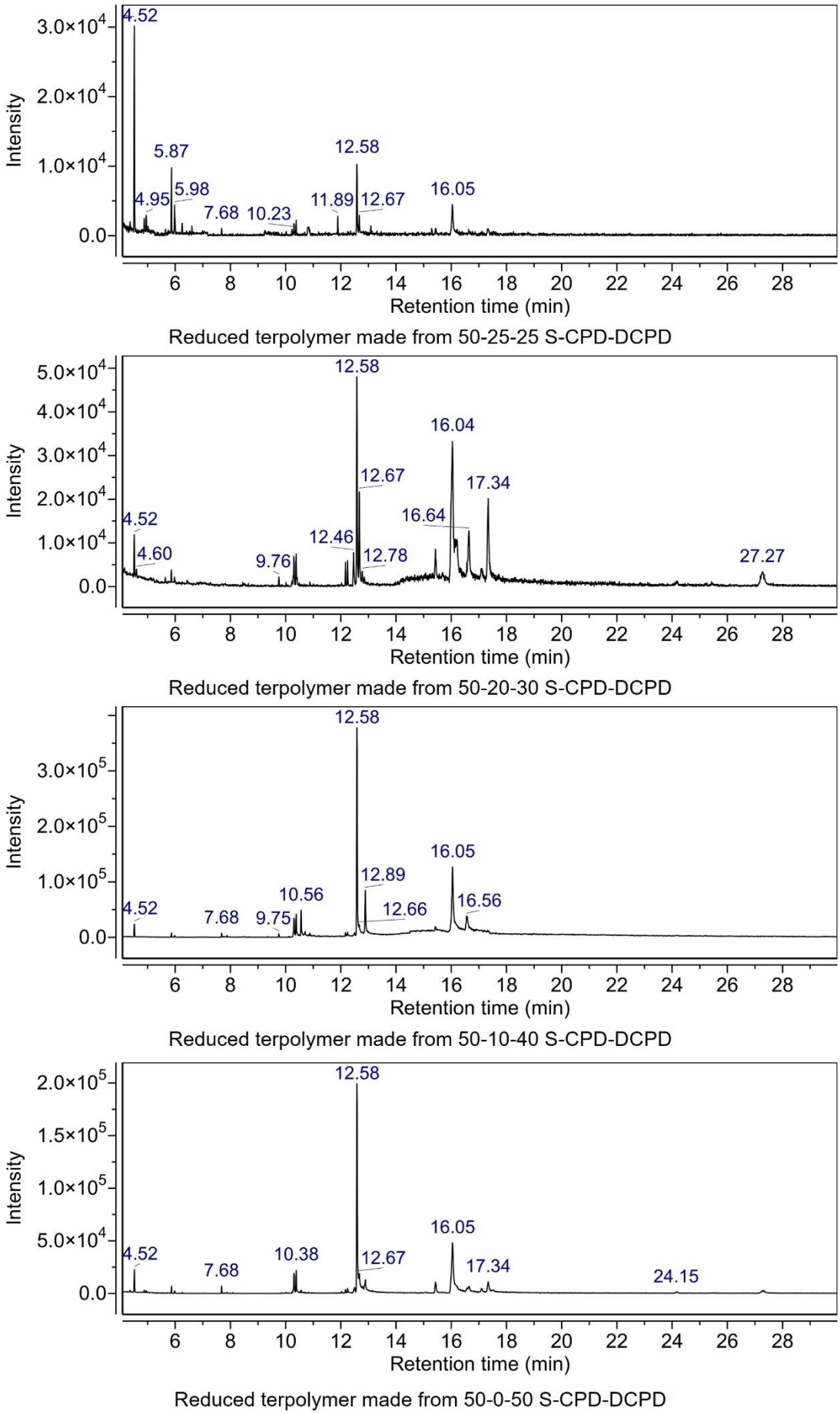

Figure 2.23: Chromatograms for terpolymers made from sulfur, CPD and DCPD which have been reduced with sodium borohydride.

The chromatograms will be split into six different groups to assign all the peaks and explain how they could form. To do this, an overlay of the 50-50-0 S-CPD-DCPD and the 50-0-50 S-CPD-DCPD polymers will be used. The groups that will be split into are: 4-7 mins, 7-9 mins, 9-12 mins, 12-14 mins, 14-19 mins and 19-30 mins. Both peaks were scaled using their largest peak.

The region between 4 and 7 minutes contains three main peaks. Two of these are impurities from the solvent and can be ignored. The peak at 5.65 minutes consists of a cyclopentane thiol. This molecule indicates that both alkenes in CPD reacted, and the resulting polymer was reduced. This peak decreased with the CPD content and was not in the polymer with only DCPD.

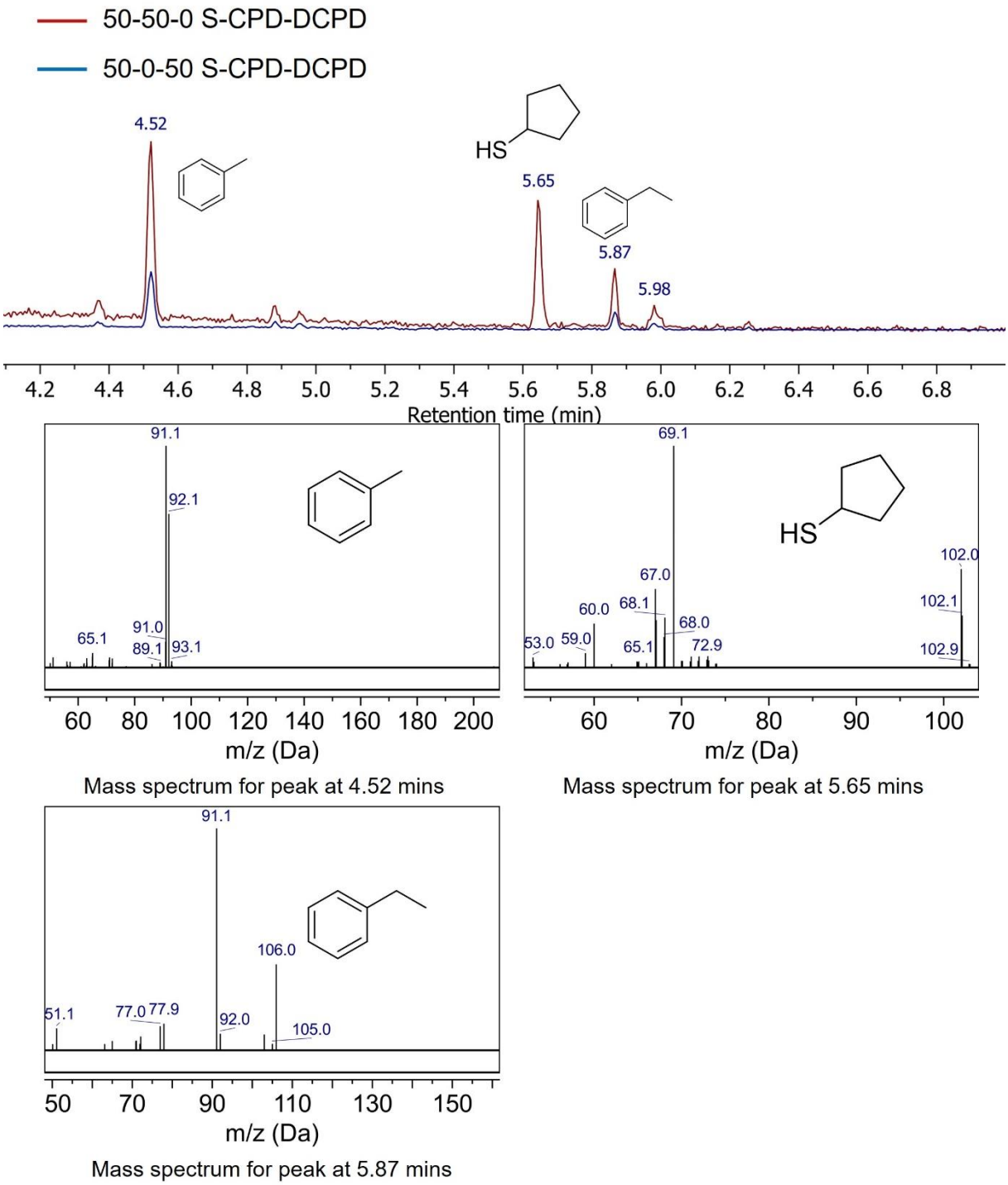

Figure 2.24: GC chromatogram from 4-7 mins for reduced terpolymers made from 50-50-0 S-CPD-DCPD and 50-0-50 S-CPD-DCPD. Mass spectra for each of the labelled peak are shown.

The region between 7 and 9 minutes shows five main peaks. One at 7.68 minutes was only present in the polymers with high DCPD content. This peak corresponds to a DCPD molecule. It is possible that this was formed in the reduction or that there was unreacted DCPD in the polymer structure. The other four peaks all have the same mass spectrum. They correspond to a cyclopentane dithiol. The four peaks likely represent isomers of the dithiol. These peaks were only present in the samples with high CPD content.

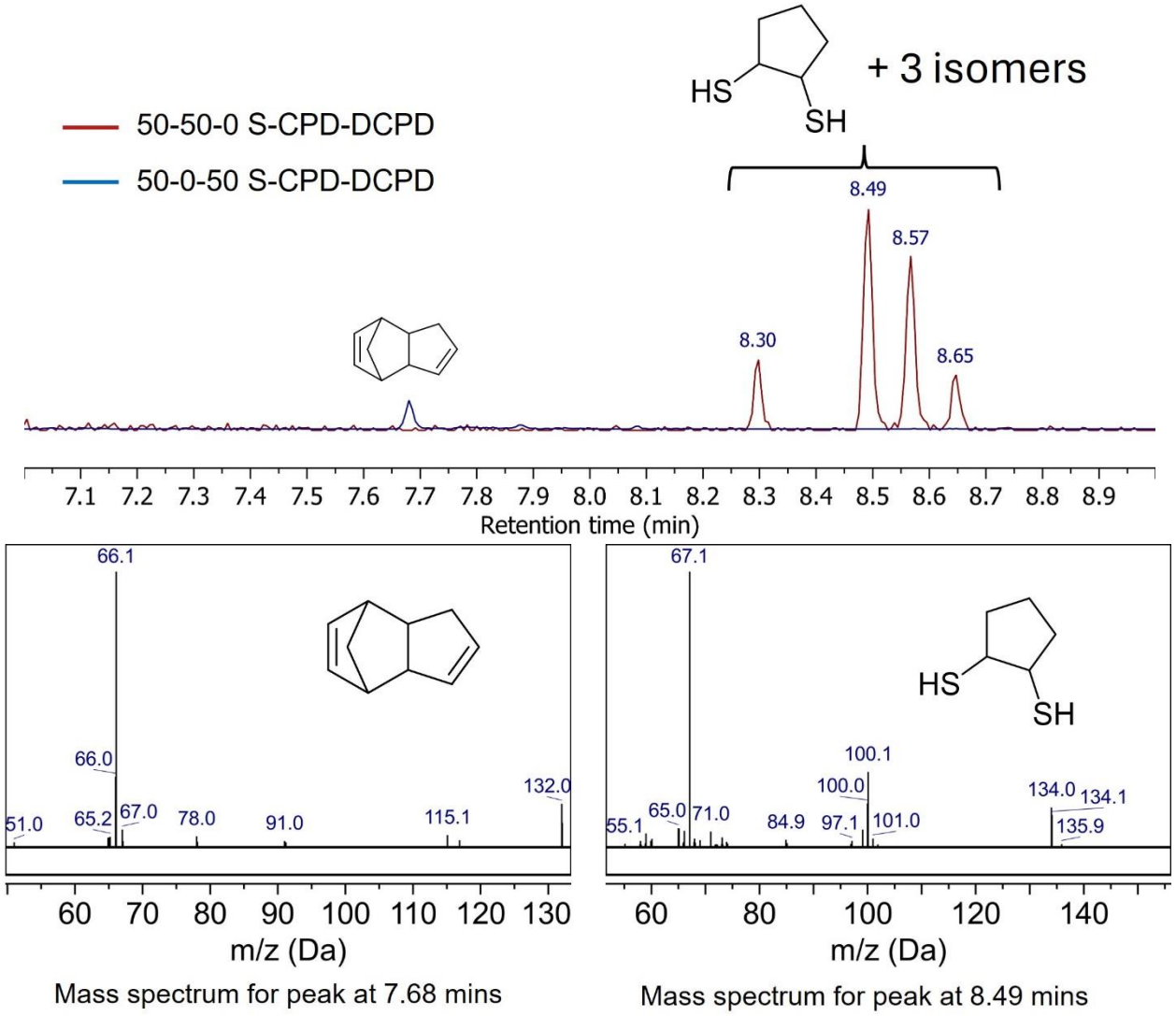

Figure 2.25: GC chromatogram from 7-9 mins for reduced terpolymers made from 50-50-0 S-CPD-DCPD and 50-0-50 S-CPD-DCPD. Mass spectra for each of the labelled peak are shown.

The region between 9 and 12 minutes contains several peaks. The terpolymers with high DCPD only showed two peaks in this region. They both have the same mass and correspond to DCPD with one alkene and a thiol. These peaks indicate that the less reactive alkene on DCPD did not react. The polymers with higher CPD content show four peaks corresponding to cyclopentane trithiol. Again, these peaks confirm that both alkenes on the cyclopentadiene reacted to form the polymer. There was also a peak corresponding to a pentane cyclic trisulfide which could also form from the reduction. There was another peak at 10.57 minutes with a mass of 132 which could not be identified.

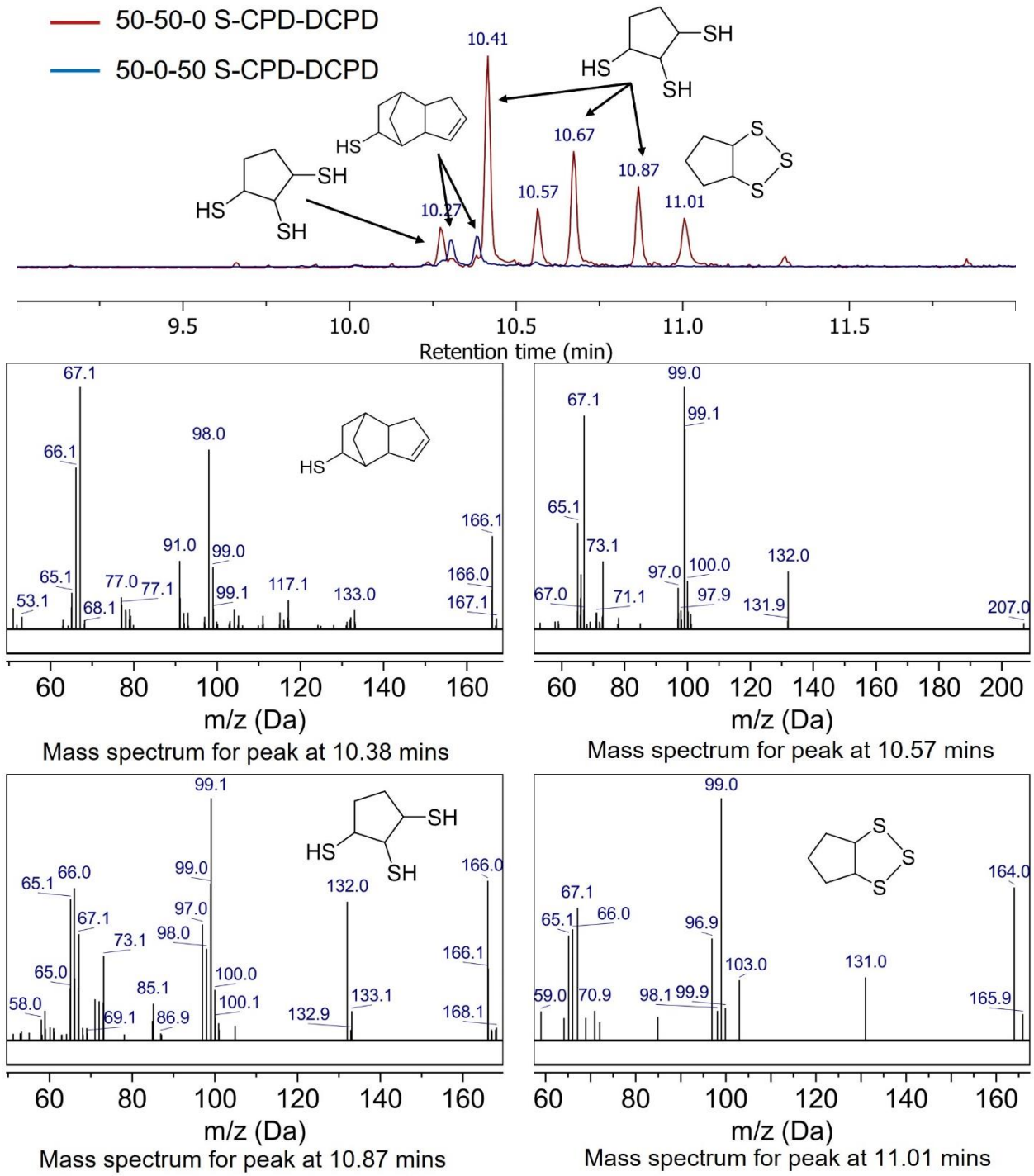

Figure 2.26: GC chromatogram from 9-12 mins for reduced terpolymers made from 50-50-0 S-CPD-DCPD and 50-0-50 S-CPD-DCPD. Mass spectra for each of the labelled peak are shown.

The region from 12 to 14 minutes had three main peaks. These peaks were very large and were the major peaks for most of the terpolymer. For the terpolymer made with only sulfur and DCPD, the major peak was a dithiol of DCPD with one alkene. This indicates that the less reactive alkene did not react in the polymerisation. However, the terpolymer which was made with only sulfur and CPD showed a dithiol DCPD with no alkenes. This indicates that DCPD can form from the reaction with CPD but when it does, it is much less likely to have alkenes. The largest peak in the chromatogram for the polymer made from sulfur and CPD was the peak at 12.67 minutes. This peak corresponded to the cyclopentane tetrathiol and indicates that both alkenes of CPD reacted with sulfur.

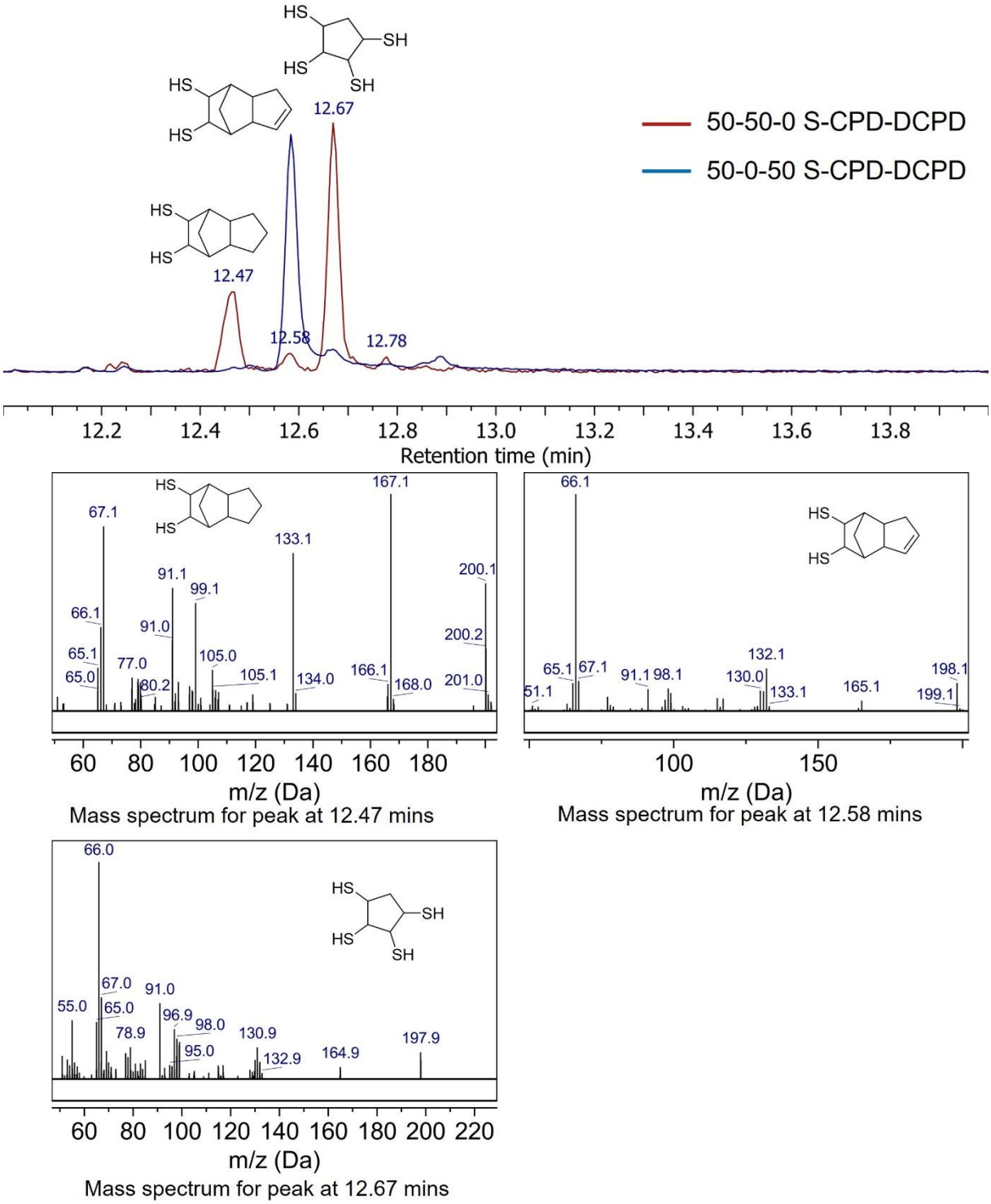

Figure 2.27: GC chromatogram from 12-14 mins for reduced terpolymers made from 50-50-0 S-CPD-DCPD and 50-0-50 S-CPD-DCPD. Mass spectra for each of the labelled peak are shown.

The region between 14 and 19 minutes only had peaks corresponding to DCPD molecules. The polymer made only from sulfur and DCPD had only a peak corresponding to a cyclic trisulfide of DCPD with one alkene. Interestingly, the polymer prepared with sulfur and CPD also showed 4 peaks corresponding to trithiols of DCPD with no alkenes. These peaks were significantly reduced in the polymer made without CPD.

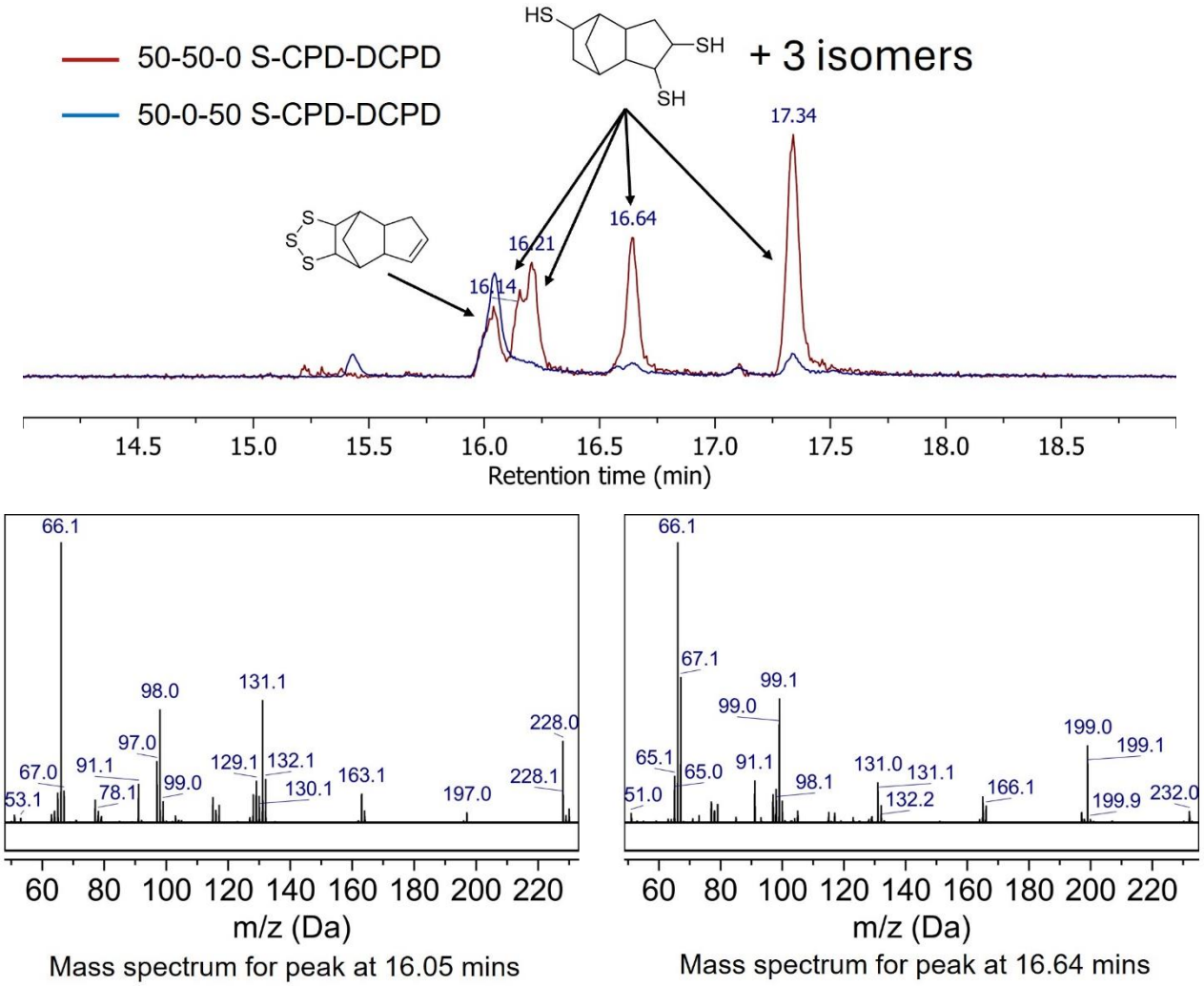

Figure 2.28: GC chromatogram from 14-19 mins for reduced terpolymers made from 50-50-0 S-CPD-DCPD and 50-0-50 S-CPD-DCPD. Mass spectra for each of the labelled peak are shown.

The region between 19 and 30 minutes only showed one peak. This peak corresponded to the tetrathiol of DCPD with no alkenes. Like in the other regions, this peak was larger in the terpolymer made from sulfur and CPD.

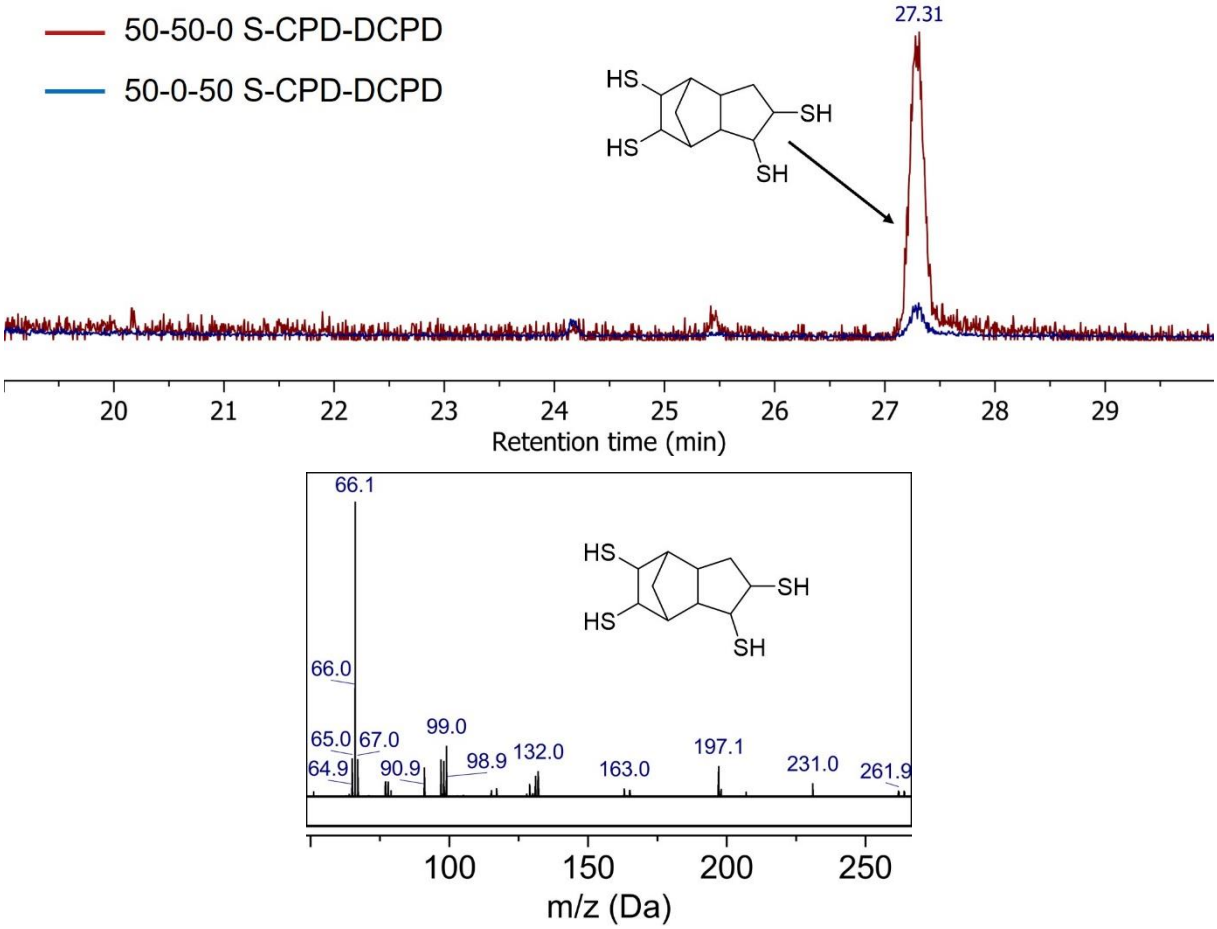

Figure 2.29: GC chromatogram from 19-30 mins for reduced terpolymers made from 50-50-0 S-CPD-DCPD and 50-0-50 S-CPD-DCPD. Mass spectra for each of the labelled peak are shown.

The results of the reduced terpolymers were very interesting. The polymers made with a large amount of DCPD converged towards only peaks that still have the less reactive alkene. This indicates that only the more reactive alkene of DCPD was participating in the reaction with sulfur. This two stage reaction of DCPD with sulfur had been seen before in several publications.[15, 20, 21] However, the peaks that corresponded to DCPD with an alkene were significantly reduced in the polymers made from CPD, despite containing peaks for fully saturated DCPD. It's possible that this is because the CPD could first react with sulfur then undergo an Diels Alder reaction with another molecule of CPD. This would leave only the more reactive alkene of DCPD which could then undergo a reaction with sulfur.

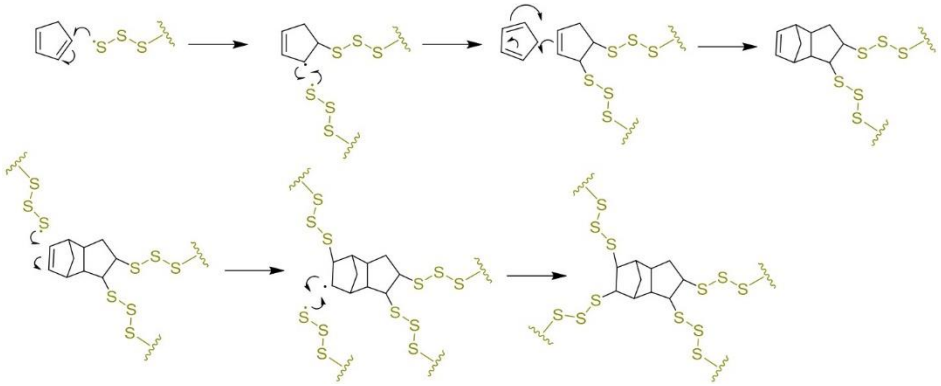

Figure 2.30: Reaction between sulfur and CPD with subsequent Diels Alder reaction.

Analysis of terpolymers with FTIR

The reduction experiments showed that the polymers with DCPD had more alkenes in the polymer structure than the polymers made with CPD. To investigate this and how this affected the infrared spectrum, thin windows of the polymers were prepared and tested using FTIR. These windows were very thin and do not give an indication of the overall transmission of a thick sample but they do allow for the major absorptions of the polymer to be observed. The results of the FTIR study confirms the findings of the reduction experiments. The peaks that correspond to alkenes (3050 cm^{-1}) were much larger in the samples with added DCPD. There was still a small peak at this location in the sample made from only CPD, this is likely from DCPD impurity in the CPD or DCPD that was formed in situ during the reaction. The samples with less added DCPD appeared to be much simpler in the LWIR region (1428 cm^{-1} – 714 cm^{-1}), potentially due to the reduced abundance of alkenes.

Free standing windows of the terpolymers were prepared using a similar method as the cure time samples. The polymers were processed with a heated press to prepare thin free-standing films with a thickness ranging from 180 µm - 220 µm to analyse by transmission FTIR analysis.

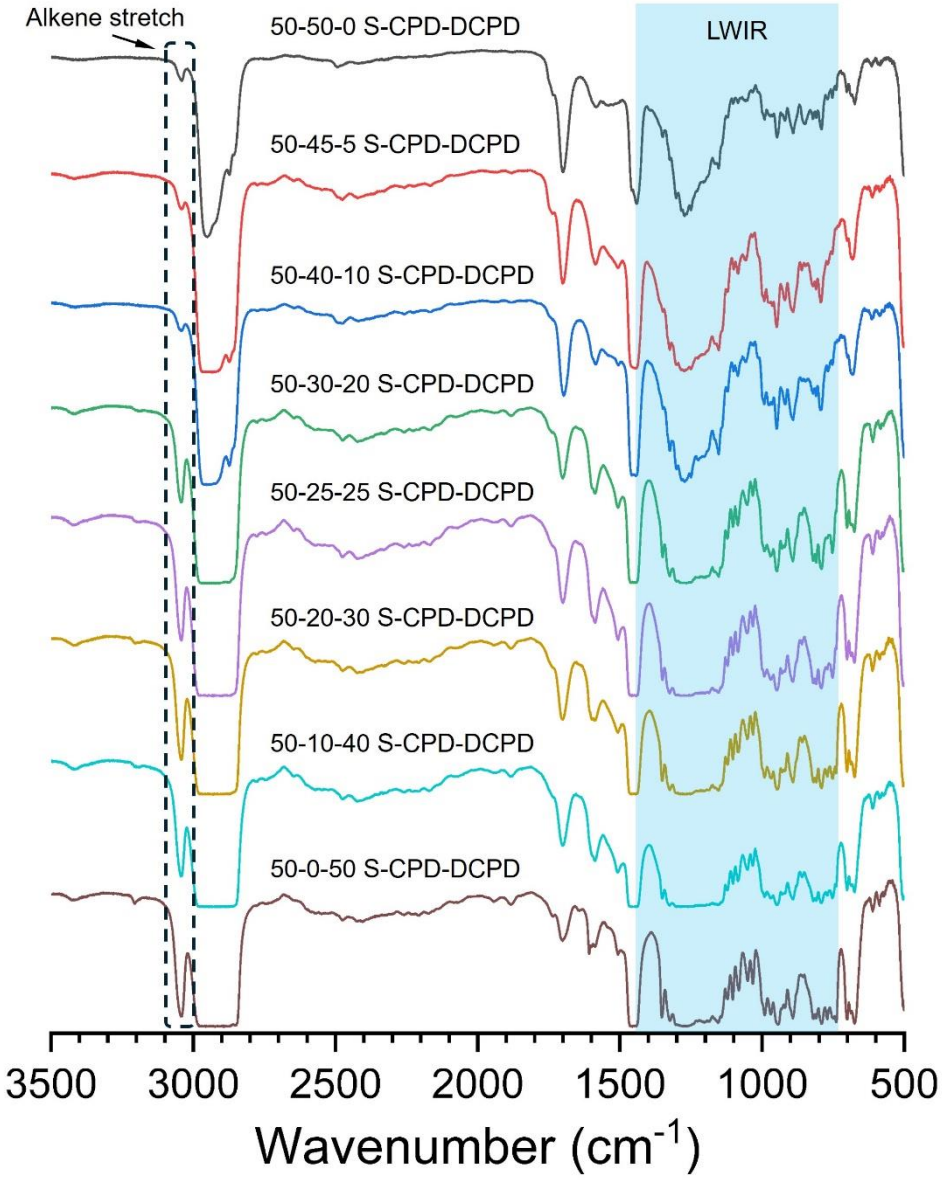

Figure 2.31: FTIR spectra of thin films of terpolymers prepared from sulfur, CPD and DCPD.

Long wave infrared transparency of terpolymers

The effect of dicyclopentadiene on the long wave infrared transparency of the polymer is extremely important for its use in infrared imaging. The focus of this thesis is long wave infrared imaging which is between the region of 7 µm – 14 µm. This region is very susceptible to changes in chemical structure of the polymer. To test the long wave infrared transmission of the terpolymers, 1 mm thick polymer samples were prepared for every composition. The samples were tested for transmission in the mid- and long-wave infrared regions using a Perkin Elmer Frontier FTIR spectrometer. In transmission mode, the polymer samples were tested in the wavelength range of 2 µm to 20 µm over a total of 16 scans.

The transmission of the samples sharply decreased as the DCPD content increased. As discussed in the previous sections. When DCPD is present in the reaction, the less reactive alkene is often still present in the polymer. These alkenes would likely lead to an increase in the unique vibrational modes in the LWIR region as was observed in the FTIR analysis section. In a recent paper by Lee, You and colleagues, a thiolated version of DCPD was used in a reaction with sulfur. It was found that using this molecule resulted in a polymer with no unreacted alkenes and an increased LWIR transmittance.[22] When only CPD was used in the reaction, the number of alkenes in the final polymer was significantly reduced. The findings of the thin film FTIR experiments showed that the LWIR region of the polymers with more CPD was much simpler. These results can also be observed in the thicker samples as only the samples with more CPD show transmission in this region. The overall transmission for the terpolymers was quite low as only 50 % sulfur was used but still gives a good indication on the effect of DCPD.

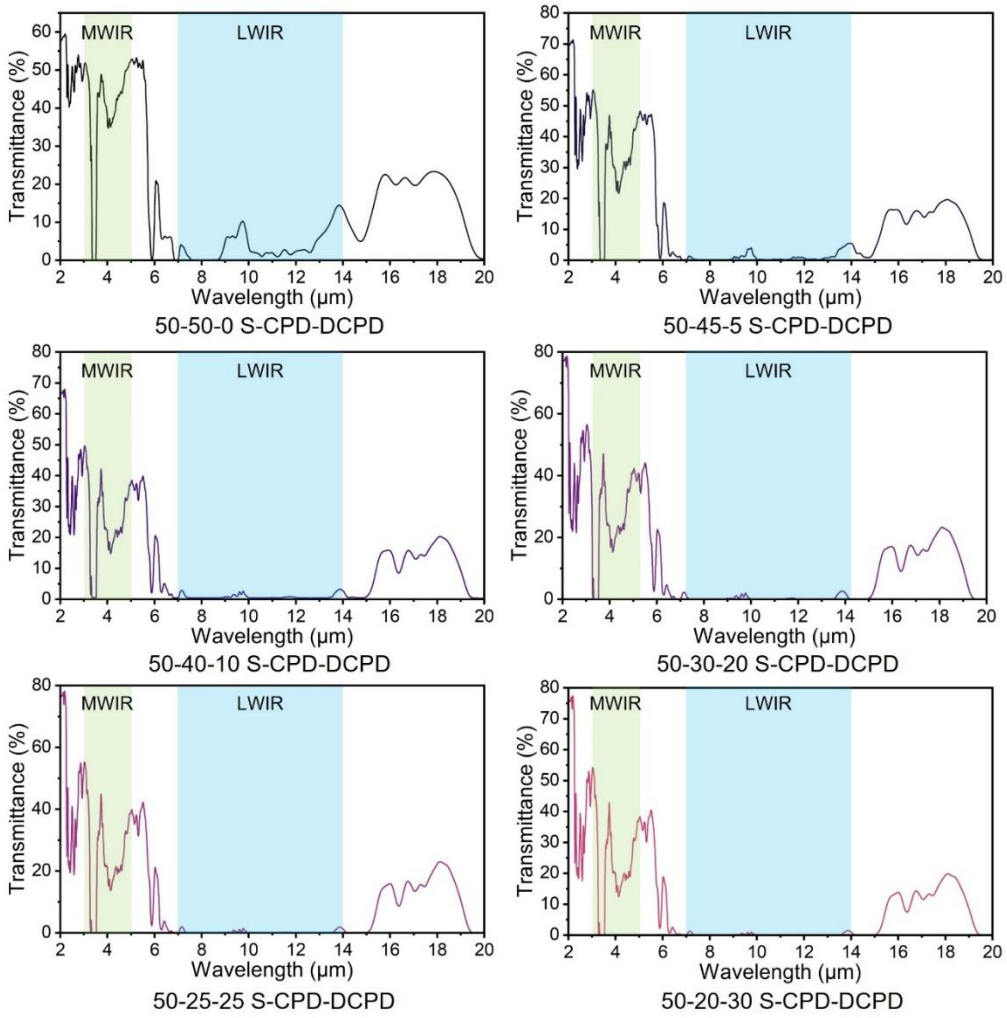

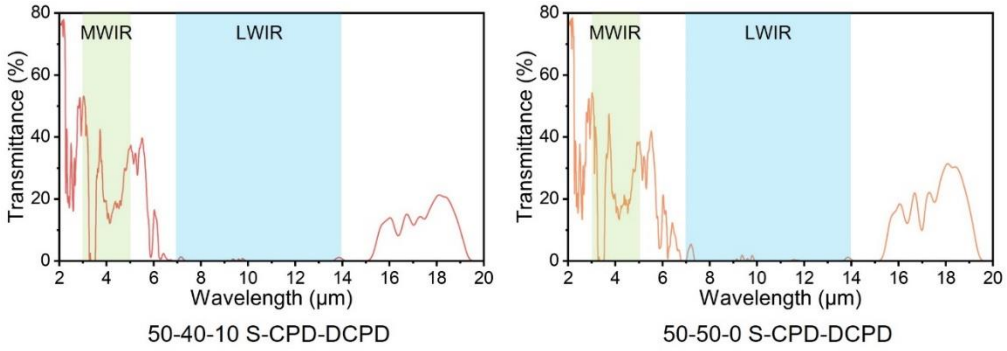

Figure 2.32: FTIR transmission spectra of 1 mm thick terpolymer samples made from sulfur, CPD and DCPD.

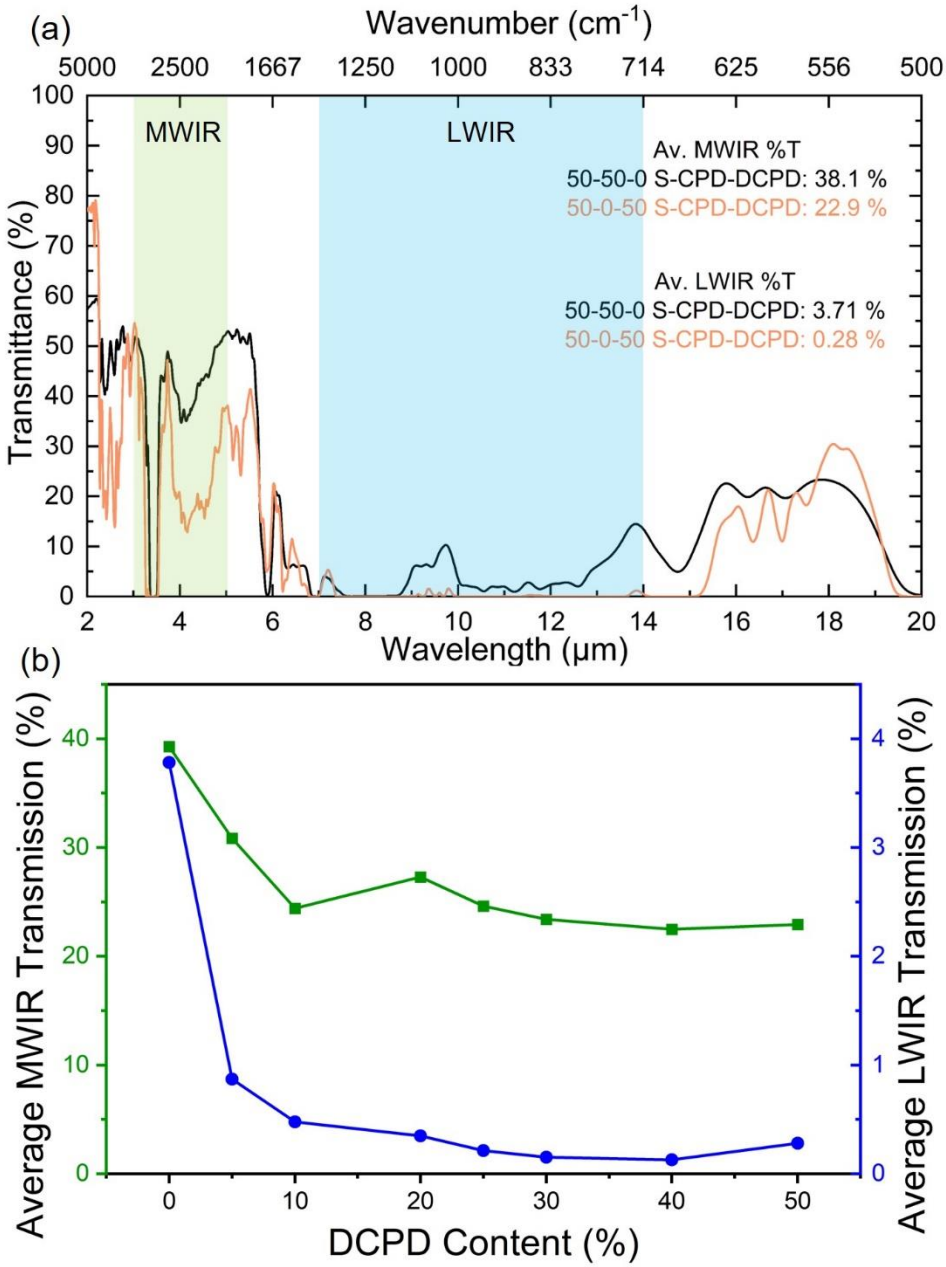

Figure 2.33: (a) FTIR plot showing of 1 mm thick polymers made from sulfur and CPD and another made from sulfur and DCPD. (b) Plot showing the average MWIR (3 μm - 5 μm) and LWIR (7 μm - 14 μm) of terpolymers made from sulfur, CPD and DCPD. All terpolymers had 50 % sulfur, the DCPD content is labelled and the CPD content is equal to 50- DCPD percentage.

Synthesis of polymer using gas phase cyclopentadiene

Gas phase method

The terpolymer experiments gave a lot of information about the effect of DCPD on the performance of the polymer. It was found that when DCPD was added at the start of the reaction, it would often only react at one alkene, leaving the second alkene in the polymer. This was found to have detrimental effect on the long wave infrared transmission of the polymer. While cyclopentadiene was found to form DCPD during the reaction, this DCPD was fully saturated and is believed to have a smaller effect on the polymer. Therefore, it was essential to remove any DCPD from the reaction and prevent its incorporation into the polymer. To achieve this, a new reactor was developed. This reactor took advantage of the higher boiling point of the DCPD to keep it separated from the reaction vessel containing sulfur.

Sulfur was added in a 2-necked round bottomed flask while the CPD was added to a second 2-necked round bottomed flask. The two round bottomed flasks were connected by a glass tube and a water-cooled condenser was added to one of them. CPD (3.00 g, 45.39 mmol) was added to the round bottomed flask with a condenser while sulfur (3.00 g, 93.75 mmol S atoms) was added to the other. A rubber septum was placed over the opening of the round bottomed flask with sulfur. Through this seal, needles for a gas pump were passed into the round bottomed flask. The inlet needle was placed in the headspace of the round bottomed flask containing sulfur, while the outlet needle was submerged in the sulfur. The pump circulated the atmosphere through the sulfur at an approximate rate of 500 mL/minute. Both round bottomed flasks were heated to 140 °C with stirring provided by a magnetic stirrer bar. The temperature used in this reaction is below the boiling point of DCPD (170 °C) but is far above the boiling temperature of CPD (41 °C). Therefore, any DCPD or other oligomers formed by heating CPD would remain in the round bottomed flask with the attached condenser and would not participate in the reaction with sulfur. Due to the much lower boiling point of CPD, it was able to pass through the glass tube into the round bottomed flask with sulfur. In this round bottomed flask, the CPD was constantly cycled through the sulfur to react and form a polymer. The reaction was heated for two and a half hours at 140 °C. Over this time, the sulfur would darken to a very dark viscous prepolymer. The prepolymer would then be transferred to a silicone mold and cured in a 140 °C oven for 24 hours to cure.

When the gas phase reactor was used, the polymers had the same black opaque appearance. The polymers were often soft and flexible at room temperature, indicating a low glass transition. Using this method, polymers could be prepared with sulfur content ranging from 40 % to 67 %, however, in samples with more than 60 % sulfur, visible sulfur blooming occurred over several days.

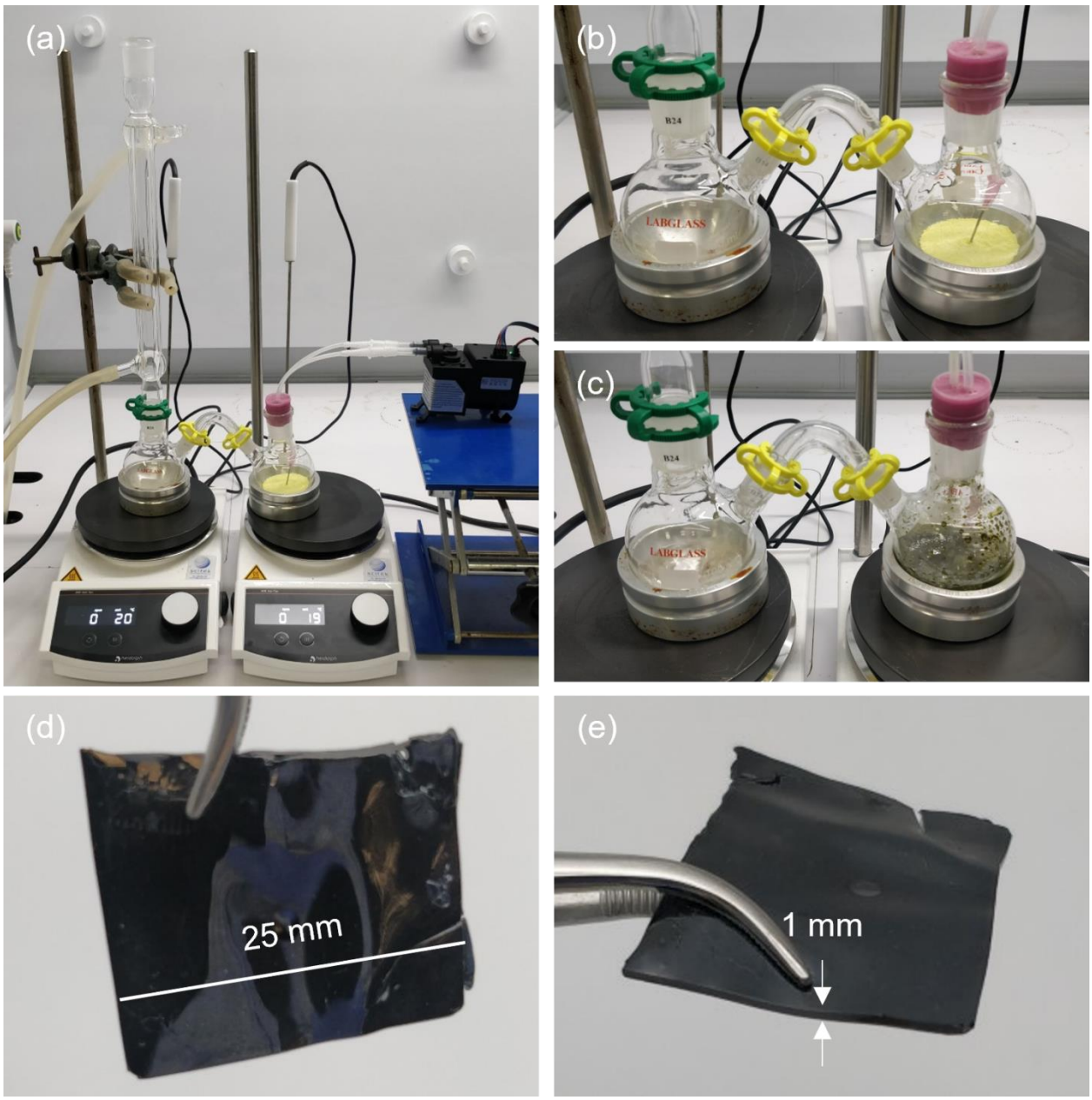

Figure 2.34: Images showing the gas phase method of polymer synthesis. (a) 2 round bottom flask set up with cyclopentadiene in left flask and sulfur in the right flask. (b) Close up of round bottomed flask before reaction. Cyclopentadiene is in the left flask and sulfur is in the right flask. The needle from the gas pump outlet is submerged in the sulfur and the pump inlet is in the headspace. (c) Image of prepolymer before being poured into silicone mold. (d) Polymer after curing. (e) Side view of polymer after curing.

Reduction of cyclopentadiene and dicyclopentadiene based sulfur polymers

To understand the chemical structure, the polymer made with the gas phase method was reduced using $NaBH_4$ with the same method as described in the terpolymer section. A polymer was also reduced using the reflux method with a sulfur content of 67 %. These polymers were compared with the polymer made using only sulfur and DCPD.

The polymer prepared using the gas phase method shows no peaks which correspond to DCPD thiols. Even the peaks corresponding to fully saturated DCPD are not visible. This indicates that by using the gas phase method, the formation of DCPD in the polymer structure can be completely removed. The polymer with 67 % sulfur which was prepared through the reflux method does show some peaks for DCPD. All the peaks that correspond to DCPD are completely saturated with no alkenes. The peaks for DCPD are also much smaller than in the polymers with 50 % sulfur. This indicates that higher sulfur polymers may favour the reaction between sulfur and CPD over the Diels Alder reaction to form DCPD. As described in the terpolymer section, the polymer prepared with only DCPD mainly shows peaks for unsaturated DCPD which has only reacted at the more reactive alkene. All the major peaks in the GC-MS for this polymer are not present in any of the other polymers. To see the mass spectra for the individual peaks, refer to the terpolymer section.

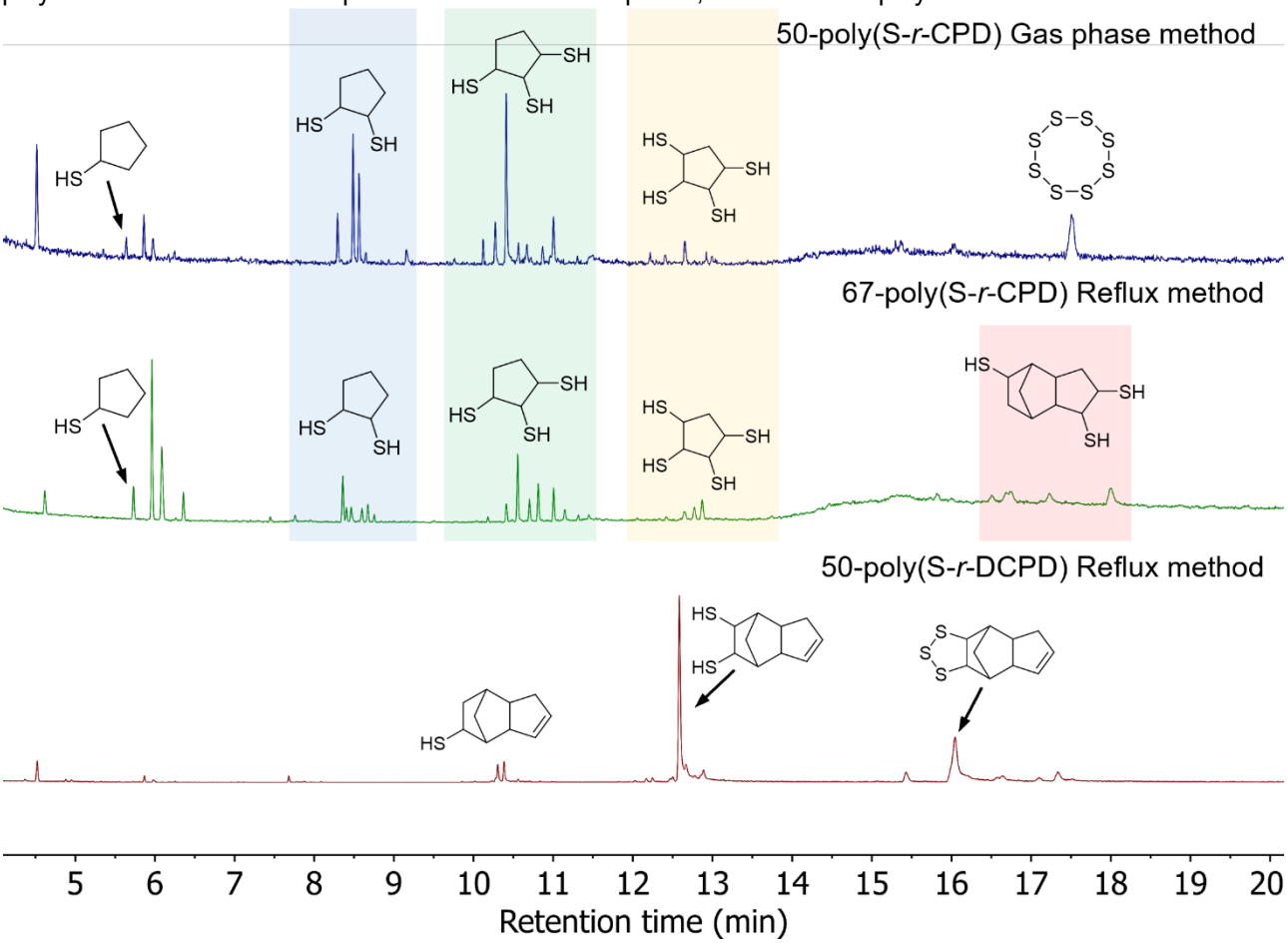

Figure 2.35: GC-MS chromatograms for polymers that were reduced by sodium borohydride. The top chromatogram is for a polymer of sulfur and CPD prepared using the gas phase method. The middle chromatogram is for a polymer of sulfur and CPD prepared using the reflux method. The bottom chromatogram is for a polymer of sulfur and DCPD prepared using the reflux method.

Solid state NMR of cyclopentadiene and dicyclopentadiene based sulfur polymers

Acknowledgements: This section was done by Martin Johnston. He performed all NMR experiments and assisted with data analysis.

To gain further understanding of the structure of the polymers, solid state NMR was used. The same three samples that were analysed in the reduction experiments were tested. These samples were the 50-poly(S-*r*-CPD) prepared using the gas phase method, the 67-poly(S-*r*-CPD) prepared using the reflux method and the 50-poly(S-*r*-DCPD) prepared using the reflux method. A 400 MHz NMR spectrometer NMR operating at 100 MHz was used with a 4 mm rotor spinning at 5 kHz. An acquisition time of 15 ms and a CP of 4 ms was used for all samples. However, due to the different mobility of the molecules within the polymers, the relaxation time needed to be changed for each sample. For the 50-poly(S-*r*-DCPD) and 67-poly(S-*r*-CPD) sample, a relaxation time of 2 s was appropriate. The 50-poly(S-*r*-CPD) polymer made using the gas phase method required a relaxation time of 30 seconds.

The solid-state NMR gave very broad peaks but all three polymers showed a large peak around 50 ppm. The most informative section of the NMR plots is the alkene region around 135 ppm. This region would show a peak if there were alkenes present in the polymer. As can be seen in the figure below, only the polymer made with DCPD showed a significant peak in this region. There was a very small bump in the spectrum for the polymer made in the gas phase but it was very minor. This gives further evidence that the polymers with DCPD do not react at both alkenes using this method but when the polymers are prepared from CPD, no alkenes remain after the reaction.

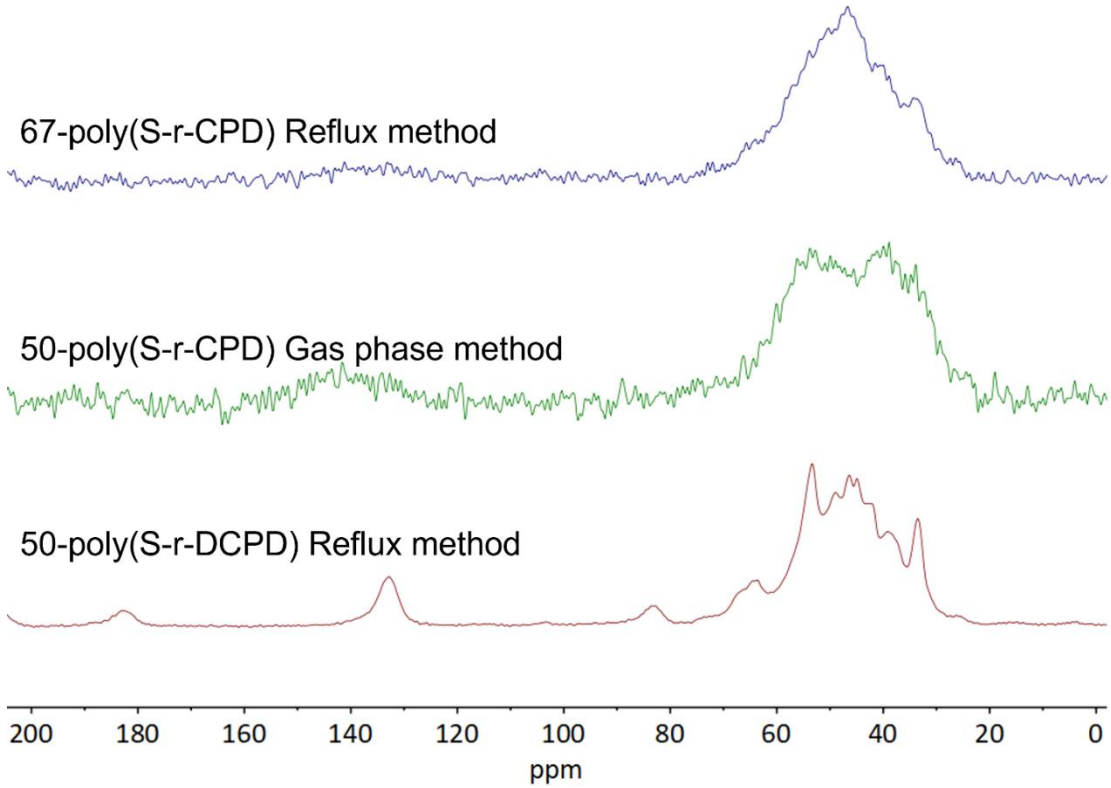

Figure 2.36: Solid state NMR spectra for the 67-poly(S-r-CPD) made using the reflux method, 50-poly(S-r-CPD) prepared using the gas phase method, and 50-poly(S-r-DCPD). The peaks at 82 ppm and 182 ppm in the NMR spectrum for the 50-poly(S-r-DCPD) polymer are spinning side bands and occur at 5000 Hz from the alkene peak.

Discussion of polymer structure

At this point, there is a lot of evidence about the structure of the polymers prepared using the different synthesis methods. The polymers made using DCPD as a monomer reacted only at the more strained alkene. The other alkene remained unreacted. This can be seen in the FTIR data which shows a peak at 3060 cm^{-1} as well as the reduced GC-MS experiments and the solid-state NMR experiments.

When the polymers were made using cyclopentadiene and sulfur, the composition of the polymer depended on the synthesis method used. When using the reflux method, the polymer mostly consisted of cyclopentadiene in which both alkenes had reacted with sulfur. However, there was a small amount of DCPD in the polymer structure. This DCPD was found to be completely saturated and both alkenes had reacted with sulfur. It was hypothesised that the DCPD formed when a CPD molecule reacted with sulfur at one alkene then participated as a dienophile with another CPD molecule. This would result in a DCPD in which the less reactive alkene has already reacted with sulfur. A mechanism for this reaction can be seen in the terpolymer section. The amount of DCPD in the polymer appears to decrease with increasing sulfur content, indicating a competing reaction between the Diels Alder reaction and the reaction between CPD and sulfur.

When the gas phase method was used with CPD, the polymer structure was much simpler. The polymer only showed evidence of CPD which had reacted at both alkenes with sulfur. There was no evidence of any DCPD in the polymer structure. However, there was some unreacted sulfur found within the polymer structure. It is possible that DCPD plays a role in stabilising the polymer, leading to greater thermal properties and a higher upper limit to sulfur content.

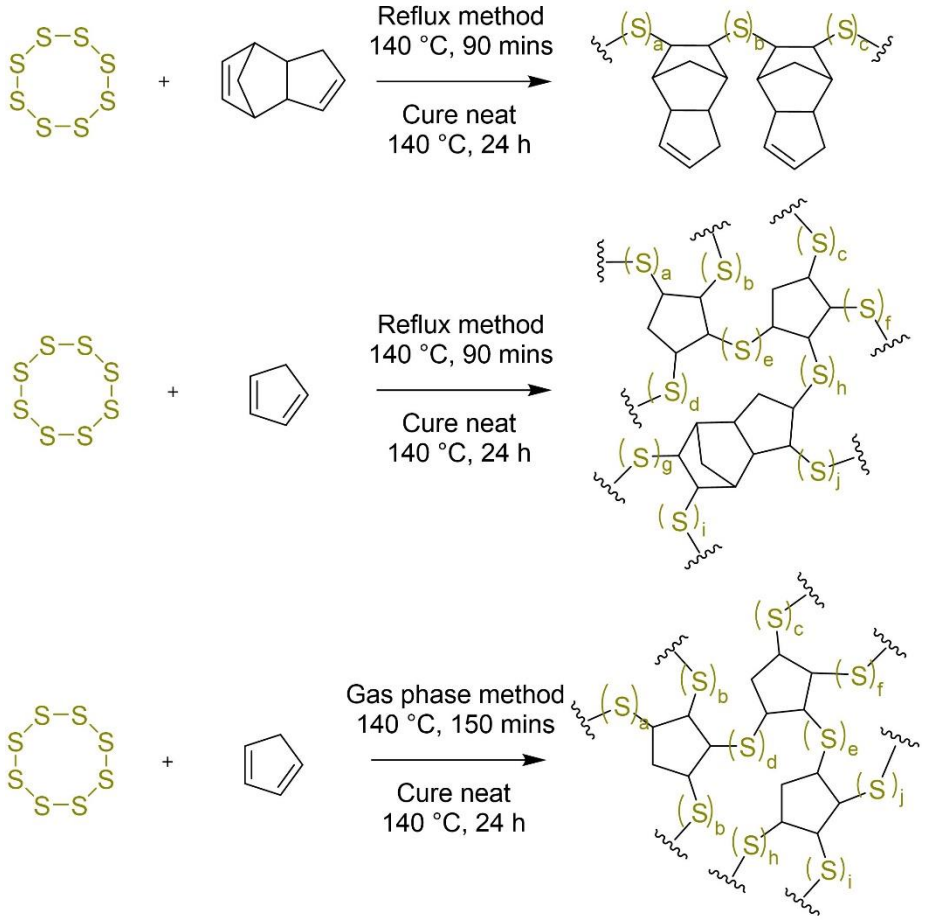

Figure 2.37: Polymer structures for polymers made with DCPD or CPD using either the reflux method or the gas phase method.

Comparisons between Gas phase and reflux method

Glass transition temperature by DSC

With the structure of the polymers prepared by both the reflux and gas phase method well understood, the next stage was to investigate any changes in properties of the two materials. This was important to find which would be more appropriate for use in thermal imaging applications.

First the glass transition temperature was tested by DSC. This is important as it indicates whether the material will be flexible or rigid at room temperature. The polymers prepared through both methods were analysed by DSC using a Perkin Elmer DSC 8000. Starting from 30 °C, the polymer was cooled to -50 °C at 5 °C/ min under nitrogen. The temperature was then cycled twice from -50 °C to 150 °C. To find the glass transition temperature, the inflection point of the change in baseline was determined for every scan and averaged.

The polymers prepared with the reflux method had a greater glass transition temperature than the polymer made with the gas phase method. It is possible that this is because the gas phase method prevents the formation of any DCPD in the polymer. DCPD is well known to improve the glass transition temperature of polymers.[21] The polymer prepared through the gas phase method also showed a melting peak for sulfur, indicating that there was unreacted sulfur in the polymer matrix. This confirms the findings of the reduction experiments.

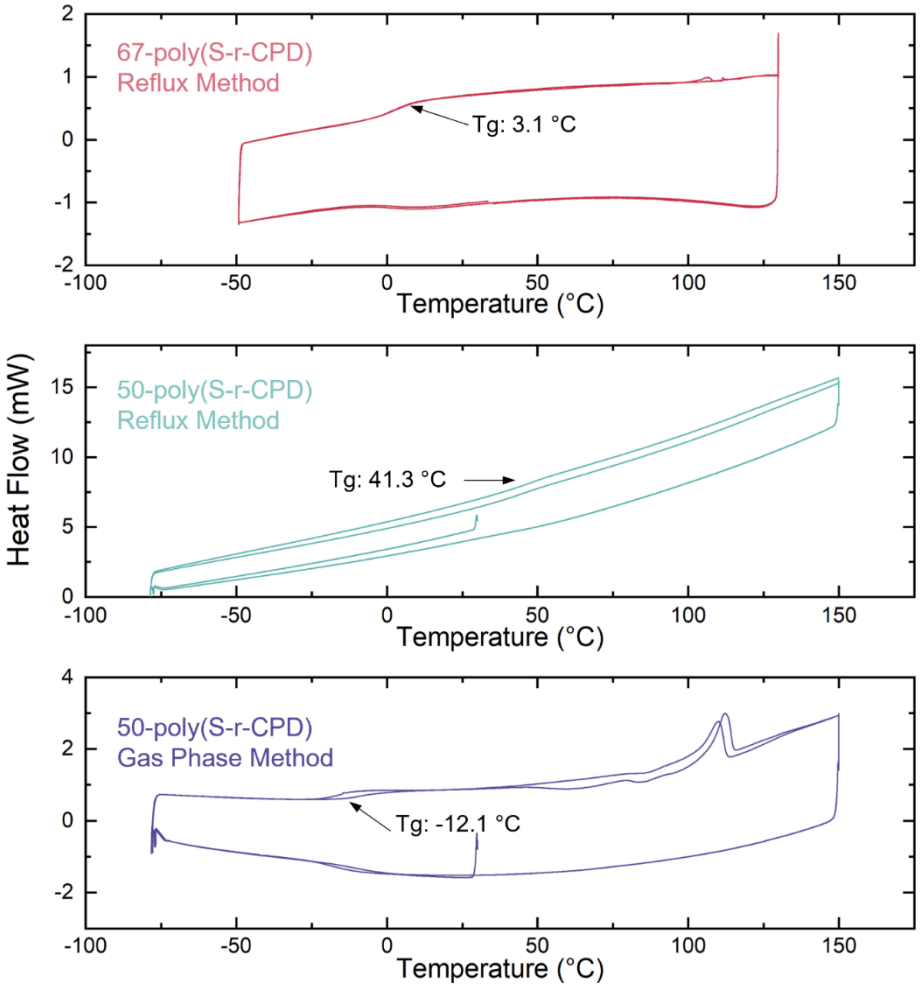

Figure 2.38: Differential scanning calorimetry of polymers prepared from CPD using either the reflux method or gas phase method.

Compression modulus with sulfur content

To test any differences in mechanical properties, the polymers prepared using both the reflux and gas phase methods were tested for compressive strength. A range of samples were prepared with different sulfur contents to test how properties changed with composition. For the reflux method, samples were prepared with sulfur contents of 40 %, 50 %, 60 %, 67 %, 70 % and 80 %. For the gas phase method, samples were prepared with sulfur contents of 40 %, 50 %, 60 % and 67 %. All samples were cured into cylinders with a diameter of 10 mm using a silicone mould. After curing, the top and bottom surfaces were sanded to give a flat surface and reduce surface irregularity. These samples were tested on a TA Q800 dynamic mechanical analyser using a two-plate compression apparatus. The samples were compressed with a force ramp rate of 3 N/min to a maximum of 18 N at room temperature. After testing, the compression modulus was calculated using the slope of the elastic portion of the stress-strain curve.

Sulfur polymers can often bloom crystals of sulfur over time. To test if this would lead to a change in mechanical properties, the samples made with the reflux method were tested both immediately and after one week. Any changed in properties were investigated. The samples prepared with the gas phase method were only tested after one week.

The 40, 50 and 60 % sulfur samples prepared with the reflux method were all below their glass transition temperature and were brittle while the 67, 70 and 80 % sulfur samples were all above their glass transition and displayed soft and compressible properties. This resulted to a greatly increased compression modulus. In general, the compression modulus of the polymers decreased with increasing sulfur content. This is consistent with most findings in literature.[23] The 70 % and 80 % samples both showed a compression modulus below 1.5 Mpa initially but after one week, it increased to over 4. These samples visibly bloomed, with sulfur crystals visible on the surface. This increase in compression modulus was likely due to sulfur acting as a bulk filler material which prevented compression of the polymer material. Therefore, the maximum amount of sulfur that could be stabilised by the polymer is likely 67 %.

The samples prepared with the reflux method showed the same trends. However, all the sulfur contents were flexible at room temperature due to the lower glass transition temperature of the polymers prepared with the gas phase method. As the sulfur content increased, the compression modulus decreased. The sample with 67 % sulfur showed blooming after one week and like the samples made with the reflux method, this resulted in an increase in compression modulus. This gives a maximum stable sulfur content of 60 % for the gas phase method. In general, the samples made with the gas phase method had a lower compression modulus. This is likely due to the DCPD which forms in the reflux method. The DCPD could act as a rigid crosslinker, improving mechanical performance of the polymer. These results show that the reflux method has greater thermal and mechanical performance than the polymers made with the gas phase method.

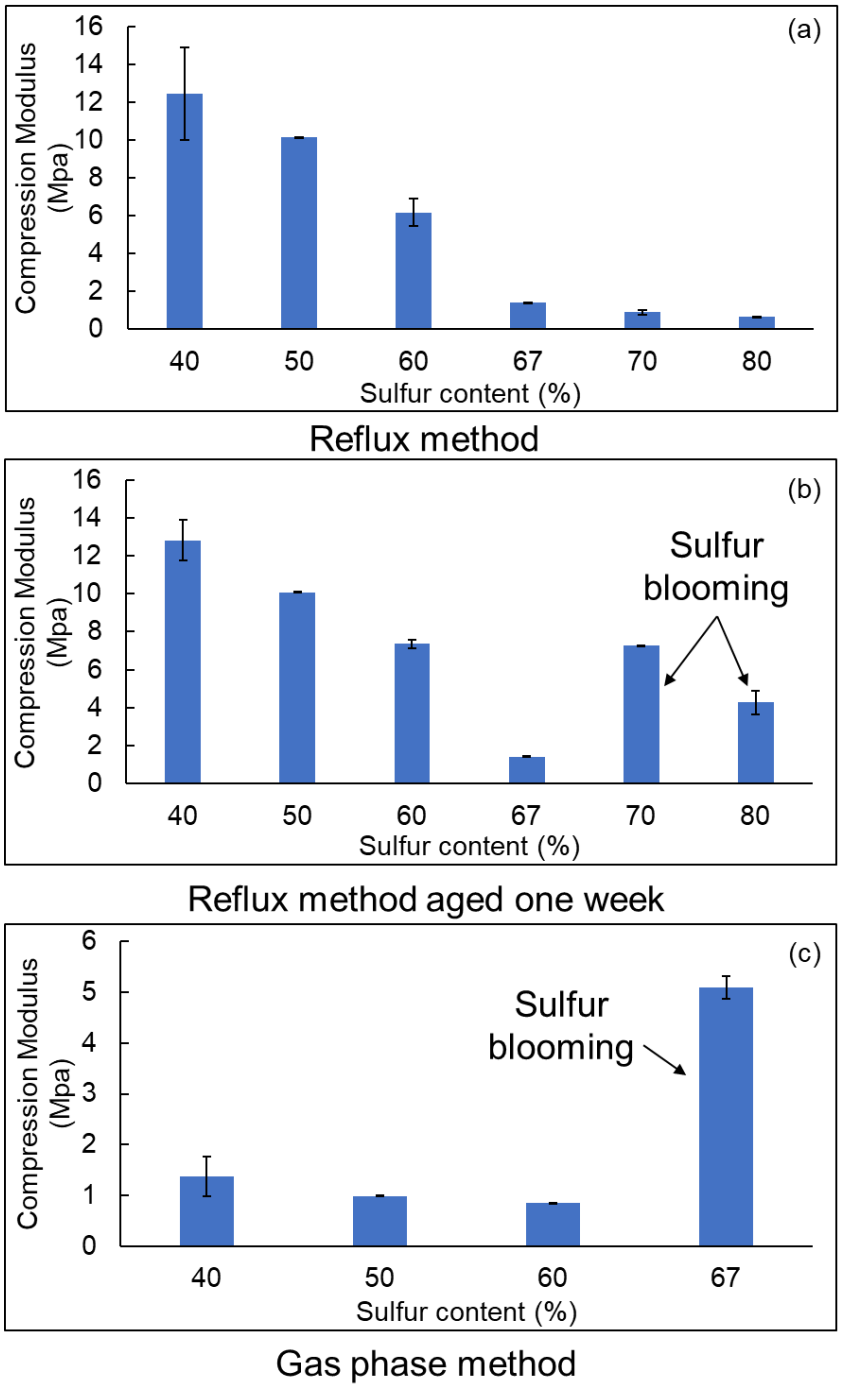

Figure 2.39: (a) Compression modulus of polymers prepared from cyclopentadiene and sulfur using the reflux method. The 40, 50 and 60 % sulfur samples were all below their glass transition temperature and were brittle while the 67, 70 and 80 % sulfur samples were all above their glass transition and displayed soft and compressible properties. (b) Compression modulus of polymers prepared from cyclopentadiene and sulfur using the reflux method that have been aged one week. The 70 and 80 % sulfur samples became brittle due to sulfur blooming. (c) Compression modulus of polymers prepared from cyclopentadiene and sulfur using the gas phase method. All samples were aged one week, the 67 % sulfur samples showed signs of sulfur blooming and became brittle.

Preparation of silicone mould for optical testing

After testing the thermal and mechanical properties of the polymers, they were tested for optical properties. For these tests, it was important that all samples had a very precise thickness to give repeatable results that can be directly compared between samples. To achieve this, a mould was designed so polymers can be cured to always give a width of 1 mm and have the appropriate size and shape for infrared transmission testing. To produce this mould, 1 mm thick glass slides were used as a negative. A 3D printed part was designed to hold up to 9 glass slides. These glass slides were positioned in another 3D printed part so that they were 5 mm from the bottom of a 35 mm wide, 65 mm long and 30 mm deep opening. Optionally, small 3D printed parts could be added to each glass slide to make a larger opening to pour the prepolymer into the mould. A heat resistant silicone resin (Pinkysil) was poured around the glass slides to prepare a mould. This silicone resin consisted of two parts which were mixed in a one-to-one ratio. Each part was measured out to approximately 23 mL and mixed for 3 minutes. After mixing, the resin was poured into the mould negative and left to cure for two hours. This mould would produce polymer windows with dimensions of 25 mm x 25.4 mm x 1 mm. To remove the polymer from the mould, the silicone was cut with a scalpel.

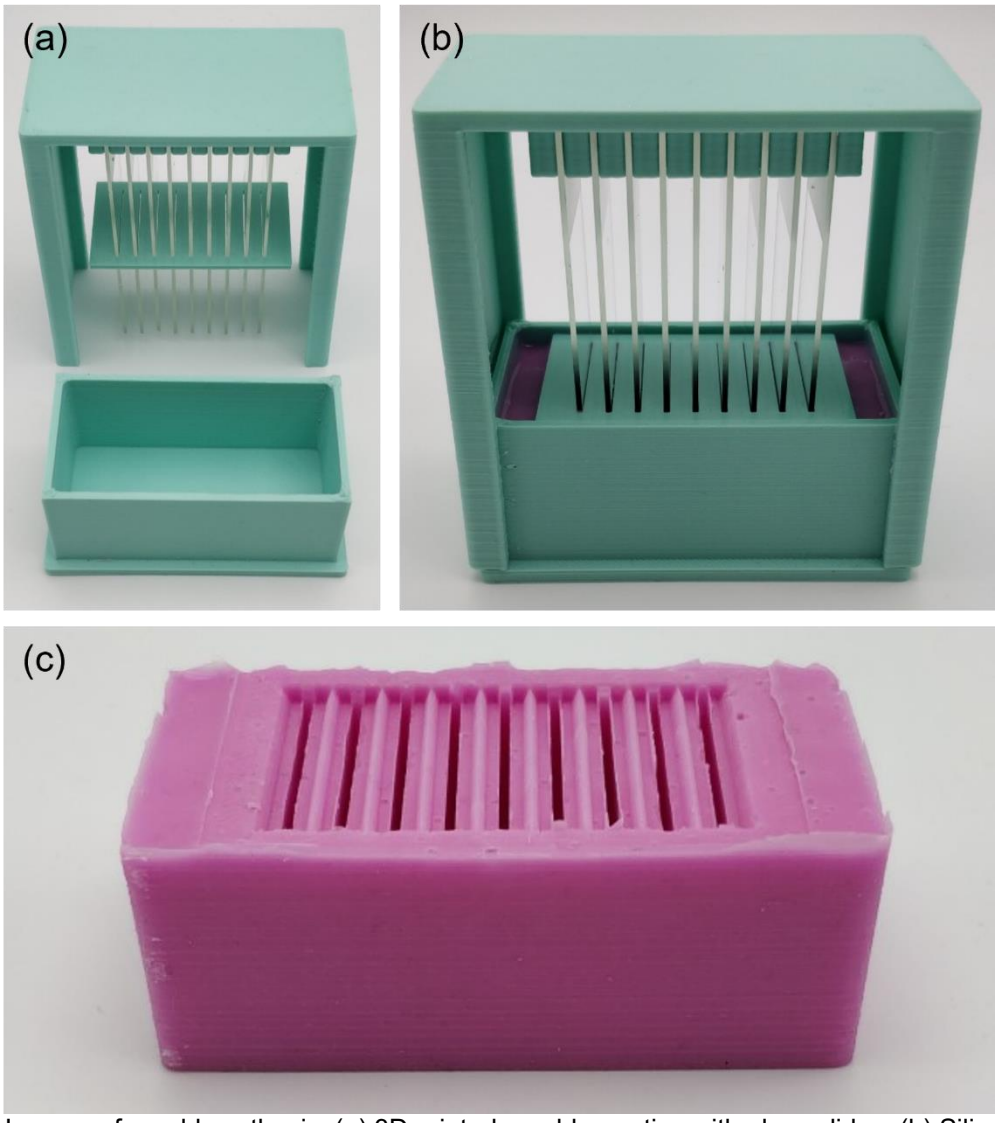

Figure 2.40: Images of mould synthesis. (a) 3D printed mould negative with glass slides. (b) Silicone mould in negative. (c) Final silicone mould.

Refractive index by specular reflectance

The refractive index of sulfur and the 67-poly(S-*r*-CPD) polymers were tested using specular reflectance. It was not possible to test the polymers made with the gas phase method as they were not shape persistent and would deform in the mount used to take the specular reflectance measurements. The polymers were found to possess an excellent refractive index which was between 1.85 and 1.9 over the entire region tested. This refractive index would allow for high power optics with less material than a lower RI polymer.[24]

Specular reflectance spectra of the 67-poly(S-r-CPD) polymer (mid- and near-IR measured consecutively without re-mounting the sample) were recorded on a Bruker Vertex v80 instrument (Bruker, Billerica, MA, USA) using the 1513/QA attachment under vacuum at an angle from the surface normal of 15°. Spectra were referenced to the reflectivity of an aluminium mirror. The samples in this study deform easily and thus care was taken to ensure the specular reflection was aligned with the detector. Even with this care, the reflectance spectrum varied in intensity when remounted due do slight variations of the reflected beam off non-parallel surface. Thus, several measurements were made of the same sample and the highest reflectance was use for subsequent analysis, and the reflectance values should be considered a lower limit. The wavenumber dependent phase shift spectrum was determined by applying the Kramers-Kronig transform using the spectrometer software (OPUS V7.2, Bruker). The complex refractive index, $\eta = n + ik$, spectrum was subsequently calculated from the phase shift and reflectance spectra using the equations given by Galeener et al.[25] The Kramers-Kronig transform was performed between 500 and 10,000 cm^{-1}.

The reflectance spectrum < 1500 cm^{-1} is very similar to that reported previously, both in terms of the specular reflectance value and the spectrum showing minima at ~1300, 950, 900 cm^{-1}.[26] As noted by these authors, the absorptivity (attenuation) index is small throughout this region, and this is confirmed by our Kramers-Kronig analysis which suggests the absorptivity index remains < 0.01 throughout the entire region. Thus, the reflectivity values are almost exclusively governed by the real part of the refractive index. It should be noted that using different spectral limits to perform the Kramers Kronig resulted in fluctuations in the absorptivity index spectrum but made no discernible differences in the refractive index spectrum. Our spectrum covers a wider range than Fuller et al and shows a weak feature at 3500 cm^{-1} that was not observed previously.[26]

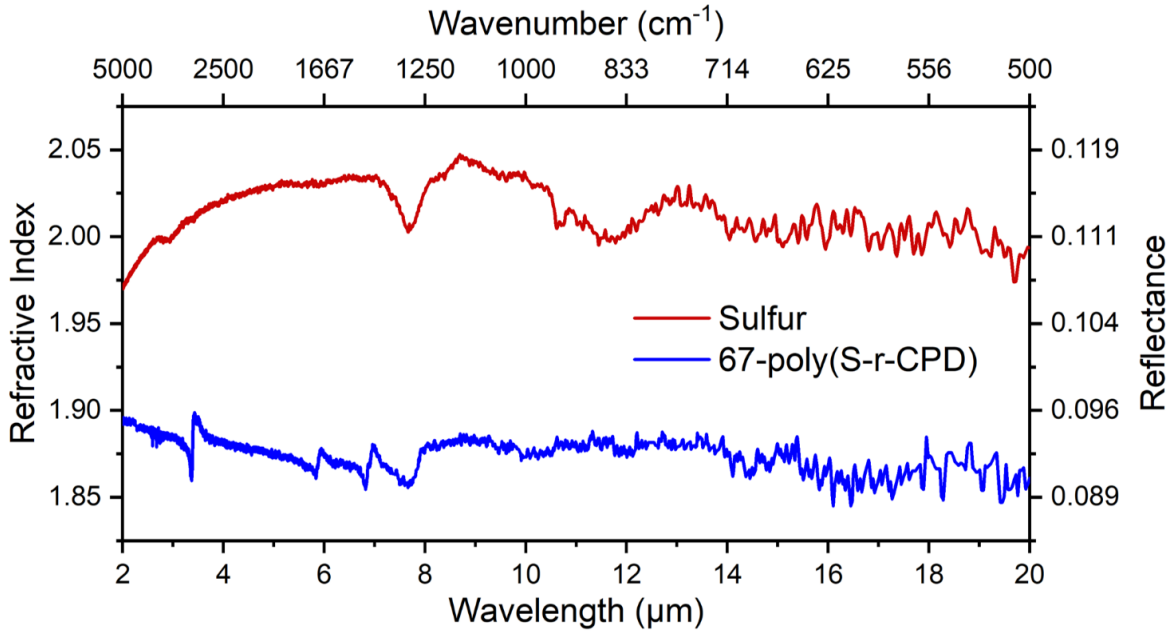

Figure 2.41: Refractive index and reflectance of sulfur and 67-poly(S-*r*-CPD).

Infrared transmission through windows with different sulfur contents

The infrared transmission was one of the most important features of the polymers made from CPD. This would indicate if they would be useful as an optic in thermal imaging systems. To test the infrared transmission, 1 mm thick samples were prepared with a range of sulfur contents. The same compositions were used as those tested in the compression analysis. For the reflux method, the sulfur content varied from 40 % to 80 % while for the gas phase method, the sulfur content varied from 40 % to 67 %. 1 mm thick polymer samples were tested for transmission in the mid- and long-wave infrared regions using a Perkin Elmer Frontier FTIR spectrometer. In transmission mode, the polymer samples were tested in the wavelength range of 2 μm to 20 μm over a total of 16 scans. The average transmittance was calculated by integrating over the region and dividing by the wavelength range. For the MWIR region, the plot was integrated between 3 μm and 5 μm and divided by 2 μm. For the LWIR region, the plot was integrated between 7 μm and 14 μm and divided by 7 μm.

The samples made using the gas phase method showed a much greater transmission in the LWIR region than those made using the reflux method. This is likely due to the reflux method possessing DCPD in the polymer structure. This would increase the unique vibrational modes and lead to decreased transmission. Some peaks corresponding to DCPD could be observed in the polymers prepared through the reflux method, particularly at lower sulfur content. These can most easily be seen at around 5 μm. As described earlier, the polymers prepared through the reflux method showed greater DCPD content in polymers with less sulfur.

The polymers made with both methods showed the same general trend with increasing sulfur content. As the sulfur content increased, the polymers showed greater transmission in both the MWIR and LWIR regions. However, when the sulfur content was too high, the polymers became unstable and sulfur blooming would occur. This was explored in the compression testing section. The samples with 70 % and 80 % sulfur in the reflux method and 67 % sulfur in the gas phase method all showed signs of sulfur blooming. This sulfur blooming resulted in significant decreases in the transmission of the polymers at shorter wavelengths. The effect of the sulfur blooming was reduced at longer wavelengths and therefore affected the MWIR region more than the LWIR region. As can be seen in the following pages, the average transmission in the LWIR region continued to improve with sulfur content but the average transmission in the MWIR decreased in samples with sulfur blooming.

The infrared transmission testing showed that the gas phase method gave the greatest transmission in the LWIR region. Therefore, for thermal imaging, it would likely give the greatest thermal resolution. However, the samples made with the reflux method had greater thermal and mechanical properties and could contain more sulfur without blooming. The application may dictate whether the compromise of mechanical performance is outweighed by the improvement in infrared transmission.

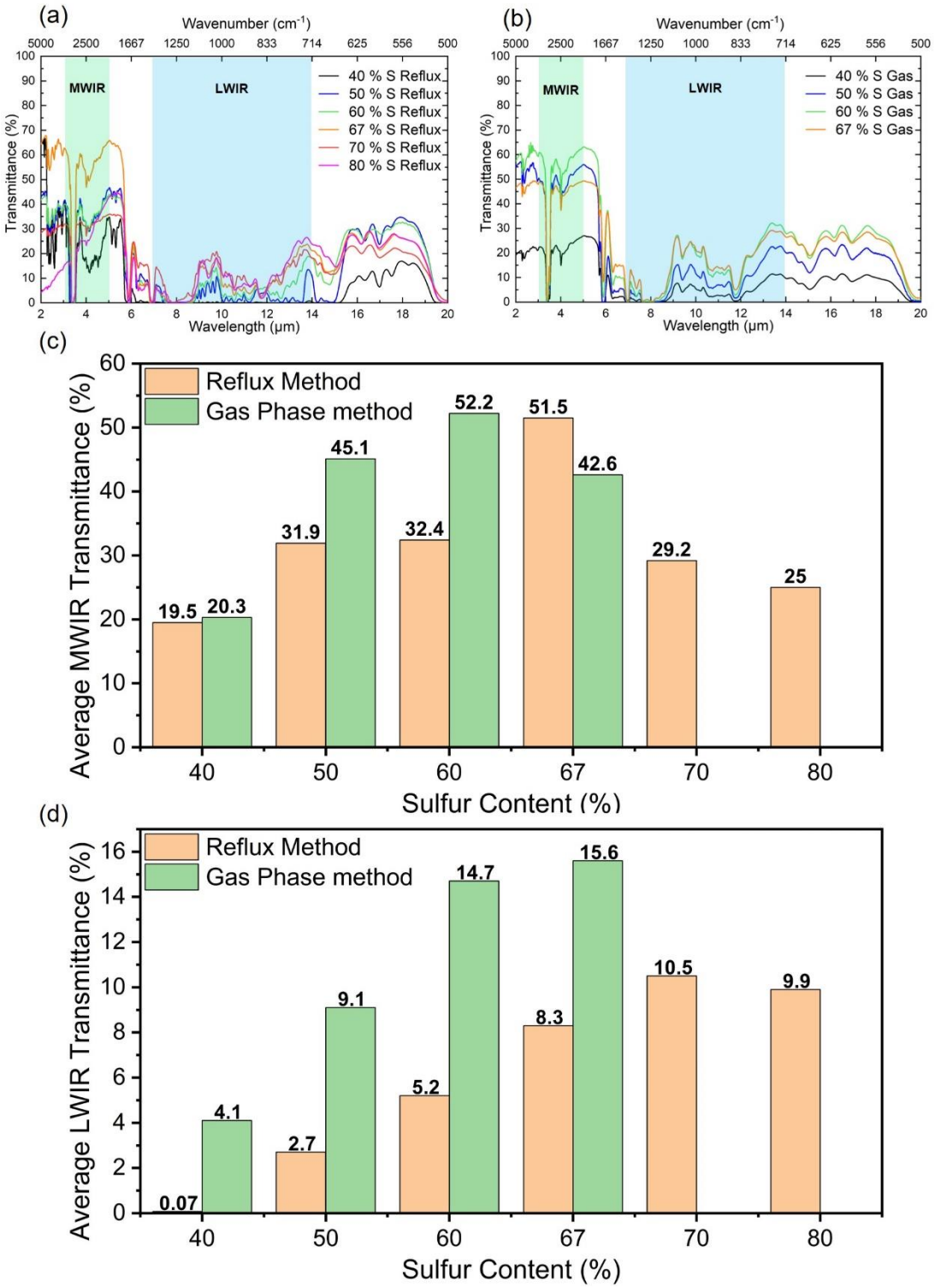

Figure 2.42: Infrared transmission spectra from 2-20 μm for samples made from the reflux method with sulfur content varying from 40 % to 80 %. Infrared transmission spectra from 2-20 μm for samples made from the gas phase method with sulfur content varying from 40 % to 67 %. Average LWIR transmission for polymers prepared from both the reflux and gas phase methods. Average MWIR transmission for polymers prepared from both the reflux and gas phase methods.

Extinction coefficient of polymers made through reflux method

To determine the effect of thickness on the transmission of the 67-poly(S-*r*-CPD) polymer, it was prepared at a range of thicknesses varying from 0.2 mm to 1.0 mm. This was achieved by using glass covers slips as a negative to form a silicone mould. The 67-poly(S-*r*-CPD) prepolymer was then poured into the silicone mould and cured. All polymer samples were tested for infrared absorbance. The extinction coefficient was calculated by the slope of the absorbance against thickness for each data point.

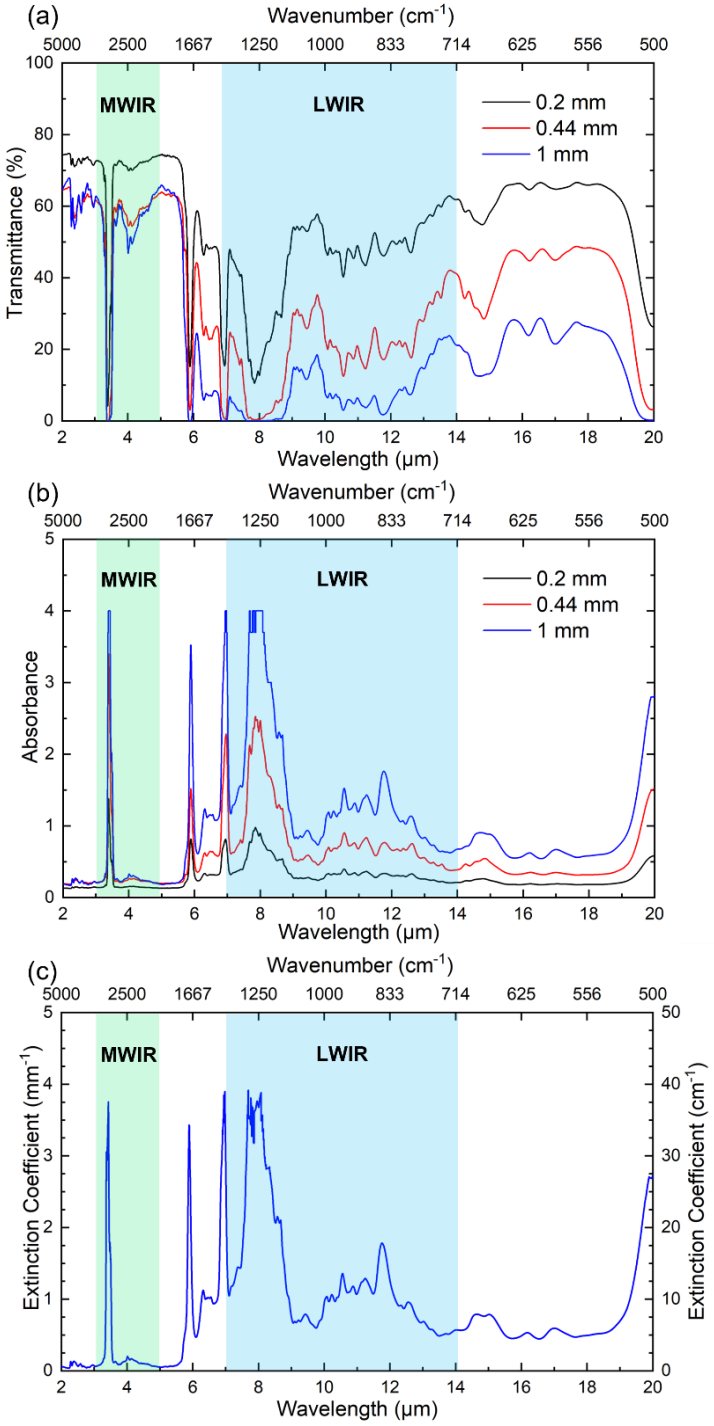

Figure 2.43: (a) FTIR spectra of freestanding 67-poly(S-*r*-CPD) films at three different thicknesses showing percent transmission. (b) FTIR spectra of freestanding 67-poly(S-*r*-CPD) films at three different thicknesses showing absorbance. (c) Extinction coefficient for 67-poly(S-*r*-CPD) polymer between a wavelength of 2 μm and 20 μm.

Thermal imaging through polymer windows

A FLIR E6 infrared camera was used to investigate the transparency of the polymer windows to infrared radiation. The spectral range of this camera is from 7.5 µm to 13 µm which makes all images in the long wave infrared region. Two types of images were taken, both using the warmth from a gloved hand to produce infrared radiation. The first image that was taken had the polymer sample in a 3D printed holder which was positioned approximately 30 cm from the camera lens. A gloved hand was then put behind the sample so that some of it was blocked by the polymer window. This image gives a good indication of how the polymer window affects the image quality. The FLIR camera also has an optical camera which shows the positioning of the sample. Note that due to how close the sample is to the camera, there is some parallax shifting in the visible image.

The polymers made with both the reflux method and the gas phase method both had enough transparency to image using a human hand. This is very rare for a polymer of this thickness as most polymers will absorb in the LWIR region.

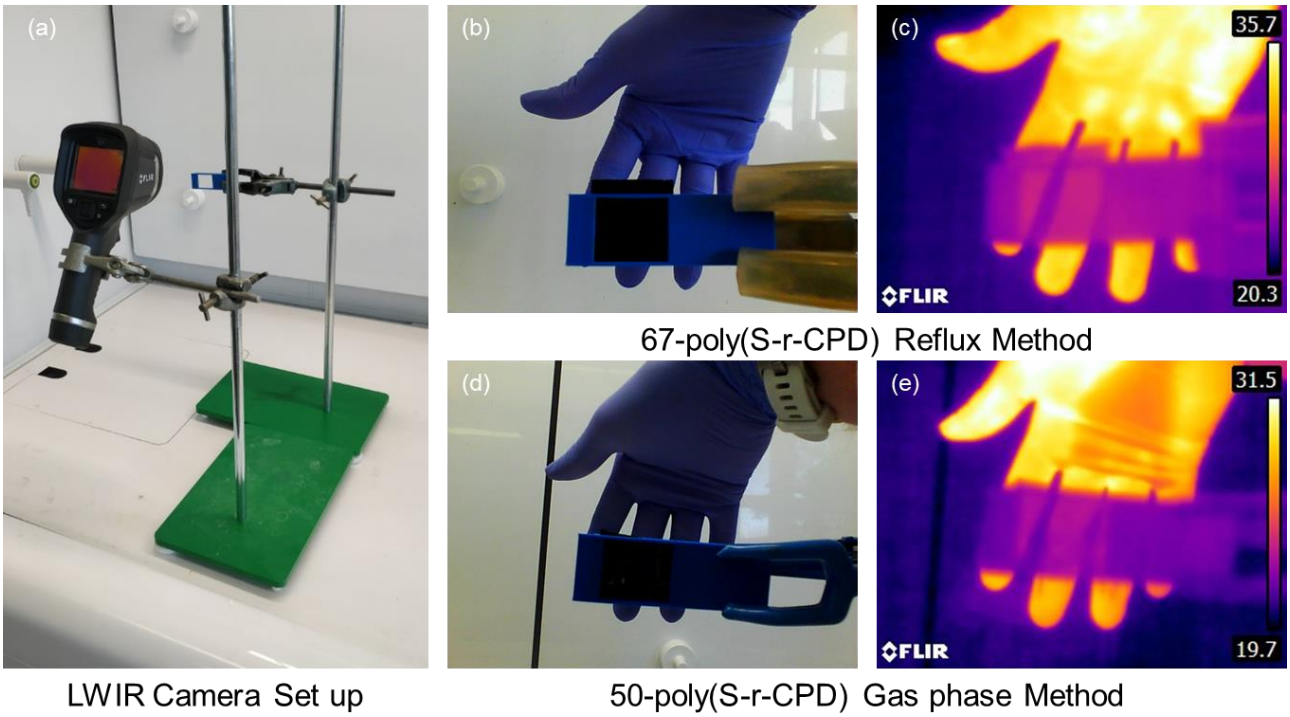

Figure 2.44: Images showing the thermal imaging of polymer. (a) Image of camera and sample holder. (b) optical image of 67-poly(S-*r*-CPD) polymer made with the reflux method in holder with a gloved hand behind. (c) Long wave infrared image through 1 mm thick 67-poly(S-*r*-CPD) made with the reflux method. (d) Optical image of 50-poly(S-*r*-CPD) made with the gas phase method. (e) Long wave infrared image through 1 mm thick 67-poly(S-*r*-CPD) made with the gas phase method.

The second type of image that was taken was one in which the 1 mm thick polymer completely blocked the lens of the camera, and an image was taken through the polymer. This gives an indication of the quality of images that could be taken when the polymer is used as a window or lens. A 3D printed mount was made to hold the polymer in front of the lens. Being able to see any image through a polymer of this thickness is very rare. The polymer samples are particularly impressive as they can image a human hand despite only approximately 15 °C difference from the surrounding environment. While subjective, the images through the polymer made with the reflux method appear to have a greater resolution. Some blurring occurred with the gas phase method. As described earlier, the polymer prepared with the gas phase method has some unreacted sulfur in its structure. This sulfur may scatter light as it passes through the polymer. The scattering of light is likely what is responsible for the blurring of the LWIR images that are taken through the polymer prepared through the gas phase method.

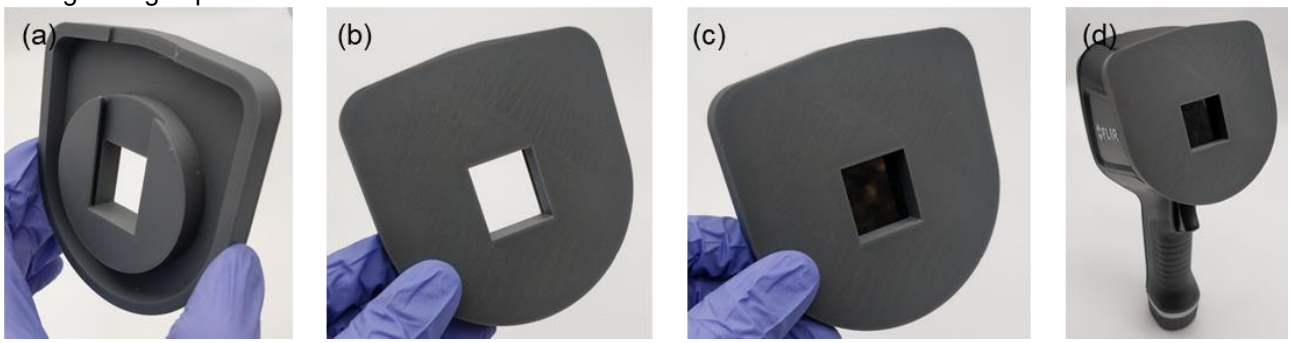

Figure 2.45: Images showing the mount used to hold polymer sample to FLIR camera. (a) Back of mount with no polymer sample. (b) Front of mount with no polymer sample. (c) Front of mount with polymer sample inserted. (d) Mount attached to FLIR camera with polymer sample inserted.

Below are images of a hand taken through a 1 mm thick sample of 67-poly(S-r-CPD) prepared through the reflux method and 50-poly(S-r-CPD) prepared using the gas phase method.

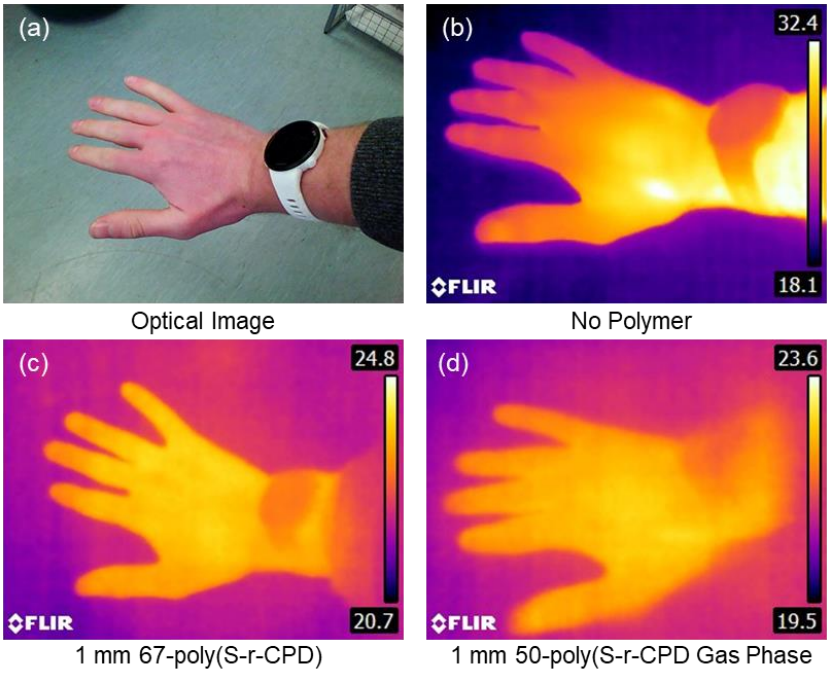

Figure 2.46: (a) Visible image of hand. (b) Long Wave Infrared image of hand with FLIR E6 camera and no polymer sample. (c) Long Wave Infrared image of hand with FLIR E6 camera through 1 mm thick 67-poly(S-r-CPD) prepared through the reflux method. (d) Long Wave Infrared image of hand with FLIR E6 camera through 1 mm thick 50-poly(S-r-CPD) prepared through the gas phase method.

Due to the high transmission of the polymer and the good resolution of images that could be taken through it. It was possible to image a person.

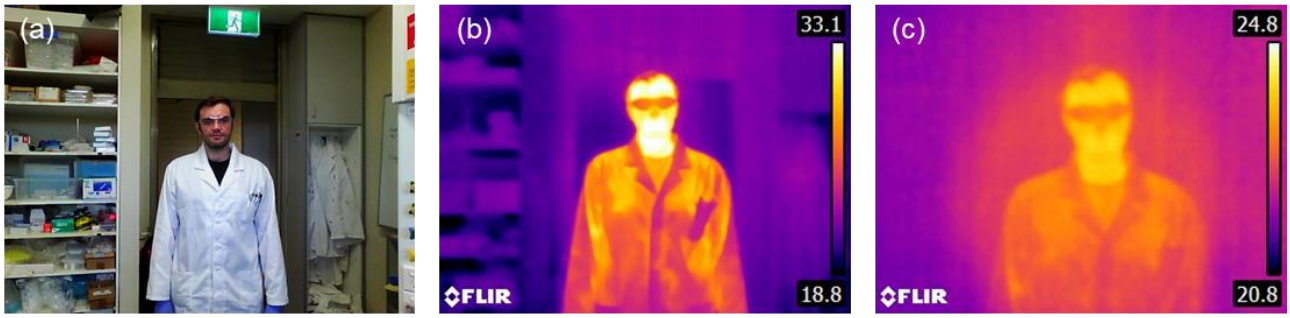

Optical image | No Polymer | 1 mm thick 67-poly(S-r-CPD)

Figure 2.47: (a) Optical image of person. (b) LWIR image of person with no polymer. (c) LWIR image of person through a 1 mm thick sample of 67-poly(S-r-CPD) prepared through the reflux method. Dr Max Mann is thanked for permission to use his image.

Comparison with 1,3-diisopropenylbenzene sulfur polymer

Polymer synthesis using 1,3-Diisopropenylbenzene and comparison

The performance of the polymers prepared using sulfur and cyclopentadiene was excellent. Particularly the transmittance in the long wave infrared region (7 μm – 14 μm). To gain an understanding of how the polymers compared with other sulfur-based polymers which had been developed in the literature, a comparison with some of the top performing polymers was made.

The standard benchmark for sulfur-based polymers is the first one described by Pyun in 2013.[27] This polymer was prepared using a reaction between elemental sulfur and 1,3-diisopropenylbenzene. 1 mm thick windows of this polymer were prepared to test against the polymers made from cyclopentadiene. A polymer made from sulfur and 1,3-diisopropenylbenzene (DIB) was prepared using the method outlined by Pyun[28] with only a slight modification to allow for appropriately shaped polymer pieces for infrared transmission testing. Two polymer compositions were prepared so they could be compared with the cyclopentadiene polymer. The first polymer composition had the same mass ratio of sulfur to the crosslinker as the optimised CPD polymer 67-poly(S-r-CPD) while the second composition had the same molar ratio (Approximately 4:1, S:DIB). A total mass of 5 grams was used for both compositions. The first polymer composition used 3.33 g of sulfur and 1.67 g of DIB and will be referred to as 67-poly(S-r-DIB) while the second used 2.21 g of sulfur and 2.79 g of DIB and will be referred to as 44-poly(S-r-DIB). The 67-poly(S-r-CPD) polymer made with the reflux method was used as a comparison as it showed better image quality than the polymers made with the gas phase method.

Sulfur was added to a 21 ml vial with a magnetic stirring rod and added to an aluminium heating block at 185 °C. The sulfur was left for 3 minutes over which time it became an orange liquid. DIB was then added by pipette to the molten sulfur and the reaction was left for an additional 8 minutes. Over this time, the mixture would change to a deep red, viscous prepolymer as sulfur reacted with DIB. In the original method described by Pyun, the reaction is left to vitrify, which happens after 9-11 minutes from when the DIB is added, depending on composition. This method was modified slightly to allow for 1 mm thick polymer windows to be produced. Instead of allowing the prepolymer to completely vitrify in the scintillation vial, it was transferred to a preheated silicone mould after 8 minutes and added to a 185 °C oven for an additional 3 minutes. After this time, the polymer was removed from the oven and allowed to cool to room temperature before removal from the mould.

The polymers had a deep red colour and were slightly transparent. The 67-poly(S-r-DIB) was soft and clearly had a glass transition below room temperature while 44-poly(S-r-DIB) was brittle and glassy. This was confirmed by DSC which found the 67-poly(S-r-DIB) polymer to have a glass transition of approximately 8 °C while the 44-poly(S-r-DIB) polymer had a glass transition temperature of approximately 29 °C.

Note that a significant amount of gas was produced when DIB was added to the sulfur so this reaction should only be done in a fume hood.

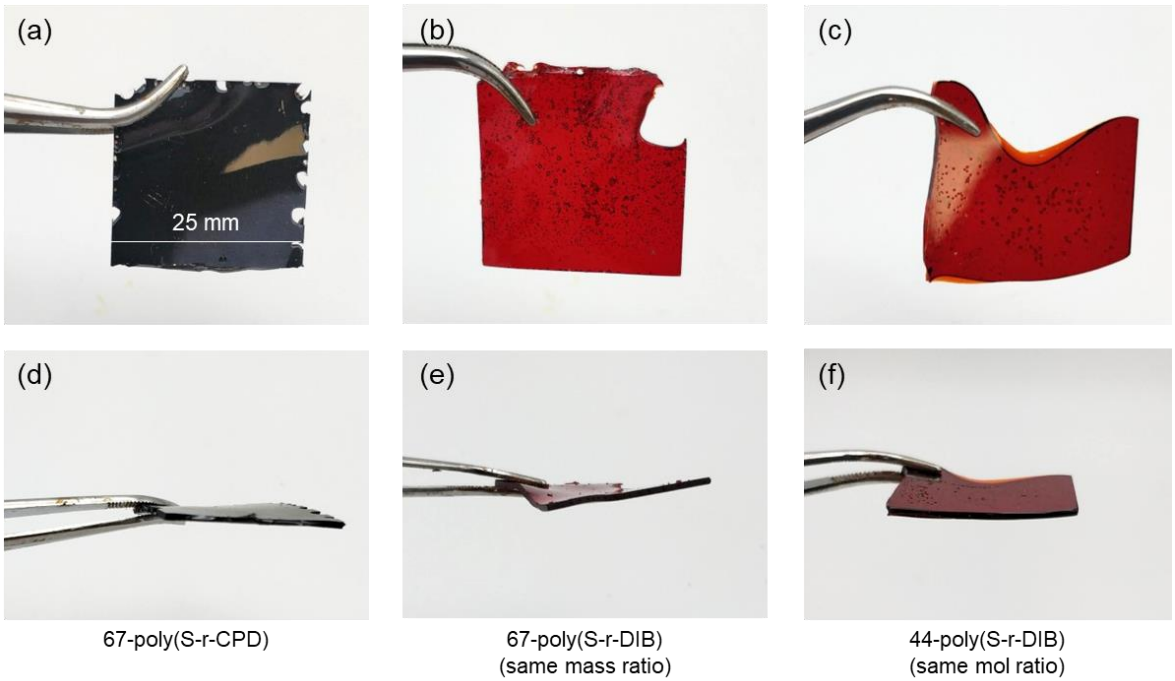

Figure 2.48: Images showing 67-poly(S-*r*-CPD) made by the reflux method, 67-poly(S-*r*-DIB) and 44-poly(S-*r*-DIB).

All polymers had the same thickness of 1 mm, allowing for direct comparison of the infrared transmission and imaging capabilities. The polymers were first tested subjectively by imaging through the polymers using a FLIR E6 thermal camera. A 3D printed sample holder was prepared which allowed for all 3 polymers to be imaged at the same time for a comparison.

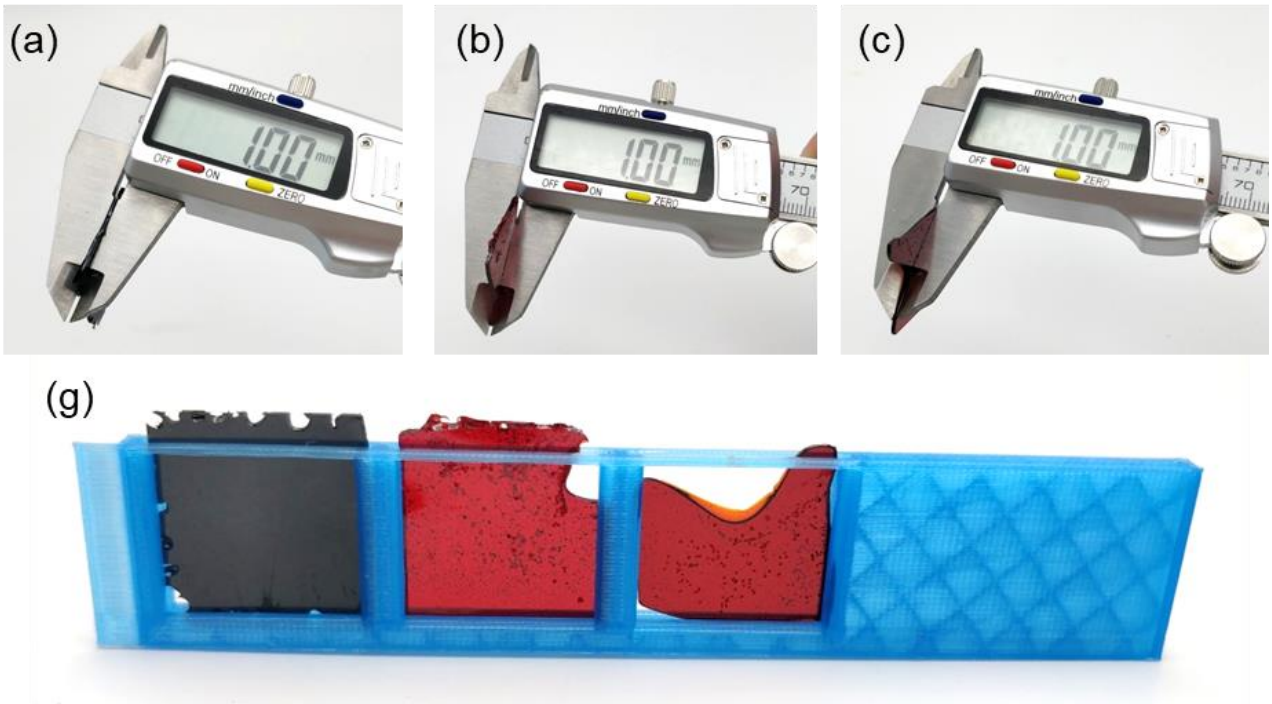

Figure 2.49: (a) 1 mm thick 67-poly(S-r-CPD) prepared with the reflux method in callipers. (b) 1 mm thick 67-poly(S-r-DIB) in callipers. (c) 44-poly(S-r-DIB) in callipers. (g) All 3 samples in 3D printed sample holder.

Below are the visible and LWIR images through the CPD and DIB polymers. Both compositions of DIB showed some transparency in the visible images as the fingers could be seen through the polymer, while the CPD polymer was completely opaque. However, the opposite was true in the LWIR images as the CPD polymer was transparent while both DIB polymers showed no transparency in this region. This allowed for the fingers to be seen through the 1 mm thick 67-poly(S-r-CPD) polymer but not through either of the DIB polymers in the LWIR image.

The polymers were also tested using the mount which covered the entire lens of the camera. This mount is described in the thermal imaging through polymer windows section above. As expected, the 67-poly(S-r-CPD) polymer was transparent in the LWIR region and allowed imaging of a hand while both compositions of DIB did not have enough transmission to be able to image a human hand. This is what would be expected for most polymer compositions as absorbance in the LWIR region is very common for polymers.

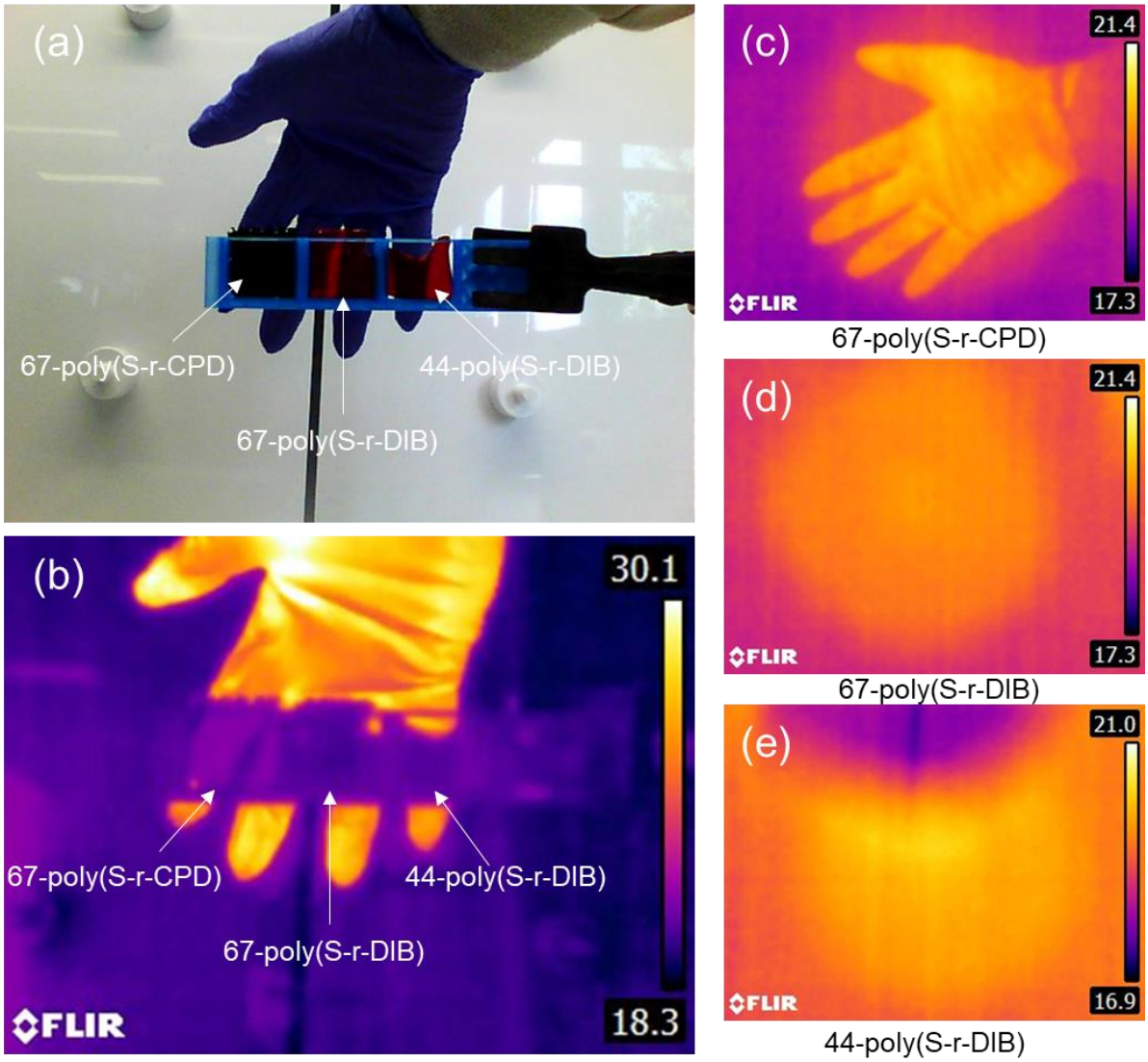

Figure 2.50: (a) Photo of hand behind 1 mm thick 67-poly(S-r-CPD) and DIB polymers with the same mass ratio and molar ratio. (b) LWIR image from 7.5 μm to 13 μm of the 1 mm thick polymer samples taken using a FLIR E6. (c) Gloved hand imaged through 1 mm thick 67-poly(S-r-CPD) polymer using camera mount to completely cover lens. (d) Gloved hand imaged through 1 mm thick 67-poly(S-r-DIB) polymer using camera mount to completely cover lens. (e) Gloved hand imaged through 1 mm thick 44-poly(S-r-DIB) polymer using camera mount to completely cover lens.

UV-Vis-NIR analysis of polymers

The UV-Vis-NIR spectrum was measured using a Perkin Elmer Lambda 950 UV-Vis-NIR spectrometer. The 1 mm thick polymers prepared from both DIB and CPD were tested. The CPD polymers both had 67 % sulfur and varied in their synthesis method. One was prepared using the reflux method and one was prepared using the gas phase method. The DIB polymers were both prepared using an inverse vulcanization method but one had 67 % sulfur and the other had 44 % sulfur. The DIB polymer with 67 % sulfur had the same mass ratio of sulfur while the one with 44 % sulfur had the same mole ratio.

The visible portion of the spectrum is shown in the plot below. For this plot, it was defined as 380 nm to 700 nm. As can be seen, both polymers prepared with CPD show no transmission in the visible region. They only begin to transmit around 1000 nm. This explains why they are completely opaque to visible light and have a black appearance. The samples made from DIB both show transmission starting from around 580 nm. This indicates that these polymers will allow yellow and red light through which explains their distinct red colour. In general, the polymers prepared with DIB had a greater transmittance in the near IR region (defined as 700 nm to 2000 nm). This indicates that the polymers prepared with DIB may be more suited to NIR imaging then MWIR or LWIR.

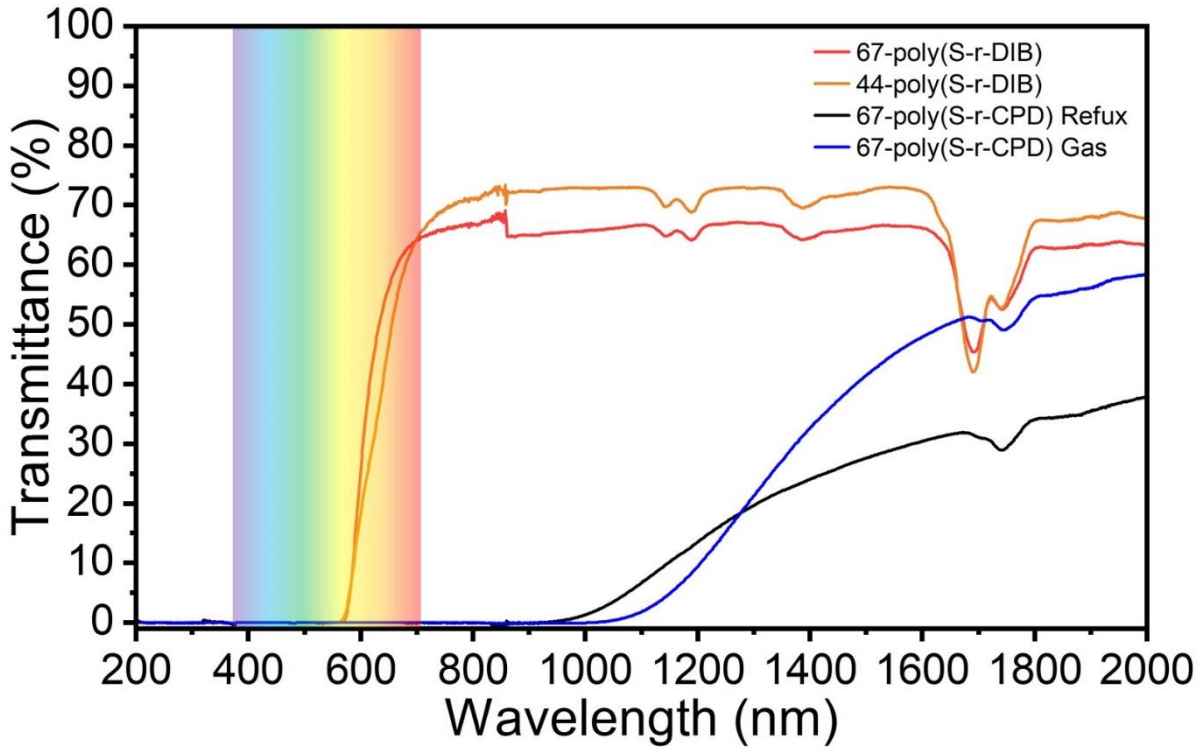

Figure 2.51: UV-Vis-NIR specta collected using a Perkin Elmer Lambda 950 UV-Vis-NIR spectrometer showing the transmission of 1 mm thick polymers prepared with CPD and DIB. Two polymers were prepared using CPD, both had a sulfur content of 67 %. One was prepared with the reflux method while the other was prepared with the gas phase method. Two polymers were prepared from DIB both using the same inverse vulcanization method. One had 67 % sulfur which was the same mass ratio of sulfur as the CPD polymers and one had 44 % sulfur which was the same mole ratio as the CPD polymers.

Comparison of FTIR and UV-Vis-NIR of polymers

To quantitatively compare the transmission of the polymers, the FTIR spectrum for each polymer was collected. A Perkin Elmer Frontier FTIR was used to analyse the polymers made from DIB and from CPD. Both the reflux method and the gas phase method for CPD synthesis was tested.

As can be seen in the plot below, the polymers prepared with CPD had much greater transmission over the entire MWIR and LWIR regions. This explained why images can be taken through them with the LWIR camera. The transmission of these polymers is very promising and indicates they would be suitable for applications in thermal imaging. A larger comparison can be found in chapter 4 which compares the polymers prepared with CPD, the ones that were developed in chapter 3 which have a norbornane core and a range of polymers from literature.

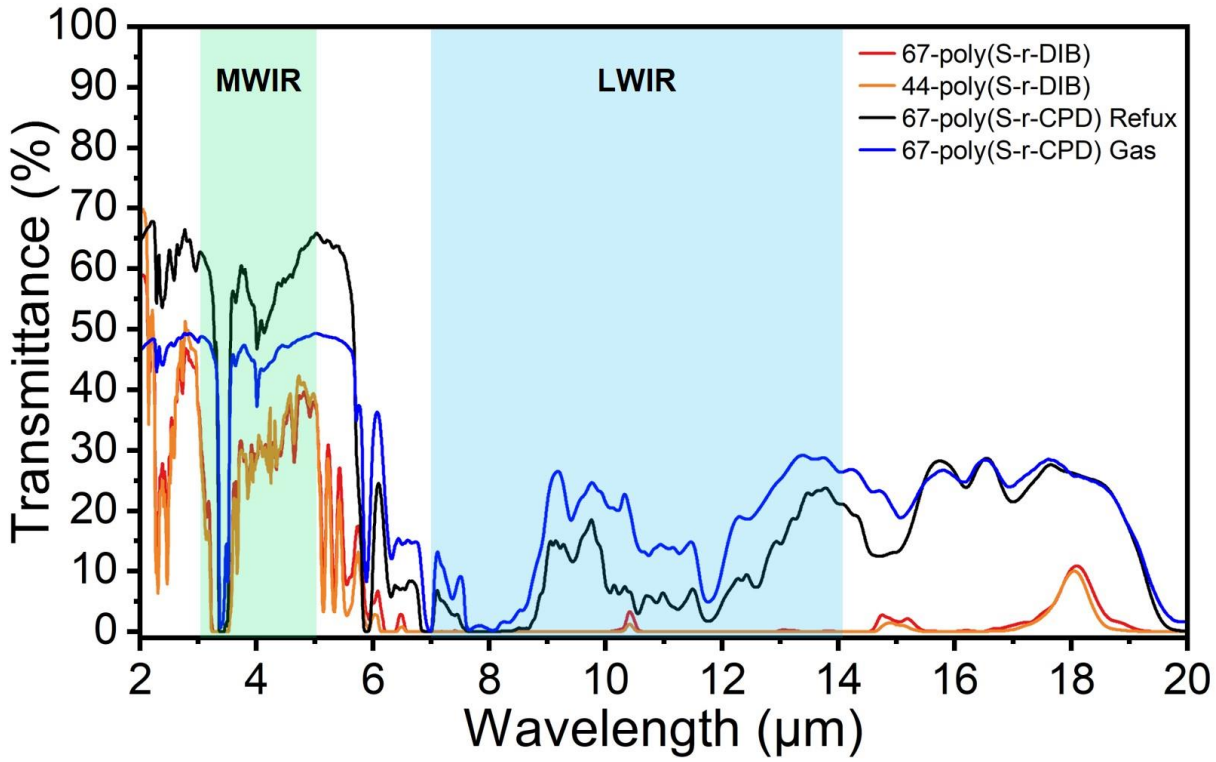

Figure 2.52: FTIR spectra collected using a Perkin Elmer Frontier FTIR showing the transmission of 1 mm thick polymers prepared with CPD and DIB. Two polymers were prepared using CPD, both had a sulfur content of 67 %. One was prepared with the reflux method while the other was prepared with the gas phase method. Two polymers were prepared from DIB both using the same inverse vulcanization method. One had 67 % sulfur which was the same mass ratio of sulfur as the CPD polymers, and one had 44 % sulfur which was the same mole ratio as the CPD polymers.

Chapter conclusions

The main goals of this chapter were to develop a polymerisation reaction between sulfur and cyclopentadiene, fully characterise the polymer structure and investigate its potential for use in thermal imaging. These goals were particularly difficult as cyclopentadiene is a very volatile monomer. At the time that this work was done, no polymerisations of this type had been reported using such a volatile monomer. This was because the reaction would use molten sulfur as both a reagent and a solvent. As sulfur does not melt until around 115 °C, most reactions required monomers which were liquid at this temperature.

To overcome the issue of the volatility of CPD, two new reactors were developed. The reflux method utilised a simple reflux set up to react sulfur with CPD. The gas phase method utilised a two-vial reaction set up to convert cyclopentadiene into a gas and pump it through molten sulfur. These polymerisations with CPD were the first inverse vulcanization reactions utilising molten sulfur and a gaseous monomer.

The chemical structure of the polymers was characterised by reducing them with sodium borohydride and analysing the soluble thiols by GC-MS. It was found that the chemical structure of the polymers depended on the synthesis method. The polymers made using the reflux method were found to have DCPD in their structure. However, this DCPD was fully saturated but when DCPD was used as a monomer, it was found to only react at the more strained alkene. When the reaction was performed using the gas phase method, no DCPD could be found in the polymer structure. GC-MS of the reduced polymer found only the expected CPD thiols, indicating a clean reaction with no side products. Solid state NMR and FTIR were used as complementary techniques and confirmed the results of the reduction experiments.

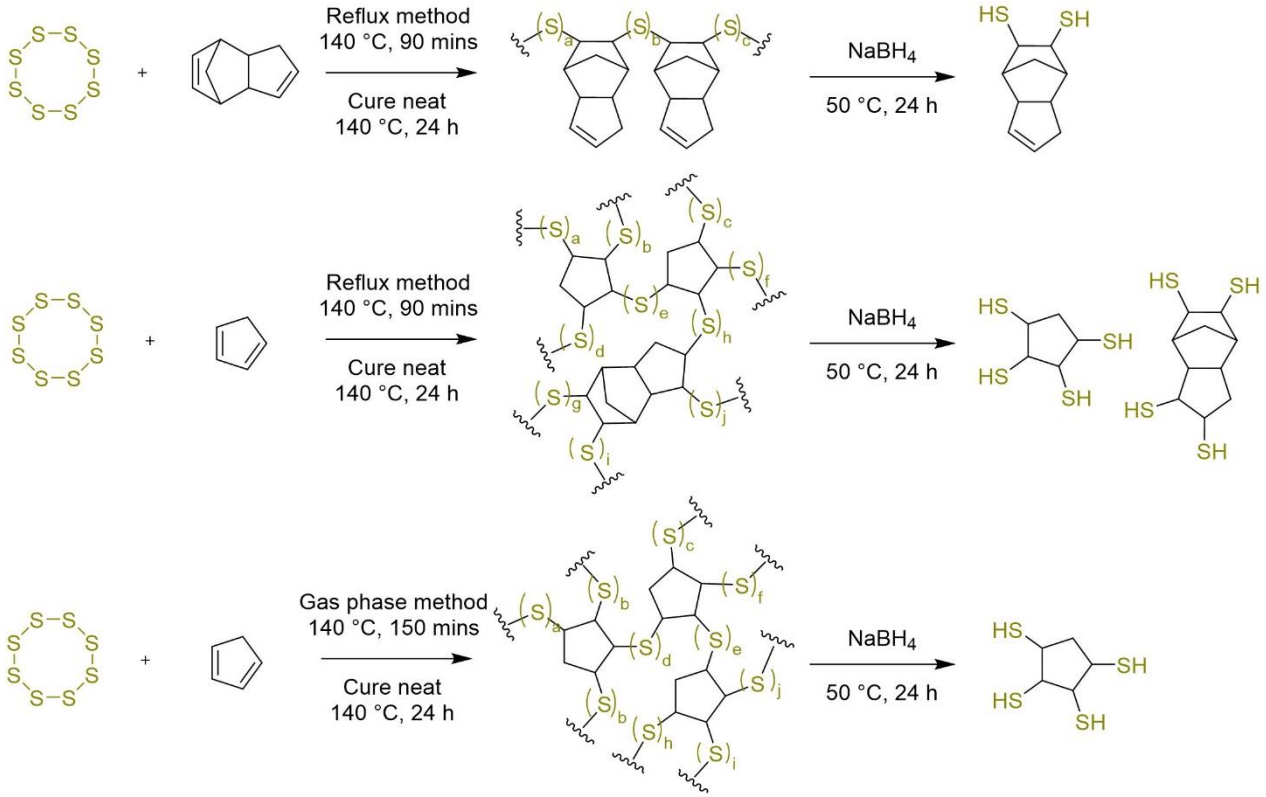

Figure 2.53: Reactions between sulfur and DCPD or CPD using the reflux method and the gas phase method. The polymer structure is shown as well as the major products when the polymer was reduced with sodium borohydride and analysed by GC-MS.

In a series of experiments, it was found that when DCPD impurities were present in the CPD, it would become incorporated into the polymer structure. As described above, this DCPD was found to only react at one alkene. This resulted in alkenes being present in the final polymer. The effect of these alkenes on the polymer properties were investigated and it was found that they significantly reduced the infrared transparency of the polymers. However, the incorporation of DCPD was found to result in an increase in thermal stability.

When polymers were prepared using the gas phase method, DCPD was eliminated from the polymer structure. As predicted by the experiments with DCPD, this resulted in a significant improvement in infrared transparency, making the polymer have the greatest long wave infrared transparency of any in literature at the time. However, this improvement in optical properties came at the expense of the thermal properties. The polymers prepared using the gas phase method had a significantly reduced glass transition temperature and were found to contain unreacted sulfur in the polymer structure.

The polymers prepared using CPD showed excellent transmission over the long wave infrared region. This allowed for thermal images to be taken through the polymers, even at a thickness of 1 mm. Due to the high sulfur content of the polymers, they were also found to possess a refractive index above 1.85. This is extremely impressive for a polymer and would allow for optics to be made smaller, thinner and lighter while maintaining the same optical power. These properties were explored further in chapter 4 where the polymers developed in this chapter were used to prepared windows and a range of lenses for use in thermal imaging.

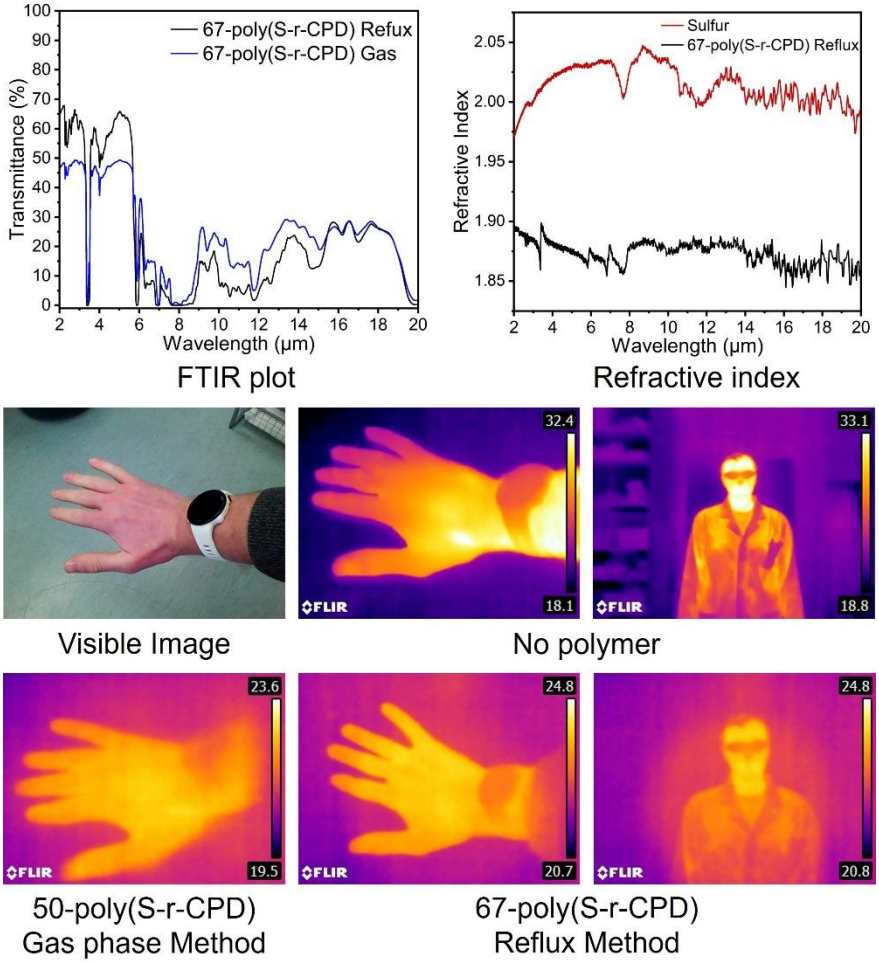

Figure 2.54: (top) FTIR and Refractive index plots for polymers prepared from a reaction between sulfur and CPD. (bottom) LWIR images through 1 mm thick polymers along with a visible image and images with no polymer window.

Chapter 2 references

(1) Tonkin, S. J.; Pham, L. N.; Gascooke, J. R.; Johnston, M. R.; Coote, M. L.; Gibson, C. T.; Chalker, J. M. Thermal Imaging and Clandestine Surveillance using Low-Cost Polymers with Long-Wave Infrared Transparency. *Advanced Optical Materials* **2023**, *11* (16), 2300058. DOI: https://doi.org/10.1002/adom.202300058.

(2) Meem, M.; Banerji, S.; Majumder, A.; Vasquez, F. G.; Sensale-Rodriguez, B.; Menon, R. Broadband lightweight flat lenses for long-wave infrared imaging. *Proceedings of the National Academy of Sciences* **2019**, *116* (43), 21375-21378. DOI: 10.1073/pnas.1908447116.

(3) Tristan S. Kleine, R. S. G., Dennis L. Lichtenberger, Michael E. Mackay, Kookheon Char,; Robert A. Norwood, J. P. 100th Anniversary of Macromolecular Science Viewpoint: High Refractive Index Polymers from Elemental Sulfur for Infrared Thermal Imaging and Optics. *ACS Macro Lett.* **2020**, *9*, 245-259.

(4) Hwang, J. H.; Kim, S. H.; Cho, W.; Lee, W.; Park, S.; Kim, Y. S.; Lee, J.-C.; Lee, K. J.; Wie, J. J.; Kim, D.-G. A Microphase Separation Strategy for the Infrared Transparency-Thermomechanical Property Conundrum in Sulfur-Rich Copolymers. *Advanced Optical Materials* **2023**, *n/a* (n/a), 2202432. DOI: https://doi.org/10.1002/adom.202202432.

(5) Kaneda, R.; Takahashi, T.; Takiguchi, M.; Hijikata, M.; Ito, H. Optical properties of high-density polyethylene in injection press molding for IR system lenses. *Polymer Engineering & Science* **2018**, *58* (5), 632-641. DOI: https://doi.org/10.1002/pen.24592.

(6) Boyd, D. A.; Nguyen, V. Q.; McClain, C. C.; Kung, F. H.; Baker, C. C.; Myers, J. D.; Hunt, M. P.; Kim, W.; Sanghera, J. S. Optical Properties of a Sulfur-Rich Organically Modified Chalcogenide Polymer Synthesized via Inverse Vulcanization and Containing an Organometallic Comonomer. *ACS Macro Letters* **2019**, *8* (2), 113-116. DOI: 10.1021/acsmacrolett.8b00923.

(7) Zhang, Y.; Pavlopoulos, N. G.; Kleine, T. S.; Karayilan, M.; Glass, R. S.; Char, K.; Pyun, J. Nucleophilic Activation of Elemental Sulfur for Inverse Vulcanization and Dynamic Covalent Polymerizations. *Journal of Polymer Science Part A: Polymer Chemistry* **2019**, *57* (1), 7-12. DOI: https://doi.org/10.1002/pola.29266.

(8) Wu, X.; Smith, J. A.; Petcher, S.; Zhang, B.; Parker, D. J.; Griffin, J. M.; Hasell, T. Catalytic inverse vulcanization. *Nature Communications* **2019**, *10* (1), 647. DOI: 10.1038/s41467-019-08430-8.

(9) Zhang, B.; Gao, H.; Yan, P.; Petcher, S.; Hasell, T. Inverse vulcanization below the melting point of sulfur. *Materials Chemistry Frontiers* **2020**, *4* (2), 669-675, 10.1039/C9QM00606K. DOI: 10.1039/C9QM00606K.

(10) Dodd, L. J.; Omar, Ö.; Wu, X.; Hasell, T. Investigating the Role and Scope of Catalysts in Inverse Vulcanization. *ACS Catalysis* **2021**, *11* (8), 4441-4455. DOI: 10.1021/acscatal.0c05010.

(11) Kim, D. H.; Jang, W.; Choi, K.; Choi, J. S.; Pyun, J.; Lim, J.; Char, K.; Im, S. G. One-step vapor-phase synthesis of transparent high refractive index sulfur-containing polymers. *Science Advances* **2020**, *6* (28), eabb5320. DOI: 10.1126/sciadv.abb5320.

(12) Pople, J. M. M.; Nicholls, T. P.; Pham, L. N.; Bloch, W. M.; Lisboa, L. S.; Perkins, M. V.; Gibson, C. T.; Coote, M. L.; Jia, Z.; Chalker, J. M. Electrochemical Synthesis of Poly(trisulfides). *Journal of the American Chemical Society* **2023**, *145* (21), 11798-11810. DOI: 10.1021/jacs.3c03239.

(13) Jia, J.; Liu, J.; Wang, Z.-Q.; Liu, T.; Yan, P.; Gong, X.-Q.; Zhao, C.; Chen, L.; Miao, C.; Zhao, W.; et al. Photoinduced inverse vulcanization. *Nature Chemistry* **2022**, *14* (11), 1249-1257. DOI: 10.1038/s41557-022-01049-1.

(14) Yan, P.; Zhao, W.; McBride, F.; Cai, D.; Dale, J.; Hanna, V.; Hasell, T. Mechanochemical synthesis of inverse vulcanized polymers. *Nature Communications* **2022**, *13* (1), 4824. DOI: 10.1038/s41467-022-32344-7. He, L.; Yang, J.; Jiang, H.; Zhao, H.; Xia, H. Mechanochemistry Enabled Inverse Vulcanization of Norbornadiene for Optical Polymers and Elastomeric Materials. *Industrial & Engineering Chemistry Research* **2023**, *62* (25), 9587-9594. DOI: 10.1021/acs.iecr.3c00801. Tedjini, R.; Viveiros, R.; Casimiro, T.; Bonifácio, V. D. B. Iron-free mechanochemical limonene inverse vulcanization. *RSC Mechanochemistry* **2024**, *1* (2), 176-180, 10.1039/D3MR00002H. DOI: 10.1039/D3MR00002H.

(15) Mann, M.; Zhang, B.; Tonkin, S. J.; Gibson, C. T.; Jia, Z.; Hasell, T.; Chalker, J. M. Processes for coating surfaces with a copolymer made from sulfur and dicyclopentadiene. *Polymer Chemistry* **2022**, *13* (10), 1320-1327, 10.1039/D1PY01416A. DOI: 10.1039/D1PY01416A.

(16) Dale, J. J.; Petcher, S.; Hasell, T. Dark Sulfur: Quantifying Unpolymerized Sulfur in Inverse Vulcanized Polymers. *ACS Applied Polymer Materials* **2022**, *4* (5), 3169-3173. DOI: 10.1021/acsapm.2c00304.

(17) Tonkin, S. J.; Gibson, C. T.; Campbell, J. A.; Lewis, D. A.; Karton, A.; Hasell, T.; Chalker, J. M. Chemically induced repair, adhesion, and recycling of polymers made by inverse vulcanization. *Chemical Science* **2020**, *11* (21), 5537-5546, 10.1039/D0SC00855A. DOI: 10.1039/D0SC00855A.

(18) Gibson, C. T.; Ridings, C. R.; Blok, A. J.; Shearer, C. J.; Andersson, G. G.; Ellis, A. V. Morphological changes of sintered polydopamine coatings. *Surface topography: metrology and properties* **2019**. DOI: 10.1088/2051-672X/ab06eb.

(19) Levandowski, B. J.; Houk, K. N. Theoretical Analysis of Reactivity Patterns in Diels–Alder Reactions of Cyclopentadiene, Cyclohexadiene, and Cycloheptadiene with Symmetrical and Unsymmetrical Dienophiles. *The Journal of Organic Chemistry* **2015**, *80* (7), 3530-3537. DOI: 10.1021/acs.joc.5b00174.

(20) Zhang, B.; Petcher, S.; Hasell, T. A ternary system for delayed curing inverse vulcanisation. *Chemical Communications* **2019**, *55* (72), 10681-10684, 10.1039/C9CC04380B. DOI: 10.1039/C9CC04380B. Parker, D. J.; Jones, H. A.; Petcher, S.; Cervini, L.; Griffin, J. M.; Akhtar, R.; Hasell, T. Low cost and renewable sulfur-polymers by inverse vulcanisation, and their potential for mercury capture. *Journal of Materials Chemistry A* **2017**, *5* (23), 11682-11692, 10.1039/C6TA09862B. DOI: 10.1039/C6TA09862B.
(21) Smith, J. A.; Wu, X.; Berry, N. G.; Hasell, T. High sulfur content polymers: The effect of crosslinker structure on inverse vulcanization. *Journal of Polymer Science Part A: Polymer Chemistry* **2018**, *56* (16), 1777-1781. DOI: https://doi.org/10.1002/pola.29067.
(22) Lee, M.; Jang, S. G.; Yeo, H.; Park, J.-J.; Moon, B.; You, N.-H. Structural Effect of Cyclic Olefin Cross-Linkers on Long-Wave Infrared-Transmitting Sulfur Polymers. *Macromolecules* **2024**, *57* (6), 2905-2914. DOI: 10.1021/acs.macromol.4c00018.
(23) Ghumman, A. S. M.; Nasef, M. M.; Shamsuddin, M. R.; Abbasi, A. Evaluation of properties of sulfur-based polymers obtained by inverse vulcanization: Techniques and challenges. *Polymers and Polymer Composites* **2021**, *29* (8), 1333-1352. DOI: 10.1177/0967391120954072. Diez, S.; Hoefling, A.; Theato, P.; Pauer, W. Mechanical and Electrical Properties of Sulfur-Containing Polymeric Materials Prepared via Inverse Vulcanization. *Polymers* **2017**, *9* (2), 59.
(24) Zhou, Y.; Zhu, Z.; Zhang, K.; Yang, B. Molecular Structure and Properties of Sulfur-Containing High Refractive Index Polymer Optical Materials. *Macromolecular Rapid Communications* **2023**, *44* (23), 2300411. DOI: https://doi.org/10.1002/marc.202300411.
(25) Galeener, F. L.; Leadbetter, A. J.; Stringfellow, M. W. Comparison of the neutron, Raman, and infrared vibrational spectra of vitreous *Physical Review B* **1983**, *27* (2), 1052-1078. DOI: 10.1103/PhysRevB.27.1052.
(26) Fuller, K. A.; Downing, H. D.; Querry, M. R. Infrared optical properties of orthorhombic sulfur. *Appl. Opt.* **1991**, *30* (28), 4081-4093. DOI: 10.1364/AO.30.004081.
(27) Chung, W. J.; Griebel, J. J.; Kim, E. T.; Yoon, H.; Simmonds, A. G.; Ji, H. J.; Dirlam, P. T.; Glass, R. S.; Wie, J. J.; Nguyen, N. A.; et al. The use of elemental sulfur as an alternative feedstock for polymeric materials. *Nature Chemistry* **2013**, *5* (6), 518-524. DOI: 10.1038/nchem.1624.
(28) Simmonds, A. G.; Griebel, J. J.; Park, J.; Kim, K. R.; Chung, W. J.; Oleshko, V. P.; Kim, J.; Kim, E. T.; Glass, R. S.; Soles, C. L.; et al. Inverse Vulcanization of Elemental Sulfur to Prepare Polymeric Electrode Materials for Li–S Batteries. *ACS Macro Letters* **2014**, *3* (3), 229-232. DOI: 10.1021/mz400649w.

Chapter 3 – Synthesis and polymerisation of norbornane based cyclic sulfides to prepare optical polymers

Publications and patents from chapter 3

Yan, P.; Zhao, W.; Tonkin, S. J.; Chalker, J. M.; Schiller, T. L.; Hasell, T. Stretchable and Durable Inverse Vulcanized Polymers with Chemical and Thermal Recycling. Chemistry of Materials 2022, 34 (3), 1167-1178. DOI: 10.1021/acs.chemmater.1c03662.[1]

Chalker, J.; Tonkin, S.; Patel, H. Methods for making cyclic sulfide and polysulfide monomers, Australia application number: 2025900891, Filed 19 March 2025.

Chapter introduction

In the previous chapter, a high-performance polymer was developed with excellent long-wave infrared transmission. This polymer was designed with a cyclopentadiene organic core, which gave a highly crosslinked polymer when reacted with sulfur. Due to the organic monomer being small and highly unsaturated, the polymer could incorporate a large relative proportion of sulfur while maintaining a short average sulfur chain length. This gave a polymer with excellent refractive index and long-wave infrared transmission.

This chapter will focus on the development of a polymer which is superior to the cyclopentadiene based polymer in some ways and complimentary in others. This new polymer utilises a norbornane group as the organic portion of the polymer. The cyclopentadiene polymer, while possessing excellent transmission in the long-wave infrared region, was black and completely opaque to visible light. For some applications, this could be utilised to great effect. For example, an opaque polymer with long-wave infrared transparency could be very valuable for concealment and protection of a thermal camera. This application is explored in detail in chapter 4 using a window of the polymer to conceal a thermal camera from visible light while still allowing it to be used in the long-wave infrared region. However, in some applications, a material which is also transparent to visible light may be more practical. Many thermal imaging cameras possess both a visible and long-wave infrared sensor to image in both regions simultaneously. For these cameras, a material which is transparent in both the visible and the long-wave infrared regions would be valuable to act as a protective window or optic that could be used by both sensors. One of the goals of this chapter was to develop a complementary material which was transparent in both the visible and long-wave infrared region.

Another goal of this chapter was to develop a polymer with a high glass transition temperature. The cyclopentadiene polymer had a glass transition temperature of 4.5 °C. This meant that at room temperature, the polymer would be soft and flexible. There are many applications where this would be an advantage. Using the example of an opaque polymer sheet to conceal a camera, using a flexible material would allow for it to be easily placed over a reinforcing mesh or be bent into a shape. Using a material above its glass transition temperature also prevents it from shattering upon impact, allowing it to function more effectively as a protective screen. While these applications are useful, most lenses use a brittle, glass like material for several key reasons. The first is that brittle materials are much less likely to flex or warp when pressure is applied. This means they can be mounted into a holder for a camera without any changes in geometry. For a lens, any

change in geometry could lead to significant changes in optical performance. Furthermore, polymer lenses are often used below their glass transition temperature to prevent significant changes in shape with variations in temperature. This means that a polymer with a high glass transition temperature would have a much greater effective temperature range. For these reasons, it would be valuable to develop a complementary material with a high glass transition temperature.

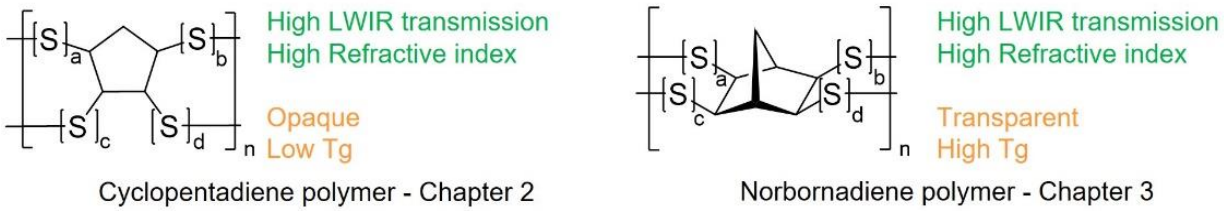

Figure 3.1: Structural diagrams of cyclopentadiene and norbornadiene polymers with properties listed.

The initial motivation for the norbornadiene polymer came from some pioneering research by Norwood, Pyun and co-workers.[2] They performed computational research on a range of polymer analogues and found that polymers with a norbornane core would have excellent LWIR transmission and a high glass transition temperature. They were not able to prepare this polymer due to the volatility of norbornadiene making the reaction with molten sulfur very difficult.[2] Instead, the authors performed a nickel catalysed [2+2] cycloaddition to prepare a dimer of norbornadiene. While this polymer was calculated to sacrifice some LWIR transmission, it could be reacted directly with sulfur to prepare a high glass transition polymer which was also transparent in the visible region. This polymer was found to possess enough LWIR transmission to image a 100 °C hotplate through a 1.3 mm thick window.

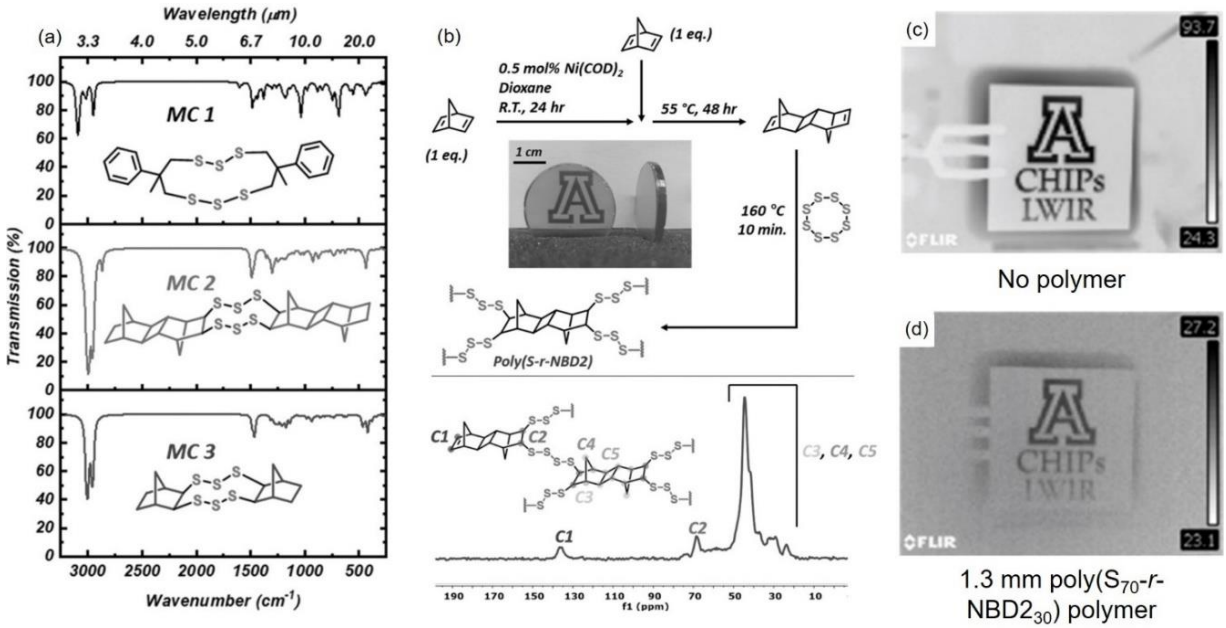

Figure 3.2: Work by Norwood, Pyun and co-workers on the computational analysis, synthesis and testing of a poly(S-*r*-NBD2) polymer. (a) Computational screening of three different model systems showing DFT-calculated FTIR spectra. (b) Synthesis of NBD2 by nickel-catalysed [2+2] cycloaddition of norbornadiene followed by a reaction with sulfur and ^{13}C CP-MAS spectrum of poly(S_{50}-*r*-$NBD2_{50}$). (c) Control image through taken with FLIR LWIR camera in "black hot" mode of 100 °C hotplate with PMMA mask. (d) LWIR image taken through 1.3 mm thick poly(S_{70}-*r*-$NBD2_{30}$) polymer window. Modified with permission from.[2]

While the authors were not able to prepare a polymer with the norbornane core, they were able to demonstrate the potential of sulfur-based polymers with a norbornane core. The Pyun group went on to use the NBD2 polymer to prepare a polymer lens which could be used with a commercial LWIR detector.[3] This will be explored further in chapter 4.

In another publication authored by He, Xia and co-workers, the norbornane based polymer was attempted to be prepared using mechanochemistry.[4] In this paper, a ball mill was used to react sulfur and NBD. While they were able to prove that a reaction had occurred, unfortunately, the characterisation of the obtained material was extremely limited. From the characterisation data available in the paper, it appears that there was some rearrangement of the norbornane core. In this chapter, a polymer was prepared directly from a monomer containing the rearrange norbornane core. This polymer contained several characteristic features that allow its identification. The rearranged norbornane core has a cyclopropane group which gives characteristic FTIR peaks above 3000 cm^{-1} and around 800 cm^{-1}. These peaks are present in the polymer prepared by mechanochemistry and can clearly be seen in the FTIR spectrum. This, combined with the low glass transition temperature of 51 °C indicates that a rearrangement likely occurred. The rearrangement of the norbornane core is a difficult issue to avoid. To prepare the desired polymer with a norbornane core, the issue of the volatility of NBD and the rearrangement must be addressed.

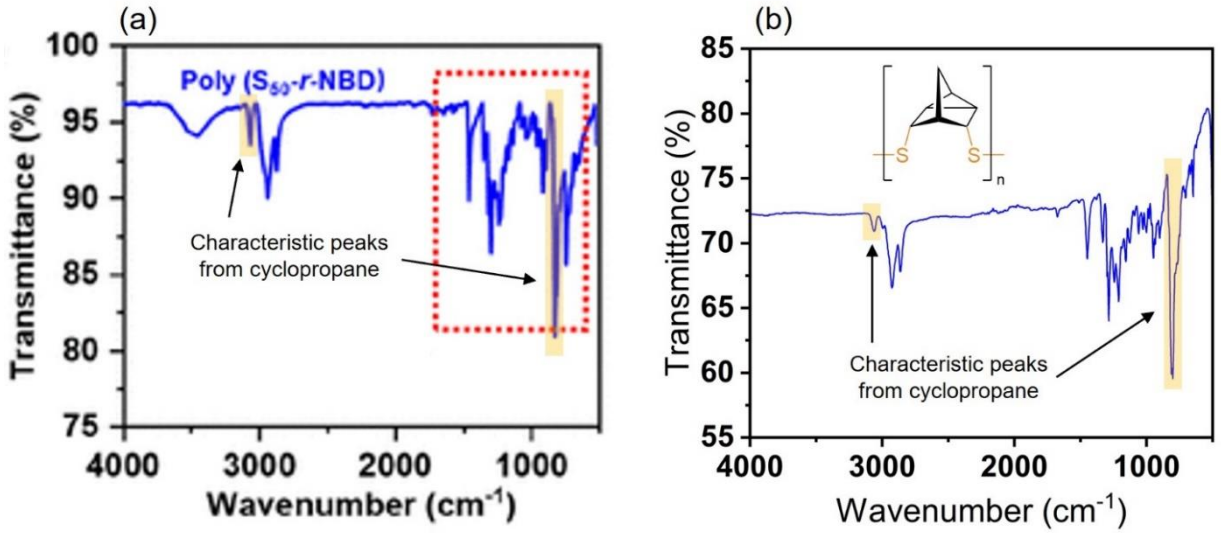

Figure 3.3: (a) FTIR plot of polymer prepared by mechanochemistry. Modified with permission from.[4] (b) FTIR plot from polymer prepared directly from rearranged norbornane disulfide prepared later in this chapter. The characteristic peaks for the cyclopropane group were present in both, indicating that the polymer prepared by mechanochemistry had some rearrangement of the norbornane core.

This chapter will explore the synthesis and characterisation of the polymer with a norbornane core while avoiding the issues of rearrangement and NBD volatility. Following the successful synthesis of the target polymer, this chapter will investigate its potential as a material for use in thermal imaging. To do this, the polymer was tested for refractive index, LWIR transmission and thermal properties, including glass transition temperature. By the conclusion of this chapter, a consistent method for the synthesis of the polymer would be developed, the rearrangement of norbornadiene would be fully understood and all the required characterisation would be complete to allow for the use of the polymer as a material to prepare optics for thermal imaging. This would then lead to the use of the polymer in chapter 4 as a custom lens in a thermal imaging camera using a commercial detector.

Solventless reaction between sulfur and norbornadiene

Polymer synthesis

To make the norbornane based polymer, a direct inverse vulcanization reaction using sulfur as both a solvent and a monomer was first attempted. In this reaction, norbornadiene (NBD) was added directly to molten sulfur like the reactions described in chapter 2. This reaction was expected to have issues as Pyun stated that “due to the volatility of NBD (boiling point: ≈89 °C), these compounds could not be used with liquid sulfur in the inverse vulcanization process (T>130 °C).”[2] To confirm these statements, it was first tested using the same methods that were used for cyclopentadiene in chapter 2.

For this reaction, sulfur (3g, 93.75 mmol S atoms) was added to a 21 mL vial with a magnetic stirrer. The vial was connected to a condenser and lowered into a 140 °C oil bath. The sulfur was heated with constant stirring for three minutes, over which time it melted into a yellow liquid. NBD (2.160 g, 23.44 mmol, 2.38 mL) was slowly added by volumetric pipette through the top of the condenser. The ratio of sulfur to NBD corresponds to a sulfur mass percentage of 58 % and an average sulfur rank of 2. Within 4-5 minutes of the adding the NBD, the sulfur completely vitrified to a soft yellow solid. NBD would still visibly reflux on the surface of the sulfur but would no longer mix with the bulk material. Over time, the surface would slowly darken while the sulfur underneath remained a yellow solid. After 90 minutes of heating, the material was removed from the vial and cured in a silicone container at 140 °C for 24 hours. This gave a material that ranged from yellow to black with clear sections of unreacted sulfur.

While a reaction between sulfur and NBD did occur, it was not possible to control the reaction and ensure a homogeneous product. This confirmed the findings of Pyun and showed that the reaction requires a solvent or other controls to ensure that a stable polymer can be formed.

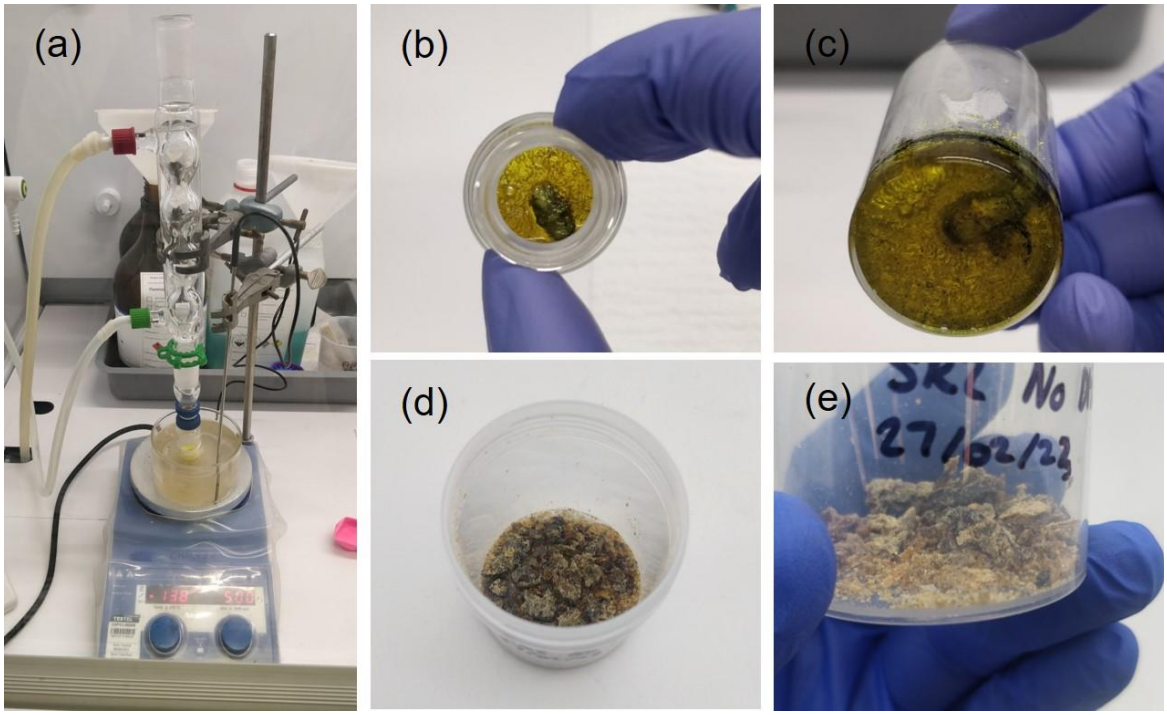

Figure 3.4: Images showing solventless reaction between sulfur and norbornadiene with 58 % sulfur. (a) Reaction set up showing condenser and sulfur in vial. (b-c) images showing vitrified material after addition of norbornadiene. (d-e) Images showing material from solventless reaction after curing for 24 hours at 140 °C.

Characterisation of material made from solventless reaction

The material from the solventless reaction between sulfur and NBD was analysed by differential scanning calorimetry (DSC), thermal gravimetric analysis (TGA) and elemental analysis. DSC was used to see any crystalline sulfur that may be present in the material. This would indicate an incomplete reaction. Crystalline monoclinic sulfur shows a large endothermic peak at around 119 °C in a DSC thermogram. DSC could also show the glass transition of any polymeric material, however, for highly crosslinked polymers, the glass transition is often difficult to see. A Perkin Elmer DSC 8000 was used to analyse the material. Starting at room temperature, the material was cooled to -60 °C then heated to 100 °C at a heating rate of 10 °C/min. Following this, the material was cooled to -60 °C again, before being heated to 150 °C. A clear sulfur melting peak is observed around 115 °C, indicating the presence of crystalline sulfur.

TGA was used to analyse the thermal degradation of the material. Sulfur based polymers often show a characteristic two step degradation. The onset of the first is generally between 250 °C and 300 °C while the second occurs at 350 °C to 400 °C. The presence of a second mass loss indicates that there are some crosslinked portions of the material as elemental sulfur will only show a single mass loss with an onset of approximately 250 °C. A TGA Perkin Elmer 8000 was used to analyse the material. Starting at room temperature, the material was heated to 800 °C at a heating rate of 20 °C/min under nitrogen atmosphere. As can be seen, there are two mass losses, indicating that there is some portion of the material which is crosslinked.

Elemental analysis gives the ratio of sulfur to carbon and hydrogen in the material. Elemental analysis was performed by the chemical analysis facility at Macquarie University using a Vario Micro cube elemental analyser. Both the surface where the NBD would reflux on the sulfur and the bottom were analysed by elemental analysis. The surface had a lower sulfur content than expected with only 42 % while the bottom was over 95 % sulfur. This indicates that the NBD did not mix through the sulfur after it vitrified.

The characterisation of the reaction without solvents shows that a well-defined polymer could not be formed. There was clear inhomogeneity caused by the premature vitrification. As this polymer was intended to be used for optical applications, there could not be any crystalline sulfur or it would cause reflections and dispersion of light, significantly affecting optical performance. However, the TGA results show that there was a reaction occurring and some polymer did form. This gave some indication that a homogeneous polymer could be formed if the issue of vitrification is addressed. The next few reactions attempted to solve this issue by doing this reaction in a solution using a range of solvent systems.

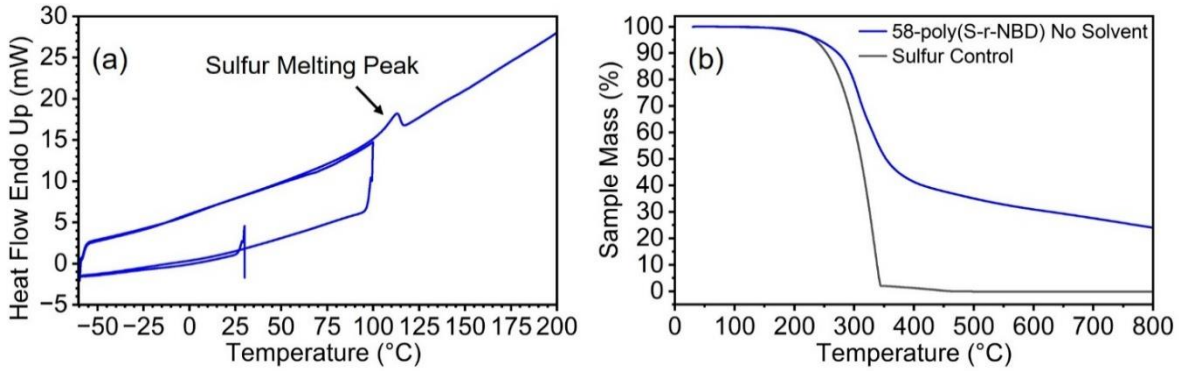

Figure 3.5: (a) DSC thermogram of 58 % sulfur NBD polymer showing sulfur melting peak. (b) TGA thermogram of 58 % sulfur BND polymer and a sulfur control.

Solution phase reactions between sulfur and norbornadiene

Effect of dimethylformamide on trisulfides

The reaction between norbornadiene and sulfur was not successful when done neat. It was believed that this was because the reaction would proceed quickly and form a crosslinked polymer. The polymer would then quickly vitrify and not allow any further stirring or the incorporation of additional NBD. A potential way to combat this would be to keep the polymer in solution as low molecular weight intermediates. If this could be achieved, the issue of premature vitrification would not be as likely to occur and all the norbornadiene could react with the sulfur before the polymer is cured.

The issue with doing inverse vulcanization reactions in solution is that most crosslinked sulfur-based polymers show very little solubility in most solvents.[5] Interestingly, these polymers did show some solubility in polar nucleophilic solvents like DMF, pyridine, DMA or NMP.[6-8] This was investigated further by Peiyao Yan from the Hasell group.[7] In this study, a range of polymers with differing crosslinking density were prepared to use as model polymers. These polymers were prepared using an inverse vulcanization reaction between sulfur and Span 80 giving a linear polymer. The linear polymer could then be reacted with bisphenol A diglycidyl ether (BADGE) to crosslink it. These polymers possessed excellent mechanical properties and controllable crosslinking, making them perfect to test the effect of polar nucleophilic solvents.

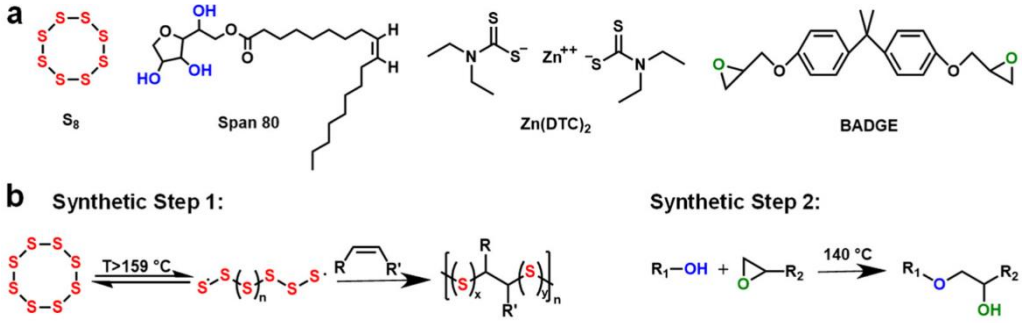

Figure 3.6: Polymer synthesis for crosslinked sulfur-based polymers based on Span 80 and BADGE. Used with permission from.[7]

As expected, the polymers were not soluble in most common solvents like THF, chloroform, acetone and ethyl acetate. However, they were soluble in DMF and pyridine. Interestingly, after being dissolved in DMF, the polymers became soluble in THF. If the polymer was then cured at either 80 °C or 140 °C, it became insoluble in THF again. This indicated that the DMF was causing a change in the chemical structure of the polymer. Using GPC, the molecular weight was determined before and after the polymers were added to DMF. It was found that the molecular weight of the polymers was significantly reduced after addition to DMF. This was attributed to the sulfur-sulfur bonds being broken by the DMF, resulting in a reduction in the crosslinking and molecular weight of the polymer.

Interestingly, if the polymers were cured in DMF, the molecular weight did not change, this indicated that the DMF was continuously breaking sulfur-sulfur bonds in the polymers. However, if the polymers were removed from DMF and cured at either 80 °C or 140 °C for 8 hours, they returned to their original crosslinking density with no changes to chemical structure, glass transition temperature or mechanical properties. This represents an interesting way to recycle the polymer with simple dissolution in DMF and recure at moderate temperatures.

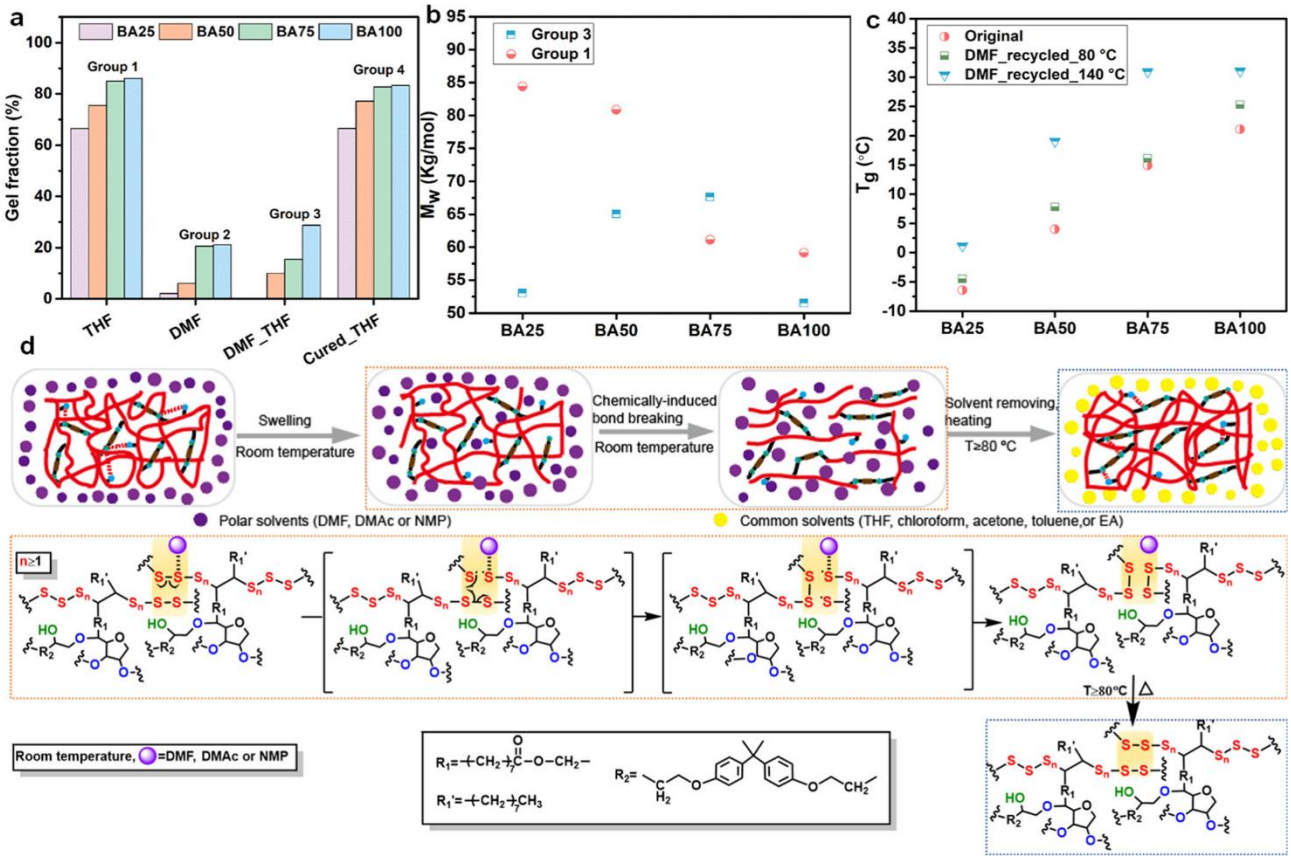

Figure 3.7: (a) The gel fraction of polymers which had been dissolved in THF, DMF or dissolved in THF after being dissolved in DMF and finally after being cured and redissolved in THF. (b) Weight average molecular weight of the THF soluble fractions both before (group 1) and after being dissolved in DMF (group 3). (c) Glass transition temperature as determined by DSC of original polymers and polymer which had been dissolved in DMF and cured at 80 °C or 140 °C for 8 hours. (d) Proposed mechanism for the recycling process. Figure used with permission from.[7]

The DMF induced recycling may be particularly applicable to the reaction between NBD and sulfur. If DMF can chemically break sulfur-sulfur bonds within the polymer, then it may prevent any premature vitrification. This would all for all NBD to react with sulfur and form oligomers. After this stage, the DMF could be removed, and the oligomers could be cured. As evidenced by the findings of this paper, the polymer should be able to fully cure after being removed from the DMF.

Disulfide and trisulfide crossover experiments

To determine if dimethylformamide (DMF) or similar solvents could break sulfur-sulfur bonds, a model study was designed using di and trisulfides. These molecules contain similar sulfur-sulfur bonds to those in sulfur polymers but can be analysed by GC-MS to determine any changes in structure. Dimethyl and dipropyl trisulfide were selected as the model trisulfides. If a metathesis reaction were to occur, it would be expected that methyl propyl trisulfide would form. This molecule was used to determine if the reaction could occur.

A total of four solvents were tested. They were dimethylformamide (DMF), dimethylacetamide (DMA), N-Methyl-2-pyrrolidone (NMP) or tetrahydrofuran (THF). DMF, DMA, and NMP are all aprotic, nucleophilic and polar. At the time, it was thought that these solvents could undergo a nucleophilic metathesis reaction.[6] This mechanism has since been disproven by subsequent studies in the Chalker lab but these solvents still induce a metathesis reaction in trisulfides. THF was chosen as a control which was not as nucleophilic. Finally, another control with no solvent was used to test if the sulfides could react neat.

The experiment was performed using both disulfides and trisulfides. The weakest sulfur-sulfur bond in disulfides is much stronger than in trisulfides.[9] By using both, it can be determined if the metathesis reaction can occur in shorter disulfides or only in trisulfides, giving an indication of the strength of S-S bond that could be broken in the reaction. This is important as it may affect the practical use of these reactions. Below is a potential mechanism for the radical metathesis reaction. It should be noted that in this thesis, the mechanism for this reaction was not fully investigated. The reaction is likely much more complicated than the radical mechanism shown below. This radical mechanism has also been disproven in experiments by in the Chalker lab in EPR studies but the mechanism is shown here to illustrate the original hypothesis and reasoning.

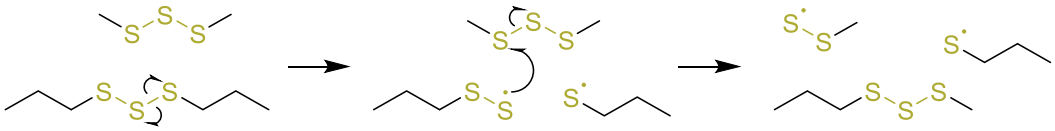

Figure 3.8: Potential mechanism for radical induced trisulfide metathesis reaction of trisulfides.

Four 15 mL reaction tubes were prepared and 1.2 mmol of either (DMF), (DMA), (NMP) or (THF) was added to each vial by volumetric pipette. A control with no solvent was also prepared. 1.2 mmol of dimethyl trisulfide and dipropyl trisulfide was added to each vial, along with a magnetic stirrer. All vials were left to react with light stirring for 24 hours at room temperature. After 1 and 24 hours, 10 µL was removed from each vial and made up to 1 mL with chloroform. This solution was analysed by GC-MS using an Agilent 5975C series GC-MS system. A 29.4 m x 250 µm x 0.25 µm, 5 % phenyl methyl silox column was used with a helium mobile phase. 1 µL of sample was injected with a split ratio of 60:1. All samples were run with the same method which used a gas flow rate of 1.2 mL/min and an initial temperature of 30 °C. This temperature was held for three minutes before being ramped to 250 °C at 20 °C/min. The temperature was then held at 250 °C for an additional three minutes. This same procedure was repeated but with the trisulfides replaced with dimethyl and dipropyl disulfide.

When no solvent was used, there was no significant reaction in either the disulfides or trisulfides at room temperature over 24 hours. There was a small peak in the trisulfides at 8.4 minutes. This peak is caused by an impurity in the dipropyl trisulfide sample and corresponds to dipropyl disulfide. This control shows that a solvent is required to give a reaction.

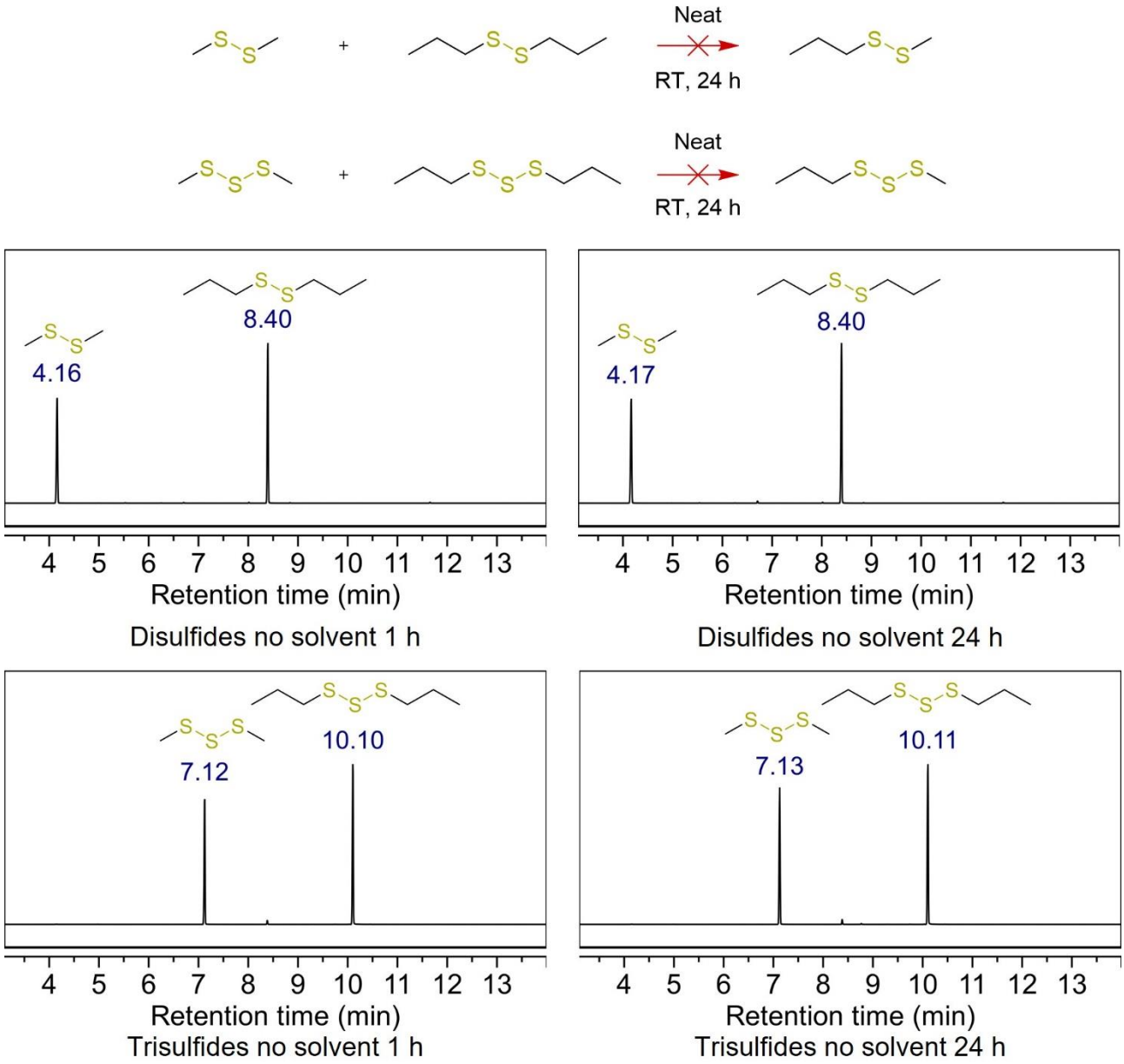

Figure 3.9: Reactions between dimethyl and dipropyl disulfide or trisulfide with no solvent. No reaction was observed over 24 hours at room temperature.

When DMF is added with disulfides, no new products are formed. There is very little change between one hour and 24 hours which indicates that no reaction is taking place. When reacted with trisulfides, a new peak is formed which corresponds to methyl propyl trisulfide, indicating that a reaction had taken place. DMF is still present which indicates that it is not consumed in the reaction. This reaction is very rapid and appears to reach equilibrium within an hour with no further change in the ratio of the trisulfides after 24 hours.

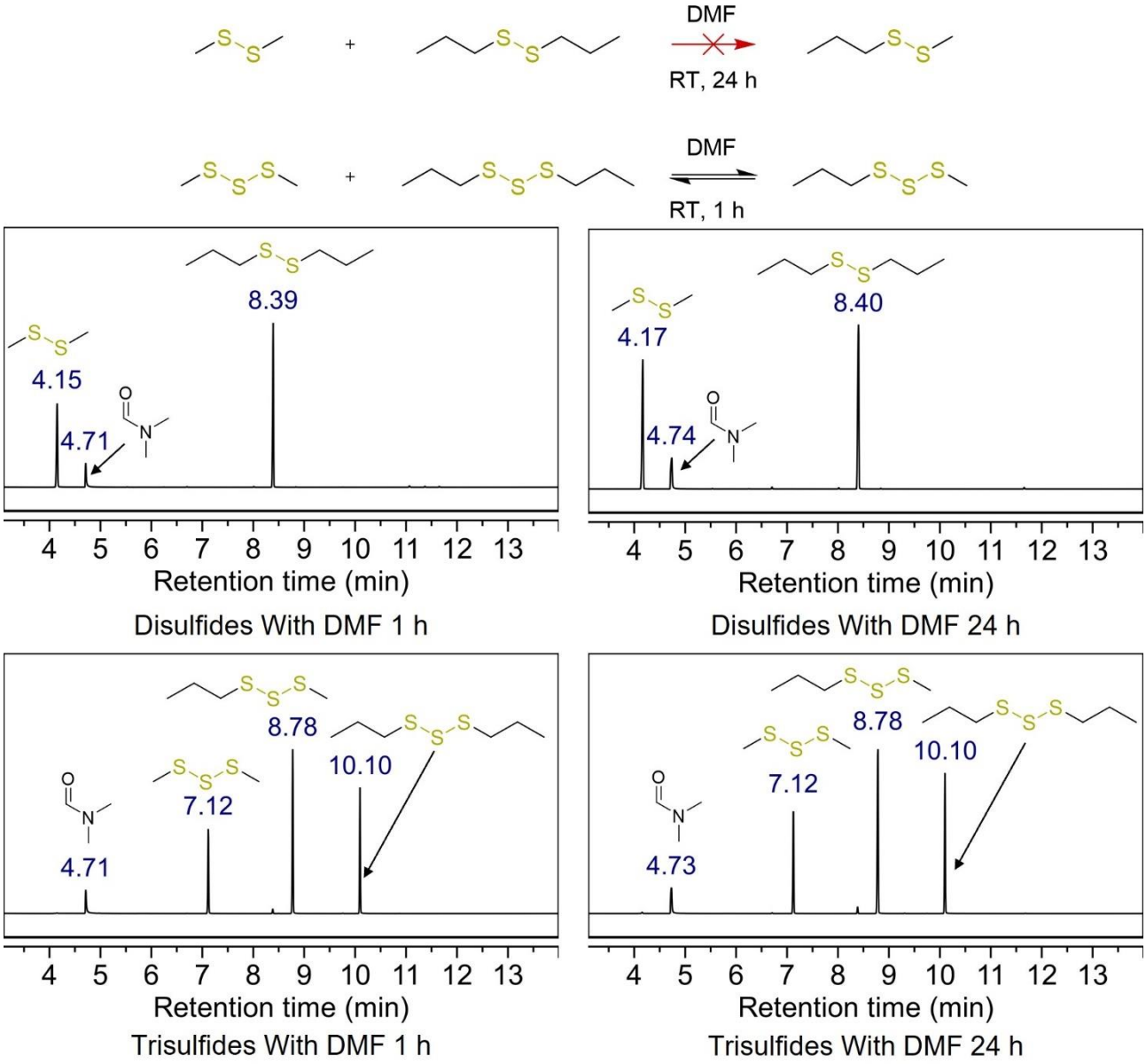

Figure 3.10: Reactions between dimethyl and dipropyl disulfide or trisulfide using DMF as a solvent. No reaction was observed over 24 hours at room temperature in the disulfides. The trisulfides showed a rapid reaction and the formation of methyl propyl trisulfide within an hour. There was no change in the ratio of the trisulfides after 24 hours.

Like DMF, a rapid reaction is seen in the trisulfides when DMA is used as a solvent. Again, there was no reaction in the disulfides. This confirms that this reaction is not unique to DMF and can occur in other solvents. The reaction appears to have already reached equilibrium after an hour so like DMF, the reaction is very quick.

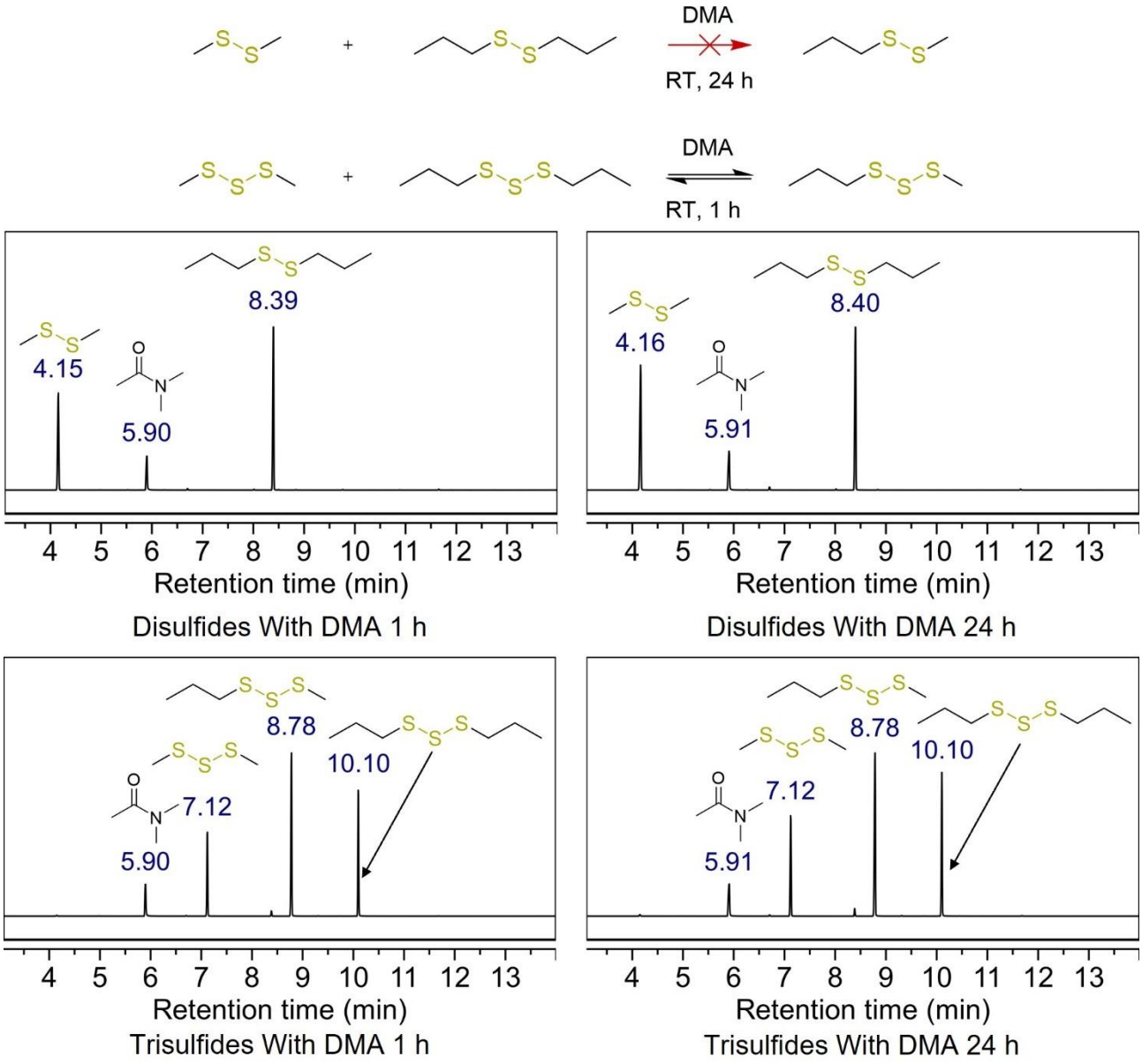

Figure 3.11: Reactions between dimethyl and dipropyl disulfide or trisulfide using DMA as a solvent. No reaction was observed over 24 hours at room temperature in the disulfides. The trisulfides showed a rapid reaction and the formation of methyl propyl trisulfide within an hour. There was no change in the ratio of the trisulfides after 24 hours.

The same trends were observed when NMP was used as the solvent. There was no reaction in the disulfides but a rapid reaction in the trisulfides which did not consume the NMP. NMP has a slighly different structure to DMF or DMA but is still polar and nucleophilic and shows the same trends.

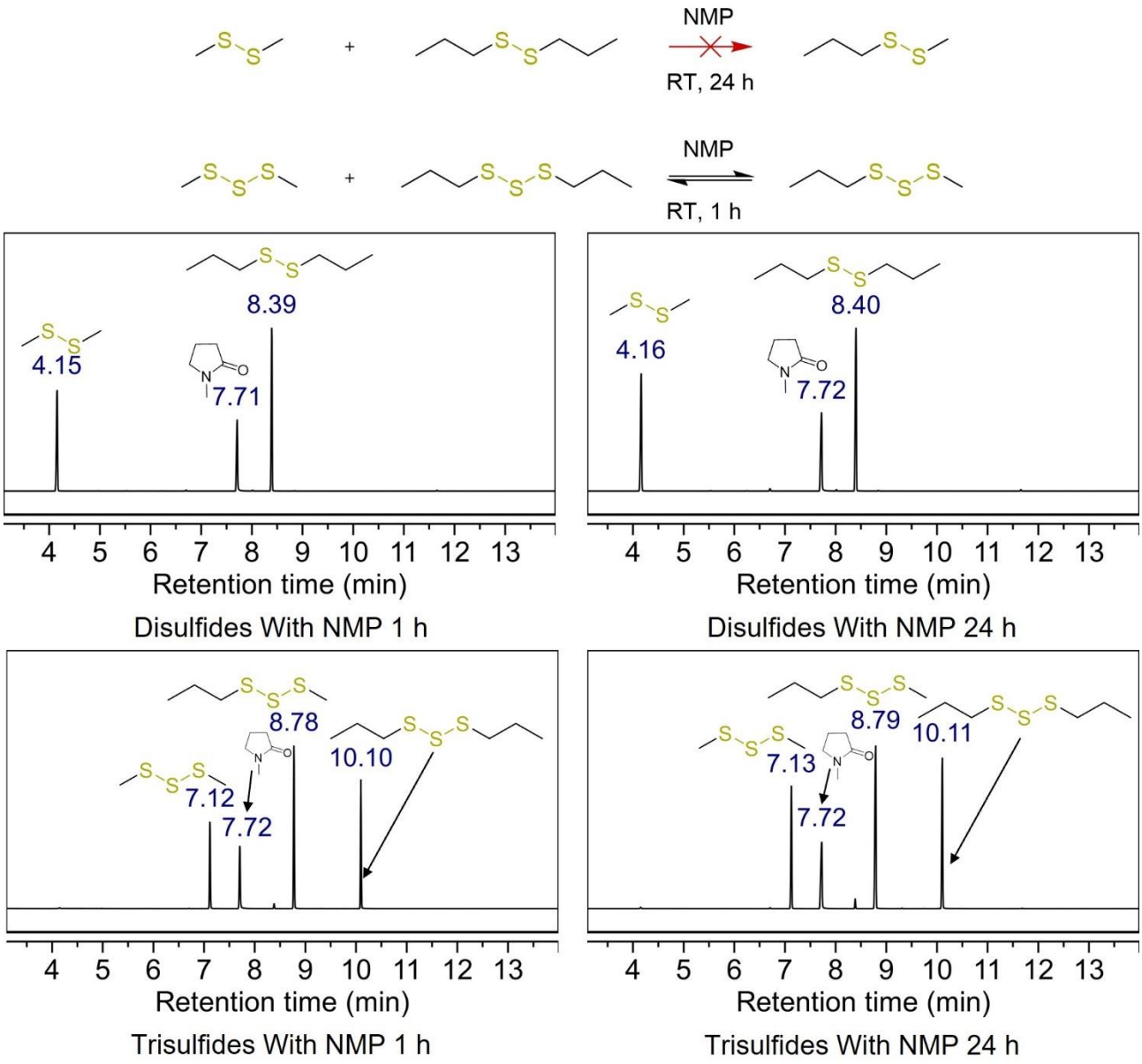

Figure 3.12: Reactions between dimethyl and dipropyl disulfide or trisulfide using NMP as a solvent. No reaction was observed over 24 hours at room temperature in the disulfides. The trisulfides showed a rapid reaction and the formation of methyl propyl trisulfide within an hour. There was no change in the ratio of the trisulfides after 24 hours.

When THF was added instead of DMF, DMA or NMP, the reaction proceeded differently. With disulfides, there was again no reaction. In the reaction with trisulfides, there was no significant reaction within an hour but after 24 hours, there was a considerable amount of the cross over product formed. This indicates that a reaction could occur but was much slower than with DMF, DMA or NMP. The products do not appear to be at equilibrium after 24 hours in this reaction as the methyl propyl trisulfide peak is much smaller than the other trisulfides. This indicates that the reaction may take several days to reach an equilibrium. These results are important as THF is not nucleophilic like the other solvents used. This indicates that non nucleophilic solvents can induce a reaction, but it is much slower. THF could not be resolved due to its high volatility and similar retention time to chloroform.

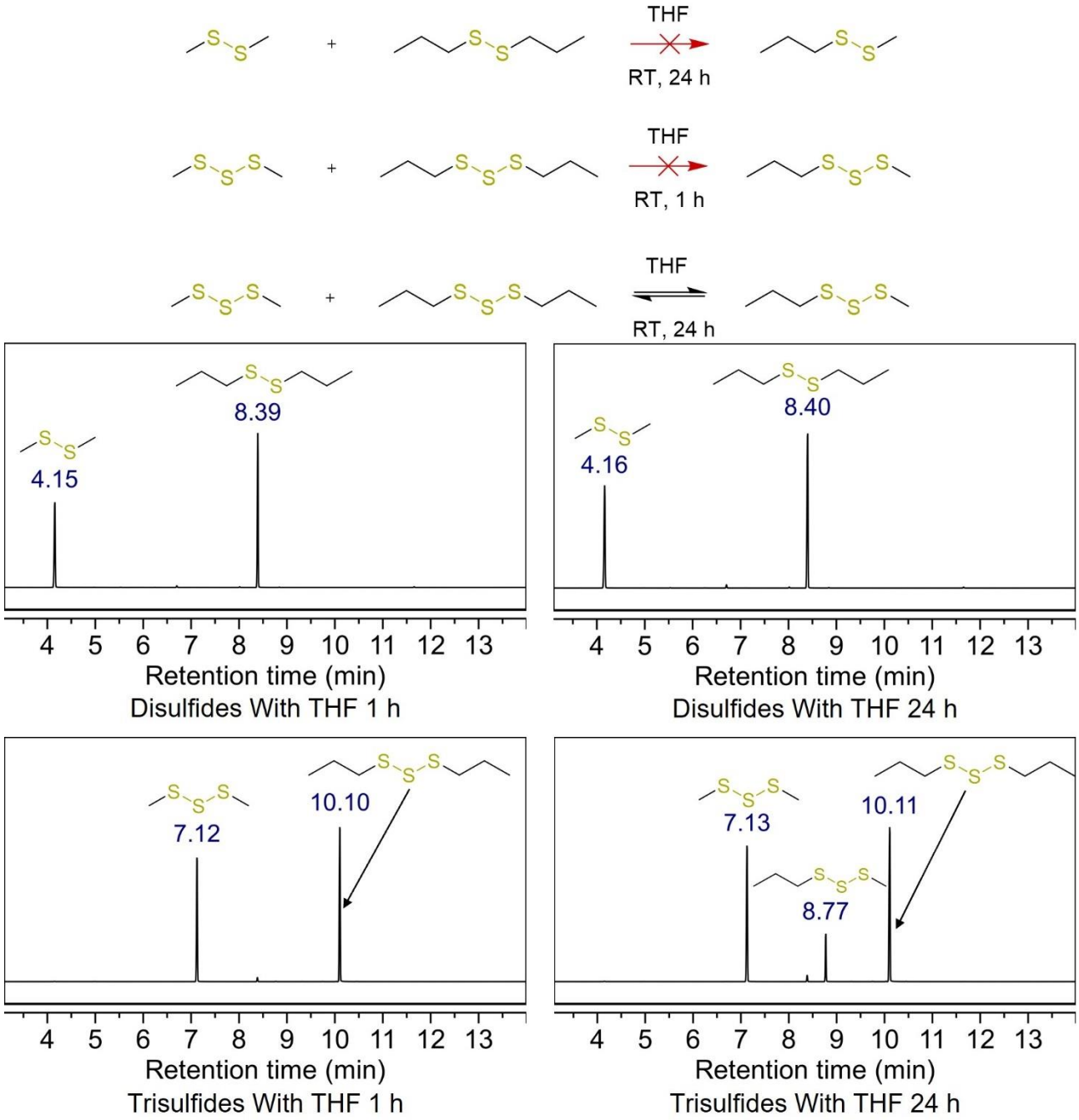

Figure 3.13: Reactions between dimethyl and dipropyl disulfide or trisulfide using THF as a solvent. No reaction was observed over 24 hours at room temperature in the disulfides. The trisulfides showed no reaction after an hour. After 24 hours, there was some formation of methyl propyl trisulfide, indicating a very slow reaction at room temperature.

After seeing the results of the trisulfide model system, it was clear that a reaction was taking place. However, the mechanism for this reaction was unclear. To test if a radical reaction was occurring, the same reactions were repeated but with a small amount (10 mol %) of (2,2,6,6-tetramethylpiperidin-1-yl)oxyl (TEMPO) added. The stabilised radical on TEMPO would quench any radical that may be formed during the metathesis reaction. This would significantly reduce the rate of reactions involving radicals as they will be quenched shortly after being formed. If DMF or the other solvents were inducing or stabilising a radical reaction, a significant decrease in the amount of methyl propyl trisulfide would be expected when TEMPO is added. However, if the mechanism was ionic, there would only a small change in the rate of methyl propyl trisulfide formation.

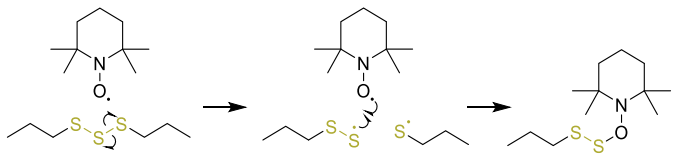

Figure 3.14: Potential mechanism for TEMPO quenching radical metathesis reaction in trisulfides.

The same method as described earlier was used with the only change being that 0.12 mmol (10 mol %) of TEMPO was first added to the reaction tubes before any reactants were added. All samples were again tested by GC-MS using the same method as the experiments without TEMPO.

As expected, when the reaction was done neat with TEMPO, there was no reaction in either the di or trisulfides after 24 hours at room temperature. The TEMPO was not consumed in the reaction. This indicates that TEMPO does not induce a metathesis reaction in either the di or trisulfides.

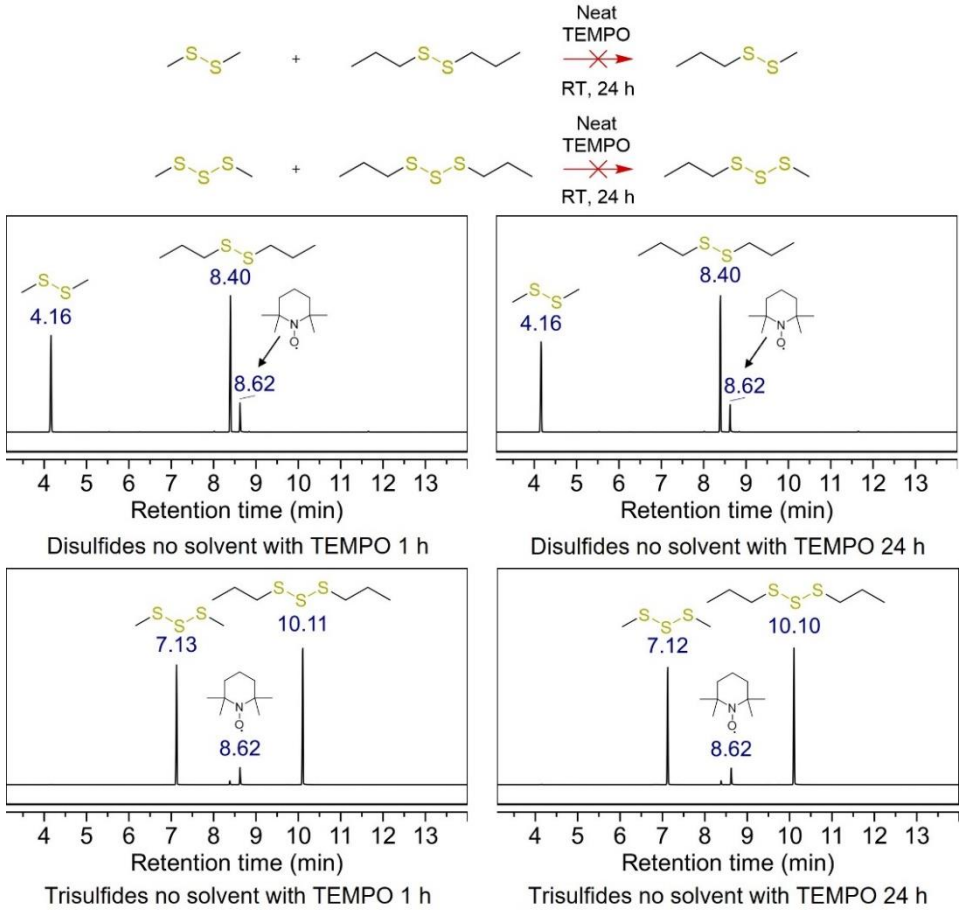

Figure 3.15: Reactions between dimethyl and dipropyl disulfide or trisulfide neat with 10 mol % TEMPO. No reaction was observed over 24 hours at room temperature.

When the reaction is done in DMF with TEMPO, there is no observed reaction in either the disulfides or trisulfides. This indicates that the TEMPO is preventing the reaction in the trisulfides, suggesting a radical mechanism. Another possibility is the TEMPO is participating in a redox reaction of some reactive intermediate.

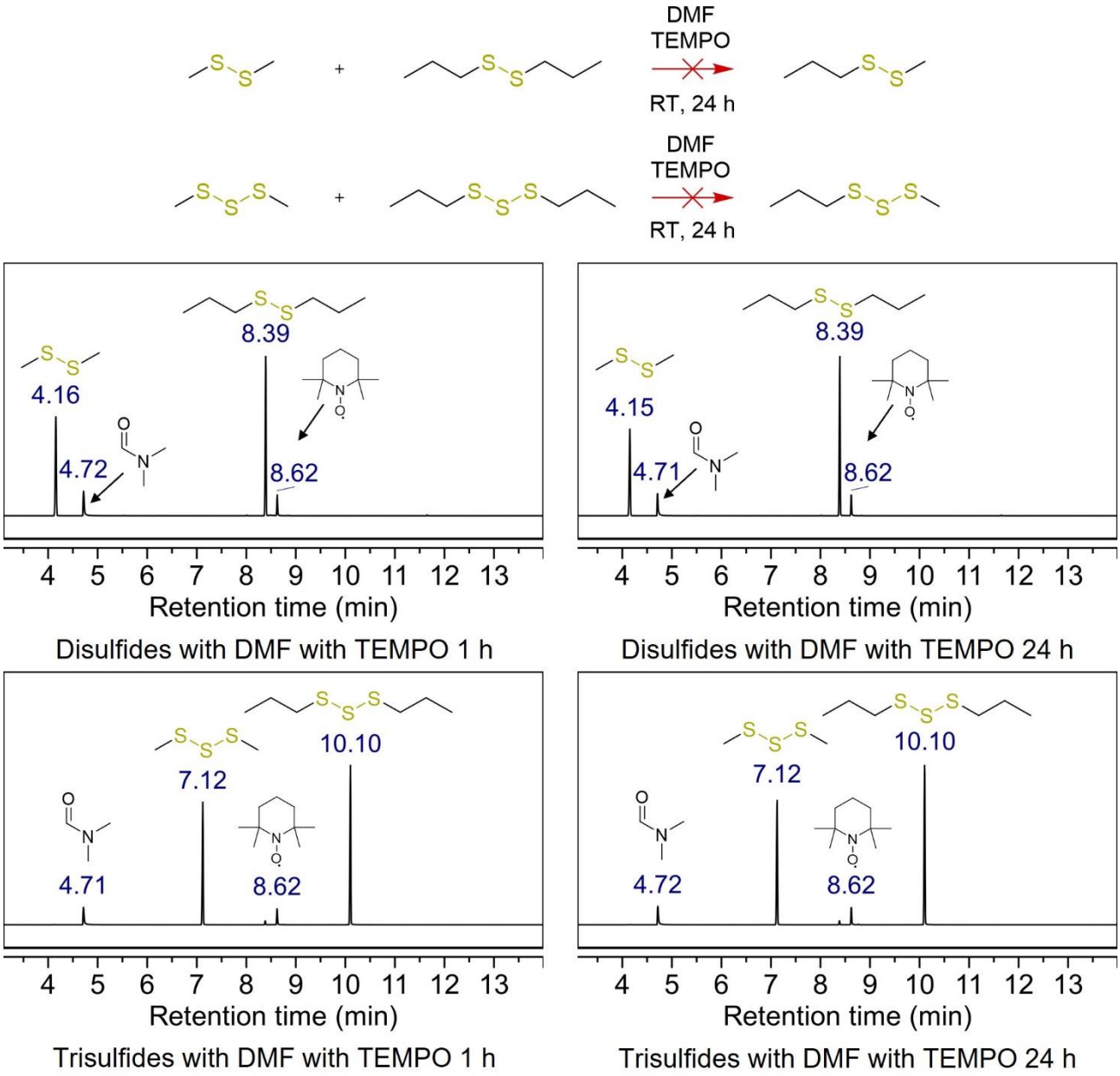

Figure 3.16: Reactions between dimethyl and dipropyl disulfide or trisulfide with 10 mol % TEMPO in DMF. No reaction was observed over 24 hours at room temperature.

Like DMF, there was no reaction in DMA when TEMPO was added. A very small peak can be seen at 8.77 minutes in the trisulfide reaction which does correspond to methyl propyl trisulfide. This potentially indicates that the reaction can still occur but is significantly reduced by the TEMPO.

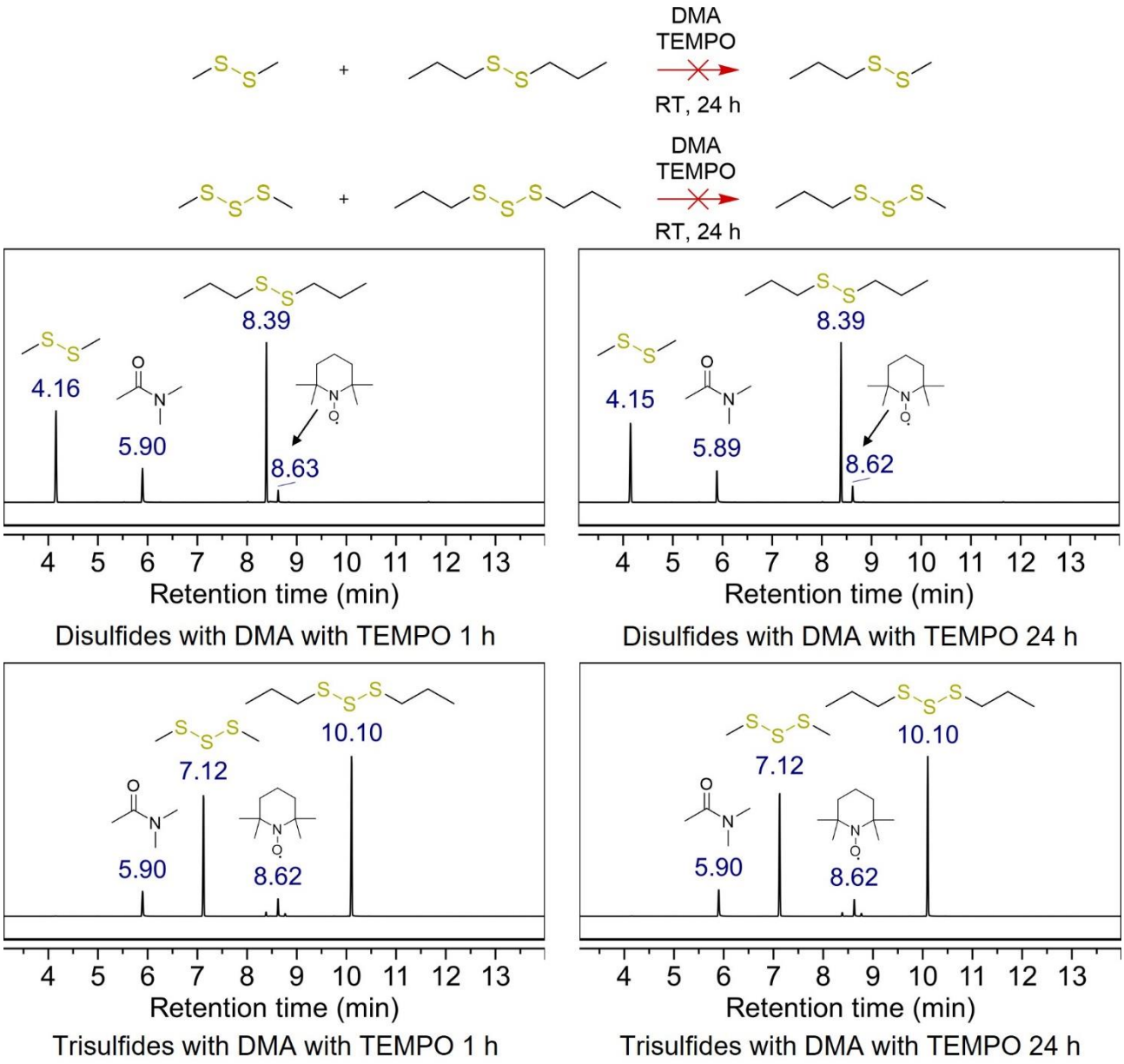

Figure 3.17: Reactions between dimethyl and dipropyl disulfide or trisulfide with 10 mol % TEMPO in DMA. No significant reaction was observed over 24 hours at room temperature.

In NMP, the reaction seemed very similar to DMA. A very small peak is observed at 8.77 minutes in the trisulfide reaction but the reaction is significantly slowed by the TEMPO.

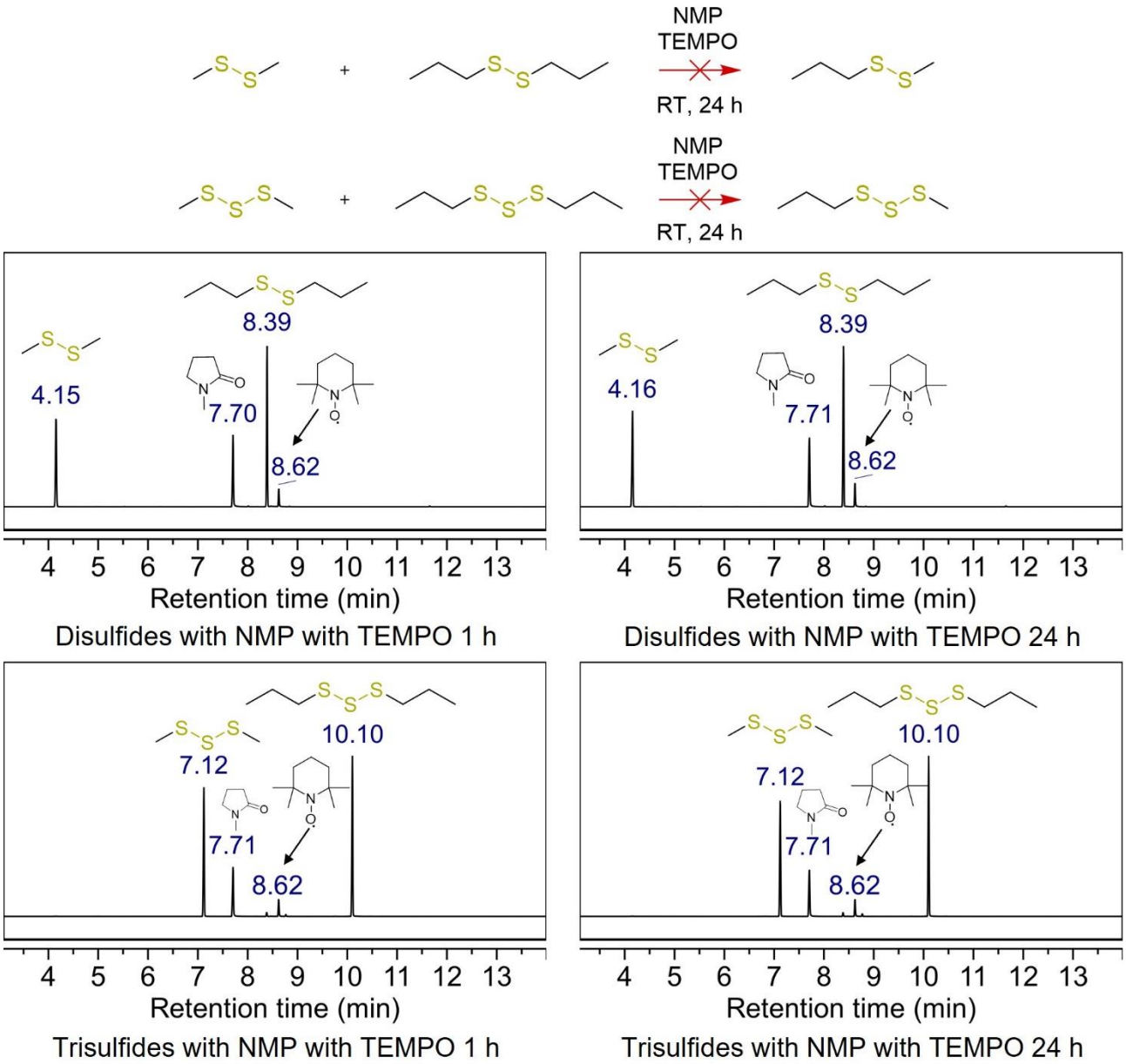

Figure 3.18: Reactions between dimethyl and dipropyl disulfide or trisulfide with 10 mol % TEMPO in NMP. No significant reaction was observed over 24 hours at room temperature.

When THF was used as a solvent, there was no reaction in either the disulfides or the trisulfides.

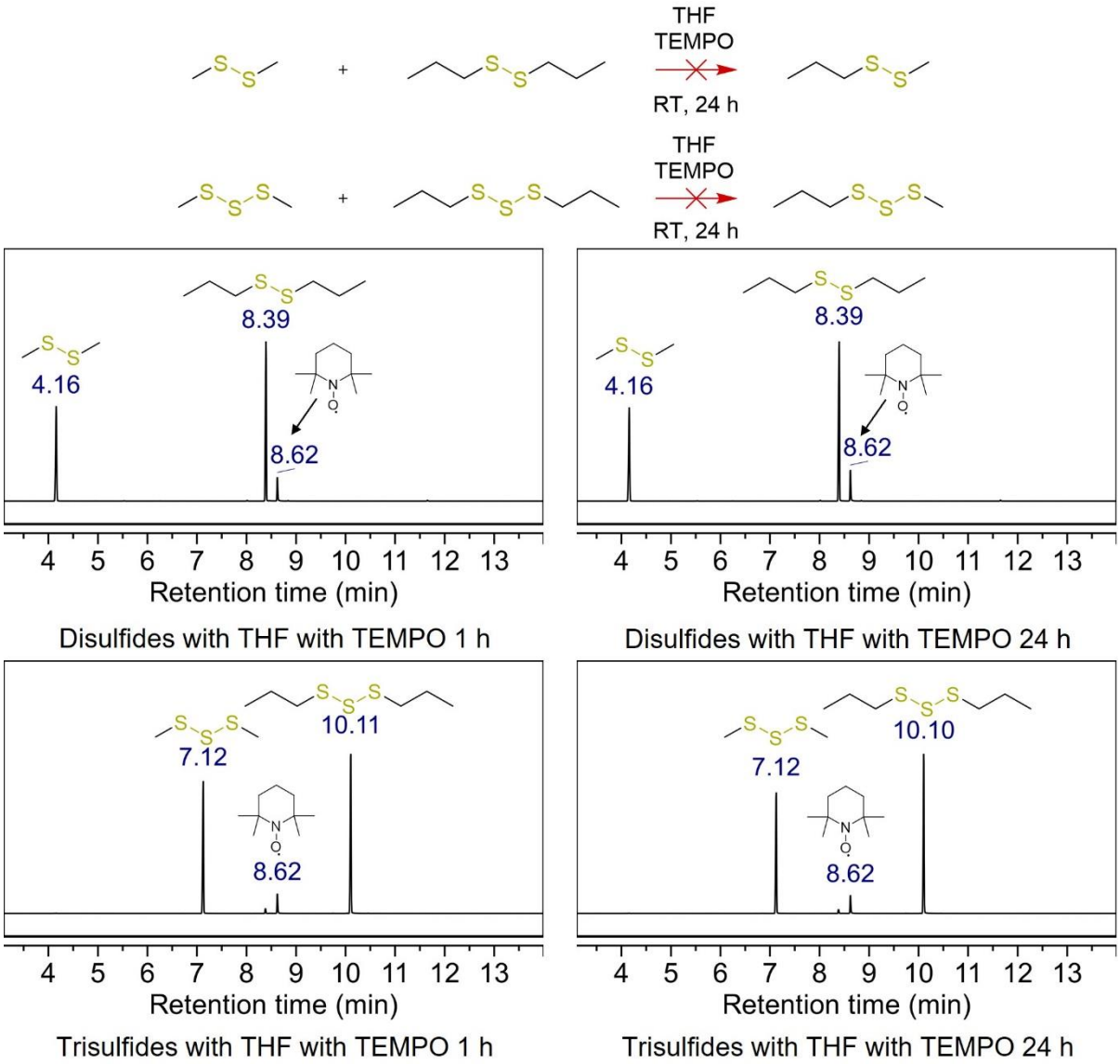

Figure 3.19: Reactions between dimethyl and dipropyl disulfide or trisulfide with 10 mol % TEMPO in THF. No significant reaction was observed over 24 hours at room temperature.

The di and trisulfide experiments show several key findings about the reactivity of sulfur-sulfur bonds. The trisulfide experiments show that DMF, DMA and NMP can induce a metathesis reaction in trisulfides. The formation of methyl propyl trisulfide indicates that sulfur-sulfur bonds were not only broken but new sulfur-sulfur bonds were formed. This occurred quickly as the three trisulfide products appeared to reach equilibrium within an hour for all these solvents. When the trisulfides were added neat, no reaction occurred, indicating that the solvent was required for a reaction to take place. The disulfide experiments had no reaction which shows that a sulfur rank of three or more is required for DMF, DMA or NMP to induce a reaction.

At first, it was believed that this reaction occurred by an anionic mechanism as THF did not induce a reaction within an hour while all the nucleophilic solvents showed a fast reaction. However, over 24 hours, THF did induce a trisulfide metathesis reaction. This indicates that it may be a mechanism that is stabilised by DMF, DMA or NMP and to a lesser extent by THF. The TEMPO experiments provide more evidence for a radical mechanism as trisulfide metathesis for all reactants was significantly reduced when TEMPO was added. However, it is likely that the mechanism is much more complicated than this and requires further testing.

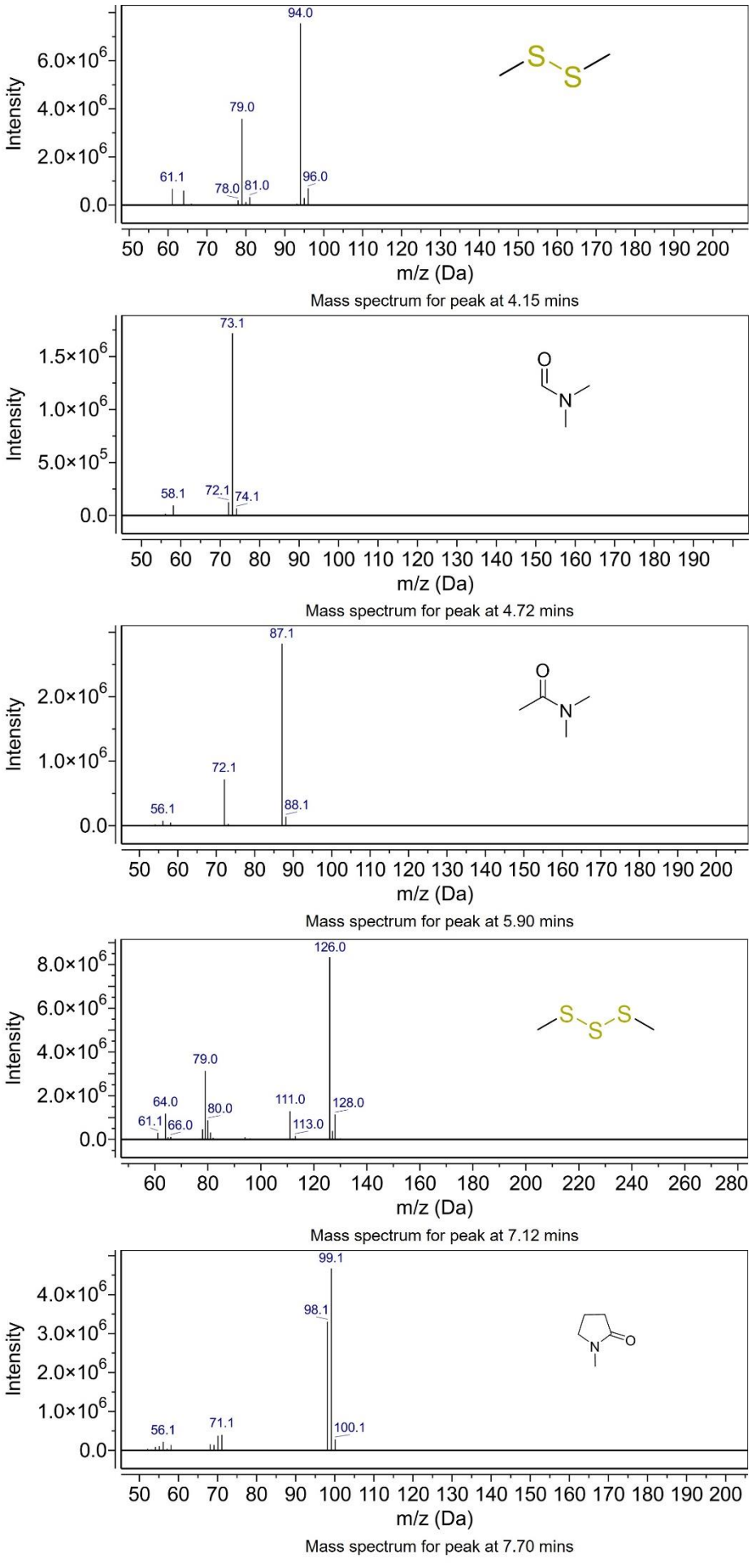

Figure 3.20: Mass spectra for di and trisulfide experiments.

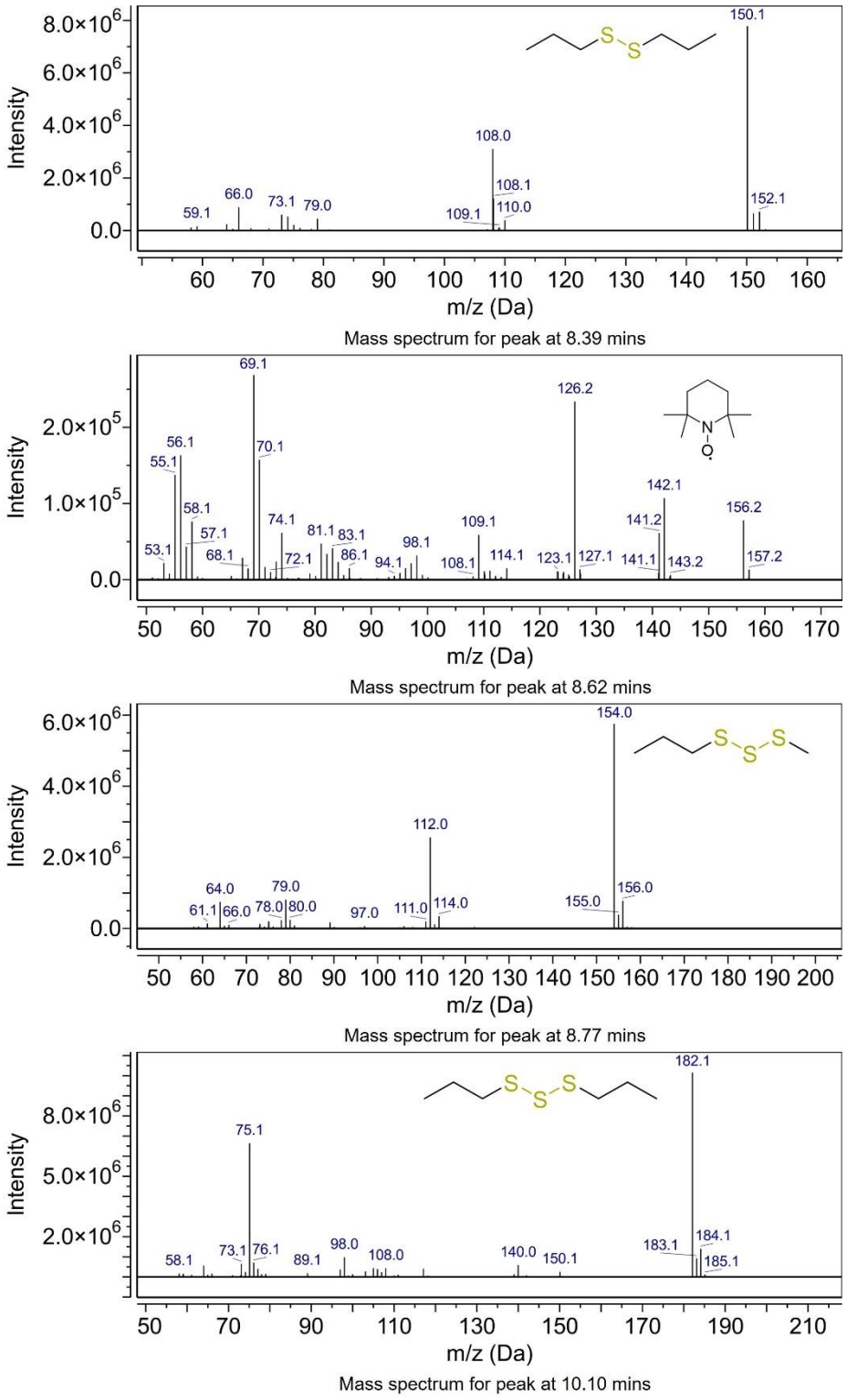

Figure 3.21: Mass spectra for di and trisulfide experiments.

Polymer synthesis in dimethylformamide

With the results of the model trisulfides in hand, it was believed that doing the reaction between norbornadiene and sulfur in dimethylformamide (DMF) would help to keep the molecular weight of the polymer low by constantly breaking and reforming any trisulfides in the polymer. This may prevent vitrification and prolong the reaction so that all of the norbornadiene could react. After the initial reaction, the DMF would then be removed and the polymer could be cured to give the crosslinked polymer.

The ratio of sulfur to DMF was found to be very important. If there was not enough DMF, the reaction would have a sulfur layer and a DMF layer. Due to the low solubility of sulfur in DMF, only a small portion of the sulfur would be dissolved in the DMF layers. As the reaction progressed, the sulfur layer would polymerise separetely to the dissolved sulfur. This would often lead to two distinct phases in the polymer, one from the DMF layer and the other from the sulfur layer.

To determine the appropriate ratio of sulfur to DMF, a range of reactions were performed with varying amounts of sulfur and DMF. The ratio of sulfur to DMF in these reactions varied from 3 g of sulfur and 1 mL of DMF to 0.5 g of sulfur and 10 mL of DMF. While the total amound of sulfur varied, all polymers had a sulfur composition of 58 % and were made using the same method which can be seen below.

Sulfur and DMF were added to a 21 mL vial and connected to a water-cooled condenser. The vial was lowered into a 140 °C oil bath and heated for 10 minutes with constant stirring provided by a magnetic stir bar. After 10 minutes, NBD was added down the condenser. The amount of NBD was calculated so all samples had a sulfur composition of 58 %. The samples were then left for a total of 90 minutes before being removed from heat. The DMF was then removed by rotary vacuum before being washed with water and lyophilised overnight. The samples were then added to a 140 °C oven for 24 hours to cure.

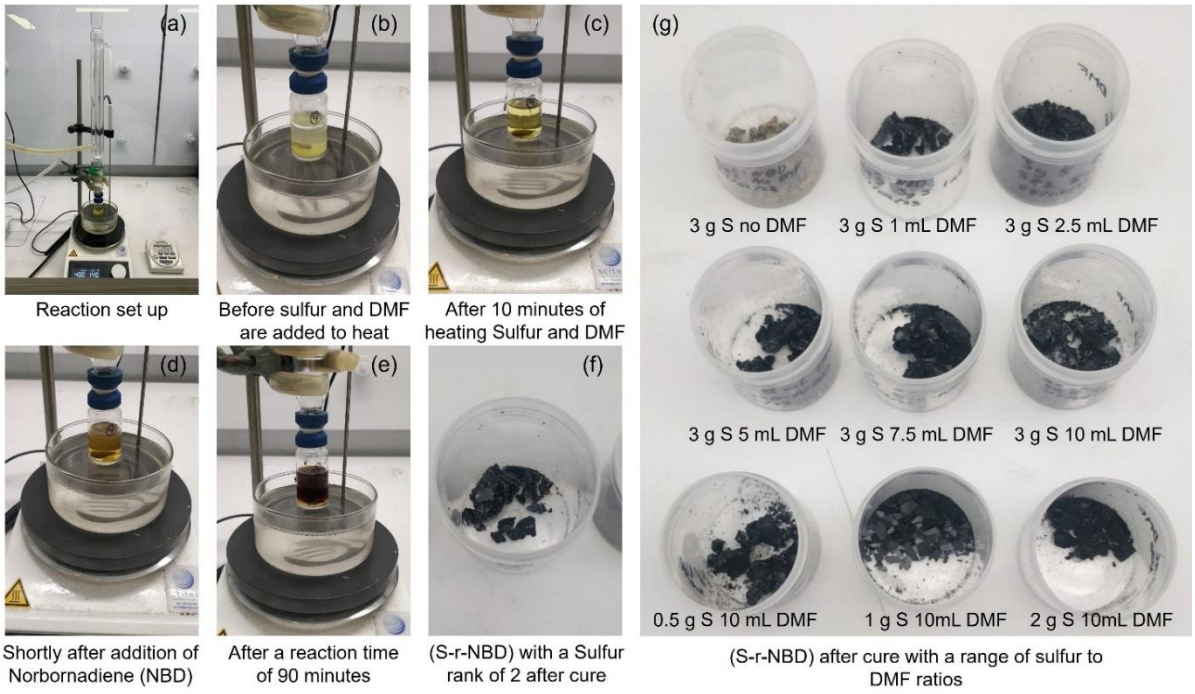

Figure 3.22: (a) Photo of reaction set up, (b) photo of sulfur and DMF before being added to 140 °C oil bath. (c) Photo of sulfur and DMF after heating for 10 minutes. (d) Photo of reaction after addition of NBD. (e) Photo of reaction after a total of 90 minutes heating. (f) Photo of polymer with a sulfur rank of 2 after cure at 140 °C for 24 hours. (g) Photo of polymers after cure with a range of sulfur to DMF ratios.

The samples with more than 3 g sulfur to 10 mL DMF had a very large sulfur layer which in some cases would vitrify and cease to stir. Only the samples with 1 g or less sulfur to 10 mL of DMF had no visible sulfur layer. In these samples, the sulfur would almost completely dissolve over ten minutes of heating at 140 °C. All samples were analysed by DSC and no crystalline sulfur was found in any sample with DMF. Every sample with DMF was distinctly different in appearance than the solventless reaction as they would all go black and had no yellow sulfur sections. The most consistent ratio of sulfur to DMF was found to be 1 g sulfur to 10 mL DMF as no precipitate was formed and no sulfur layer was present.

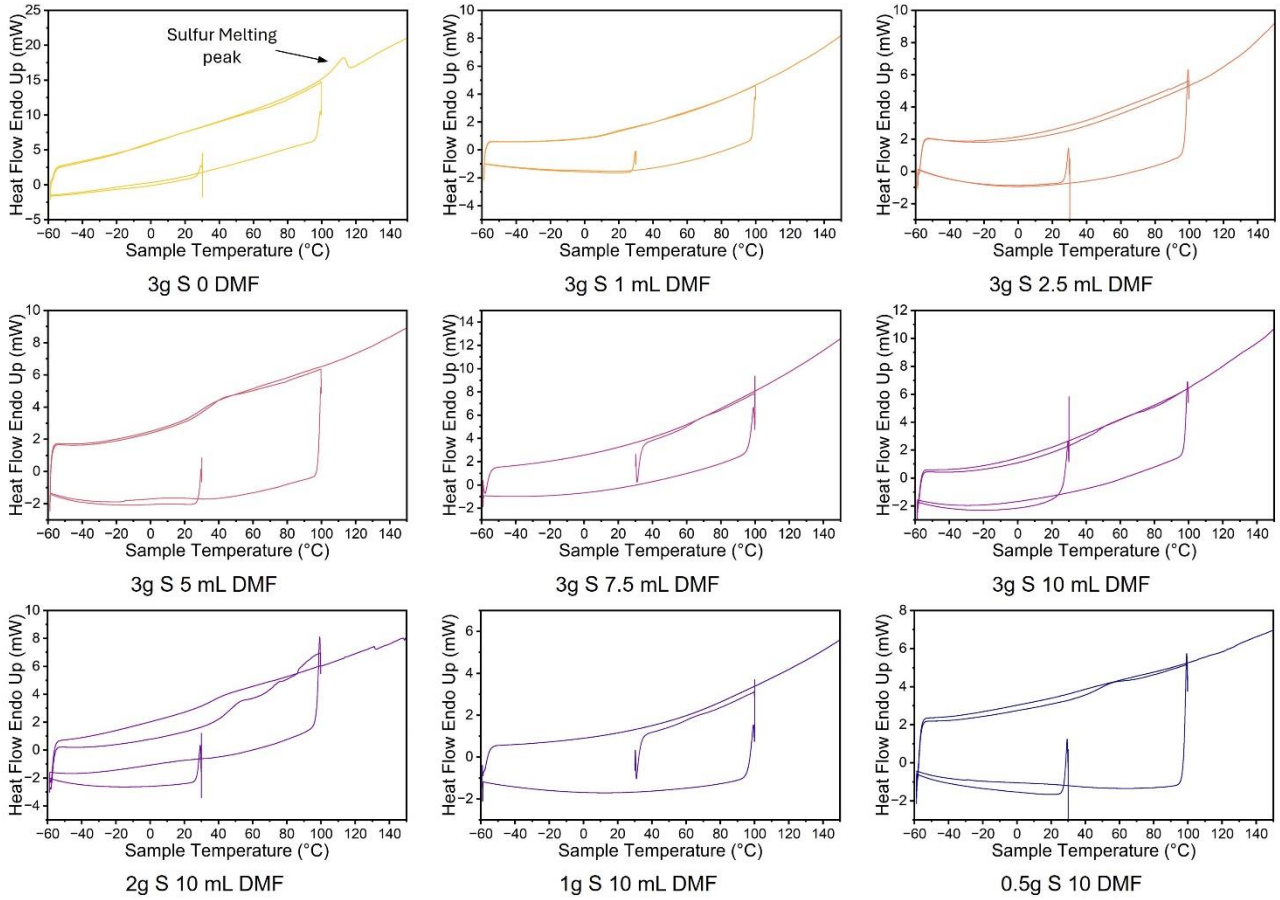

Figure 3.23: DSC chromatogram of polymers made from 58 % sulfur and 42 % NBD. All reactions apart from the top left used DMF as a solvent. The ratio of sulfur to DMF was varied for each sample.

NMR analysis of reaction in deuterated DMF

The DSC results indicated that there was no unreacted crystalline sulfur. However, it was still uncertain to what extent the alkenes in NBD have been consumed. Having an understanding of the rate of consumption of the NBD is important as this can be used to control how long the reaction is left for. To test the consumption of alkenes, the reaction was repeated in deuterated DMF using the ratio of sulfur to DMF which was determined to be most consistent.

To avoid using excess DMF, the reaction was scaled down by a factor of 10 to a DMF volume of 1 mL and sulfur mass of 100 mg. The same method was used to synthesise the polymer as described earlier. Three different reactions were run which were left for 30, 90 and 150 minutes respectively. After the time was reached, the reaction was removed from heat and allowed to cool. After cooling, a significant amount of precipitate was formed. The soluble portion was removed by pipette and added to a NMR tube. The sample was then analysed by proton NMR using a 600 MHz NMR to determine any changes in the NBD. It should be noted that only the soluble species will be present in the NMR.

After 30 minutes, there was still some NBD remaining which is most evident by the peak at 6.75 ppm. However, there are a range of new peaks between 4 and 5 ppm and below 3 ppm which were not present before the reaction. These peaks potentially indicate some rearrangement of the norbornane core but more information is required to know for certain. Some new alkene peaks also form around 6.5 ppm. After 90 minutes, all peaks corresponding to NBD have almost dissapeared along with the alkene peaks at 6.5 ppm. This indicates close to complete consumption of all alkenes in the reaction. There is very little change between 90 and 150 minutes apart from the alkene peaks reducing further. The information gathered from this experiment indicates that the reaction should be left for atleast 90 minutes before being cooled. While the polymer is cured after this point, it is important to ensure that all of the norbornadiene has been consumed as it will evaporate in the oven when curing.

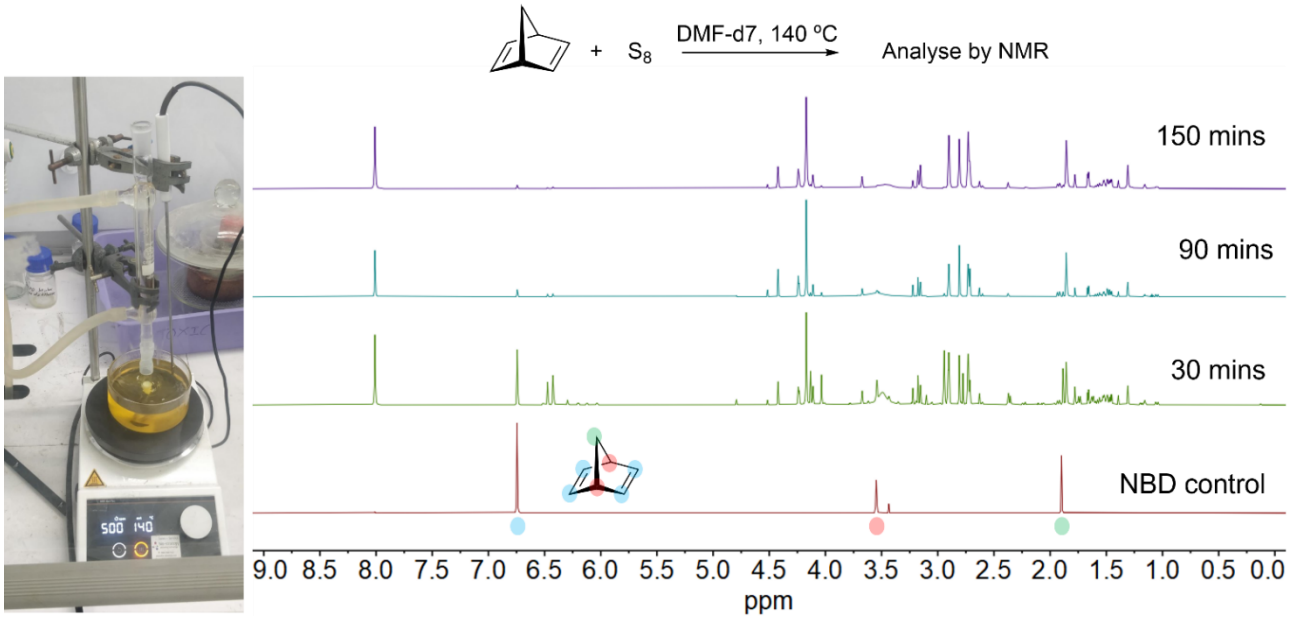

Figure 3.24: Proton NMR in deuterated DMF of a NBD control and the soluble portion of several reactions between sulfur and NBD. All reactions have a sulfur content of 58 % but were stopped after 30, 90 or 150 minutes.

Scaling up reaction in DMF and phase separation of polymer

While a reaction could be performed when using DMF as a solvent, it was found that the reaction was very prone to precipitation of a high sulfur material. This issue was most noticeable when scaling up the reaction. The reaction was scaled up to 5 grams of sulfur while maintaining the same ratio of sulfur to DMF. In this reaction, 50 mL of DMF was used with 5 g of sulfur (156.25 mmol S8). The scaled reaction was done in a 250 mL round bottomed flask. It was found that more time was required to allow the sulfur to dissolve in the DMF so the reaction was heated for 30 minutes before the NBD (7.2 g, 78.1 mmol, 7.93 mL) was added. After the addition of NBD, the reaction became cloudy before darkening over time. Due to the additional heating time at the start, the reaction was left for 120 minutes before removal from heat. The vial was then added to a rotary vacuum to remove most of the DMF. The remaining prepolymer was washed in water and lyophilised overnight. The prepolymer was then cured at 140 °C for 24 hours.

Despite using the optimised ratio of sulfur to DMF, a precipitate still formed over time in the reaction. This precipitate had a different colour and different properties to the soluble portion. The precipitate is believed to form because of the low solubility of the polymer in DMF so it will precipitate as soon as the reaction initiates. The polymer that is produced through this method has two distinct phases. One is formed from the precipitate and the other from the soluble portion. These polymer phases were both tested for elemental composition at the chemical analysis facility at Macquarie University using a Vario micro cube elemental analyser. For the polymer with a sulfur feed ratio of 58 %, the soluble portion was found to posses 62.6 % sulfur while the sulfur layer was found to posses 73.7 % sulfur. The precipitate had a very high sulfur content. This is likely due to the low solubility of sulfur in DMF. To address this, several other solvent systems were tested.

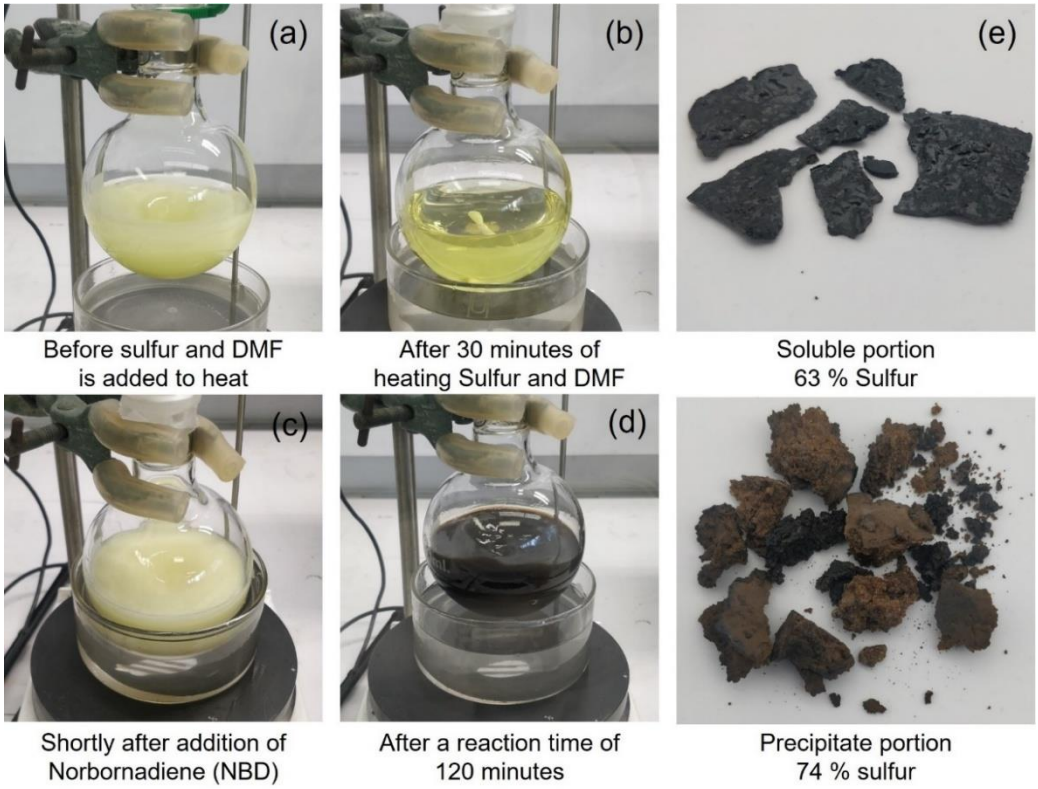

Figure 3.25: Scaled up reaction between sulfur and NBD in DMF. (a) Sulfur and DMF before being heated. (b) Sulfur and DMF after 30 minutes of heating at 140 °C. (c) Reaction after NBD is added. (d) Reaction after 120 minutes of heating. (e) Soluble and precipitate portion after reaction is completed and polymer is cured at 140 °C for 24 hours.

Polymer Synthesis in tetrachloroethylene

The reactions using DMF as a solvent were successful in preparing a polymer. However, when sulfur has poor solubility in the solvent, it can lead to precipitation and inhomogeneity of the polymers. To address this, two additional solvents were tested. The additional solvents were tetrachloroethylene (TCE) and xylenes. These solvents were selected as they can readily dissolve sulfur and they have a boiling point which is high enough to accommodate the reaction but can still be removed by rotary evaporation. Tetrachloroethylene is also nonflammable which is important as inverse vulcanization reactions are exothermic and can be very dangerous.

Tetracholoethylene does have an alkene so it is important to test if this alkene can react with sulfur. To confirm if the tetrachloroethylene can react with sulfur, several control experiments were performed where the tetrachloroethylene acts as a reactant in a typical inverse vulcanization reaction. These experiments used molten sulfur as the solvent and a ratio of two sulfur atoms for every tetrachloroethlene molecule. Two temperatures were tested, 120 °C and 170 °C. The reaction at 120 °C is below the boiling point of tetrachloroethlyene (bp: 121.1 °C) so the reaction was completely liquid. The reaction at 170 °C had molten sulfur with refluxing tetrachloroethylene like the reactions with cyclopentadiene in chapter 2 or the solventless reaction with NBD earlier in this chapter. The reaction at 170 °C is above the floor temperature of sulfur so it would be expected that there would be sulfur radicals formed. The reactions were also performed using 1 wt % zinc diethyldithiocarbamate. This is a commonly used catalyst in inverse vulcanization reactions[10]. If no reaction is observed under these conditions then it is very unlikely that sulfur and tetrachloroethylene have any reactivity.

Sulfur (3g, 93.75 mmol S atoms) and Tetrachloroethylene (7.77 g, 46.9 mmol) were added to a 21 ml vial. Two vials with the same masses of sulfur and tetrachloroethylene were measured out. 1 wt% of zinc diethyldithiocarbamate (108.8 mg) was added to one of the vials. A reflux condenser was added to each vial and they were heated to 120 °C with constant stirring. The vials were left heating and stirring for 24 hours before being removed. This same procedure was repeated at 170 °C. The sulfur dissolved in the tetrachloroethylene but no change in colour occurred. There was no visible change in the reaction over the 24-hour period.

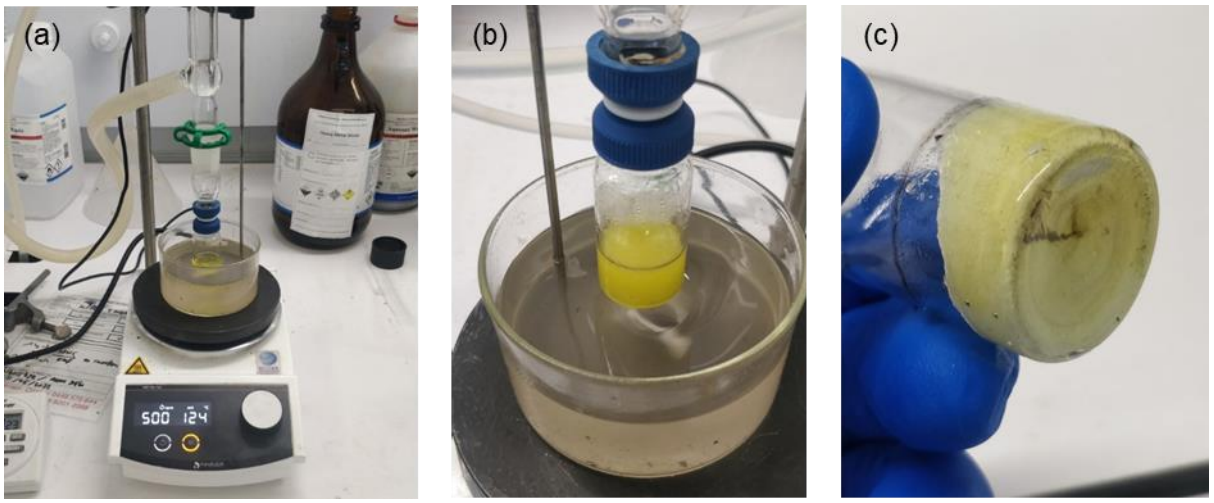

Figure 3.26: Pictures showing reaction between sulfur and tetrachloroethylene (a) reaction set up. (b) Solution during reaction. (c) After removal from heat and cooling.

After heating, a small part of the solution was poured into a silicone mould and added to an oven at 140 °C for 24 hours. The rest of the solution was left to cool. The parts that were cured had the appearance of sulfur but the samples that used zinc diethyldithiocarbamate were slightly darker. To determine how much unreacted sulfur was in the samples, they were ground into a powder and 50 mg was weighed out. 10 mL of toluene was added to each sample, and they were sonicated at 50 °C for 45 minutes. This would dissolve the sulfur and leave any high molecular weight polymers unreacted. The solution was then filtered, and the mass of any undissolved species was measured. Both the solutions with no catalyst had no undissolved species, indicating it consisted of only sulfur or very low molecular weight oligomers. The solutions with catalysts only had a maximum of 2.36 % undissolved species which is believed to be made up of mostly the catalyst. This method was adapted from a method first described by the Hasell group[11].

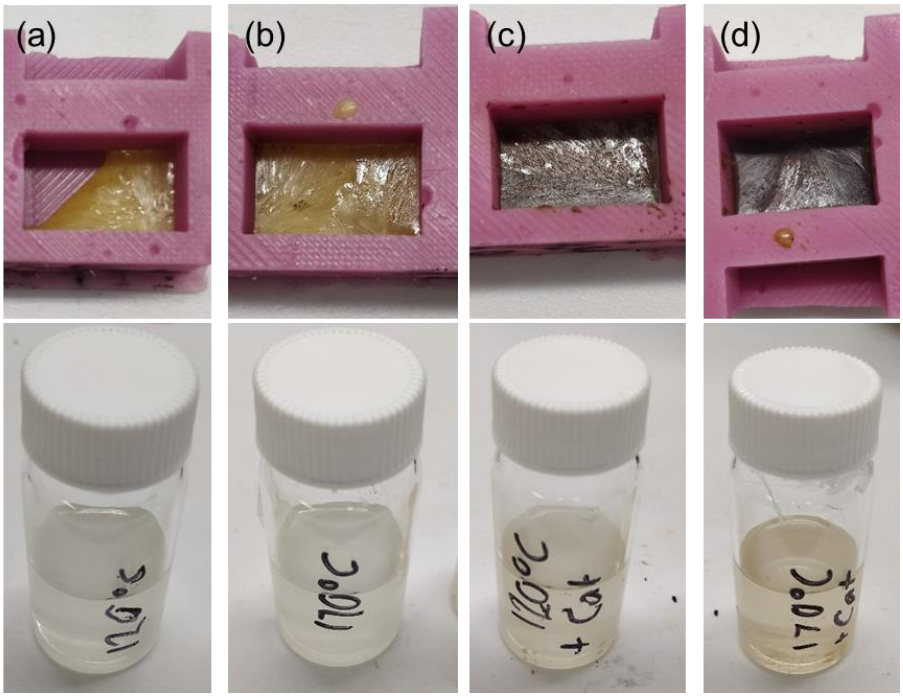

Figure 3.27: (top row) Images of cured samples of cured material from reaction between sulfur and TCE. (bottom row) Images of 50 mg of material in 10 mL of toluene. (a) 120 °C for 24 hours. (b) 170 °C for 24 hours. (c) 120 °C for 24 hours with 1 wt% of zinc diethyldithiocarbamate. (d) 170 °C for 24 hours with 1 wt% of zinc diethyldithiocarbamate.

Before being cured, an aliquot was removed from each sample. These aliquots were filtered and analysed by GC-MS. Every sample showed only Tetrachloroethylene, indicating tetrachloroethylene does not react with sulfur under the conditions used for the reaction. An injection volume of 1 µL was used with a split ratio of 60:1. A 29.4 m x 250 µm x 0.25 µm, 5% Phenyl Methyl Silox column was used with a constant flow of 1.2 mL/min helium. An initial oven temperature of 40 °C was used which was held for 3 minutes. The temperature was then increased at 50 °C/min to 250 °C where it was held for 12.8 minutes to complete the run.

These experiments indicate that tetrachloroethylene does not form any polymeric material when reacted with sulfur and the tetrachloroethylene molecule itself is unchanged.

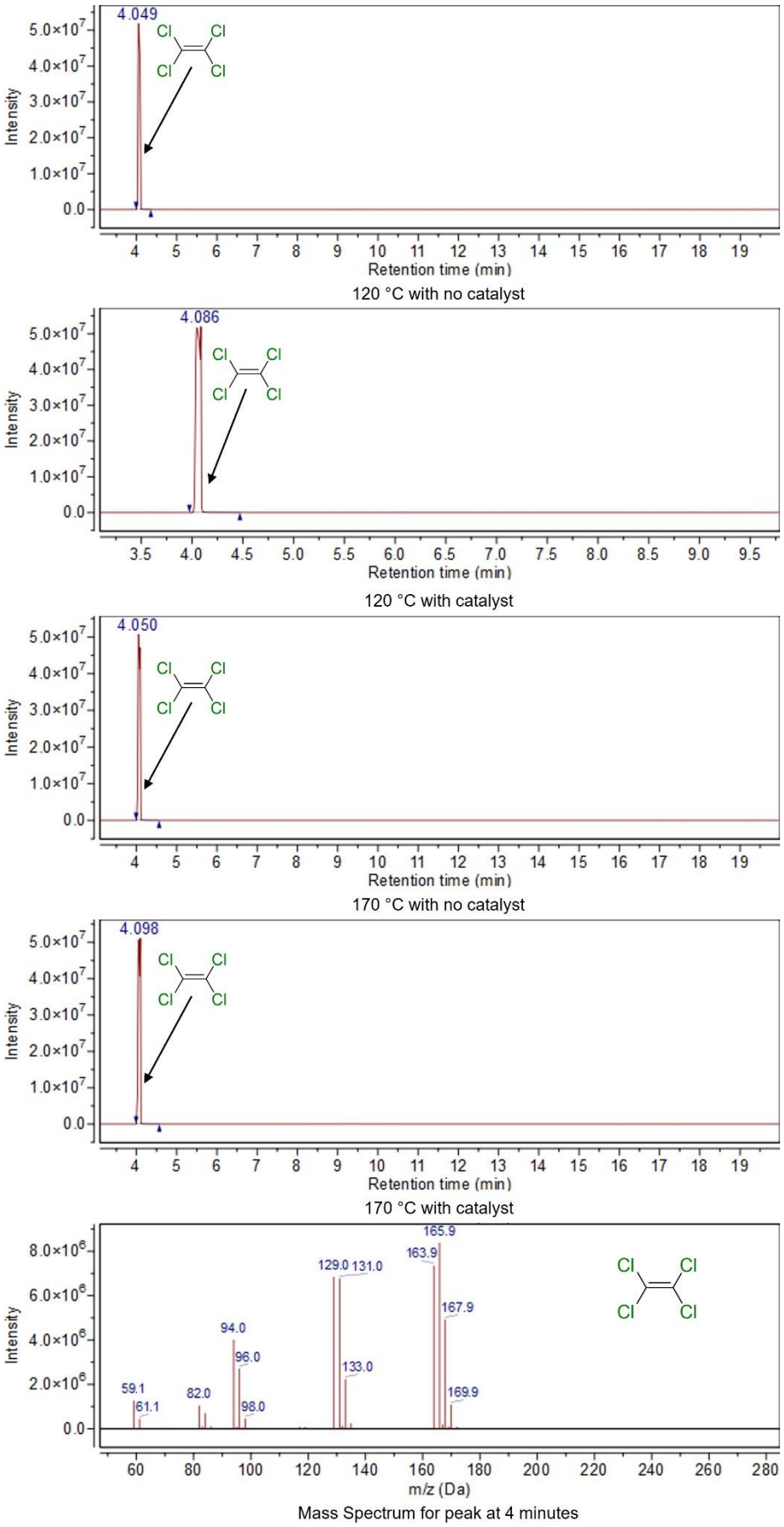

Figure 3.28: GC-MS chromatograms for reaction between tetrachloroethylene and sulfur. All reactions were done for 24 hours at either 120 °C or 170 °C. Two samples used 1 wt% of zinc diethyldithiocarbamate as a catalyst. Mass spectrum for peak at 4 minutes is shown.

With the control experiments completed, the reaction between norbornadiene and sulfur in TCE was attempted. The reaction was also performed using a mixed solvent system of DMF and TCE in a 50:50 ratio. This was to test if using DMF can alter the properties of the polymer as it is known to cause trisulfide metathesis in trisulfide model systems. For the reactions with a mixed solvent system, the same total volume was used but was made up of both solvents.

Sulfur is much more soluble in TCE than DMF, particularly at high temperatures. This allowed for 1 gram of sulfur to be used for 10 mL of TCE without any undissolved sulfur at 140 °C. Even when a mixture of the two solvents was used, the sulfur would be completely soluble at 140 °C. Sulfur (1 g, 31.2 mmol S atoms) was added into a 21 mL vial with 10 mL of TCE or 10 mL of 50-50 TCE-DMF. The vial was attached to a water cooled reflux condenser and lowered into a 140 °C oil bath. The reaction was heated for 10 minutes with constant stirring provided by a magnetic stirring bar. Over this time, the sulfur completely dissolved, giving a yellow solution. After heating for 10 minutes, NBD (0.72 g, 7.81 mmol, 0.79 mL) was added through the top of the reflux condenser using a volumetric pipette. The volume of NBD was calculated to give a polymer with 58 % sulfur. The reaction was heated for an additional 80 minutes and slightly darkened over this time to a brown colour. When using a mixed solvent of DMF and TCE, the soltion becamse much darker over the course of the reaction but there was not precipitation, even after 80 minutes of heating. After removal from heat, the TCE was removed by rotary vacuum. The prepolymer was then washed thorougly in water before being lyophilised overnight. The prepolymer was transferred into a silicone mould and added to a 140 °C oven for 24 hours to cure. After curing, the polymer took on the appearance of an orange, slightly transparent material when TCE was used as a solvent. When a mixed solvent was used, the material was significantly darker but had an orange colour when thin.

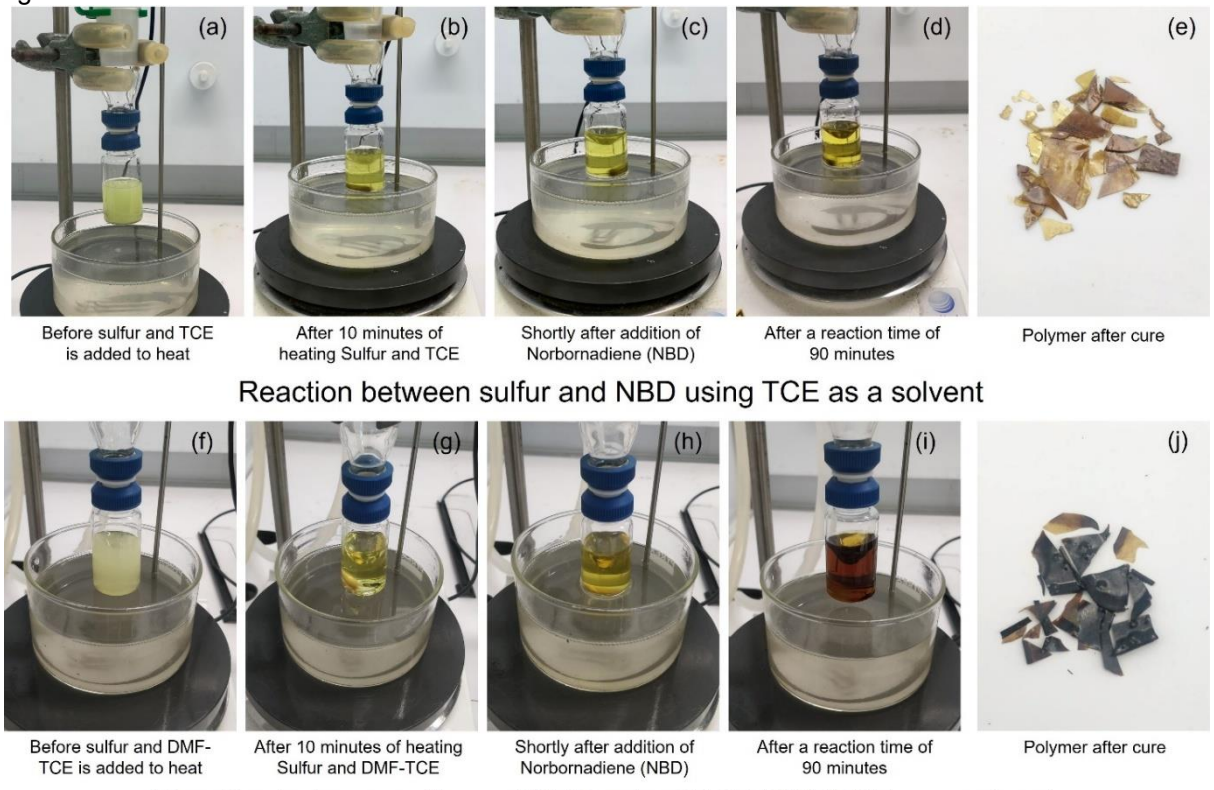

Figure 3.29:Reactions between sulfur and NBD using Tetrachloroethylene as a solvent. Both reactions used 58 % sulfur. (a-e) Reactions only using TCE as a solvent. (f-j) Reactions using 50-50 DMF-TCE as a solvent.

Polymer synthesis in xylenes

The next solvent that was tested was xylene. The advantage of using xylene as a solvent is that it has a high solubility for sulfur, particularly at high temperatures but it also has a boiling point around 140 °C. This prevents any refluxing of the solvent as the reaction progresses. Like in the reaction with TCE, two reactions were performed, one with only xylenes as a solvent and one with 50-50 DMF-xylenes as a solvent.

The xylenes used in these reactions were a mix of the ortho, meta and para isomers in a 32:100:24 ratio as analysed by GC. The xylenes were tested using the following GC-MS method. An injection volume of 1 µL was used with a split ratio of 60:1. A 29.4 m x 250 µm x 0.25 µm, 5% Phenyl Methyl Silox column was used with a constant flow of 1.2 mL/min helium. An initial oven temperature of 40 °C was used which was held for 3 minutes. The temperature was then increased at 20 °C/min to 140 °C to complete the run.

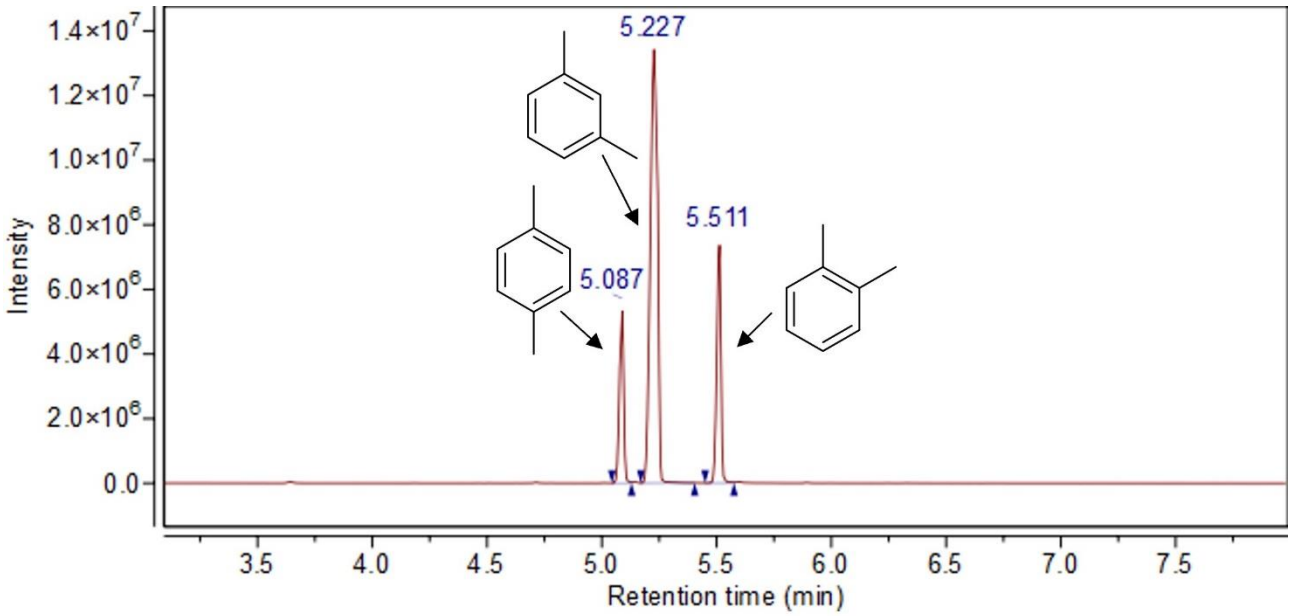

Peak	Start	RT	End	Height	Area	Area %
1	5.05	5.09	5.13	5.33×10^6	7.14×10^6	24.2
2	5.17	5.23	5.37	1.34×10^7	2.95×10^7	100
3	5.467	5.513	5.582	7.36×10^6	9.3×10^6	32

Figure 3.30: GC-MS chromatogram of xylene solvent used in reaction between sulfur and NBD. Analysis was performed on an Agilent single quadrupole GC-MS. Integration peak list was exported from Agilent MassHunter software.

Sulfur (1 g, 3.9mmol S8) was added to a 21 mL vial with 10 mL of xylene or 10 mL of 50-50 xylene-DMF. The vial was attached to a water cooled reflux condenser and lowered into a 140 °C oil bath. The vial was heated for 10 minutes with constant stirring provided by a magnetic stirring bar. Over this time, the sulfur completely dissolved, giving a yellow solution. After heating for 10 minutes, NBD (0.72 g, 7.81 mmol, 0.79 mL) was added through the top of the reflux condenser using a volumetric pipette. The reaction was heated for an additional 80 minutes. The initially yellow solution slowly darkened over time but no precipitate formed. Like in the reactions using TCE as a solvent, the solution went much darker when DMF was included in the solvent system. The vial was then removed from heat and xylene was evaporated using a rotary evaporator. The prepolymer was then washed thorougly in water before being lypholised overnight. The prepolymer was then transferred into a silicone mould and added to a 140 °C oven for 24 hours to cure. The polymer material was brittle and dark brown. When thin, it was slightly transparent but more opaque than the reactions in TCE. The polymer sample made in a 50-50 xylene-DMF solvent system was much darker than when xylene was the only solvent.

The experiments using TCE or xylene as solvents were successful in eliminating the issue of polymer inhomogenuity. When these solvents were used, either as the only solvent or when mixed with DMF, there was no precipitation and the entire reaction was one phase. Due to this, the batch to batch consistency was greatly improved and the final polymer was consistent in structure.

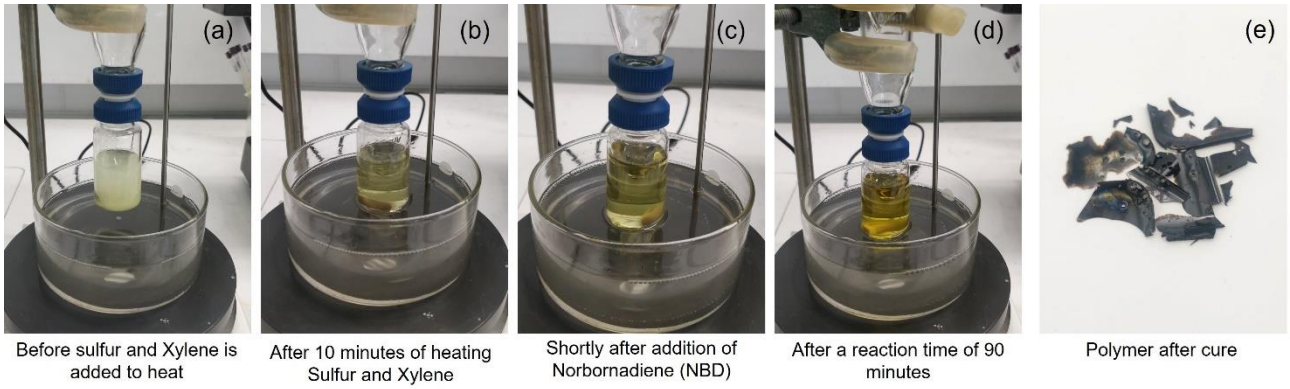

Figure 3.31:Reactions between sulfur and NBD using xylene as a solvent. Both reactions used 58 % sulfur. (a-e) Reactions only using xylene as a solvent. (f-j) Reactions using 50-50 DMF-xylene as a solvent.

Elemental analysis of polymers made in different solvents

At this point, a consistent method for producing a polymer from the reaction between sulfur and norbornadiene had been made. However, it was important to find which solvent system gives a polymer which was closest to what was desired. The feed ratio for every reaction had 58 % sulfur and 42 % norbornadiene. There were many factors that may result in a polymer with a different sulfur content to the feed ratio. If the reaction was not complete and there was still unreacted norbornadiene when the solvents were removed, the norbornadiene would also be removed. It is also possible that norbornadiene would be left on the glassware as it refluxes. These factors would both result in a greater sulfur content in the final polymer than the feed ratio. Each of the polymers prepared with different solvents were tested to find which was closest to the feed ratio.

Elemental analysis of the polymers prepared in different solvents was done at the chemical analysis facility at Macquire University using a Vario MICRO cube elemental analyser. Each of the polymers made from a reaction between sulfur and NBD in different solvents were tested in triplicate for CHNS analysis. The material made without any solvent was also tested. This sample was not homogeneous and was much darker near the top of the reaction than at this bottom due to poor mixing. For this reaction, samples were taken from the top and from the bottom to test homogeneity. For the reactions that used DMF as a solvent, three samples were taken. One was from the precipitate that formed from the sulfur layer of the scaled-up reaction, one from the soluble portion and one from the optimised reaction which had very little precipitate. While elemental analysis is usually accurate for carbon and hydrogen, the sulfur content in the polymers was far above the calibration standards used. Due to this extrapolation, there was some inconsistency in the values obtained and the data should only be considered as approximate.

As expected, the sulfur content of the material made from the solventless reaction varied greatly between the top and the bottom. The sample from the top of the reaction was only 42 % sulfur while the sample taken from the bottom was over 95 % sulfur. This indicates that the norbornadiene was not reaching to the bottom of the sulfur when stirring ceased. Elemental analysis confirmed that the polymers that were made using DMF/Xylene were closest to the feed ratio. When made using this solvent system, there were also no issues with precipitation so DMF/Xylene was selected as the best solvent system moving forward.

Table 3.1: Elemental analysis for polymers made from a reaction between sulfur and norbornadiene. All reactions had the same feed ratio of 58 % sulfur. Elemental analysis was performed at the chemical analysis facility at Macquire University.

Sample	Carbon (%)	Hydrogen (%)	Sulfur (%)
Feed ratio	38.3	3.7	58
No Solvent top	52.9	5.0	42.1
No solvent bottom	4.1	0.39	95.5
DMF Precipitate	23.9	2.3	73.7
DMF soluble	33.9	3.5	62.6
DMF optimised	31.9	3.1	65.1
Xylene	18.6	1.7	79.6
DMF/Xylene	32.5	3.3	64.2
TCE	10.6	0.96	88.5
DMF/TCE	24.6	2.4	73.0

Thermal gravimetric Analysis of polymers made in different solvents

While the elemental analysis gave an idea of the sulfur content, the results were not very consistent as the polymers had a much greater sulfur content than the calibration standards used. To confirm the results of the elemental analysis, thermal gravimetric analysis (TGA) was performed on each of the polymers. TGA gives the thermal stability of the polymers under an inter atmosphere. When analysing sulfur polymers, the high sulfur material is usually lost first. After this, the carbon-based material remains. The final mass of material that is left at 800 °C gives a good indication of the proportion of the polymer which is organic based. This should follow the same trends as the elemental analysis and indicate the sulfur content of the polymer.

A Perkin Elmer 8000 thermal gravimetric analyser (TGA) was used to investigate the thermal degradation of each of the polymer samples prepared with sulfur and NBD in different solvents. All samples had the same feed ratio of 58 % sulfur and 42 % NBD. The DMF only sample used the optimised ratio of sulfur to DMF. Each polymer sample was fully cured and ground into a powder before testing. All samples were tested from 30 °C to 800 °C at a temperature ramp rate of 20 °C/min under a nitrogen atmosphere. At 800 °C, the atmosphere was switch to air and held for 10 minutes to burn off any remaining polymer before cooling.

All polymer samples had no loss until around 150 °C. After this point, the tetrachloroethylene and DMF sample showed a small mass loss. This is likely due to evaporation of solvent that became trapped in the polymer. All polymer samples showed a mass loss between 300 °C and 400 °C. This is likely due to the loss of high sulfur regions of the polymer. This mass loss is shifted to a higher temperature than in the sulfur control, indicating the sulfur is stabilised in a polymer structure. After this mass loss, there is a gradual decrease in mass as temperature increases. The gradual loss is likely due to the loss of some organic material. The final mass before 800 °C roughly shows the same trend as the elemental analysis with the higher carbon polymers having a greater final mass. TGA confirms the result of the elemental analysis that the polymer prepared in a solvent system of 50-50 DMF-Xylene contains the lowest sulfur content and is likely the best solvent system.

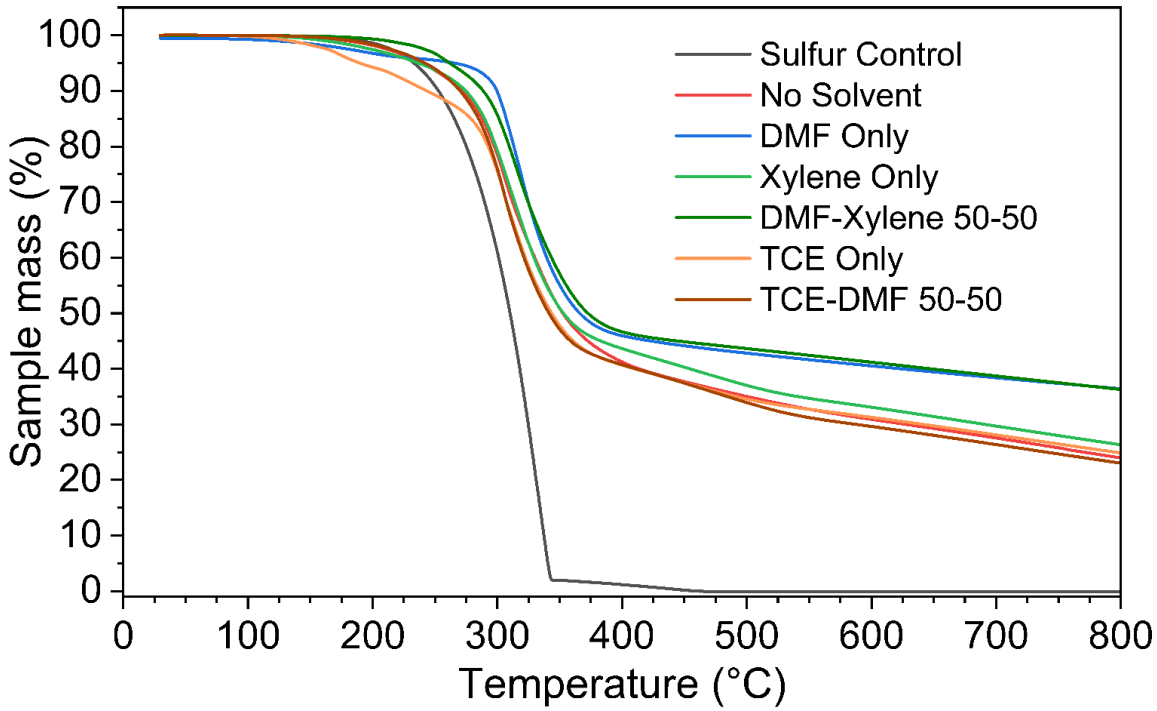

Figure 3.32: Thermal gravimetric analysis of polymers prepared from a reaction between sulfur and norbornadiene tested on a Perkin Elmer 8000 TGA. All samples had a 58 % sulfur content.

Characterisation of polymers with a range of sulfur contents

Polymer synthesis in DMF-Xylene solvent with a range of sulfur contents

The next part of this project was to use the optimised solvent system to prepare polymers with a range of compositions and test for thermal and optical properties. To do this, the reaction between sulfur and NBD in a solvent system of 50-50 DMF-xylene was scaled up five times. Then a range of polymers were prepared with sulfur contents ranging from 41 % to 86 %. In total, 9 polymer samples were prepared sulfur contents of 41 %, 58 %, 67 %, 74 %, 81 %, 83 %, 85 % and 86 %. These sulfur contents were selected so that the average sulfur rank would range from 1 to 9. The exact sulfur rank is likely higher than this as some rearrangements have been observed in this reaction. The method used for the synthesis of these polymers is below.

Sulfur (5 g, 156.25 mmol S atoms) was added to a 250 mL round bottomed flask with 50 mL of 50-50 DMF-xylene. The flask was connected to a condenser and added to a 140 °C oil bath. The flask was heated for 30 minutes with constant stirring, over which time, the sulfur would completely dissolve. NBD was then added down the condenser. The volume of NBD was varied to give the desired sulfur content. The reaction was continued for an additional 90 minutes after the addition of NBD. The solvents were then mostly removed by rotary vacuum to give a black prepolymer. The prepolymer was washed thoroughly in water before being lyophilised overnight. The polymers were not immediately cured as prepolymers were used in the following experiments.

The prepolymers were soft and would flow when heated above 50 °C. All prepolymers were black solids apart from the 85 % and 86 % samples. These were a yellow colour and had the appearance of sulfur. These samples were not used for future tests. The 41 % sulfur sample did not flow when heated and was more difficult to mould or manipulate.

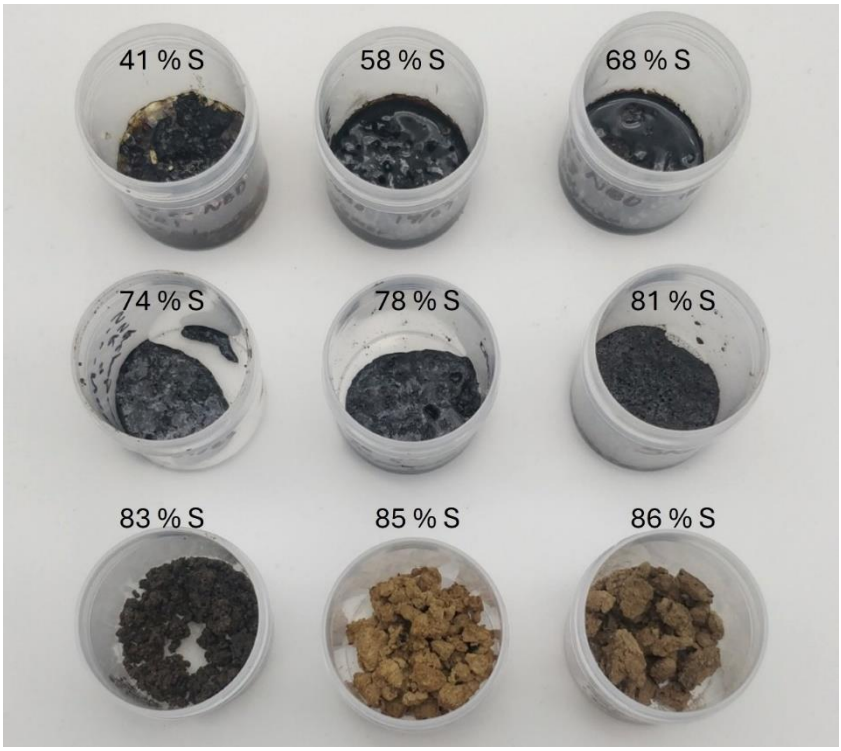

Figure 3.33: Picture showing a range of prepolymers prepared from a reaction between sulfur and norbornadiene in a solvent system of DMF-Xylene. The sulfur content of each prepolymer is displayed.

Prepolymer Stability

The prepolymer was tested for long term stability to investigate if it would remain stable without being cured. A stable prepolymer would be useful as it could be made and stored then only moulded into a part when required. A common issue with polymers made from sulfur is the formation of crystalline sulfur. This could be caused by unreacted sulfur which is embedded in the polymer matrix or it could be caused by backbiting of sulfur chains within the polymer to reform octahedral sulfur. Uncured prepolymers are particularly vulnerable to this, as they are likely not fully reacted, resulting in longer sulfur chains than a fully cured polymer. To test if crystalline sulfur would form over time, the 58 % sulfur prepolymer was analysed by DSC over a period of three months. If crystalline sulfur was reforming, a melting peak at approximately 115 °C would be evident. All tests were performed on a Perkin Elmer Agilent DSC 8000.

The DSC method involved heating the sample from 30 °C to 100 °C at 25 °C/min. The temperature was then held isothermally at 100 °C for one minute. This step is to remove any thermal history in the sample. The temperature was then decreased to -60 °C at 25 °C /min where it was again held for one minute. After this, the temperature was increased to 150 °C at 25 °C/min. A nitrogen atmosphere was maintained for the entire run.

The prepolymer was tested at 2 days, 1 week, 2 weeks, 1 month, 2 months and 3 months after synthesis. There was no crystalline sulfur melting peak in the 2-day sample, indicating that there was no unreacted sulfur. The prepolymer had a glass transition temperature of -21.8 °C. This is much lower than the fully cured polymer, indicating that it had not reacted completely. Over three months at room temperature, the glass transition temperature of the prepolymer increased from -21.8 °C to -6.3 °C. This potentially indicates that the prepolymer is not fully stable. One possible explanation for this increase in glass transition temperature is backbiting of the sulfur chains. If backbiting occurs, it would be expected that the average length of the sulfur chains in the polymer would decrease as cyclic sulfur species are formed. A decrease in the length of the sulfur chains would result in an increase in glass transition temperature. It would be expected that this would also result in a peak forming at approximately 115 °C due to the melting of crystalline octahedral sulfur. None of the samples show a clear peak but the 1-month sample shows a very small peak at approximately the correct temperature.

This study indicates that the prepolymer may have some stability over a period of three months. However, there is a slight shift in glass transition temperature, indicating a change in structure. For this reason, all future experiments were carried out using prepolymer which was less than one week old.

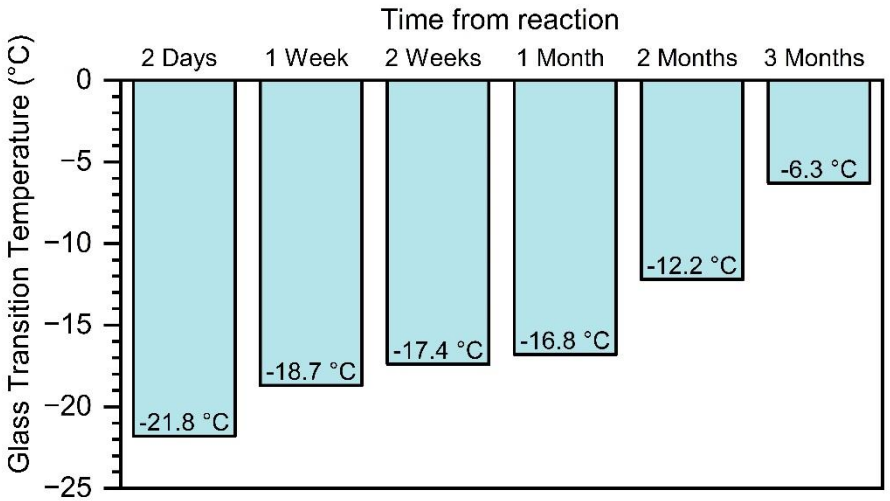

Figure 3.34: Plot showing the glass transition temperature of a 58 % sulfur 42 % NBD prepolymer over time.

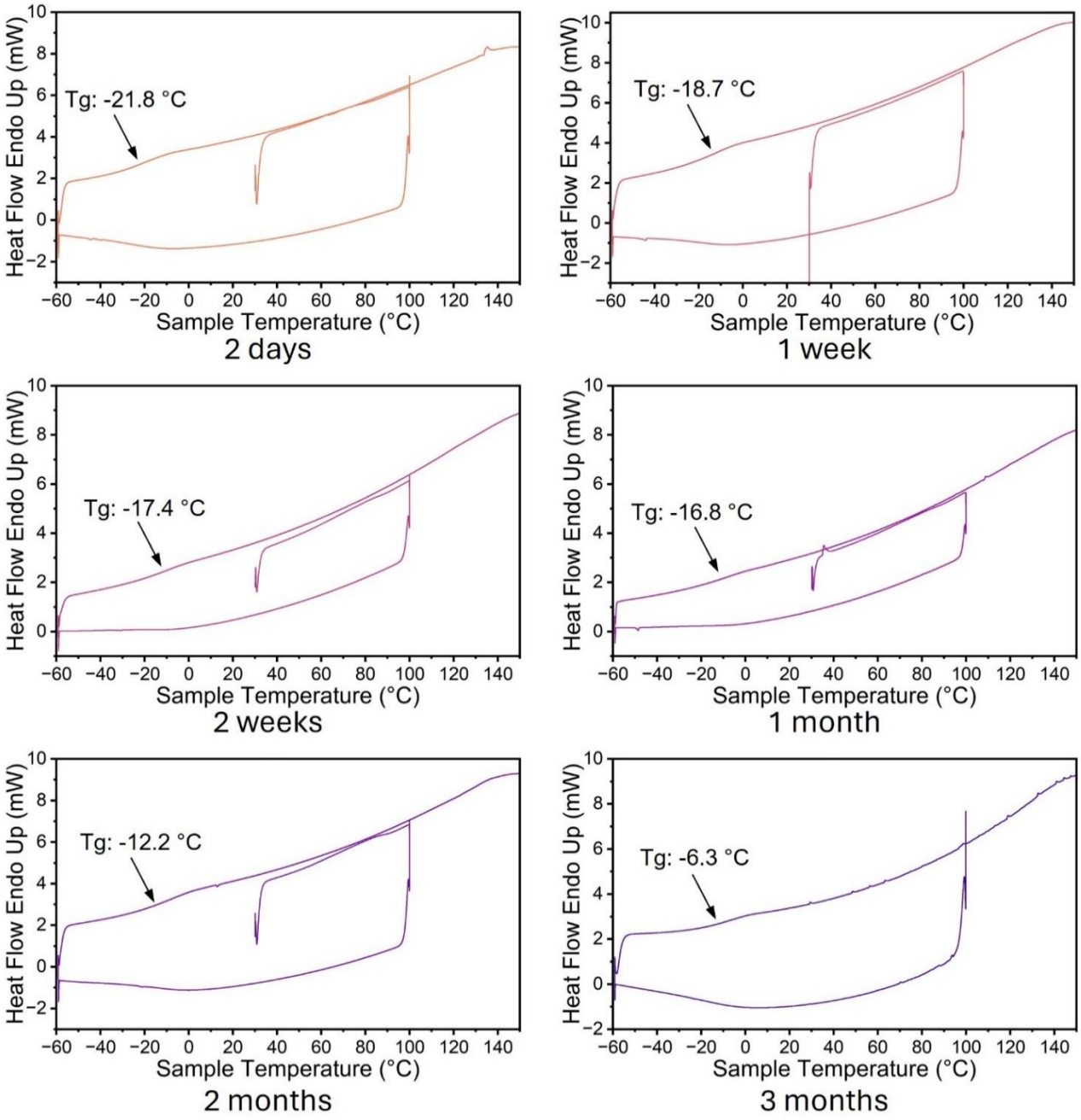

Figure 3.35: DSC thermogram for prepolymers prepared from sulfur and NBD in a solvent system of DMF-xylene 50-50. The prepolymers were left uncured between 2 days and 3 months before being tested. The glass transition as determined by the inflection point on the second positive temperature ramp is displaced for each sample.

Cure study of polymer prepared from NBD and sulfur

The prepolymers were in the form of a soft, malleable, and sometimes tacky solid. A study was conducted to investigate if there is a temperature at which the prepolymers will flow into a mould but will not fully cure. This would allow for the prepolymer to be heated to this temperature and moulded into a specific geometry when required. It was also important to investigate a temperature in which the polymer can be fully cured and ensure that no further reaction will occur.

First the temperature at which the prepolymer would flow was determined qualitatively. It was found that the prepolymer required temperatures above 60 °C to flow. Above 110 °C, the polymer would flow but quickly harden and form a solid. It was determined that a temperature between 60 °C and 110 °C would likely be the best for moulding of the prepolymer

To confirm the results of this experiment quantitatively, the cure of the 58 % sulfur prepolymer was tested at several different temperatures. Prepolymer samples were placed into a silicone mould. A total of seven samples for each temperature were prepared. The samples were placed into an oven at either 70 °C, 85 °C, 100 °C or 140 °C. Samples were removed at 30 minutes, 1 hour, 2 hours, 4 hours, 8 hours, 16 hours, and 24 hours. Another sample was not placed in the oven.

Each of the samples were tested for glass transition temperature using a Perkin Elmer DSC 8000 with the same method as the prepolymer stability study. When cured at 140 °C, the glass transition temperature of the polymer quickly increased and seemed to reach a maximum of 115 °C between 8 and 16 hours. When the cure temperature was between 70 °C and 110 °C, the glass transition temperature increased much slower and never reached full cure. This experiment indicates that 70 °C is an appropriate temperature to allow the prepolymer to flow into a mould, then curing could be done at 140 °C for at least 16 hours. For all moulding experiments, 70 °C was used with a cure temperature of 140 °C.

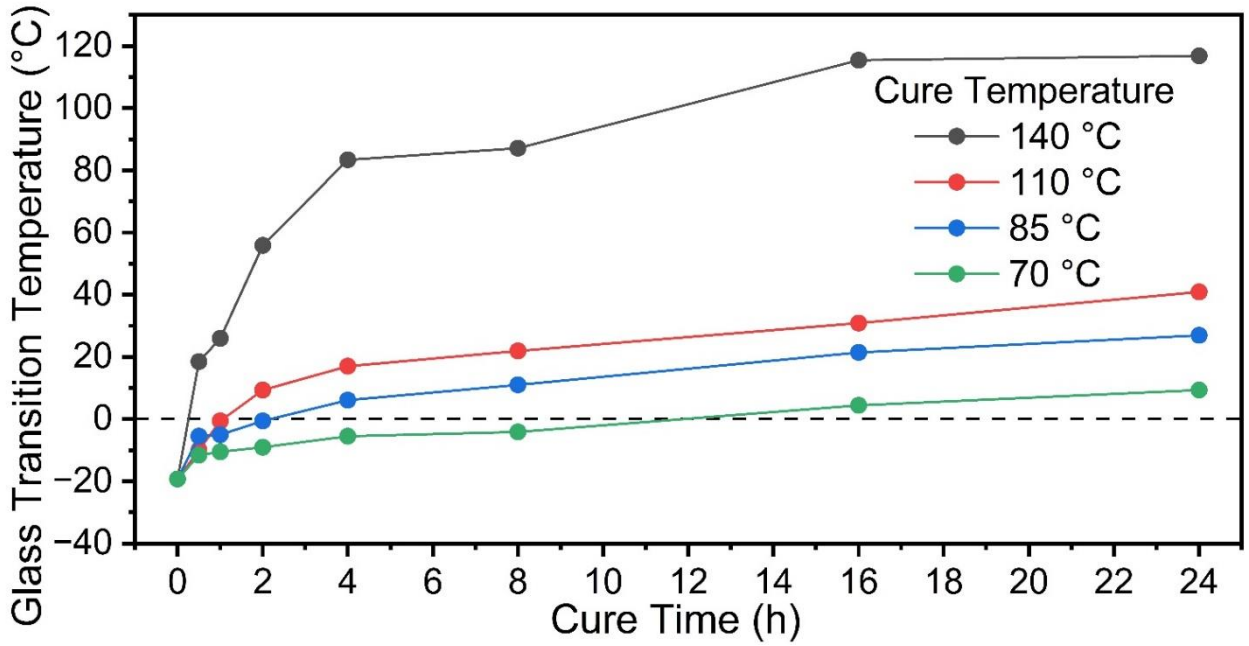

Figure 3.36: Glass transition temperature as measured by DSC of a 58 % sulfur, 42 % NBD prepolymer when cure time and temperature is varied.

Glass transition temperature by dynamic mechanical thermal analysis

To test glass transition temperature, it is often important to use multiple techniques. DSC is useful but can be insensitive to glass transitions while dynamic mechanical thermal analysis (DMTA) is much more sensitive but requires greater sample preparation.[12] The following experiments will test the polymers using both techniques.

Using the results of the cure study, the polymers were moulded into samples which could be tested for glass transition temperature using a TA Q800 dynamic mechanical thermal analyser. Polymer samples were moulded into rectangular prisms with dimensions of 65 mm by 5 mm by 2.5 mm. To make the mould, a negative was 3D printed with these dimensions. A silicone resin was poured into the 3D printed negative and left to cure for two hours. After this point, the silicone was removed from the negative to be used.

As discussed in the cure study section, the prepolymers would flow when heated above 60 °C. This was utilised to mould the prepolymers into the correct geometry for the dual cantilever clamp in the DMTA. The silicone mould was first heated to 70 °C. The prepolymer was then heated and poured into the mould. To reduce the chance of air bubbles forming in the prepolymer, it was poured into one end of the mould and allowed to flow to the other. Due to the high viscosity of the polymer, it was necessary to push it into the mould with a spatula. The mould and prepolymer was left in the oven at 70 °C for an additional 30 minutes to allow the prepolymer to take the shape of the mould. If needed, more prepolymer would be added to ensure the sample had a consistent height. The mould and prepolymer were then added to an oven at 140 °C for 24 hours to cure. This was done for the samples ranging from 58 % sulfur to 83 % sulfur. The 41 % sulfur prepolymer did not flow when heated and could not be moulded.

To test the glass transition temperature, a multifrequency temperature sweep was used on the DMTA with a dual cantilever clamp. The polymer sample was added into clamp and cooled to -10 °C. After equilibrating, it was heated at 3 °C/min until 150 °C. The glass transition was determined from the temperature of the centre of the tan delta peak. The glass transition temperature decreased with increasing sulfur content which is common for sulfur polymers.[13]

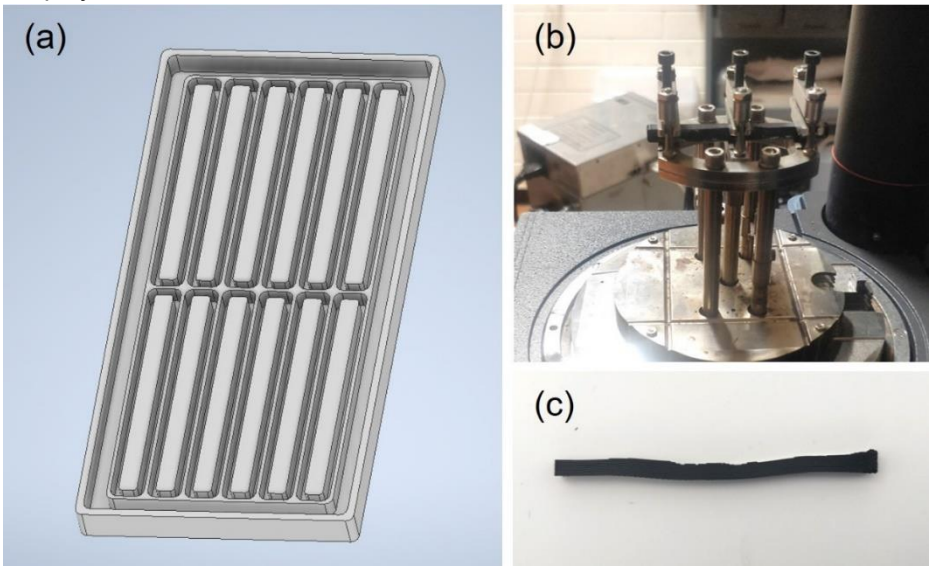

Figure 3.37: Images showing the testing of sulfur polymers with dynamic mechanical thermal analysis. (a) Image of negative that was 3D printed to make silicone mould. (b) Polymer sample in dual cantilever clamp of TA Q800 dynamic mechanical analyser. (c) sample after multifrequency temperature sweep.

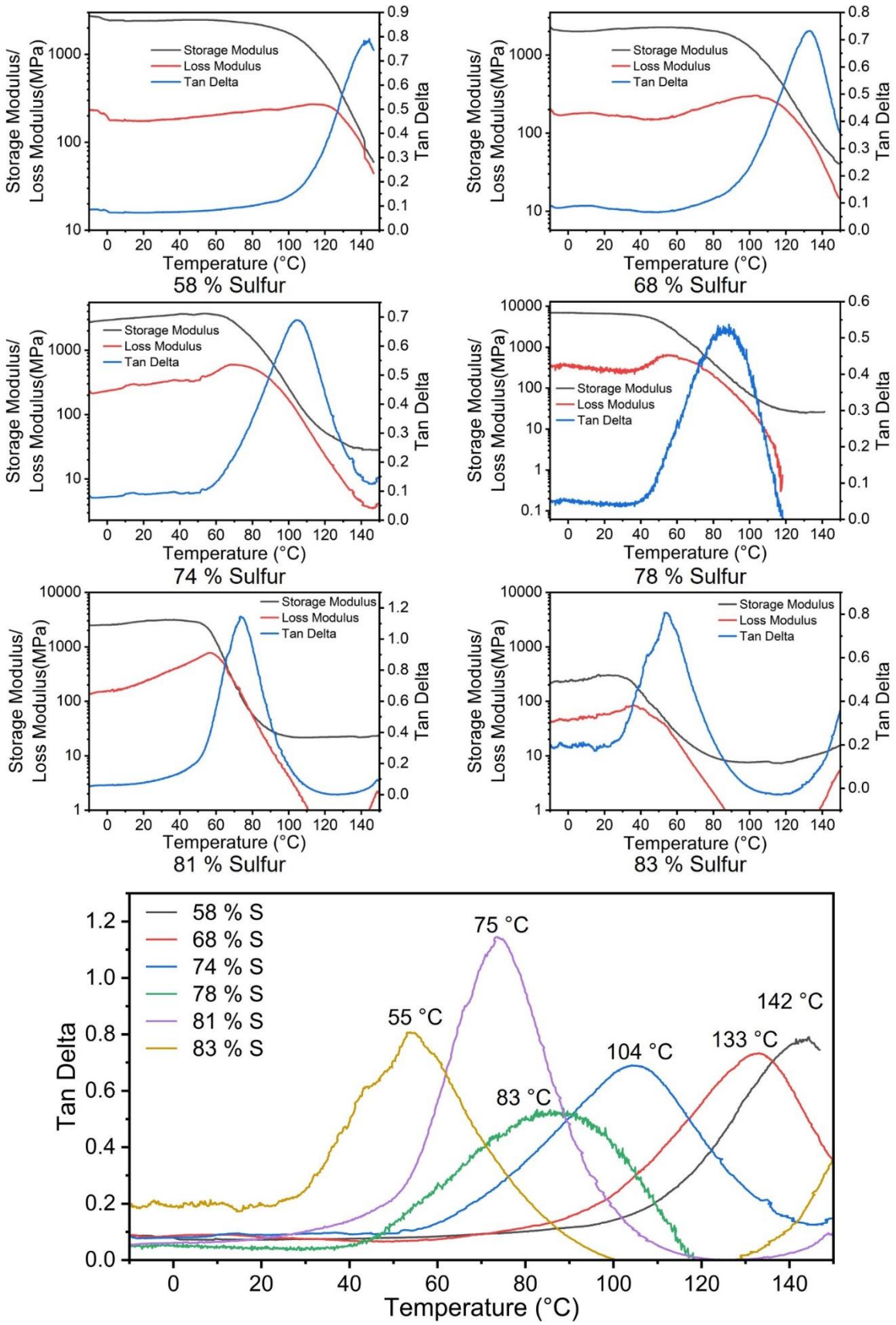

Figure 3.38: DMTA thermograms for polymers of sulfur and NBD that were made in a solvent system of 50-50 DMF-xylene. A cantilever bending clamp was used with a multifrequency temperature sweep from -10 °C to 150 °C The sulfur content of the prepolymers ranged from 58 % to 83 %. Bottom plot shows the tan delta for each polymer sample.

Glass transition temperature by Differential Scanning Calorimetry

To confirm the results of the DMTA experiments, a method was developed to cure the prepolymer in the DSC. In this method, the uncured prepolymer was placed into a DSC. The samples were first heated to 100 °C for 1 minute to remove any thermal history. Following this, the temperature was decreased to -60 °C at 25 °C/min and held for 1 minute before increasing to 140 °C. This step allowed for the initial glass transition temperature to be determined. After this, the temperature was held at 140 °C for an hour to cure the prepolymer before another temperature sweep to -60 °C. The process of curing for an hour at 140 °C before a temperature sweep was repeated for 24 hours. This allowed for the measurement of the glass transition temperature over the full cure of the polymer.

Using this method to investigate the cure of the polymer had many advantages over curing the polymer in an oven and investigating the fully cured material in the DSC. First, it gives many data points at multiple cure times without requiring multiple DSC samples to be prepared. Secondly, the glass transition temperature of a highly crosslinked polymer can be difficult to resolve in a DSC but the prepolymer usually has a very clear transition. It is much easier to trace the trend of increasing glass transition temperature then to find a transition in a fully cured polymer. This reduces the ambiguity and inconsistency in glass transition temperature that is often the case with DSC.

When comparing the results of the 58 % sulfur sample when cured in the DSC and cured in the oven, they follow a very similar trend. As the sulfur in the sample increased, the time to reach full cure and the final glass transition temperature decreased. The only sample that showed a crystalline sulfur melting peak was the 83 % sulfur sample. This indicates that there is unreacted sulfur in the polymer and this is an upper limit to the sulfur content of the polymer. The glass transition temperature was lower than the values obtained by DMTA but followed the same trends.

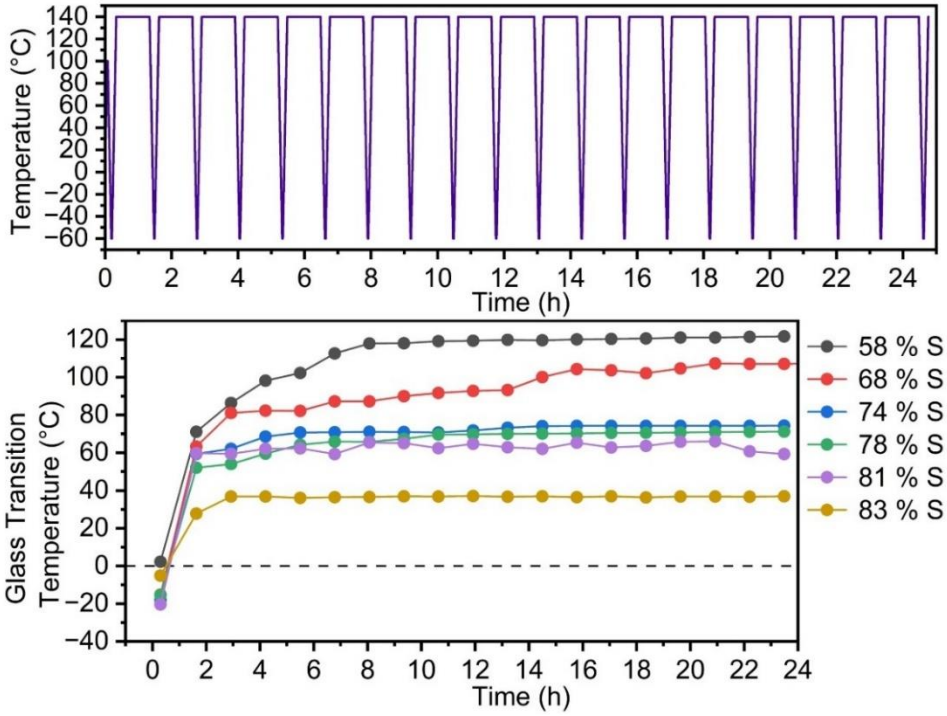

Figure 3.39: Temperature profile of DSC method and glass transition temperature against cure time in DSC for polymers made from sulfur and norbornadiene in different ratios. All polymers were made in a solvent system of 50-50 DMF-xylene.

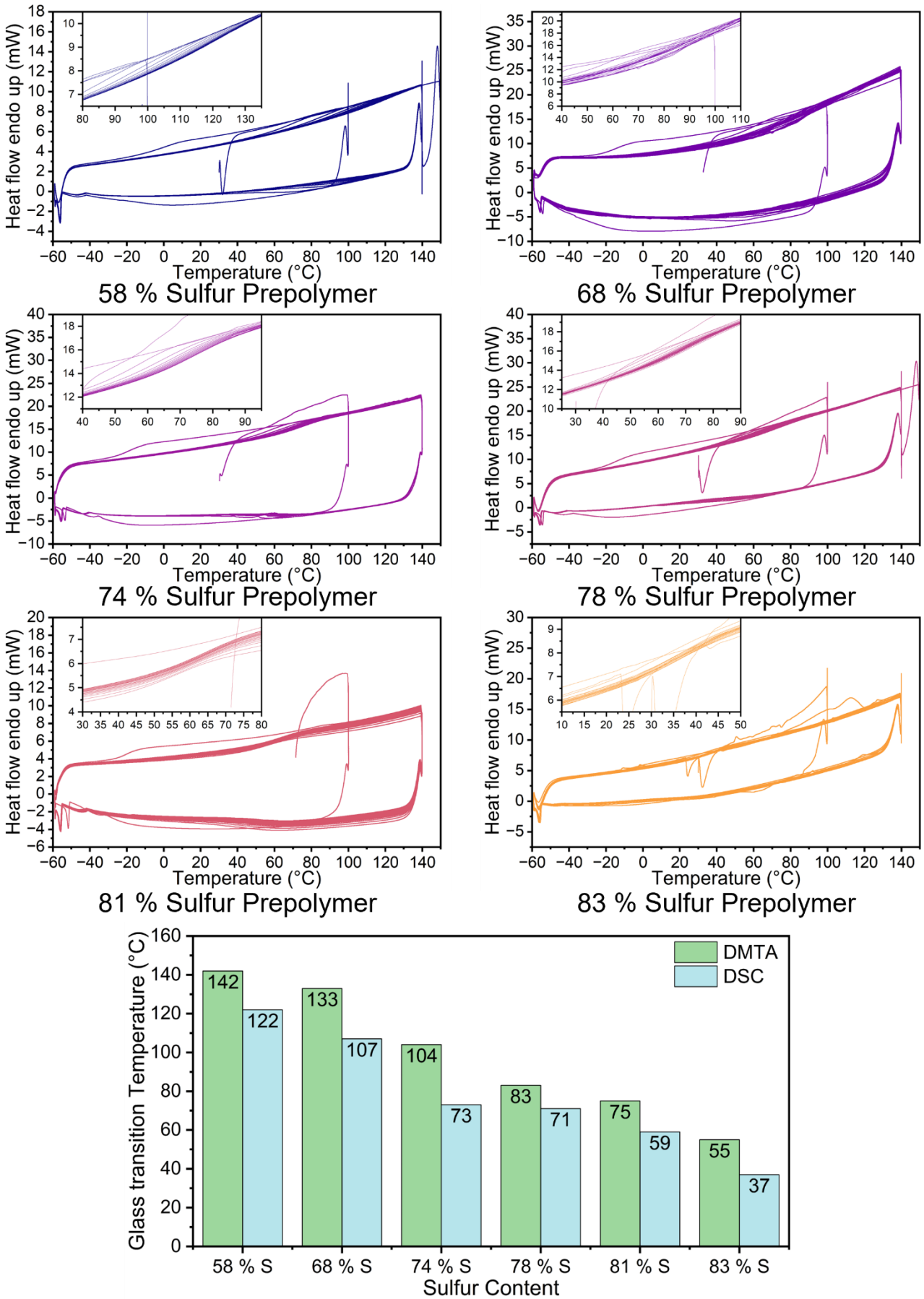

Figure 3.40: DSC thermograms for prepolymers of sulfur and NBD that were made in a solvent system of 50-50 DMF-xylene. The sulfur content of the prepolymers ranged from 58 % to 83 %. Plot showing the glass transition temperature obtained by DMTA and DSC.

Reactive compression moulding of polymers into windows

At this point, the thermal properties of the polymer were well understood. However, little was known about the optical properties. To investigate the optical properties, windows of known thickness and high surface quality were needed. When testing optical transparency, several thicknesses are required such that effect from reflection can be reduced. As the thickness of the sample does not affect reflection off the surface, the change in transmission between samples of different thicknesses can be attributed to absorption. To test optical properties of the polymers, three different window thicknesses were used.

The polymer windows were prepared using a technique first pioneered by Nicholas Lundquist known as reactive compression moulding[9, 14, 15]. In this technique, the polymer is ground into a fine powder and placed in a heated press. The polymer is then heated, usually above its glass transition temperature, while a large force is applied to compress it into a sheet or window. What is unique about reactive compression moulding is that crosslinked sulfur polymers which do not melt can still form strong sheets. The high strength of the sheets is due to the S-S bonds metathesis in the polymer leading to new covalent bonds between polymer particles. This creates a homogeneous polymer sheet. Reactive compression moulding is a versatile technique that can be used to prepare high strength composites[9], confine toxic sorbents[14] or create magnetic responsive materials[15].

To prepare the polymer windows, a custom reactive compression moulding die was machined by the engineering staff at Flinders University. This custom die was necessary to control the thickness and geometry of the polymer sheets prepared by reactive compression moulding. The die was designed on Autodesk Inventor and machined from aluminium. The die consisted of a push rod, an outer sleeve, two polished disks and several thickness determining rings. When assembled, the sample could be put between two discs which fit into the outer sleeve with a clearance of 0.1 mm. A ring could be selected to vary how far the push rod can extend into the sleeve, altering the thickness of the polymer sheet. This ring could be placed under the sleeve to aid in removal of the sample after compression. A dry PTFE spray was used as a mould release agent to ensure the samples did not stick to the aluminium disks. A shim with an insert of 15 mm was placed into the press to give windows that are appropriately sized for infrared transmission testing.

Each of the polymers made from norbornadiene and sulfur were compressed into windows of three thicknesses. The die was preheated to 140 °C and the cured polymer was crushed into a powder. A temperature of 140 °C was used as it was above the glass transition temperature of all the polymers (apart from the 58 % sulfur polymer when tested by DMTA) but is far below the degradation temperature of the polymer. Approximately 500 mg of polymer was loaded into the aluminium die and added to a heated press. 20 Mpa of pressure was applied for 10 minutes. The aluminium die was then removed from the press and left to cool. After cooling to approximately 40 °C, the polymer window was removed from the press. Each composition was compressed into three thickness: 0.75 mm, 1 mm, and 1.1 mm.

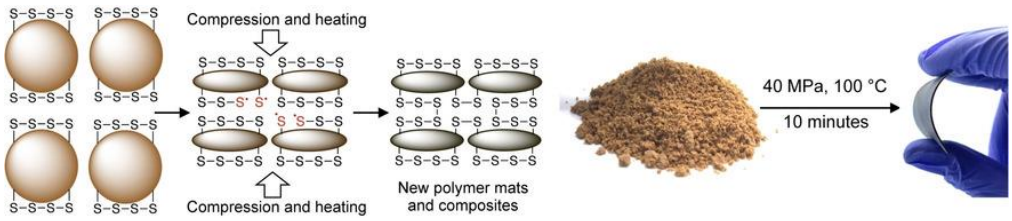

Figure 3.41: Image showing process of reactive compression moulding. Used with permission from.[9]

Infrared transparency of sulfur and norbornadiene polymer with sulfur content

To test the infrared transparency of the polymers, they were tested from a wavelength of 2 μm to 20 μm using a Perkin Elmer Frontier FTIR. The transmittance was integrated over the mid wave-infrared (MWIR, 3 μm – 5 μm) and the long-wave infrared (LWIR, 7 μm – 14 μm) then divided by the wavelength range to obtain an average.

The polymer showed very poor transmission in the LWIR region. It showed almost no transmission over the whole region in the samples with less than 75 % sulfur. This was unexpected as the polymer had been predicted computationally to possess a high transmission in the long wave infrared region. These results indicated that there may be some side reactions occurring that create unwanted products which absorb in the LWIR region.

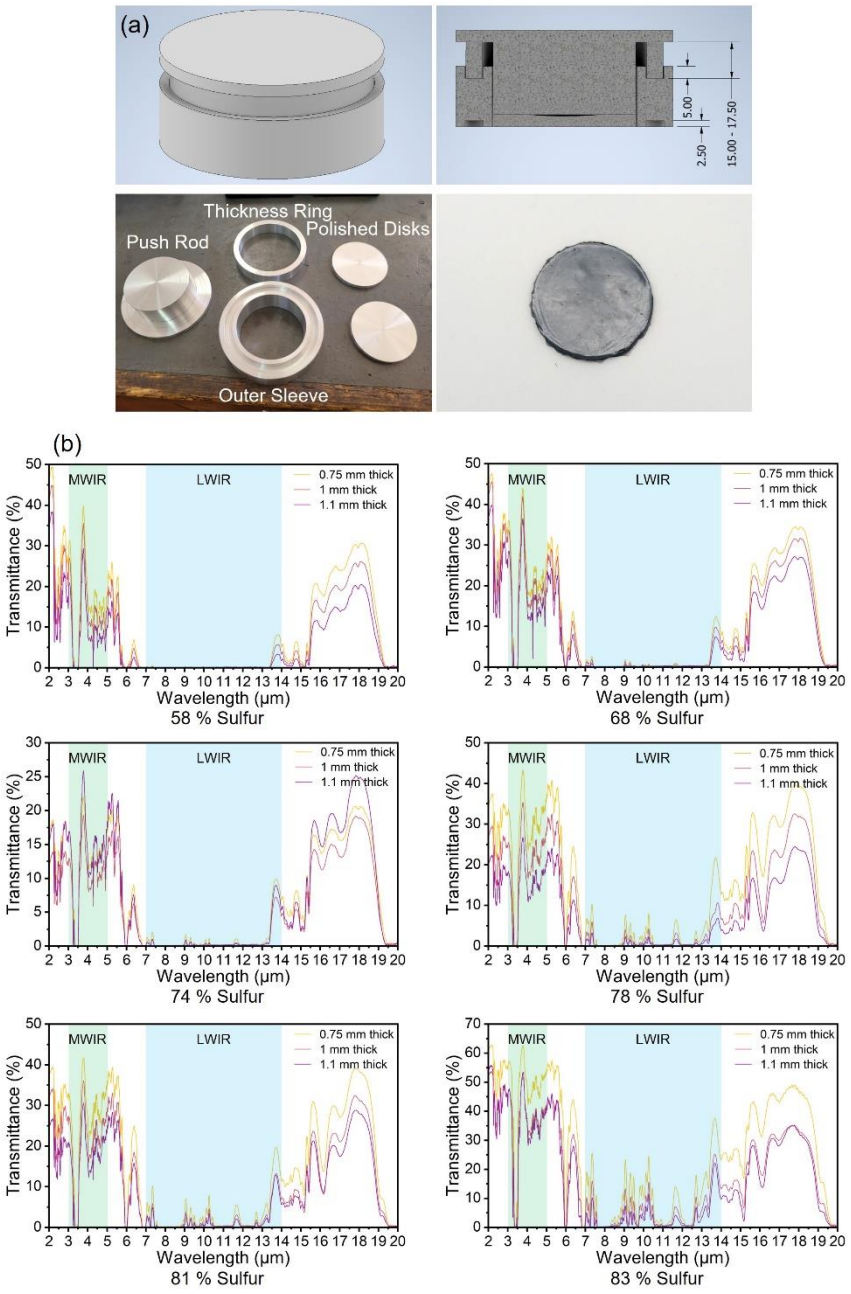

Figure 3.42: (a) Aluminium die used for making polymer windows. (b) FTIR spectra for polymers made from NBD and sulfur at 3 different thicknesses and a range of sulfur contents. All spectra were taken using a Perkin Elmer Frontier FTIR. The MWIR and LWIR regions are labelled at 3 μm - 5 μm and 7 μm - 14 μm respectively.

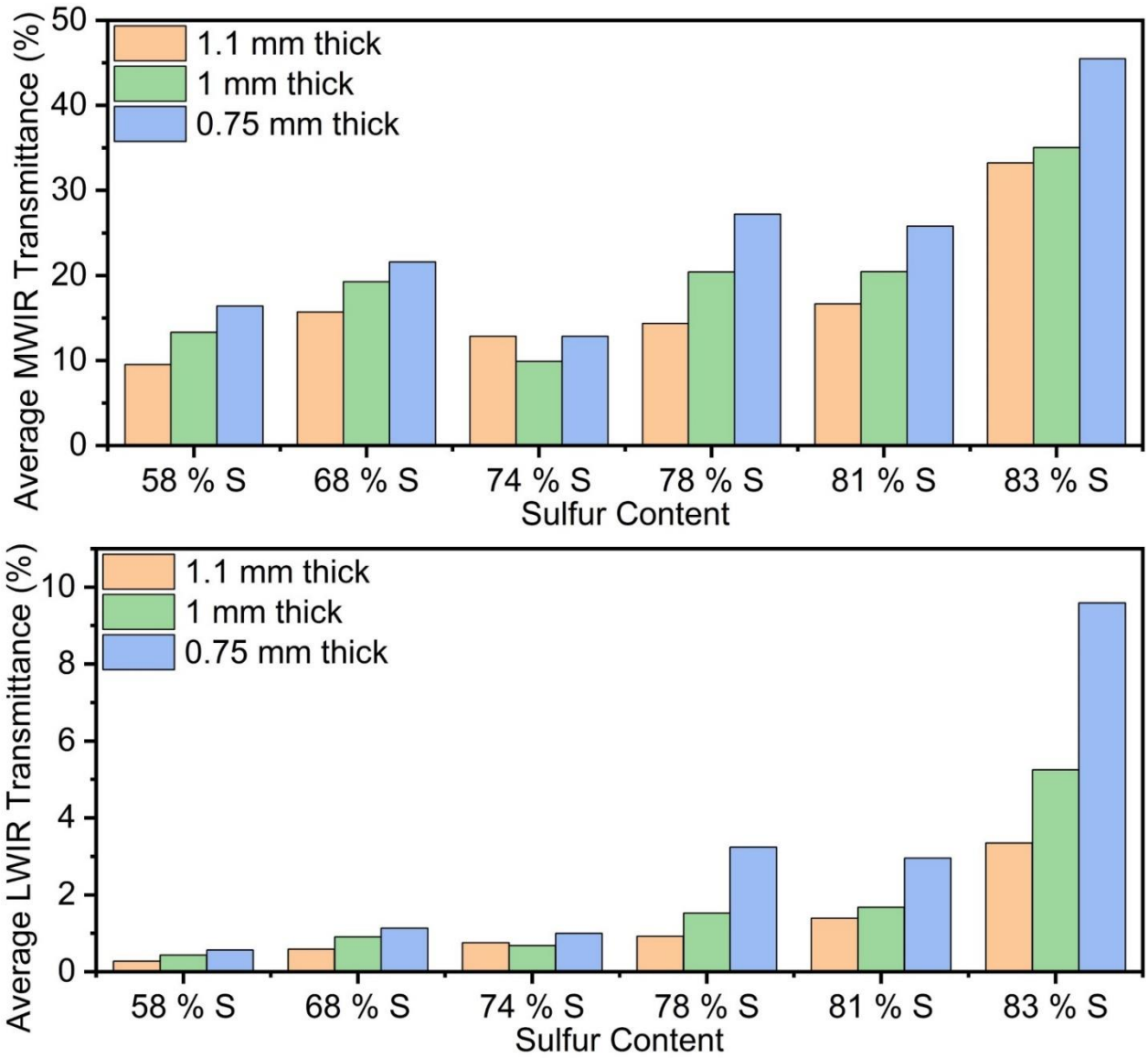

Figure 3.43: Average MWIR and LWIR transmittance for polymers made from NBD and sulfur in a solvent system of 50-50 DMF-xylene at 3 different thicknesses and a range of sulfur contents. The average MWIR transmittance is calculated by integrated the transmittance plot between 3 μm and 5 μm before dividing by the wavelength range. The average LWIR transmittance is calculated by integrated the transmittance plot between 7 μm and 14 μm before dividing by the wavelength range.

Refractive index with sulfur content

Along with the transmission of the material, the refractive index is very important. Materials with a greater refractive index can be used to make smaller, lighter or more practical optics[16]. Sulfur has a high molar refraction relative to carbon[17] and can therefore impart a high refractive index on a material. Each of the polymers were tested for refractive index using their specular reflectance.

Specular reflectance was measured using a Bruker Vertex v80 instrument with the 1513/QA attachment for each of the polymers prepared from norbornadiene and sulfur in DMF/Xylene. The 1 mm thick samples were tested with an angle from the surface normal of 15 ° under vacuum. All samples were referenced using the reflectance spectrum of an aluminium mirror. A Kramers-Kronig transform was applied using the OPUS V7.2 software to find the wavenumber dependent phase shift spectrum. The refractive index was then calculated using the real portion of the complex refractive index, $\eta = n + ik$.

As the sulfur content of the samples increased, the reflectance and refractive index increased. This would be expected as the sulfur atom is large and unpolarizable when compared to carbon[17], leading to an increase in refractive index.

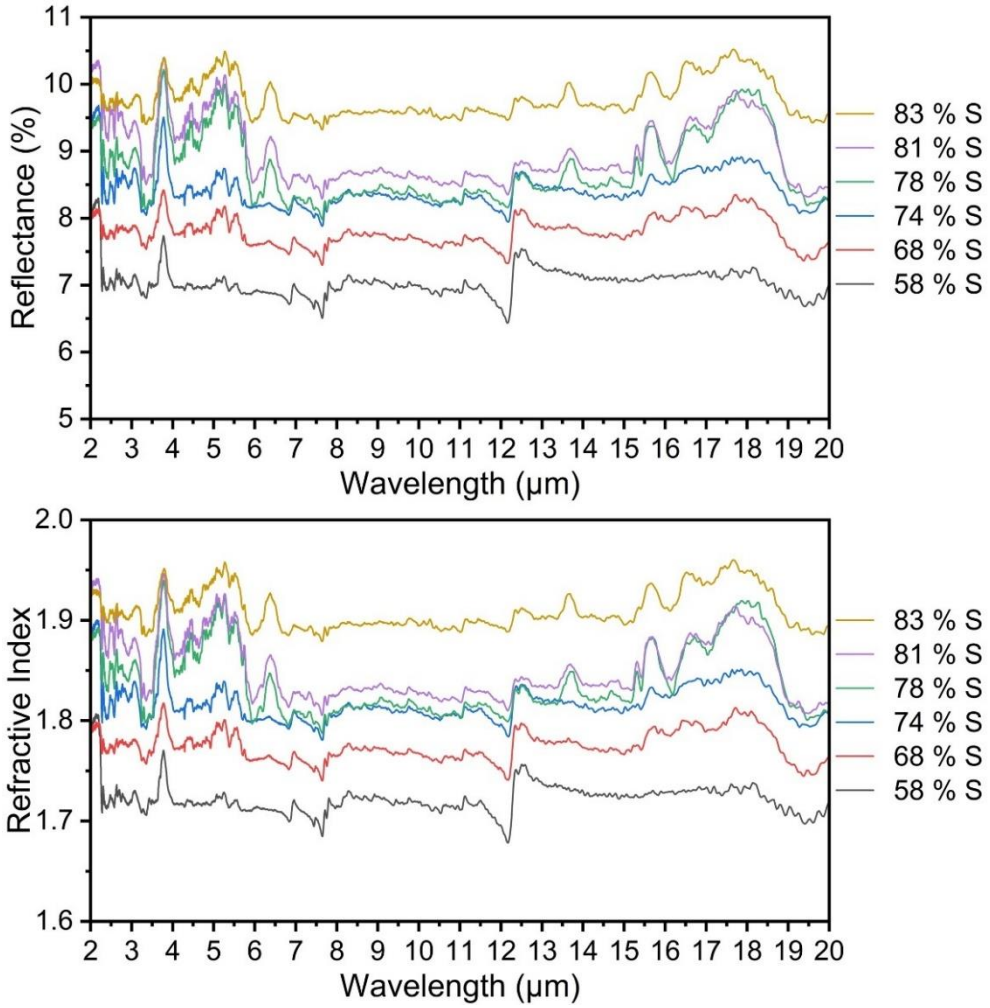

Figure 3.44: Reflectance and refractive index spectra of polymers made from sulfur and norbornadiene in a solvent system of 50-50 DMF-xylene. All spectra were obtained on a Bruker Vertex v80 using the 1513/QA attachment. An angle from the surface normal of 15 ° was used with all spectra reference against an aluminium mirror. The refractive index was determined by first taking the Kramers-Kronig transform of the reflectance spectra of each sample then taking the real portion of the complex refractive index, $\eta = n + ik$.

Synthesis and isolation of norbornadiene cyclic sulfides

Extraction of hexane soluble intermediates

While the thermal and optical properties of the polymers could be measured effectively, the chemical structure was still unknown. The chemical characterisation was made more difficult by the low solubility of the polymers in almost any solvents when fully cured. The NMR results of the reaction in deuterated DMF along with the GC-MS of the reduced polymer indicated that there may be some side reactions taking place, but the intermediates had not been extracted or isolated. The following experiment was performed to extract any intermediates and investigate them by GC-MS.

Elemental sulfur (5g, 19.5 mmol S8) was added to a 250 mL two necked round bottom flask along with a magnetic stirrer, DMF (50 mL) and xylene (50 mL). A condenser was added to the main neck of the flask and the other was sealed with a rubber septum. The reaction was then heated at 140 °C for 30 minutes with constant stirring at 600 rpm. Over this time, the sulfur completely dissolved in the solvents to form a deep orange liquid. Norbornadiene (3.98 mL, 39.13mmol) was added using a syringe through the rubber septum. Immediately after the addition of NBD, a 1 mL aliquot of the reaction mixture was removed using a needle through the rubber septum and added to a glass vial. This was the 30-minute sample. Aliquots were taken every 15 minutes until a total time of 120 minutes then again at 24 hours. The aliquots were left to cool before deionised water (2 mL) and hexane (2 mL) was added. This caused any polymeric material to precipitate and combine in the water/DMF (bottom) layer. 100 µL of the hexane/xylene layer (top) was filtered through cotton wool and added to a GCMS vial. The aliquot was diluted to 1 mL with hexane before being filtered and analysed on a Perkin Elmer Agilent GC-MS.

All samples were analysed using the same GCMS method. An injection volume of 1 µL was used with a split ratio of 60:1. A 29.4 m x 250 µm x 0.25 µm, 5% Phenyl Methyl Silox column was used with a constant flow of 1 mL/min helium. An initial oven temperature of 100 °C was used which was held for 3 minutes. The temperature was then increased at 5 °C/min to 200 °C. Following this, the temperature was increased at 20 °C/min to 250 °C. Any GC-MS chromatograms with longer resonance times were held at 250 °C. The GC chromatograms and mass spectra all major peaks can be seen on the following pages.

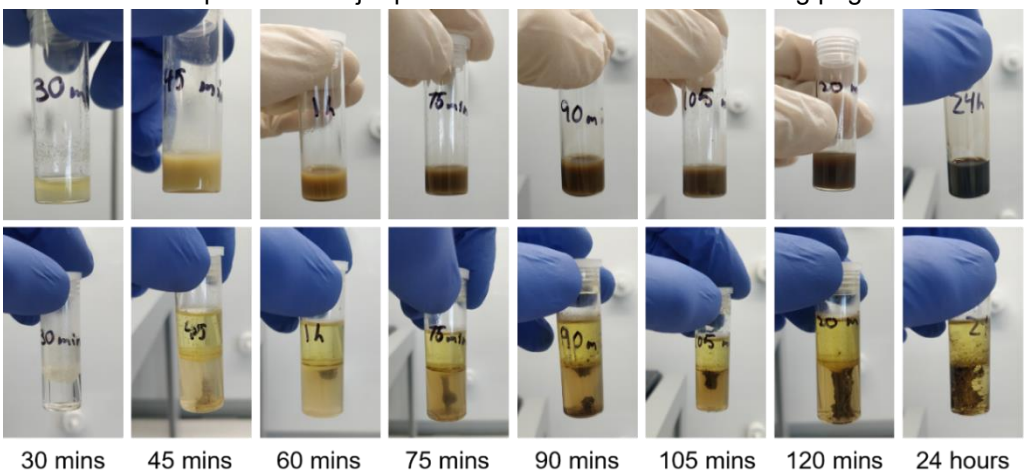

Figure 3.45: Samples taken from reaction between sulfur and NBD. The reaction was left for a total of 24 hours with aliquots removed every 15 minutes for the first 120 minutes then another at 24 hours. The top row shows the aliquots directly after being removed from the reaction. The bottom row is after 2 mL of deionised water and 2 mL of hexane was added.

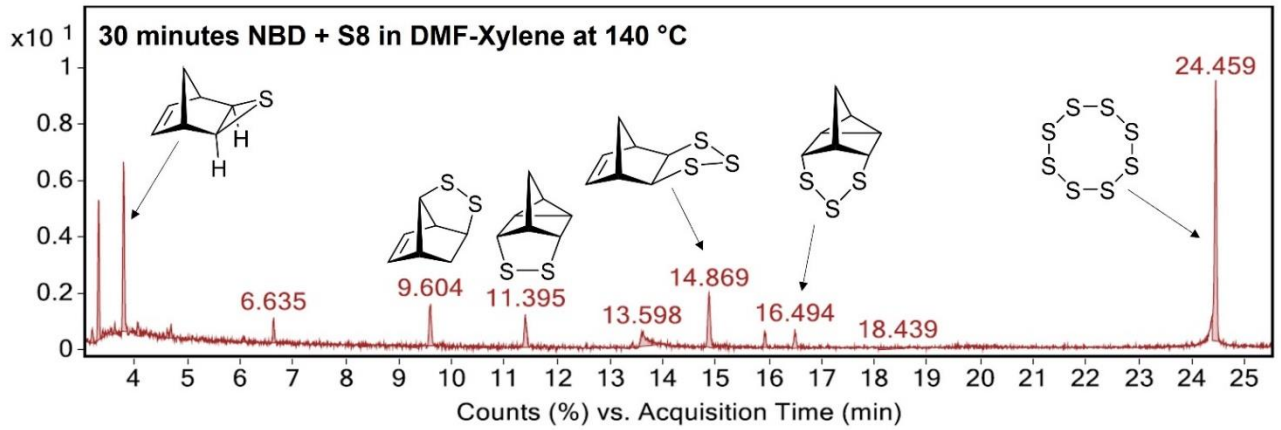
x10 1
30 minutes NBD + S8 in DMF-Xylene at 140 °C
6.635
9.604
11.395
13.598
14.869
16.494
18.439
24.459
Counts (%) vs. Acquisition Time (min)

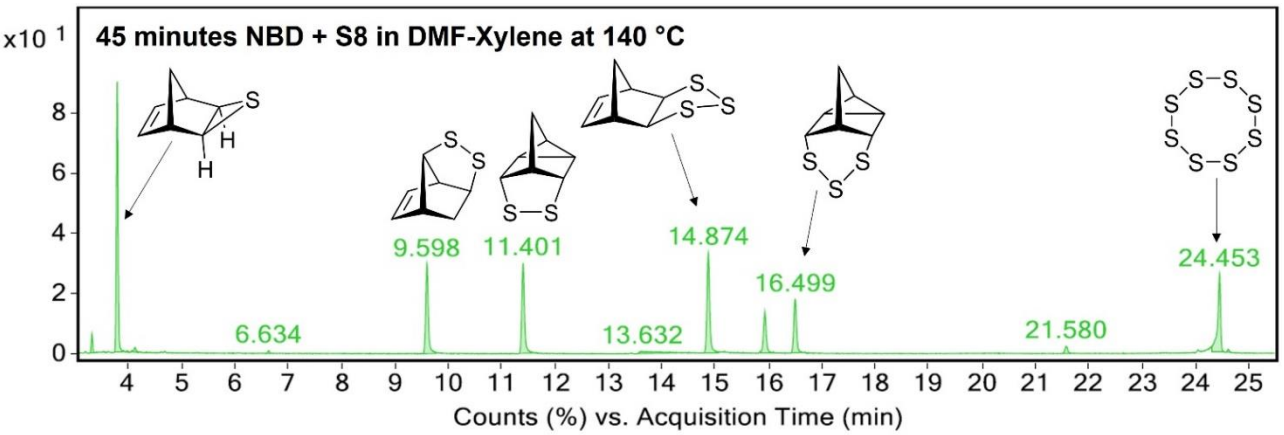
x10 1
45 minutes NBD + S8 in DMF-Xylene at 140 °C
6.634
9.598
11.401
13.632
14.874
16.499
21.580
24.453
Counts (%) vs. Acquisition Time (min)

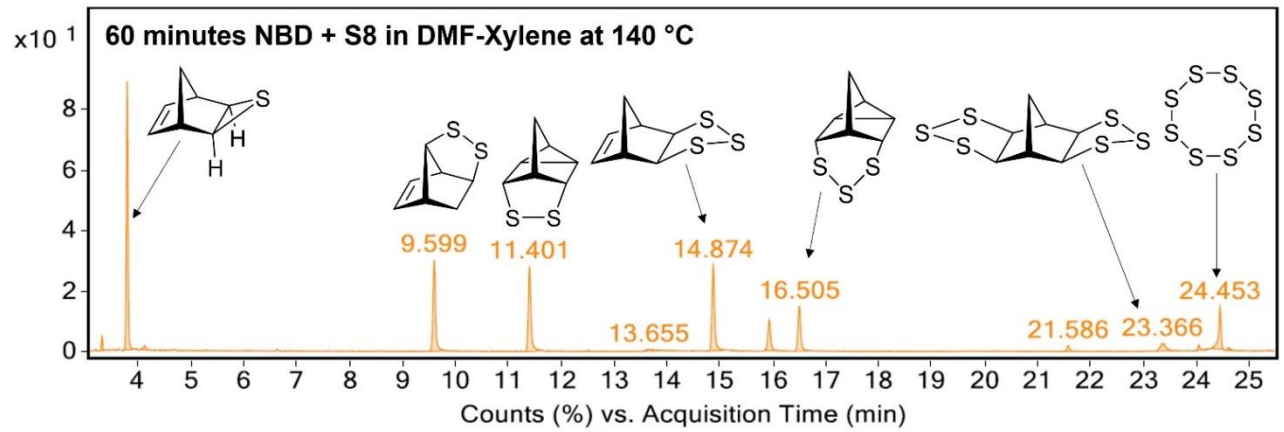
x10 1
60 minutes NBD + S8 in DMF-Xylene at 140 °C
9.599
11.401
13.655
14.874
16.505
21.586
23.366
24.453
Counts (%) vs. Acquisition Time (min)

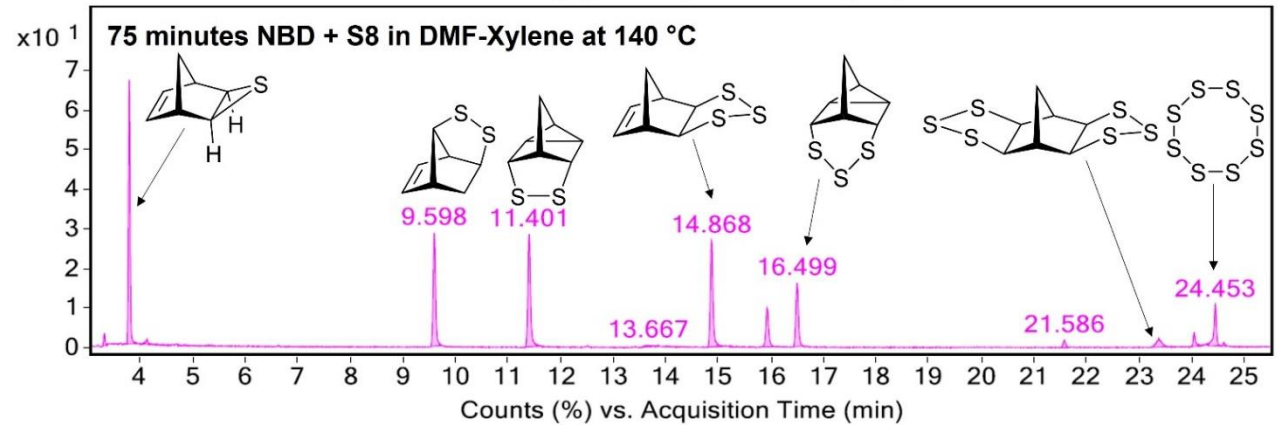
x10 1
75 minutes NBD + S8 in DMF-Xylene at 140 °C
9.598
11.401
13.667
14.868
16.499
21.586
24.453
Counts (%) vs. Acquisition Time (min)

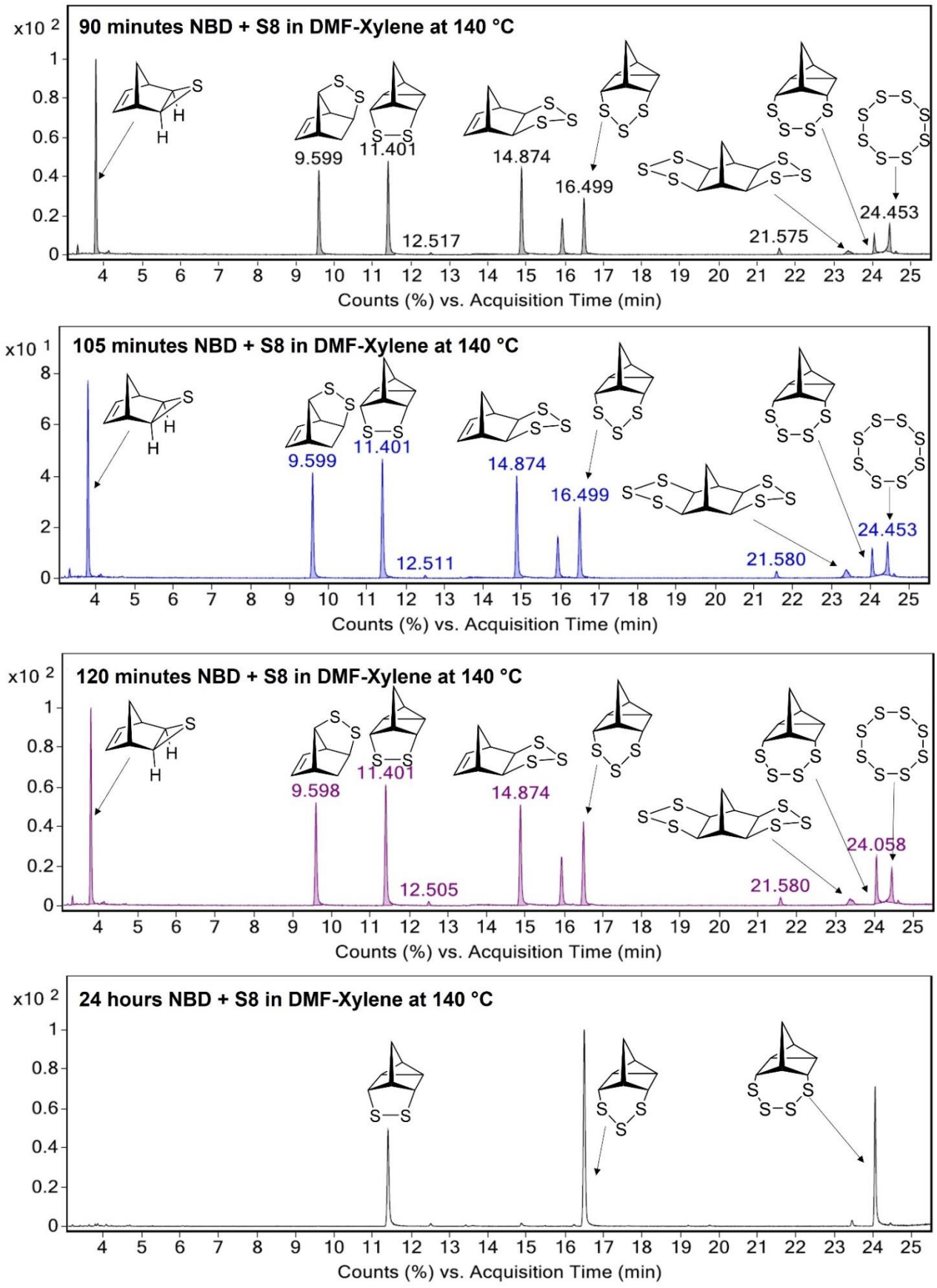

Figure 3.46: GC chromatograms for extracted products of sulfur and NBD reaction at different reaction times.

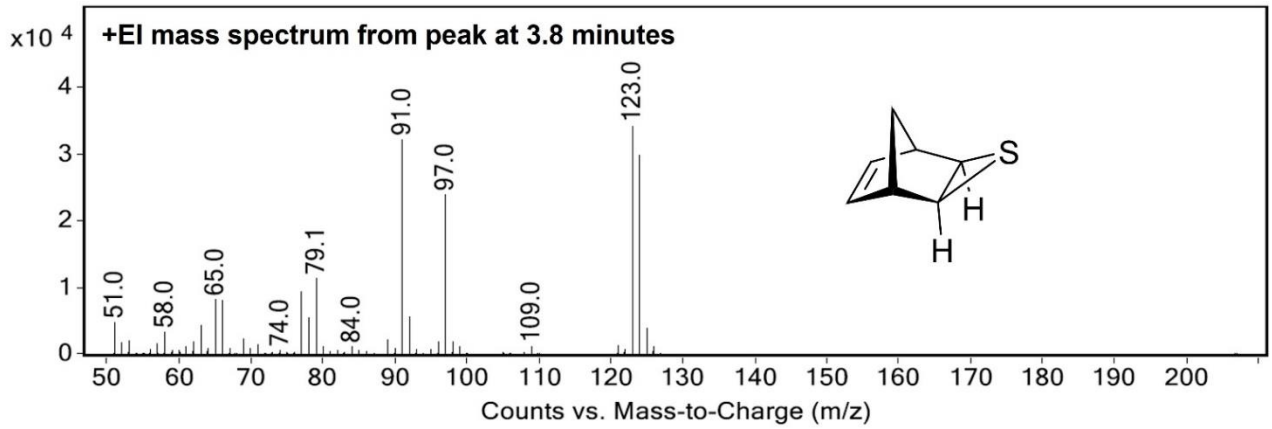
x10 4
+EI mass spectrum from peak at 3.8 minutes
123.0
91.0
97.0
79.1
65.0
58.0
51.0
74.0
84.0
109.0
S
H
H
Counts vs. Mass-to-Charge (m/z)

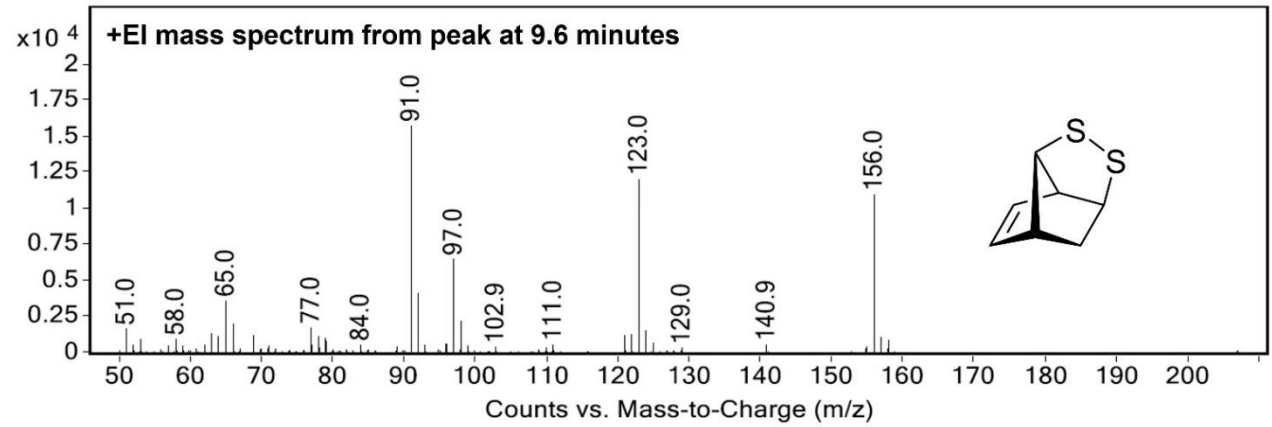
x10 4
+EI mass spectrum from peak at 9.6 minutes
91.0
123.0
156.0
97.0
65.0
51.0
58.0
77.0
84.0
102.9
111.0
129.0
140.9
S
S
Counts vs. Mass-to-Charge (m/z)

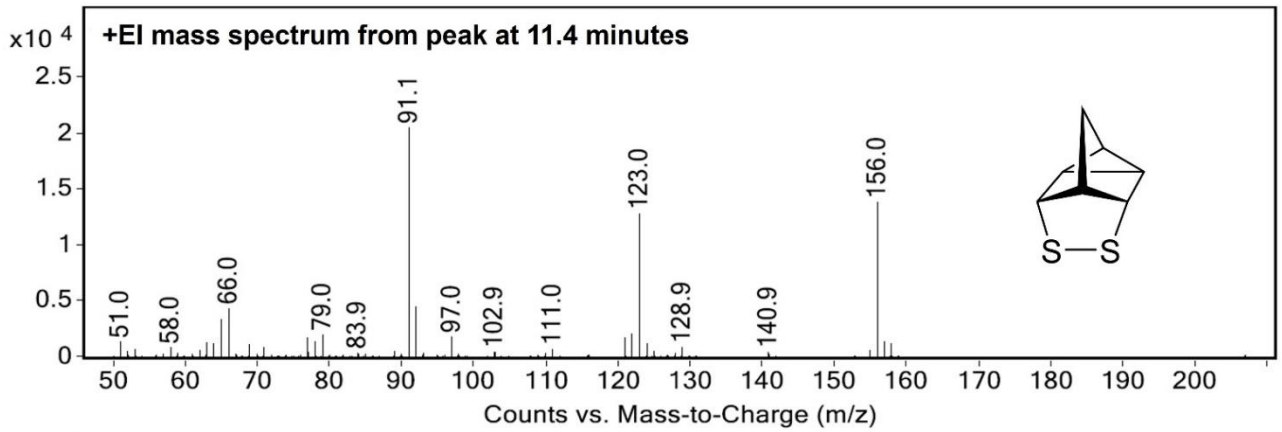
x10 4
+EI mass spectrum from peak at 11.4 minutes
91.1
123.0
156.0
66.0
51.0
58.0
79.0
83.9
97.0
102.9
111.0
128.9
140.9
S—S
Counts vs. Mass-to-Charge (m/z)

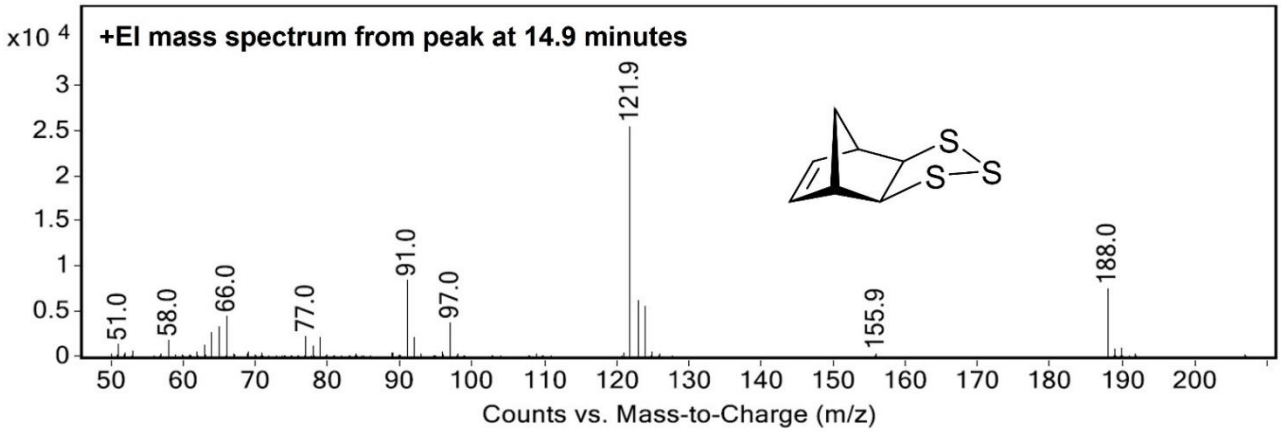
x10 4
+EI mass spectrum from peak at 14.9 minutes
121.9
91.0
188.0
66.0
97.0
77.0
51.0
58.0
155.9
S
S—S
Counts vs. Mass-to-Charge (m/z)

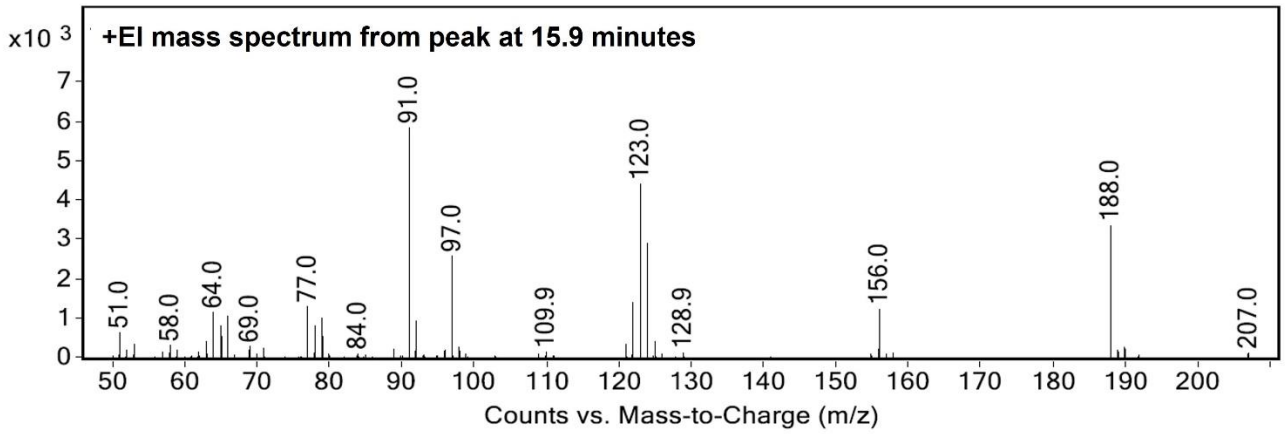
x10 3
+EI mass spectrum from peak at 15.9 minutes
91.0
123.0
188.0
97.0
156.0
51.0
58.0
64.0
69.0
77.0
84.0
109.9
128.9
207.0
Counts vs. Mass-to-Charge (m/z)

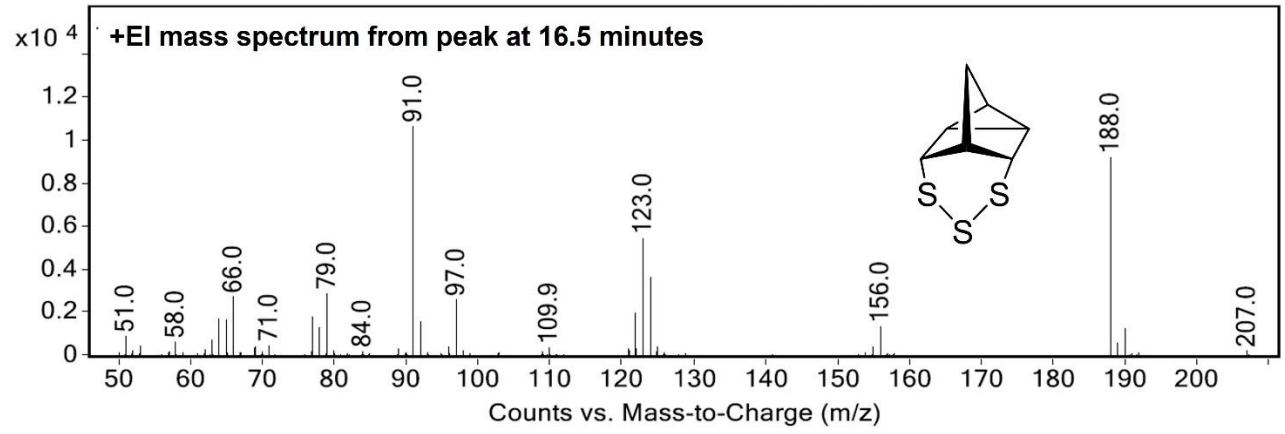
x10 4
+EI mass spectrum from peak at 16.5 minutes
91.0
188.0
123.0
S
S
S
66.0
79.0
51.0
58.0
71.0
84.0
97.0
109.9
156.0
207.0
Counts vs. Mass-to-Charge (m/z)

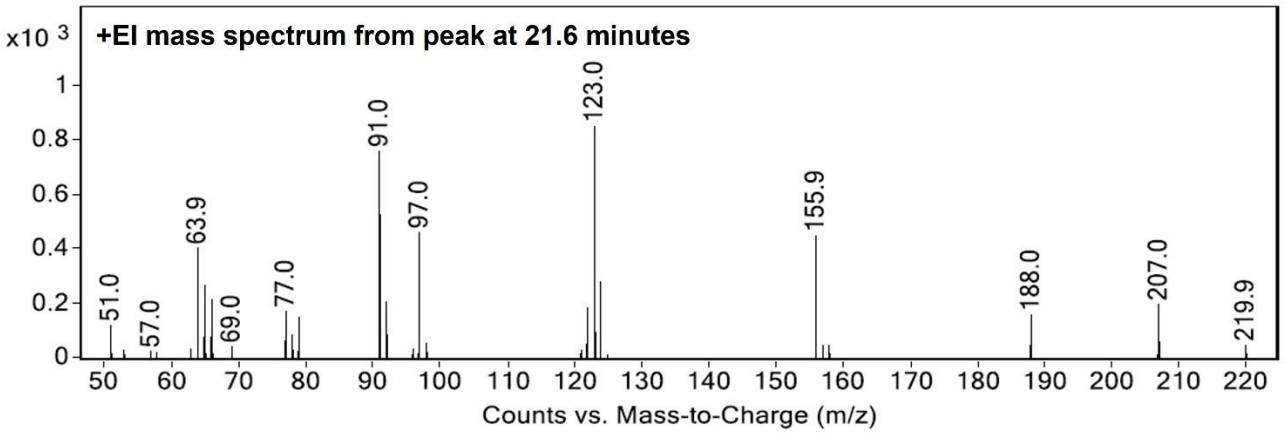
x10 3
+EI mass spectrum from peak at 21.6 minutes
123.0
91.0
155.9
63.9
97.0
51.0
57.0
69.0
77.0
188.0
207.0
219.9
Counts vs. Mass-to-Charge (m/z)

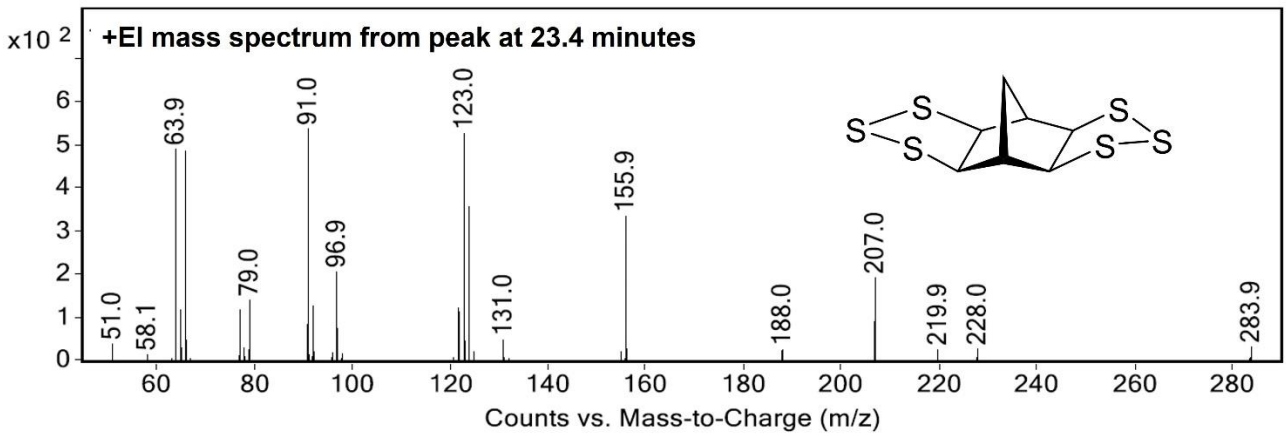
x10 2
+EI mass spectrum from peak at 23.4 minutes
63.9
91.0
123.0
155.9
S
S
S
S
S
79.0
96.9
207.0
51.0
58.1
131.0
188.0
219.9
228.0
283.9
Counts vs. Mass-to-Charge (m/z)

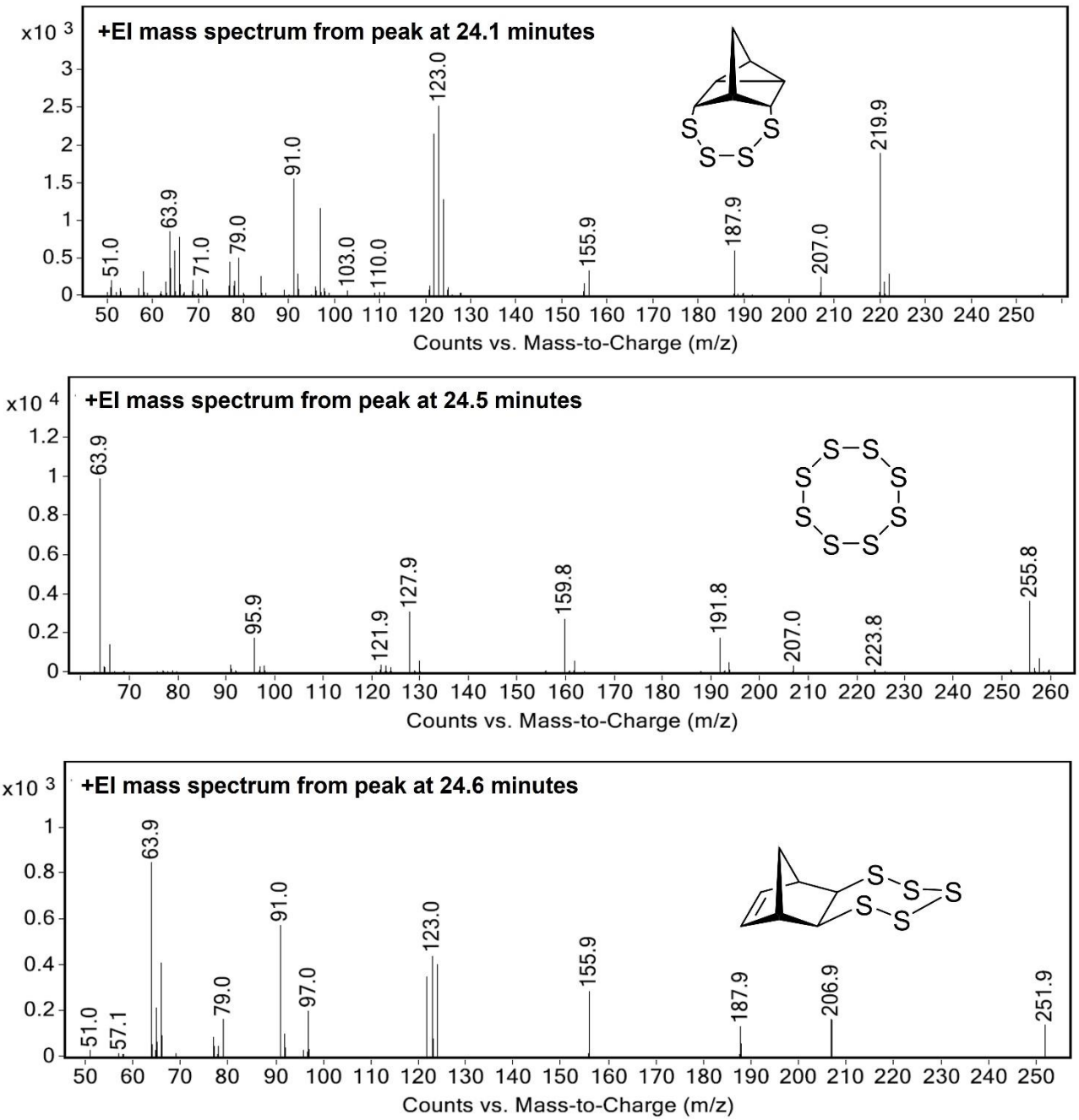

Figure 3.47: Mass spectra from major peaks in GCMS chromatograms of the extracted products from a reaction between sulfur and norbornadiene.

Discussion of results from the extracted cyclic intermediates

The hexane soluble intermediates from the reaction between NBD and sulfur gave a lot of information about the reaction and the potential structure of the polymer which was formed. There were many products which could be resolved by GC-MS, some were expected, and others indicate side reactions or alternative mechanisms. All the observed molecules along with their mass and GC retention time can be seen below.

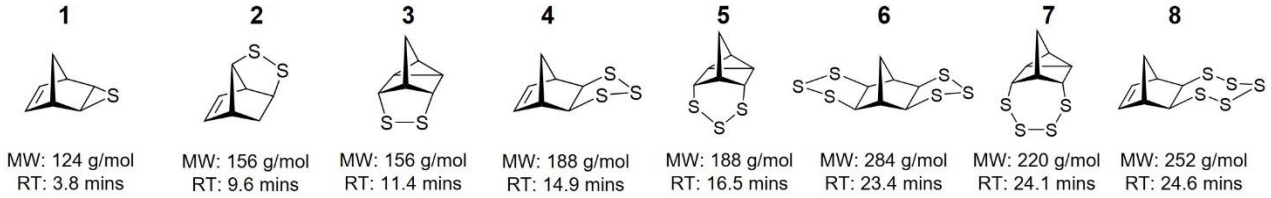

Figure 3.48: All hexane soluble products observed by GC-MS from reaction between sulfur and NBD.

There were molecules which had no change to the norbornane organic core where one or both alkenes had reacted with sulfur as expected. These molecules all had cyclic sulfur rings with either 1, 3 or 5 sulfur atoms. While not possible to confirm by GC-MS, it was confirmed by X-ray crystallography that the sulfur rings were all exo to the bridge head apart from those with a cyclopropane group. These intermediates indicate that a typical inverse vulcanisation reaction may have occurred where the alkene was attacked by a sulfur radical to form carbon sulfur bonds. When being described in any further descriptions, these molecules with an alkene will be referred to as **1**, **4** or **8** for norbornene epi, tri and penta sulfide respectively. The molecule where both alkenes had reacted to form a trisulfide ring will be referred to as norbornane bistrisulfide. The norbornane bistrisulfide molecule is only observed in the reactions that were longer than 60 minutes (30 minutes after the addition of NBD). This indicates that while the first alkene may react very rapidly, it may take some time for the second alkene to react. The relative concentration of the bistrisulfide molecule quite small, however, there are several factors that may affect how much is observed in the GC chromatogram. Firstly, it was found that the molecule was not stable in the high temperatures of the GC, leading to a range of additional peaks which eluted after 25 minutes and were not visible in the GC method used. Secondly, as there were two cyclic sulfur rings in this molecule, it means it would have crosslinked structure when polymerised. This may result in it becoming trapped within the polymer structure and would not be soluble in the hexane layer. All the observed intermediates are likely in an equilibrium between a polymerised and the cyclic product due to the dynamic nature of sulfur bonds at high temperature. They would only be observed in the hexane layer in the cyclic structure so the observed concentration likely depends on how easily they could be removed from the polymer structure. The norbornane bistrisulfide molecule would have to form two cyclic structures instead of only one like all the other molecules which would likely decrease the chance of it being released from the polymer structure and decreasing its concentration in the solvent.

There were also some molecules that indicate rearrangement of the norbornane core or deprotonation. There were several molecules which possessed a cyclopropane group. These molecules have a cyclic sulfur structure with 2, 3 or 4 sulfur atoms. Norbornadiene is known to go through a rearrangement to form quadricyclane, usually through a light induced, intramolecular [2+2] cycloaddition.[18] This molecule has seen extensive use in energy storage applications. In this rearrangement, the same cyclopropane group is observed. During the reaction between NBD and sulfur, it is likely that a similar reaction occurs. Although here it is proposed to be initiated initiated by a sulfur radical attacking an alkene. This would form a carbon radical on the NBD molecule which could result in an intramolecular rearrangement to form the observed cyclopropane

group. The molecules containing this group were very common and increased with reaction time. All other isolated intermediated decreased over time. This is likely because the other intermediates all had an alkene which could still react. As time went on, this alkene would allow them to become incorporated into the polymer structure. The molecules with a cyclopropane group could only form two sulfur chains when in the polymer structure and would likely exist in an equilibrium between the cyclic and polymeric forms. This is why they can be observed even after a 24-hour reaction time.

Finally, there was a molecule with an alkene and a sulfur chain to the bridge carbon in the norbornene. The mechanism for how the molecule is formed is not fully understood but it is believed to have formed from a hydride shift from the bridging carbon to one of the outer carbons. This mechanism can be seen in the figure below. According to computational analysis, the bond dissociation energy of the C-H bond on the bridge carbon is the weakest.[19] This molecule still had an alkene which could react further and was therefore not seen after a reaction time of 24 hours. There were two peaks in the GC-MS chromatograms which could not be identified. One at 15.9 minutes and the other at 21.6 minutes. While these molecules could not be isolated and characterised by NMR, it is likely that these peaks belong to the tri and tetra sulfide variants of the molecule with a sulfur chain to the bridge carbon. The mass spectra had the correct molecular weight and fragmentation pattern for these molecules.

The presence of molecules **3**, **5** and **7** in the polymer structure would likely introduce a range of absorptions in the LWIR region which may explain the poor performance of the material in the optical transmission testing. Later in this thesis, it was found that the cyclopropane structure gives a very large absorption at around 12.4 μm. While molecule **2** does not introduce any additional functional groups, it does lose the symmetry of the molecule. Several papers have shown that symmetry is important for long wave infrared transmission as it reduces the unique modes of vibration.[20] Therefore, it is important to prevent these structures from becoming incorporated into the polymer structure to improve the optical performance.

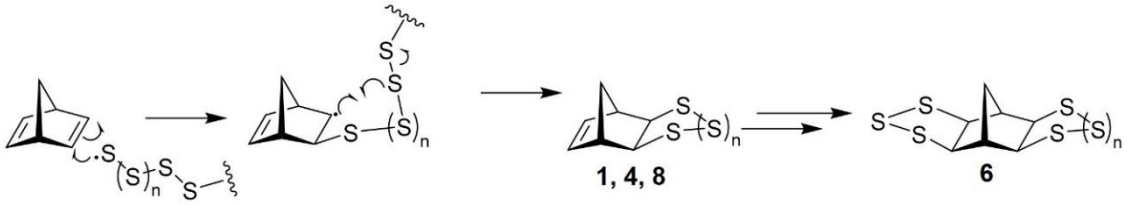

Proposed mechanism for formation of 1, 4, 6 and 8

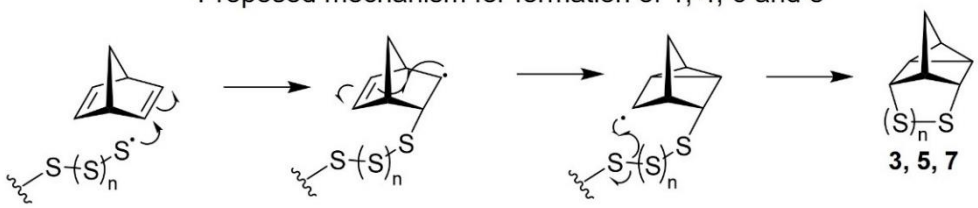

Proposed mechanism for formation of 3, 5 and 7

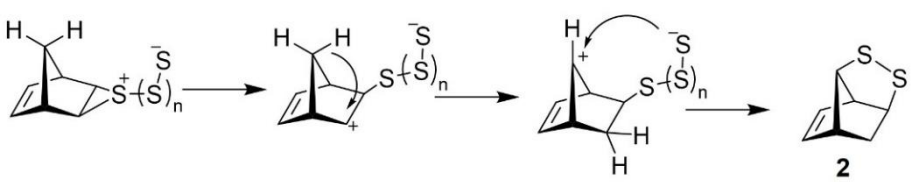

Proposed mechanism for formation of 2

Figure 3.49: Proposed mechanisms for the formation of hexane soluble cyclic sulfide intermediates.

Developing a method to isolate cyclic sulfide intermediates

After the cyclic sulfide intermediates were first found in the reaction between sulfur and NBD, a method was developed to synthesise and isolate them. This would allow for a full characterisation using NMR, GC-MS and X-ray crystallography and it may be possible to use the cyclic sulfides as monomers in future reactions.

The reaction temperature was first optimised for maximum yield of the hexane soluble intermediates. All reactions were performed using the same method, reaction conditions and molar ratio of sulfur to norbornadiene. Reaction temperatures from 80 °C to 120 °C were tested to optimise the crude yield of hexane soluble intermediates. For each reaction, a 50 mL round bottomed flask was charged with sulfur (945 mg, 3.69 mmol S8), norbornadiene (1 mL, 0.906 g, 9.83 mmol) and 10 mL of DMF. This gave a ratio of 3 sulfur atoms per NBD molecule. A magnetic stirrer was added to each flask. The reaction was left for 90 minutes, over which time, the solution went black. After this time, the solution was poured into a beaker containing 50 mL of hexane and 50 mL of distilled water. This caused any polymeric material to precipitate and combine into the water layer. The solution was filtered over celite, and the filtrate was collected. The filtrate was washed three times with 50 mL of distilled water to remove any DMF. The solution was dried with magnesium sulphate and filtered into a round bottomed flask. The hexane was removed by rotary vacuum and the crude yield was measured. The products were analysed by GC-MS and proton NMR to ensure all solvent had been removed. The samples using a temperature of less than 120 °C had a large amount of unreacted sulfur at the bottom of the flask which resulted in a reduced yield with 5.17 % and 8.65 % for the 80 °C and 100 °C respectively. The 120 °C sample was found to have the greatest crude yield of 12.2%.

A catalyst was tested to improve the crude yield of hexane soluble products. Using the same method as above, the reactions were repeated at 120 °C with and without a $[Ni(NH_3)_6]Cl_2$ catalyst. 2 mol % (45.6 mg, 197 µmol) of the catalyst was added at the start of the reaction. The sulfur in the samples with the catalyst dissolved much faster and the solution went black within 3 minutes. The yield of the reaction increased from 12.2 % to 24.9 % using the catalyst.

To further improve the yield, the reaction was repeated with 10 mL of toluene added at the start to help dissolve the sulfur. When toluene was added, there was no unreacted sulfur after 90 minutes and a reduced amount of insoluble polymer. Using toluene increased the crude yield from 25 % to 60.5 %. This was found to be the most optimised method for crude yield of hexane soluble products and was used in future experiments.

The optimised method was slightly different to the method used in the polymerisation as it used a lower temperature (120 °C instead of 140 °C), included the use of a $[Ni(NH_3)_6]Cl_2$ catalyst and used 50-50 toluene-DMF instead of 50-50 xylene-DMF. The lower temperature resulted in greatly reduced polymer and more soluble intermediates. Toluene was used instead of xylene as it has a lower boiling point which aided in its removal by rotary vacuum. Despite these differences, all the major intermediates from the polymerisation reaction were found in the optimised reaction.

There was a change in the relative proportion of the intermediates under the different reaction conditions. At lower temperatures and without the catalyst, norbornene episulfide (molecule 1) was the major product. At the higher temperature and with the catalyst, the relative proportion of norbornene trisulfide (molecule 4) increased

greatly to become the major product. This is likely because in the more optimised reactions, all the sulfur would dissolve, leading to an increase in the high sulfur molecules.

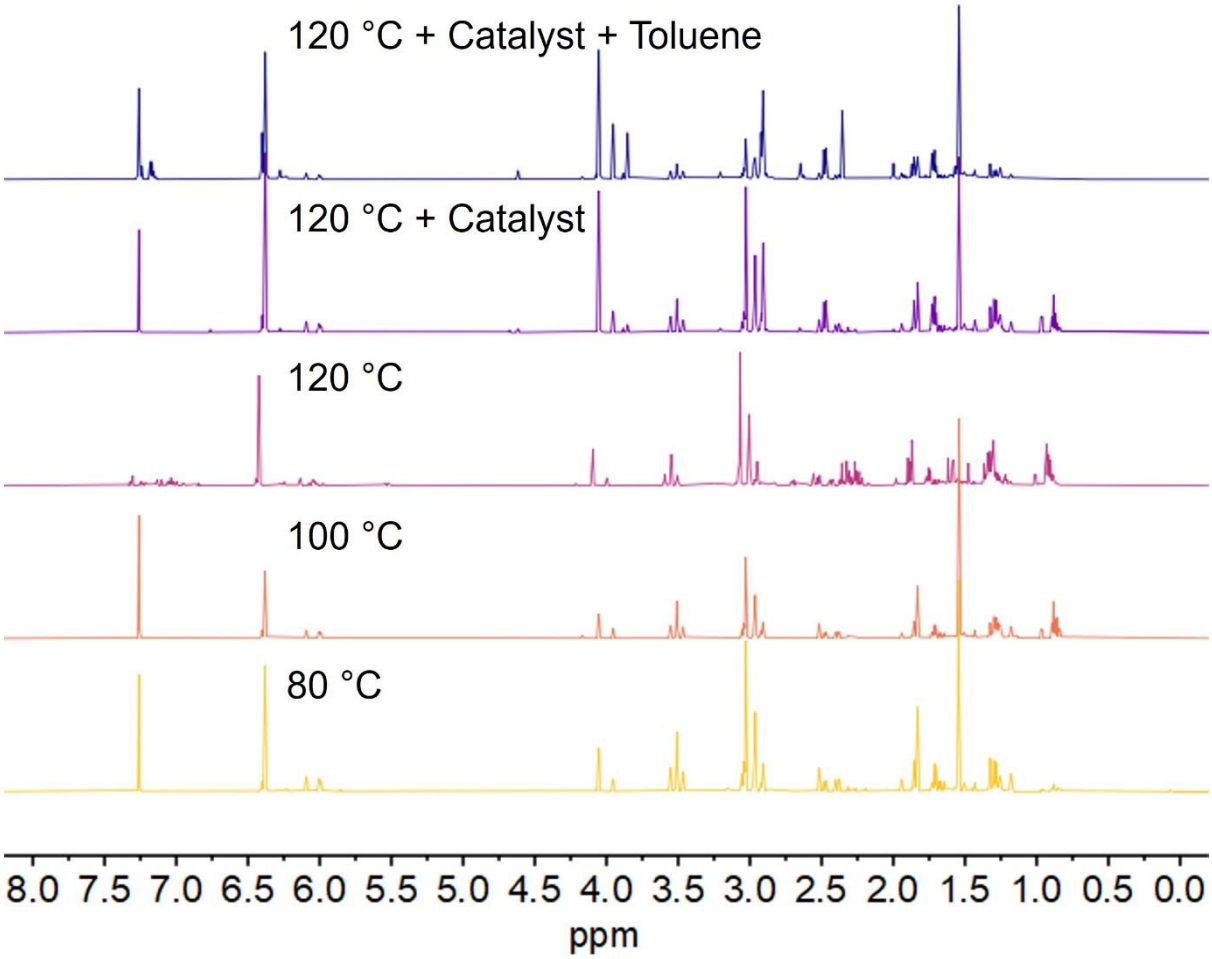

Figure 3.50: Proton NMR of crude samples obtained from the reaction between sulfur and norbornadiene under different conditions. All samples had the same reaction time (90 minutes), mass of sulfur (945 mg), mass of norbornadiene (0.906 g) and solvent (DMF, 10 mL). The two top samples had $[Ni(NH_3)_6]Cl_2$ at a loading of 2 mol % and the top sample has an additional 10 mL toluene in the solvent.

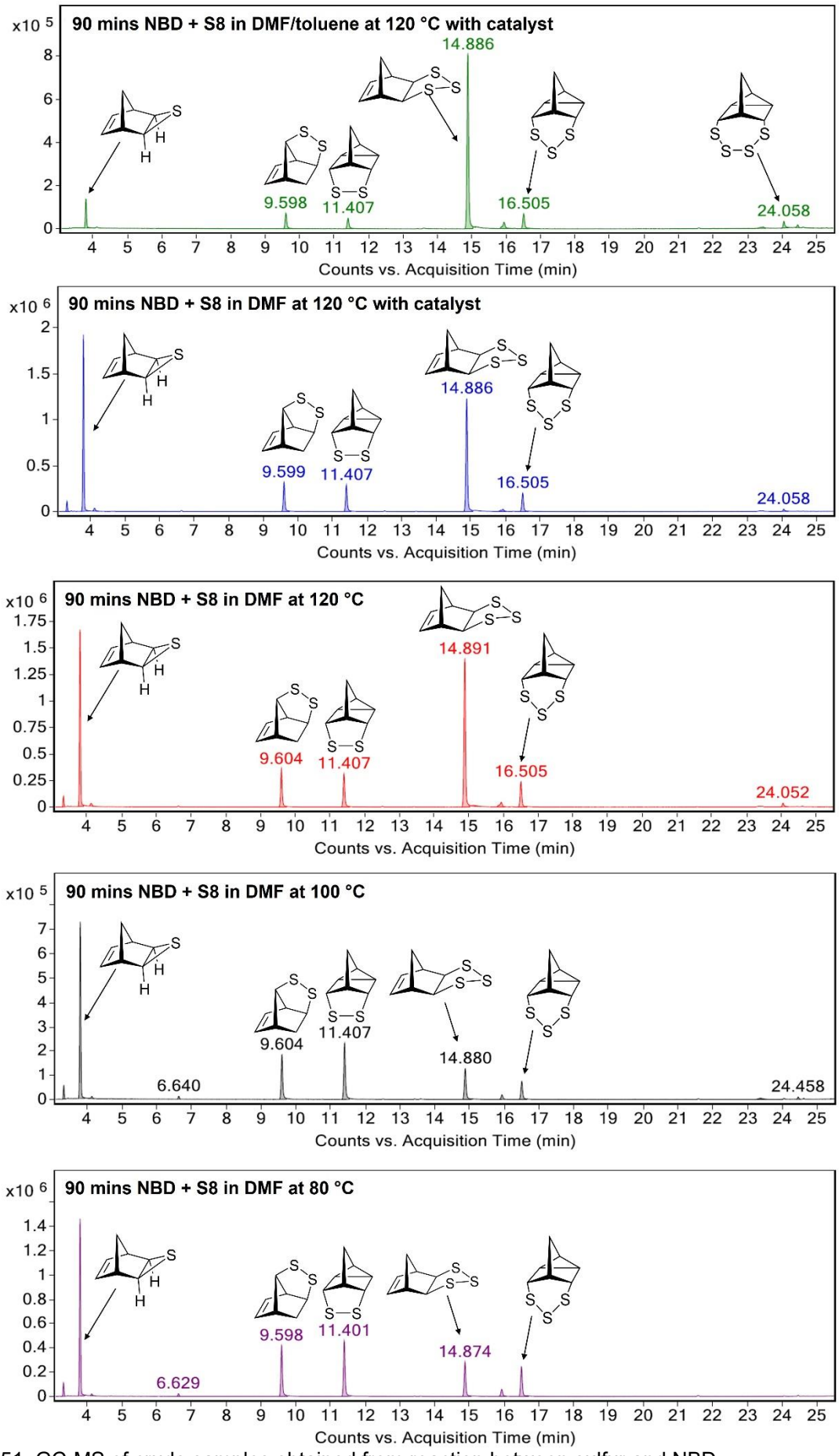

Figure 3.51: GC-MS of crude samples obtained from reaction between sulfur and NBD.

Scaling up reaction to produce intermediates

Using the optimised conditions for crude yield, the reaction was scaled up by a factor of 5. This was necessary so that the intermediates could be isolated at a scale that was appropriate for analysis and any further reactions.

A 250 mL round bottomed flask was charged with sulfur (4.725 g, 18.43 mmol S8), norbornadiene (5 mL, 4.53 g, 49.15 mmol) and $[Ni(NH_3)_6]Cl_2$ (228 mg, .984 mmol). 50 mL of DMF and 50 mL of toluene were added along with a magnetic stirrer. The reaction was heated to 120 °C and left for 90 minutes. Following this, the solution was poured into a beaker containing 250 mL of hexane and 250 mL of distilled water. This caused any polymeric material to precipitate and combine into the water layer. The solution was then filtered over celite, and the filtrate was collected. The orange-coloured filtrate was washed three times with 250 mL of distilled water to remove any DMF. The solution was then dried with magnesium sulphate and filtered into a round bottomed flask. The hexane was removed by rotary vacuum and a crude yield of 59.7 % was obtained. NMR and GCMS of the crude products showed a very similar distribution of products as the optimised small-scale reaction.

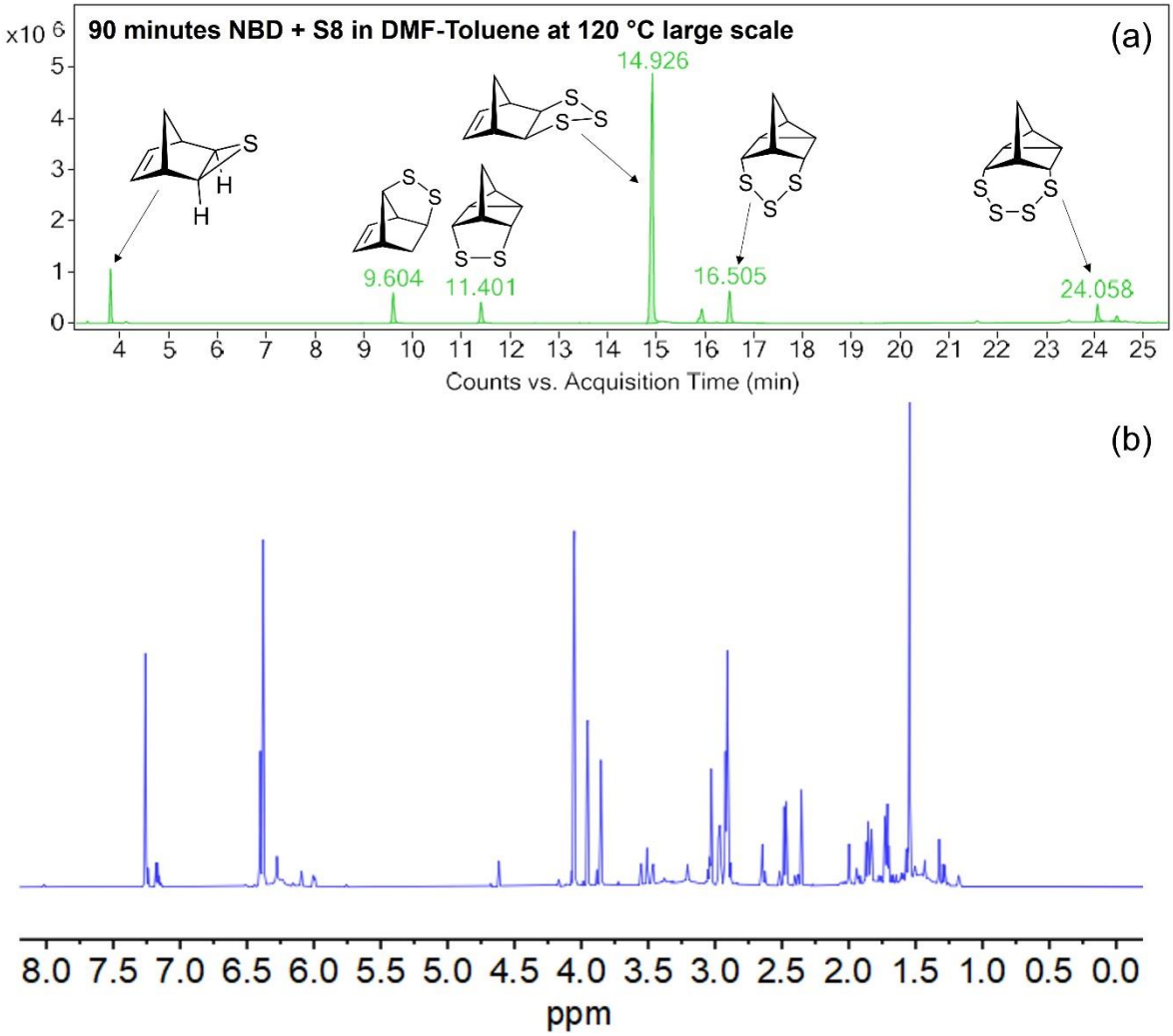

Figure 3.52: Analysis of crude products obtained from scaled up reaction between norbornadiene and sulfur in DMF-toluene using 2 mol % $[Ni(NH_3)_6]Cl_2$. (a) GCMS chromatogram of hexane soluble crude products. (b) Proton NMR in deuterated chloroform of hexane soluble crude products.

Purification of intermediates

The products of the scaled-up reaction were isolated using flash chromatography over silica gel using hexane as a mobile phase. This was done so they could be characterised fully and so they could be investigated as monomers.

The first fraction to elute was a mixture of mostly norbornene epi, tri and penta-sulfide (**1**, **4** and **8**). These would usually be produced in a ratio of 0.24: 1: 0.4 of **1**: **4**: **8**. **4** and **8** could be separated by growing crystals overnight at 4 °C from the neat solution. **1** remained as an oil which was be decanted to remove it from the crystals. The crystals of **1** and **3** could then be washed with cold hexane. In some samples, a small amount of the **8** could be isolated by washing the crystals in chloroform and filtering the solution. The crystal of **8** is only soluble in chloroform with extended sonication while the crystal of **4** dissolves readily. **8** could not be detected by GCMS as it would degrade to form **4** and sulfur in the column. **1** has not been isolated as it would always have some impurity of **4** and **8**. The GCMS and NMR characterisation of each fraction along with the isolated products are shown below.

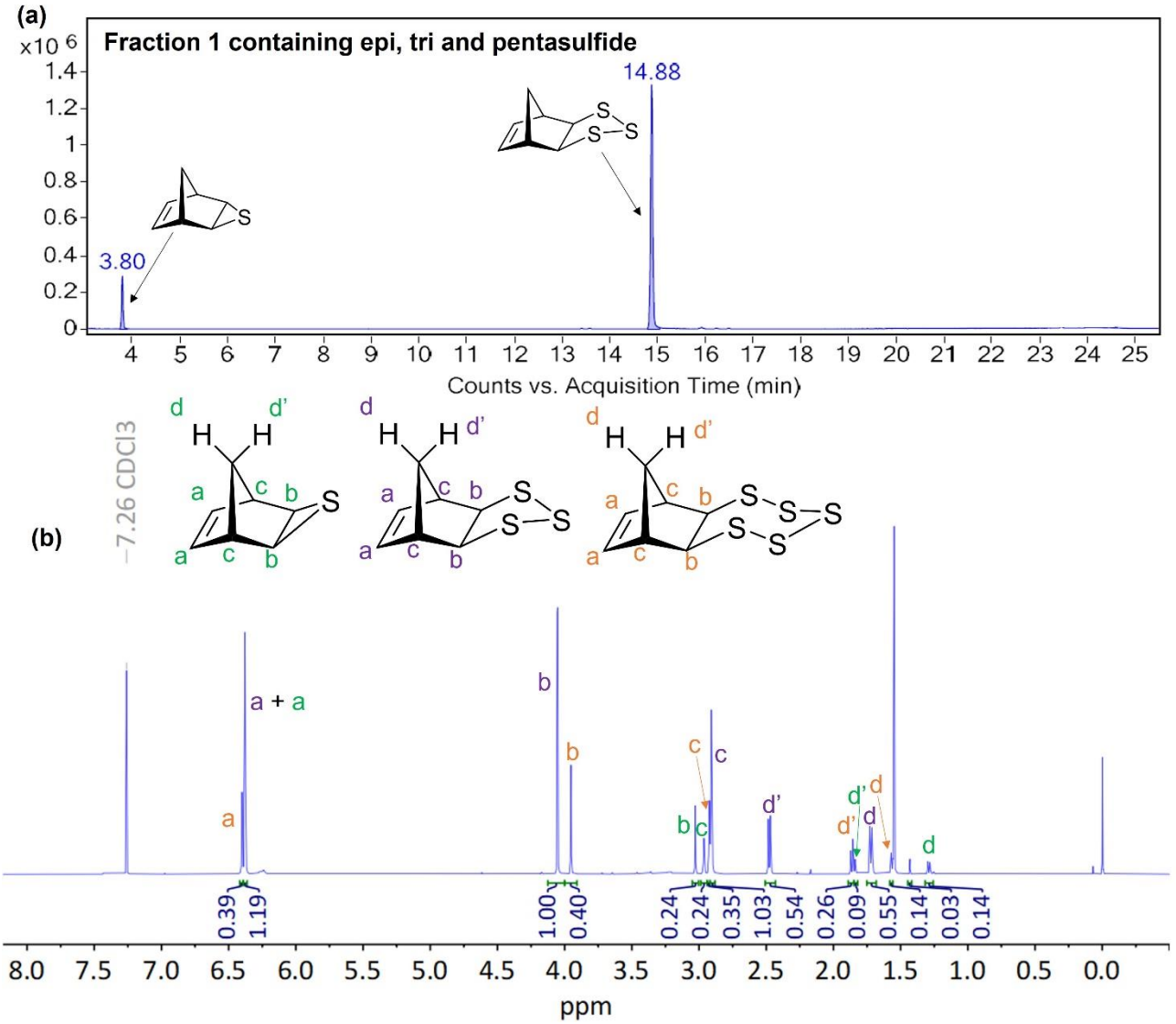

Figure 3.53: Fraction one from column of polysulfides. (a) GCMS chromatogram from fraction one. (b) Proton NMR in deuterated chloroform of fraction one.

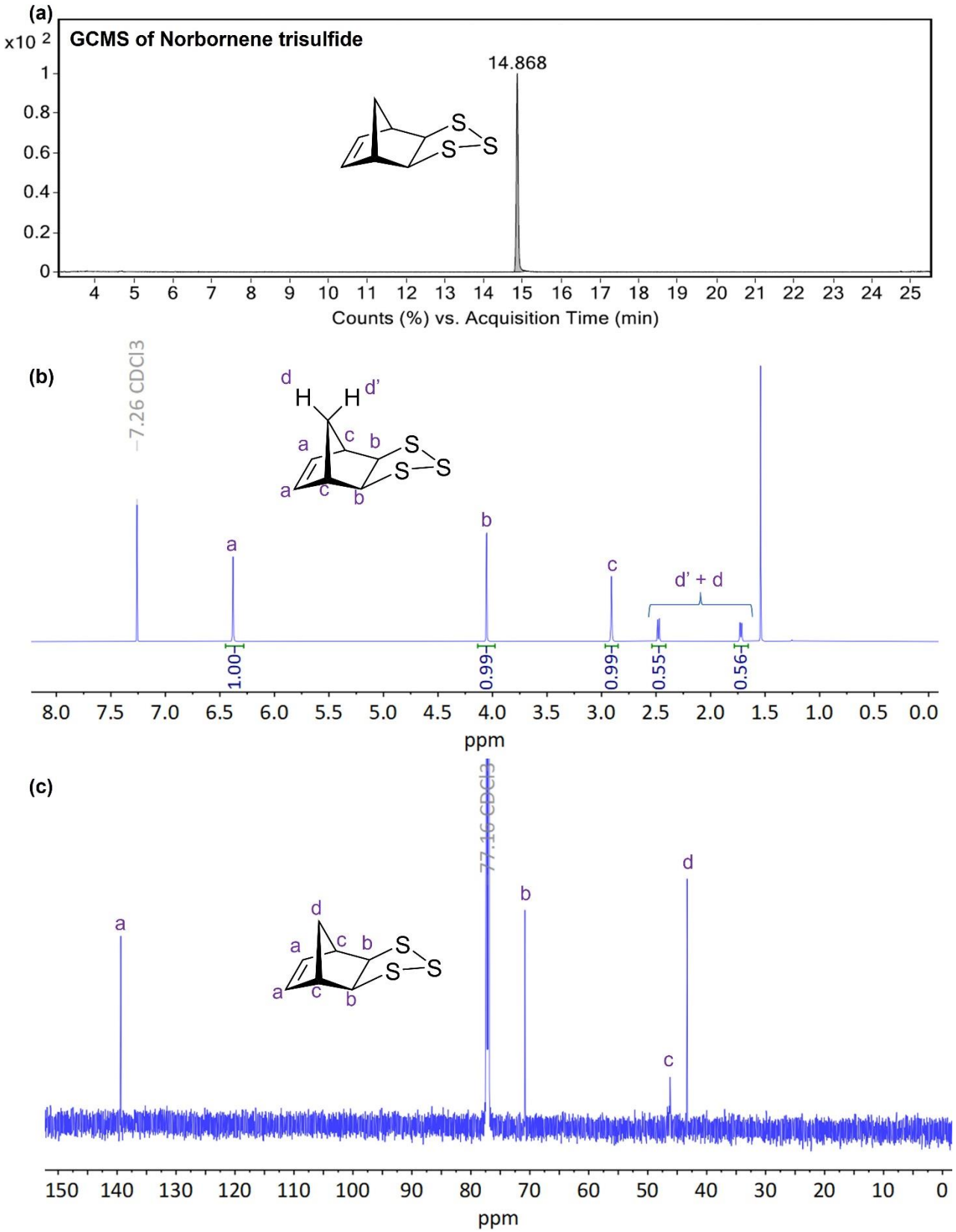

^{1}H NMR (600 MHz, CDCl3) δ 6.38 (m, 2H), 4.05 (d, J = 1.9 Hz, 2H), 2.91 (m, 2H), 2.48 (ap. d, J = 9.3, 1H), 1.72 (m, 1H). **^{13}C NMR** (151 MHz, $CDCl_3$) δ 139.38, 70.81, 46.21, 43.32

Figure 3.54: Analysis of norbonene trisulfide (molecule **4**). (a) GCMS of **4**. (b) proton NMR of **4** in deuterated chloroform. (c) carbon thirteen NMR of **4** in deuterated chloroform.

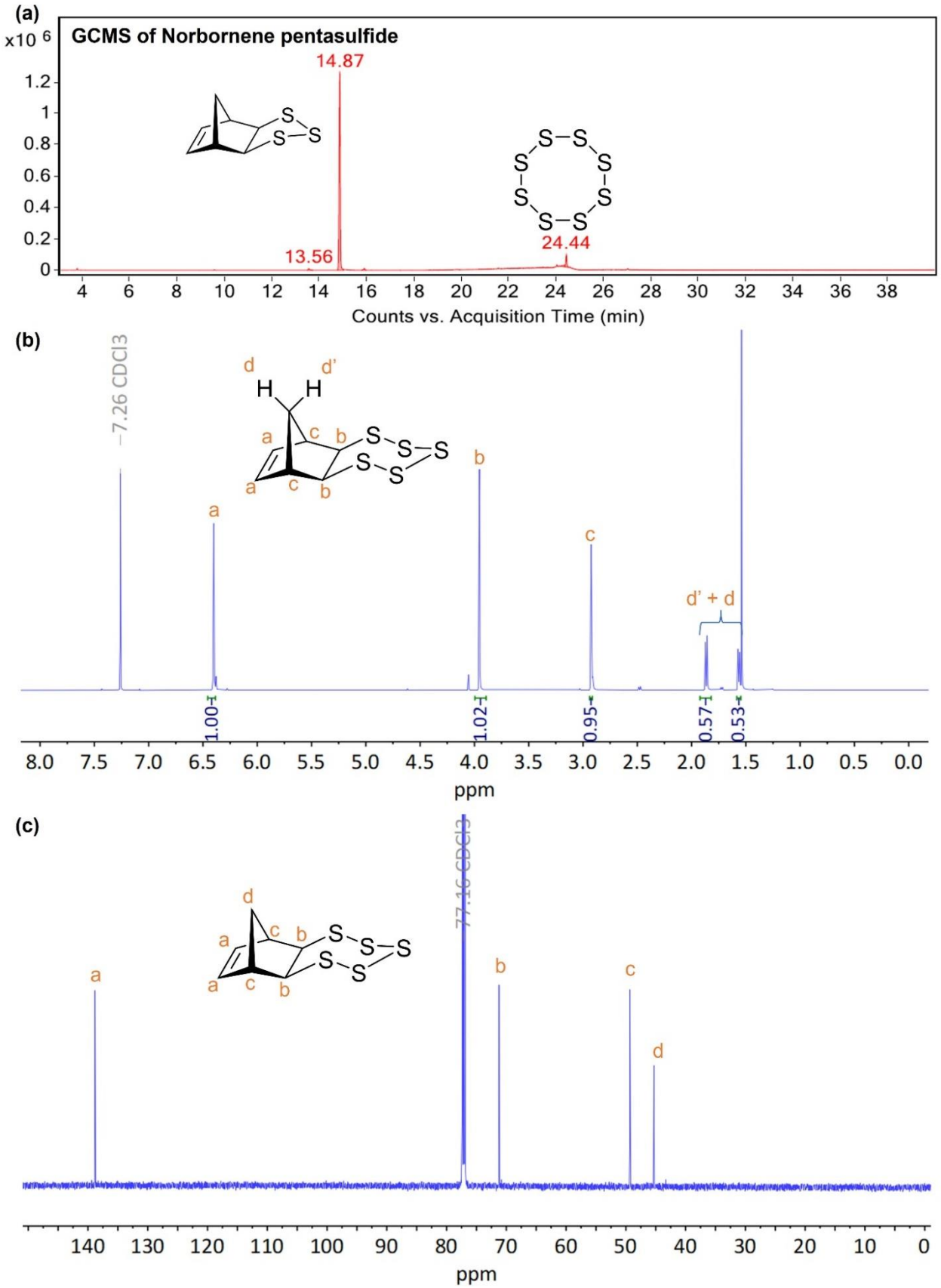

^{1}H NMR (600 MHz, CDCl3) δ 6.40 (m, 2H), 3.95 (d, J = 2.0 Hz, 2H), 2.92 (m, 2H), 1.86 (ap. d, J = 9.4, 1H), 1.56 (m, 1H). **^{13}C NMR** (151 MHz, CDCl3) δ 138.83, 71.22, 49.33, 45.29.

Figure 3.55: Analysis of norbonene pentasulfide (molecule **8**). (a) GCMS of **8**. (b) proton NMR of **8** in deuterated chloroform. (c) carbon thirteen NMR of **8** in deuterated chloroform.

The second fraction contained the molecules **2** and **5**. This corresponds to the molecule with the sulfur chain to the bridge carbon and the trisulfide rearranged product. This fraction also contained norbornane bistrisulfide (molecule 6) but this could be removed by growing crystals in a dilute solution in hexane. Further purification of this fraction could not be done as it formed a yellow gel over a period of 24 hours which was no longer soluble in chloroform or hexane. The NMR peaks match those reported by Paul Bartlett and Tirthankar Ghosh.[21]

Figure 3.56: Image of yellow gel formed from fraction 2 over 24 hours.

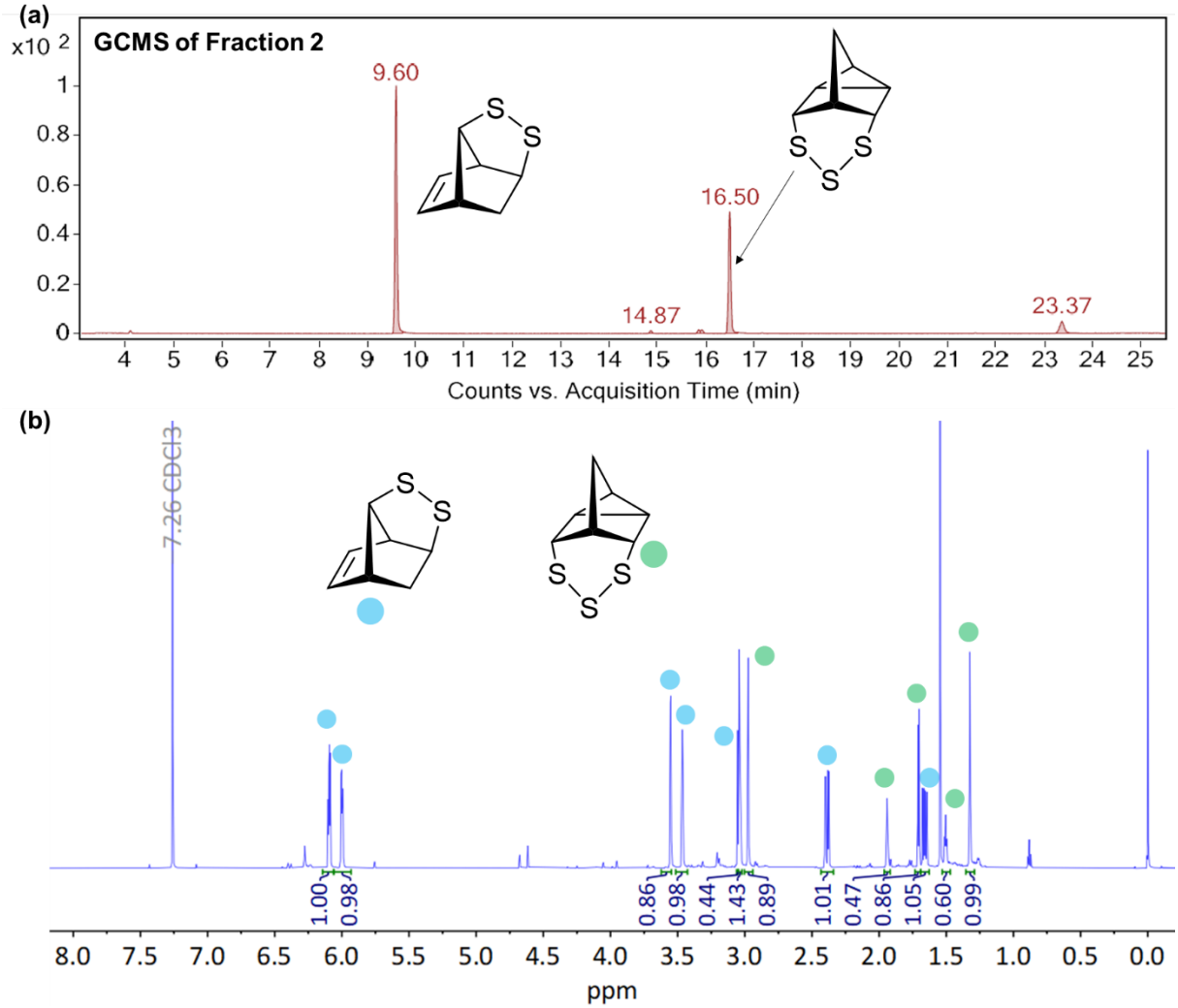

Figure 3.57: Analysis of fraction 2. (a) GCMS of fraction 2. (b) Proton NMR of fraction 2.

The third fraction contained mostly norbornane bistrisulfide (molecule **6**). Crystals of the product would form on the tubes used for the column overnight at room temperature. **6** was not stable in the GC-MS column and gave a very broad peak at around 26 minutes and a range of sharper peaks. When using the method, the relative amount of the **6** formed was low and yields were typically less than 5 %. In the optimised method for synthesis of norbornadiene bistrisulfide section, a new method was developed to improve this yield.

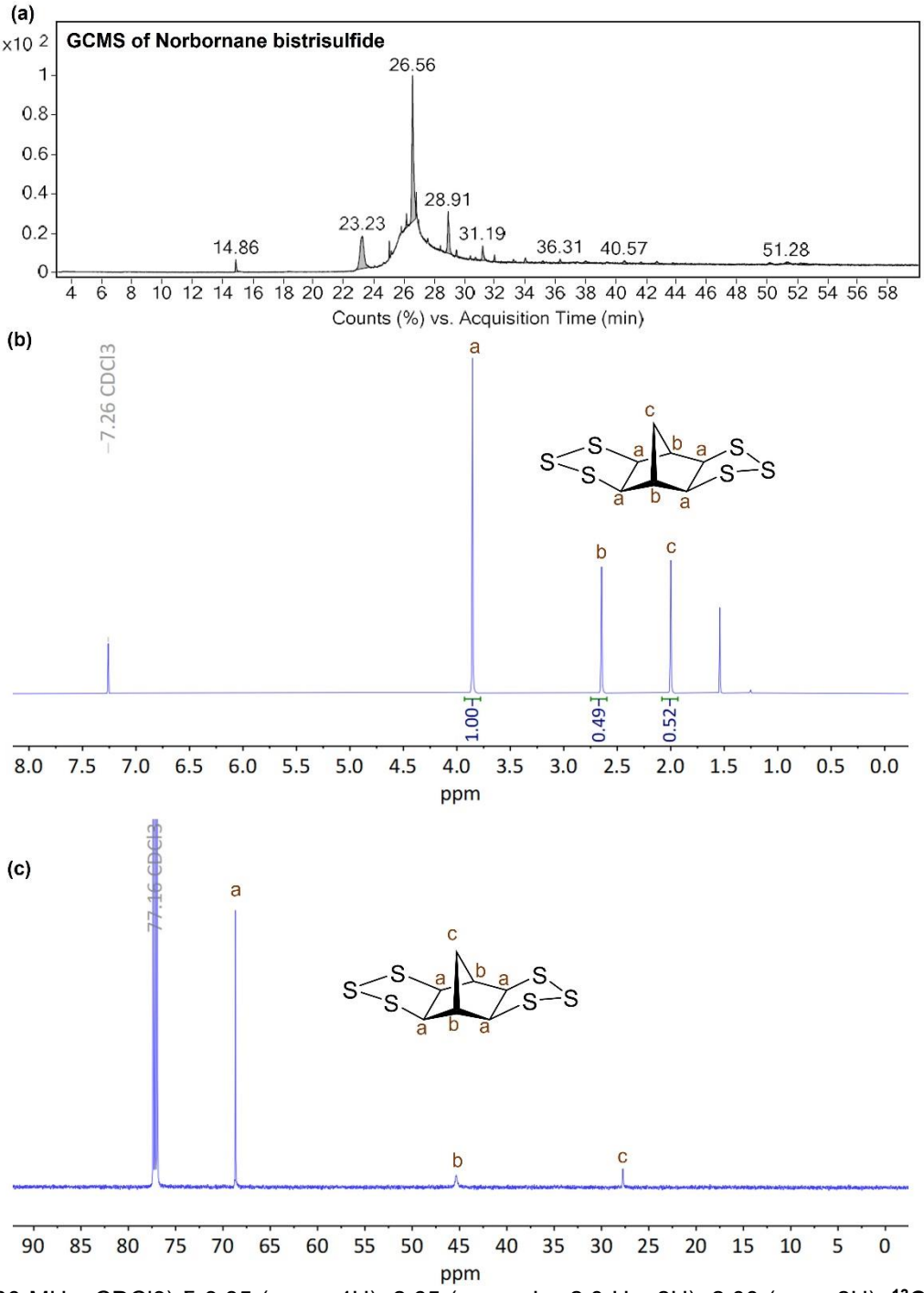

^{1}H NMR (600 MHz, CDCl3) δ 3.85 (ap. s, 4H), 2.65 (ap. s, J = 2.0 Hz, 2H), 2.00 (ap.s, 2H). **^{13}C NMR** (151 MHz, CDCl3) δ 68.68, 45.35, 27.74.

Figure 3.58: Analysis of norbonane bis trisulfide (molecule **6**). (a) GCMS of **6**. (b) proton NMR of **6** in deuterated chloroform. (c) carbon thirteen NMR of **6** in deuterated chloroform.

The fourth fraction contained mostly molecule **3** which is the rearranged product with a disulfide ring. There was a very small impurity which mostly consisted of **7** which is the rearranged product with a tetrasulfide ring. Over several days, **3** would crystalise out of the neat solution.

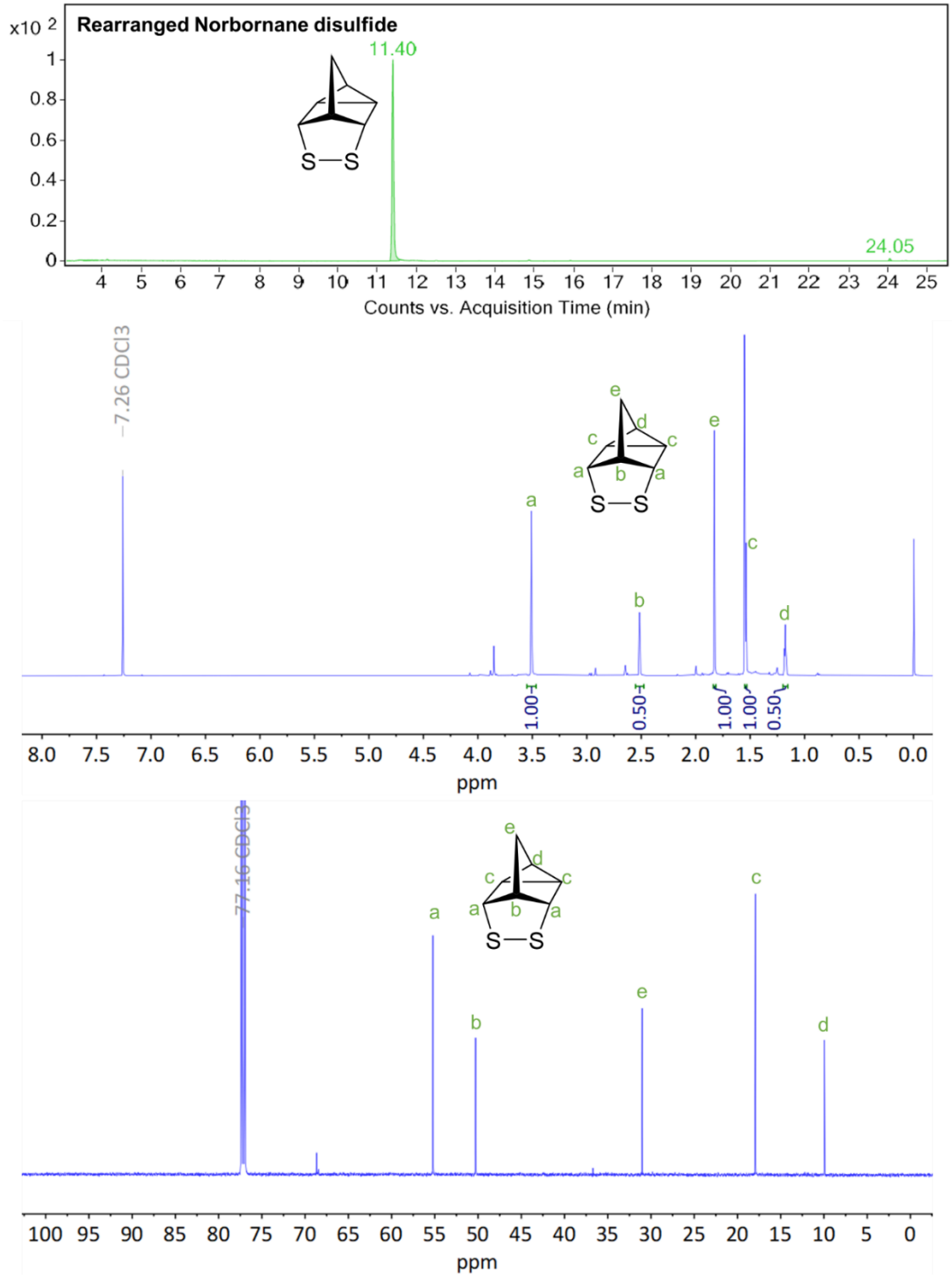

^{1}H NMR (600 MHz, CDCl3) δ 3.51 (m, 2H), 2.52 (m, 1H), 1.83 (t, J = 1.5 Hz, 2H), 1.54 (ap. d, J = 5.0, 2H), 1.18 (td, J = 5.0, 1.2 Hz, 1H). **^{13}C NMR** (151 MHz, CDCl3) δ 55.22, 50.28, 31.01, 17.93.

Figure 3.59: Analysis of rearranged norbonane disulfide (molecule **3**). (a) GCMS of **3**. (b) proton NMR of **3** in deuterated chloroform. (c) carbon thirteen NMR of **3** in deuterated chloroform.

Optimised method for synthesis of norbornane bistrisulfide

While the method above was effective in isolating most of the other intermediates, norbornane bistrisulfide (molecule **6**) could only be prepared in a small quantity at a relatively low yield. This molecule was also of interest to use as a monomer for a polymerisation reaction. If it were to be used as a monomer, a large quantity would be required. It would also be advantageous to prepare it without needing column separation to reduce wasted solvent and allow for easier large-scale synthesis. For these reasons, the method to prepare **6** was modified. The optimised method used a reaction time of 24 hours and molar ratio of 6 sulfur atoms for every norbornadiene molecule. These modifications were found to favour **6** over the other intermediates.

A 250 mL round bottomed flask was charged with sulfur (9.450 g, 36.875 mmol S8), norbornadiene (5 mL, 4.53 g, 49.15 mmol) and $[Ni(NH_3)_6]Cl_2$ (228 mg, .984 mmol). 50 mL of DMF and 50 mL of toluene were added along with a magnetic stirrer. The vial was attached to a condenser and heated at 120 °C for 24 hours. Following this, the solution was poured into a beaker containing 250 mL of hexane and 250 mL of distilled water. This caused any polymeric material to precipitate and combine into the water layer. The solution was then filtered over celite, and the filtrate was collected. The orange-coloured filtrate was washed three times with 250 mL of distilled water to remove any DMF. The solution was then dried with magnesium sulphate and filtered into a round bottomed flask. The washing and filtering steps were done quickly as **6** would start to precipitate. The round bottomed flask was sealed and left overnight. Norbornane bistrisulfide would precipitate as a yellow powder. After the norbornane bistrisulfide fully precipitated (usually 24 hours) the hexane solution was carefully poured out of the vial. Most of the NBBTS would stick to the side of the glass and the hexane was poured carefully to avoid any loss. Toluene was then added to the round bottomed flask to dissolve **6,** some sonication was required to remove it from the side of the glassware. The solution was then poured into a vial, and the toluene was removed by rotary evaporation.

NMR indicated that **6** precipitated with a molecule consisting of a trisulfide ring on one side of the norbornane and a pentasulfide ring on the other. The precipitate had a melting point of 172 °C. If a pure crystalline sample was required, a hot recrystalisation in hexane gave pure norbornane bistrisulfide with a melting point of 179 °C. A maximum yield of 9.48 % was obtained.

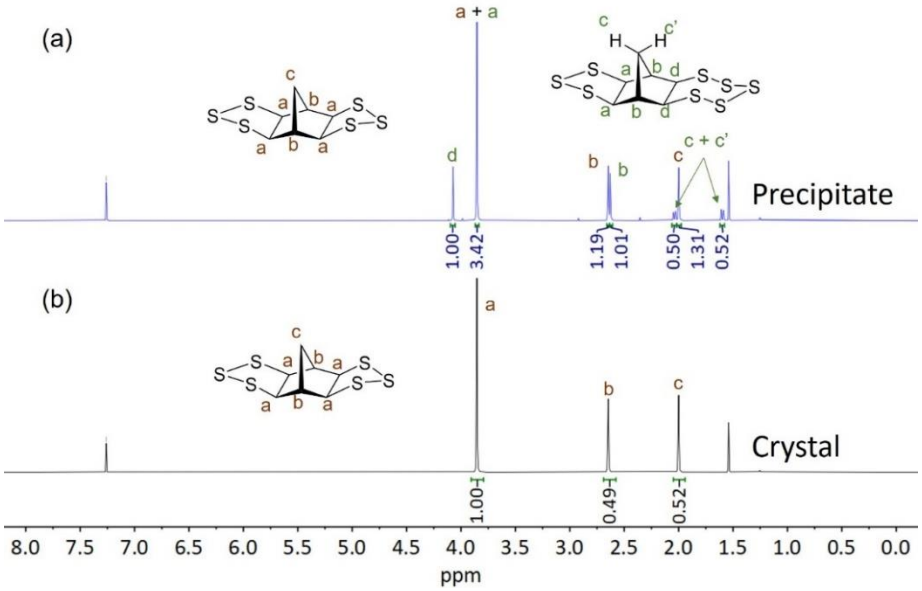

Figure 3.60: (a) Proton NMR of precipitate showing both molecule **6** and an impurity. (b) Proton NMR of a crystal of **6**.

X-Ray Crystallography

Acknowledgements: Jasmine People is thanked for contributing to preparing the crystals for **4** and **6**, Witold Bloch for assisting with mounting of the crystals and analysis of X-ray diffraction data and Steven Tsoukatos for collecting diffraction data.

Crystals of norbornene trisulfide (**4**), norbornene pentasulfide (**8**), norbornane bistrisulfide (**6**), and the rearranged molecule with a disulfide (**3**) were prepared and analysed on the Australian Synchrotron. The data showed that the sulfur chain was exo to the bridge in **4**, **8** and **6**, indicating that sulfur attacks the less hindered exo side of NBD.

Single crystals were mounted in paratone-N oil on a nylon loop. X-ray diffraction data was collected at 100(2) K on the MX-1 or MX-2 beamline of the Australian Synchrotron (λ = 0.7107 Å).[22] Structures were solved by direct methods using SHELX[23] and refined with SHELXL[24] and ShelXle[25] as a graphical user interface. All non-hydrogen atoms were refined anisotropically and hydrogen atoms were included as invariants at geometrically estimated positions.

Table 3.2: X-ray experimental data for molecules **4**, **6**, **8**, and **3.**

	NBTS (4)	**NBBTS (6)**	**NBPS (8)**	**ReNBDS (3)**
CCDC number	2289708	2289709	2305218	2305219
Empirical formula	$C_7H_8S_3$	$C_7H_8S_6$	$C_7H_8S_5$	$C_7H_8S_2$
Formula weight	188.31	284.49	252.43	156.25
Crystal system	Orthorhombic	Monoclinic	triclinic	monoclinic
Space group	Pbcn	$P2_1/c$	P-1	P 21/m
***a* (Å)**	42.045(8)	6.7640(14)	9.0240(18)	5.8750(12)
***b* (Å)**	7.7730(16)	13.008(3)	9.921(2)	9.2290(18)
***c* (Å)**	9.6930(19)	12.204(2)	11.724(2)	6.527(2)
α (º)	90	90	87.16(3)	90
β (º)	90	100.82(3)	71.21(3)	108.75(3)
γ (º)	90	90	86.85(3)	90
Volume ($Å^3$)	3167.8(11)	1054.7(4)	991.6(4)	335.12(15)
Z	16	4	4	2
Density (calc.) (mg/m^3)	1.579	1.792	1.691	1.548
Absorption coefficient (mm^{-1})	0.849	1.243	1.107	0.686
F(000)	1568	584	520.0	164.0
Crystal size (mm^3)	0.17 x 0.15 x 0.12	0.25 x 0.21 x 0.18	0.23 x 0.12 x 0.11	0.22 x 0.08 x 0.07
θ range for data collection (º)	0.969 to 27.882	2.310 to 27.882	1.836 to 28.597	3.296 to 28.506
Reflections collected	46785	15666	12602	4165
Observed reflections [R(int)]	3673 [0.0385]	2510 [0.0538]	3247[0.0361]	720
Goodness-of-fit on F^2	1.105	1.080	1.081	1.083
R_1 [I>2σ(I)]	0.0300	0.0301	0.0373	0.0306
wR_2 (all data)	0.0806	0.0768	0.0990	0.0902
Largest diff. peak and hole (e.Å-3)	0.388 and -0.389	0.614 and -0.530	1.213 and -0.465	0.293 and -0.510
Data / restraints / parameters	3673 / 0 / 181	2510 / 0 / 119	3433/0/217	720/0/46

Thermal Ellipsoid plots

Norbornene trisulfide – Molecule **4**

Yellow crystals of norbornene trisulfide were grown overnight from a neat solution of fraction one at 4 °C. The crystals were washed with cold hexane to remove any norbornene episulfide. This gave crystals of both norbornene trisulfide and norbornene pentasulfide. The trisulfide could be easily recognised as it was yellow while the pentasulfide was clear. The structure was solved in the orthorhombic space group Pcbn and refined to an R1 value of 3 %. The asymmetric unit contains two norbornene trisulfide molecules. The melting point of the crystal was 138 °C.

Figure 3.61: Image of norbornene trisulfide asymmetric unit with all non-hydrogen atoms shown as ellipsoids at the 50 % probability level.

Norbornene pentasulfide – Molecule **8**

White crystals of norbornene pentasulfide were grown overnight at 4 °C from a neat solution of fraction one. This gave both the norbornene trisulfide and norbornene pentasulfide. To separate the pentasulfide, the crystals were washed with chloroform. This would cause the trisulfide crystals to desolve, leaving only the norbornene pentasulfide crystals. The structure was solved in the triclinic space group P1 and refined to an R1 value of 3.63 %. The asymmetric unit contains two norbornene pentasulfide molecules. The melting point of the crystal was 93 °C.

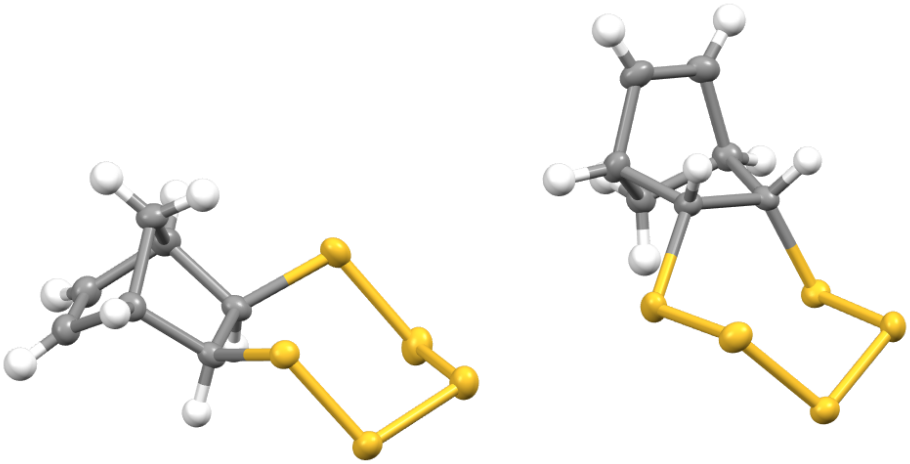

Figure 3.62: Image of norbornene pentasulfide asymmetric unit with all non-hydrogen atoms shown as ellipsoids at the 50 % probability level.

Norbornane bistrisulfide – molecule **6**

Yellow crystals of norbornane bistrisulfide were grown directly from hexane after separation by flash chromatography. The structure was solved in the monoclinic space group $P2_1c$ and refined to an R1 value of 3.01 %. The asymmetric unit contains a single norbornane bistrisulfide molecule. The melting point of the crystal was 179 °C

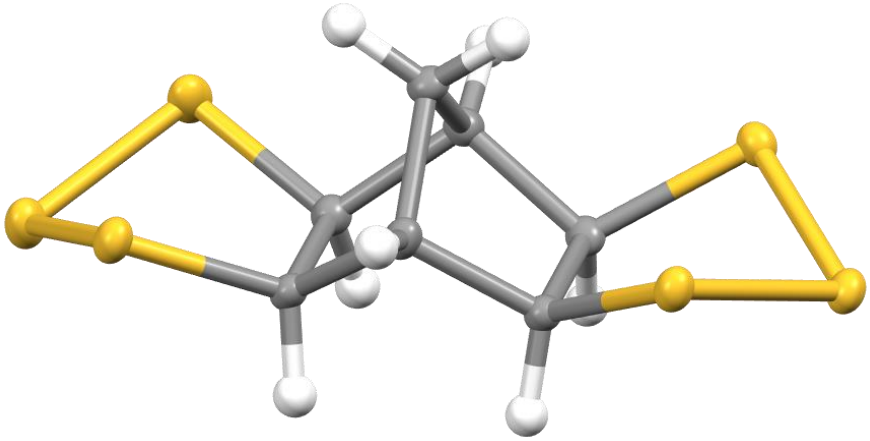

Figure 3.63: Image of norbornane bistrisulfide asymmetric unit with all non-hydrogen atoms shown as ellipsoids at the 50 % probability level.

Rearranged norbonane disulfide – molecule **3**

Crystals of the rearranged norbornane disulfide formed from the neat solution over several days at room temperature. The structure was solved in the monoclinic space group $P2_1/n$ and refined to an R1 value of 3.1 %. The asymmetric unit contains a single rearranged norbornane disulfide molecule. The melting point of the crystal was 63 °C.

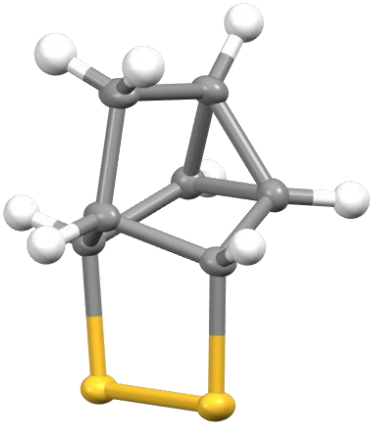

Figure 3.64: Image of a rearranged norbornane disulfide asymmetric unit with all non-hydrogen atoms shown as ellipsoids at the 50 % probability level.

Polymerisation using cyclic sulfides as monomers

Polymerisation method

With the methods to produce and isolate the cyclic sulfides in hand, it was then investigated if they could be used as monomers. This was an important as it may reduce some of the issues encountered when NBD was used directly in the reaction with sulfur. It was hypothesised that by starting with a cyclic sulfide already in place, it may prevent the rearrangement to form molecule **3**, **5** or **7**. Furthermore, if the cyclic sulfides are already built into the molecule, the stereochemistry will not change. This would increase the symmetry of the organic portions of the polymer, potentially resulting in greater long wave infrared transmission. Polymers prepared using the isolated intermediates may also be valuable to characterise the chemical structure of the polymer prepared from NBD as they could be used as a comparison.

The sulfides that were used as monomers were the norbornene trisulfide (**4**), the norbornane bistrisulfide (**6**) and the rearranged norbornane disulfide (**3**). These products could be synthesised in great enough yield and purity for the reaction. Along with the pure sulfides, another set of reactions were performed using molecules **1**, **4**, and **8** in the same ratio as the reaction solution. This ratio was determined by proton NMR as 0.24: 1: 0.4, **1**: **4**: **8**. The combined sulfides was important as may be more practical to scale up the reaction if the monomers did not need to be isolated before the reaction.

The purified sulfides were reacted under similar conditions as the optimised reaction between norbornadiene and sulfur. For each sulfide, four reactions were done. One where the sulfides were heated neat with no added sulfur. Another where the sulfides were heated in a solvent system of 50-50 DMF-Xylene with no added sulfur. These reactions were done to see if the sulfides could undergo a homopolymerisation, potentially by ring opening of the cyclic sulfide ring. Two more reactions were done where sulfur was added to determine if any alkenes could react to form a crosslinked polymer. The samples made with **4** or the combination of **1**, **4** and **8** had sulfur added to give approximately 66 % sulfur which is very close to the amount of sulfur in the samples using **6.** The polymers made with **3** had sulfur added to give an average sulfur rank of 4.

All reactions were done with 100 mg of reactants. The sulfides were added to a vial with a stir bar. 1 mL of DMF and Xylene was added to the reactions in the samples with solvent and sulfur was added to the appropriate samples. The mass of the sulfides and sulfur to make 100 mg is summarised in the table below. The vials were then added to a preheated oil bath at 140 °C and heated with stirring for 90 minutes. After this time, they were removed from the oil bath and the magnetic stir bar was extracted. Any solvent was evaporated using rotary evaporation and the samples were added to a preheated oven at 140 °C for 24 hours to cure.

These reaction conditions had to be modified when **6** was used due to its high melting point. When heated at 140 °C, the crystals would not melt. For the NBBTS samples without solvent, they were first heated to 185 °C for 5 minutes before following the same method as the other samples.

Table 3.3: Table showing mass of sulfides and sulfur used in polymerisation reactions using purified sulfides.

Sample	Sulfide mass	Sulfur mass	Sulfur Content (%)
4 No S No Sol	100 mg	0	51 %
4 With S No Sol	69 mg	31 mg	66 %

4 No S With Sol	100 mg	0	51 %
4 With S With Sol	69 mg	31 mg	66 %
1, 4 and 8 No S No Sol	100 mg	0	51 %
1, 4 and 8 With S No Sol	68.5 mg	31.5 mg	66 %
1, 4 and 8 No S With Sol	100 mg	0	51 %
1, 4 and 8 With S With Sol	68.5 mg	31.5 mg	66 %
6 No S No Sol	100 mg	0	67 %
6 With S No Sol	87 mg	13 mg	72 %
6 No S With Sol	100 mg	0	67 %
6 With S With Sol	87 mg	13 mg	72 %
3 No S No Sol	100 mg	0	41 %
3 With S No Sol	71 mg	29 mg	58 %
3 No S With Sol	100 mg	0	41 %
3 With S With Sol	71 mg	29 mg	58 %

All samples showed a significant change after the reaction forming a brittle material after cure. The reactions using **4**, **6** and the combination of sulfides made a yellow-orange glassy material when no solvent was used. When DMF-Xylene was added, the samples were much darker orange but were still brittle and glassy. The samples made with **3** formed a dark brown material. There was no obvious difference in colour or physical properties between the neat and solvent samples for the rearranged norbornane disulfide. There was also no obvious difference when additional sulfur was added.

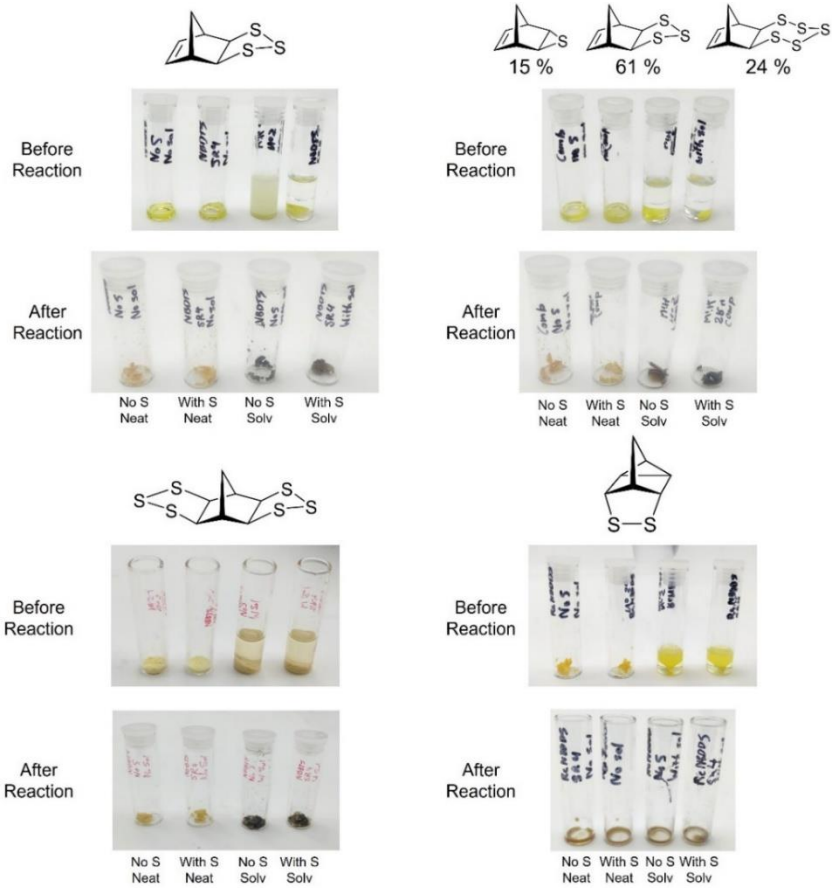

Figure 3.65: Images showing the reactions using isolated cyclic sulfides. The solvent system used in this reaction was 50-50 DMF-Xylene.

Method to prepare polymer with norbornane bistrisulfide

Molecule **6**, norbornane bistrisulfide, had a much greater melting point than any of the other cyclic sulfides. The melting point of the crystal was 179 °C. It was the only molecule which had a melting point higher than the temperature used in the polymerisation reaction (140 °C). This lead to some difficulties when performing the polymerisations and required a different method to be prepared. For reactions where the polymer did not need to be cast, the reaction temperature could simply be increased to 185 °C for 5 minutes to melt the monomer and initiate the reaction. After this, the standard polymerisation method as described above could be used. This was successful and made stable polymers, however, at these elevated temperatures, the reaction only had a liquid working time of approximately 10 seconds. After this point, the polymer would vitrify and could not be moulded. For polymers with no added sulfur, a method to improve the working time has not yet been found. These polymer compositions would require reactive compression moulding or other post cure manufacturing methods. However, for higher sulfur compositions, a method was developed to prepare polymers which could be cast and moulded into a variety of complex forms. This method is described below.

To make a castable polymerisation reaction, molten sulfur was used as a solvent for the reaction using molecule **6**. By doing this, the working time of the reaction could be increased to approximately 3 minutes. While still short, this working time was appropriate for moulding of the polymer into windows, and even complex lenses which will be described in chapter 4. This method would only work with sulfur contents of 80 % or greater as it relies on dissolving the monomer in sulfur. The standard method that is described here for a 750 mg reaction, however, reactions as large as 10 g have been successfully performed. It was later discovered that due to the short working time, bubbles would become trapped in the polymer. After many experiments, it was found that these bubbles were caused by moisture in the sulfur. To prevent this, the molten sulfur was degassed.

Sulfur (300 mg, 1.17 mmol S8) was measured into a 5 mL vial. The vial was added to a preheated oil bath at 140 °C. The sulfur was left for 3 minutes to melt. After this point, the vial was transferred to a preheated vacuum oven at 140 °C. A vacuum of approximately 2 mbar was pulled in the oven and the molten sulfur was left for 30 minutes. After degassing the sulfur, the pressure was returned to ambient, and the sulfur was transferred back to the 140 °C oil bath. **6** (445 mg, 1.56 mmol) for 81 % S polymer or (267 mg, 0.94 mmol) for 85 % S polymer was poured into the vial. **6** would rapidly dissolve in the molten sulfur over approximately 15 seconds. 15 seconds after **6** was added, the reaction was stirred with a heated metal spatula. The reaction was stirred carefully to prevent trapping gasses which would cause bubbles in the polymer. The reaction was stirred for a total of 30 seconds (stirring was stopped at a reaction time of 45 seconds). After a total reaction time of 60 seconds, the prepolymer was poured into a silicone mould which had been preheated to 140 °C. The mould was then placed in a 140 °C oven where it was left for 24 hours to cure. Further experimentation showed that a cure time of 1 hour is appropriate but all polymers in this thesis were cured for a full 24 hours. Below are some images of a polymer windows prepared using this method.

Figure 3.66: Images of polymer windows made from 81 % sulfur norbornane bistrisulfide polymer.

ATR-FTIR of polymers made with purified norbornadiene sulfides

After preparing polymers from the isolated cyclic intermediates, it was important to understand their chemical composition and how this affects their optical properties. To do this, each of the polymers were analysed by ATR-FTIR. FTIR is very important as it can show any major absorptions in the long wave infrared region which would indicate the polymer's suitability for thermal imaging applications.

The FTIR spectrum of all norbornadiene sulfides and polymers were tested using a Bruker Vertex 80 V Spectrometer using the ATR attachment. The polymers were first ground into a fine powder using a mortar and pestle before being analysed. All samples were tested under vacuum from 5000 cm^{-1} to 500 cm^{-1} over a total of 30 scans.

Controls of all the purified sulfides were first ran. The norbornene trisulfide (**4**), pentasulfide (**8**) and the control of the combined sulfides (**1**, **4**, **8**) were very similar. These molecules could react in two ways. It is possible that the polymerisation reaction occurs as a ring opening polymerisation which only utilises the cyclic sulfur ring. If this were the case, it would be expected that any alkene peaks remain unchanged after the reaction. If they reduce or dissapear, it can be determined that a reaction had occurred at the alkene, likely leading to a crosslinked polymer. The alkene peaks are visible around 3050 cm^{-1} and a strong peak at 730 cm^{-1}.

The norbornane bistrisulfide (**6**) control did not posses any of alkene peaks as expected and was very simple in the long wave infrared region. This indicates it may be a good material to use for thermal imaging applications. The rearranged norbornane disulfide control had several characteristic peaks from the cyclopropane structural unit. Two at 3120 cm^{-1} and 3060 cm^{-1} and another at 804 cm^{-1}. The peak at 3060 cm^{-1} can sometimes overlap with the alkene peak from the norbornene sulfides but the bending peak at 804 cm^{-1} is very useful for identifying the presence of the cyclopropane unit. This peak was used to determine if any rearrangement occurred in any of the polymerisations.

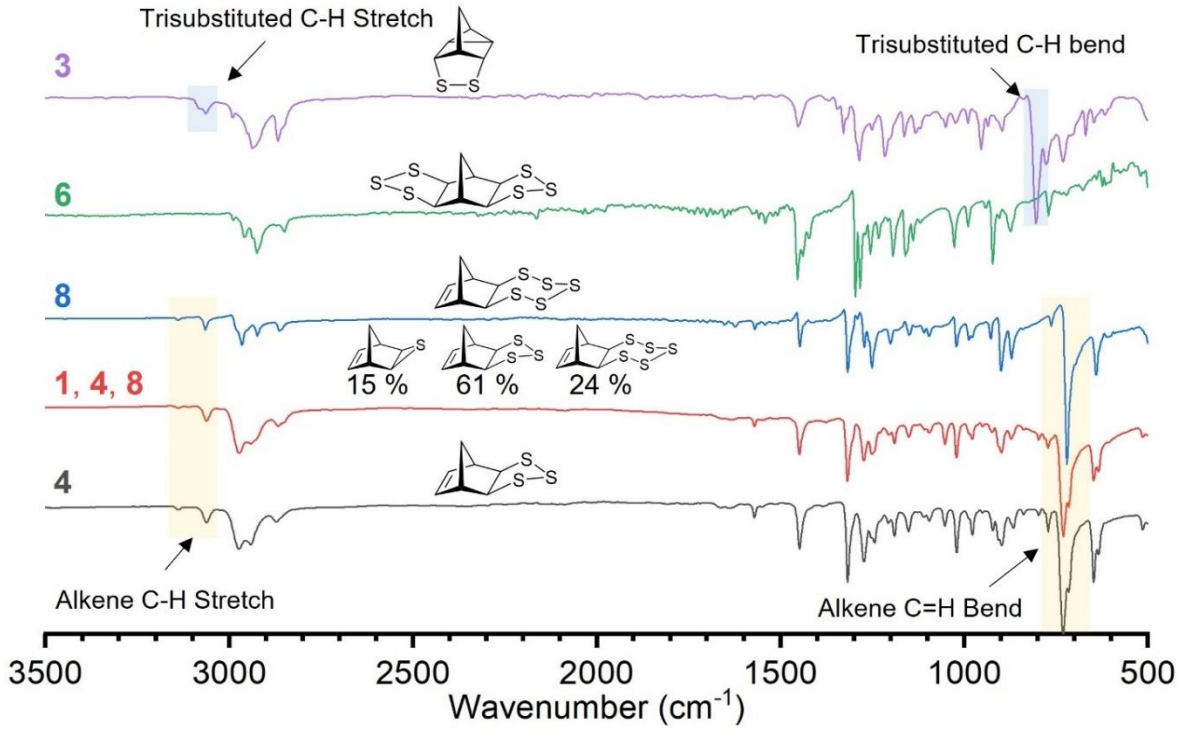

Figure 3.67: ATR-FTIR spectra of purified sulfide products from the reaction between norbornadiene and sulfur. All spectra ran on a Bruker Vertex 80 V under vacuum.

The polymers made from **4** had very similar infrared spectra to the polymerisation with **1**, **4** and **8** in a ratio of 0.21: 1: 0.4. They both showed very little change in the alkene peaks when no sulfur was added. When sulfur was added to the reaction, the alkene peaks decreased in intensity. This was more noticeable in the sample with a solvent of DMF-Xylene as the alkene peaks were almost completely consumed. These results show that when no additional sulfur as added, the reaction likely proceeds through a ring opening polymerisation. However, when additional sulfur is added into the reaction, the alkene can react.

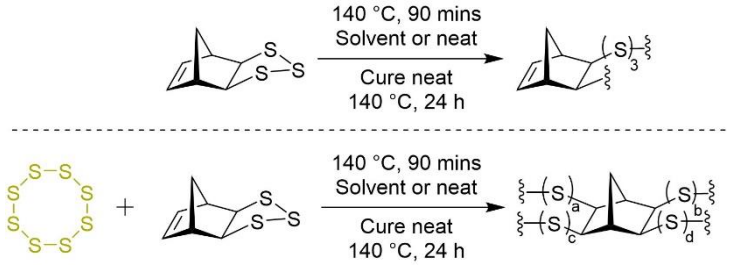

Figure 3.68: Polymerisation reactions using norbornene trisulfide (**4**).

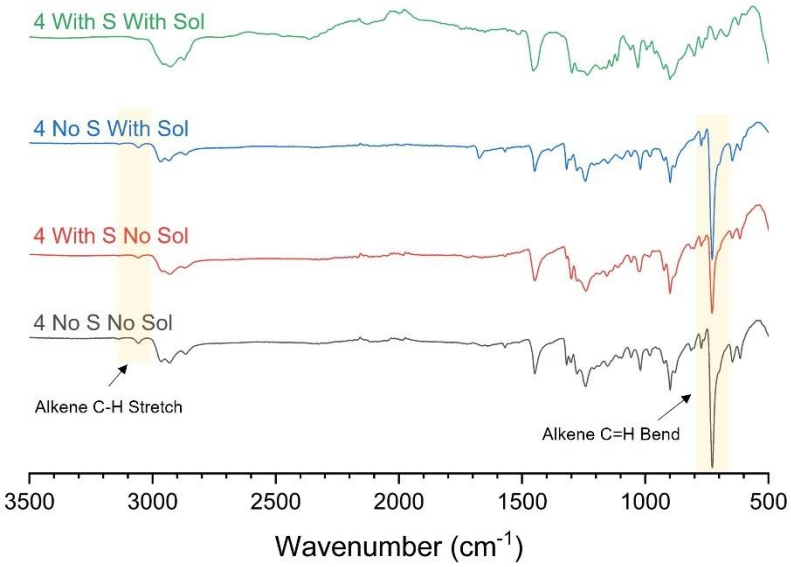

Figure 3.69: ATR-FTIR spectra of polymers made from **4**. Samples with sulfur have approximately 66 % sulfur. The solvent was 50-50 DMF-Xylenes.

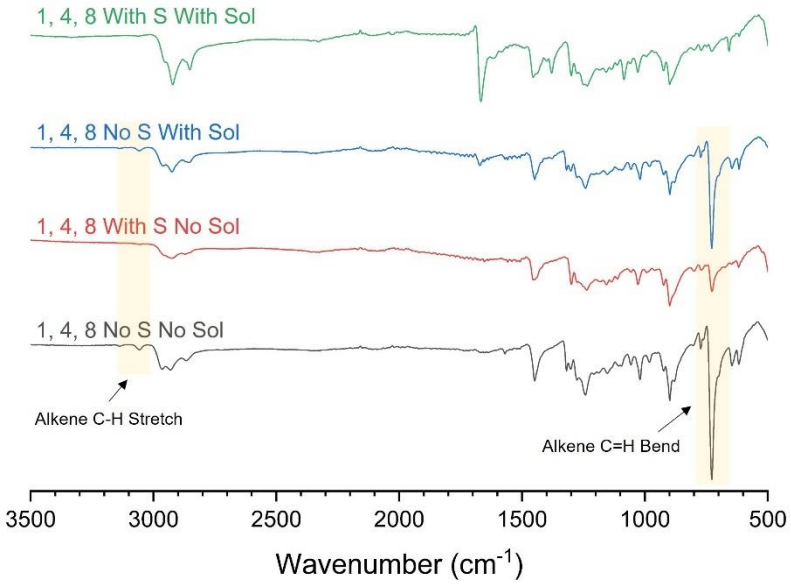

Figure 3.70: ATR-FTIR spectra of polymers made from **1**, **4**, **8** in a 24:100:40 ratio. Samples with sulfur have approximately 66 % sulfur. The solvent was 50-50 DMF-Xylenes.

When **6** was polymerised, the sharp peaks broadened slightly but there was no significant change in peaks. This indicates that there may have been ring opening polymerisation but no change to the organic parts. The polymers made from **3** all had the same FTIR spectra. This indicates that there is very little difference in the organic portion of the polymers. The large peak at 800 cm^{-1} is visible in all samples, indicating that there was no change to the cyclopropane unit.

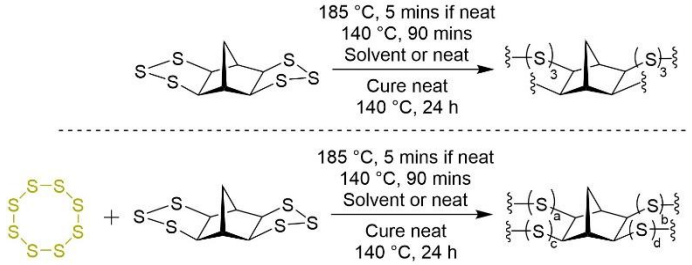

Figure 3.71: Polymerisation reactions using norbornane bistrisulfide (**6**).

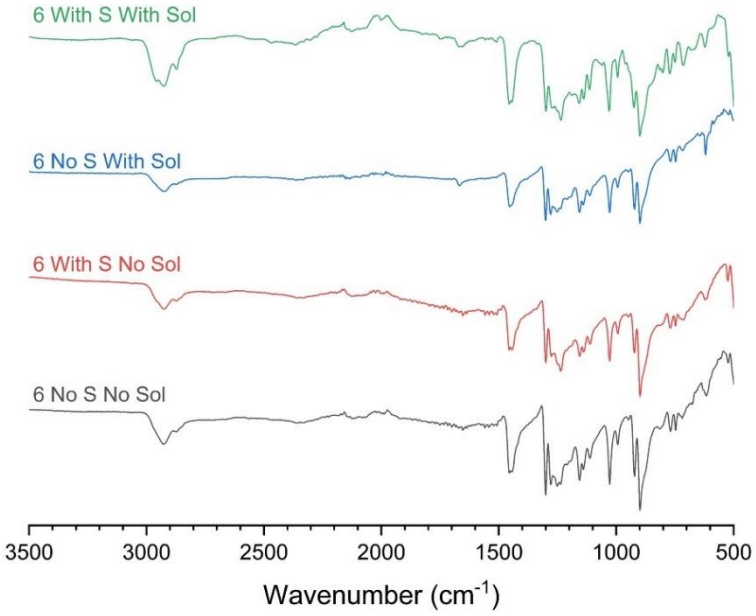

Figure 3.72: ATR-FTIR spectra of polymers made from **6**. Samples with sulfur have approximately 72 % sulfur. The solvent was 50-50 DMF-Xylenes.

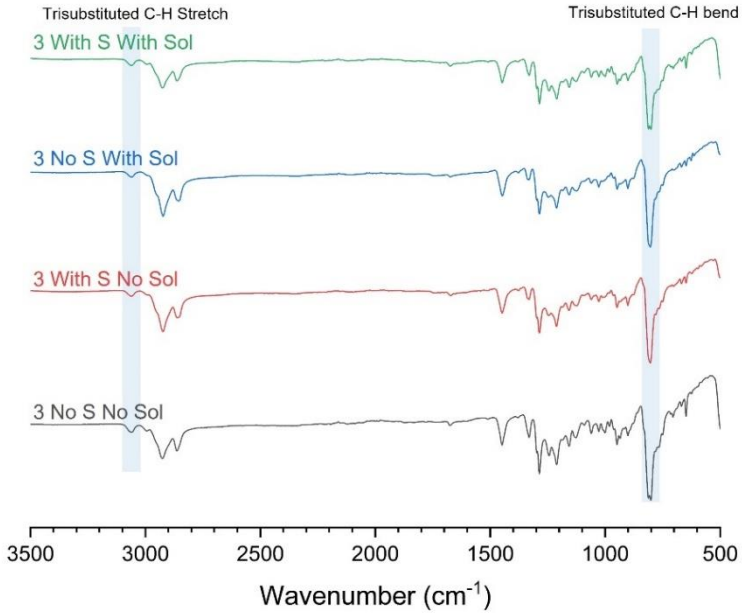

Figure 3.73: ATR-FTIR spectra of polymers made from **3**. Samples with sulfur have approximately 58 % sulfur. The solvent was 50-50 DMF-Xylenes.

The polymers made with norbornadiene and sulfur in a range of solvents were analysed by ATR-FTIR on the Bruker Vertex 80 V under vacuum. All of them had a peak at around 800 cm^{-1} and another at 3060 cm^{-1}. This indicates that there are some rearranged products in the structure. When the polymer made using norbornadiene and sulfur was plotted against the polymers made with the purified sulfides, its appears to match the polymer made from **3**. These findings may explain why the polymers prepared directly from NBD did not have as high long wave infrared transmittance as expected. If there is a significant amount of rearrangement, the polymer performance would not match the calculated performance. These results indicate that to make a polymer with a norbornane core, the polymerisation must use monomers with a cyclic sulfide structure. In particular, monomers **4** and **6** were the most promising.

When the solvent had DMF, a peak was observed at 1670 cm^{-1}. There was an additional peak in the sample in tetrachloroethylene at around 900 cm^{-1}, these peaks may be from excess solvent trapped in the polymer.

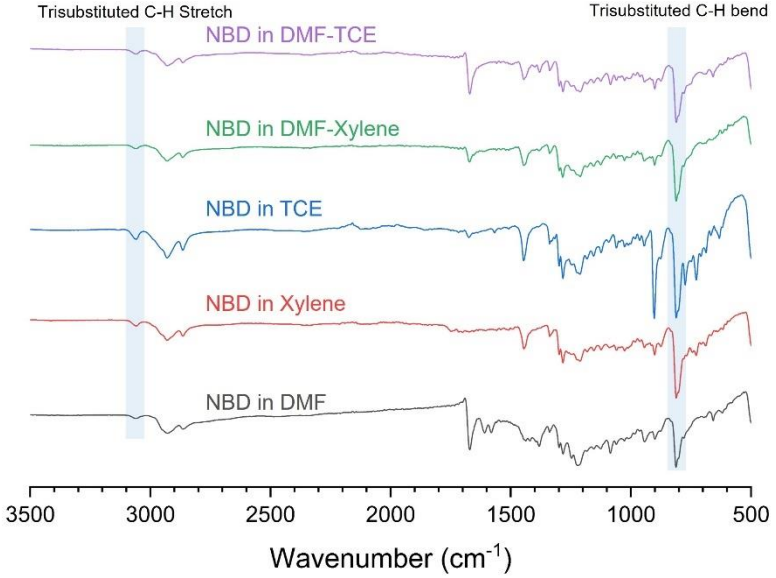

Figure 3.74: ATR-FTIR spectra of polymers made from NBD in a range of solvent systems.

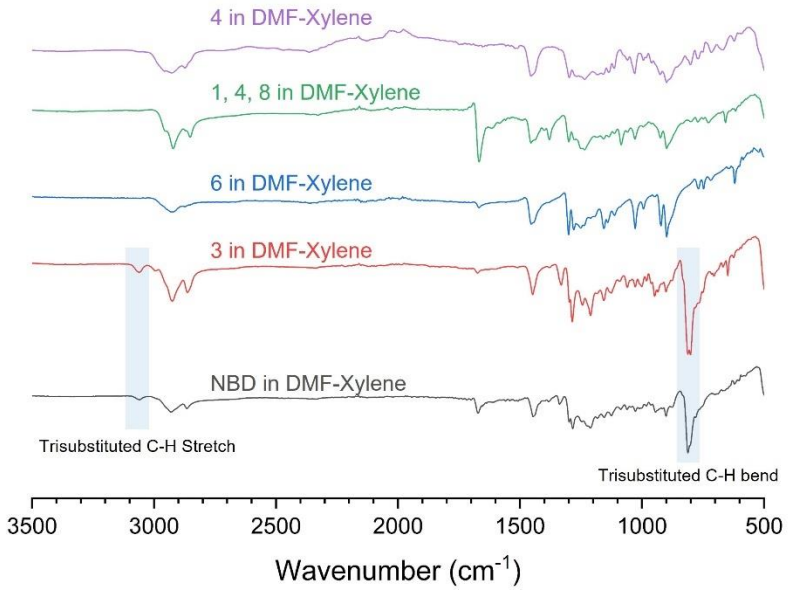

Figure 3.75: ATR-FTIR spectra of polymers made from different sulfide starting materials, all samples used a solvent system of 50-50 DMF-Xylene.

Reduction of polymers and analysis with GC-MS

While the FTIR data gave some understanding of structure of the polymers, a complementary technique would be useful to fully characterise them. The polymers were not soluble in almost any organic solvents, but they could be reduced by lithium aluminium hydride ($LiAlH_4$) to break them into soluble organic thiols. These thiols give a lot of information about the organic portions of the polymer.

30 mg of the polymer was ground into a powder and added to a flame dried vial and capped. The vial was purged with nitrogen. A 1 M solution of $LiAlH_4$ in anhydrous tetrahydrofuran (THF) was prepared and 2.2 mL was injected into the vial. The reaction was left for 24 hours with constant stirring. After this time, the round bottomed flask was added to an ice bath to cool. 5 mL of 1 M hydrochloric acid (HCl) was injected slowly to quench the reaction. 5 mL of hexane was then injected into the round bottomed flask and stirred for an additional hour. The organic layer was separated and analysed by GC-MS using an agilent single quadropole GC-MS.

When the polymers made using norbornene trisulfide (**4**) were reduced, the GC-MS chromatograms showed the same trends as the FTIR data. When no sulfur was added, the major peak was a norbornene dithiol. This peak indicates that the alkene on the **4** did not react. There were two very small peaks that corresponded to the tetrathiol, indicating that the alkene can react but it is very unlikely.

Two samples were reduced which consisted of **4** with added sulfur. One had a total of approximately 66 wt% sulfur while the other had approximately 81 wt% sulfur. In the sample with 66 wt% sulfur, the largest peak shifted to the tetrathiol. This indicates that a large portion of the alkene has reacted, complimenting the FTIR data. This sample also showed a peak for a trithiol which could be produced when the tetrathiol is further reduced by lithium aluminium hyrdide. The peak for the dithiol with an alkene is still present, indicating that not all of the alkene had reacted.

The sample with 81 % sulfur only showed peaks with no alkenes. It had the tetra, tri and dithiol peaks, indicating that the tetrathiol had been reduced. There was also a peak which corresponded to an episulfide molecule which was only present in this sample. The results of the reduced polymers prepared from **4** indicated that when no sulfur was added, the polymerisation follows a ring opening polymerisation and does not react at the other alkene. When sulfur was added, the other alkene could also react, likely increasing the crosslinking of the polymer considerably. At some point between 66 wt% and 81 wt% sulfur, all of the alkenes in the reaction would be consumed.

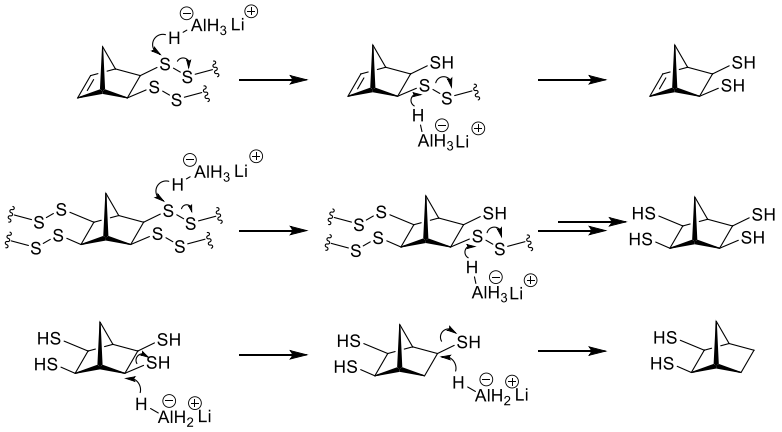

Figure 3.76: Mechanism for the reduction of several potential polymers to give molecules observed in GC-MS.

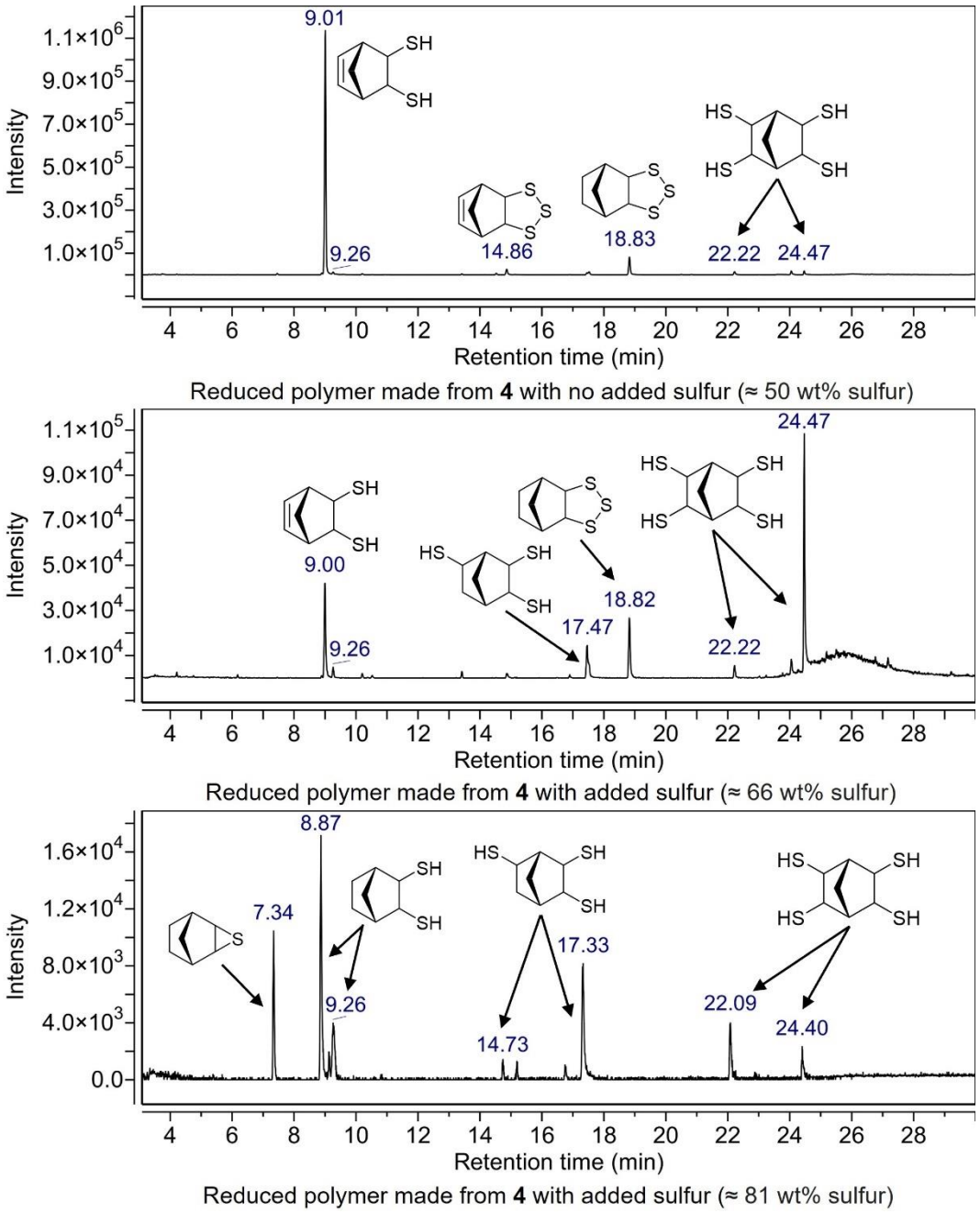

Figure 3.77: GC-MS chromatograms for polymer made from norbornene trisulfide (**4**) after being reduced by lithium aluminium hydride. All polymers were prepared from a neat reaction.

Four samples made from norbornane bistrisulfide (**6**) were reduced with lithium aluminium hydride and analysed by GC-MS. Three of the samples were from neat reactions with differing amounts of sulfur and one was polymerised in a solvent system of 50-50 DMF-xylene. All samples showed the tetrathiol product. They also showed other products of further reduction. None of the chromatograms showed peaks for alkenes or rearrangement.

The chromatogram for the polymer made in a solvent system of 50-50 DMF-Xylene was dominated by the tetrathiol peak. The peaks from the further redced tri and di thiols were significantly reduced. The reason for this is uncertain although it may indicate that the polymer structure has a greater homogenuity.

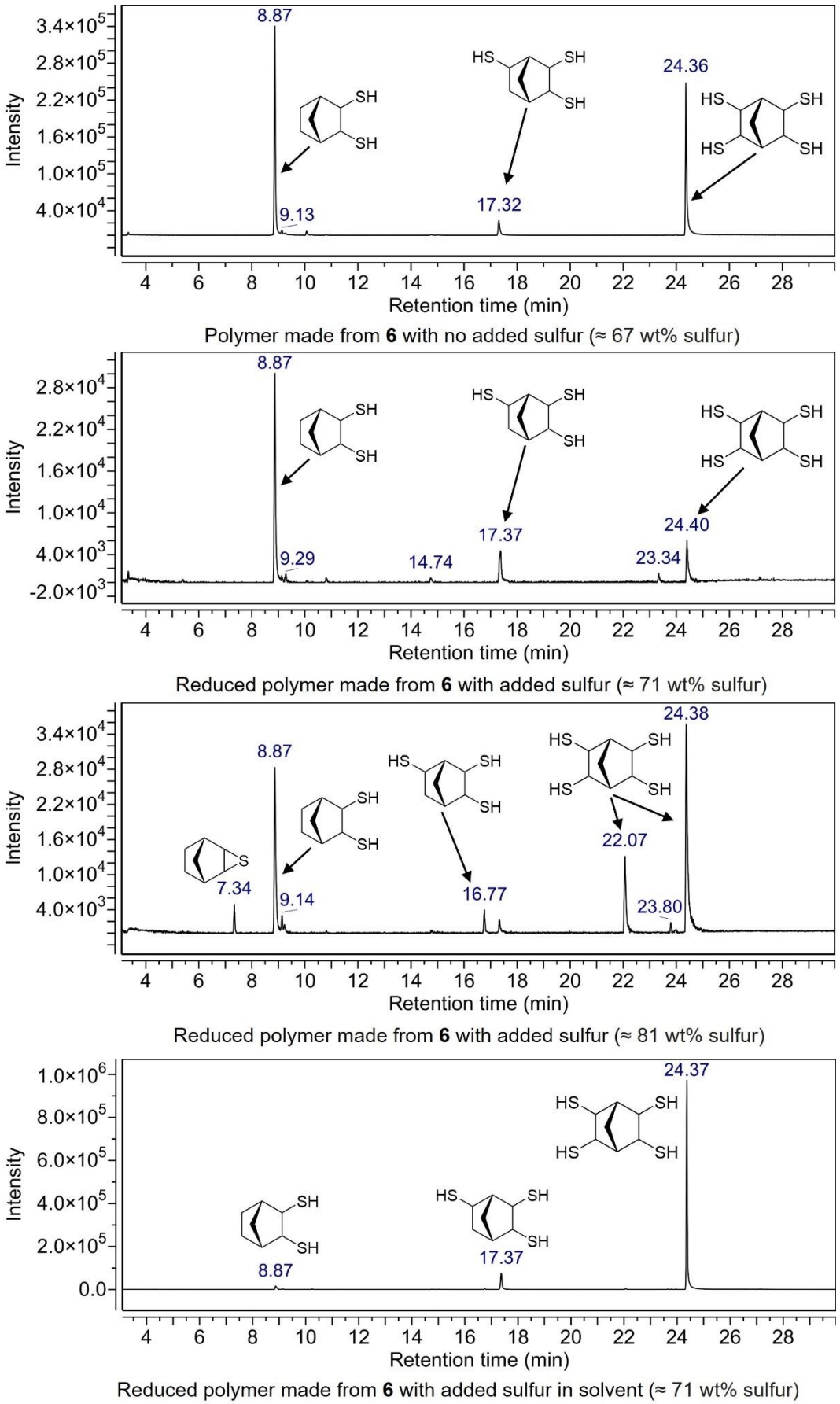

Figure 3.78: GC-MS chromatograms for polymer made from norbornane bistrisulfide (**6**) after being reduced by lithium aluminium hydride. The last spectra which used a solvent system of 50-50 DMF-Xylene, all others were neat.

One polymer prepared from the rearranged norbornane disulfide (**3**) was reduced with lithium aluminium hydride. The polymer prepared neat with no added sulfur was reduced. The chromatogram was very simple for this polymer. There were only three peaks. Two of them were assigned to the rearranged disulfide that has been reduced to a dithiol. The two peaks likely represent different isomers. The other peak is the rearranged disulfide its self. It's possible that this molecule is stable enough to not be further reduced by the lithium aluminium hydride when it is formed.

As there are many peaks with a retention time of around 9 minutes, an overlay plot between 8.5 minutes and 9.5 minutes was made. The chromatograms from the reduced polymers made from **3**, **4** and **6** with no added sulfur were all combined. While the retention times were very similar, none of the peaks overlap. The peaks in this region correspond to norbornane dithiol, two peaks for the rearranged norbornane dithiol and another peak for the norbornene dithiol. These results show that the polymers made from **4** and **6** do not rearrange. It also shows that polymers made from **3** do not revert back to the norbornane core during the reaction.

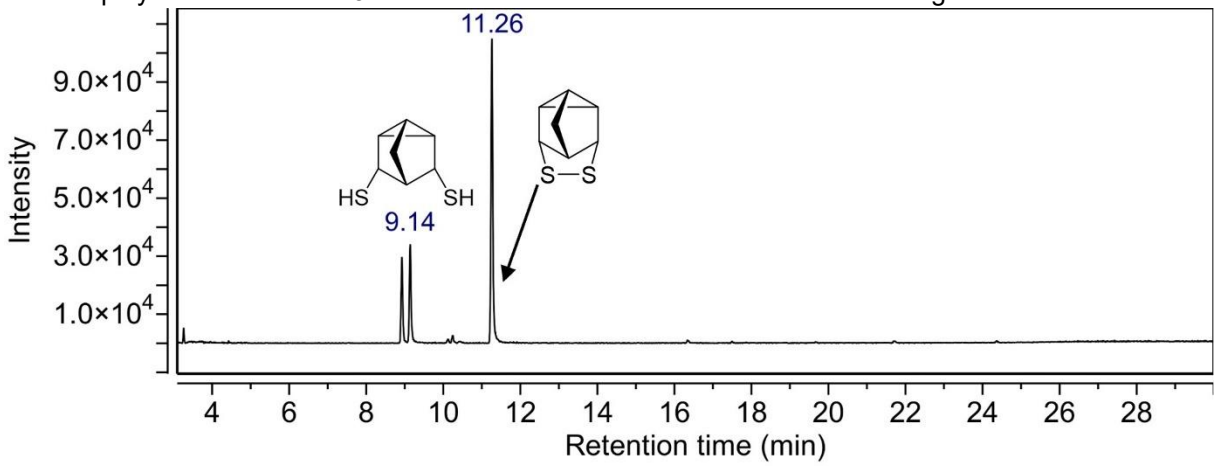

Reduced polymer made from **3** with no added sulfur (≈ 42 wt% sulfur)

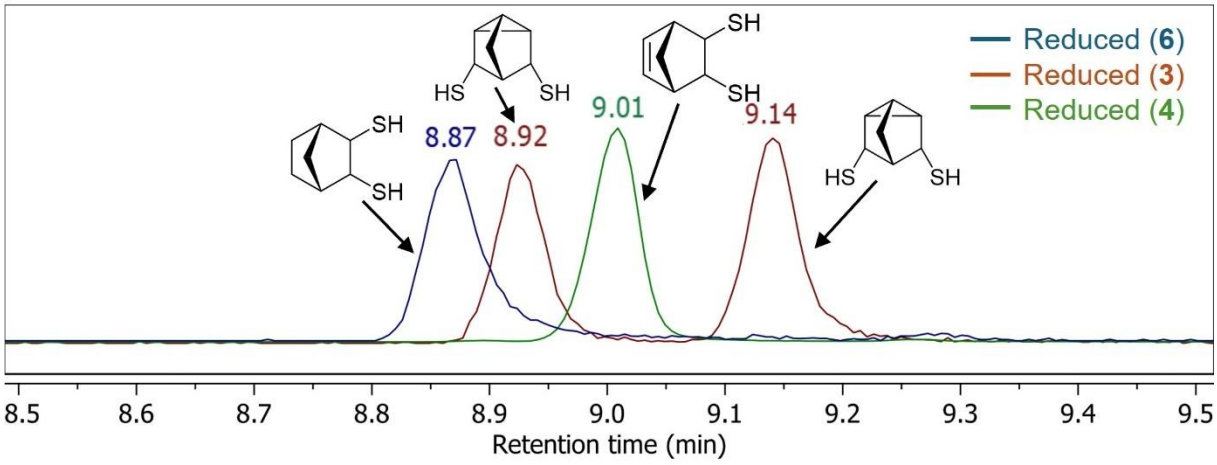

Over lay of reduced polymers made from **3, 4** and **6** with no added sulfur

Figure 3.79: (top) GC-MS chromatogram for polymer made from rearranged norbornane disulfide (**3**) after being reduced by lithium aluminium hydride. (bottom) Overlay of chromatograms from reduced polymers made from **3**, **4** and **6** between a retention time of 8.5 minutes to 9.5 minutes.

The polymers made direcly from NBD in a range of solvent systems were also redced with lithium aluminium hydride and analysed by GC-MS. These polymers all clearly showed peaks for the rearranged product, confirming the findings of the FTIR data. While the rearranged molecule was the major peak, they did show some very small peaks for the tetrathiol or trithiol in some cases. The polymers prepared direcly from NBD also showed two peaks at 10.24 and 8.77 minutes. These peaks were not present when the polymer was prepared with any of the cyclic sulfides. While it can not be confirmed from the mass spectrum alone, it is possible that these peaks are from the molecule which formed a cyclic sulfide to the bridge carbon (molecule 2).

The results of the reduced polymer experiments show that the polymers prepared directly from NBD in a range of solvents had a very significant amount of rearrangement. The presence of the tetrathiol indicates that a small amount of the reaction proceeded as expected which may aid in crosslinking the polymer but the bulk properties are likely to be dominated by the rearranged structure. This explains why the optical properties are not as good as expected. These experiments show that to achieve the desired chemical structure of the polymer, monomer **4** or **6** should be used.

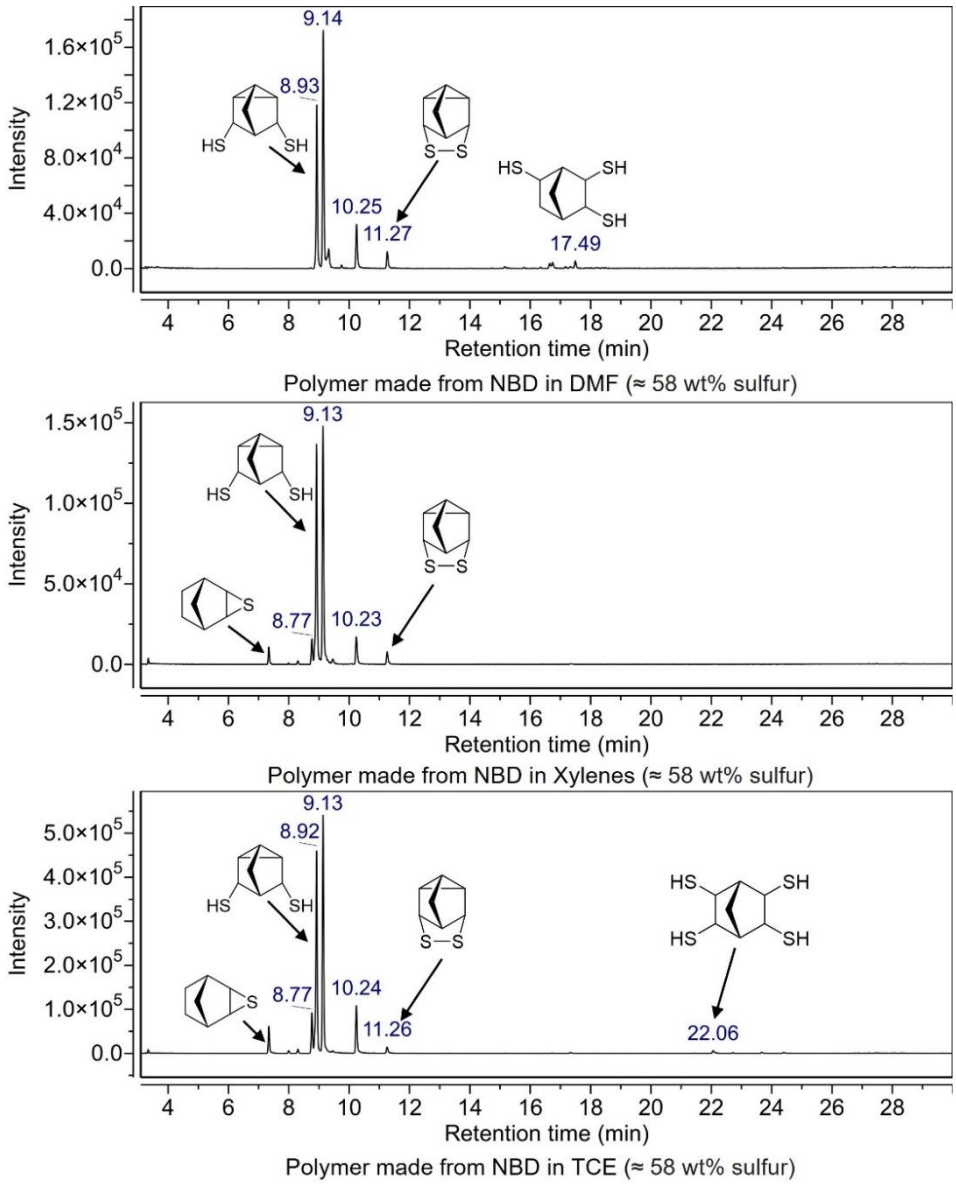

Figure 3.80: GC-MS chromatograms for polymers made from NBD in a range of solvents after being reduced by lithium aluminium hydride.

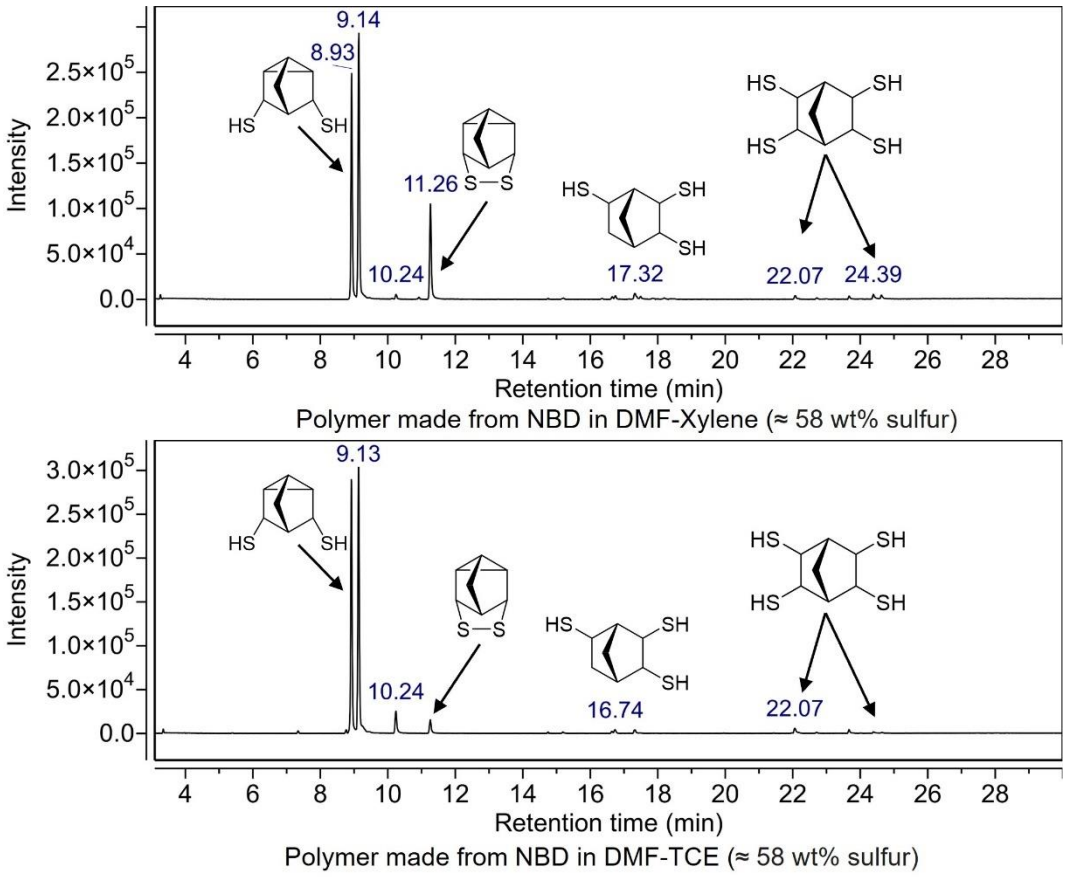

Figure 3.81: GC-MS chromatograms for polymers made from NBD in a range of solvents after being reduced by lithium aluminium hydride.

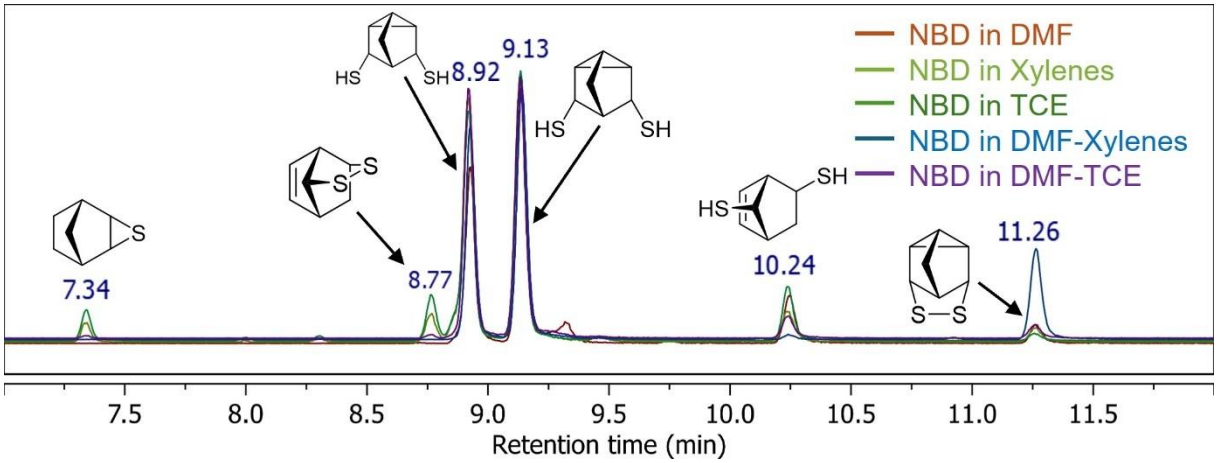

Figure 3.82: Overlay of GC-MS chromatograms for polymers made from NBD in a range of solvents after being reduced by lithium aluminium hydride between a retention time of 7 and 12 minutes.

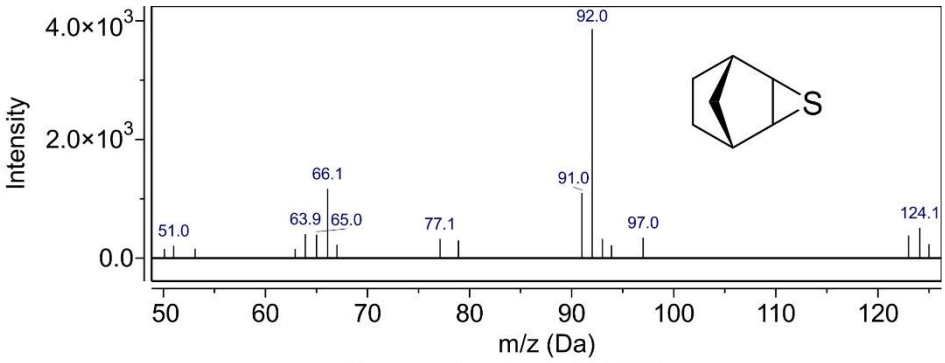

Mass spectrum for peak at 7.34 mins

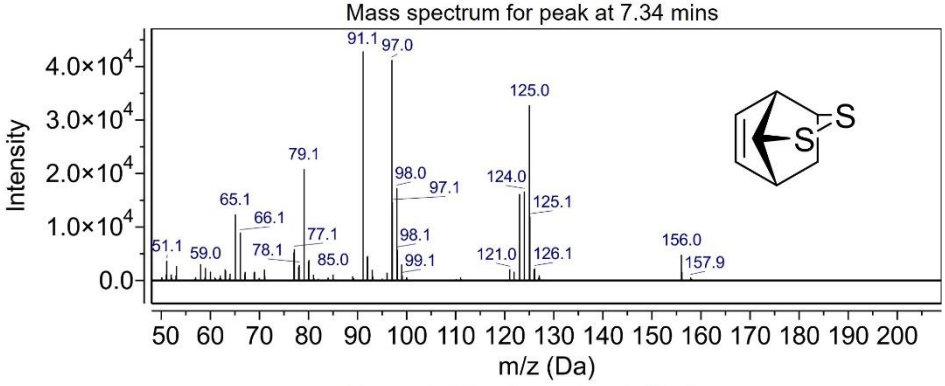

Mass spectrum for peak at 8.77 mins

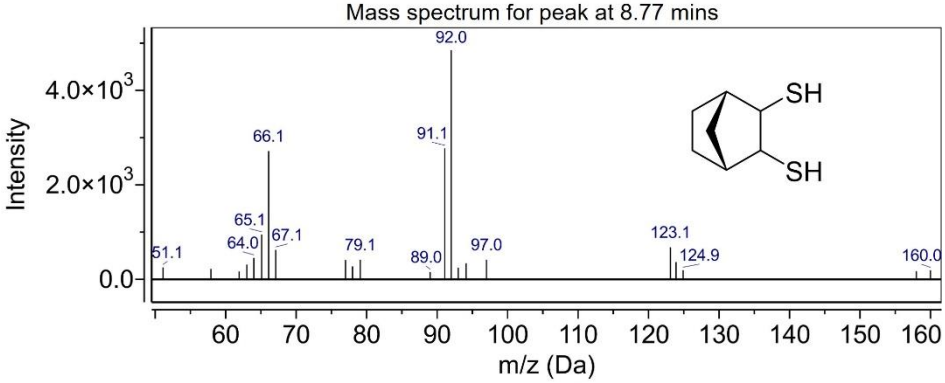

Mass spectrum for peak at 8.87 mins

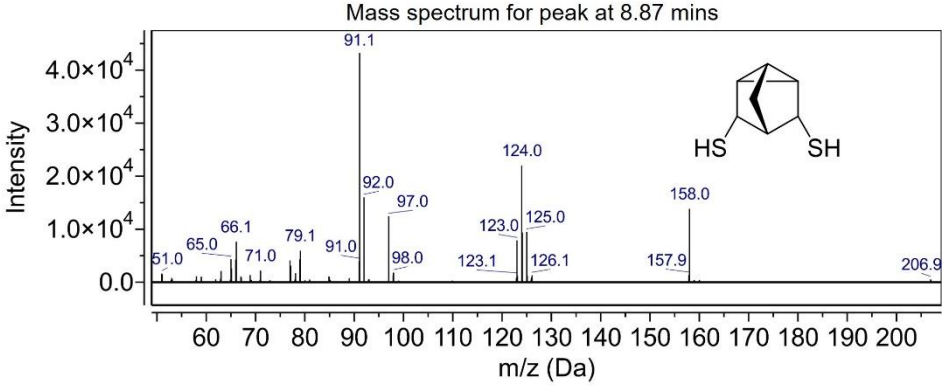

Mass spectrum for peak at 8.92 mins

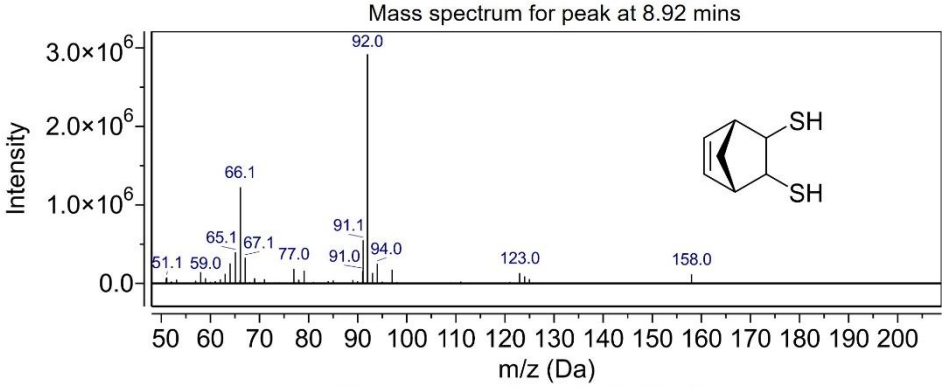

Mass spectrum for peak at 9.01 mins

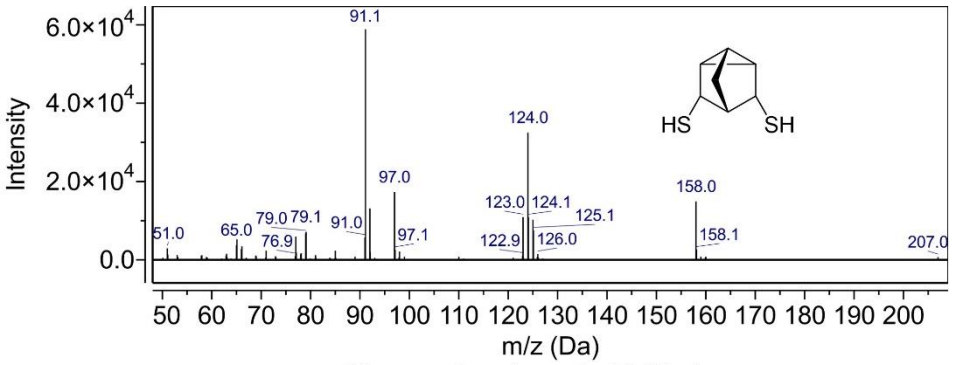

Mass spectrum for peak at 9.14 mins

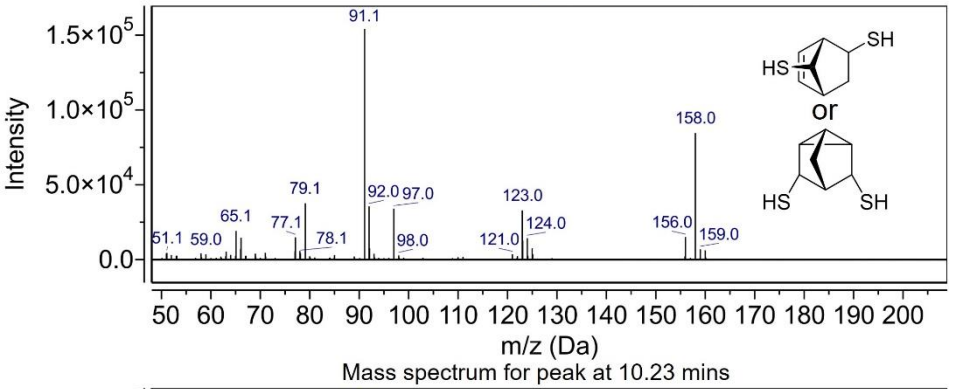

Mass spectrum for peak at 10.23 mins

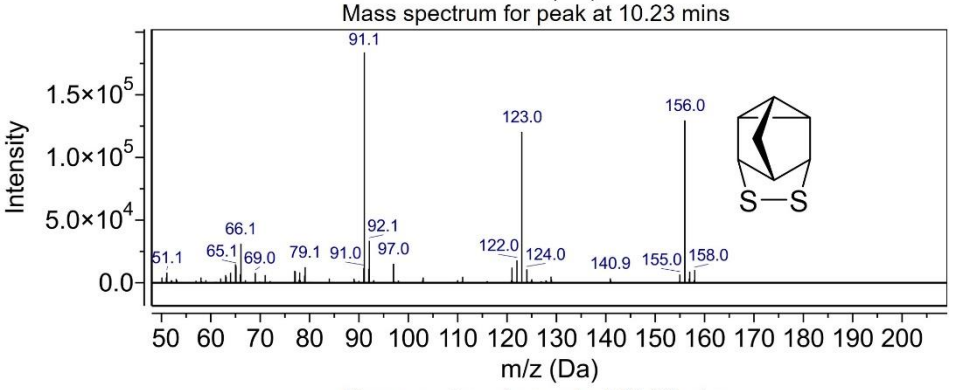

Mass spectrum for peak at 11.26 mins

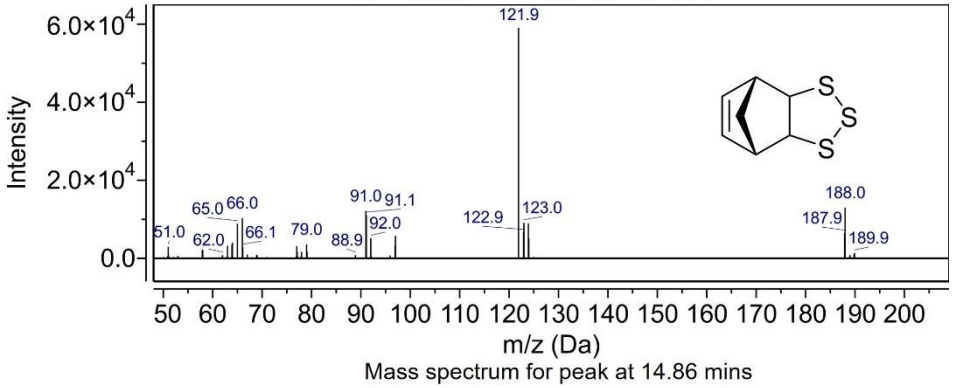

Mass spectrum for peak at 14.86 mins

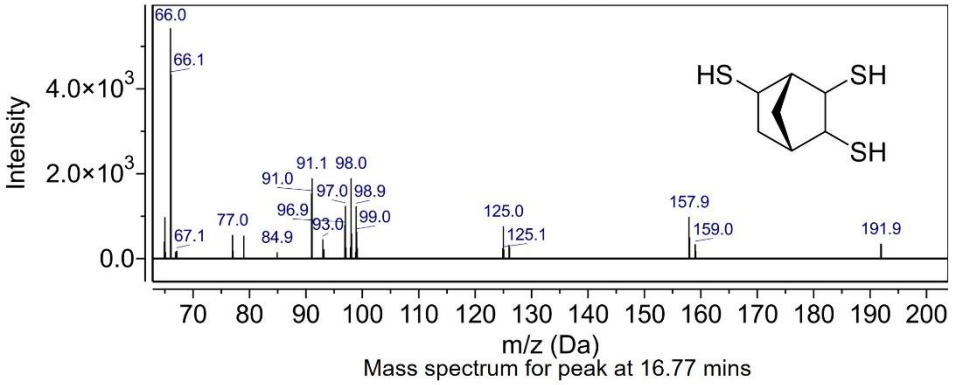

Mass spectrum for peak at 16.77 mins

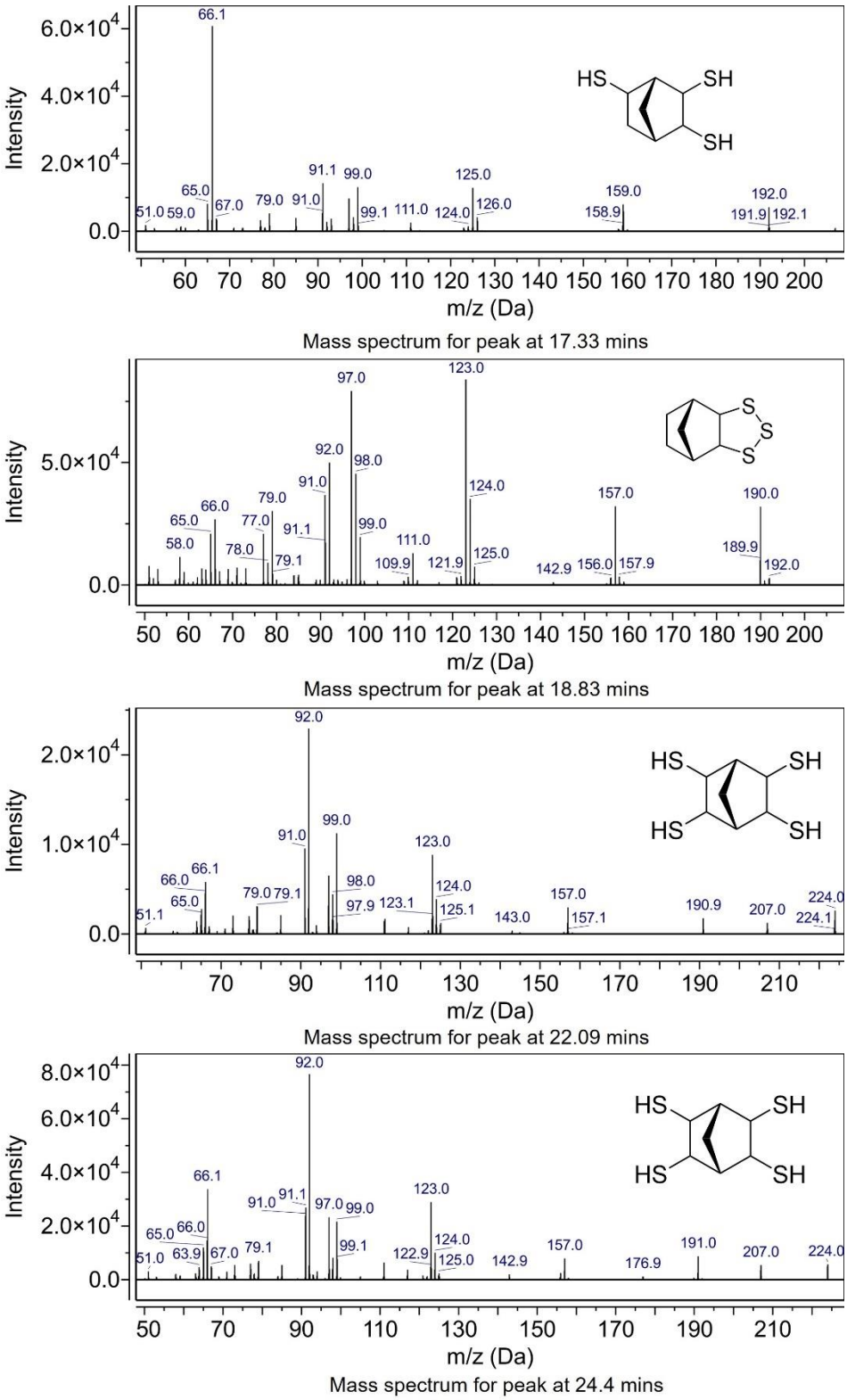

Figure 3.83: Mass spectra for all GC-MS data of polymers reduced with lithium aluminium hydride.

Solid state NMR of polymer made from norbornane bistrisulfide

Aknowledgements: The solid state NMR experiments would not have been possible without Martin Johnston. He assisted with sample preparation, running the experiments and data analysis.

The polymer made using monomer **6** was chosen as the most promising to use for any thermal imaging applications as it gave the desired polymer without the risk of any rearrangement or unreacted alkenes. To understand the polymer structure further, the monomer and two polymers with different sulfur contents were analysed using carbon-13 cross polarisation solid state NMR. Like in solution NMR, the monomer had three peaks at around 70 ppm, 47 ppm and 31 ppm. In the polymer samples, these peaks were still observed but they were significantly broader and shifted to a higher chemical shift. The broadening of the peaks indicated that polymerisation had occurred, leading to a range of chemical environments rather than the well defined trisulfide. The shifting of the peaks, particularly peak b, is likely due to increased sulfur content in the polymers relative to the monomer. No peaks were observed below 25 ppm apart from a spining side band. The peaks from cyclopropane are usually observed in this region, providing more evidence that no rearrangment occurred.

The samples were ground into a powder and packed into a 4 mm sample tube. A 400 MHz NMR spectrometer NMR operating at 100 MHz was used with a magic angle spin rate of 5 kHz. The NMR was calibrated using the 29 ppm peak of adamantane. All samples were analysed by cross polarisation magic angle spinning solid state NMR.

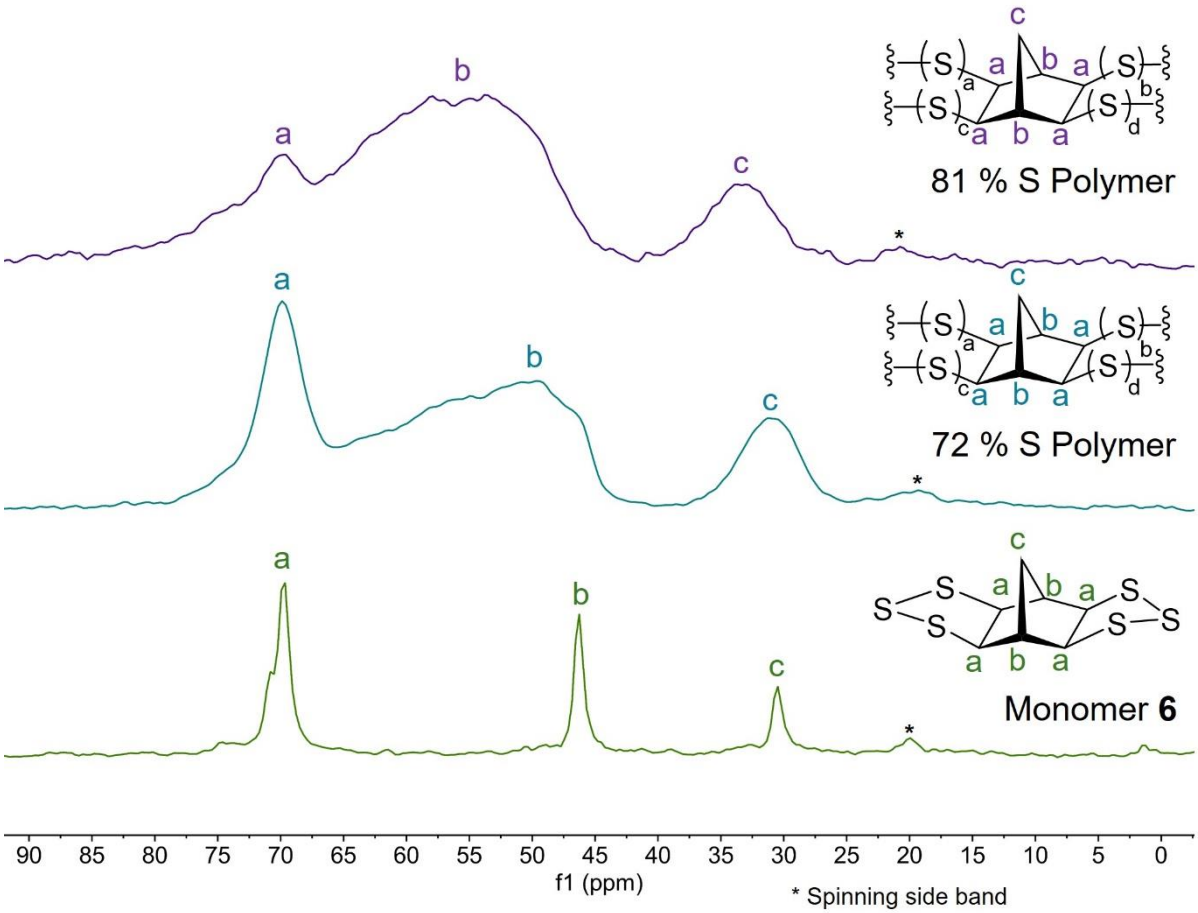

Figure 3.84: Cross polarisation, magic angle spinning, solid state NMR of monomer **6** and two polymers of different sulfur contents.

Raman spectroscopy of polymer made from norbornane bistrisulfide

Aknowledgements: Christopher Gibson ran all of the Raman experiments. The dipropyl di, tri and tetrasulfides were synthesised and prepared by Thomas Nicholls and Harshal Patel.

At this point, the organic portion of the polymer is well known. When monomer **4** or **6** is used, there is no rearrangement of the norbornane core or side reactions. To fully understand the polymer, the sulfur portion of the polymer must also be analysed. Raman spectroscopy can be used to understand the number of sulfur atoms in each chain of the polymer.[26] It can also be used to indicate if there is any crystalline sulfur in the sample.[27] To analyse the sulfur portions of the polymers, the polymers made from monomer **6** were analysed along with a dipropyl di, tri and tetrasulfides and a sulfur control. The dipropyl sulfides were used to understand where the expected peaks would be for a sulfur chain of 2, 3 or 4 sulfur atoms. The these peaks would indicate the relative proportion of the different sulfur chain lengths in the polymer. The sulfur control allowed for the peaks of elemental sulfur to be determined. By comparing this spectrum to the polymer samples, the presence of any unreacted elemental sulfur could be determined.

Raman spectra were collected using a Witec alpha 300R Raman microscope at an excitation laser wavelength of 785 nm with a 40X objective. A 600 groves/mm grating was used which gives a spectral resolution of approximately 3 to 4 cm^{-1}. The x-axis was cailibrated to the 520.6 cm^{-1} peak for silicon. Approximately 10 samples were taken for each sample with an integration time per spectra between 10 and 20 seconds with 2 to 3 accumulations.

When compared with the monomer, the polymers made from **6** have much broader peaks. There was a lot of flurescence which has been reported for sulfur polymers in literature.[26] The flurescence was much more severe in the samples which were synthesised in solvent. There is a correlation between darker samples and a greater flurescence in literature[26] which could explain why the samples made in solvent had a greater flurescence. Despite this, the sample made in solvent and neat all had the same peaks. None of the polymer samples had the characteristic peaks for crystalline sulfur, indicating that there was no unreacted sulfur in the polymer matix.

Most of the major peaks from the monomer were still present in the polymers but some were slightly shifted. The major peak at 510 cm^{-1} shifted to 490 cm^{-1} in the polymers. This major peak was from the trisulfide linkages in the monomer or polymer. The shift to a lower wavenumber has been observed in literature when a cyclic trisulfide is opened to form a linear trisulfide.[28] The shift in the wavenumber of this peak was confirmed by comparing it to dipropyl sulfides with 2, 3 or 4 sulfur atoms. When compared with the Raman spectra of these sulfides, the major peak of the polymers appeared to correspond with the dipropyl trisulfide peak. There was a shoulder at approximately 508 cm^{-1} which could indicate some disulfide linkages or potentially some cyclic trisulfides end groups. While there was no clear peak in the polymers which corresponded to the dipropyl tetrasulfide major peak, it did have a broad shoulder which could potentially indicate higher sulfur chains. These results indicated that the cyclic trisulfide from the monomer opened up to form linear sulfur chains which likely had a distribution of chain lengths with the most common number of sulfur atoms per chain being three. These results differ from polymers prepared electrochemically or photochemically from trisulfides which only form trisulfide linkages.[28] It is possible that thermal reactions allow for S-S bond metathesis, leading to a range of sulfur chain lengths within the polymer.

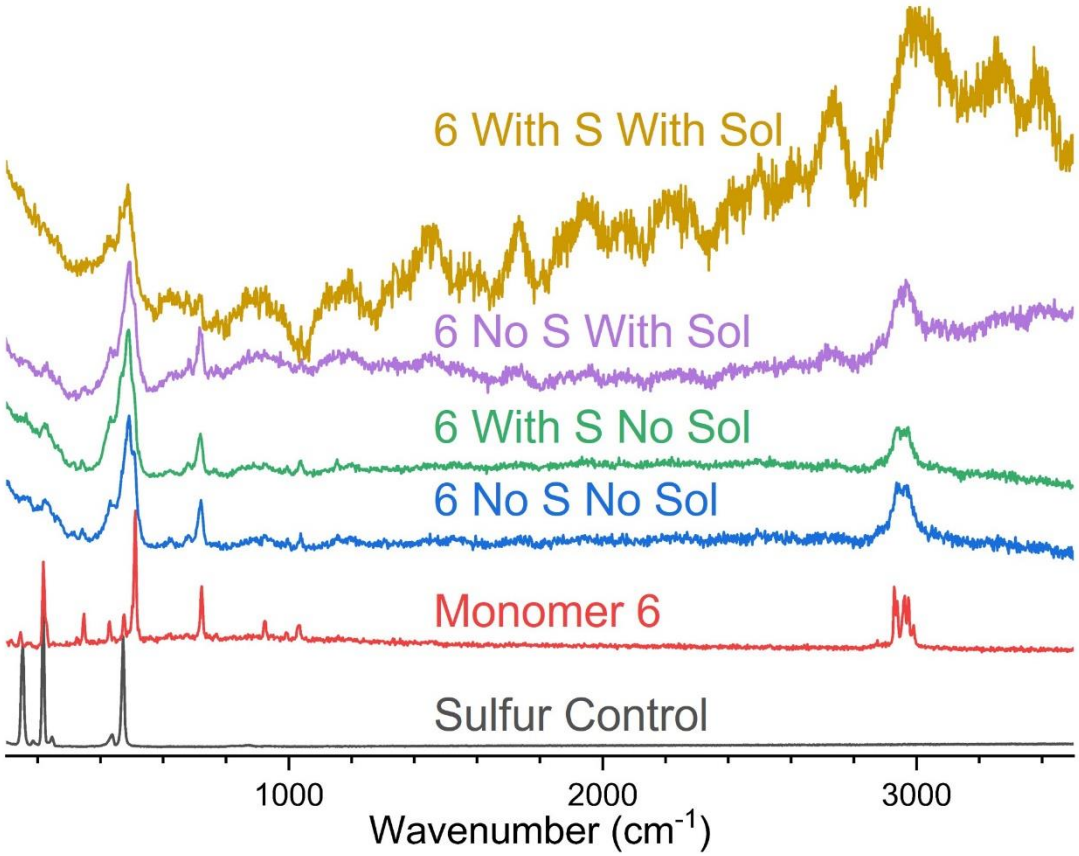

Figure 3.85: Raman spectra for a sulfur control, norbornane bistrisulfide (**6**) and polymers made using **6**.

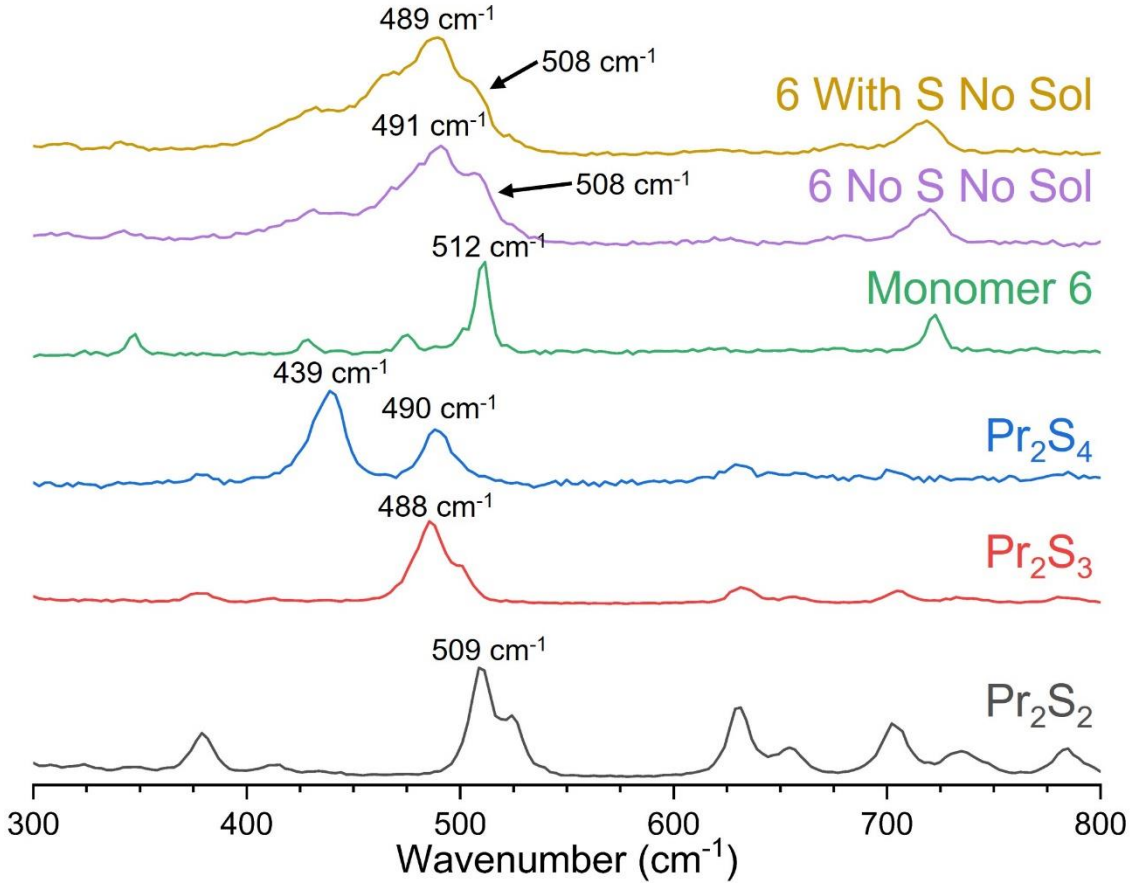

Figure 3.86: Raman spectra of dipropyl di, tri and tetrasulfide, norbornane bistrisulfide (**6**) and polymers made using **6.**

Thermal gravimetric analysis of polymers

The thermal properties of the polymers were investigated using TGA and DSC. All polymers prepared from the isolated cyclic monomers were tested.

A TGA Perkin Elmer 8000 was used to analyse the thermal degradation of all the polymers. Starting at 30 °C, the sample was heated to 800 °C at 20 °C/min under a 35 mL/min flow of nitrogen. At 800 °C, the gas was switched to air at 20 mL/min to burn off any remaining material.

All samples showed a mass loss at around 300 °C. This mass loss started earlier and was slightly larger in all the samples with added sulfur. The samples with added sulfur also had less remaining material at 800 °C. This is consistent with the TGA results from the polymers made directly from NBD. The samples made with **4** and a combination of **1**, **4** and **8** had very similar degradation patterns. Some samples had a slight mass loss before 800 °C in the samples that were polymerised in a solvent. This is attributed to trapped solvent in the polymer.

The polymers made from the **3** had a different degradation pattern to the other polymers. They had an additional mass loss which started around 130 °C. This mass loss would be approximately 15 % of the total sample mass. This indicates that these polymers were less thermally stable and could likely be attributed to these polymers not possessing any crosslinking groups.

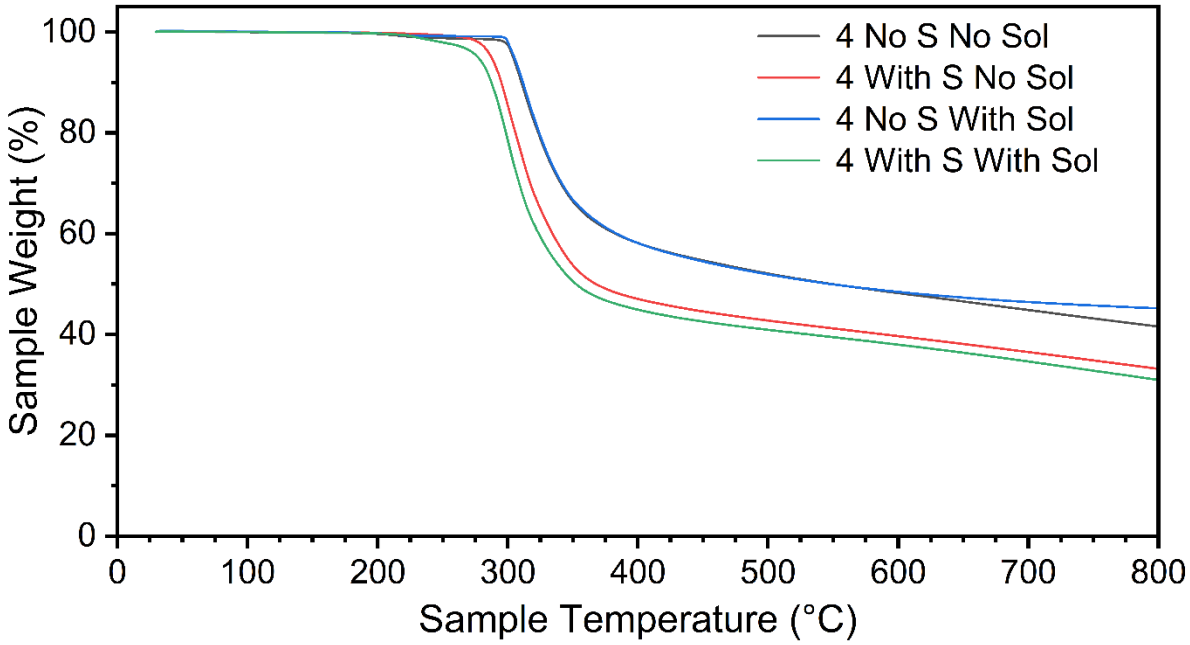

Figure 3.87: Thermal gravimetric analysis of polymers made from norbornene trisulfide (**4**). The samples with S had additional sulfur to give a sulfur content of 66 %. The samples with sol were reacted in a solvent system of 50-50 DMF/xylene.

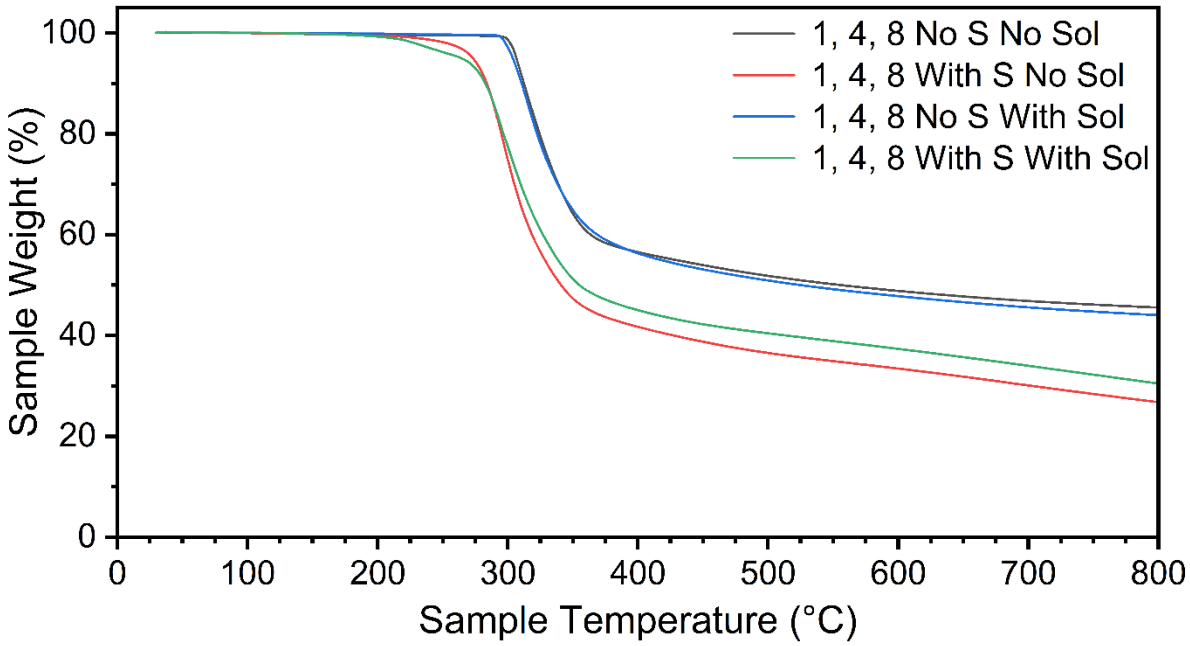

Figure 3.88: Thermal gravimetric analysis of polymers made from norbornene epi, tri and penta sulfide (**1, 4, 8**) in a 24: 100: 40 ratio. The samples with S had additional sulfur to give a sulfur content of 66 %. The samples with sol were reacted in a solvent system of 50-50 DMF/xylene.

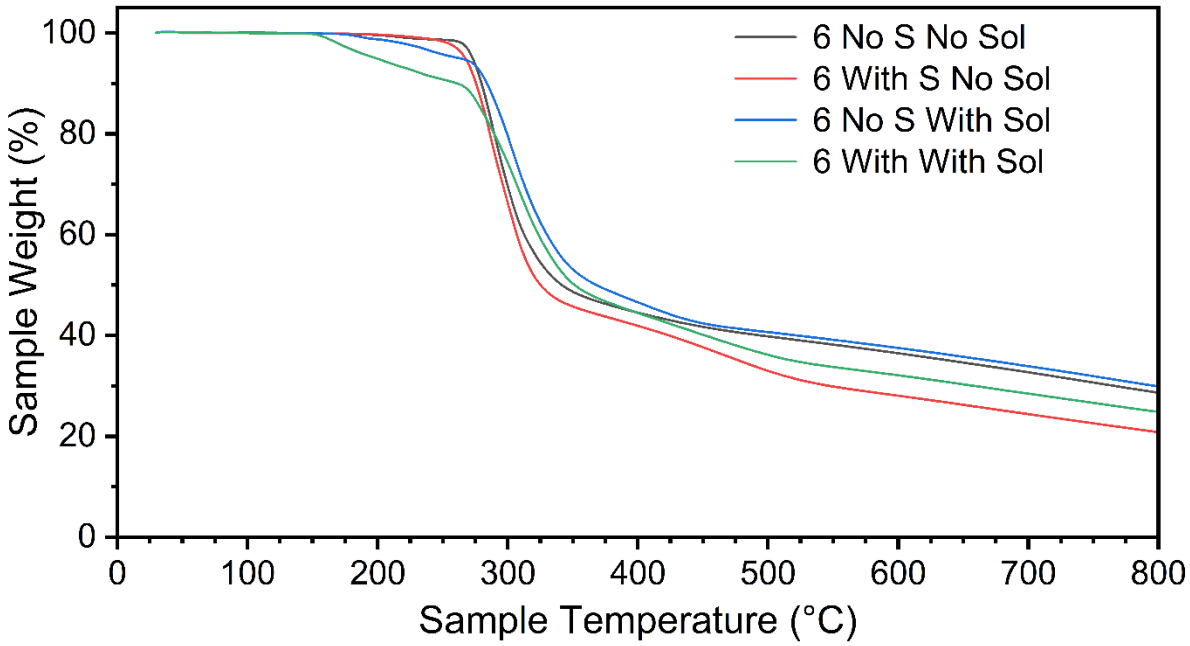

Figure 3.89: Thermal gravimetric analysis of polymers made from norbornane bistrisulfide (**6**). The samples with S had additional sulfur to give a sulfur content of 67 %. The samples with sol were reacted in a solvent system of 50-50 DMF/xylene.

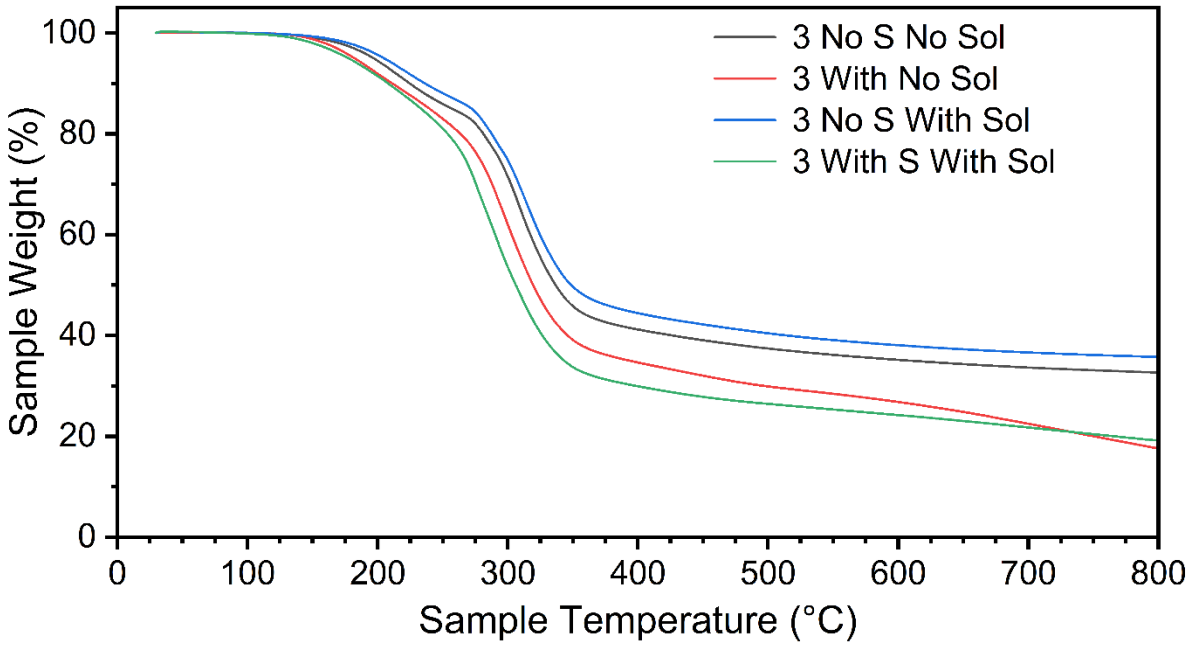

Figure 3.90: Thermal gravimetric analysis of polymers made from rearranged norbornane disulfide (**3**). The samples with S had additional sulfur to give a sulfur content of 58 %. The samples with sol were reacted in a solvent system of 50-50 DMF/xylene.

Differential scanning calorimetry of polymers made from sulfides

Each of the polymers made with cyclic sulfides were tested by differential scanning calorimetry (DSC) to find glass transition temperatures or any other thermal properties. The samples were analysed at the ANFF Queensland node using a Mettler Toledo DSC. Several of the samples were analysed using a TA DSC.

All samples were run using the same method. The samples were first heated from room temperature to 100 °C at 25 °C/min and held for 1 minute. This step was to remove any thermal history in the samples. The temperature was then decreased to 0 °C at 25 °C/min where it was again held for 1 minute. The temperature was then increased to 200 °C at 25 °C/min. All samples were under a constant stream of nitrogen. The samples that were run on the TA DSC followed the same method but the samples were only cooled to 40 degrees.

The glass transition temperatures of the polymer made from norbornene trisulfide (**4**) was very high, ranging from 148 °C to 196 °C. Interestingly, the glass transition temperature increased when **4** was polymerised with additional sulfur. Usually, the glass transition temperature of sulfur polymers decreases with increasing sulfur content.[13] It is possible that this was due to the alkene reacting with additional sulfur, leading to more crosslinking and a higher glass transition temperature. No samples had any crystalline sulfur melting peaks.

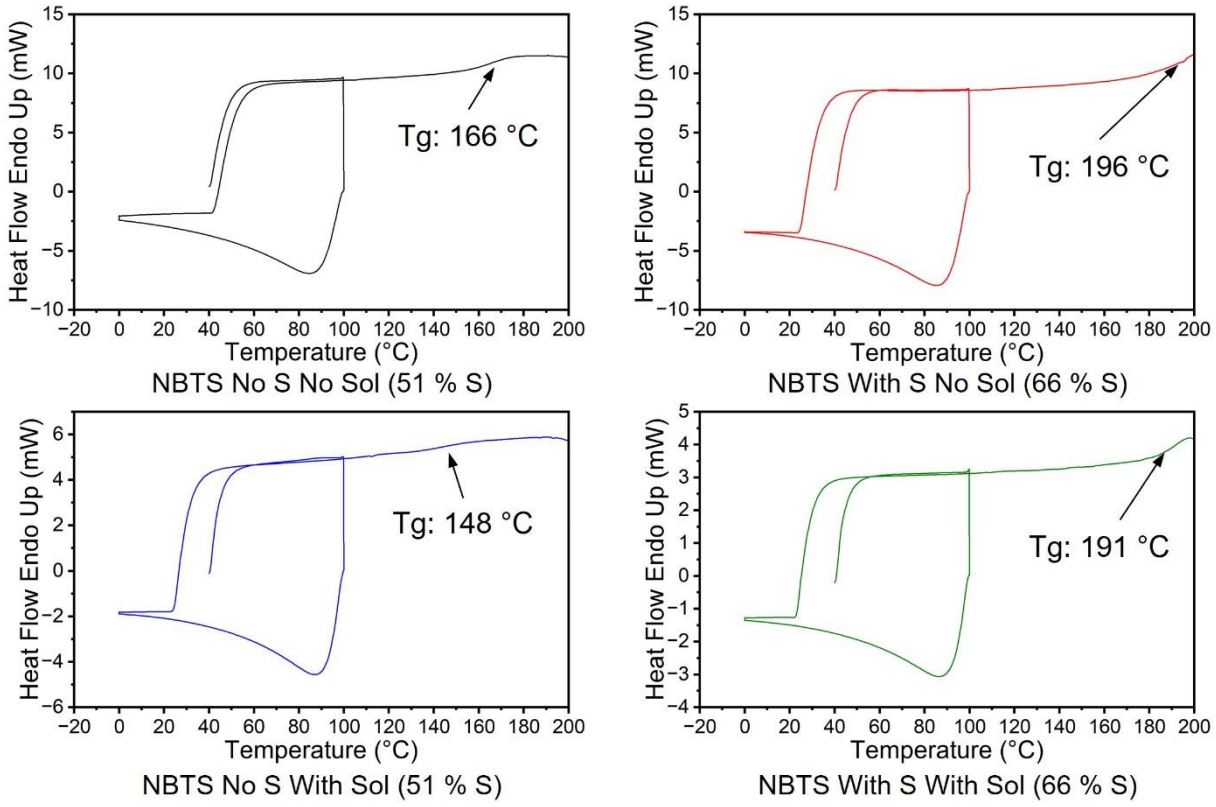

Figure 3.91: Differential scanning calorimetry of polymers made from norbornene trisulfide (**4**). The samples with sulfur had a total sulfur content of 66 %. The samples with sol were reacted in a solvent system of 50-50 DMF/xylene.

The polymers made from a combination of norbornene epi, tri and penta sulfide (**1**, **4**, **8**) were very similar to those prepared from **4**. Just like the samples made with only **4,** the samples with added sulfur had a greater glass transition temperature. The samples made in solvent had a slightly decreased glass transition temperature than those made neat.

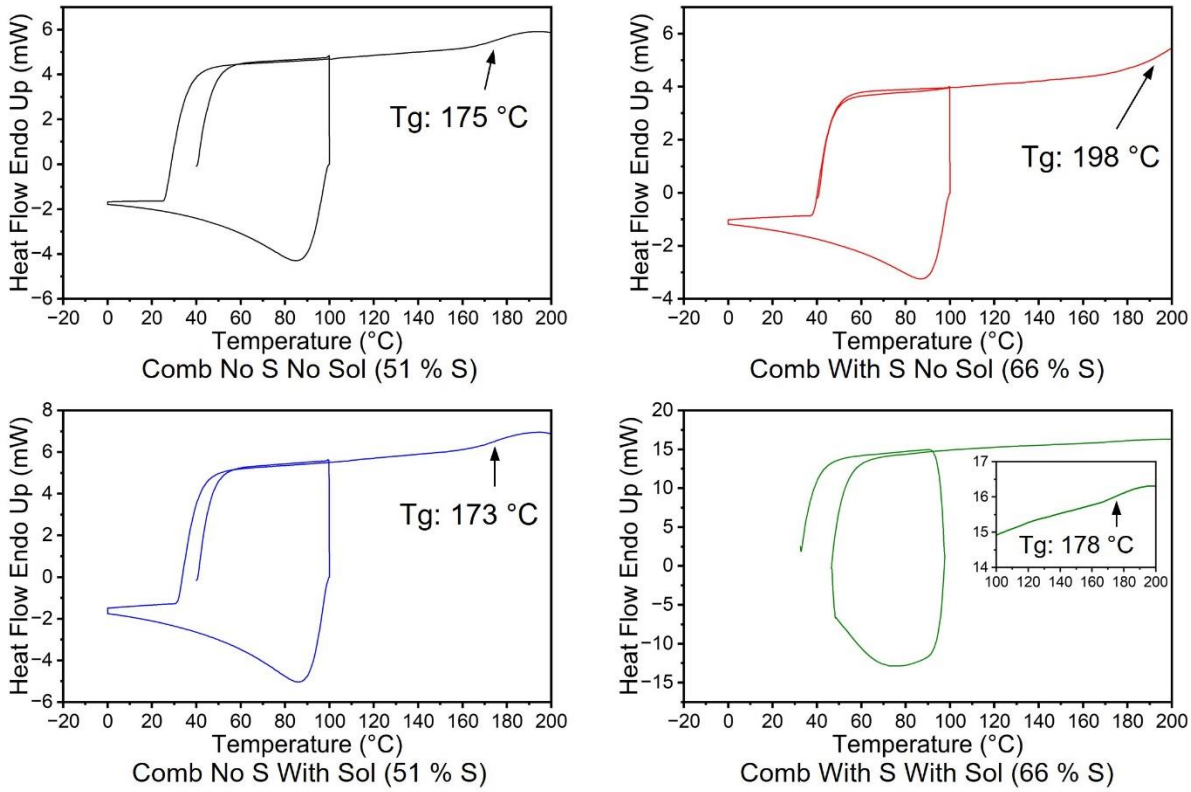

Figure 3.92: Differential scanning calorimetry of polymers made from a combination of (**1**, **4**, **8**) in a 24: 100: 40 ratio. The samples with sulfur had a total sulfur content of 66 %. The samples with sol were reacted in a solvent system of 50-50 DMF/xylene.

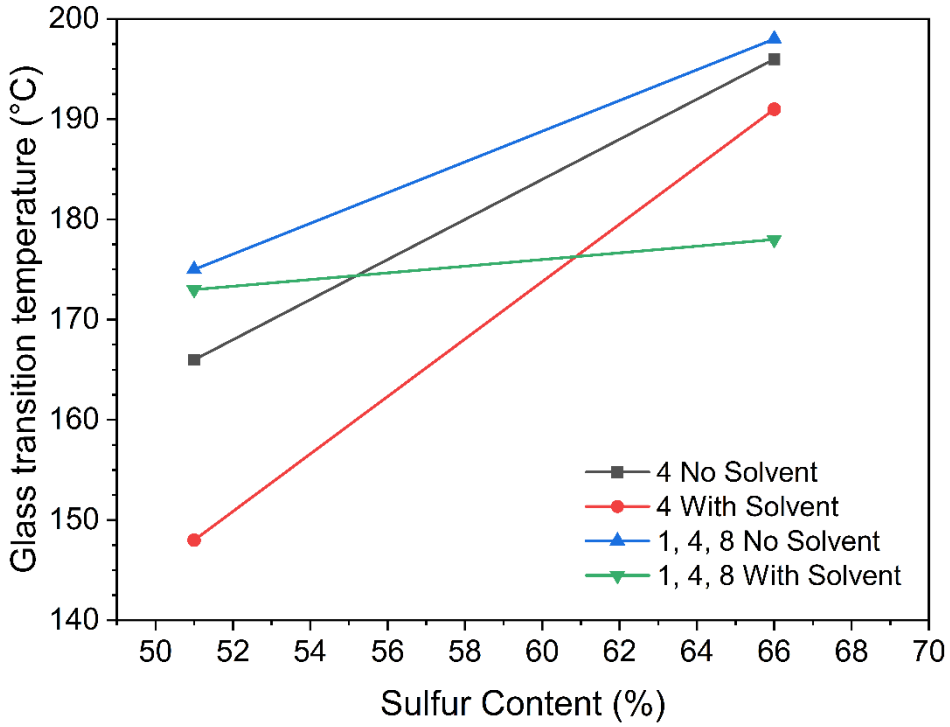

Figure 3.93: Glass transition temperature of polymers made from **4** or a combination of **1**, **4**, **8** in a ratio of 24: 100: 40.

The samples made with norbornane bistrisulfide (**6**) had a very high glass transition temperature. Unlike those made from **4** or a combination of **1**, **4**, **8**, a decrease in glass transition temperature was observed with increasing sulfur content. This is likely because the polymers are already crosslinked as **6** has two trisulfide rings. The samples made in a solvent of 50-50 DMF-Xylene had a slightly decreased glass transition temperature than those made neat.

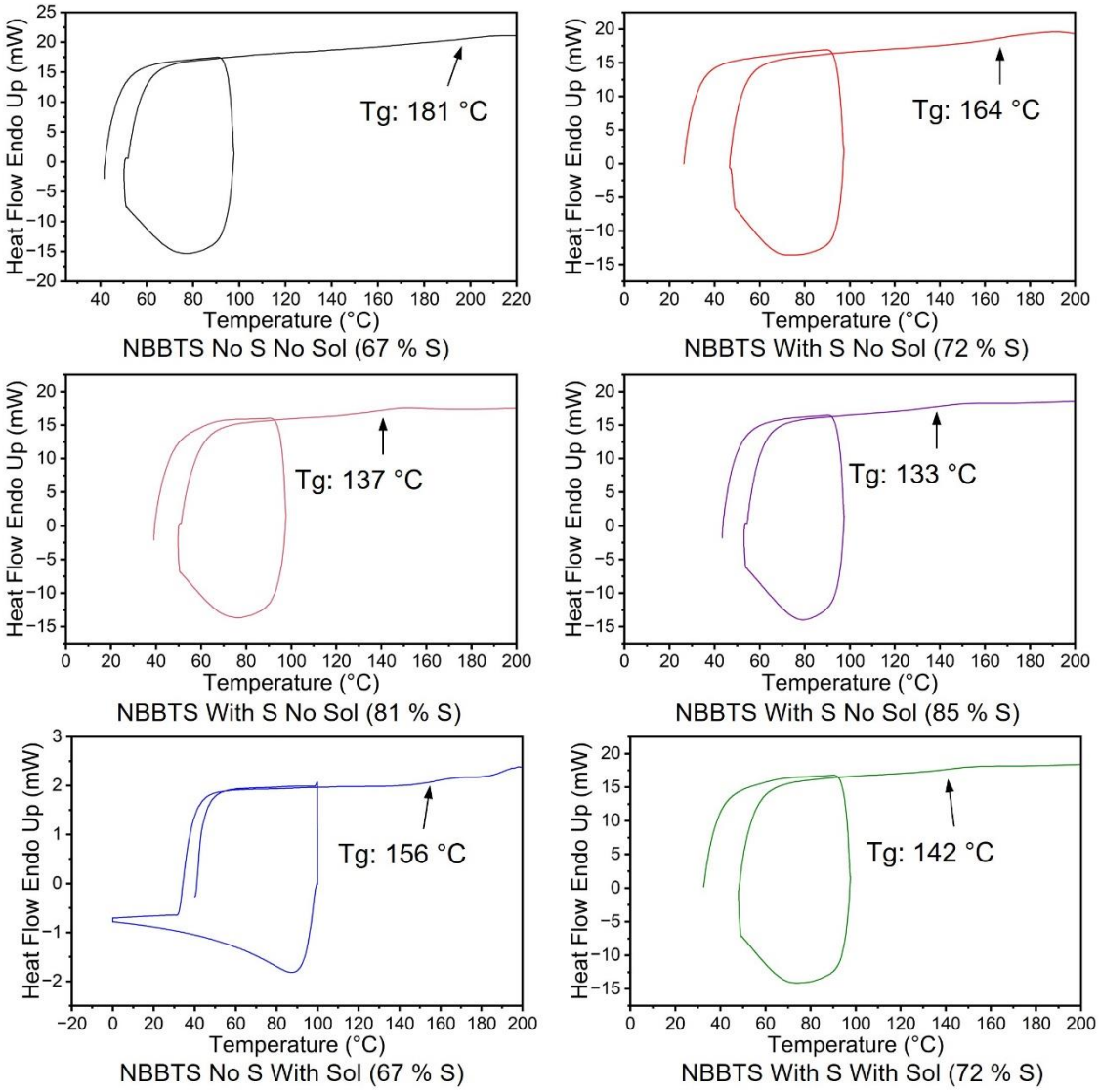

Figure 3.94: Differential scanning calorimetry of polymers made norbornane bistrisulfide (**6**) The samples with sol were reacted in a solvent system of 50-50 DMF/xylene.

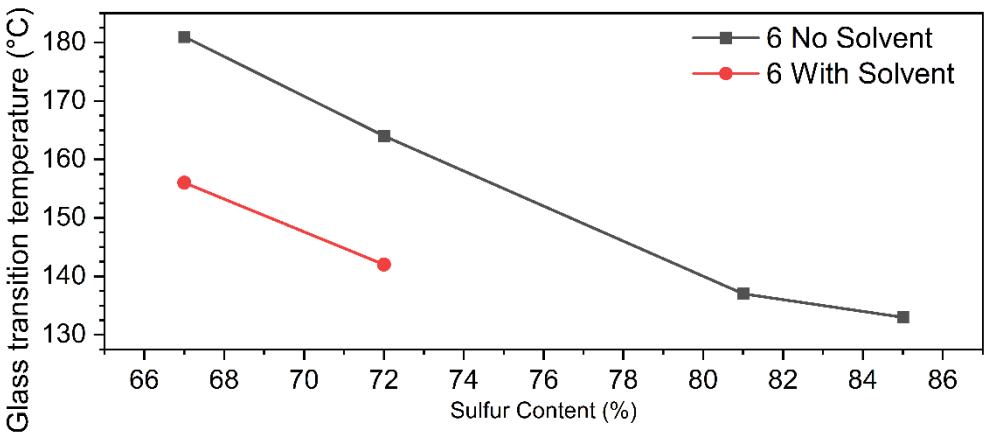

Figure 3.95: Glass transition temperature of polymers made from **6.**

The polymers prepared from the **3** were very different to all the other polymers. All the samples showed a melting peak in the first heating run. This potentially indicates that there was some unreacted monomer in these samples as **3** melts around this temperature. The samples also didn't show a clear glass transition temperature in the with S no Sol or No S with Sol samples. The other two samples had a glass transition temperature around 122 °C

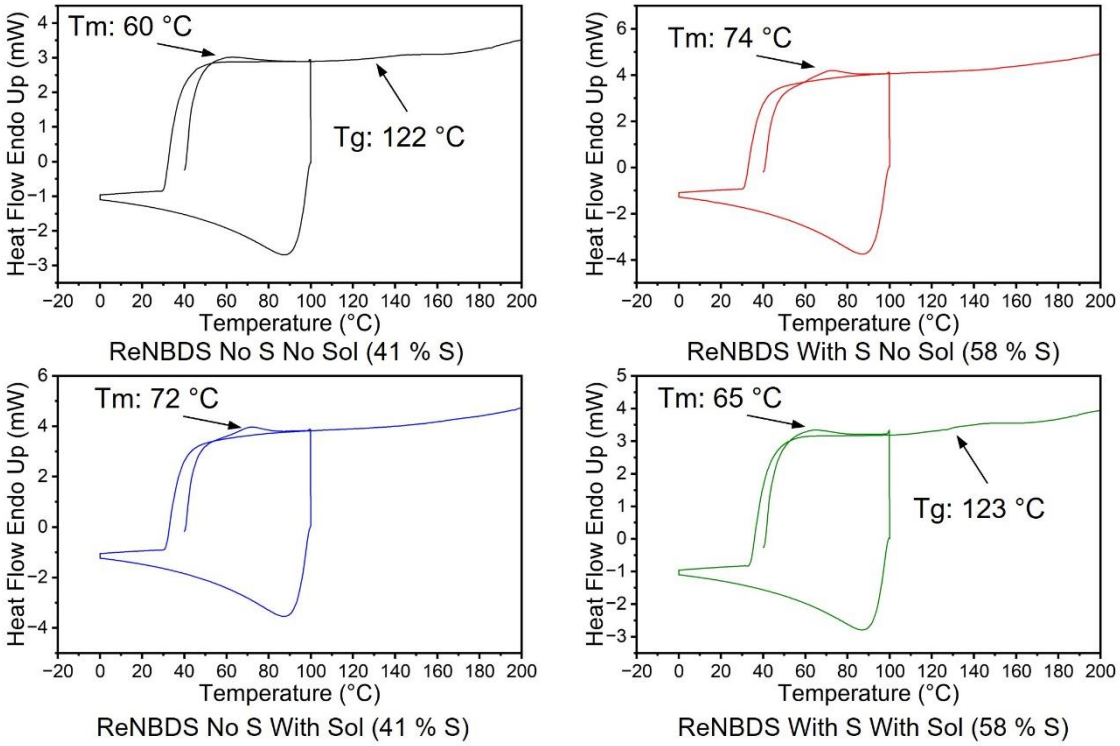

Figure 3.96: Differential scanning calorimetry of polymers made rearranged norbornane disulfide (**3**) The samples with sol were reacted in a solvent system of 50-50 DMF/xylene

Window formation using polymer made from norbornene bistrisulfide

With the chemical and thermal properties in hand, the optical properties of the polymer was further explored. The polymers made from norbornane bistrisulfide (**6**) were selected to test as they had excellent thermal properties and unlike those prepared from **4**, there was no chance of alkenes in the polymer after the reaction.

Due to the very high glass transition temperature of the polymers prepared from **6,** reactive compression moulding was not possible. Instead, the polymers were moulded directly into a window for testing. Casting of polymers prepared from **6** was not trivial. As the monomer is a solid at room temperature, to polymerised it neat, it must be heated to above 179 °C. At this temperature, the reaction occurs very rapidly, only allowing several seconds to cast the polymer. This made it not possible to mould polymers made from **6** without any sulfur. However, it was found that **6** would dissolve in molten sulfur at 140 °C. At this reduced temperature, the reaction would occur slower but would still only allow a working time of approximately 3 minutes. Using this method, only polymers with a sulfur content of above 80 % could be produced as this is the minimum amount of molten sulfur to fully dissolve **6**. Two different polymers were made into windows, one with 81 % sulfur and the other with 85 % sulfur.

A window with three thicknesses was prepared for the polymers made from **6**. To prepare this window, a silicone mould was first made. The negative for the mould was made using glass cover slips. The cover slips were glued together so that there were 3 different thicknesses in one piece. The three thicknesses were 1 mm, 0.75 mm and 0.55 mm. The glass piece was placed in a 3D printed part which held it upright. Silicone resin was then poured into the 3D printed part and left for two hours to cure. When fully cured, the silicone resin was taken out of the 3D printed part and the glass negative was removed.

The polymerisation reaction was done using the following method. Sulfur (300 mg, 1.17 mmol S8) was measured into a vial with a magnetic stirrer. The vial was added to a preheated oil bath at 140 °C. The sulfur was left for 3 minutes to melt. **6** (445 mg, 1.56 mmol) for 81 % S polymer or (267 mg, 0.94 mmol) for 85 % S polymer was poured into the vial. **6** would rapidly dissolve in the molten sulfur. The reaction was heated in the oil bath 1 additional minute. Stirring was done manually with a heated metal spatula. The reaction was stirred carefully to prevent trapping gasses which would cause bubbles in the polymer. The prepolymer then poured into the mould which had been preheated to 140 °C. To reduce bubbles, the prepolymer was poured from one end and allowed to fill into the mould. The mould was then placed in a 140 °C oven where it was left for 24 hours to cure.

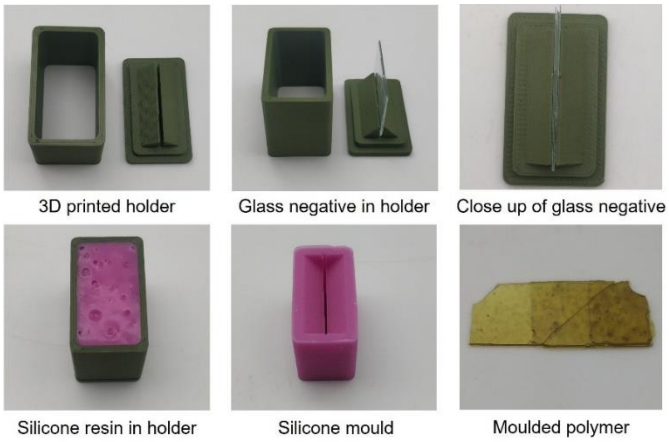

Figure 3.97: Images for synthesis of polymer windows.

The polymer windows made form **6** were used to take long wave infrared images. Using a FLIR E6 long wave infrared camera, images were taken through the polymer windows. This camera uses the wavelength range of 7.5 μm to 13 μm. This puts it completely within the long wave infrared region. At each of the three thicknesses, the polymer window was placed in front of the thermal camera lens. An image of a hand was then taken. Each thickness of both sulfur compositions had enough transparency to image a human hand which is very rare for a polymer. For both polymers, the thinner samples gave better thermal resolution, likely due to reduced absorptions of the polymer.

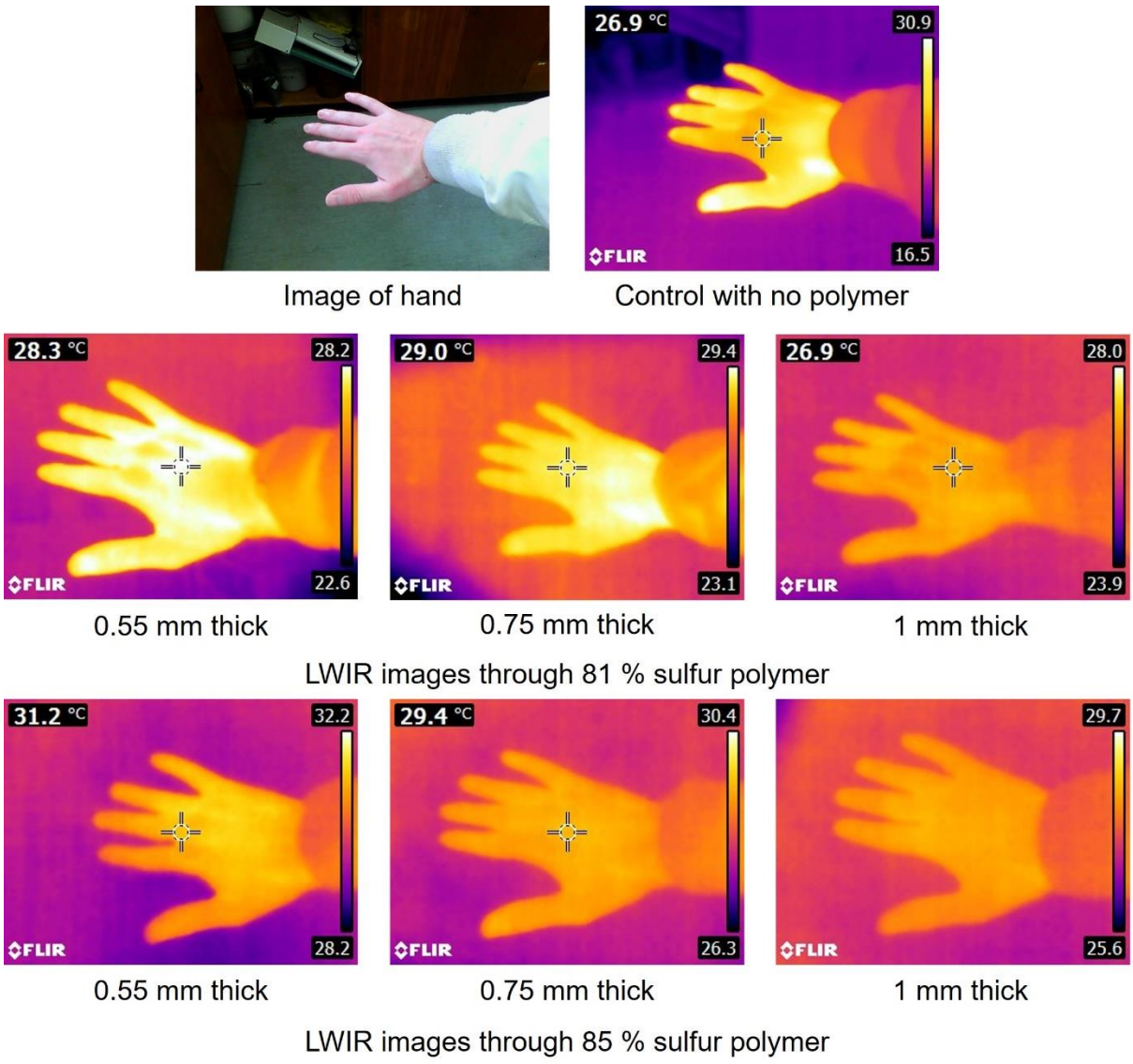

Figure 3.98: Visible and long wave infrared image of a hand taken with FLIR E6 Thermal camera. LWIR images using FLIR E6 camera with polymers prepared using **6** at different thicknesses covering the lens.

Infrared transparency of norbornene bistrisulfide polymer

While the images through the polymers prepared from **6**, to objectively know the optical performance of the polymer, the infrared spectrum is needed. The transparency of the polymers was tested from a wavelength of 2 μm to 20 μm using a Perkin Elmer Frontier FTIR. The transmittance was integrated over the mid wave infrared (3 μm – 5 μm) and the long wave infrared (7 μm – 14 μm) then divided by the wavelength range to obtain an average.

The transmittance of both the MWIR and LWIR region was much greater in the polymers prepared with **6** than the polymers prepared directly from NBD. The Transmittance in the LWIR region was particularly impressive, with the SR 8 sample displaying greater than 21 % average transmittance at 1 mm thick.

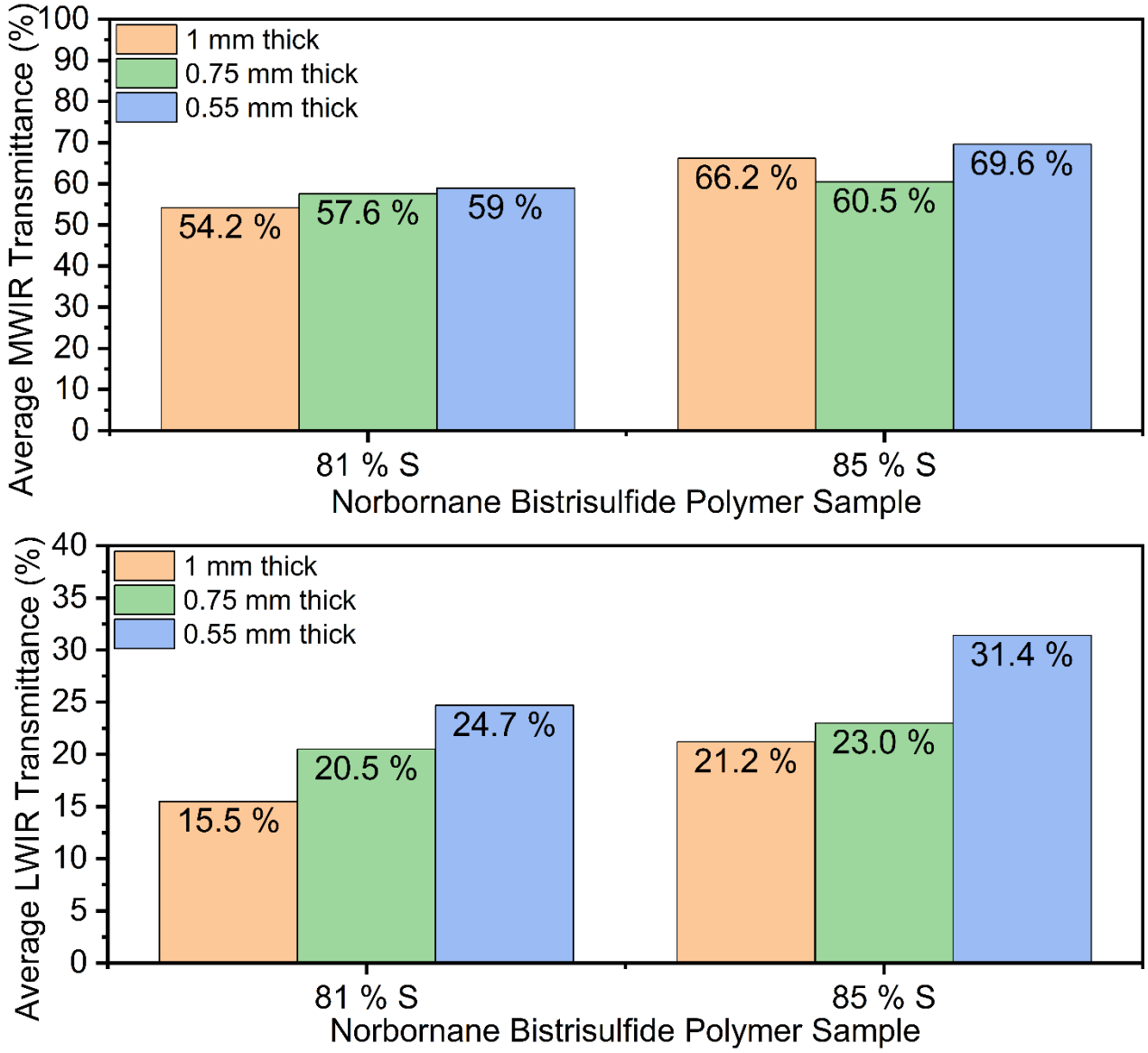

Figure 3.99: Average MWIR and LWIR transmittance for polymers made from norbornane bistrisulfide and sulfur at two different sulfur contents. The average MWIR transmittance is calculated by integrated the transmittance plot between 3 μm and 5 μm before dividing by the wavelength range. The average LWIR transmittance is calculated by integrated the transmittance plot between 7 μm and 14 μm before dividing by the wavelength range.

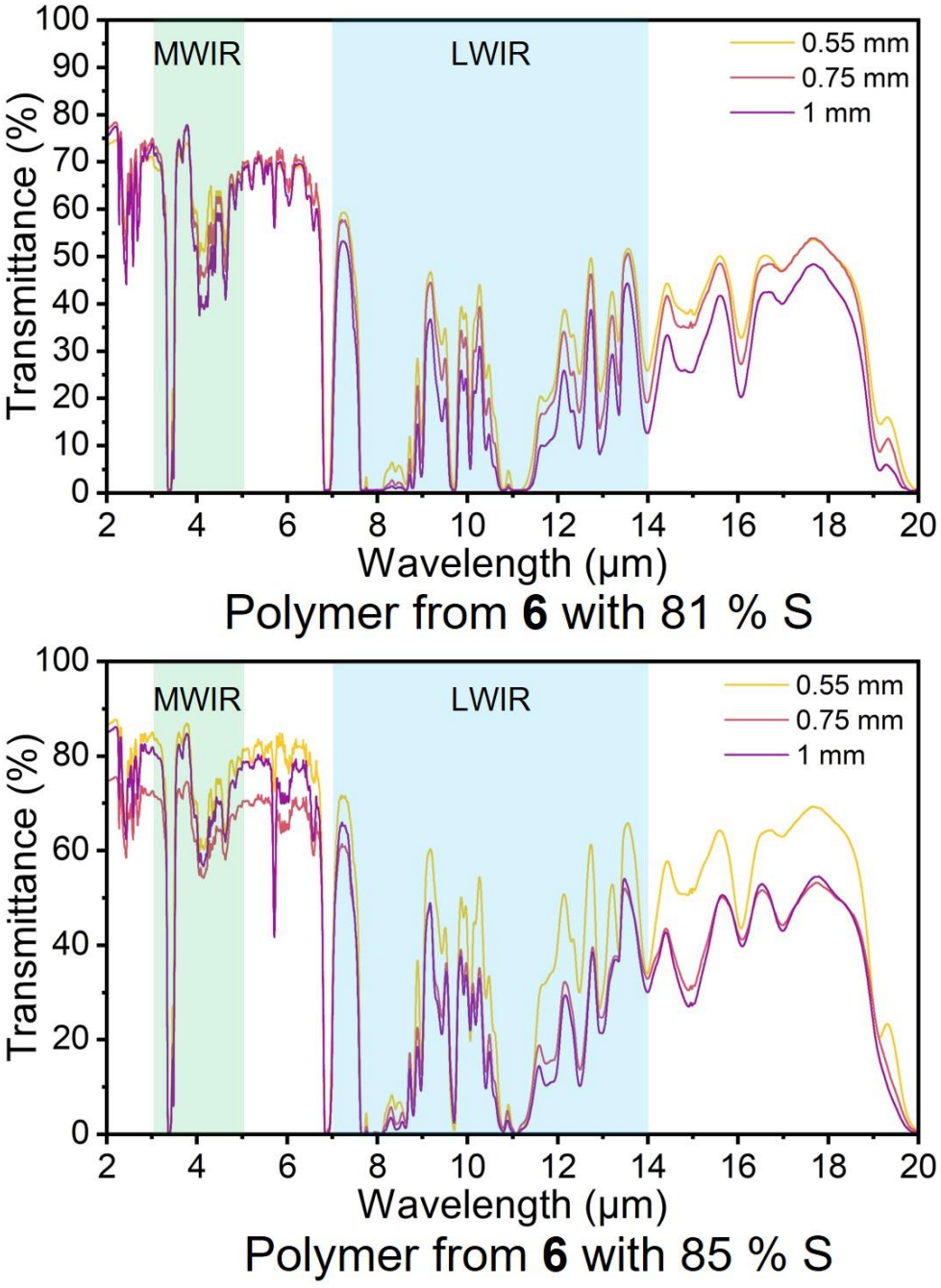

Figure 3.100: FTIR spectra for polymers made from norbornane bistrisulfide (**6**) and sulfur at three different thicknesses. All spectra were taken using a Perkin Elmer Frontier FTIR. The MWIR and LWIR regions are labelled at 3 μm -5 μm and 7 μm -14 μm respectively.

Refractive index testing of norbornene bistrisulfide polymer

To test the refractive index of the polymers prepared from **6,** the specular reflectance of the polymer was measured and converted to refractive index using a Kramers-Kronig transform. It was found that the window thickness and surface roughness were vitally important when measuring reflectance. When thin windows (less than 2 mm thick), the reflectance spectrum would show a similar pattern to the transmittance spectra. This was likely due to light transmitting through the surface, reflecting off the bottom surface before being collected by the sensor. Due to these effects, the sample geometry was carefully considered. Two changes were made to the samples which allowed excellent transmission spectra to be obtained. The first was to make a very thick sample. Cylinders of the polymer were made with a diameter of 25 mm and a thickness of 10 mm. This thickness ensured that very little light would transmit through the entire sample. The other change was that only one face of the polymer cylinder was polished. On the other face, the polymer was scratched with course sandpaper (80 grit). This made an inconsistent surface which would scatter the light and prevent it from reflecting towards the sensor. After these changes, the reflectance spectra improved greatly and no longer showed effects of transmitted light.

The top surface of the polymer sample was polished using sandpaper with a range of grits. Starting at 200 grit, the surface was sanded flat. Follow this, the sample surface was wet and dry sanded with micro mesh polishing kit with sandpaper grits from 1500 to 12000. Following this, a micro gloss polish with a 1-micron abrasive crystal was applied to the surface.

Specular reflectance spectra were measured using a Bruker Vertex v80 instrument with the 1513/QA attachment for the polymers prepared from **6** and sulfur. An angle from the surface normal of 15 ° was used under vacuum. The sample was referenced using the reflectance spectrum of an aluminium mirror. A Kramers-Kronig transform was applied using the OPUS V7.2 software to find the wavenumber dependent phase shift spectrum. The refractive index was then calculated using the real portion of the complex refractive index, η = n + ik.

For many applications, the dispersion or change in refractive index with wavelength is very important. The dispersion of a material is defined in the visible region by the Abbe number. The Abbe number uses the refractive index at the Fraunhofer's C (656.3 nm), d (587.6 nm) and F (486.1 nm) spectral lines to quantify the dispersion of the material. For long wave infrared transparent materials, the V-number is more commonly used. Materials that are used for thermal imaging are mostly interested in light between 7 and 14 microns so instead of using the Fraunhofer's spectral lines, the refractive index at 8 μm, 10 μm and 12 μm are used. To calculate the V-number, the following equation is used.

$$V = \frac{n(10) - 1}{n(8) - n(12)}$$

Where V is the V-number and n(x) is the refractive index a x μm. The polymer had a very high average refractive index over the long wave infrared region (7 μm - 14 μm) of 1.871 and a V-number of 314. This V-number classifies it as a crown glass with very long dispersion, a useful property for lenses and other optics.

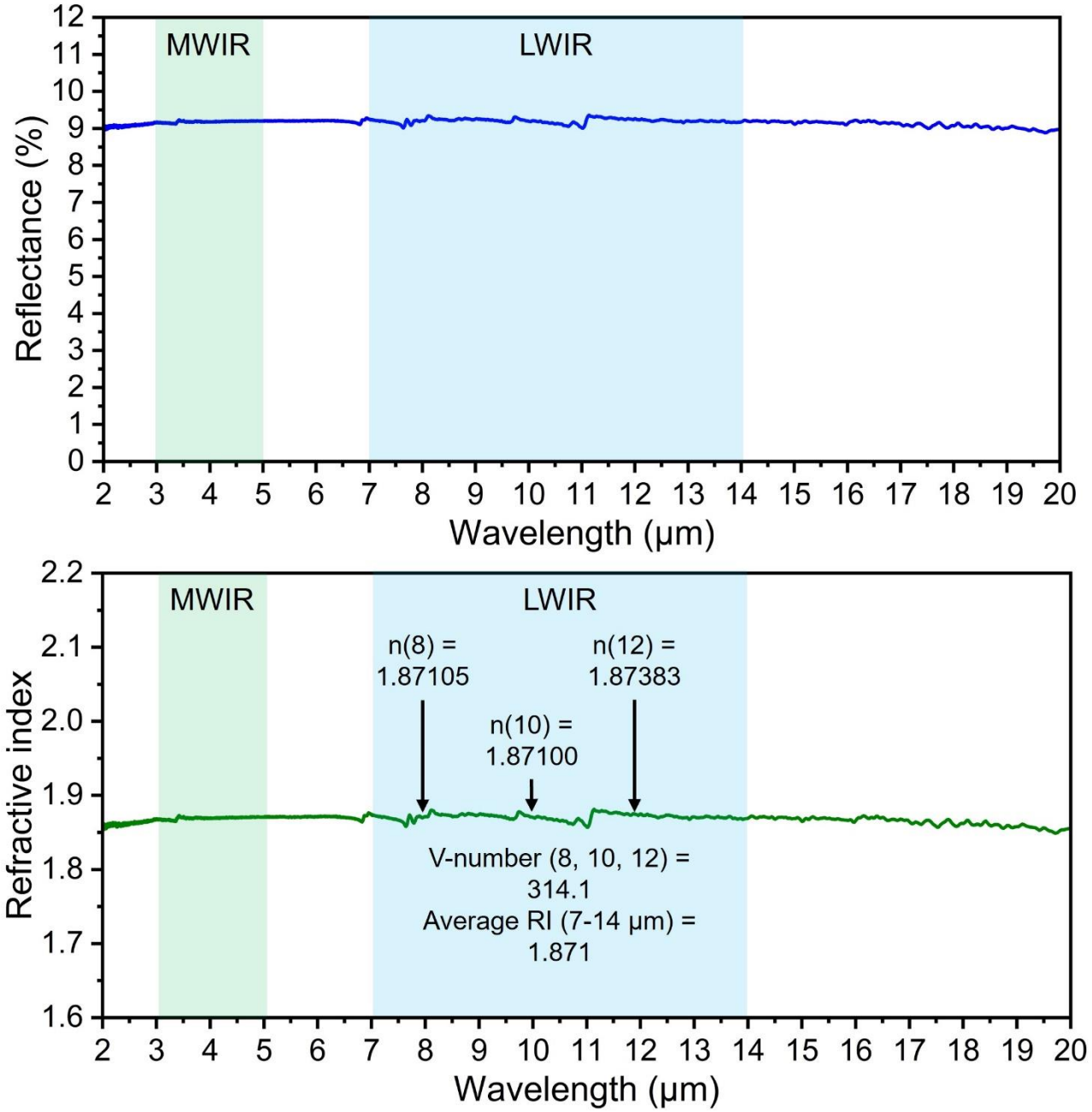

Figure 3.101: Reflectance and refractive index spectra of polymers made from sulfur and norbornane bistrisulfide (**6**). All spectra were obtained on a Bruker Vertex v80 using the 1513/QA attachment. The V-number was calculated using the equation above and the refractive index at 8 μm, 10 μm and 12 μm.

Chapter conclusions

This chapter investigated the development of a sulfur-based polymer with a norbornane core. Initial attempts to synthesise this polymer involved the direct polymerisation of norbornadiene with sulfur. When using NBD, it was found that the reaction required a solvent system to prevent premature vitrification, leading to inhomogeneity of the polymer. After investigating several solvent systems, it was found that using DMF and xylenes in a 50-50 ratio gave a consistent polymer and eliminated all the issues with the solventless reaction.

Characterisation of the polymers prepared in solvent directly from NBD and sulfur found that they had a very high glass transition and refractive index but a very poor long wave infrared transmission. Further analysis of the chemical composition of these polymers indicated that this may be due to rearrangement of the norbornane core. This rearrangement gave a molecule with a cyclopropane group which was found to introduce many vibrational modes in the LWIR region, explaining the poor transmission.

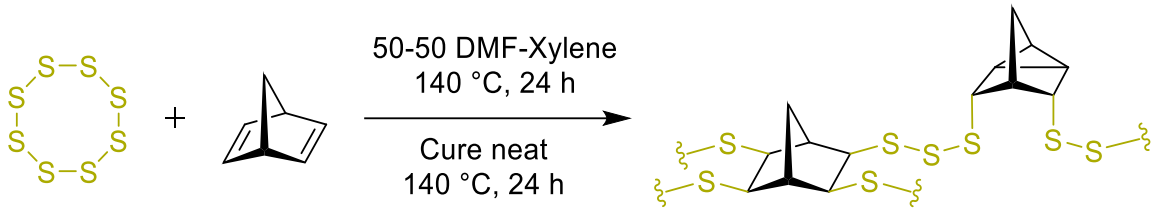

Figure 3.102: Reaction between sulfur and NBD in a solvent system of 50-50 DMF-Xylene.

After the reactions directly with NBD, a new approach was taken to prepare the desired polymer. The hexane soluble intermediates of the reaction were isolated, and it was found that the reaction produced several cyclic sulfide intermediates. In a series of experiments, these intermediates were isolated and fully characterised. One of these intermediates was a norbornane molecule with two cyclic trisulfide rings (molecule **6**). To avoid the issue of rearrangement, it was found that the polymer could be prepared using **6** giving a polymer with no rearrangement or side reactions. Solid state NMR, FTIR, Raman and reduction experiments all showed that the norbornane core structure was preserved while the trisulfide ring participated in a ring opening polymerisation when either neat or with additional sulfur.

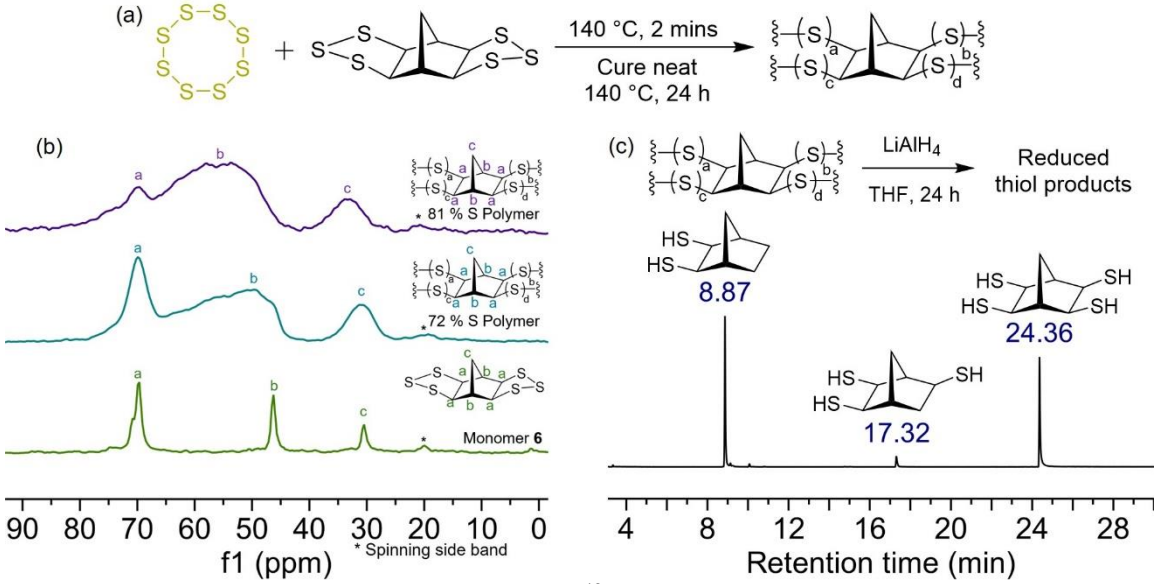

Figure 3.103: (a) Reaction between **4** and sulfur. (b) ^{13}C CP-MAS of the monomer and polymers with two different amounts of sulfur. (c) Reduction of polymer with $LiAlH_4$ and GC chromatogram of reduced thiol products.

With a method to synthesise the desired polymer from **6**, several polymers were prepared with varying sulfur contents. These polymers were tested to determine their suitability in thermal imaging applications. The glass transition temperature of all the polymers prepared from **6** was very high, ranging from 181°C to 133°C, decreasing with increased sulfur content (67 wt% - 85 wt%). This made the polymer brittle and glassy, making it well suited for use as a lens or other optics.

The materials prepared from **6** also possessed exceptional transmission in the long wave infrared region. Windows of three different thickness and two different sulfur contents were prepared. The long wave infrared transmission was measured for all the windows. The transmission for the 1 mm thick windows was 15.5 % and 21.5 % for polymers with 81 % and 85 % sulfur respectively. This transmission is among the best for any polymers and allows for high quality images of relatively low temperature objects like people. The polymers also possessed a refractive index of above 1.87, indicating that they could be used to prepare high powered lenses and other optics.

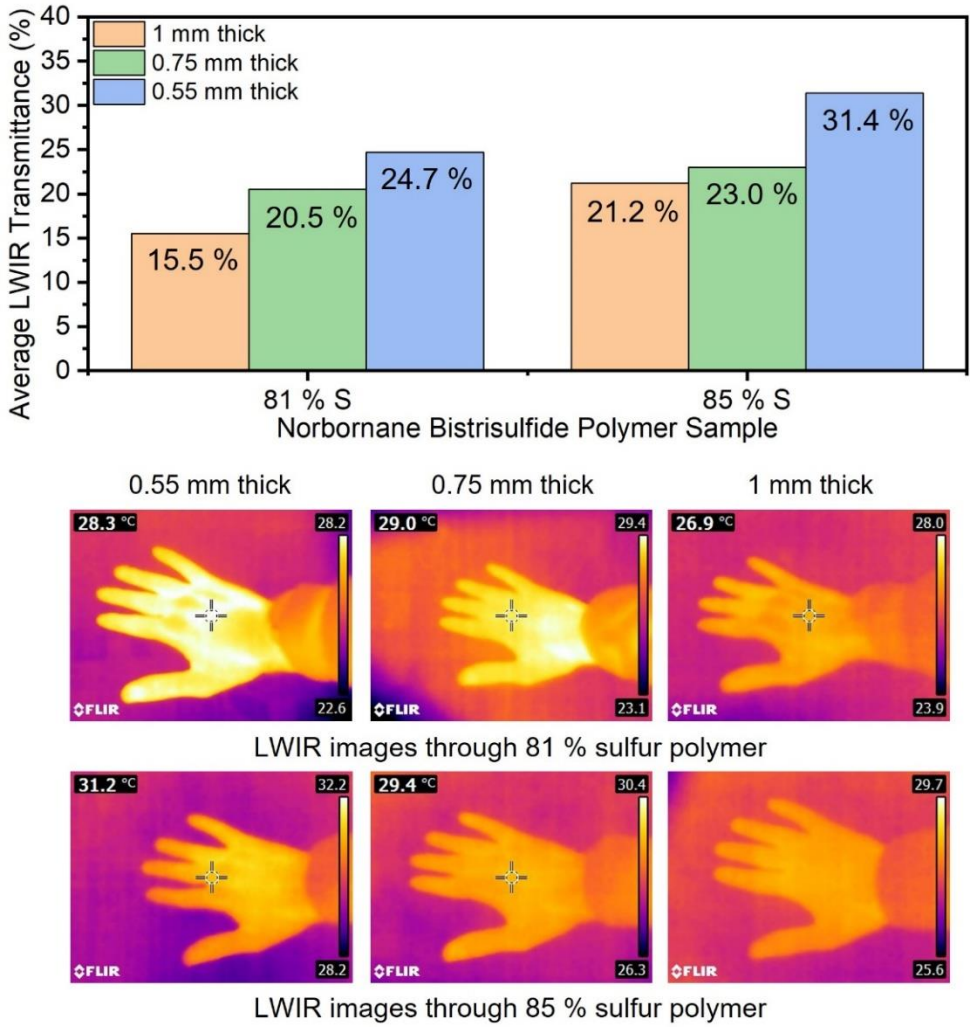

Figure 3.104: Average LWIR (7 µm -14 µm) transmission for polymers made from **6** and thermal images taken through windows of different thicknesses.

This chapter found that to prepare high performance sulfur polymers, it was important to prevent any rearrangement or side reactions. This was achieved by first preparing cyclic trisulfides which can then be used as monomers in a ring opening polymerisation. The polymers prepared in this chapter showed excellent potential for use in thermal imaging. This application was explored in detail in chapter four.

Chapter 3 references

(1) Yan, P.; Zhao, W.; Tonkin, S. J.; Chalker, J. M.; Schiller, T. L.; Hasell, T. Stretchable and Durable Inverse Vulcanized Polymers with Chemical and Thermal Recycling. *Chemistry of Materials* **2022**, *34* (3), 1167-1178. DOI: 10.1021/acs.chemmater.1c03662.
(2) Kleine, T. S.; Lee, T.; Carothers, K. J.; Hamilton, M. O.; Anderson, L. E.; Ruiz Diaz, L.; Lyons, N. P.; Coasey, K. R.; Parker Jr., W. O.; Borghi, L.; et al. Infrared Fingerprint Engineering: A Molecular-Design Approach to Long-Wave Infrared Transparency with Polymeric Materials. *Angewandte Chemie International Edition* **2019**, *58* (49), 17656-17660. DOI: https://doi.org/10.1002/anie.201910856.
(3) Molineux, J.; Lee, T.; Kim, K. J.; Kang, K.-S.; Lyons, N. P.; Nishant, A.; Kleine, T. S.; Durfee, S. W.; Pyun, J.; Norwood, R. A. Fabrication of Plastic Optics from Chalcogenide Hybrid Inorganic/Organic Polymers for Infrared Thermal Imaging. *Advanced Optical Materials* **2024**, *12* (7), 2301971. DOI: https://doi.org/10.1002/adom.202301971.
(4) He, L.; Yang, J.; Jiang, H.; Zhao, H.; Xia, H. Mechanochemistry Enabled Inverse Vulcanization of Norbornadiene for Optical Polymers and Elastomeric Materials. *Industrial & Engineering Chemistry Research* **2023**, *62* (25), 9587-9594. DOI: 10.1021/acs.iecr.3c00801.
(5) Orme, K.; Fistrovich, A. H.; Jenkins, C. L. Tailoring Polysulfide Properties through Variations of Inverse Vulcanization. *Macromolecules* **2020**, *53* (21), 9353-9361. DOI: 10.1021/acs.macromol.0c01932. Scheiger, J. M.; Hoffmann, M.; Falkenstein, P.; Wang, Z.; Rutschmann, M.; Scheiger, V. W.; Grimm, A.; Urbschat, K.; Sengpiel, T.; Matysik, J.; et al. Inverse Vulcanization of Norbornenylsilanes: Soluble Polymers with Controllable Molecular Properties via Siloxane Bonds. *Angewandte Chemie International Edition* **2022**, *61* (16), e202114896. DOI: https://doi.org/10.1002/anie.202114896. Chalker, J. M.; Worthington, M. J. H.; Lundquist, N. A.; Esdaile, L. J. Synthesis and Applications of Polymers Made by Inverse Vulcanization. In *Sulfur Chemistry*, Jiang, X. Ed.; Springer International Publishing, 2019; pp 125-151.
(6) Tonkin, S. J.; Gibson, C. T.; Campbell, J. A.; Lewis, D. A.; Karton, A.; Hasell, T.; Chalker, J. M. Chemically induced repair, adhesion, and recycling of polymers made by inverse vulcanization. *Chem. Sci.* **2020**, *11* (21), 5537.
(7) Yan, P.; Zhao, W.; Tonkin, S. J.; Chalker, J. M.; Schiller, T. L.; Hasell, T. Stretchable and Durable Inverse Vulcanized Polymers with Chemical and Thermal Recycling. *Chem. Mater.* **2022**, *34* (3), 1167.
(8) Huang, Y.; Liu, Y.; Si, G.; Tan, C. Self-Healing and Recyclable Vulcanized Polyisoprene Based on a Sulfur-Rich Copolymer Cross-Linking Agent Derived from Inverse Vulcanization. *ACS Sustainable Chemistry & Engineering* **2024**, *12* (6), 2212-2224. DOI: 10.1021/acssuschemeng.3c05929.
(9) Lundquist, N. A.; Tikoalu, A. D.; Worthington, M. J. H.; Shapter, R.; Tonkin, S. J.; Stojcevski, F.; Mann, M.; Gibson, C. T.; Gascooke, J. R.; Karton, A.; et al. Reactive Compression Molding Post-Inverse Vulcanization: A Method to Assemble, Recycle, and Repurpose Sulfur Polymers and Composites. *Chemistry – A European Journal* **2020**, *26* (44), 10035-10044. DOI: https://doi.org/10.1002/chem.202001841 (acccessed 2024/01/18).
(10) Wu, X.; Smith, J. A.; Petcher, S.; Zhang, B.; Parker, D. J.; Griffin, J. M.; Hasell, T. Catalytic inverse vulcanization. *Nature Communications* **2019**, *10* (1), 647. DOI: 10.1038/s41467-019-08430-8.
(11) Dale, J. J.; Petcher, S.; Hasell, T. Dark Sulfur: Quantifying Unpolymerized Sulfur in Inverse Vulcanized Polymers. *ACS Applied Polymer Materials* **2022**, *4* (5), 3169-3173. DOI: 10.1021/acsapm.2c00304.
(12) Rahman, M. S.; Al-Marhubi, I. M.; Al-Mahrouqi, A. Measurement of glass transition temperature by mechanical (DMTA), thermal (DSC and MDSC), water diffusion and density methods: A comparison study. *Chemical Physics Letters* **2007**, *440* (4), 372-377. DOI: https://doi.org/10.1016/j.cplett.2007.04.067. Bikiaris, D.; Prinos, J.; Botev, M.; Betchev, C.; Panayiotou, C. Blends of polymers with similar glass transition temperatures: A DMTA and DSC study. *Journal of Applied Polymer Science* **2004**, *93* (2), 726-735. DOI: https://doi.org/10.1002/app.20531. Ramis, X.; Cadenato, A.; Morancho, J. M.; Salla, J. M. Curing of a thermosetting powder coating by means of DMTA, TMA and DSC. *Polymer* **2003**, *44* (7), 2067-2079. DOI: https://doi.org/10.1016/S0032-3861(03)00059-4.
(13) Smith, J. A.; Wu, X.; Berry, N. G.; Hasell, T. High sulfur content polymers: The effect of crosslinker structure on inverse vulcanization. *Journal of Polymer Science Part A: Polymer Chemistry* **2018**, *56* (16), 1777-1781. DOI: https://doi.org/10.1002/pola.29067. Zheng, B.; Zhong, L.; Wang, X.; Lin, P.; Yang, Z.; Bai, T.; Shen, H.; Zhang, H. Structural evolution during inverse vulcanization. *Nature Communications* **2024**, *15* (1), 5507. DOI: 10.1038/s41467-024-49374-y. Kleine, T. S.; Nguyen, N. A.; Anderson, L. E.; Namnabat, S.; LaVilla, E. A.; Showghi, S. A.; Dirlam, P. T.; Arrington, C. B.; Manchester, M. S.; Schwiegerling, J.; et al. High Refractive Index Copolymers with Improved Thermomechanical Properties via the Inverse Vulcanization of Sulfur and 1,3,5-Triisopropenylbenzene. *ACS Macro Letters* **2016**, *5* (10), 1152-1156. DOI: 10.1021/acsmacrolett.6b00602.
(14) Lundquist, N. A.; Chalker, J. M. Confining a spent lead sorbent in a polymer made by inverse vulcanization prevents leaching. *Sustainable Materials and Technologies* **2020**, *26*, e00222. DOI: https://doi.org/10.1016/j.susmat.2020.e00222.

(15) Lundquist, N. A.; Yin, Y.; Mann, M.; Tonkin, S. J.; Slattery, A. D.; Andersson, G. G.; Gibson, C. T.; Chalker, J. M. Magnetic responsive composites made from a sulfur-rich polymer. *Polymer Chemistry* **2022**, *13* (39), 5659-5665, 10.1039/D2PY00903J. DOI: 10.1039/D2PY00903J.
(16) Macdonald, E. K.; Shaver, M. P. Intrinsic high refractive index polymers. *Polymer International* **2015**, *64* (1), 6-14. DOI: https://doi.org/10.1002/pi.4821. Naccarato, F.; Ricci, F.; Suntivich, J.; Hautier, G.; Wirtz, L.; Rignanese, G.-M. Searching for materials with high refractive index and wide band gap: A first-principles high-throughput study. *Physical Review Materials* **2019**, *3* (4), 044602. DOI: 10.1103/PhysRevMaterials.3.044602.
(17) Mazumder, K.; Voit, B.; Banerjee, S. Recent Progress in Sulfur-Containing High Refractive Index Polymers for Optical Applications. *ACS Omega* **2024**, *9* (6), 6253-6279. DOI: 10.1021/acsomega.3c08571.
(18) Hemauer, F.; Steinrück, H.-P.; Papp, C. The Norbornadiene/Quadricyclane Pair as Molecular Solar Thermal Energy Storage System: Surface Science Investigations. *ChemPhysChem* **2024**, *25* (9), e202300806. DOI: https://doi.org/10.1002/cphc.202300806 (acccessed 2024/07/21). Jacovella, U.; Carrascosa, E.; Buntine, J. T.; Ree, N.; Mikkelsen, K. V.; Jevric, M.; Moth-Poulsen, K.; Bieske, E. J. Photo- and Collision-Induced Isomerization of a Charge-Tagged Norbornadiene–Quadricyclane System. *The Journal of Physical Chemistry Letters* **2020**, *11* (15), 6045-6050. DOI: 10.1021/acs.jpclett.0c01198. Orrego-Hernández, J.; Dreos, A.; Moth-Poulsen, K. Engineering of Norbornadiene/Quadricyclane Photoswitches for Molecular Solar Thermal Energy Storage Applications. *Accounts of Chemical Research* **2020**, *53* (8), 1478-1487. DOI: 10.1021/acs.accounts.0c00235. Petersen, A. U.; Hofmann, A. I.; Fillols, M.; Mansø, M.; Jevric, M.; Wang, Z.; Sumby, C. J.; Müller, C.; Moth-Poulsen, K. Solar Energy Storage by Molecular Norbornadiene–Quadricyclane Photoswitches: Polymer Film Devices. *Advanced Science* **2019**, *6* (12), 1900367. DOI: https://doi.org/10.1002/advs.201900367 (acccessed 2024/07/21).
(19) Chen, J.; Liu, M.; Zhu, Y.; Jin, K.; Tian, Z.; Yang, L.; Zhou, C.-W. Oxidation of norbornadiene: Theoretical investigation on H-atom abstraction and related radical decomposition reactions. *Propulsion and Power Research* **2023**, *12* (1), 104-113. DOI: https://doi.org/10.1016/j.jppr.2023.02.001. Wang, H.; Zhang, B.; Gong, S.; Wang, L.; Zhang, X.; Liu, G. Experimental and modeling studies of quadricyclane and 2-ethylnorbornane pyrolysis from atmospheric to high pressure. *Combustion and Flame* **2021**, *226*, 163-181. DOI: https://doi.org/10.1016/j.combustflame.2020.11.042.
(20) Lee, M.; Oh, Y.; Yu, J.; Jang, S. G.; Yeo, H.; Park, J.-J.; You, N.-H. Long-wave infrared transparent sulfur polymers enabled by symmetric thiol cross-linker. *Nature Communications* **2023**, *14* (1), 2866. DOI: 10.1038/s41467-023-38398-5. Boyd, D. A.; Nguyen, V. Q.; McClain, C. C.; Kung, F. H.; Baker, C. C.; Myers, J. D.; Hunt, M. P.; Kim, W.; Sanghera, J. S. Optical Properties of a Sulfur-Rich Organically Modified Chalcogenide Polymer Synthesized via Inverse Vulcanization and Containing an Organometallic Comonomer. *ACS Macro Letters* **2019**, *8* (2), 113-116. DOI: 10.1021/acsmacrolett.8b00923. Ye, P.; Hong, Z.; Loy, D. A.; Liang, R. UV-curable thiol-ene system for broadband infrared transparent objects. *Nature Communications* **2023**, *14* (1), 8385. DOI: 10.1038/s41467-023-44273-0.
(21) Bartlett, P. D.; Ghosh, T. Sulfuration of the norbornene double bond. *The Journal of Organic Chemistry* **1987**, *52* (22), 4937-4943. DOI: 10.1021/jo00231a020.
(22) Cowieson, N. P.; Aragao, D.; Clift, M.; Ericsson, D. J.; Gee, C.; Harrop, S. J.; Mudie, N.; Panjikar, S.; Price, J. R.; Riboldi-Tunnicliffe, A.; et al. MX1: a bending-magnet crystallography beamline serving both chemical and macromolecular crystallography communities at the Australian Synchrotron. *J Synchrotron Radiat* **2015**, *22* (1), 187-190. DOI: 10.1107/s1600577514021717 PubMed. Aragao, D.; Aishima, J.; Cherukuvada, H.; Clarken, R.; Clift, M.; Cowieson, N. P.; Ericsson, D. J.; Gee, C. L.; Macedo, S.; Mudie, N.; et al. MX2: a high-flux undulator microfocus beamline serving both the chemical and macromolecular crystallography communities at the Australian Synchrotron. *J Synchrotron Radiat* **2018**, *25* (3), 885-891. DOI: doi:10.1107/S1600577518003120.
(23) Sheldrick, G. SHELXT - Integrated space-group and crystal-structure determination. *Acta Crystallographica Section A* **2015**, *71* (1), 3-8. DOI: doi:10.1107/S2053273314026370.
(24) Sheldrick, G. M. Crystal structure refinement with SHELXL. *Acta Crystallogr C Struct Chem* **2015**, *71* (Pt 1), 3-8. DOI: 10.1107/s2053229614024218 From NLM.
(25) Hubschle, C. B.; Sheldrick, G. M.; Dittrich, B. ShelXle: a Qt graphical user interface for SHELXL. *Journal of Applied Crystallography* **2011**, *44* (6), 1281-1284. DOI: doi:10.1107/S0021889811043202.
(26) Dodd, L. J.; Lima, C.; Costa-Milan, D.; Neale, A. R.; Saunders, B.; Zhang, B.; Sarua, A.; Goodacre, R.; Hardwick, L. J.; Kuball, M.; et al. Raman analysis of inverse vulcanised polymers. *Polymer Chemistry* **2023**, *14* (12), 1369-1386, 10.1039/D2PY01408D. DOI: 10.1039/D2PY01408D.
(27) Ward, A. T. Raman spectroscopy of sulfur, sulfur-selenium, and sulfur-arsenic mixtures. *The Journal of Physical Chemistry* **1968**, *72* (12), 4133-4139.
(28) Pople, J. M. M.; Nicholls, T. P.; Pham, L. N.; Bloch, W. M.; Lisboa, L. S.; Perkins, M. V.; Gibson, C. T.; Coote, M. L.; Jia, Z.; Chalker, J. M. Electrochemical Synthesis of Poly(trisulfides). *Journal of the American Chemical Society* **2023**, *145* (21), 11798-11810. DOI: 10.1021/jacs.3c03239.

Chapter 4 - Long wave infrared optics prepared from sulfur-based polymers

Publications and patents from this chapter

Tonkin, S. J.; Pham, L. N.; Gascooke, J. R.; Johnston, M. R.; Coote, M. L.; Gibson, C. T.; Chalker, J. M. Thermal Imaging and Clandestine Surveillance using Low-Cost Polymers with Long-Wave Infrared Transparency. Advanced Optical Materials 2023, 11 (16), 2300058. DOI: https://doi.org/10.1002/adom.202300058.[1]

Chalker, J.; Tonkin, S. Organic polysulfide polymers and uses thereof. Australian application number: 2024902135, Filed 10 July 2024.

Chapter introduction

So far in this thesis, several different methods to prepare high sulfur polymers have been investigated. From these chapters, two main polymer compositions have been found to be most promising for long wave infrared imaging. The first was the cyclopentadiene based polymer from chapter two. The second was the norbornane bistrisulfide based polymer from chapter three. These polymers both have distinct advantages and disadvantages which could be exploited to prepare a range of optics to be used in thermal imaging applications. The main goal of this chapter was to find unique applications that specifically suit the unique properties of each polymer. Following this, a demonstration of each application would be developed to show a proof of concept for how these polymers could be used in the thermal imaging industry.

The main advantages of the cyclopentadiene based polymer is that it is cheap to produce, can be practically moulded into a variety of geometries and transparent to LWIR radiation while being opaque to visible light. This is a unique mix of attributes which could be used in applications not possible with any other material. The featured application for this polymer was a large sheet which could be placed around a thermal camera to provide protection from the environment, humans or wildlife. Furthermore, as the polymer was opaque to visible light, it could be used to conceal the camera from visible light while not affecting its operation. Due to the low cost of the polymer, and the ease of manufacturing using compression moulding, this sheet could be very large which would be cost prohibitive using germanium for all but the most funded industries. The other attribute of this polymer that made it well suited to this application was that the glass transition temperature could be varied by altering the sulfur content. High sulfur compositions would be flexible while lower sulfur compositions would be brittle due to a lower glass transition temperature. For applications where protection from impacts would be common, a most flexible protective sheet would be more appropriate but for applications where the polymer would be load bearing or under pressure, a more rigid, brittle polymer would be preferred.

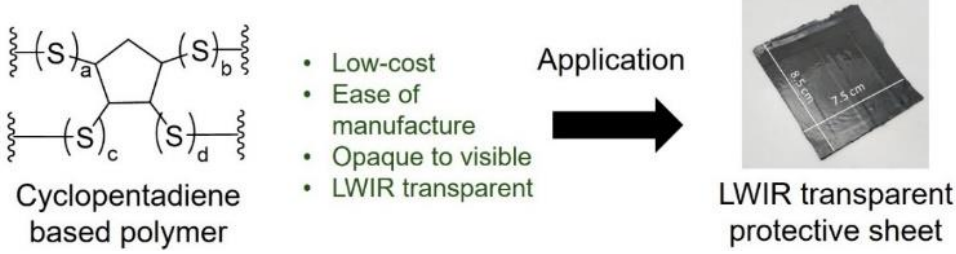

Figure 4.1: Key features of the cyclopentadiene polymer and an application explored in this chapter.

The featured application of the norbornane bistrisulfide based polymer was in the preparation of low-cost polymer lenses to be integrated into a thermal imaging system. The norbornane bistrisulfide polymer had a high glass transition temperature, making it brittle and able to maintain the geometry of a complex lens. It also possessed an excellent transmission in the long wave infrared region, making it perfect to use as a lens. The lenses prepared in this chapter are the first free standing polymer lenses to be able to image objects below 60 °C when integrated into a thermal camera. This facilitated imaging of people or low temperature objects and provides a proof of concept that these polymers could replace expensive germanium or zinc selenide lenses.

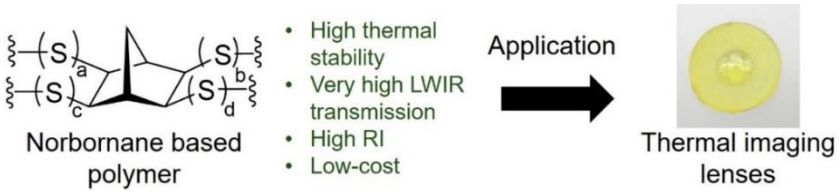

Figure 4.2: Key features of the norbornane bistrisulfide polymer and an application explored in this chapter.

A full overview of the highest performing polymers will be given in the following section. The LWIR transmittance of the best polymers from literature will be compared with the polymers described so far in this thesis. However, there was one paper that warranted further investigation. The paper was published in 2023 by the Pyun and Norwood groups.[2] This paper utilised sulfur-based polymers based on either a dimer of norbornadiene which they called NBD2 or diisopropenyl benzene, a commonly used monomer in inverse vulcanization. With the use of diamond point turning, a positive of a Fresnel lens with a focal length of 10 mm and a pupil diameter of 5 mm was machined from PMMA. This positive was then used to prepare a PDMS mould which could then be used to cast the polymer. When cast, the polymers took the geometry of the Fresnel lens. Following this, the Fresnel lenses were used with a thermal camera to investigate the quality of the imaging.

The paper is an excellent example of the integration of a sulfur polymer into an imaging system. The lenses showed promise however, there were some limitations. The first was the relatively low transmission of the polymer meant that imaging below 60 °C was not possible with free standing lenses. They were able to prepare thin film Fresnel lenses which were approximately 100 µm thick. However, these lenses were not free-standing and required a NaCl backing. There is a need for a free-standing polymer lens that could be used for thermal imaging of objects at ambient temperatures. If this could be achieved, it could replace germanium or silicon lenses which are currently used in thermal imaging systems.

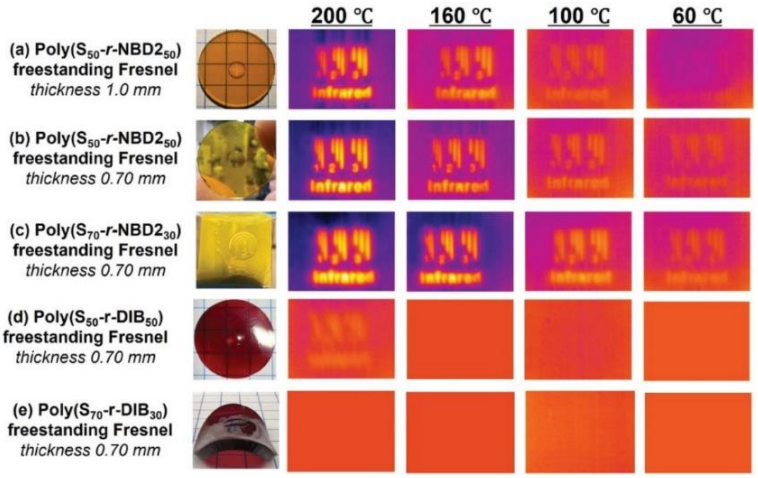

Figure 4.3: A range of free-standing Fresnel lenses prepared with different sulfur-based polymers and their imaging of a target at different temperatures. Used with permission from.[2]

Comparison between polymers prepared in chapter 2 and 3 and literature

Over this thesis so far, three polymers have been found to be the most promising for long wave infrared imaging. The two polymers made from cyclopentadiene in chapter 2 and the norbornane based polymer prepared from the bistrisulfide in chapter 3. To gain an understanding of the performance of the polymers, the long wave infrared transparency was compared to the best performing polymers from literature. Below is an overview of the polymers that were used in the comparisons. The polymer made from the reflux method in chapter 2 will be considered as a separate polymer from the one made by the gas phase method as the chemical structure was slightly changed.

A total of eight polymer compositions were selected to compare with the ones developed in this thesis. The first four polymer compositions were produced through conventional inverse vulcanization reactions. The next two were prepared using a thiol-ene type reaction. The final two utilised a polycondensation reaction and a photo induced thio-ene/-yne reaction. Polymers made from 1, 3-diisopropenyl benzene (DIB) were the first inverse vulcanized polymers to be proposed as potentially applicable for infrared imaging.[3] In chapter 2, this polymer was synthesised and compared with the cyclopentadiene polymer. It will again be used in this comparison. The DIB polymer was first synthesised in 2013, so it gives an understanding on how far the performance of these polymers has improved over the last ten years. The polymer prepared from 1, 3, 5-triisopropenylbenzene (TIB) was developed with the goal of improving upon the IR transmittance and refractive index of DIB as it could incorporate more sulfur into its structure without compromising thermomechanical properties.[4] While DIB and TIB show some promise as LWIR transparent materials, they were not intended to be used for this application. All the other polymers in this comparison were designed for the main purpose of long wave infrared imaging.

The next polymer in this comparison was prepared using norbornadiene 2, a dimer of norbornadiene (NBD2). This monomer was used after a DFT calculation study by the Pyun group indicated it would show high transmittance in the long wave infrared region.[5] The Pyun group predicted that a polymer with a norbornane core would have excellent transmission in the long wave infrared region, however, they were not able to synthesise the predicted polymer. In their paper, they stated that the volatility of norbornadiene made the reaction impossible. This is what led to the project that was described in chapter 3. As they were not able to synthesise a polymer from norbornadiene directly, they prepared a dimer using a nickel catalysed [2+2] cycloaddition. The dimer was then used in an inverse vulcanization reaction to form the polymer that was used in this comparison.

Another well-designed polymer included in this comparison was one based on Tetravinyltin (TVSn). In this paper, the authors incorporated a tin atom in the polymer structure to increase the transmittance in the LWIR region.[6] This pushed many of the absorptions of the polymer outside of the long wave infrared region giving the polymer excellent transmission. This polymer showed the greatest transmission of any published sulfur-based polymer until 2023.

The next two polymers in the comparison utilised monomers with thiols. These thiols were predicted to react in a thiol-ene type reaction with elemental sulfur when heated. These polymers were published in 2023 and 2024 and represent some of the highest long wave infrared transparent polymers in the literature. Both polymers were developed by the You group. The first polymer utilised benzene trithiol (BTT) as a symmetric

crosslinker with sulfur. In the paper, the author claims that the symmetric nature of the monomers reduced the number of unique vibrational modes in the long wave infrared region, leading to excellent transmittance.[7] The second polymer utilised dicyclopentadiene which had thiol groups replace the alkenes (TCDSH). This allowed them to prepare a dicyclopentadiene based polymer with no alkenes or side reactions.[8] As discussed in chapter 2, dicyclopentadiene based polymers show very poor transmission in the long wave infrared region when an alkene is present in the polymer structure. The approach used by this group was very effective in ensuring that only the fully saturated dicyclopentadiene was in the polymer structure.

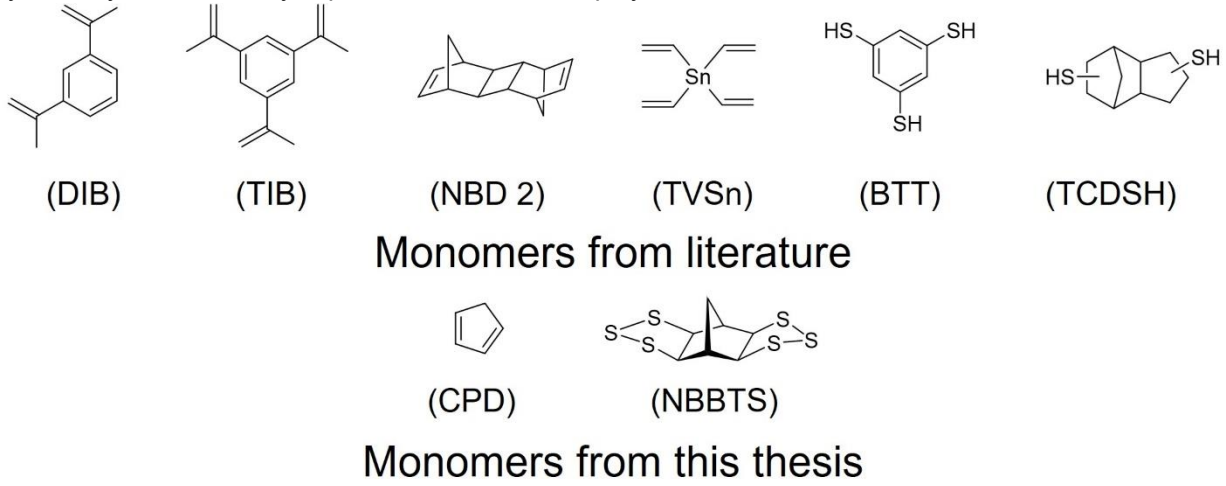

Figure 4.4: Monomers from polymers used in comparison with a reported infrared spectrum of a 1 mm thick free-standing window.

The polymers made from the six monomers in the figure above were all prepared into a window with a thickness of 1 mm. This allowed them to be directly compared. However, there were two polymers which were only reported as a 200 µm window. These polymers were compared to each other and the cyclopentadiene polymer prepared through the reflux method. Poly(phenylene polysulfide) networks were produced through the polycondensation of p-Diiodobenzene.[9] 2,3-bis((2-mercaptoethyl)thio)-1-propanethiol (BMETP) and its derivatives were used in a photo induced thiol-ene/-yne reaction.[10] Three R groups were produced but only the Allyl will be used in this comparison as it showed the greatest transmittance.

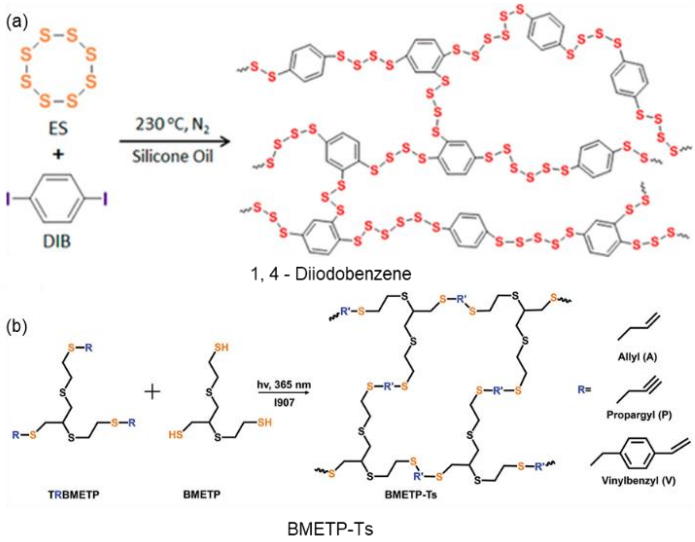

BMETP-Ts

Figure 4.5: (a) Reaction between sulfur and p-Diiodobenzene to produce a Poly(phenylene polysulfide). Modified with permission from[9](b) Thiol-ene/-yne reaction with BMETP and its derivatives to produce a high sulfur polymer modified with permission from.[10]

To accurately compare these polymers, factors such as thickness had to be considered. While thickness of the selected polymers varied, most literature sources presented the infrared transmission spectra for either a 1 mm or 200 µm thick sample. Samples of the polymers developed in this thesis of the same thickness were prepared to use as comparisons. A 1 mm thick sample was prepared for both all polymers using a silicone mould with a 1 mm thick glass slide as a negative. This same process was not appropriate for freestanding films at a thickness of 200 µm as the high viscosity of the prepolymer meant it did not flow into the extremely thin mould. This would result in an inconsistent thickness and bubbles in some cases. To overcome this issue, a different process was used. To produce the 200 µm thick window, a heated press was used to compress the polymer to the desired thickness. A 25 x 25 mm square was cut out of a 200 µm thick PTFE sheet. This was used to control the shape and thickness of the polymer window. 210 mg of cured 67-poly(S-r-CPD) was ground into a powder and placed into the opening in the Teflon sheet. The sheet and polymer were then placed in a heated press and the press was heated to 140 °C. After the temperature had reached 140 °C (approximately 15 minutes), the polymer was compressed to 10 Mpa for 35 minutes. After this time, the sample was removed from the press and allowed to cool. Both the 1 mm and 200 µm thick polymer samples were tested for infrared transmission between 2 µm and 20 µm using a Perkin Elmer Frontier FTIR spectrometer. A 200 µm sample was only prepared for the 67-poly(S-*r*-CPD) polymer made through the reflux method.

To quantitatively compare the polymers from literature, the transmission data had to be extracted from the available publications. An image of an infrared spectrum of each polymer window was downloaded from the publications of each polymer. The infrared spectrum for the highest performing composition was used. For most polymers, this was the composition with the highest sulfur content. A Matlab script was then developed which could directly extract the raw data from the plot. After data extraction, the script would integrate over any regions of interest to get the average transmittance of the sample in the region. The mid wave infrared (3µm - 5µm) and long wave infrared (7µm – 14 µm) regions were used to compare samples. The accuracy of the Matlab script was confirmed using infrared transmission plots of known polymers. The average transmission over the long wave infrared region was found to have an error of less than 5 %. The Matlab script can be seen below.

```
imshow S-r-TVSn.PNG                         %Show Image
wavelmin = 1.3;                             %Wavelength range
wavelmax = 19.3;
Tmin = 0;                                   %Transmission range
Tmax = 100;

[x,y,P] = impixel;
xorigin = x(1);                             %First click on origin
xpixelmax = x(2);                           %Then max value of X axis
yorigin = y(1);
ypixelmax = y(3);                           %Then max Y axis
D = [x y];                                  %This gives raw data

n = numel(x);
wavel = zeros(n-3:1);
Transm = zeros(n-3:1);

%Converts pixel values to wavelength and transmission
for i = 4:n
    wavel(i-3) = wavelmin+((x(i)-xorigin)/(xpixelmax-xorigin)*(wavelmax-wavelmin));
    Transm(i-3) = Tmin+((yorigin-y(i))/(yorigin-ypixelmax)*(Tmax-Tmin));
end
```

```
imshow S-r-TVSn.PNG                          %Show Image
wavelmin = 1.3;                              %Wavelength range
wavelmax = 19.3;
Tmin = 0;                                    %Transmission range
Tmax = 100;

[x,y,P] = impixel;
xorigin = x(1);                              %First click on origin
xpixelmax = x(2);                            %Then max value of X axis
yorigin = y(1);
ypixelmax = y(3);                            %Then max Y axis
D = [x y];                                   %This gives raw data

n = numel(x);
wavel = zeros(n-3:1);
Transm = zeros(n-3:1);

%Converts pixel values to wavelength and transmission
for i = 4:n
    wavel(i-3) = wavelmin+((x(i)-xorigin)/(xpixelmax-xorigin)*(wavelmax-wavelmin));
    Transm(i-3) = Tmin+((yorigin-y(i))/(yorigin-ypixelmax)*(Tmax-Tmin));
end


plot(wavel,Transm);                          %Check graph

%This section finds the integration over the LWIR region
LWIRmin = 7;                                 %Range to be integrated
LWIRmax = 14;
error = 0.1;

a = find(abs(wavel-LWIRmin)<error,1);        %Finds index range
b = find(abs(wavel-LWIRmax)<error,1);

LWIRWL = wavel(a:b);
LWIRTR = Transm(a:b);

Integral = trapz(LWIRWL,LWIRTR);             %Integrates over region
AvLWIR = Integral/(LWIRmax-LWIRmin);         %Averages over the region
```

Figure 4.6: Matlab script used to extract data from FTIR plots of sulfur polymers.

The plot below shows the infrared spectrum of the polymers prepared from DIB and TIB as well as the CPD based polymers developed in chapter 2 and the norbornadiene based polymer from chapter 3. Both the reflux method and the gas phase methods for synthesising the CPD polymer are shown here. The norbornadiene based polymer is labelled as poly(S-*r*-NBBTS) as it was prepared using the norbornane bistrisulfide (NBBTS) monomer. In chapter 3, this polymer was labelled as poly-**6**.

The CPD and NBBTS based polymers showed far greater transmittance than the polymers prepared from DIB and TIB, particularly in the LWIR region. This was expected as these polymers were not initially designed for use at infrared transparent materials. Poly(S-r-NBBTS) had the greatest transmission over almost the entire region from 2 μm to 20 μm. This indicates that it would be very well suited for use as a long wave infrared transparent lens or window used in thermal imaging. As explained in chapter 2, the gas CPD based polymer prepared through the gas phase method showed greater transmission in the LWIR region. This was likely due to reduced DCPD content in the polymer.

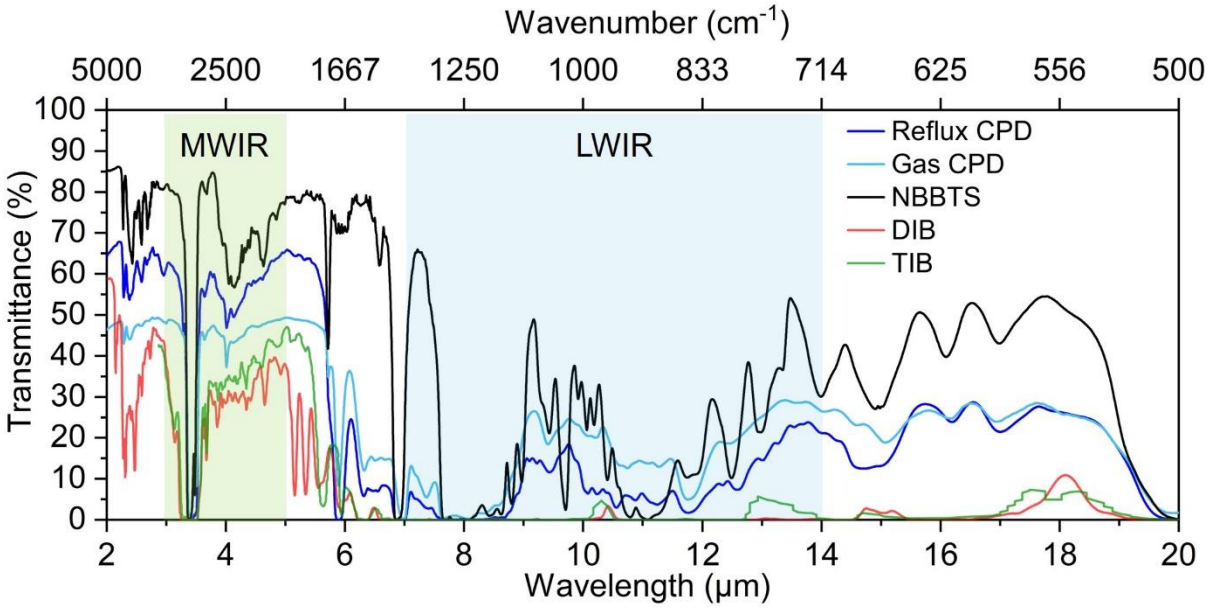

Figure 4.7: Infrared spectra for 1 mm thick polymer windows. Plotted polymers are: 67-poly(S-*r*-CPD) prepared through the reflux and gas phase methods, 85-poly(S-*r*-NBBTS), 67-poly(S-*r*-DIB)[3] and 70-poly(S-*r*-TIB).[4]

The next plot shows the polymers developed in this thesis compared with polymers prepared from NBD2 and TVSn. These polymers show much greater LWIR transparency than the ones prepared from DIB or TIB. This indicates a significant improvement in the field between 2013 and 2019. Overall, the CPD and NBBTS polymers showed greater transmittance in the long wave infrared region than those prepared from NBD2 and TVSn. Although at some wavelengths, the TVSn polymer showed greater transmission than the CPD based polymers

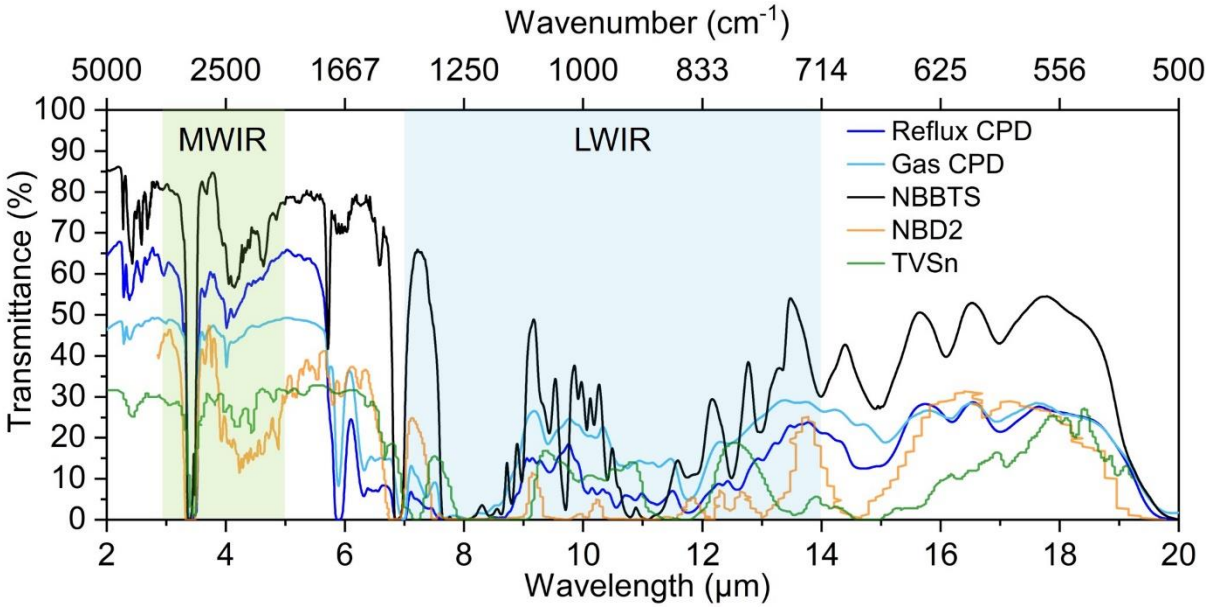

Figure 4.8: Infrared spectra for 1 mm thick polymer windows. Plotted polymers are: 67-poly(S-*r*-CPD) prepared through the reflux and gas phase methods, 85-poly(S-*r*-NBBTS), 70-poly(S-*r*-NBD2)[5] and 70-poly(S-*r*-TVSn).[6]

The next plot shows the polymers prepared from thiol-ene reactions using BTT or TCDSH. These polymers show excellent transmittance, particularly in the long wave infrared region. These are the state-of-the-art polymers with the greatest performance for long wave infrared transmission in the literature. The polymer prepared from BTT has a greater transmission than both polymers prepared from CPD. In some areas, particularly from 8 µm to 11 µm, it shows greater transmission than poly(S-*r*-NBBTS)**.** Although poly(S-*r*-NBBTS) has greater transmission from 11 µm to 14 µm. While not as transparent as the polymer made from BTT, TCDSH also showed excellent long wave infrared transmission, with similar properties to the cyclopentadiene polymer prepared through the reflux method.

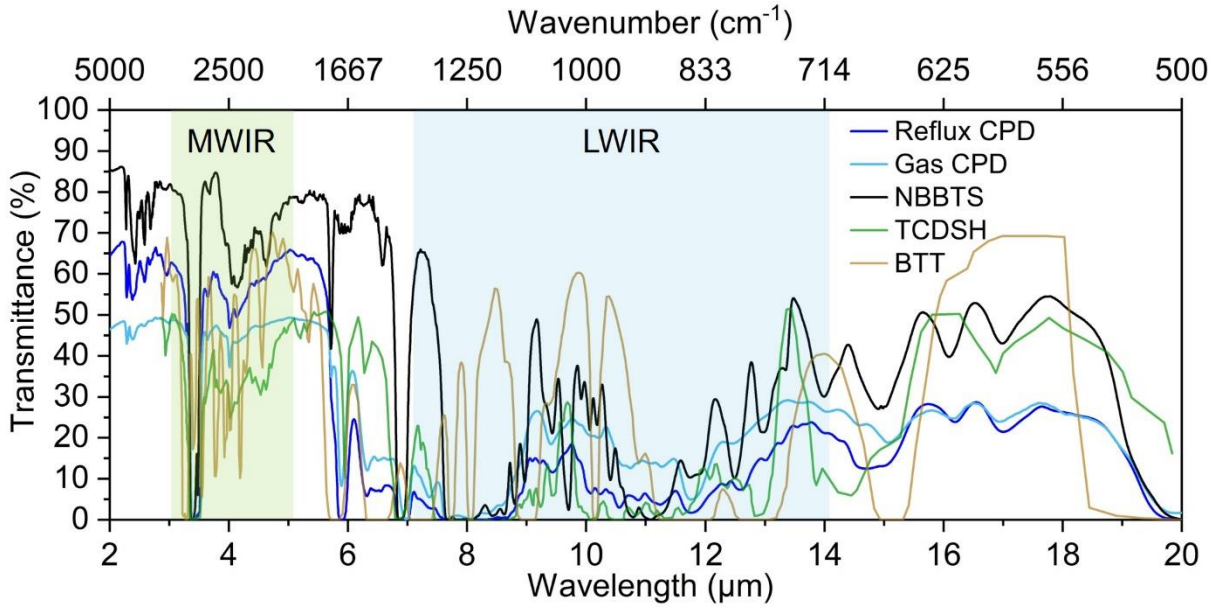

Figure 4.9: Infrared spectra for 1 mm thick polymer windows. Plotted polymers are: 67-poly(S-*r*-CPD) prepared through the reflux and gas phase methods, 85- poly(S-*r*-NBBTS), 70 % S TCDSH[8] and 82 % S BTT.[7]

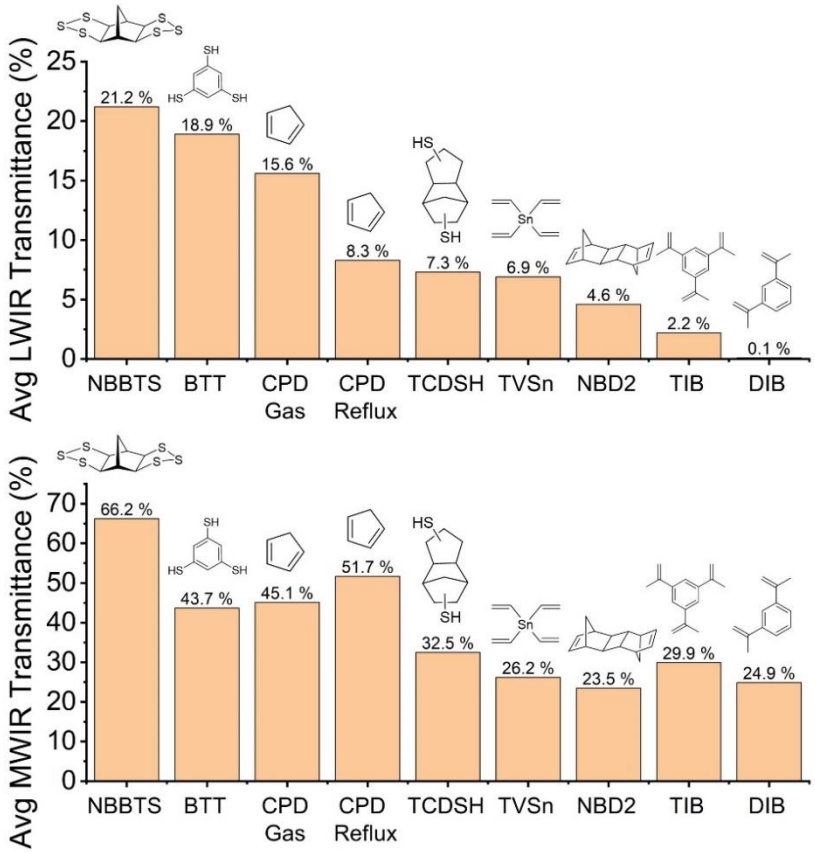

Figure 4.10: Average LWIR and MWIR transmittance of 1 mm thick sulfur polymers.

The average over the MWIR (3 µm -5 µm) and the LWIR (7 µm – 14 µm) was taken from the integration of the transmittance plot divided by the wavelength range. The top performing polymers were the poly(S-*r*-NBBTS) and 70 % S BTT, followed by the CPD based polymers. Both poly(S-*r*-NBBTS) and BTT have benefits and drawbacks. poly(S-*r*-NBBTS) has excellent thermal properties, with a glass transition temperature of 133 °C but requires an additional process to prepare the monomer. BTT on the other hand has a one-step reaction process but produces H_2S gas and displays some peaks which correspond to thiols in the polymer. This could result in a bad odour or unwanted reactivity. Both polymers have excellent infrared performance and could likely see use in the thermal imaging industry.

The polymers which only reported a 200 µm thick window were also compared. Only the CPD polymer prepared using the reflux method was compressed into a 200 µm window for this comparison. As can be seen, all three of the polymers show transmission in the long wave infrared region. The 67-poly(S-*r*-CPD) showed the greatest overall transmission. This can be clearly seen in the plot average transmission data.

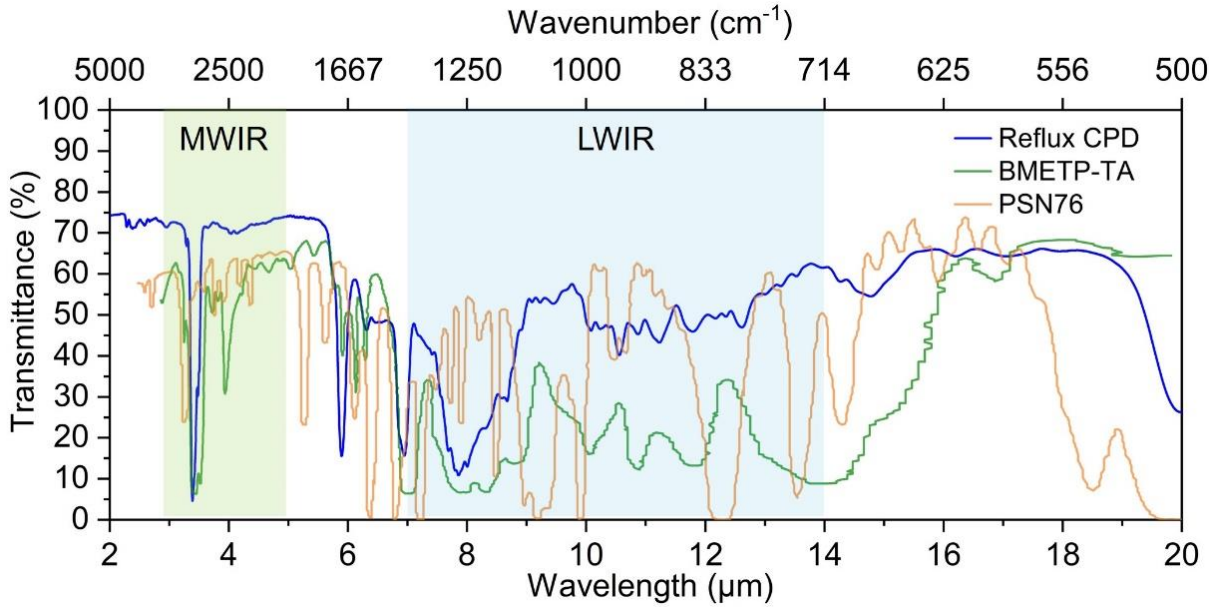

Figure 4.11: Infrared spectra for 200 µm thick polymer windows. Plotted polymers are: 67-poly(S-*r*-CPD) prepared through the reflux methods, BMETP-TA[10] and PSN76[9].

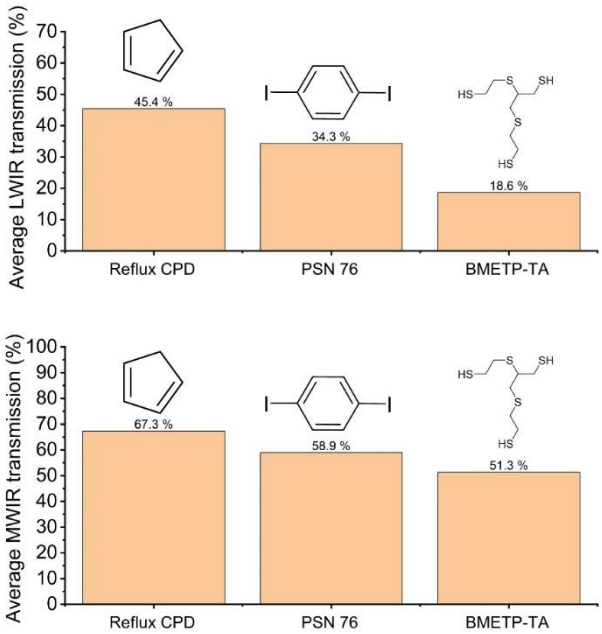

Figure 4.12: Average LWIR and MWIR transmittance of 200 µm thick sulfur polymers

Surveillance and protection of thermal camera with polymer window

Poly(S-*r*-CPD) polymer synthesis

The next sections will use the poly(S-*r*-CPD) polymer to make a polymer window and a range of lenses. While the synthesis and characterisation of this polymer was described in detail in chapter 2, it will be repeated in this chapter for clarity. For all applications, the 67 % sulfur polymer was used as this was found to possess the greatest transmission of LWIR light without having any issues with sulfur blooming. The reflux method was used over the gas phase method as the polymer had a greater glass transition temperature. This made it more practical to use and ensured that the lens would maintain its focal length. The method used to prepare this polymer can be seen below.

For all reactions, CPD was first prepared directly from DCPD by distillation using the following method. 20 g of DCPD was weighed and added to a 100 mL round bottomed flask with a magnetic stirrer. The round bottomed flask was added to a standard distillation set up with a water-cooled condenser and slowly heated to 180 °C. Another 100 mL round bottomed flask was used as an outlet to collect the CPD. The outlet round bottomed flask was cooled with an ice bath to reduce the rate of the Diels Alder conversion back to DCPD. The CPD was used immediately after distillation to reduce the chance that DCPD was reformed. The CPD would be keep in a freezer and tested by NMR before every use. If the proportion of DCPD was above 2 % by NMR, the CPD would be distilled again at 70 °C to separate it from DCPD.

Sulfur (3.00 g, 93.56 mmol S atoms) was added to a 21 mL vial with a magnetic stirrer. A threaded adapter was used to attach this vial to a water-cooled condenser. An oil bath and oven were preheated to 140 °C and the sulfur was lowered into the oil bath for three minutes. Over this time, the sulfur would melt to form a yellow liquid. CPD (1.5 g, 22.69 mmol) was added with a volumetric pipette down the reflux condenser. The CPD was added in 150 µL additions every 3 minutes to prevent rapid cooling of the sulfur. The reaction was left for 90 minutes at 140 °C with constant stirring. Over this time, the sample would slowly darken and increase in viscosity. The sample was then poured into a silicone mould and cured in an oven at 140 °C for 24 hours. After curing, the polymer was left at room temperature to cool before being removed from the silicone mould.

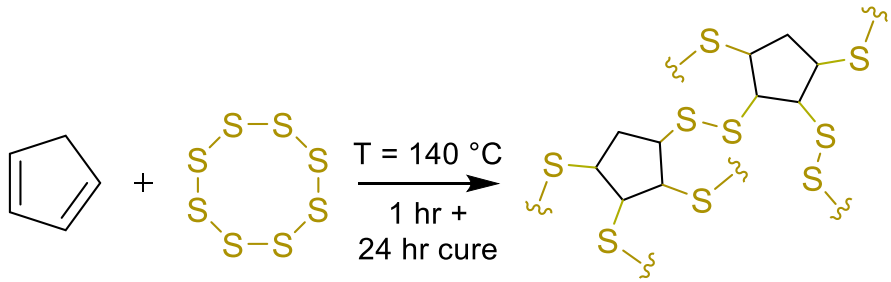

Figure 4.13: Reaction between cyclopentadiene and sulfur to form 67-poly(S-*r*-CPD).

Reactive compression moulding of polymer window

The first application that was explored using the sulfur-based polymers developed in this thesis was a window used to protect and conceal a thermal camera. Thermal cameras are often used for surveillance or monitoring of wildlife due to their ability to image in low light.[11] These applications often require the camera to be controlled from environmental factors like light or direct sunlight. However, there are very few materials which could be used to encase a thermal camera which would not block the long wave infrared radiation from entering. The materials which could be used, like germanium, are extremely expensive, both in raw material costs and in manufacturing.[12] Due to the large size of the casings required, these materials are often far too expensive to be practically used in any but the most highly funded applications. A material which was extremely cheap and easily processable would be very valuable in to use to protect and conceal a thermal camera.

While the polymers prepared with CPD showed reduced transmission compared to the NBBTS based polymers, they did have several advantages. The first is that it could be made using a very simple reaction with low-cost monomers. This means that the raw cost of producing the polymer is very low. They also have the advantage of high processability. The CPD based polymers have been shown to be melt processable in their prepolymer stage or mouldable using reactive compression moulding. This makes it perfectly suited to be used as a low-cost material to protect or conceal a camera. Due to how inexpensive the material is, it could be used as a disposable window which protects the costly thermal camera from any damage and is then replaced. The ease of processing and low cost also makes it possible to prepare large polymer windows which would not be possible with other materials.

Another advantage that polymers prepared with CPD have is that they are completely opaque to visible light. In some applications, this may be a drawback since any optic prepared with the CPD polymers could only be used with infrared light while a transparent optic may be used in the visible region as well. However, there are many applications where it would be a benefit to be opaque to visible light while being transparent in the infrared region. This would be a major advantage for the application of a casing to protect a polymer camera. If a polymer window was made with the CPD polymer, it could be used to block all visible light from entering while not preventing a thermal camera from imaging through. This could be used to conceal or protect a thermal imaging camera without affecting it’s use.

While many optical applications require brittle, rigid materials which do not bend or flex with force, a protective window may benefit from some flexibility. Flexible materials can often survive impact better than brittle materials as they can absorb the impact without shattering. The polymers made from CPD could be prepared with a glass transition temperature above or below room temperature by adjusting the sulfur content as explained in chapter 2. Therefore, it could be used to prepare flexible, shock resistant windows or rigid windows with more structural integrity. In this thesis, the 67-poly(S-*r*-CPD) polymer was used. This polymer had a glass transition temperature below room temperature, so it was soft and flexible, but it was shape persistent. This made it perfect for a protective window as it would not shatter when impacted but it could also be bent into a shape to suit the camera being protected. The reflux method was used despite its lower long wave infrared transmission due to its greater thermal stability and mechanical properties.

To explore the use of the CPD polymer as a low-cost window to protect and conceal a thermal camera, it was compressed into a sheet using a heated press. This manufacturing technique was used as it is scalable and

demonstrates that a large quantity of these polymer windows could be prepared at a relatively low cost. In this method, the polymer could be prepared in multiple batches and stored as a pellet or powder. When required, it could then be compressed into the geometry required for the window. This is a significant advantage as it would allow for the synthesis to be scaled up while the window formation could be distributed and prepared when required. Below is the method used to prepare the window for the following section.

Three 4.5 g batches of the 67-poly(S-r-CPD) polymer were prepared using the reflux method. For more details on the synthesis of this polymer, see chapter 2. Reactive compression moulding was then used to combine all three batches into one piece. 10 grams of the polymer from three batches was ground into a powder and added to an 85 mm by 85 mm heated press. Baking paper was used to ensure the polymer could be removed from the aluminium press afterwards. The press was heated to 140 °C and compressed to 30 Mpa for 10 minutes. After this time, the polymer was allowed to cool, and it was removed from the press. The polymer sheet was cut into an 85 mm by 75 mm sheet as it would often have some irregularity around the outside of the press. The thickness of the sheet was 0.83 mm, and the final mass was 7 g.

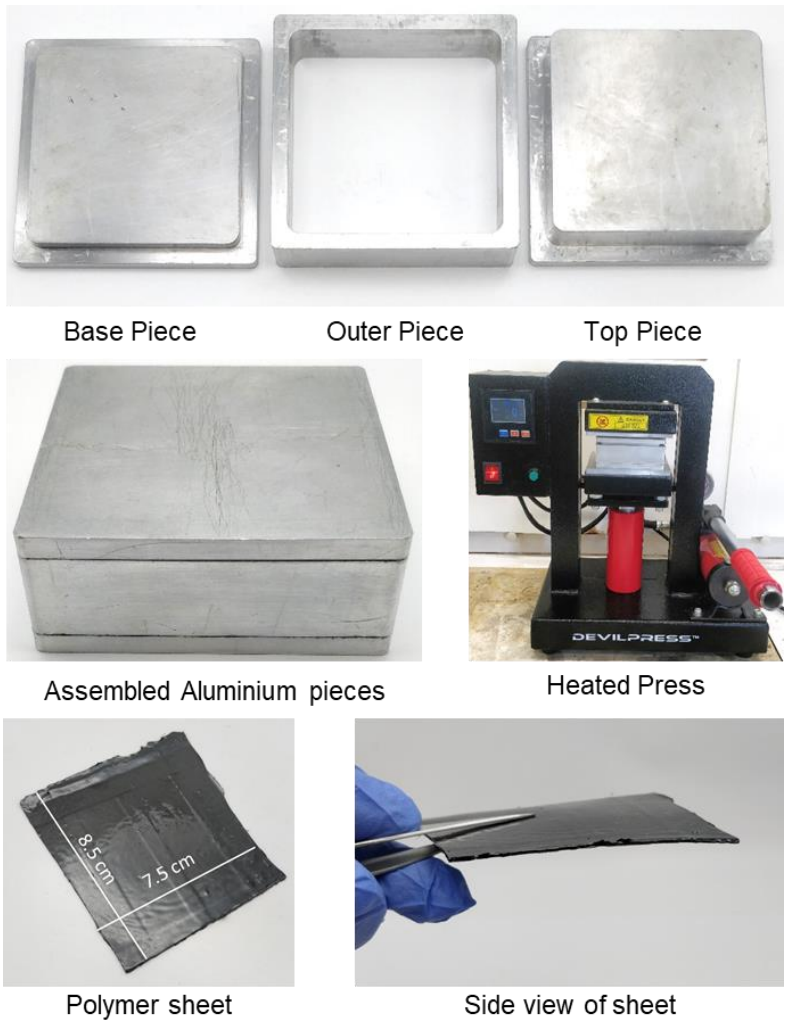

Figure 4.14: Images of heated press and 67-poly(S-r-CPD) polymer sheet.

Design of casing for FLIR E6 thermal imaging camera

To investigate the polymer window as a window to protect and conceal a thermal camera, a casing was made to cover a FLIR E6. The FLIR E6 is a hand operated thermal camera that uses the wavelength range of 7.5 µm – 13 µm. For the application of security or animal observation, it would be much more likely that a remotely controlled camera would be used. This would allow it to be completely concealed inside the casing and its operation would be unobservable from the outside without another thermal camera. However, to demonstrate the application, the casing for the camera had openings in the back to allow for images to be manually taken and observed on the screen.

The casing was designed on Autodesk Inventor. The camera main body of the camera was first modelled to aid in the casing design. The casing had two main parts. The bottom part included a slot to hold the FLIR E6 which was then held in place using zip ties around the handle portion. There was also a large opening at the back to allow for access to the trigger on the camera. The bottom part of the casing had parts designed to allocate an M4 nut and bolt to attach to the top part of the casing. The top part of the casing would cover the screen and allow for a polymer window to be placed in front of the lens of the camera. It had an opening at the back so that any images could be inspected manually. The casing had an opening with a 60 mm diameter in front of the camera lens. There was a slot designed to accommodate the reactive compression moulded window to cover this opening. The casing was 3D printed using black poly lactic acid (PLA) using a Creality CR-10S Pro.

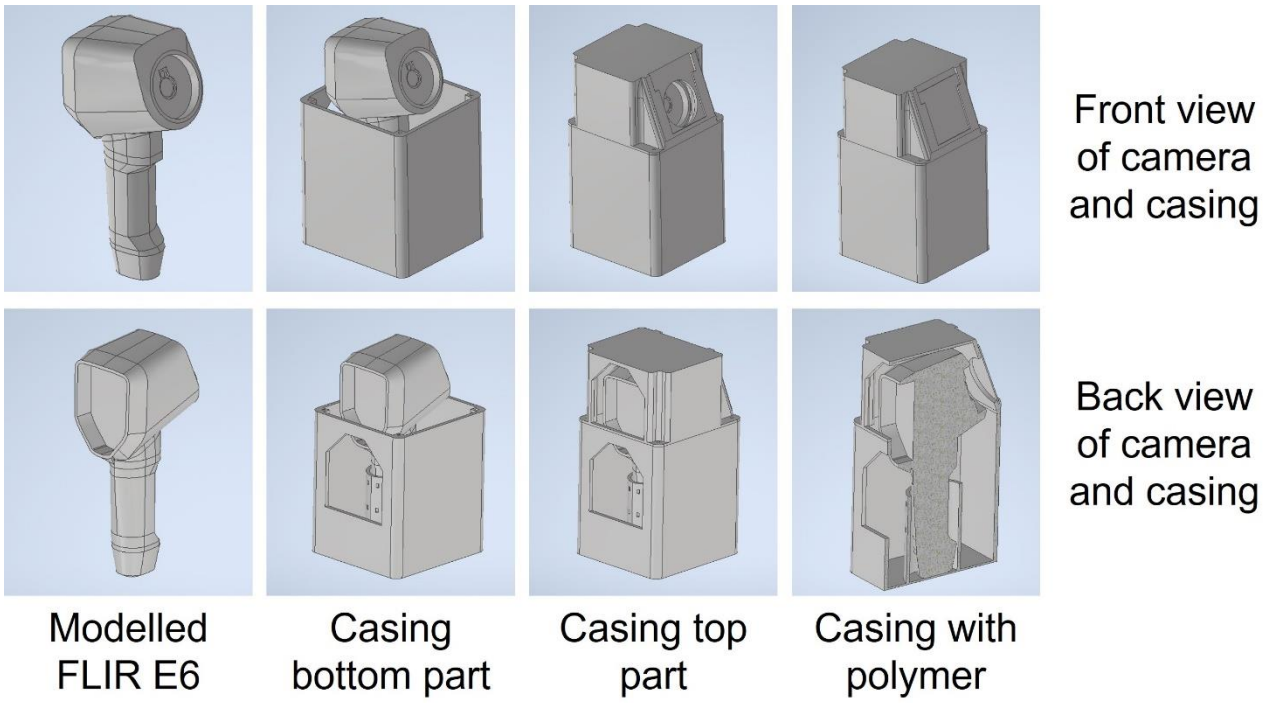

Figure 4.15: Design of casing for FLIR E6 on Autodesk Inventor.

Imaging using FLIR E6 through polymer window

After the casing was 3D printed, the camera was inserted into the bottom part and secured with zip ties. After this, the top part of the casing was attached and bolted on using four M4 bolts. The polymer window was then inserted into the slot in the casing.

To test the imaging through the window, it was used to image the infrared radiation given off by several animals. This demonstrates the potential of thermal imaging through a protective polymer window for wildlife surveillance. Here Shep deserves an acknowledgement for being a good boy and letting his photo be taken. The chickens also deserve an acknowledgement since they had their sleep interrupted to model for some photos. To demonstrate the use of thermal imaging in low light environments, a photo of some chickens was taken at night. Both the visible image and the thermal image is shown in the figure below. As can be seen, there was not enough light to observe the chickens with the visible camera, but they could be seen clearly using the thermal camera through the polymer window.

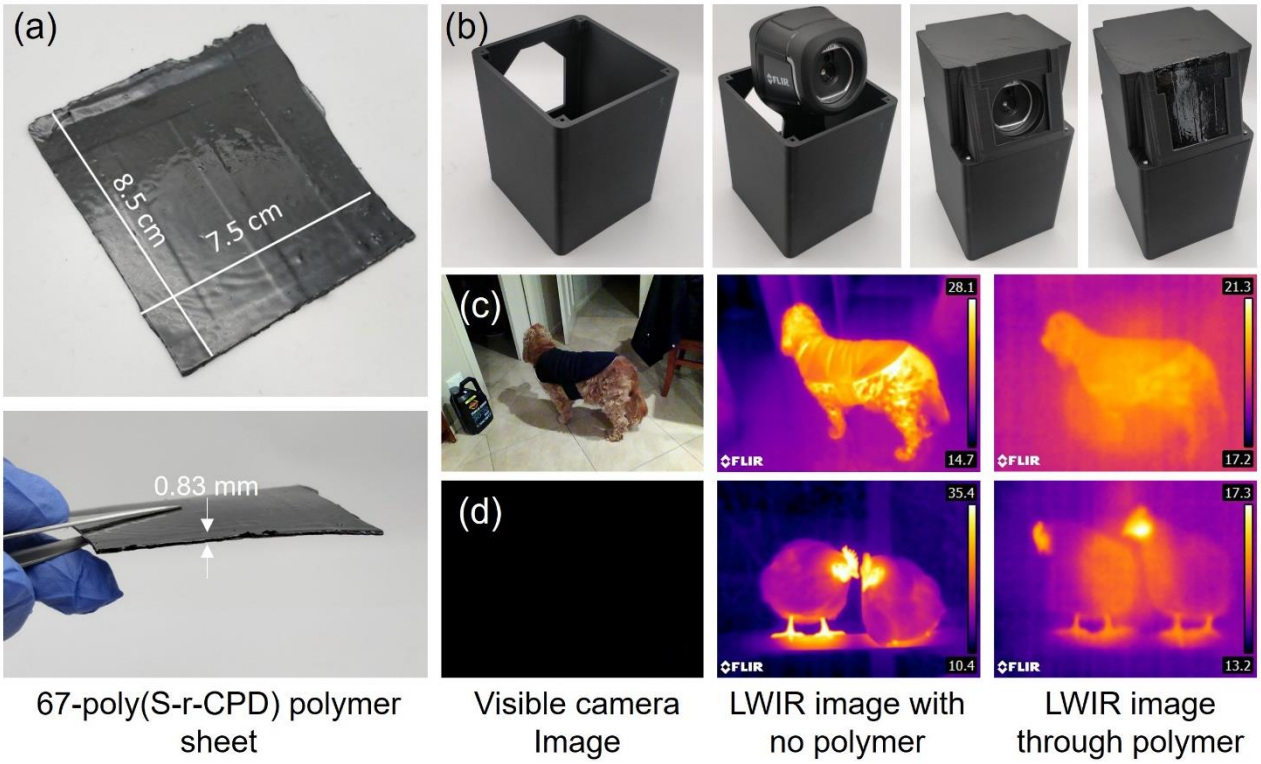

Figure 4.16: Long wave infrared transparent polymer window and imaging using FLIR E6. (a) Polymer window made from 67-poly(S-*r*-CPD) prepared using the reflux method and compressed into a sheet with thermal imaging. (b) 3D printed casing to cover FLIR E6 and hold polymer window. (c) Visible, LWIR control image and LWIR image through polymer window of dog. (d) Visible, LWIR control image and LWIR image through polymer window of chickens at night.

Plano concave and plano convex lenses from cyclopentadiene based polymer

Mould and lens preparation

After testing the use of the polymer as a transparent window, the polymer was used to prepare several lenses. The cyclopentadiene based polymer had a very high refractive index for a polymer. Over the long wave infrared region, it was approximately 1.875. Such a high refractive index allows for the preparation of lenses that are smaller or lighter than if they were made using materials with a lower refractive index.[13]

To utilise the high refractive index of the polymer, a plano concave and a plano convex lens was made. These lenses were not optimised for any particular sensor or imaging system but instead were used to demonstrate the ability for the polymer to be used to prepare an optical component.

Explanation of lenses

To prepare these lenses, moulds were prepared using a silicone resin. The moulds were made using a glass negative. The negatives were purchased in a kit from Livingstone International. This kit had several lenses, each with a diameter of 50 mm. The concave lens with a focal length of 300 mm and the convex lens with a focal length of -300 mm were used. The glass used in these lenses had a refractive index of 1.52, giving them a radius of curvature of 155 mm for both lenses. To prepare an open top mould, the glass lenses were placed with their plano side down and silicone resin was poured over them. The resin was left for approximately two hours to cure before the glass lenses were removed.

The open top moulds gave the correct radius but no control over the thickness of the sample. For this reason, the polymer lenses had a different thickness to the original glass negative. The exact thickness of the plano convex and plano concave lenses is described in the following sections. The open top moulds were also found to give poor control over the top surface of the polymer. When cured in this mould, the polymer would form a meniscus, giving the top surface a slight convex radius. For this reason, open top moulds were not used in any future lenses. These lenses were a good proof of concept and showed that light could be manipulated and focused using the polymer.

To cast the polymer in the lens moulds, they were first preheated to 140 °C. The cyclopentadiene polymer was then prepared using the reflux method described in chapter two. For both lenses, the composition with 67 % sulfur was used. After the reaction, the molten prepolymer was poured into the lens moulds. For the plano convex lens, two 4.5 g batches of the polymer were used while the plano concave lens used three. The polymer and moulds were then left to cure for 24 hours at 140 °C. After curing, the polymer and moulds were left to cool to room temperature before being removed from the mould. While the surface of the lenses was found to be optical quality directly after removal from the mould, they were polished before any imaging. To polish the lenses, a small amount of an aluminium oxide polish material was applied to a microfibre cloth. The lens surfaces were gently polished by hand on both the plano and curved sides.

When accounting for the higher refractive index of the cyclopentadiene polymer, the lenses had an effective focal length of 177 mm or -177 mm for the convex and concave lenses respectively. Given the 50 mm diameter of the lenses, this gave an f-number of f/3.54. Most thermal cameras use lenses with focal lengths of less than

1.5 to maximise the amount of light reaching the sensor and give a greater thermal sensitivity. The f-number of these lenses is likely too high to act as a stand alone lens in an imaging system but could still be used to magnify or reduce images for a thermal camera. For this reason, the lenses were used in combination with the FLIR E6 thermal camera which already had a germanium focussing lens. The plano convex and plano concave lenses were simply placed in front of the FLIR E6 to magnify or reduce the images respectively.

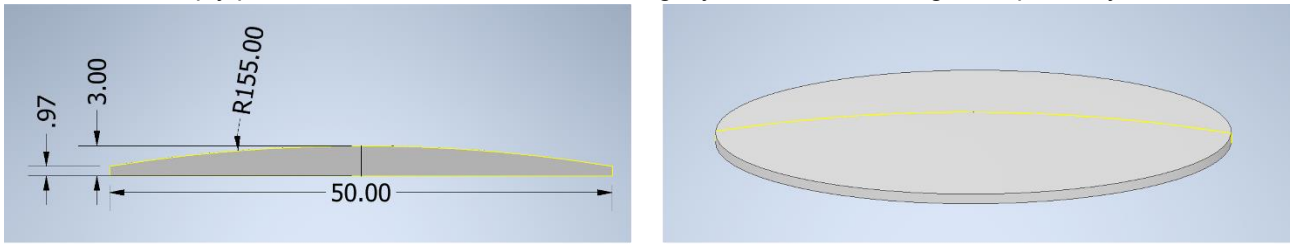

Plano Convex lens

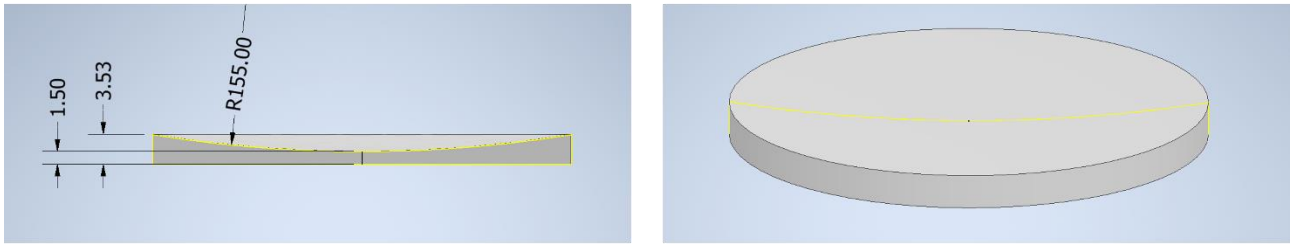

Plano Concave lens

Figure 4.17: Images showing cross section and diagonal view of plano convex and plano concave lens negatives.

Imaging through plano concave lens with FLIR E6

The plano concave lens was tested first. This lens had a centre thickness of 1.5 mm and an edge thickness of 4 mm. Due to the thickness and relatively high f-number, this lens did not transmit enough light to image objects less than 50 °C. Instead, it was used to image a hotplate with an oil bath and a soldering iron. These images were used to show a reduction in the image. To image the hotplate and oil bath, a FLIR E6 was placed in a clamp approximately 30 cm above a 100 °C oil bath. The lens was then placed between the oil bath and the camera to take an image. While the quality of the image is poor, a clear reduction in the image can be seen. The image of the oil bath was reduced to 83 % of its original diameter.

The image of the soldering iron was taken by holding the soldering iron and FLIR E6 in clamps approximately 30 cm apart. The soldering iron was heated to 250 °C and allowed to equilibrate for 5 minutes. After that, the lens was then placed in front of the soldering iron and an image was taken. The image of the soldering iron was noticeably reduced when the plano concave lens was placed in front.

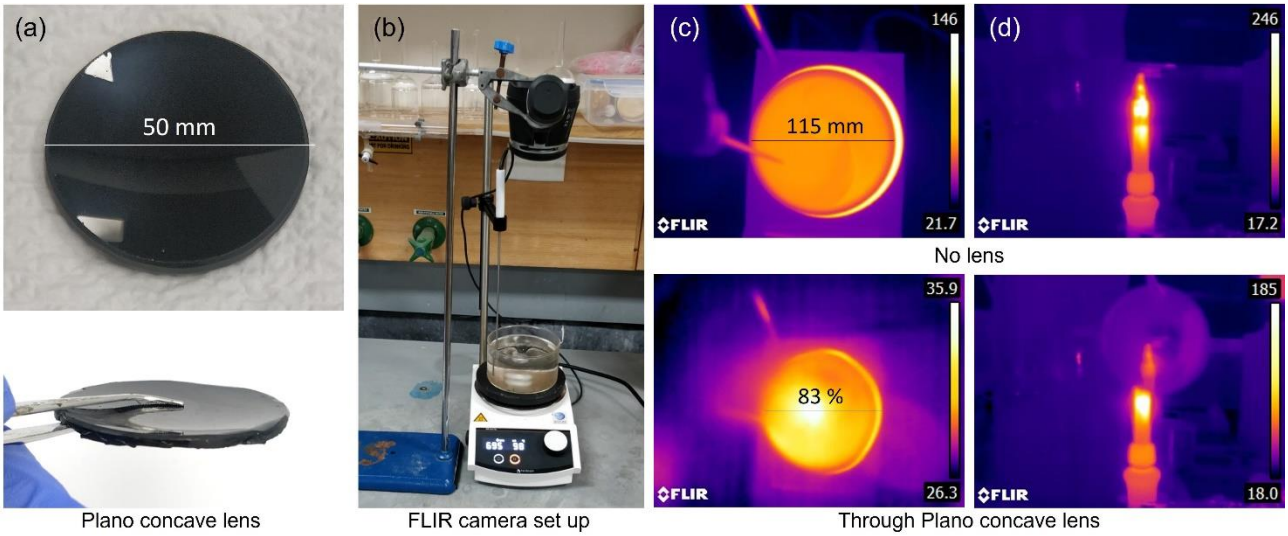

Figure 4.18: Images of plano concave lens made from 67-poly(S-*r*-CPD). (a) photos of plano concave lens from the top and side view. (b) Set up of FLIR E6 camera to image hotplate and oil bath. (c) Long wave infrared image of 100 °C hotplate and oil bath taken using FLIR E6 with and without plano concave lens. (d) Long wave infrared image of 350 °C soldering iron with and without plano concave lens.

Design and 3D printing of masks for imaging through plano convex lens

The imaging experiments with the plano concave lens were a good proof of concept and showed the ability of the poly(S-*r*-CPD) polymer to be used in imaging applications. However, to allow for a greater understanding of the capacity of the lenses, several masks were prepared. These masks were prepared on Autodesk inventor and 3D printed using PLA filament on a Creality Cr-10S pro. Two masks were made to just produce images and demonstrate the magnification of the lens. The first was a kangaroo and the second was a Flinders University logo. The other masks were designed to have features of known dimensions so that the magnification could be quantified. These masks were also designed to have features that would be too small to resolve without the lens. One of these masks had 10 slits, all with a length of 50 mm and width of 2 mm. These slits were separated by gaps which decreased in width from 3.5 mm to 0.4 mm. The smallest gap between the slits is very difficult to make out with the infrared camera, however, with the lens, it could be clearly seen. The next mask was similar with had an array of 3 mm by 3 mm square. These squares had a gap which varied from 3 mm to 0.25 mm. With no lens, the smallest gaps could not be resolved, however, with the aid of the plano convex lens, even the smallest gaps could be observed. The final mask had four different shapes on it. These shapes were designed to quantify the magnification of the image. The dimensions of the different shapes can be seen in the figure below.

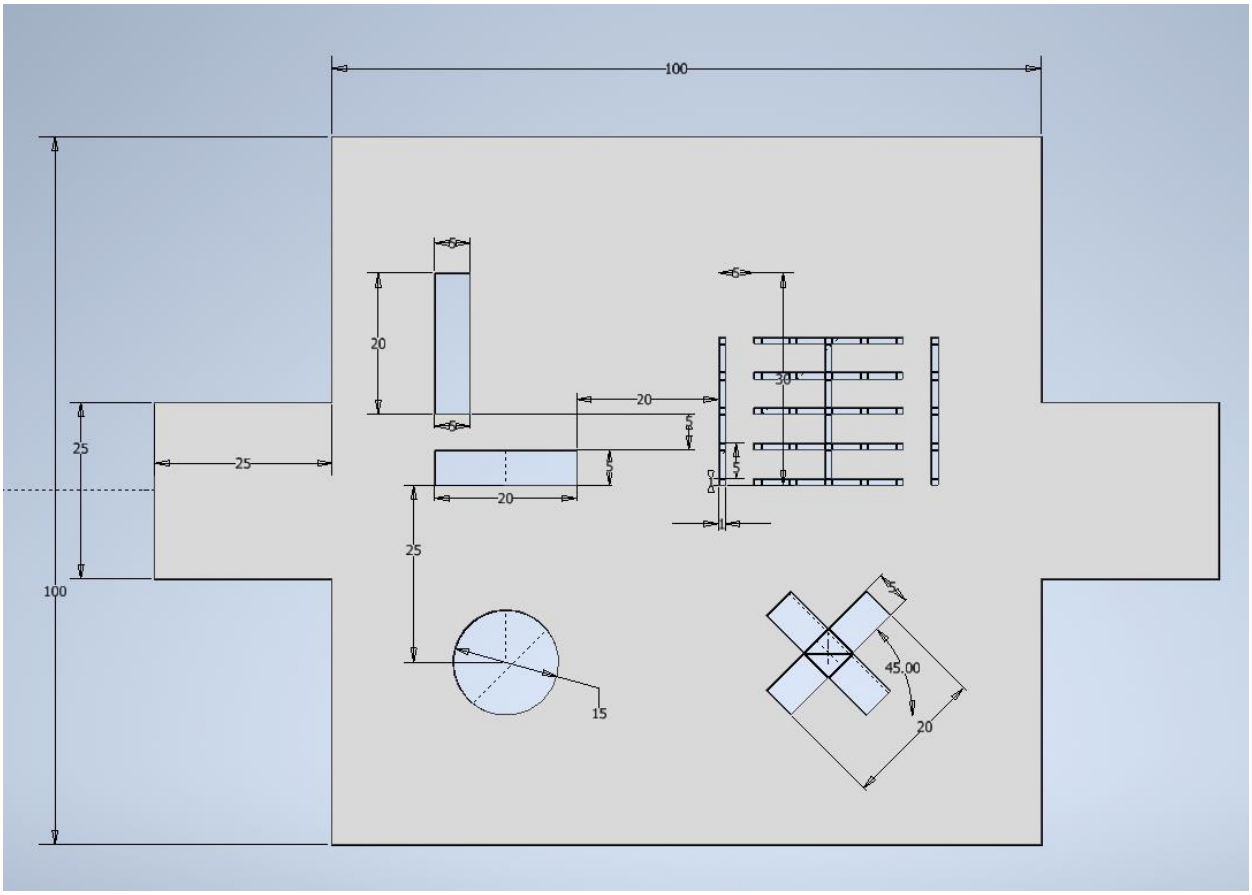

Figure 4.19: Sketch from Autodesk Inventor showing the dimensions of a mask used to investigate plano convex lens.

To use the masks, a 150 °C hot plate was used as a radiation source. The masks were placed approximately 5 cm from the hot plate. A FLIR E6 infrared camera was placed 30 cm from the mask. The lens was then positioned between the camera and the mask so that the image was in the best focus. A photo of the hotplate and camera set up can be seen in the figure below.

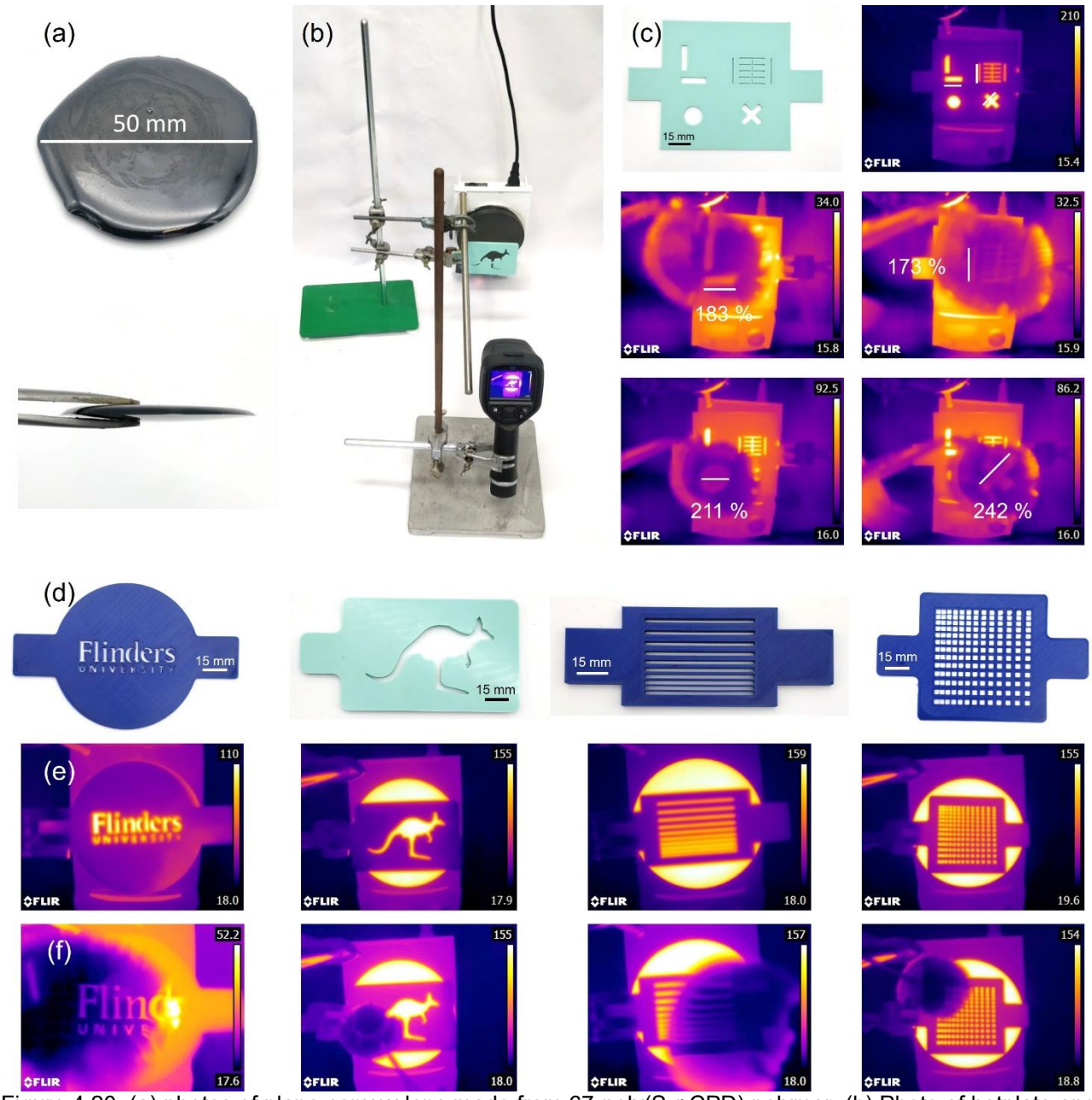

Figure 4.20: (a) photos of plano convex lens made from 67-poly(S-*r*-CPD) polymer. (b) Photo of hotplate and FLIR E6 thermal camera set up with kangaroo mask. (c) Photo of mask with different shapes for investigating magnification of the lens. (d) Photos of masks used for imaging with plano convex lens. (e) Control images of all masks taken with FLIR E6 thermal camera and no polymer lens. (f) Images of all masks taken with FLIR E6 thermal camera using the 67-poly(S-r-CPD) polymer lens for magnification.

Fresnel Lens from cyclopentadiene based polymer

Mould synthesis and preparation of lens

To prepare a Fresnel lens, an injection mould was produced in which the polymer could be moulded on all sides. The mould was produced from a polydimethylsiloxane rubber with a shore hardness of 55A. The silicone used was M4670A/B and was purchased from Barnes. It was found that a silicone rubber with a high hardness was necessary for the injection mould to prevent warping due to the pressure of the injected prepolymer. This silicone rubber had a working time of 45 minutes and a cure time of 24 hours at room temperature.

To produce the injection mould, an acrylic Fresnel lens was used as a negative. This lens had a diameter of 66 mm, a thickness of 1.52 mm, a groove density of 1 groove per millimetre and a focal length of 185 mm. The circular focussing section was in the centre of a 76.2 mm square. When accounting for the higher refractive index of the sulfur-based polymer, the focal length of this lens was 110 mm. One of the corners of the positive was cut to near the focussing section of the lens to allow for alignment of the two-sided mould.

The Injection mould was produced by placing the lens negative in the centre of an aluminium piece with a square shaped opening and a side length of 85 mm. A 20 mL glass syringe was placed on the top of the non-focussing section of the lens positive and the Luer lock was secured in place with modelling clay. Two glass pipettes were also placed on the other two corners of the lens on the non-focussing sections and secured with modelling clay. These were used to create holes in which the air could escape when the polymer was injected. Three balls of modelling clay were placed on the space left by the cut part of the lens positive. These were used to create an indent which could be used to align the completed mould. 90 g (81 g part A, 9 g part B) of silicone rubber was mixed and poured into the opening and left to set. After the silicone rubber was set, the syringe and pipettes were removed, and the aluminium piece was flipped upside down. The silicone mould was pushed to the bottom of the aluminium piece and the clay used to make the alignment indents was removed. Another 90 g (81 g part A, 9 g part B) of silicone rubber was mixed and poured into the opening and left to set. After the silicone rubber was set, both parts were removed from the aluminium piece and separated. The lens positive and any modelling clay was removed to leave a cavity of the lens.

To produce the polymer Fresnel lens, four batches of the 67-poly(S-r-CPD) polymer were produced simultaneously using reflux method described earlier. The two parts of the mould were assembled and a 20 mL syringe was added to the corresponding hole. The mould was placed in an oven and preheated to 140 °C. Thee plunger was removed from the syringe and all four batches of 67-poly(S-r-CPD) were added without curing. The mould was returned to the oven for 10 minutes at 140 °C to ensure a consistent temperature throughout the prepolymer. The mould was then removed from the oven and the plunger was inserted into to the syringe. Using heat proof gloves, the syringe plunger was pressed down until the prepolymer flowed into the mould and could be seen in both outlets. The entire mould was then placed back into the oven at 140 °C and cured for 24 hours. After curing, the polymer lens was removed by separating the two mould parts. The excess polymer was cut off using a scalpel to leave a circular Fresnel lens.

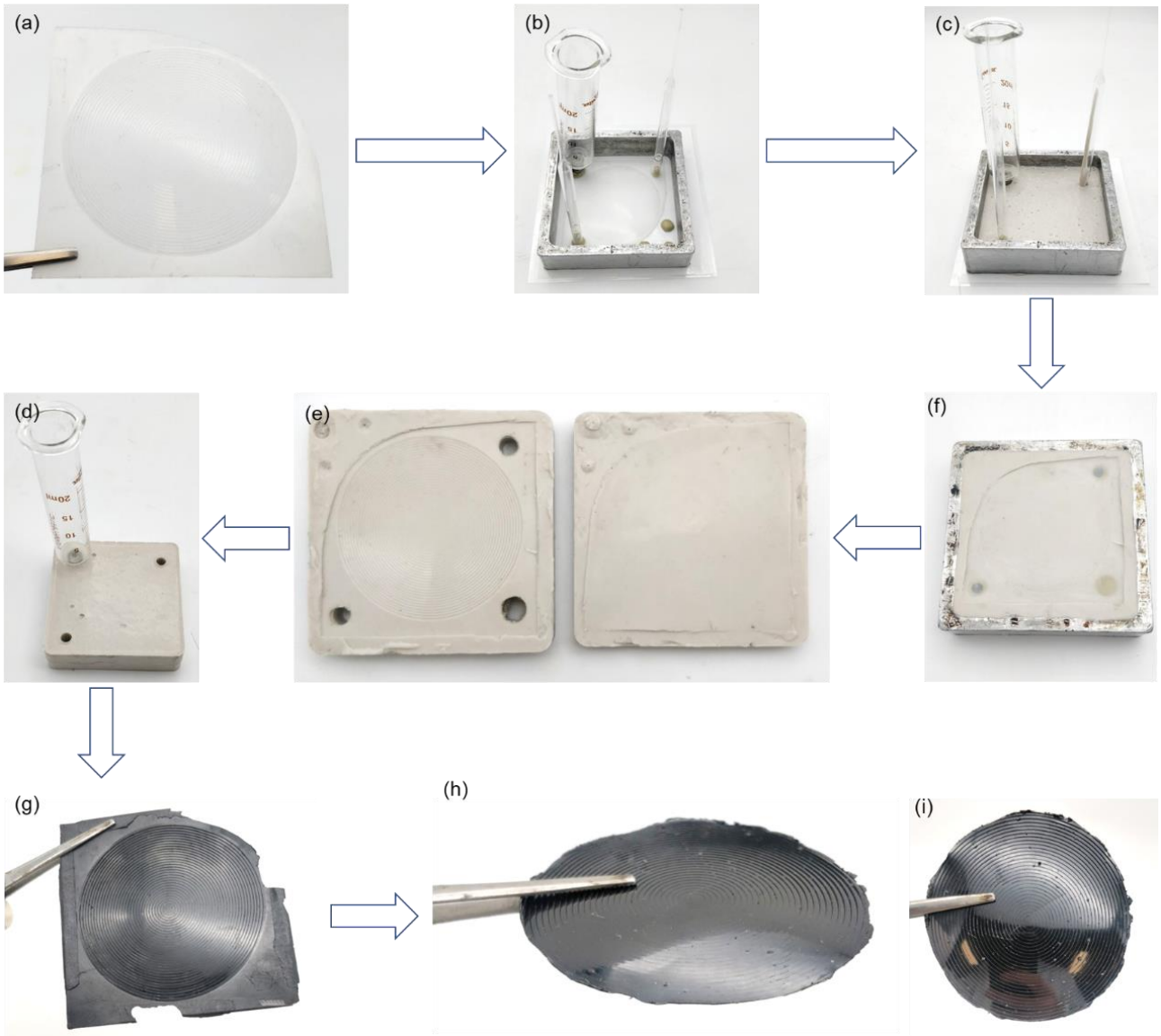

Figure 4.21: (a) Fresnel lens positive made from acrylic. (b) Syringe and pipettes secured to lens positive using modelling clay in an aluminium piece. (c) After 90 g of M4670A/B silicone was added and allowed to cure. (f) After syringe and pipettes were removed from silicone and the mould is flipped upside down. (e) Two silicone pieces after cure. (d) Assembled injection mould with syringe. (g) 67-poly(S-r-CPD) after being cured in injection mould. (h-i) Fresnel lens after excess was removed.

Imaging through Fresnel lens with FLIR E6

The Fresnel lens was imaged using the same FLIR E6 infrared camera that was used for the plano convex and concave lenses. Three different tests images were taken. A 150 °C hotplate was imaged with the lens to quantify the magnification of the lens. Following this, the mask with several shapes was placed in front of the hotplate and images of the circle and cross shapes were taken. Following this, a 300 °C soldering iron was used as a heat source. The Fresnel lens was then placed in front of the soldering iron to take an image.

When compared with the plano convex and plano concave lenses, the quality of images through the Fresnel lens was much better. This is likely due to the type of mould used. The plano convex and plano concave lenses were made using an open top mould. These moulds only control one face of the lens. The other face often has a poor quality as it is open to air and can form a meniscus.

The Fresnel lens is a very complicated lens and would be very difficult and costly to prepare using subtractive methods like CNC milling. This demonstrates the advantage of polymer-based lenses as a single mould made using these methods could be used to make many lenses. Using techniques like this opens up the possibility of mass manufacturing of low-cost infrared lenses.

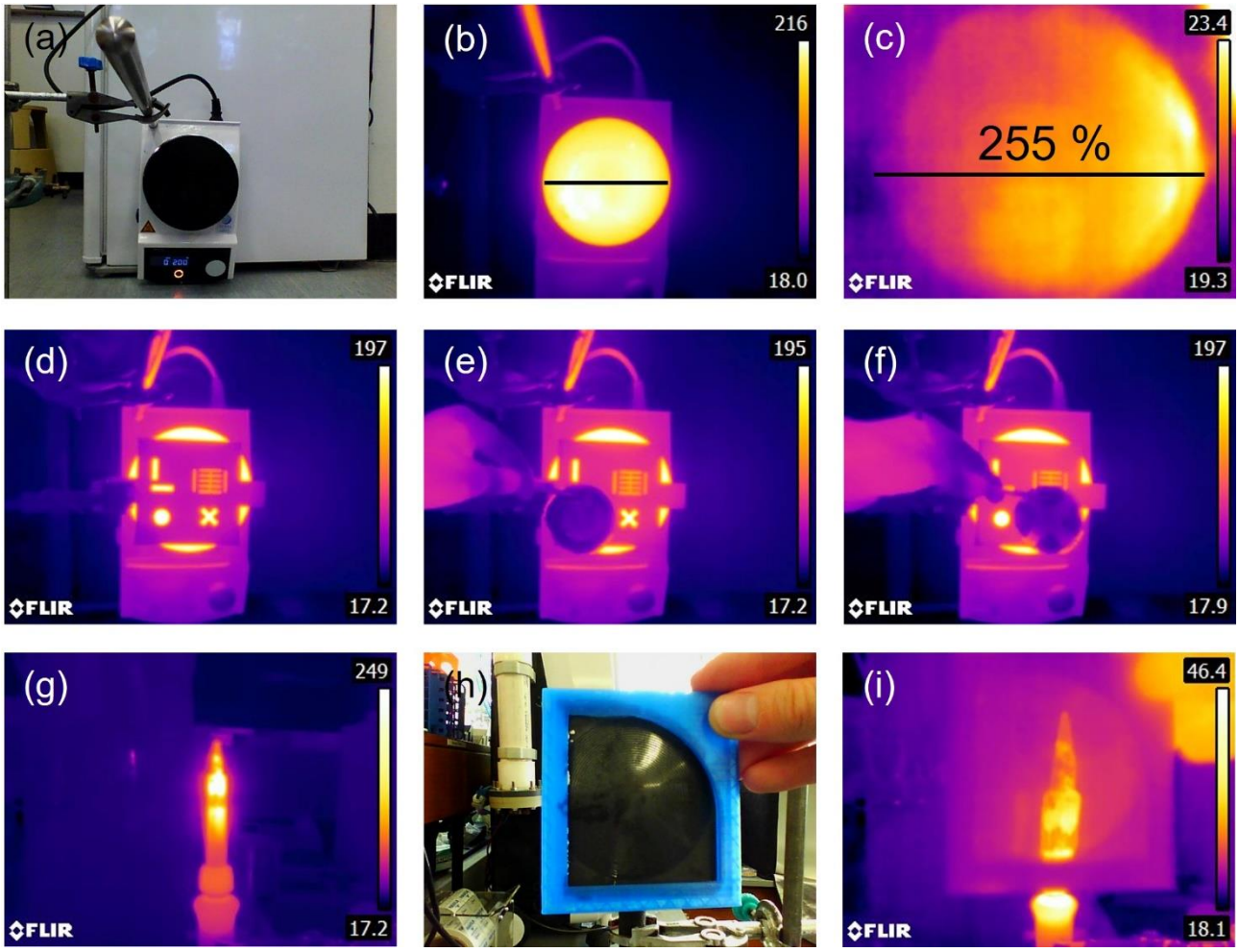

Figure 4.22: (a) Image of 150 °C hotplate used for imaging. (b) LWIR image of 150 °C hotplate taken using FLIR E6 camera. (c) LWIR image of 150 °C hotplate through Fresnel lens with magnification shown. (d) LWIR image of mask in front of 150 °C hotplate taken with FLIR E6 camera. (e-f) LWIR images of mask through Fresnel lens. (g) LWIR Image of 300 °C soldering iron taken with FLIR E6 camera. (h) Photo of Fresnel lens in holder being placed in front of soldering iron. (i) LWIR image of soldering iron taken through Fresnel lens.

Lens design and mould preparation for FLIR Lepton

Sensor considerations

The lenses and windows prepared with the cyclopentadiene polymer showed some very promising results. They could magnify light and showed the potential applications of the material. However, for all the experiments using these lenses, a FLIR E6 camera had to be used. This camera had a germanium lens which focused the LWIR radiation onto the sensor. To truly demonstrate the potential for sulfur-based polymers to act as lenses, they would need to completely replace the lens used in a thermal camera. This would allow for a stand-alone thermal camera to be made which only uses low-cost sulfur polymer-based lenses.

The first task in making a stand along thermal camera using a sulfur-based polymer was to determine what sensor to use. There were several key considerations which influenced the choice of sensor. Namely cost, size and usability. When considering all these factors, a FLIR Lepton 3.5 was found to be most applicable. Below is an explanation of how this sensor meets the desired features.

One of the major advantages of using a sulfur-based polymer over conventional infrared transparent materials is cost. Sulfur based polymers have raw material costs which are many times cheaper than germanium of zinc selenide. The manufacturing methods are also much more scalable and energy efficient. Therefore, they are most suited to applications where cameras could be made at a large scale and low cost. To align with this goal, a low-cost sensor would be most appropriate. In lower cost sensors, the lens makes up a much greater portion of the cost. Therefore, the use of a low-cost lens would have a relatively greater effect on price. The FLIR Lepton 3.5 is one of the lowest cost sensors that are commercially available, ranging from $250 - $400 AUD. With the reduced lens cost, this sensor could be used in a range of commercial applications.

A smaller sized sensor was also desired. The target applications were in smartphone integration, drone technology or commercial user products. These applications all benefit from small and light cameras. A smaller sensor also means that the lens can be thinner while still possessing the desired focal length and image circle, leading to reduced losses from absorption. The FLIR Lepton sensor has a focal plane array of 160 x 120 active pixels with a pitch of 12 µm. This gives a sensor with dimensions of 1.92 mm x 1.44 mm, making it perfectly sized for the desired applications.

Finally, the usability of the sensor was considered. The FLIR Lepton 3.5 is a development sensor. This means that it is designed to be easily modified. The shutter and lens can be removed, allowing for custom lenses to be mounted. It also comes with software which allows for calibration and testing with different lens systems. All these factors made the FLIR Lepton 3.5 a perfect choice for the sensor.

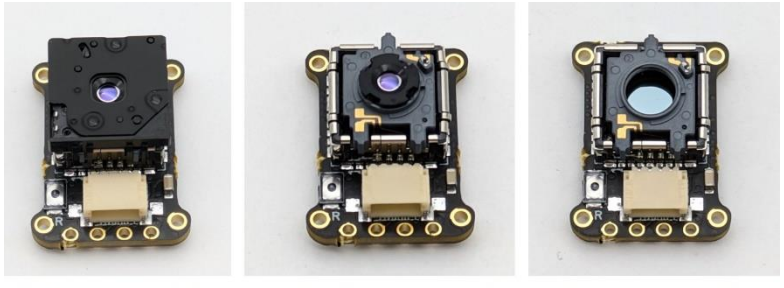

FLIR Lepton 3.5 Shutter removed Lens removed

Figure 4.23: Images of FLIR Lepton 3.5 camera with shutter and lens removed.

Lens designs

The lens design is one of the most important factors which affects the quality of images obtained with a thermal camera. There are several features of the lens which need to be considered when designing a lens for a particular application. To keep the design and manufacture simple, in this thesis, only plano convex lenses were used. Later in this chapter, the potential for more complex lens designs will be discussed. For plano convex lenses, one side has a spherical curve while the other is flat. This reduces the complexity of the design, but the focal length, f-number and thickness are still critical to achieving the desired imaging. Each of these factors are described below.

Focal length

The focal length is a value for how strongly a lens converges light. A lens with a shorter focal length will bring light into focus in a shorter distance. This has several effects on the image that would be achieved by the camera. When imaging a distant object, a lens with a shorter focal length will give a wider field of view and reduced magnification. A longer focal length will give a narrower field of view but with greater magnification. Using this knowledge, the focal length of the lens should be selected to give the desired image. The field of view (FOV) is related to the focal length (f) by the following equation. Where x is the width or height of the sensor for horizontal or vertical field of view respectively.

$$FOV = 2\arctan(\frac{x}{2f})$$

The field of view is extremely important to the application that the camera is designed for. For sensing and imaging at close ranges, a wide field of view is desired. This is because a single camera can capture a large area without needing to be manually moved. For imaging at longer ranges, a narrow field of view is more practical as it allows greater magnification, giving more detail of distant object. With the relationship between focal length and field of view in mind, a range of lenses with different focal lengths were designed. The focal lengths of the polymers ranged from 1.5 mm to 5 mm. The sensor on the FLIR Lepton 3.5 was 1.92 mm x 1.44 mm giving a range of horizontal field of views from 65 ° to 22 °.

To determine the required radius of curvature to achieve the desired focal length, the lens makers equation is used. This equation relates the radii of the two refracting surfaces (R_1 and R_2), the refractive index of the lens material (n_1), the medium (n_0) and the focal length (f).

$$\frac{1}{f} = (\frac{n_1 - n_0}{n_0})(\frac{1}{R_1} - \frac{1}{R_2})$$

As the lenses are used in air, $n_0 = 1$. The lenses used in this thesis were plano convex so $1/R_2 = 0$. Using this, the equation can be simplified and rearranged for R_1 to determine the radius required to give the desired focal length.

$$\frac{1}{f} = (n_1 - 1)\left(\frac{1}{R_1}\right)$$

$$R_1 = f(n_1 - 1)$$

F-number

The f-number is a measure of the ability for the lens to collect light. The f-number (N) is given by the ratio between the focal length (f) and the diameter of the entrance pupil of the lens (D). For the plano convex lenses, in this thesis, the entrance pupil was assumed to be the diameter of the lens as no f-stop was used in the camera design. The f-number is usually expressed as f/N where N is the f-number of the lens. The following equation shows the relationship between f-number (N), focal length (f) and the entrance pupil diameter (D).

$$N = \frac{f}{D}$$

The illumination of the image decreases with the square of the f-number. In an infrared imaging system, the thermal sensitivity is directly proportional to the illumination of the image. For this reason, most thermal imaging systems use a low f-number, usually around 1.[14] In this thesis, lenses with f-numbers ranging from 0.75 to 2 were tested. The effect of the f-number on thermal sensitivity and imaging quality was investigated.

The f-number also affects the depth of field of the camera. The depth of field is the distance between closest and furthest objects that are in focus. The depth of field (DOF) is related to the focal length of the lens (f), the f-number (N), the distance to the object (u) and the circle of confusion (c). This is given by the following equation.

$$DOF = \frac{2u^2Nc}{f^2}$$

In thermal imaging systems, particularly those using small sensors, the depth of field is usually quite large. This is because the focal length of the lens is usually short and when low resolution sensors like those used in this thesis, the circle of confusion can be relatively large. Therefore, the effect of the f-number on the depth of field is less impactful than in conventional photography. In this thesis, the difference in the depth of field of the lenses was not thoroughly investigated.

Thickness

The thickness of the lenses was also considered. While the polymers developed in this thesis have excellent transmission in the LWIR, there was still considerable absorption which was dependent on the thickness of the material. For this reason, the centre thickness of the lenses was kept as low as possible. Using some moulding techniques, several thicknesses were tested for some of the lenses. This can be seen in the two-part mould section. The standard centre thickness of the lenses was 0.8 mm.

It should be noted that the edge thickness of the lenses varied based on the focal length and diameter. This could mean that some lenses may have more spherical aberrations than others due to the increased transmission of the marginal rays of light. This could result in lenses with a smaller f-number showing an increase in spherical aberrations. The effect of this was discussed in the “comparison of lens imaging” section.

A total of 7 lenses were selected to investigate a range focal lengths and f-numbers. These lenses would allow for the viability of the polymer lenses to be investigated on the FLIR Lepton. These lenses were all plano convex and bought from Edmund Optics. The radius of the curved section was selected to give the desired focal length when accounting for the higher refractive index of the polymer over glass. These glass lenses would be used to make moulds which could be used to cast the polymer. Below is a table showing the lenses bought for investigation in this thesis. The focal length in this table accounts for the higher refractive index of the norbornane based sulfur polymer.

Table: 4.1: Data of lenses used for lenses purchased from Edmund Optics used for making moulds and casting polymer lenses.

Lens number	**Lens type**	**Radius of convex surface (mm)**	**Focal length (RI 1.87) (mm)**	**Diameter (mm)**	**F-number**	**Centre thickness**	**HFOV Lepton 3.5 (%)**
1	Plano Convex	1.28	1.5	1.5	f/1	0.8	65
2	Plano Convex	1.28	1.5	2	1/0.75	0.8	65
3	Plano Convex	1.70	2	2	f/1	0.8	51
4	Plano Convex	1.70	2	2.5	f/0.8	0.8	51
5	Plano Convex	2.12	2.5	2.5	f/1	0.8	42
6	Plano Convex	2.55	3	2.5	f/1.2	0.8	35
7	Plano Convex	4.25	5	2.5	f/2	0.8	22

The lenses purchased from Edmund Optics were selected so the effect of focal length and f-number could be investigated. There were a range of focal lengths selected from 1.5 mm and 5 mm. This would show the differences in the field of view and zoom. For two of the focal lengths, there were two different diameters for the same focal lengths. This gave a different f-number and could be used to show the difference in f-number when focal length was maintained. There were also several lenses with the same diameter and different focal lengths. Four lenses all had a diameter of 2.5 mm while the focal length ranged from 2 mm to 5 mm. These lenses would give a good understanding on how the imaging is changed while maintaining the diameter of the lens and altering the focal length. The centre thickness of all lenses was maintained at 0.8 mm. This was important so that comparisons between the lenses could be analysed. The norbornane based polymer has approximately 20 % transmission at this thickness.

The expected horizontal field of view of each lens when using the FLIR lepton was calculated using the focal length and the horizontal size of the sensor. These values were then used in the following equation which was explained in the previous section:

$$FOV = 2\arctan(\frac{x}{2f})$$

Where x is the width of the sensor and f is the focal length.

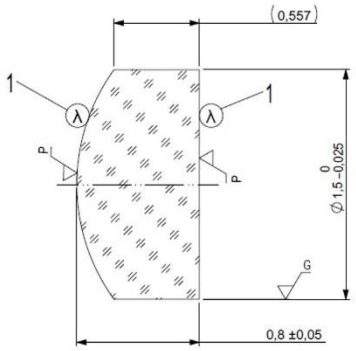

Lens 1: 1.5 mm FL, 1.5 mm Diameter

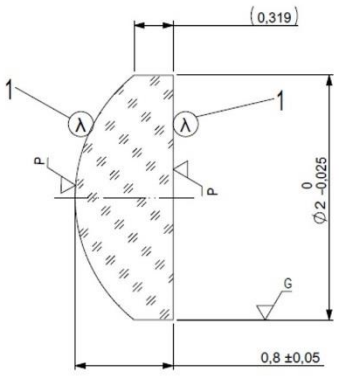

Lens 2: 2 mm FL, 1.5 mm Diameter

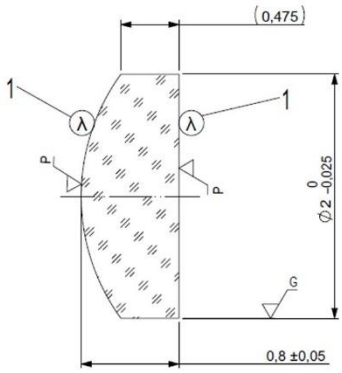

Lens 3: 2 mm FL, 2 mm Diameter

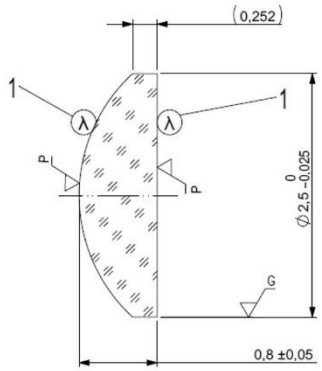

Lens 4: 2 mm FL, 2.5 mm Diameter

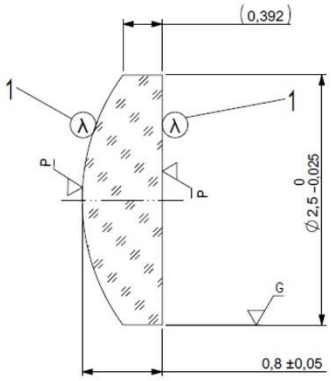

Lens 5: 2.5 mm FL, 2.5 mm Diameter

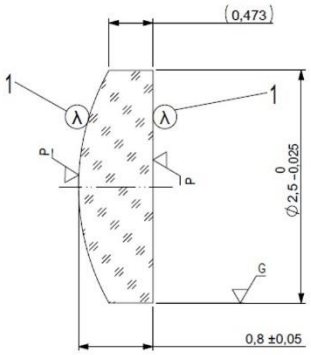

Lens 6: 3 mm FL, 2.5 mm Diameter

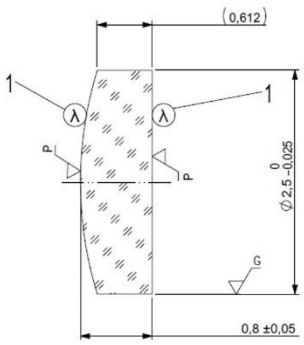

Lens 7: 5 mm FL, 2.5 mm Diameter

Figure 4.24: Diagrams showing dimensions of lenses bought from Edmund Optics to use as positives for silicone moulds.

Synthesis of Norbornane bistrisulfide polymer

The rest of this chapter will focus on optics made from the norbornane bistrisulfide polymer. While the synthesis and characterisation were covered in detail in chapter 3, it will be repeated here for added clarity. Unless otherwise stated, the 81 % sulfur composition was used. This polymer was used over the cyclopentadiene based polymer for several main reasons. The first is the much greater glass transition temperature. The norbornane based polymer with 81 % sulfur had a glass transition temperature of 137 °C. This is much greater than the cyclopentadiene polymer which had a glass transition temperature of only 3.1 °C. As the glass transition temperature is much above room temperature, this polymer acts like a brittle glass. This is very useful for making lenses as it means that it will not change its shape with pressure. It also means that the polymer can be ground or polished like a glass, allowing for high quality surfaces to be prepared. The norbornane bistrisulfide based polymer also has a very high refractive index of 1.871 and excellent transmission in the long wave infrared region making it perfectly suited for use as a lens. Below is a standard method for the synthesis of the polymer, see chapter 3 for details on the synthesis of the monomer and any polymer characterisation.

Sulfur (300 mg, 1.17 mmol S8) was measured into a 5 mL vial. The vial was added to a preheated oil bath at 140 °C. The sulfur was left for 3 minutes to melt. After this point, the vial was transferred to a preheated vacuum oven at 140 °C. A vacuum of approximately 2 mbar was pulled in the oven and the molten sulfur was left for 30 minutes. After degassing the sulfur, the pressure was returned to ambient, and the sulfur was transferred back to the 140 °C oil bath. Norbornane bistrisulfide, molecule **6** (445 mg, 1.56 mmol) was poured into the vial. **6** would rapidly dissolve in the molten sulfur over approximately 15 seconds. 15 seconds after **6** was added, the reaction was stirred with a heated metal spatula. The reaction was stirred carefully to prevent trapping gasses which would cause bubbles in the polymer. The reaction was stirred for a total of 30 seconds (stirring was stopped at a reaction time of 45 seconds). After a total reaction time of 60 seconds, the prepolymer was poured into a silicone mould which had been preheated to 140 °C. The mould was then placed in a 140 °C oven where it was left for 24 hours to cure. Further experimentation showed that a cure time of 1 hour is appropriate but all polymers in this thesis were cured for a full 24 hours. Below two images of a polymer window prepared using this method.

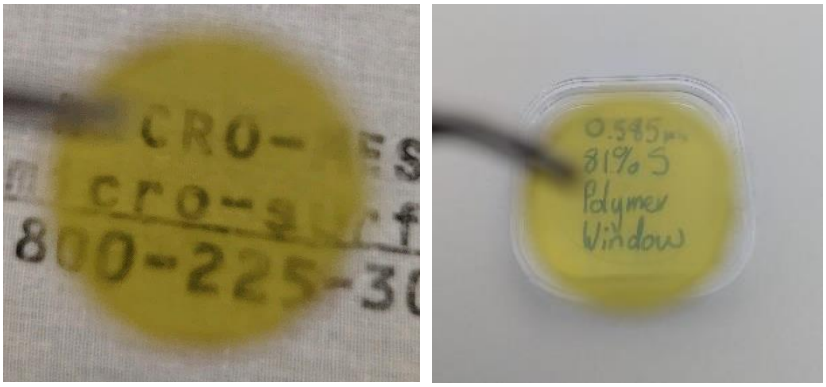

Figure 4. 25: Images of polymer window made from 81 % sulfur norbornane bistrisulfide polymer.

One-part mould design

To make the lenses from the sulfur-based polymer, a silicone mould had to first be prepared. The first and most simple mould design was a one-part mould. In this design, the glass lens would be held in a 3D printed part. This part had a base and outside part which when assembled, would allow for silicone to be poured into it. After allowing the silicone to cure, the 3D printed part could be removed to give the final mould. When using this mould, the prepolymer would be poured into the space left by the 3D printed part and the lens. Due to the 3D printed part, the lens would have some non-imaging material around the plano convex portion. This material is known as carrier material. While not necessary for imaging, the carrier material provided additional strength to the lens and aided in mounting in a holder. When using the one-part mould, the carrier material formed a square with sides of 4 mm.

After curing the polymer in the silicone mould, the mould would need to be cut open. After extracting the polymer, the lens and carrier material could be separated using an intentional weak point in the part. At this point, the thickness of the polymer would only be 300 µm. By scoring along this line with a scalpel, the lens and carrier material could be broken away from the funnel section.

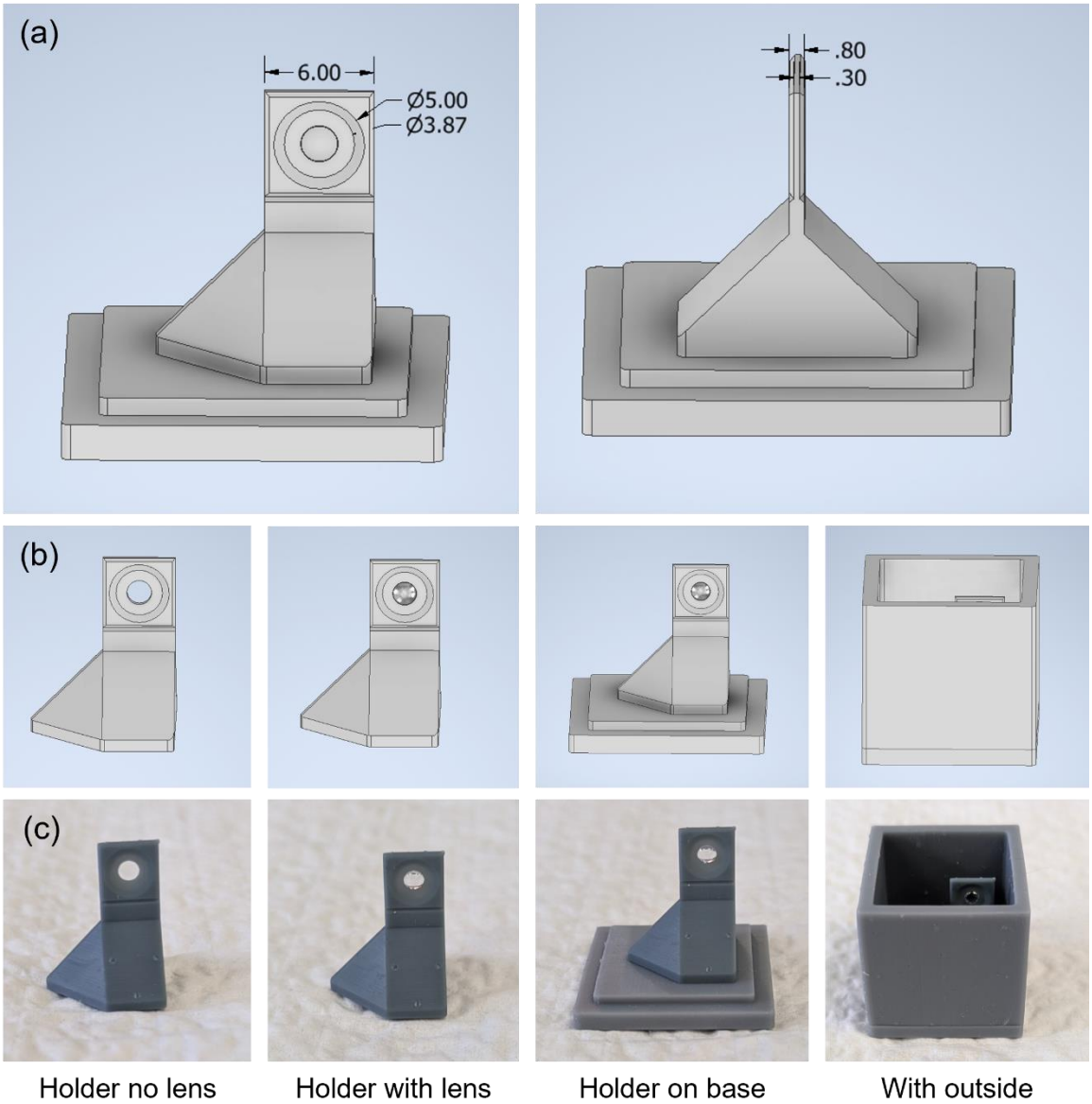

Figure 4.26: One part mould design. (a) Design with dimensions for carrier material. (b) Inventor design of design. (c) 3D printed parts for one part mould.

The 3D printed parts were made on a Phrozen Sonic mini 8k 3D printer using the 8k resin. It was found that addition cure silicone would not cure properly when in contact with the 3D printed resin. To overcome this issue, a condensation cure silicone was used instead. To make the mould, approximately 20 g of M4503 condensation cure silicone rubber from Barnes was mixed with 1 gram of T35 catalyst. This silicone had a working time of 90 minutes and a cure time of 24 hours at room temperature. It was found that this silicone did not suffer from any of the issues of poor cure that the addition silicones had. For all future moulds, this silicone was used.

While the one-part mould was simple, it had many weaknesses which lead to many failed casts. The biggest one is that the mould had no outlet for the air within the part to leave. The prepolymer was very viscous had had a short working time. For this reason, air could make its way through the polymer before it vitrified. This led many casts where the polymer would fill the funnel section but not completely fill the mould. An example of a failed cast like this can be seen in the figure below.

Several modifications to the casting method were employed to attempt to improve the consistency. Placing the mould on an angle and manually squeezing the mould to increase the size of the opening was attempted, however, these methods were inconsistent and very manual. Another modification that was made was to manually push the prepolymer into the mould using a heated spatula. While this method did allow the polymer to fill into the mould, it often led to the formation of bubbles which decreased the consistency of the cast. The final modification was to place a glass syringe into the mould before casting the polymer. The glass syringe acted as an outlet for air and would be removed once the polymer had filled the mould. This method allowed for several successful casts like the one in the figure below, however, it was very manual and slow.

The one-part mould showed that an outlet for air is very important in the mould design. For this reason, the one-part mould design was abandoned in favour for the two-part mould design in the following section.

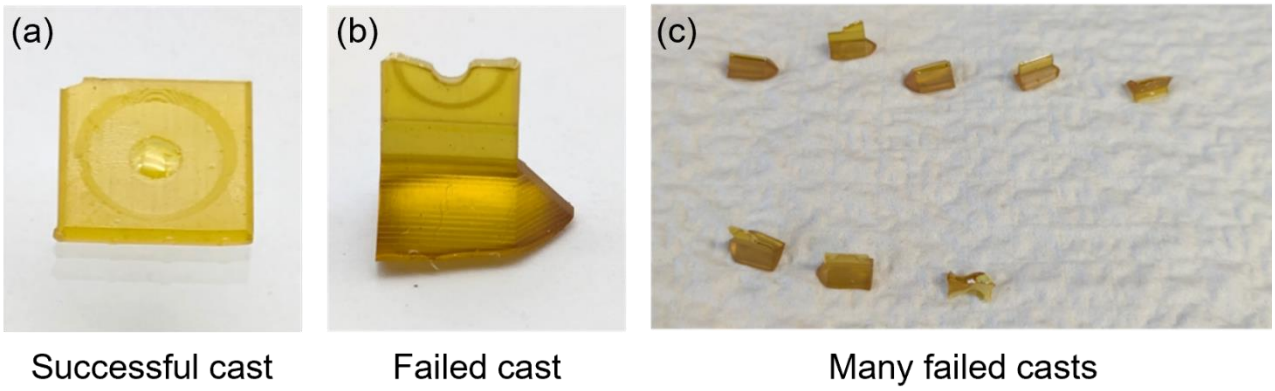

Figure 4.27: (a) A successful cast using one part mould. (b) A close up example of a failed cast. (c) many failed casts using one part mould.

Two-part mould design

To improve upon the one-part design, a new mould was designed. This mould incorporated an outlet for air which was found to be very important in the one-part design. The two-part mould had a seam down the middle so that the mould did not need to be cut open after every cast, allowing it to be reused many times over. One side of the mould would be prepared using the convex side of the glass lens from Edmund Optics. This side would also include a funnel section where the prepolymer could be poured as well as an outlet for air. The other part of the mould was completely flat. This side of the mould had no features which meant that exact alignment of the mould was not necessary. If a lens design which utilised two curved surfaces was used, the mould would need to be modified.

Unlike the one-part mould, the carrier material for the lens did not need to be square when using the two-part mould. Instead, a round carrier material was incorporated. This carrier material gave the lens a total diameter of 4 mm for all lens designs. The imaging section of the lens was only in the centre while the outside of this simply provided strength and allowed for easier mounting. The carrier material had a thickness of 0.65 mm on the outside with a sloped section between the outer edge of the lens and the thickest section of the carrier material. This design was far more practical than the one-part mould for mounting on the FLIR Lepton. When the shutter and lens are removed from the FLIR Lepton 3.5, an opening of 4.5 mm is revealed. Using the circular carrier material, there was just enough tolerance to allow for the lens and a holder to be inserted into the FLIR Lepton 3.5.

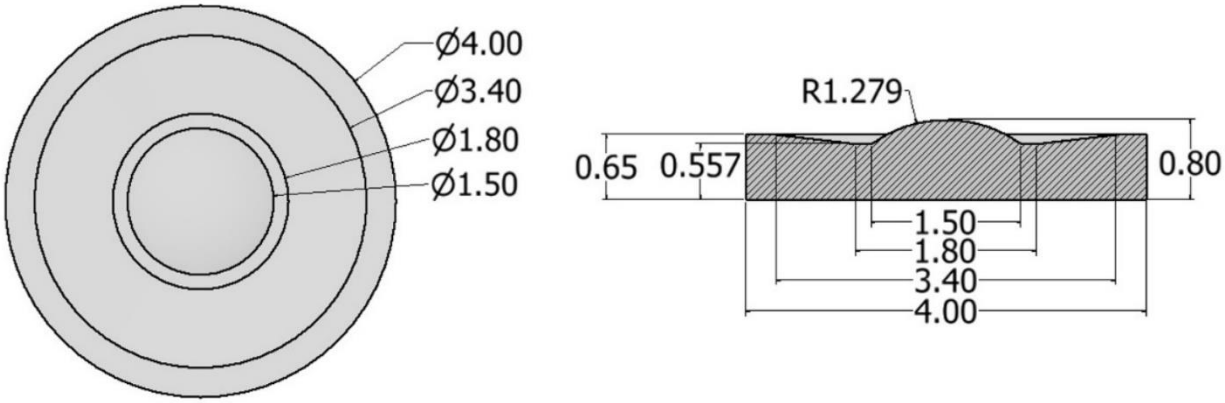

Figure 4.28: Carrier material for lenses when 2-part mould was used. (1.5 mm focal length, 1.5 mm diameter lens is shown).

To prepare the flat side of the mould, a 3D printed part was produced. This part was a simple rectangular prism with filleted edges and a 19 mm by 17 mm opening in the centre. The 3D printed part was placed on a glass slide. The glass slide provided a high-quality surface for the plano side of the lens. To prepare the silicone mould, the same condensation cure silicone from Barnes was used. When used with glass, this silicone was found to stick very strongly. To prevent this issue, a range of release agents was used. It was found that the most effective method to prevent the silicone from sticking was to mix detergent in water and submerge the glass slide in it. The water was then wiped away with a tissue, leaving a detergent layer on the glass slide. After this, the 3D printed part was placed on the glass slide and the silicone was mixed in a 95:5 ratio of part A (M4503) and B (T35) respectively. After leaving the silicone for 24 hours at room temperature to cure, it was removed from the 3D printed part and was ready for use.

To prepare the cavity side of the mould, another 3D printed part was used. This part contained the carrier material and a slot where the glass lens would sit. It also had a funnel section where the prepolymer would be poured into and an outlet for air to escape. This part was designed so that the same 3D printed piece from the flat side could be used to provide an enclosure for the silicone resin to be poured to prepare the mould.

To cast the silicone, the glass lens was first submerged in detergent water like the glass slides for the flat side of the mould. The glass lens was then pressed into the 3D printed part with the convex side facing up. The tolerance between the lens and the 3D printed part was 50 µm. This tolerance was found to be very important as a larger tolerance would have silicone flow between the lens and the part. This silicone could flow under the lens and push it up, leading to an angle between the carrier material and the lens. If the tolerance was too tight, it was difficult to insert the lens and this could also lead to similar issues where the lens is not pushed flat prior to casting the silicone. With some prototyping, it was found that 50 µm was adequate. After inserting the lens into the 3D printed part, the outside piece was added. The condensation cure silicone was then mixed and poured into the mould. After leaving the silicone for 24 hours at room temperature to cure, the outside piece was removed. To aid in the removal, some indents were made in the 3D printed part which allowed for a tool to be inserted. The silicone was then separated from the 3D printed part and any flashing was removed with a scalpel.

Figure 4.29: Design of two part mould in Autodesk Inventor.

There were many iterations of the two-part mould to find one which gave consistent casts. This next section will outline the main findings of these iterations and the considerations that should be made when making a mould of this type. The first design of this mould had a much longer path length for the prepolymer to flow. In this design, the polymer would flow down through the funnel, through a path and enter the bottom of the lens cavity. There are several advantages to this type of design. The first is that the path entering the lens cavity is very thin. This means that the excess polymer would be very easy to remove in post processing. Another advantage is that the polymer enters the cavity through the bottom, relative to gravity. As there is no injection pressure, this would ensure that all air is pushed out, preventing any trapped air bubbles. However, it was found that the prepolymer would not be able to flow all the way through the path. This is likely due to the high viscosity and very shorts working time of the prepolymer meaning it could not flow through the path before vitrification. When casting the polymer, there is not injection pressure, instead, they rely completely on gravity to fill the mould. Typical injection moulding uses pressure ranging from 70 to 112 MPa[15]. If pressure like this was used, a longer path length could be used, but for a gravity casting method, it is not feasible. Similarly, it

was found that paths that were too thin would block the flow of the prepolymer. Through several trials, it was found that the gates must be at least 0.4 mm thick to ensure consistent casting.

Another issue that was found in the prototyping process was that the lens cavity would not fill completely if it was filled from the top. As the prepolymer has no injection pressure, it will flow around the lens section rather than fill it. To prevent this, the polymer must fill from the bottom. This was, as it filled, it would displace any air from the lens cavity and fill it completely.

These issues were overcome by having the funnel section directly connected to the lens cavity from the side and an air outlet on the top. It was found that filling from the side was adequate to displace that air from the cavity and completely fill it with polymer. The connection between the funnel and the lens cavity was much larger, leading to no blockages. Furthermore, by reducing the pathlength of the polymer flow, the consistency of casts significantly improved.

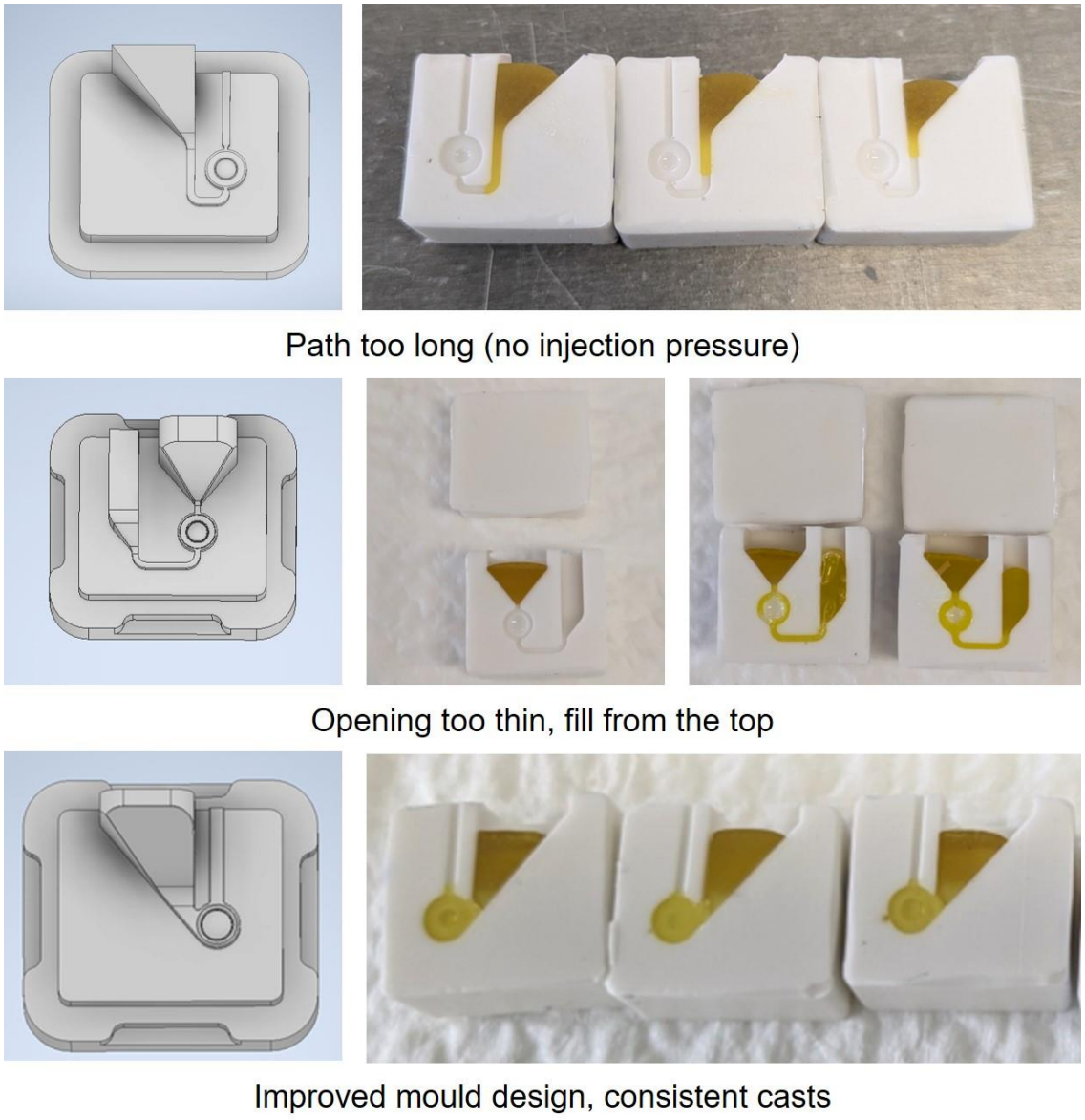

Figure 4.30: Two part mould prototyping. The top mould design had a pathlength that was too long, leading to a short shot. The second design had an opening that was too thin and also filled the cavity from the top, leading to blockages or a poor fill. The bottom designed connected the funnel section directly to the side of the lens cavity. This prevented any blockages and resulted in consistent casts.

While the consistency of the casts was improved, there was still one issue with the two-part mould design. The connection, or gate, between the funnel section and the lens cavity was very large. This meant that it was very difficult to remove the funnel without damaging the lens in the process. Another prototyping process was performed to improve the mould and post processing techniques to remove the funnel and air outlet without damaging the lens or carrier material. As the polymer was hard and brittle. It could be scored and broken like glass. These score lines worked best if they could be made straight. It was also much easier to score if there was a clear distinction between the lens carrier material and the funnel or outlet sections. This distinction was achieved by making the gate between the funnel and the carrier material decrease in thickness to only 0.4 mm, making it 0.25 mm thinner than the edge of the carrier material. The air outlet was also made thinner and the fillets connecting it to the lens cavity were removed. The thinner sections made scoring the part much easier, aiding in the removal of the funnel and outlet. After this point, the lens had only small imperfections. To remove these sections, a file was used. Another 3D printed part was used to aid in alignment of the lens for the filing.

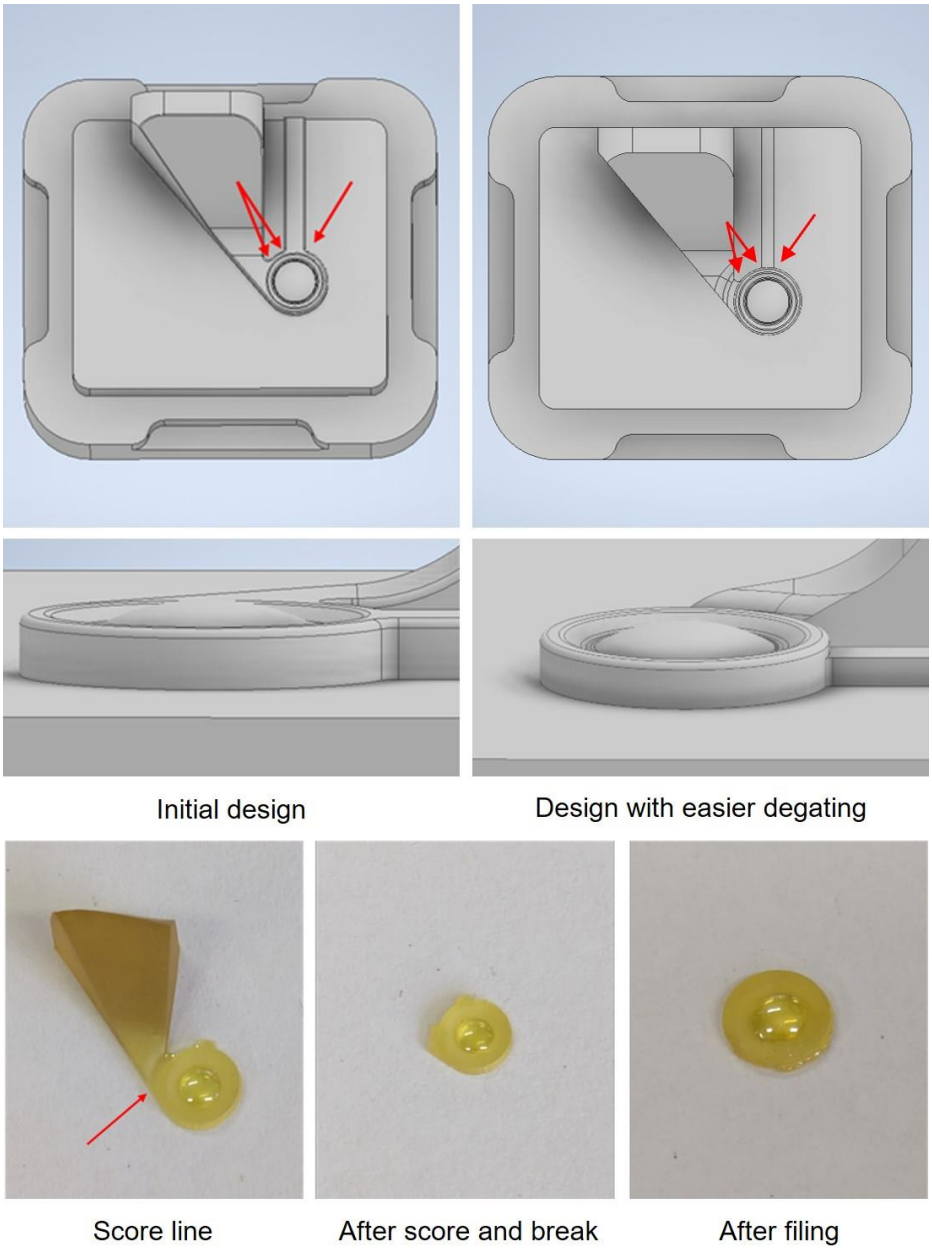

Figure 4.31: Mould prototyping to improve degating of funnel and air outlet. Red arrows indication location of scores.

Norbornane based polymer casting and lens characterisation

Casting and issues with bubbles in lenses

After optimising the two-part mould, consistent castings could be achieved. However, it was found that the polymer lenses would have a significant number of bubbles. These bubbles could be hundreds of microns in diameter and were very common. When the lenses were used, the bubbles would lead to artifacts in the images, making the lenses difficult to focus and use.

After many experiments, it was determined that the bubbles likely originated from two different sources. The first was from outgassing of the silicone mould. A condensation cure silicone resin was used to prepare the lens moulds as described in the sections above. A general reaction scheme for the condensation reaction used in silicone resins is shown below. As can be seen, alcohol is released as past of the reaction. Even after the silicone has completely cured, it can still outgas alcohol for several days. It was possible that this alcohol could be forming bubbles in the polymer. To prevent this outgassing, a post-cure degassing procedure was developed. After cure, the silicone moulds were placed in an oven at 140 °C for 2 hours. The pressure was maintained at standard atmospheric pressure. This was found to be adequate to prevent the silicone from outgassing during the reaction.

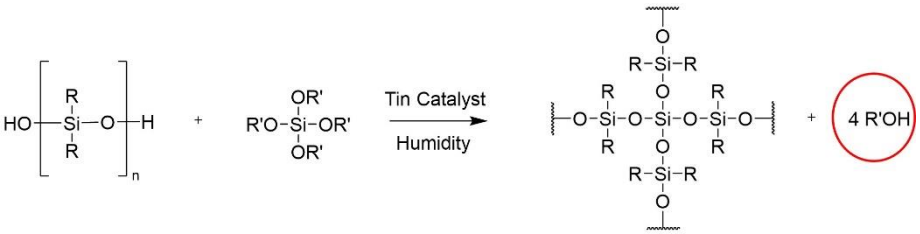

Figure 4.32: General reaction scheme for the tin catalysed cure of silicone resin.

The other source of bubbles in the polymer was found to be from the sulfur source. When the sulfur was melted and placed into a vacuum oven, it was found to form many bubbles. These bubbles were likely from moisture in the sulfur. In most inverse vulcanisation reaction, the working time is usually between 15 minutes and 3 hours. With such a long working time, the gas has time to escape without forming a bubble. However, in the reaction between norbornane bistrisulfide and sulfur, the working time in only approximately 3 minutes. This means that the gas is trapped in a bubble before it can escape the polymer matrix.

To prevent bubbles in the polymer, a degassing procedure was developed for the sulfur before the reaction. The sulfur was first melted at 140 °C with an oil bath. Following this, it was transferred to a 140 °C vacuum oven without letting it cool. The pressure in the oven was reduced to approximately 2 mbar and maintained for 30 minutes. After this, the sulfur was removed from the oven and used in the reaction while still molten. When this degassing procedure was used, no bubbles were present in any polymer lenses.

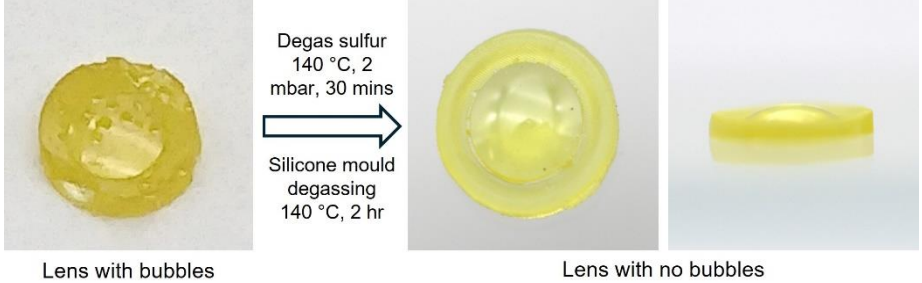

Figure 4.33: Photos of a lens with bubbles and another that was prepared using the degassing proceedures.

Photos and dimensions of all lenses

This section shows all the lenses that were prepared and detailed the dimensions and important parameters of each. All lenses have the same carrier material design apart from lens 7 which was made first and had a much thicker carrier material. All lenses were plano convex with diameters varying from 1.5 mm to 2.5 mm and focal lengths ranging from 1.5 mm to 5 mm

Focal Length	*1.5 mm*
Back Focal Length	*1.07 mm*
Lens Type	*Plano Convex*
Diameter (lens)	*1.5 mm*
F-number	*f/1*
Centre thickness	*0.8 mm*
Radius	*1.279 mm*
Edge thickness (lens)	*0.557 mm*
Carrier material diameter	*4 mm*
Carrier material edge thickness	*0.65 mm*
Refractive Index	*1.871*
Glass transition temperature	*137 °C*

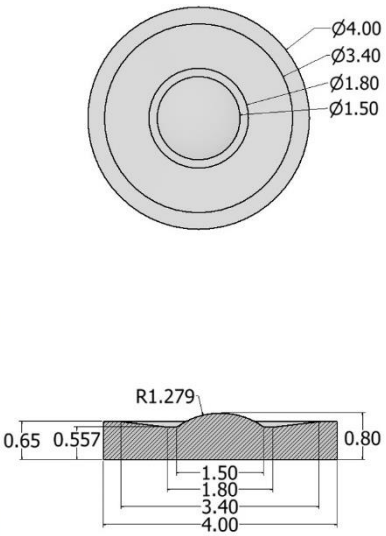

Lens 1

Focal Length	*1.5 mm*
Back Focal Length	*1.07 mm*
Lens Type	*Plano Convex*
Diameter (lens)	*2 mm*
F-number	*f/0.75*
Centre thickness	*0.8 mm*
Radius	*1.279 mm*
Edge thickness (lens)	*0.319 mm*
Carrier material diameter	*4 mm*
Carrier material edge thickness	*0.65 mm*
Refractive Index	*1.871*
Glass transition temperature	*137 °C*

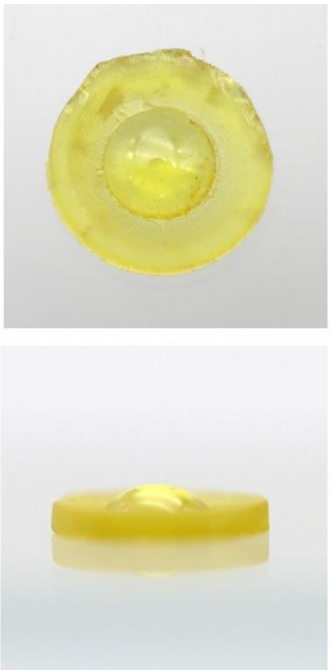

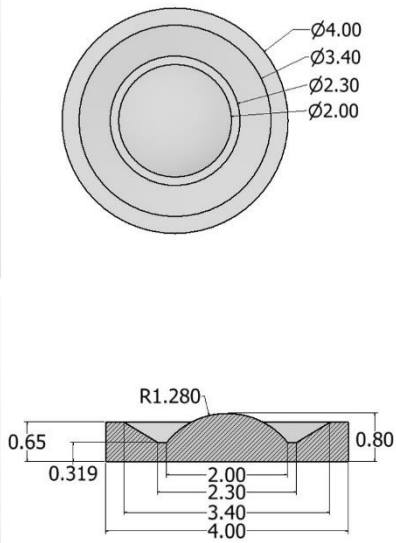

Lens 2

Figure 4.34: Images and dimensions for lens 1 and 2. All dimensions are in mm.

Focal Length	*2 mm*
Back Focal Length	*1.57 mm*
Lens Type	*Plano Convex*
Diameter (lens)	*2 mm*
F-number	*f/1*
Centre thickness	*0.8 mm*
Radius	*1.7 mm*
Edge thickness (lens)	*0.475 mm*
Carrier material diameter	*4 mm*
Carrier material edge thickness	*0.65 mm*
Refractive Index	*1.871*
Glass transition temperature	*137 °C*

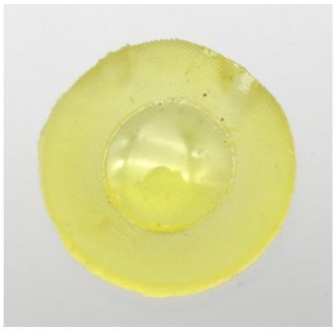

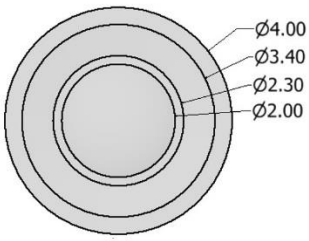

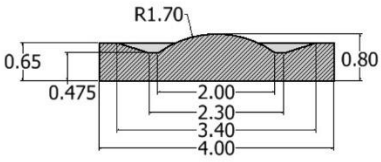

Lens 3

Focal Length	*2 mm*
Back Focal Length	*1.57 mm*
Lens Type	*Plano Convex*
Diameter (lens)	*2.5 mm*
F-number	*f/0.8*
Centre thickness	*0.8 mm*
Radius	*1.7 mm*
Edge thickness (lens)	*0.252 mm*
Carrier material diameter	*4 mm*
Carrier material edge thickness	*0.65 mm*
Refractive Index	*1.871*
Glass transition temperature	*137 °C*

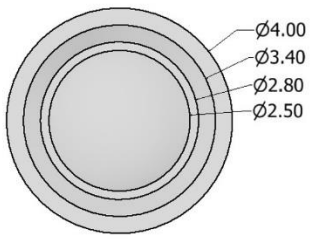

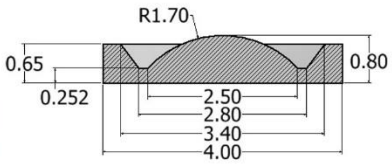

Lens 4

Figure 4.35: Images and dimensions for lens 3 and 4.All dimensions are in mm.

Focal Length	*2.5 mm*
Back Focal Length	*2.07 mm*
Lens Type	*Plano Convex*
Diameter (lens)	*2.5 mm*
F-number	*f/1*
Centre thickness	*0.8 mm*
Radius	*2.12 mm*
Edge thickness (lens)	*0.392 mm*
Carrier material diameter	*4 mm*
Carrier material edge thickness	*0.65 mm*
Refractive Index	*1.871*
Glass transition temperature	*137 °C*

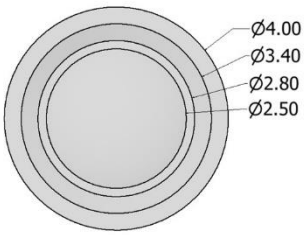

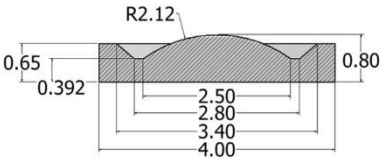

Lens 5

Focal Length	*3 mm*
Back Focal Length	*2.57 mm*
Lens Type	*Plano Convex*
Diameter (lens)	*2.5 mm*
F-number	*f/1.2*
Centre thickness	*0.8 mm*
Radius	*2.55 mm*
Edge thickness (lens)	*0.473 mm*
Carrier material diameter	*4 mm*
Carrier material edge thickness	*0.65 mm*
Refractive Index	*1.871*
Glass transition temperature	*137 °C*

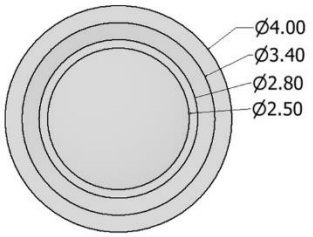

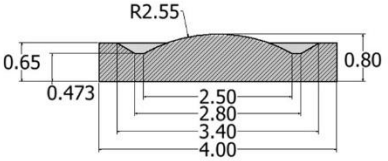

Lens 6

Figure 4.36: Images and dimensions for lens 5 and 6. All dimensions are in mm.

Focal Length	*5 mm*
Back Focal Length	*4.57 mm*
Lens Type	*Plano Convex*
Diameter (lens)	*2.5 mm*
F-number	*f/2*
Centre thickness	*0.8 mm*
Radius	*4.25 mm*
Edge thickness (lens)	*0.612 mm*
Carrier material diameter	*4 mm*
Carrier material edge thickness	*1 mm*
Refractive Index	*1.871*
Glass transition temperature	*137 °C*

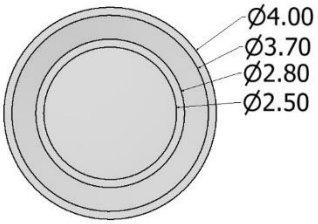

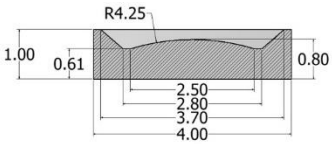

Lens 7

Figure 4.37: Images and dimensions for lens 7. All dimensions are in mm.

Confocal microscope analysis of polymer lenses

Acknowledgement: This section was done with equipment from the Australian National Fabrication Facility (ANFF) with training and guidance given by Mark Cherrill.

The surface of two polymer lenses were analysed using an OLS 5000 Confocal Microscope. This was done at the Australian National Fabrication Facility at the SA node. The main purposes of testing the surface structure were to understand the surface roughness and ensure that the radius matched the glass positive. The surface roughness is vital to the optical performance of the lens. Surface roughness can affect the reflection, scattering and transmission of light.[16] As the lenses were to be used with light between 7 μm and 14 μm, it was essential that the surface roughness was less than this, preferably sub-micron. The radius of the convex side of the lens was critical to the performance of the lens as any variation would affect the focal length and f-number of the lens. It was possible that the injection pressure or cooling effect could result in changes in the radius so this was an essential parameter to test.

To measure the radius and surface roughness of the lenses, a scan of the plano and convex sides of both lenses was performed. This scan was utilised a 20 x magnification lens. After performing a scan of both sides, the radius of curvature of the convex side was found using Gwyddion software. The surface roughness data was analysed using the OLS 5000 data analysis software. For each scan, a tilt and curvature correction was performed. Following this, surface roughness was measured over an area of the lens surface.

A range of parameters for the surface roughness were obtained. The following is an explanation of each of the parameters.[17] Sq is the root mean square height and gives the standard deviation of the distribution of height in the surface. Ssk is skewness in the roughness data. Sku is kurtosis. Sp is the maximum peak height while Sv is the minimum pit height. Sz is the maximum height. Sa is the average difference in height from the mean plane. The Sa value will be mostly used to analyse the samples roughness. Sdq is the gradient of the root mean square. Sdr is the developed interfacial area ratio.

Of the parameters outlined above, the most important of optical applications is the Sa, this gives information on the surface roughness of the samples. All surfaces Sa values of less than 0.1 μm which made them appropriate for long wave infrared imaging. The radius of the convex surfaces of both lenses was also very close to expected.

Table 4.2: Surface parameters for polymer lenses

Surface	Radius (mm)	Sq (μm)	Ssk	Sku	Sp (μm)	Sv (μm)	Sz (μm)	Sa (μm)	Sdq	Sdr (%)
Lens 7: Convex	4.22	0.119	0.454	9.661	1.184	1.585	2.769	0.082	0.211	2.489
Lens 7: Plano	N/A	0.087	0.254	6.640	1.057	1.169	2.226	0.066	.124	.906
Lens 3: Convex	1.74	0.78	.506	15.802	1.081	1.554	2.635	0.056	0.138	1.083
Lens 3: Plano	N/A	0.126	-0.255	7.564	1.714	1.883	3.596	0.096	0.270	4.327

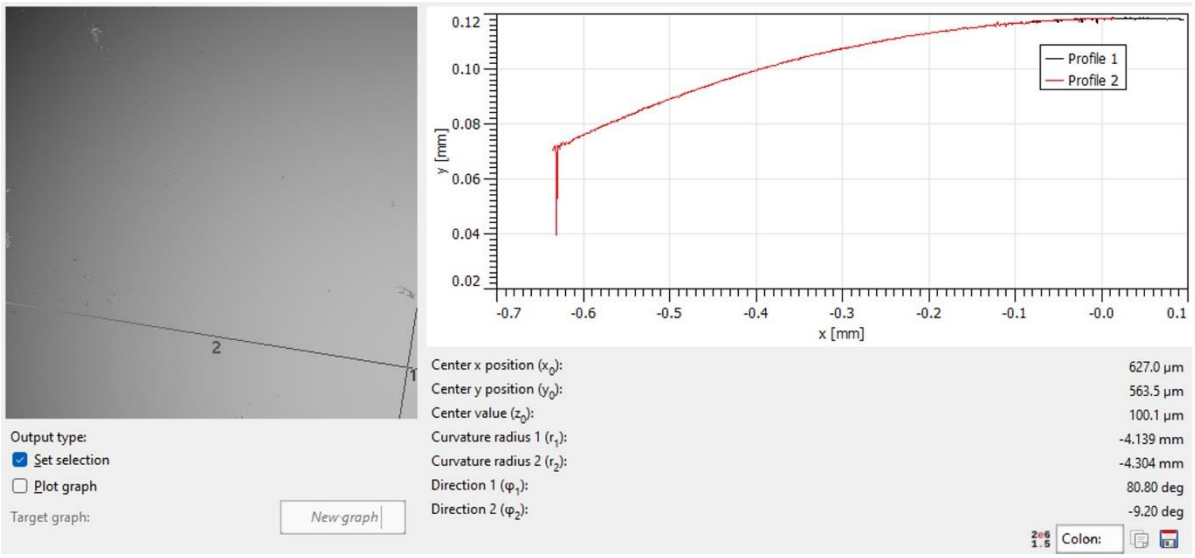

Lens 7: radius of convex surface

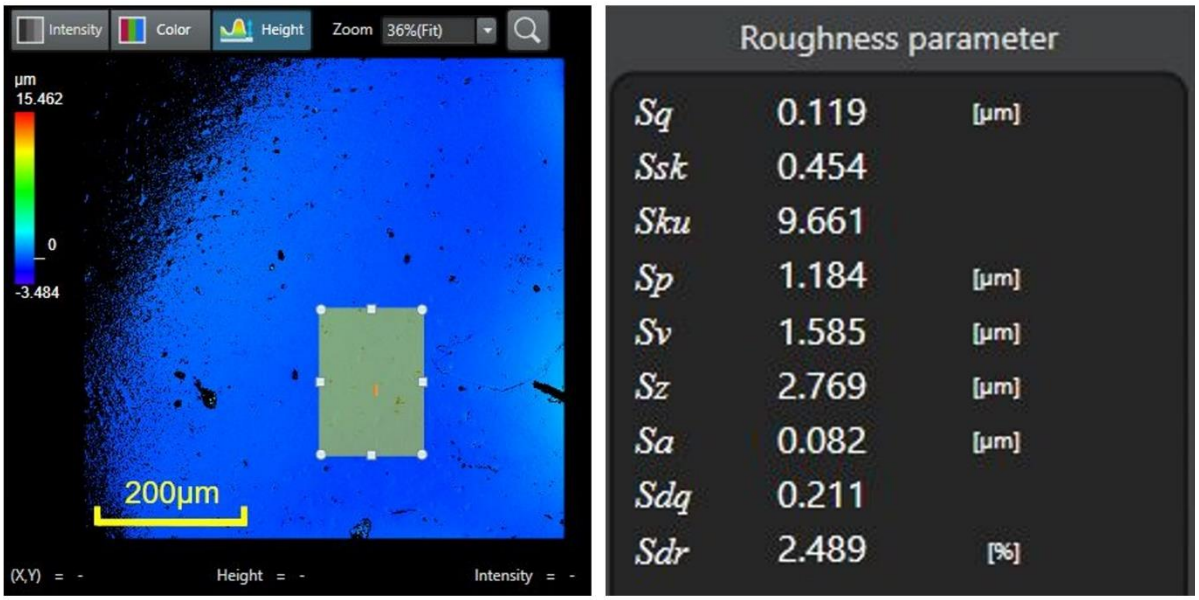

Lens 7: surface roughness of convex surface

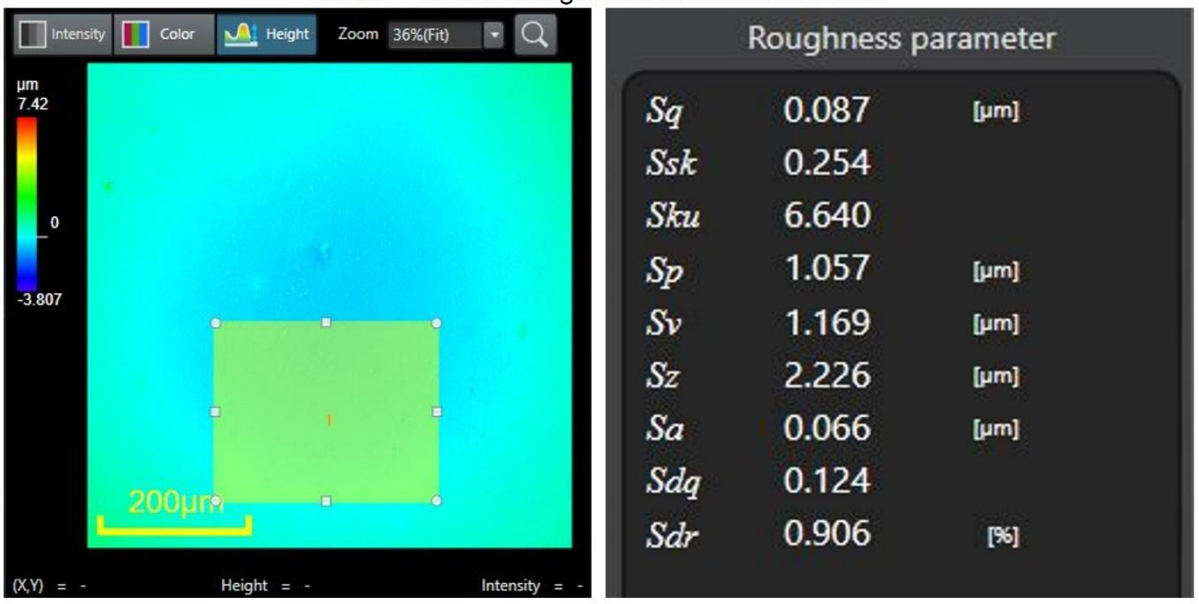

Lens 7: surface roughness of plano surface

Figure 4.38: OLS 5000 Confocal Microscope data for lens 7 (5 mm FL, 2.5 mm diameter).

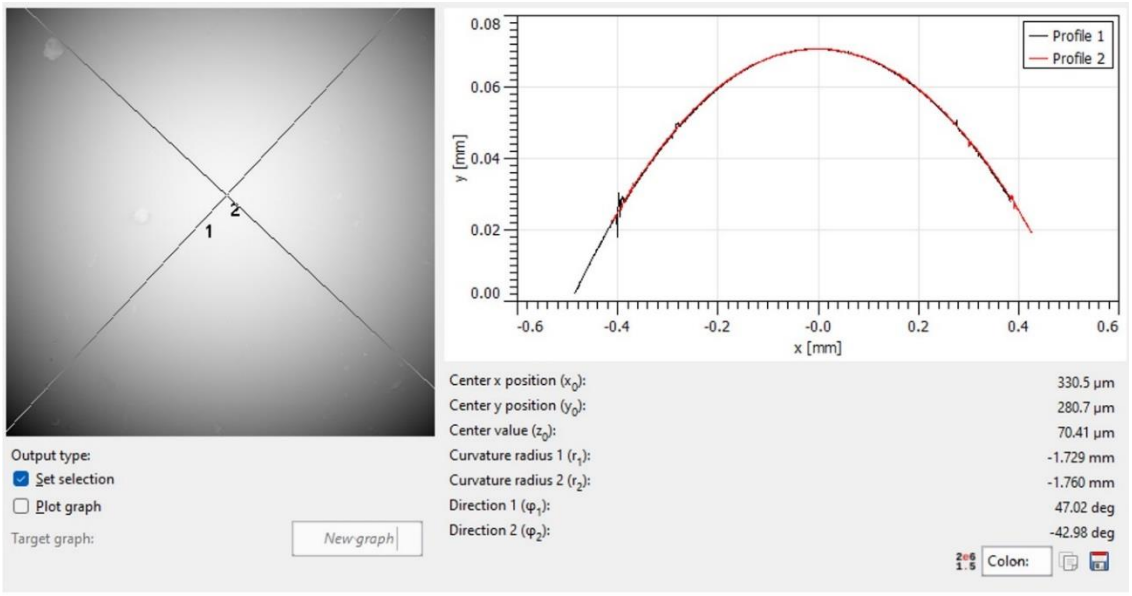

Lens 3: radius of convex surface

Lens 3: surface roughness of convex surface

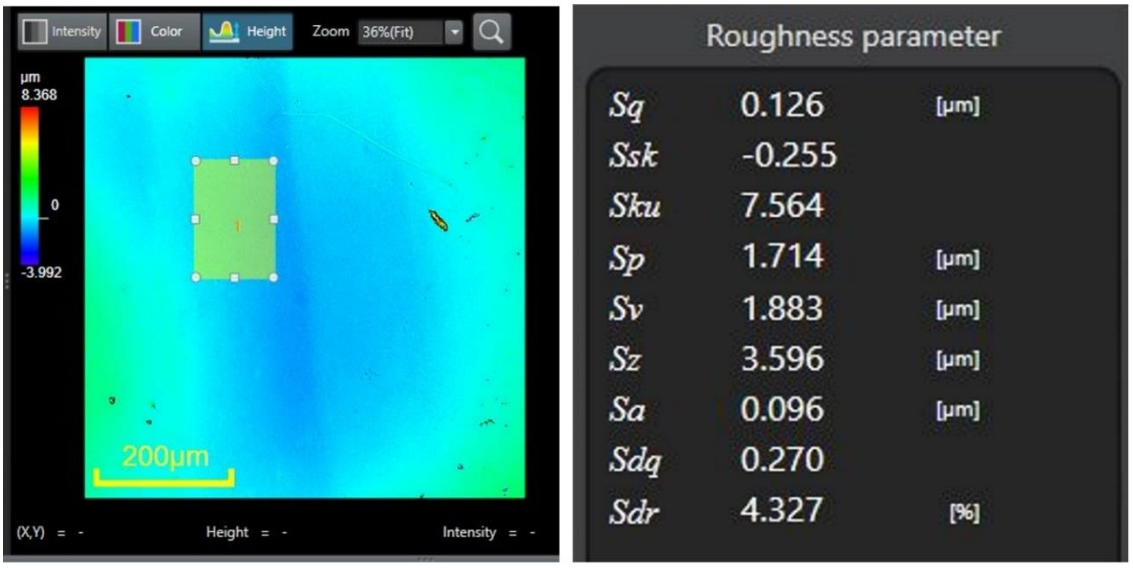

Lens 3: surface roughness of plano surface

Figure 4.39: OLS 5000 Confocal Microscope data for lens 3 (2 mm FL, 2 mm diameter).

Infrared imaging using custom lenses with commercial sensor

Lens holder design

With the lenses prepared and characterised, the next step was to integrate them into a FLIR Lepton 3.5 infrared module. This would be a very large milestone as to this point, the polymer had never been used as the sole lens in a working infrared camera. Every imaging system to this point in the thesis had used a germanium lens to focus light onto a sensor in the camera. In these systems, the polymer lenses were only used to magnify the image.

To fully integrate the lens into a camera, several factors need to be controlled. The first and most important is the distance between the sensor and the lens. Each lens has a specific back focal length. This is the distance from the back surface that the lens will focus parallel light. To achieve the optimum focus, this point should be at the sensor of the camera. The second important factor is that the stray or unfocussed light should be blocked from the sensor. If additional light reaches the sensor that has not been focussed by the lens, it will result in noise or artifacts in the image. While some of this can be removed using calibration, ideally, any light that hasn't been focussed by the lens should be blocked by an aperture before reaching the sensor. Finally, the lens needs to be held securely and be somewhat protected from damage. All these factors can be achieved using a well designed holder for the lenses.

The FLIR Lepton 3.5 had an internal thread with a pitch of 350 µm. The holder was designed to thread into this. The thread not only provided a secure fitting for the holder but also allowed for fine control of the distance from the sensor to the bottom of the holder. This was used to find the optimal focus of each lens. The holders had a hole through the middle and an opening where the lens could be placed. After inserting the lens, a press fit cap could be inserted. The cap ensured that the lens was held securely and didn't move or fall out of the holder. For all but one, the distance between the bottom edge of the holder and the sensor was maintained at 500 µm. As there was a range of focal length lenses, several different holders were prepared which controlled the height at which the lens was held. After removing the shutter and lens from the FLIR Lepton 3.5, the holder could be directly threaded into the camera, allowing the lens to be used for imaging.

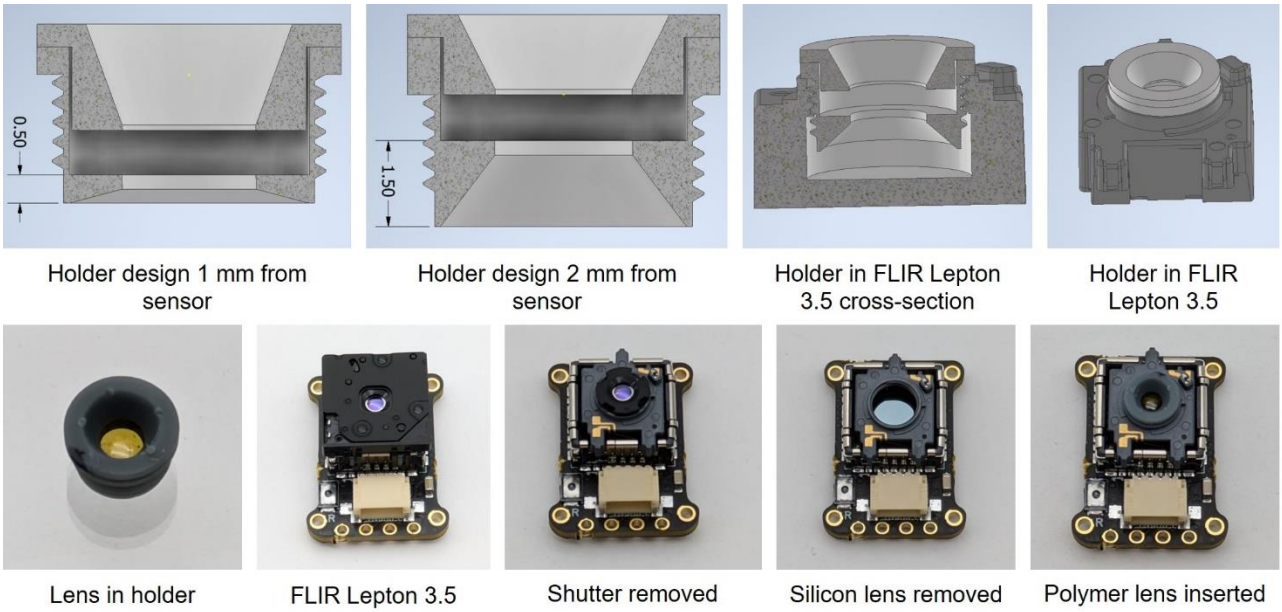

Figure 4.40: 3D printed holder designs and integration into a FLIR Lepton 3.5 thermal camera module.

Masks for imaging with FLIR Lepton 3.5

To investigate the imaging when using the polymer lenses, several masks were prepared. These masks were cut from 3 mm thick acrylic using a laser cutter. A 3D printed holder with a thread allowed these masks to be attached to an optical rail. The masks were then positioned in front of a hotplate for imaging.

Three masks were prepared. The first was a USAF 1951 resolution target. This target is designed to test the resolving power of an optical system.[18] The USAF target utilises lets of line pairs with varying thickness and separation. The maximum resolution of the camera can be determined by the smallest set of three lines which can be resolved. The number of line pairs per millimeter and the width of each line is determined by the element and group number. The group number is written next to every set of 6 lines while the element is written next to its associated group. The elements and groups used for the target as well as their dimensions can be seen in the table below. The only modification to the standard USAF 1951 target is that three square openings with side lengths of 14, 10 and 8 mm were placed instead of an extra two groups due to the limitations on the minimum dimensions of the laser cutter. It should be noted that the target is usually used with visible light and evaluates the resolution of the entire imaging system. When used in this thesis, it is evaluating the FLIR lepton 3.5 as well as the lenses.

Table 4.3: Number of line pairs per millimetre and the width of each line in the USAF 1951 optical target.[18, 19]

	Number of line pairs per millimetre		**Width of line in micrometres (μm)**	
	Group		**Group**	
Element	**-2**	**-1**	**-2**	**-1**
1	0.25	0.5	2000.0	1000.0
2	0.281	0.561	1781.8	890.9
3	0.315	0.630	1587.4	793.7
4	0.354	0.707	1414.2	707.1
5	0.397	0.794	1259.9	630.0
6	0.445	0.891	1122.5	561.2

The next mask was a custom infrared mask based off a design by the Pyun group.[2] While they were not clear on the exact dimensions of this target, it had three sets of 6 lines. For each set, three lines were horizontal and three were vertical. The widths of the lines were 1 mm, 2 mm, 3 mm for the first second and third sets respectively. The horizontal and vertical lines in each set had three different lengths with 3 mm, 7.5 mm and 12 mm and the distance between the outer edges of each group of vertical or horizontal lines was 12 mm. This target is useful to show general imaging and demonstrate the focus of the lens. The range of line widths also gives an indication on the resolution of the imaging system.

The final mask was a star mask. This mask consisted of a 60 mm diameter circle broken into 36 sectors. This gave it a 10 ° pitch with each sector being 5 °. In the centre, there was a circle with a diameter of 10 mm. This mask is useful to see any astigmatism or focusing effects.[20] If there was any warping or inconsistency in the lens focus, the sectors would no longer be straight.

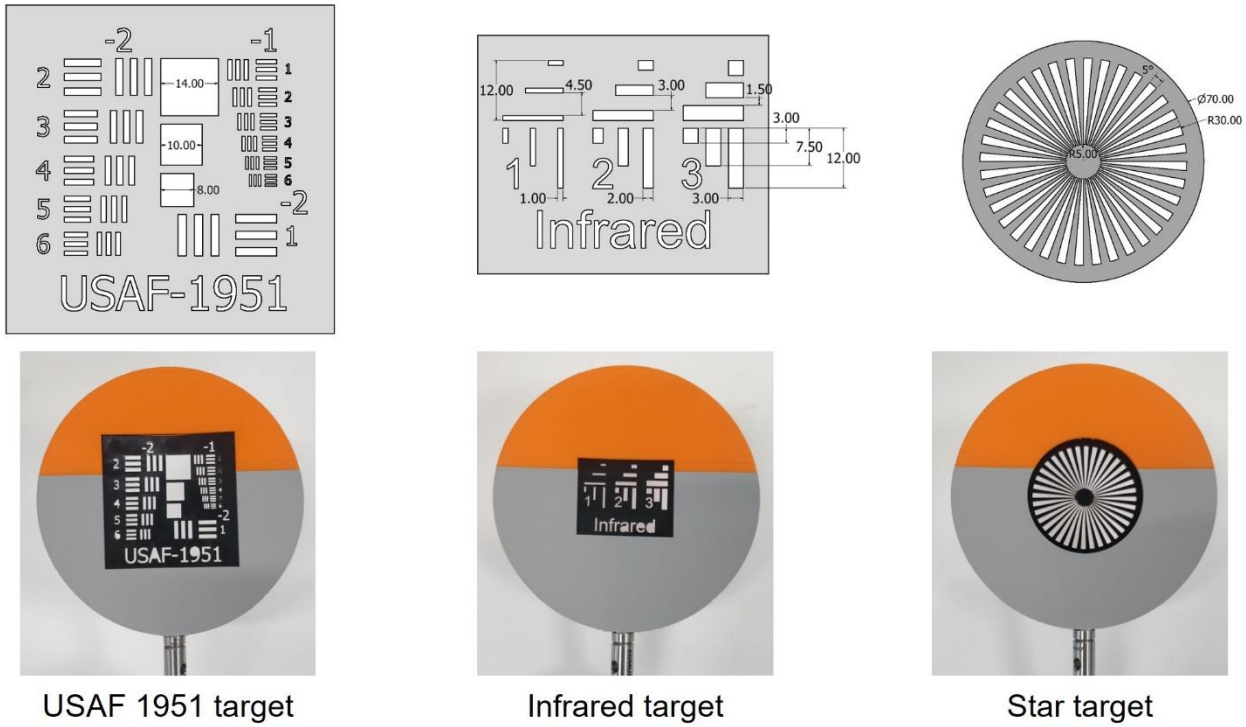

Figure 4.41: Laser cut masks for imaging using polymer lenses on the FLIR Lepton 3.5.

These masks were useful for investigating the imaging of with the polymer lenses. However, there were several limitations. The first is that the masks have a thickness. Each mask was 3 mm thick. This meant that if the mask was not perfectly aligned with the camera, the gaps may become obscured due to parallax effects. For this reason, the lines or openings may appear smaller than the dimensions of the lens. It is possible that the thickness of the masks may also block much of the non-parallel light from reaching the camera, potentially affecting the focus of the lens.

The second limitation of the masks is that they can heat up over time while being close to the heat source. As the masks heat up, they may emit long wave infrared light of their own. As this occurs, the contrast in the images of the masks may decrease. Overall, these limitations mean that the resolution and thermal sensitivity determined using these masks is likely the lower estimate.

Focal length testing

The first feature that was measured for each lens was the optimum distance between the lens and sensor. To determine this, the USAF 1951 target was placed 5 cm from a 100 °C hotplate. The FLIR Lepton 3.5 was mounted onto a 3D printed part with a thread. This allowed it to be attached to an optical rail and placed 20 cm from the mask. The FLIR lepton was plugged in to a laptop and used to take an image of the target. By using 3D printed holders, the distance between the back surface of the lens and the sensor was varied. Between each image, the holder was turned 90 °. As the thread in the FLIR Lepton 3.5 had a pitch of 350 µm, a turn of 90 ° resulted in a change in distance of 87.5 µm. A range of images were taken, and the most focused image was determined qualitatively. This distance was used for all further tests. The exact value obtained by this test is the distance from the plano surface of the lens to the highest point on the sensor.

This distance obtained in this experiment should not be considered as the exact back focal length of the lens as the FLIR Lepton 3.5 has a silicon cap before the sensor. The exact thickness of the cap and separation from the sensor is not known but it is likely on the order of several hundred microns. Despite this, the value obtained in this experiment is useful obtain the optimum focus for future tests.

In general, it was found that the longer focal length lenses gave a sharper image and had a broader range of acceptable sensor to lens images. This is likely due to their narrower field of view, making the image more magnified and increasing the number of pixels used to make up the image. The longer focal length lenses also usually had a higher f number, resulting in a decrease in spherical aberrations. This would result in a greater focus. For more explanation of the results, see the “comparisons of lens imaging” section.

For all lenses apart from lens 7, the USAF 1951 target was used. Lens 7 was tested first and used the infrared target for the focus testing and thermal sensitivity. The FLIR Lepton 3.5 camera has a wavelength range from 8 µm to 14 µm, making it completely within the long wave infrared region.

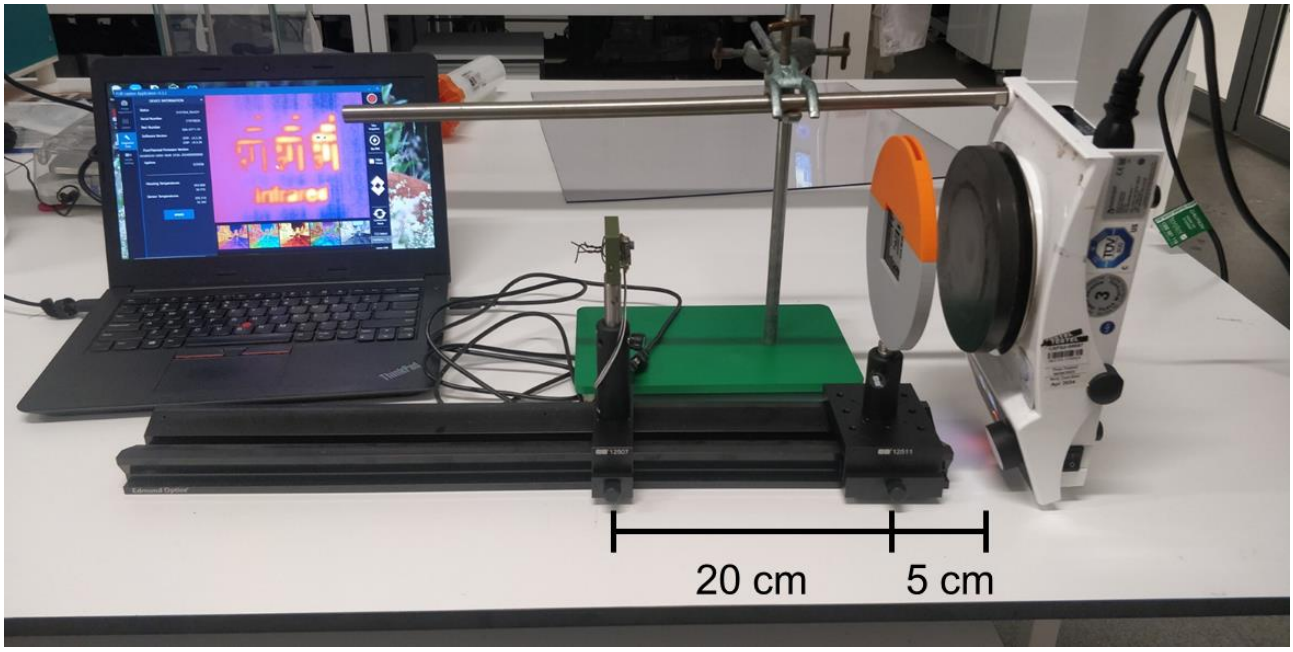

Figure 4.42: Set up used for focus testing with a 100 °C hotplate. The laser cut mask was placed 5 cm from the hotplate and the FLIR Lepton 3.5 was placed 20 cm from the mask.

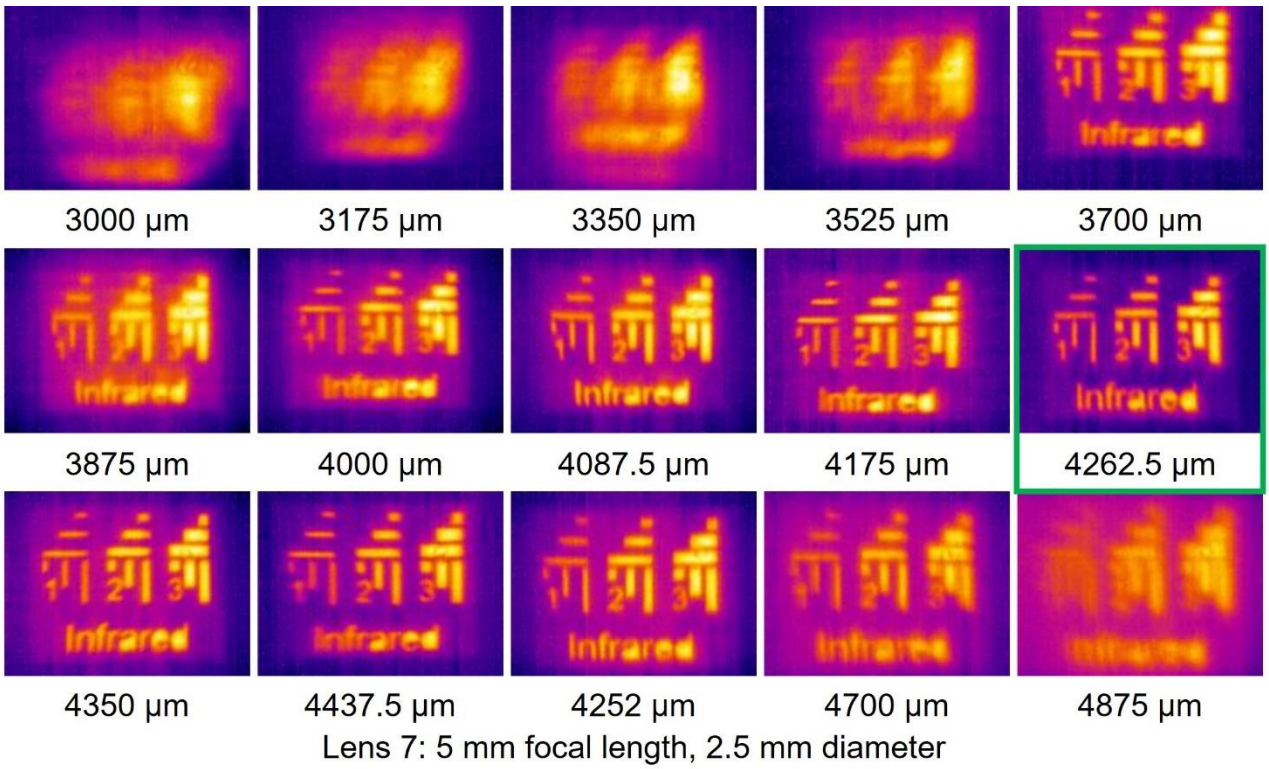

Figure 4.43: Focus testing using lens 7 on a FLIR Lepton 3.5. The distance from the back surface of the lens to the camera sensor was varied with the optimum focus found at 4262.5 µm. Testing was done with a mask placed 5 cm from a 100 °C hotplate and the thermal camera placed 20 cm from the mask.

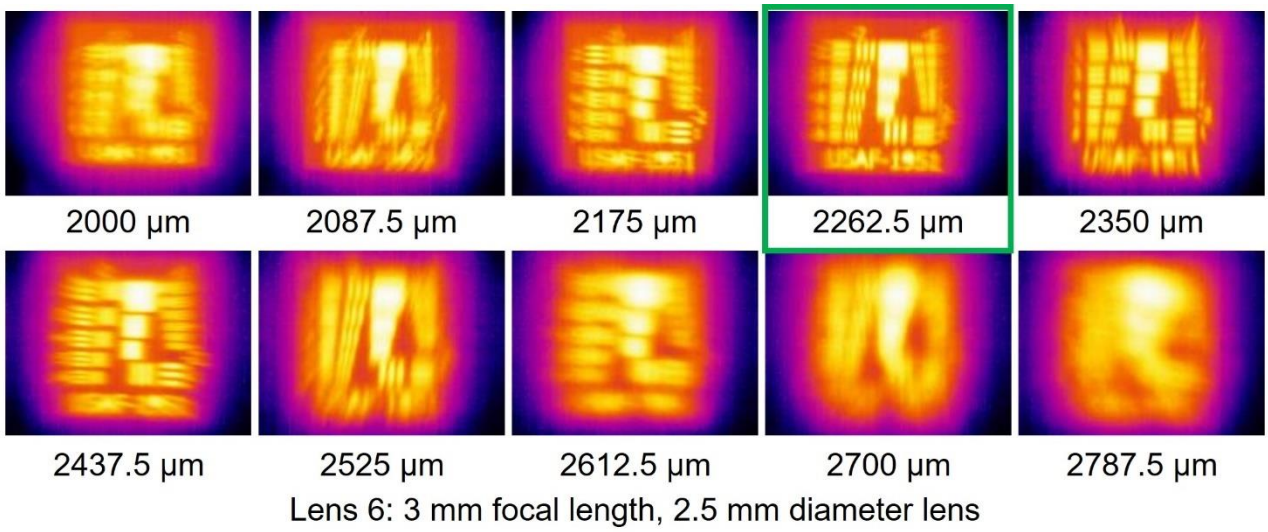

Figure 4.44: Focus testing using lens 6 on a FLIR Lepton 3.5. The distance from the back surface of the lens to the camera sensor was varied with the optimum focus found at 2262.5 µm. Testing was done with a mask placed 5 cm from a 100 °C hotplate and the thermal camera placed 20 cm from the mask.

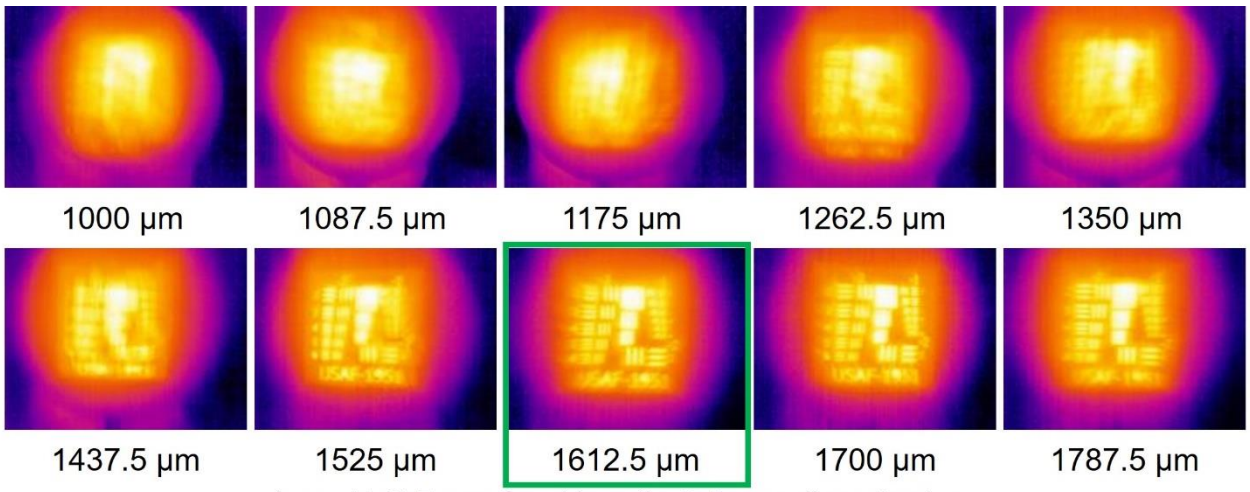

Figure 4.45: Focus testing using lens 5 on a FLIR Lepton 3.5. The distance from the back surface of the lens to the camera sensor was varied with the optimum focus found at 1612.5 µm. Testing was done with a mask placed 5 cm from a 100 °C hotplate and the thermal camera placed 20 cm from the mask.

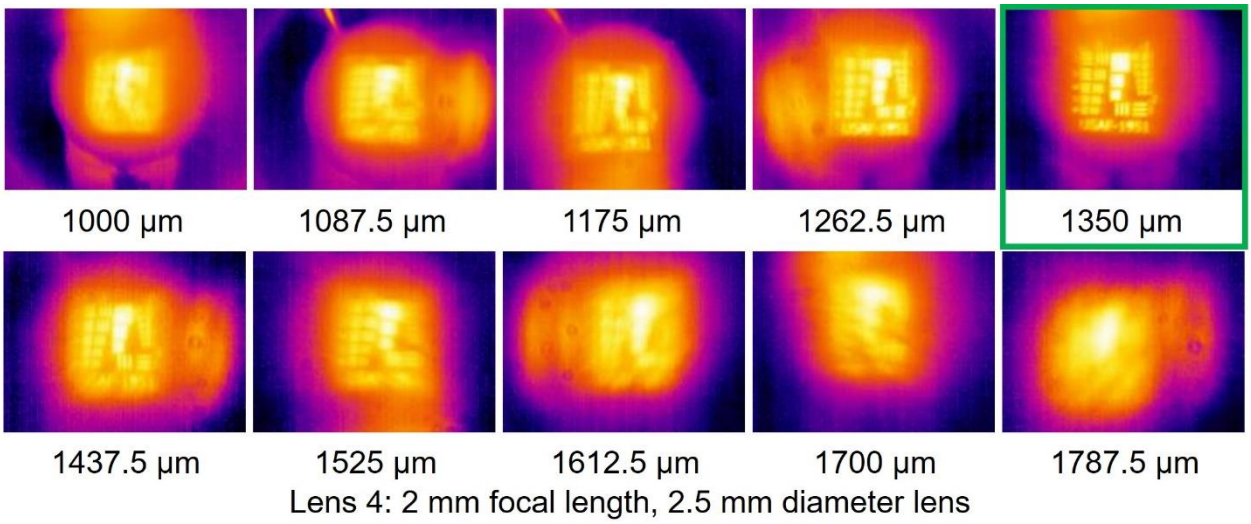

Figure 4.46: Focus testing using lens 4 on a FLIR Lepton 3.5. The distance from the back surface of the lens to the camera sensor was varied with the optimum focus found at 1350 µm. Testing was done with a mask placed 5 cm from a 100 °C hotplate and the thermal camera placed 20 cm from the mask.

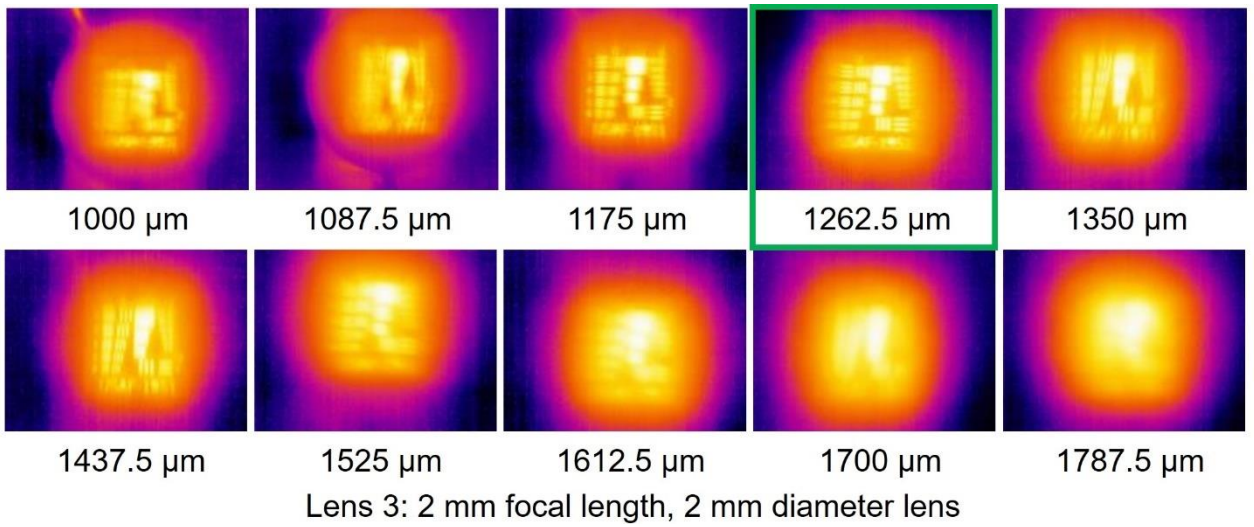

Figure 4.47: Focus testing using lens 3 on a FLIR Lepton 3.5. The distance from the back surface of the lens to the camera sensor was varied with the optimum focus found at 1262.5 µm. Testing was done with a mask placed 5 cm from a 100 °C hotplate and the thermal camera placed 20 cm from the mask.

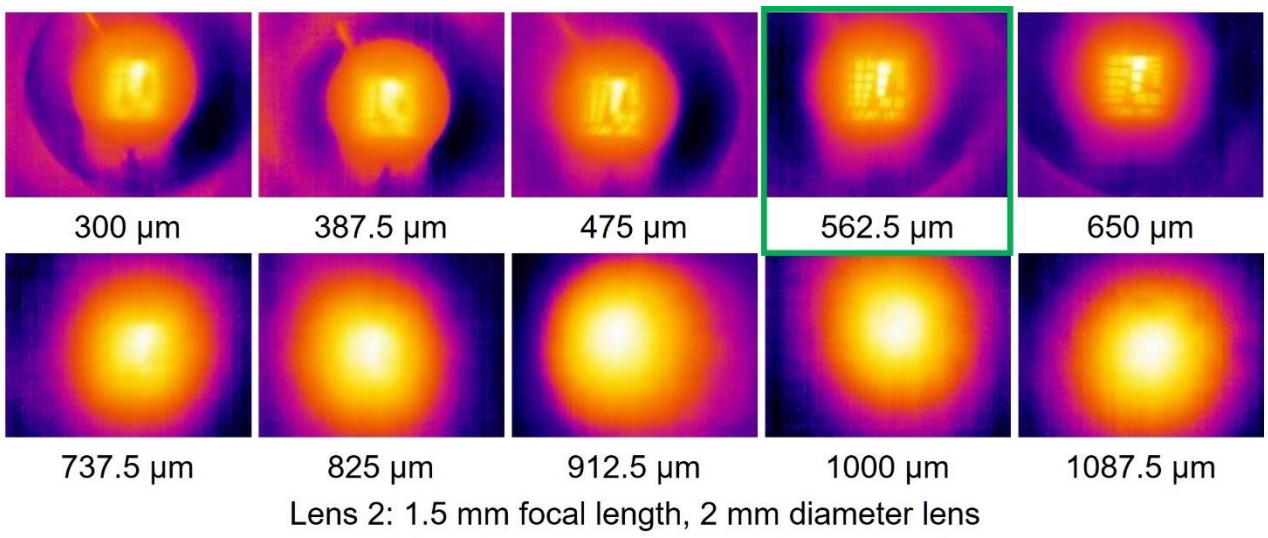

Figure 4.48: Focus testing using lens 2 on a FLIR Lepton 3.5. The distance from the back surface of the lens to the camera sensor was varied with the optimum focus found at 562.5 µm. Testing was done with a mask placed 5 cm from a 100 °C hotplate and the thermal camera placed 20 cm from the mask.

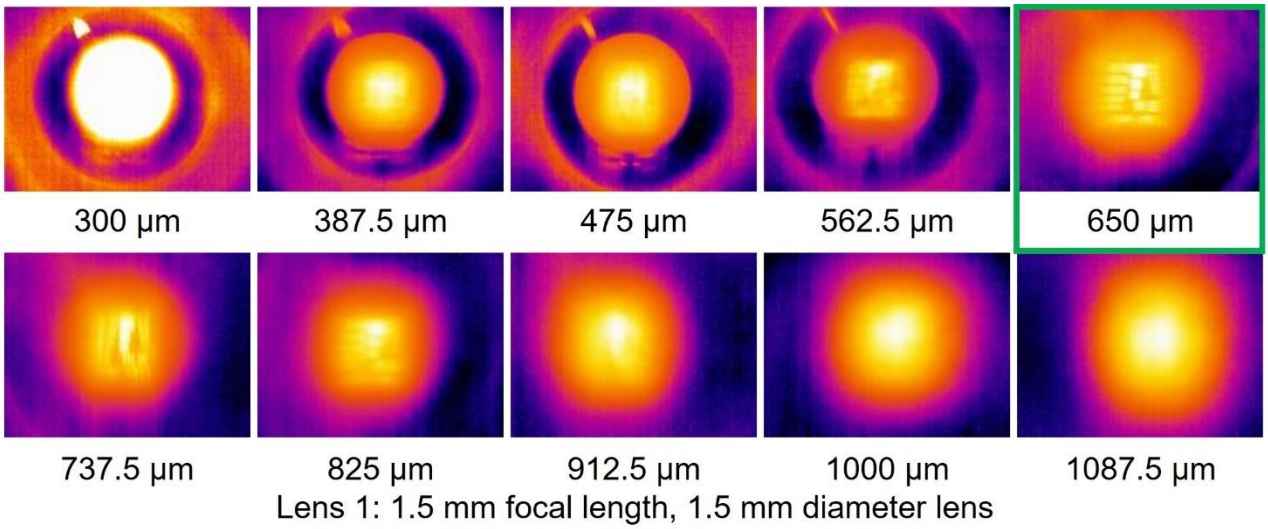

Figure 4.49: Focus testing using lens 1 on a FLIR Lepton 3.5. The distance from the back surface of the lens to the camera sensor was varied with the optimum focus found at 650 µm. Testing was done with a mask placed 5 cm from a 100 °C hotplate and the thermal camera placed 20 cm from the mask.

Thermal sensitivity testing

After finding the optimal focus for each lens, they were tested for thermal sensitivity. The same set up as the focus testing was used. However, in this case, the lens was maintained at the optimum focus using the mount and instead, the temperature of the hotplate was varied. A LWIR image was taken every 10 °C between 30 °C and 100 °C. For all tests, the room temperature was approximately 25 °C.

The thermal sensitivity testing was only quantitative as access to the intensity values for the FLIR Lepton was not possible, but it showed the lowest temperature differential at which clear images can be taken with the camera using the polymer-based lenses. In general, the thermal sensitivity followed the expected trends. The lenses with a higher f-number showed the lowest thermal sensitivity. This was expected as the intensity is inversely proportional to the square of the f-number. The lens where this was most evident was lens 7. Here the contrast in the image was much lower than the other lenses at lower temperature. An in-depth discussion of these effects can be found in the “comparisons of lens imaging” section.

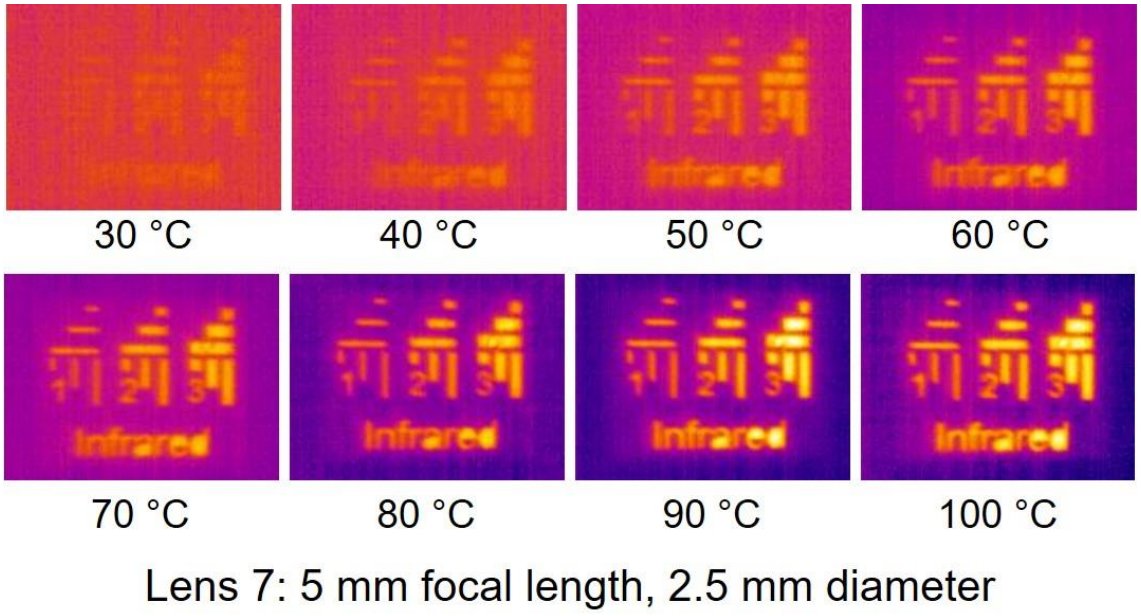

Figure 4.50: Thermal sensitivity testing of lens 7 on a FLIR Lepton 3.5.

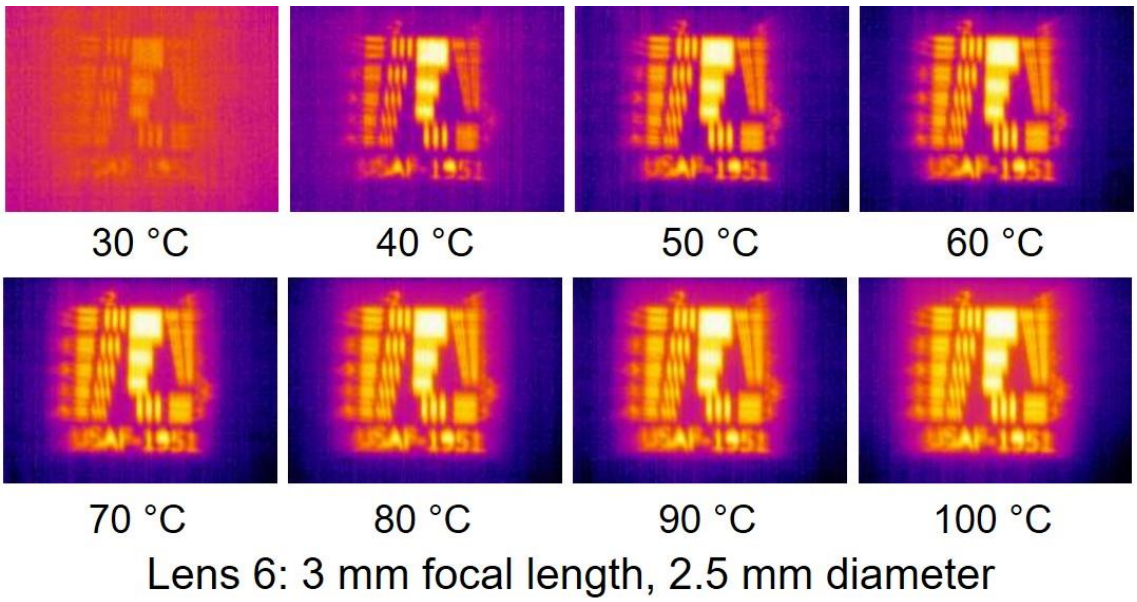

Figure 4.51: Thermal sensitivity testing of lens 6 on a FLIR Lepton 3.5.

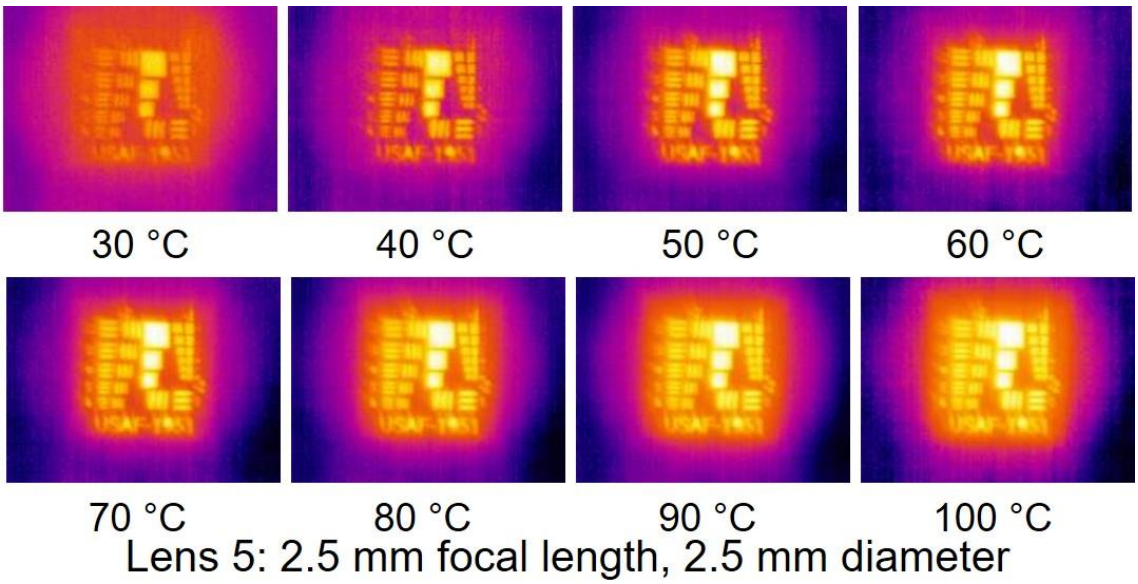

Figure 4.52: Thermal sensitivity testing of lens 5 on a FLIR Lepton 3.5.

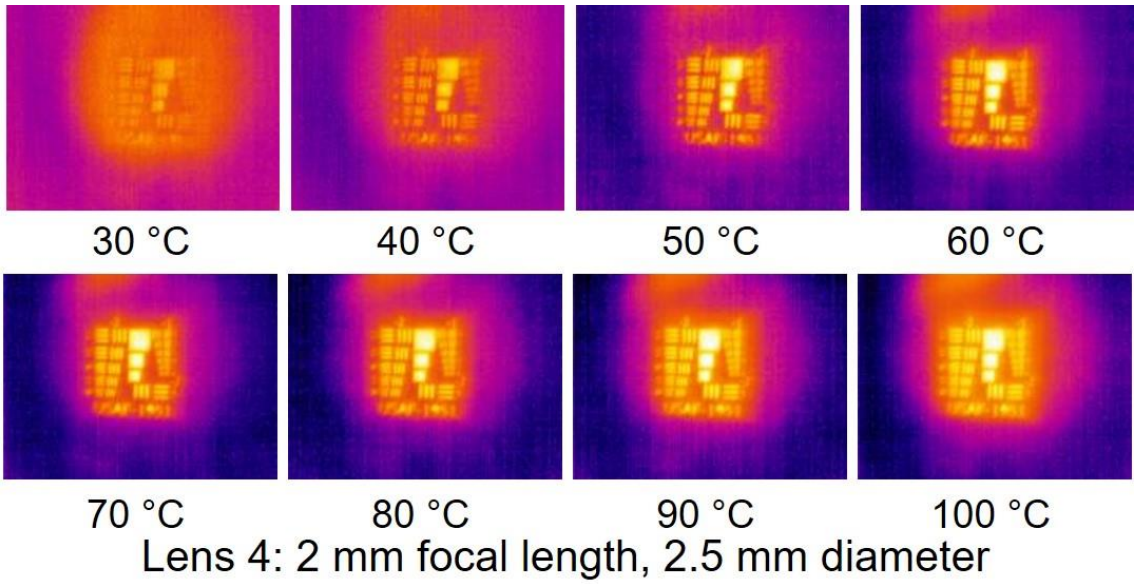

Figure 4.53: Thermal sensitivity testing of lens 4 on a FLIR Lepton 3.5.

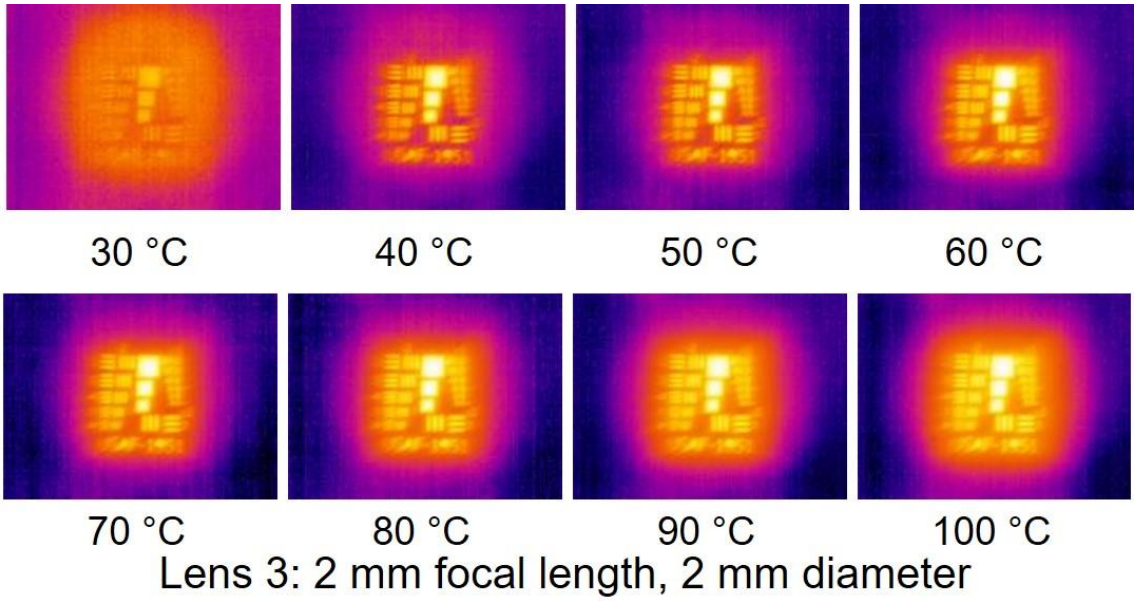

Figure 4.54: Thermal sensitivity testing of lens 3 on a FLIR Lepton 3.5.

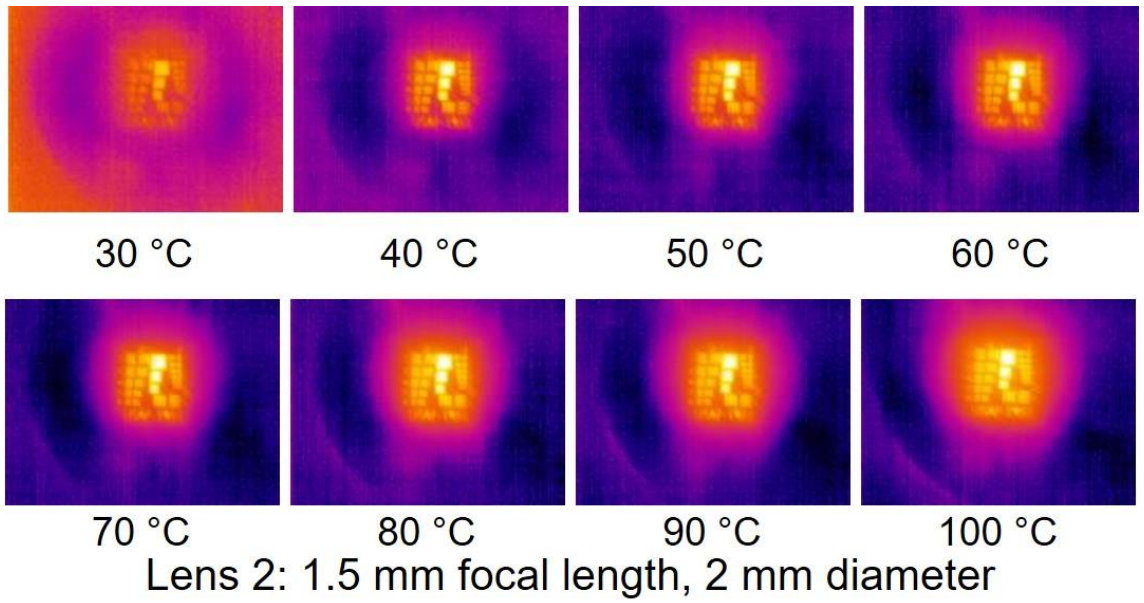

Figure 4.55: Thermal sensitivity testing of lens 2 on a FLIR Lepton 3.5.

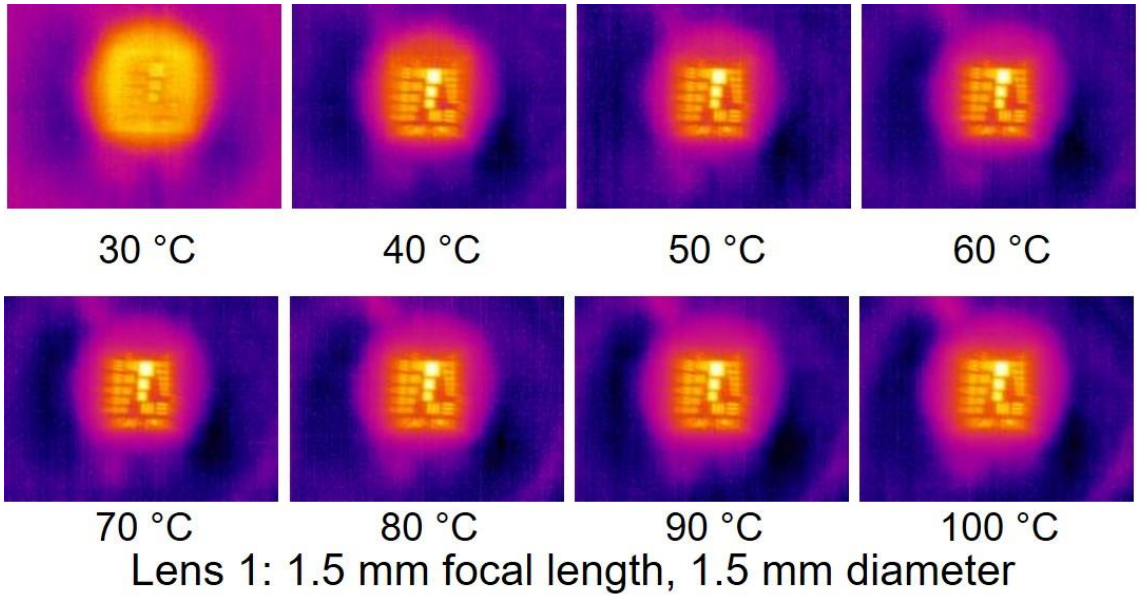

Figure 4.56: Thermal sensitivity testing of lens 1 on a FLIR Lepton 3.5.

Overview of imaging using polymer lenses on FLIR Lepton 3.5 sensor

This section is an overview of all the images taken with each of the lenses on the FLIR Lepton 3.5. The LWIR images of the masks were all taken using the same set up described in the previous two sections. The hotplate was at 100 °C for all the mask images. To go with the images of the masks, images were taken of a person and a hand. The top set of images is a control using the stock silicon doublet. This is an optimised doublet lens made from high quality silicon with an anti-reflection coating on all surfaces. The f-number of this lens is 1.1 and a focal length of 1.77 mm. While there was some loss in intensity, the images using the plano convex polymer-based lenses compare very well to the silicon doublet. This is very impressive for a polymer-based lens particularly when it is considered that they are a simple plano convex.

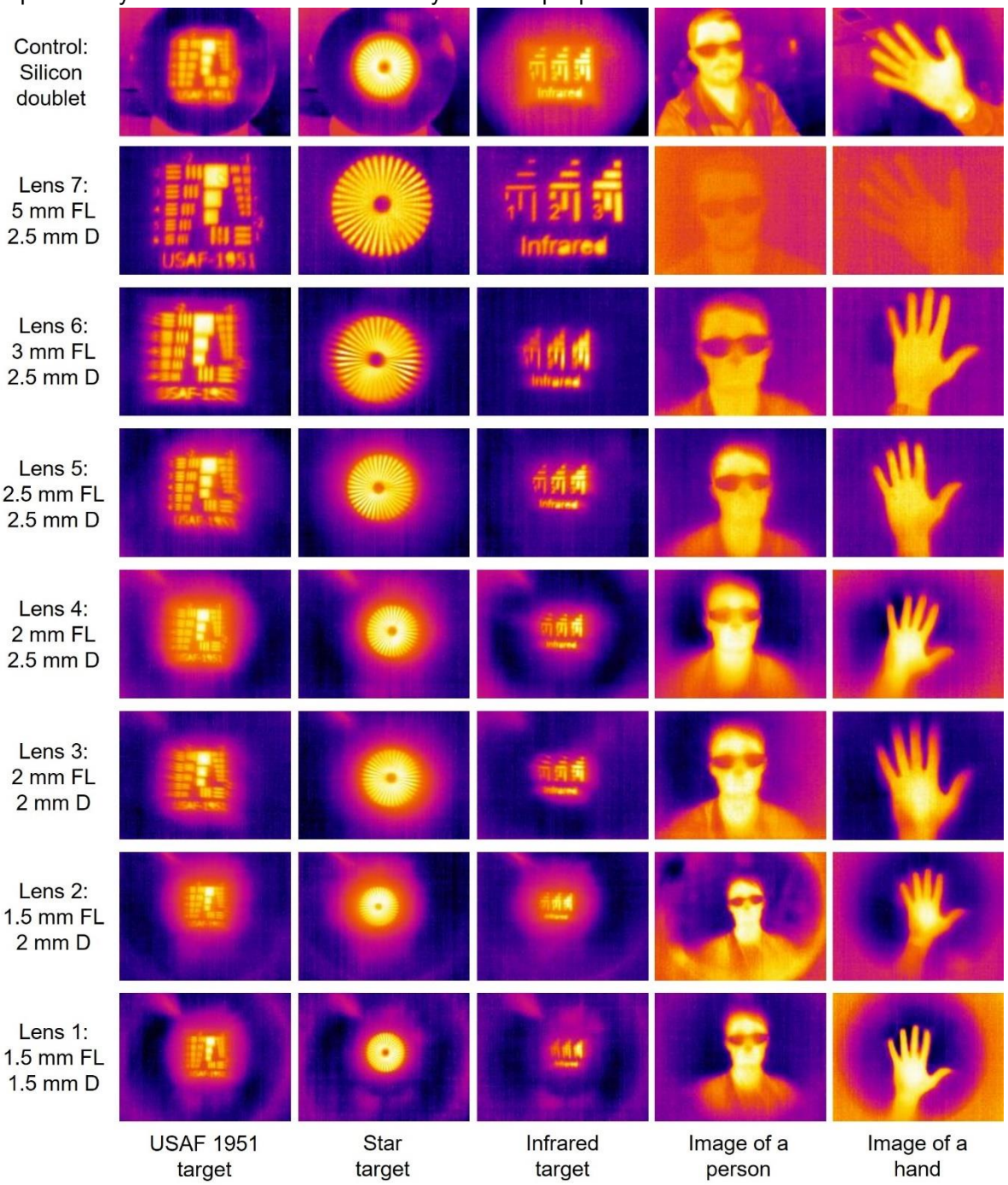

Figure 4.57: LWIR Images taken with norbornane polymer based lenses on a FLIR Lepton 3.5 thermal camera. The images of the targets were all taken using a 100 °C hotplate as a black body radiation source. The target was placed 5 cm from the hotplate and the camera was placed 20 cm from the target.

Comparisons of lens imaging

In this section, the lens imaging will be compared between lenses, with simulation and with the silicon lens. Overall, the performance of the lenses was excellent, showing clear images of a person and a range of targets. It should be noted that it is extremely rare for a polymer lens to be transparent enough to image a person due to the relatively low temperature differential with the ambient environment. Most lenses are only microns thick and often require another material to provide mechanical strength to make a free-standing lens.[2, 21] The lenses in this thesis had a centre thickness of 0.8 mm and were completely free-standing.

To understand the imaging quality, the simulated MTF of each lens was used. To simulate the MTF of each lens, they were put into Zemax Opticstudio. Using light with a wavelength of 10 µm, the MTF at three different angles were calculated. The maximum angle was derived from the horizontal angular field of view of the FLIR Lepton 3.5 when using the lens. This would correspond to the very edge of the images in the section above. The second angle was at half of the horizontal angular field of view and the third angle was paraxial to the lens (angle of 0°). The only exception to this was for lenses 1 and 2. The field of view for these lenses was partially cut off by the holder, resulting in an actual field of view of 55 °. Angles of 55 °, 27.5 ° and 0 ° were used for these lenses. It should be noted that the lenses used in this thesis were all plano convex, so significant spherical aberrations were expected. However, if the imaging matches the simulation, it gives confidence that the polymer lenses would perform as expected with more optimised lens designs.

Each MTF plot showed the diffraction limited line in black. This is the theoretical optimal focus that the lens could have. As these were plano convex lenses, they were not diffraction limited. Both the tangential and sagittal MTF plots are shown for each angle of light. Sagittal means the test lines that run parallel to the line running from the centre to the corner while the tangential lines are perpendicular. [22]The tangential lines are solid in the MTF and will be primarily used for any comparisons. To aid in the understanding of the MTF plots, a brief explanation will be given.[22-24] The y-axis of an MTF plot gives the contrast in the image. A higher contrast will give a clearer and higher quality image.[23] The x-axis is the spatial frequency. This is the number of line pairs per mm. A simplistic explanation of this is that a larger value on the x-axis indicates a smaller feature that the lens is attempting to focus onto the sensor. In general, a human eye needs a contrast of at least 0.1 to make out an image. A lens that has a higher contrast or modulus of the OTF at a particular spatial frequency will give a clearer image.

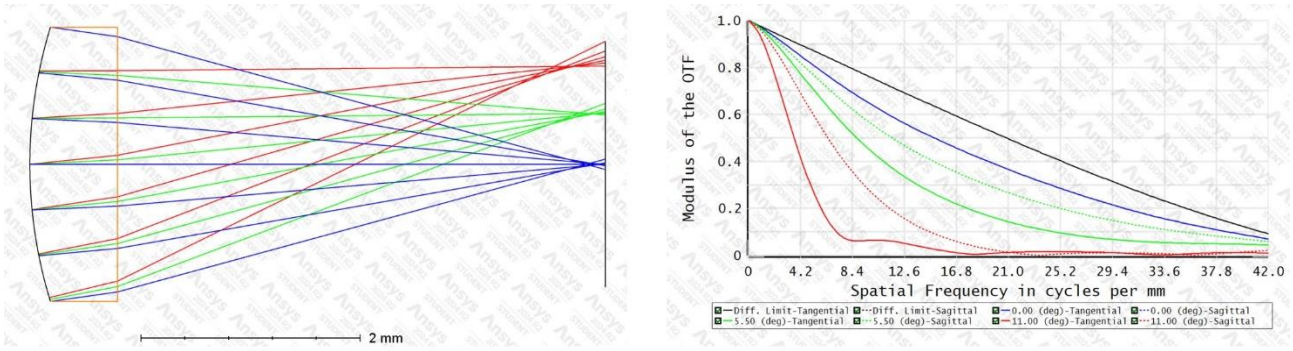

Lens 7 : 5 mm focal length, 2.5 mm diameter

Figure 4.58: Lens cross section and MTF for lens 7 which has a focal length of 5 mm giving it an f-number of f/2. MTF at angles of 0 °, 5.5 ° and 11 ° are shown.

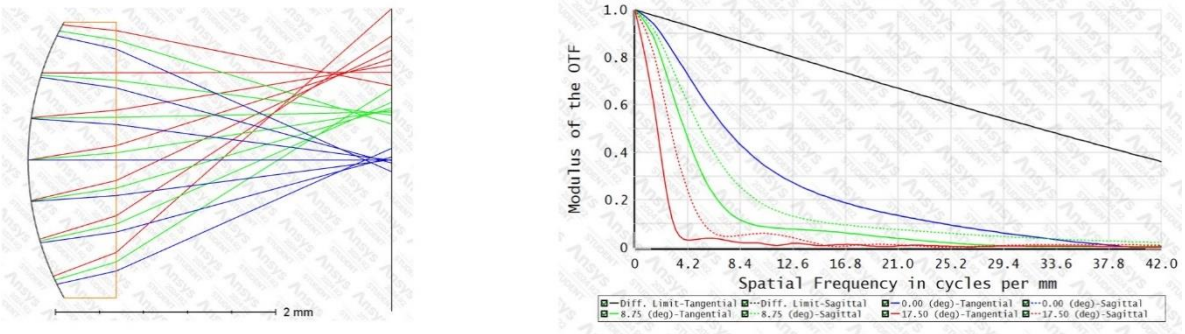

Lens 6 : 3 mm focal length, 2.5 mm diameter

Figure 4.59: Lens cross section and MTF for lens 6 which has a focal length of 3 mm giving it an f-number of f/1.2. MTF at angles of 0 °, 8.75 ° and 17.5 ° are shown.

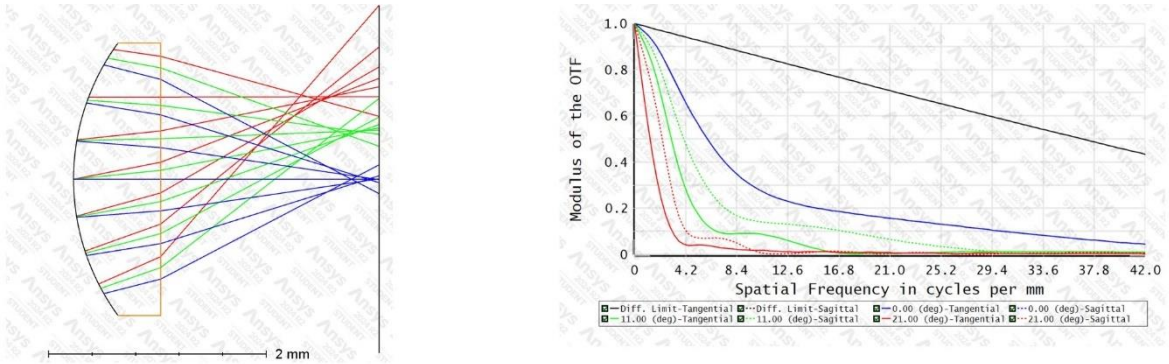

Lens 5 : 2.5 mm focal length, 2.5 mm diameter

Figure 4.60: Lens cross section and MTF for lens 5 which has a focal length of 2.5 mm giving it an f-number of 1. MTF at angles of 0 °, 10.5 ° and 21 ° are shown.

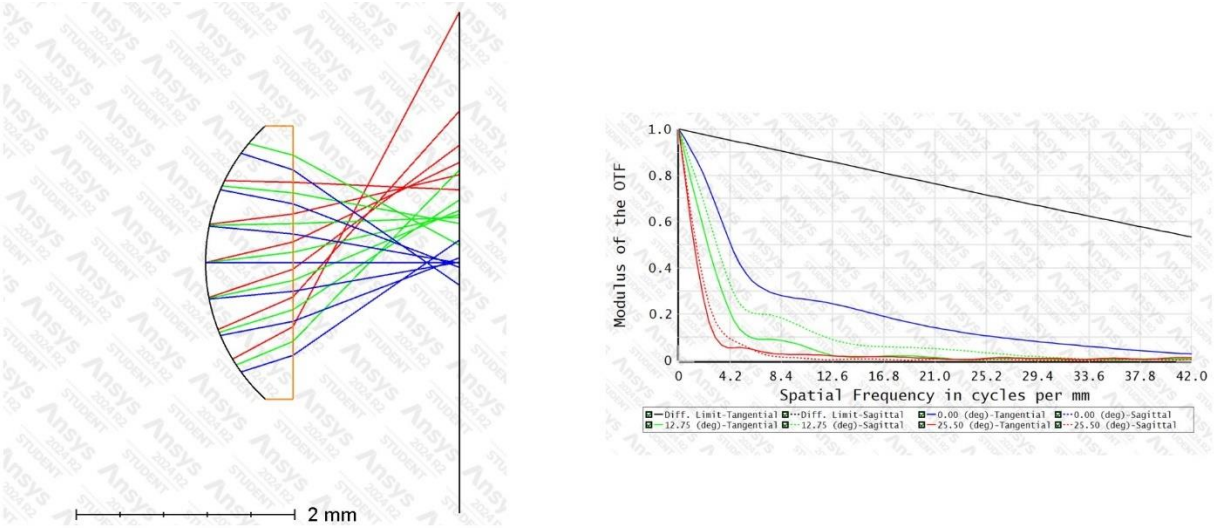

Lens 4 : 2 mm focal length, 2.5 mm diameter

Figure 4.61: Lens cross section and MTF for lens 7 which has a focal length of 2 mm giving it an f number of 0.8. MTF at angles of 0 °, 12.75 ° and 25.5 ° are shown.

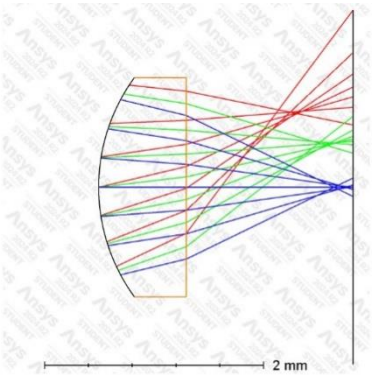

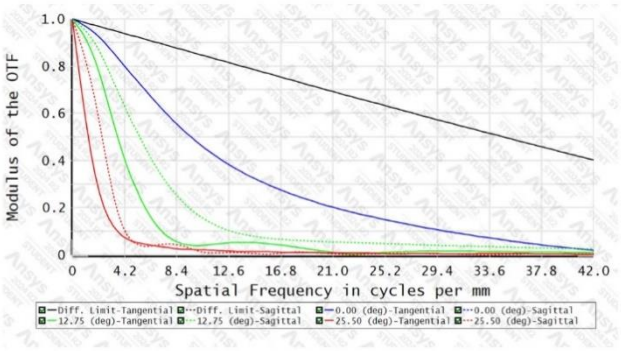

Lens 3 : 2 mm focal length, 2 mm diameter

Figure 4.62: Lens cross section and MTF for lens 7 which has a focal length of 2 mm giving it an f-number of f/1. MTF at angles of 0 °, 12.75 ° and 25.5 ° are shown.

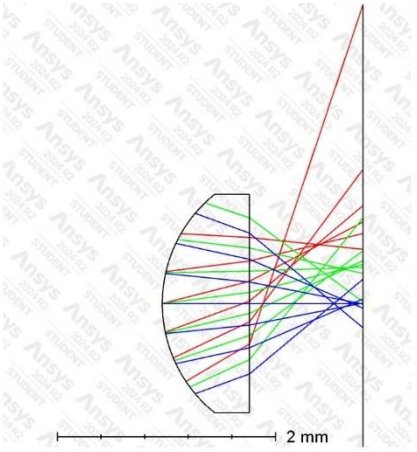

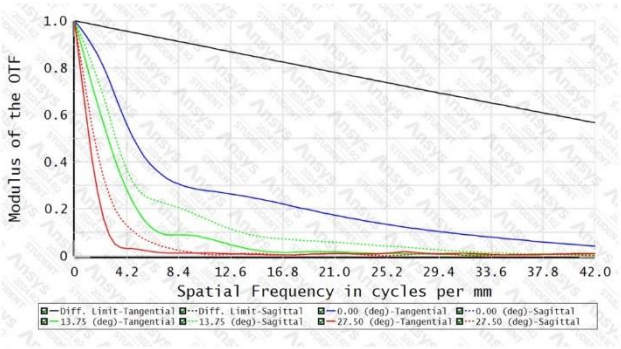

Lens 2 : 1.5 mm focal length, 2 mm diameter

Figure 4.63: Lens cross section and MTF for lens 2 which has a focal length of 1.5 mm giving it an f-number of f/0.75. MTF at angles of 0 °, 13.75 ° and 27.5 ° are shown.

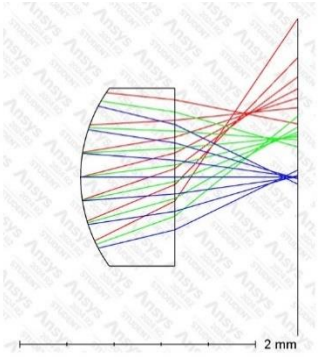

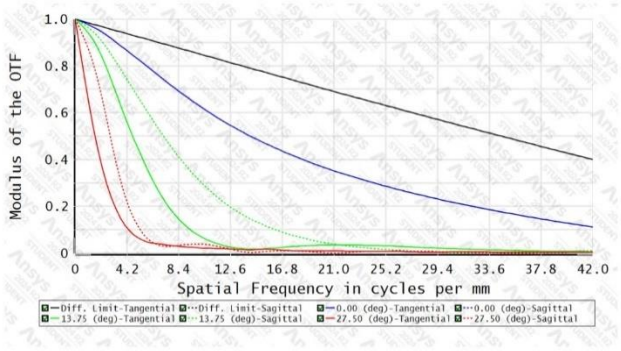

Lens 1 : 1.5 mm focal length, 1.5 mm diameter

Figure 4.64: Lens cross section and MTF for lens 1 which has a focal length of 1.5 mm giving it an f-number of f/1. MTF at angles of 0 °, 13.75 ° and 27.5 ° are shown.

The imaging with the polymer lenses indicated that the lenses with the higher f-number had greater imaging quality. This could be seen most clearly in lens 7 which showed excellent resolution of the USAF-1951 target as well as the star and infrared targets. This lens had a f-number of 2 which was much greater than any of the other lenses. The MTF plots followed the same trend. Lens 7 showed a much greater contrast than any of the other lenses. This could also be seen qualitatively in the ray diagrams as the rays of light do not spread out nearly as much in lens 7 as the other lenses.

One of the biggest factors that contribute to the improved image quality of the lenses with a higher f-number is spherical aberrations. Spherical aberrations are caused by the convex surface of the lens having a spherical surface. This means that the curve would make up part of a sphere. While this is easier for manufacturing and is very common, spherical surfacers are not optimal for imaging lenses. This is because the light that strikes the surface off-centre is not refracted to the same degree as those that strike near the centre.[25] Spherical aberrations are proportional to the fourth power of the diameter over the third power of the focal length. As the f-number is equal to the focal length over the diameter, the spherical aberrations are inversely proportional to the f-number. To visualise this effect, the cross section of lenses 4 and 3 are shown. These lenses both have a focal length of 2 mm but have different f-numbers. Lens 4 has an f-number of 0.8 while lens 3 has an f-number of 1. Only the paraxial rays are shown for clarity, but they clearly have a greater spread in lens 4.

To correct for spherical aberrations, the most common solution is to use an aspheric surface.[26] An aspheric surface does not make up a portion of a sphere but instead allows for greater control of the optical properties. While aspheric surfaces are more difficult to manufacure, they are well suited to the casting method used to prepare the polymer lenses. As many lenses could be made from one silicone mould and many moulds could be made from one lens positive, the aspheric surface would only need to be manufactured once and could be used many times over. While it was not possible to complete in this thesis due to time constraints, future lens designs should incorporate an aspheric surface to reduce the effect of spherical aberrations. In the figure below, an optimised aspheric lens with the same focal length and f-number as lens 4 is shown. This lens significantly reduces the effect of spherical aberrations.

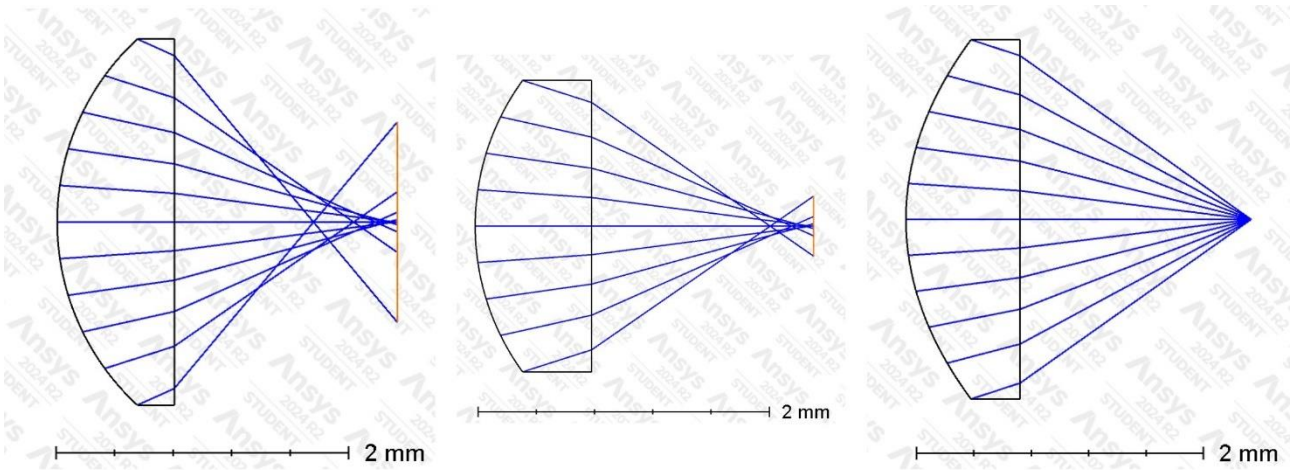

Figure 4.65: Comparison of spherical aberrations between lenses with different f-numbers and an optimised aspheric lens.

The other effect that is clear in the imaging and the MTF simulations is that the images prepared by the lenses have a decrease in quality as they near the edge of the image. This shows its self in the MTF plots as the plots at a greater angle have a lower contrast than the paraxial rays. The main reason for the reduction in image quality is Petzval field curvature. Petzval field curvature is where light at an angle does not focus at the same point as the paraxial rays. Instead, the focal pionts curve away from the focal plane as the angle increases.[27]

One way to address Petzvel field curvature is to use a curved sensor. However, this can be very expensive to manufacture.[28] Therefore, the field curvature is usually corrected with lens design. To correct the field curvature with the lens design, additional optical elements are often required. All the lenses in this thesis have a plano or flat side. To address field curvature, the most common way is to have both positive and negative surfaces. By combining these surfaces and optimising with software, the field curvature can be reduced. While it is possible to reduce field curvature with a singlet lens, often additional elements are used. This gives more surfaces and generally optimises to a higher quality lens. However, there are disadvantages to multi-element lenses like alignment of the lenses, increased losses from reflections and absorption and an increase in cost.[29] Therefore, it is usually a trade off between improved image quality and these practical issues.

Below is an image demonstrating the effect of field curvature. The cross section of lens 4 has a clear Petzval field curvature where the angled rays are not focussed in the same plane as the paraxial rays. The LWIR images show the practical effect of this as the finger is focused at the centre but unfocused at the edge. Finally, an example of a aspheric doublet which corrects for field curvature is shown. As can be seen here, the light at different angles all focus at the imaging plane. The angles used for this figure was 0 °, 10 ° and 20 °.

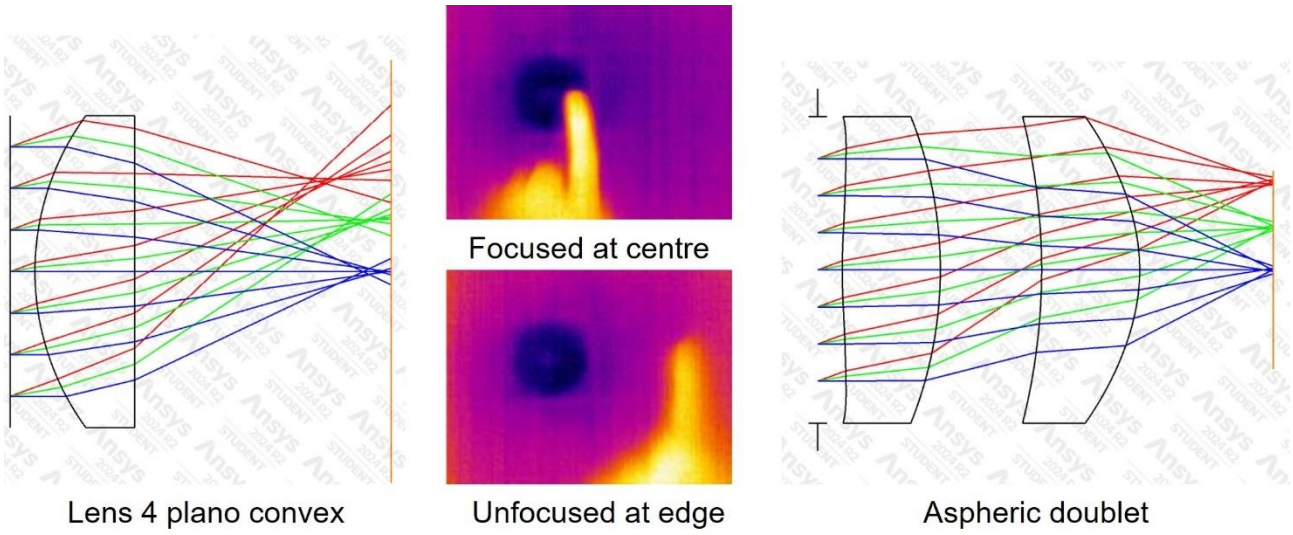

Figure 4.66: Lens 4 with parallel rays at 0 °, 10 ° and 20 ° showing Petzval field curvature. LWIR images taken on FLIR Lepton 3.5 with lens 4 showing a focused image at the centre and an unfocused image at the edge. Finally, a more optimised doublet lens which corrects for field curvature is shown with parallel rays at 0 °, 10 ° and 20 °.

Finally, the lenses show differences in the intensity of light that reaches the sensor. The lenses with a greater f number show a decrease in intensity. This is expected as the intensity of light is inversely proportional to the square of the f-number of a lens.[30] This is why the f-number is often considered as the ability for a lens to collect light. The f-number is given by the focal length divided by the diameter of the entrance pupil. For all the lenses used in this thesis, no aperture stops are used so the pupil diameter is equal to the lens diameter.

The relationship between f-number and intensity could be explained by considering two lenses with the same focal length but where one had a diameter that is twice as large as the other. The f-number of the lens with the larger diameter would be half that of the other lens. As the diameter is twice as large, the entrance pupil would have four times the area, collecting four times as much light. The same is also true of two lenses which have the same pupil diameter but where one has half the focal length. The lens with a longer focal length would have twice the f-number. While the pupil of both lenses would have the same area, the lens with a longer focal length would project an image of the same object that is twice as wide and twice as high. This means that it would be spread over four times as many pixels but the intensity at each pixel will be reduced by four times.

This effect is clear in the LWIR imaging with the polymer lenses. The lenses with a lower f-number had a significantly increased intensity. To demonstrate this, the LWIR images of a person and a hand for lenses 4, 5, 6 and 7 are shown below. These lenses all had the same diameter but differing focal lengths, resulting in f-numbers that ranged from 0.8 to 2. While the LWIR images produced by lens 4 are bright, the images produced by lens 7 barely have enough intensity to make out the image.

The intensity of light is extremely important in thermal imaging. This is because the intensity of light directly affects the thermal sensitivity of the camera.[30] Therefore, lens designs should try to keep the f-number as low as possible while still achieving an appropriate image quality.

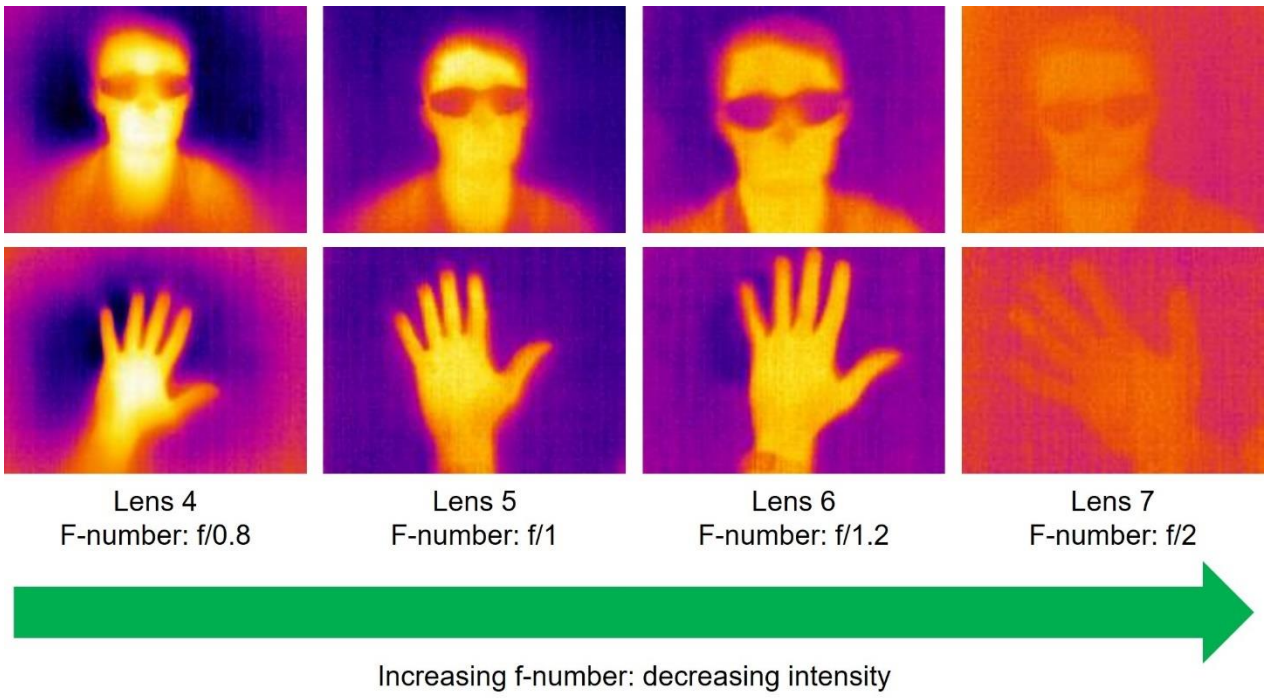

Figure 4.67: Long wave infrared images of a person and a hand with lenses 4-7 on a FLIR Lepton 3.5. The intensity of the image decreases with the square of the f-number.

Compression moulding to prepare windows and lenses

The polymer lenses were demonstrated to have fantastic imaging potential. To compliment this, a method to manufacture lenses and windows scalably and without losses in imaging quality. For this reason, a method of compression moulding was developed. Compression moulding has very major advantages over the casting method that was used to prepare all the lenses to this point. The first is a higher throughput. Compression moulding is a very scalable process with moulds which would prepare many lenses at one in automated facilities. The second is that there is minimal waste. When casting the polymer, there is a significant amount of waste due to polymer offcuts in the funnel and outlet portions of the mould. Each lens only weighed around 12 mg but over 150 mg of polymer was used to prepare each lens. If compression moulding was used, these offcuts could be ground into a powder and recycled. Damaged or scratched lenses could also be completely recycled in this same way, reducing the overall wastage. One final advantage of compression moulding is that the polymer could be prepared ahead of time and in a different scale to the moulding of the polymer. This way, the polymer could be prepared in a very large batch and prepared as pellets which could be stored and transported if required. The pellets could the be put into a compression moulding die and made into a window or lens at a different time. This is not possible with casting methods as the reaction and moulding all need to occur rapidly.

To explore the possibility of compression moulding the polymer, a heated die set from Across International was purchased. This die set had a diameter of 13 mm and could be heated to 250 °C. This die could be placed into a hydraulic press to prepare samples. The first test was to prepare a window of the polymer that could be compared to windows made by the casting method. To prepare the window, 250 mg of polymer was ground into a powder. A silicone-based release agent was applied to the core pieces of the die and the polymer was inserted. Following this the die was heated to 185 °C. It was found that if a single polymer piece was used, a temperature of 160 °C was adequate, however, for a powder, 185 °C was required. After the temperature was reached, the die was placed in a manual pellet press and compressed to 10 MPa for 30 minutes while heating was maintained. After this point, the die was removed from the press and cooled to room temperature using water cooled aluminium plates. Once the die reached room temperature, the window was extracted. The window was polished with fine sandpaper ranging from 1500 to 12000 grit and finished with a 1 µm polishing compound. After polishing, the window had a thickness of 0.585 mm.

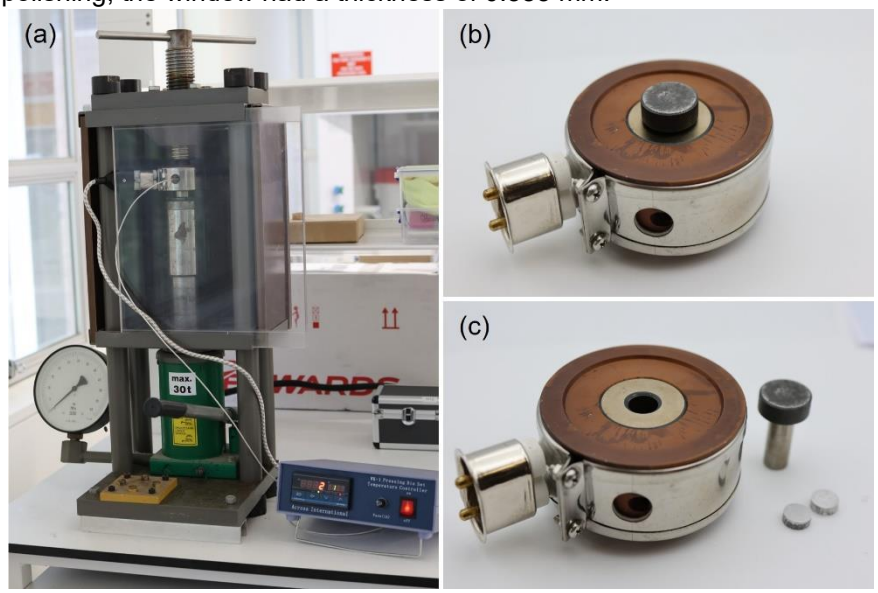

Figure 4.68: Press used for heated compression moulding. (b-c) Heated die used for compression moulding.

To test if the optical properties of the compression moulded window matched the cast windows, it was tested by transmission FTIR. Using a Perkin Elmer Frontier FTIR, the polymer window was tested for transmittance between 2 μm and 20 μm over a total of 16 scans. The average in the MWIR (3 μm – 5 μm) and the LWIR (7 μm – 14 μm) was calculated by integrating under the line and dividing by the wavelength range. The average MWIR transmission was 72.5 % and the average LWIR transmission was 28.3 %. This was greater than the cast window which had a transmission of 24.7 % for a similar thickness. The increase in transmission was attributed an improvement in the polishing procedure leading to an improved surface finish. Importantly, no optical quality was lost and there was no change in the FTIR spectrum. The window was also placed in front of the lens of a FLIR E6 thermal camera and a LWIR image was taken of a person and a hand to test image quality. The images taken through the compression moulded window were excellent.

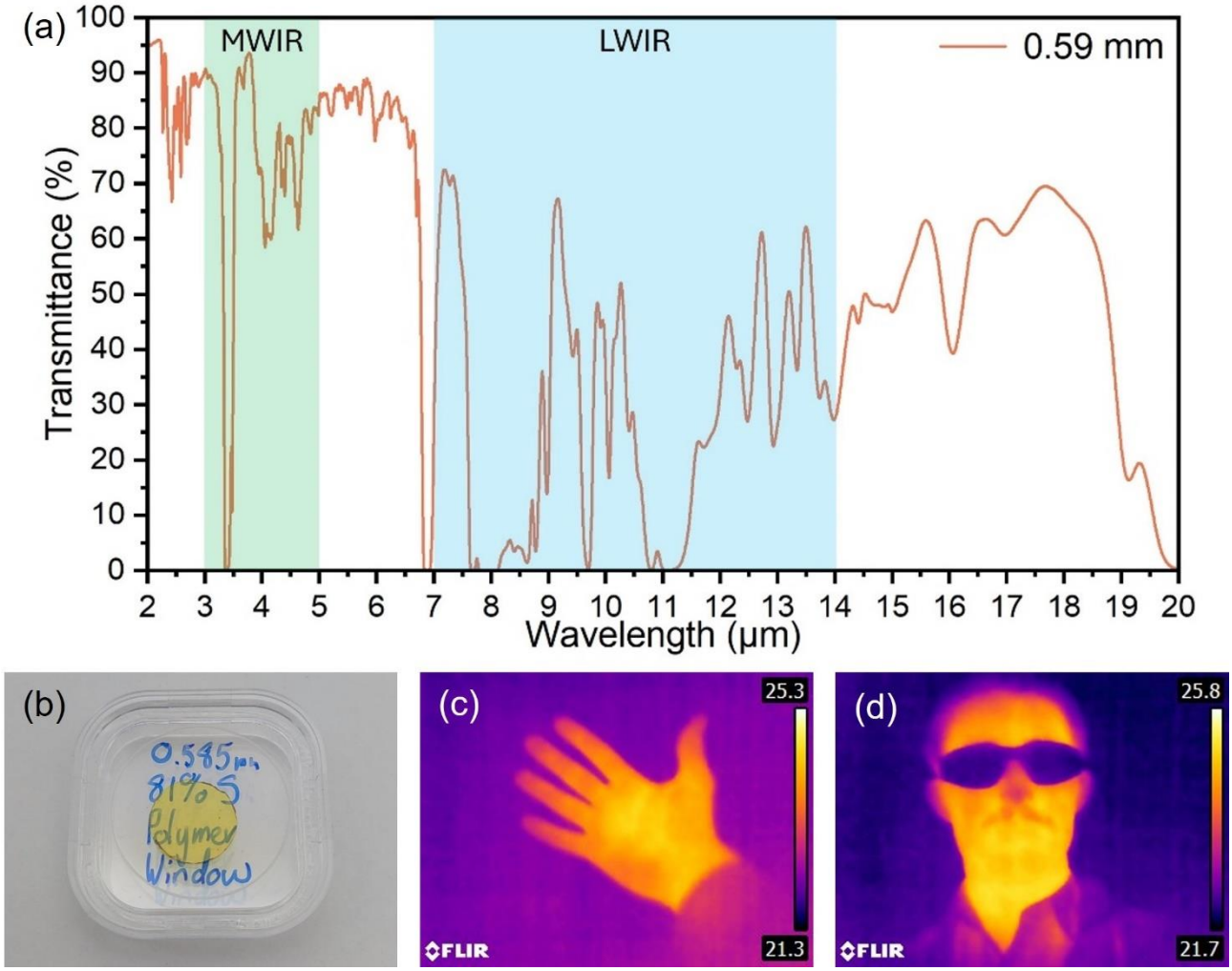

Figure 4.69: (a) FTIR spectrum of 0.585 mm thick window made from compression moulded 81 % sulfur norbornane bistrisulfide polymer window. (b) Photo of compression moulded window. (c) LWIR image of hand through compression moulded window taken with FLIR E6 thermal camera. (d) LWIR image of person through compression moulded window taken with FLIR E6 thermal camera.

After the promising results of the polymer window, some compression moulded lenses were made. To prepare the compression moulded lenses, come custom inserts were designed and machined to fit into the heated die set. One side of the insert was flat like the inserts used to make the window. The other side had five concave indents. These indents had a radius of 2.12 mm and a diameter of 2.5 mm. This design would prepare lenses with the same focal length and diameter as lens 5. Unlike the casted lenses, the compression moulded ones

did not include any carrier material. This was to aid in the removal of the polymer from the die after compression. The thickness of the lenses was controlled by the dosing of the polymer. The inserts were machined out of aluminium 7075 from JLCPCB.

To prepare the compression moulded lenses, the die inserts were sprayed with a silicone-based release agent. 150 mg of ground polymer was placed into the die, and it was heated to 185 °C. After reaching temperature, the die was placed into a manual pellet press and compressed to 10 MPa for 30 minutes. Following this, the die was cooled, and the polymer lenses were removed from the die. The 5 lenses were initially connected with a thin sheet of polymer. This was scored and removed using a scalpel to separate the lenses. These first lenses were designed only as a proof of concept and likely require improvements in surface roughness to match the cast lenses.

To test the compression moulded lenses, they were placed into a holder for the FLIR Lepton 3.5. After finding the optimal focal point for the lens by adjusting the thread, an image of a person and a hand was taken. While there was significant blurring, an image could be made. This is very promising and demonstrates the potential for lenses to be prepared using a compression moulding technique. Due to time constraints, the compression moulding could not be optimised further. However, the image quality could be significantly improved by polishing the die inserts to provide a lower surface roughness and experimenting with different release agents that leave a higher quality finish.

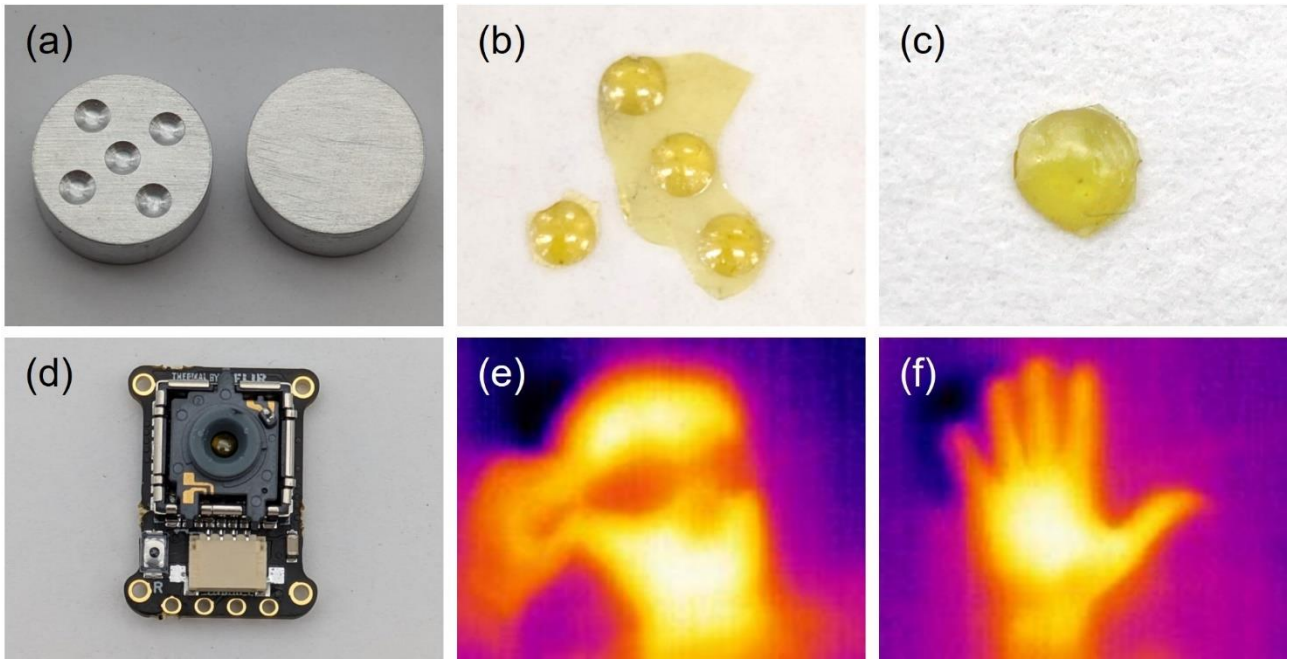

Figure 4.70: (a) Photo of custom aluminium inserts for heated press. (b) Photo of lenses after removed from mould and separation. (c) Photo of compression moulded lens made from 81 % sulfur norbornane bistrisulfide polymer. (d) Photo of FLIR Lepton 3.5 with polymer lens. (e) LWIR image of person taken with FLIR Lepton 3.5 using compression moulded lens. (f) LWIR image of hand taken with FLIR Lepton 3.5 using compression moulded lens.

Chapter conclusions

This chapter explored the application of sulfur-based polymers in long wave infrared imaging applications. It started with an overview of some of the highest performing polymers in literature. By extracting the infrared transmittance from the several papers, the long wave infrared transmittance could be compared. It was found that the cyclopentadiene based polymers from chapter 2 and the norbornane bistrisulfide polymers from chapter 3 were some of the highest performing polymers in literature.

With this knowledge in hand, the high transmission was exploited for use in thermal imaging. The cyclopentadiene based polymer was cost effective to produce, opaque to visible light and had high transmission in the LWIR region. This made it well suited to prepare a sheet which could serve to protect and conceal a thermal camera. Despite being black and blocking all visible light from reaching the camera, it was transparent to LWIR radiation, allowing the thermal camera to still be used. This camera was used to image a dog and some chickens, demonstrating a potential use for the polymer. The cyclopentadiene polymer also had the advantage of being able to vary the sulfur content to make the glass transition temperature above room temperature, making it brittle or below room temperature, making it flexible. The flexible polymer could be used as a protective screen as it would flex when impacted, rather than shattering.

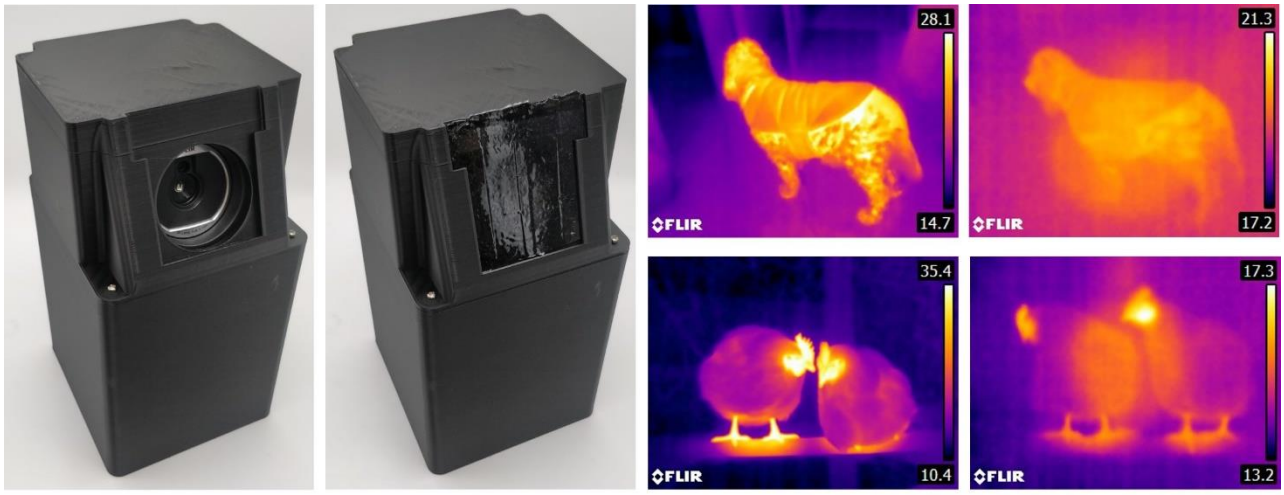

Figure 4.71: Long wave infarred transparent sheet made form 67 % sulfur cyclopentadiene polymer.

Following the application as a transparent sheet, the cyclopentadiene polymer was utilised to prepare a range of lenses. Both plano concave and convex lenses were prepared as well as an injection moulded Fresnel lens. These lenses were shown to magnify infrared light before reaching a FLIR E6 thermal camera. This was a significant milestone for the project as to this point, the sulfur-based polymers had only been used as windows sheets with no optical power.

The injection moulding of the Fresnel lens was also a very important achievement as it demonstrated a potential rough for high throughput synthesis of LWIR optics. The major advantages of sulfur-based polymers over conventional materials like germanium and zinc selenide is their relatively low cost and ease of manufacture. If this same Fresnel lens were to be prepared with germanium, it would need to be individually prepared with a CNC mill. This would be expensive and not scalable in the same way that injection moulding is. In this chapter, the cyclopentadiene polymer was demonstrated to be prepared with extremely low-cost

starting materials and could be manufactured into complex geometries using scalable methods like compression of injection moulding.

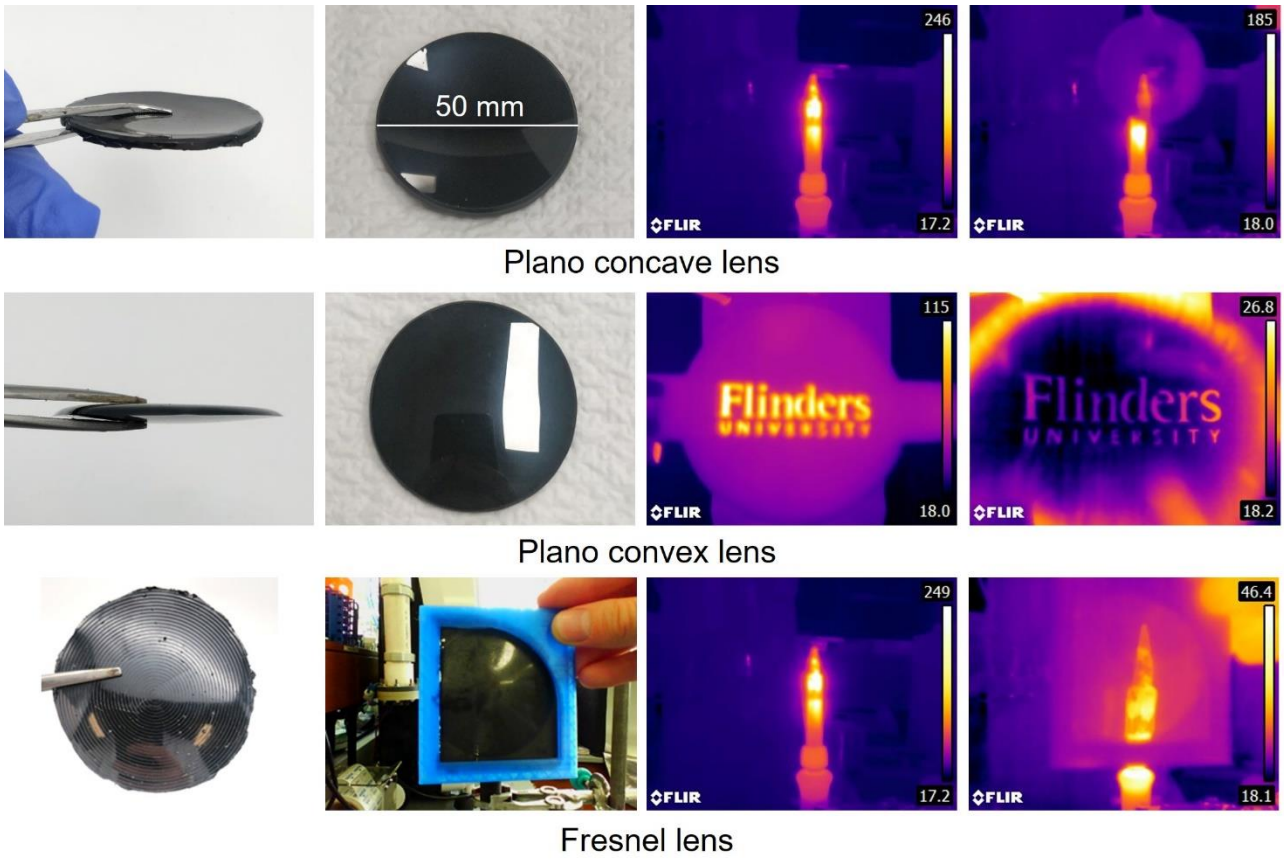

Figure 4.72: Photos and LWIR images of lenses prepared using 67 % sulfur cyclopentadiene based polymers. LWIR images were taken using a FLIR E6 thermal camera.

While the lenses and optics prepared using the cyclopentadiene polymers were an important step, they still required a germanium lens to focus light using the FLIR E6 camera. To truly demonstrate the sulfur-based polymers as optical materials for thermal imaging, a camera needed to be developed which solely utilised a polymer lens to focus all light. This would show that they could completely replace germanium, zinc selenide or silicon and provide a cost-effective solution.

To make the lenses to be used in a stand-alone camera, the norbornane bistrisulfide polymer was utilised due to its superior LWIR transmission and thermal properties. A total of seven plano convex lenses were prepared with a range of focal lengths and diameters. These lenses were shown to be able to be prepared using scalable and low-cost methods like reactive casting or compression moulding, demonstrating manufacturing methods which could be used to prepare low-cost thermal lenses.

After developing the method to prepare high quality lenses, they were integrated into a FLIR Lepton 3.5 thermal camera module. To do this, the silicon lens was removed, and a range of custom 3D printed holders were prepared. Each lens was demonstrated to be effective in focusing light onto the sensor and produced images with excellent resolution and thermal sensitivity. Due to the high transmittance of the norbornane bistrisulfide based polymer, images of a person could be taken despite the relatively low temperature differential with the environment.

Each lens was tested for thermal sensitivity and was found to be able to resolve temperature differentials of as little as 5 °C. The lenses made with the norbornane bistrisulfide polymer demonstrate that the polymer has the potential to completely replace the high cost and scarce materials conventionally used in the thermal imaging industry.

Finally, the potential improvements in lens design were discussed. While the imaging using the lenses was excellent, they did show signs of aberrations due to the simple plano convex lens geometry. Improvements like aspheric surfaces and optimised lens geometries could eliminate many of these aberrations and provide images that would rival those of high-quality silicon or germanium. These steps are relatively simple to implement and would provide immediate and significant improvements in image quality. While not a part of this thesis, work to improve the lens design, demonstrate scalability of manufacturing and integration into a range of sensors is ongoing.

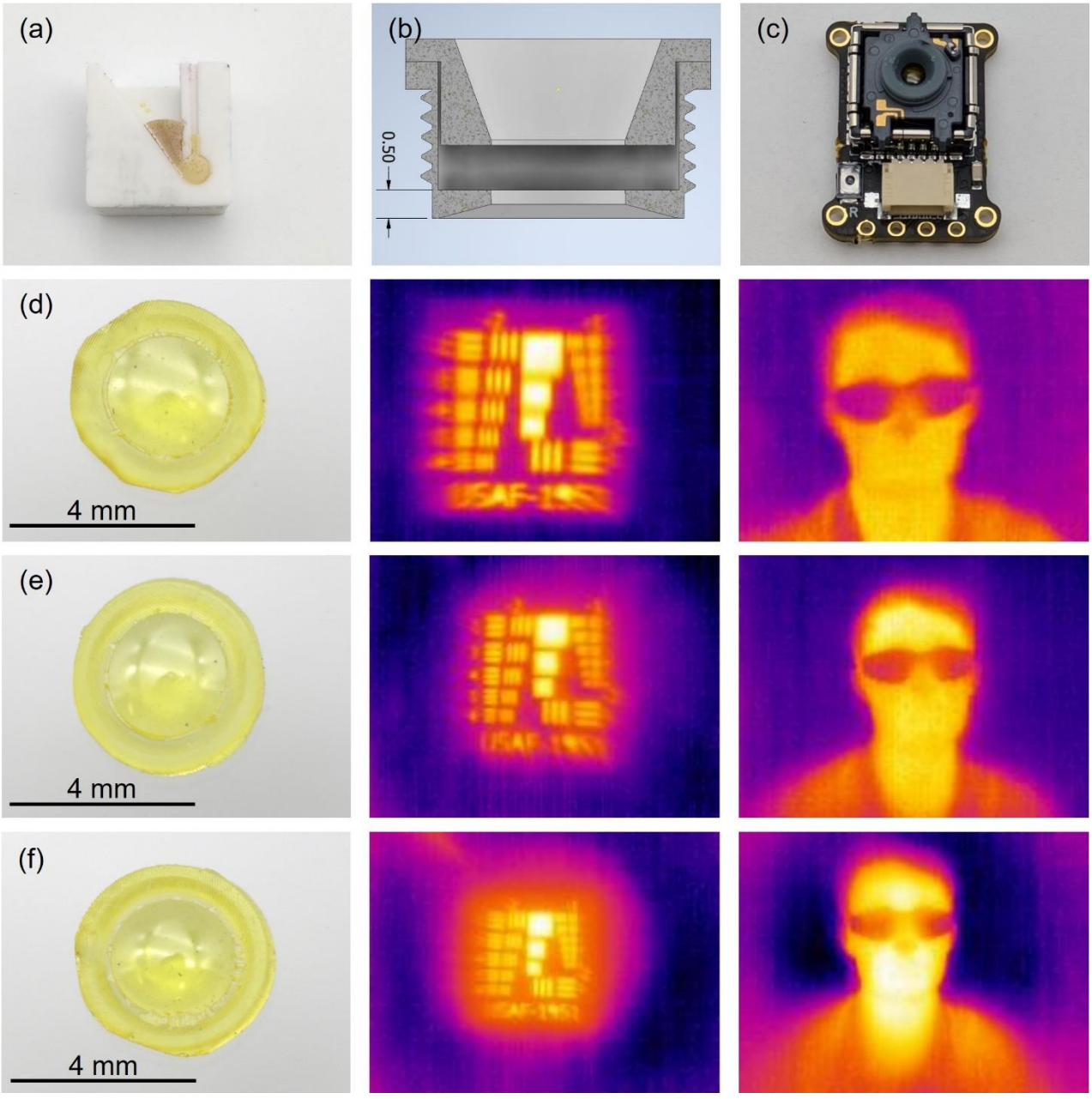

Figure 4.73: (a) Two part mould used to make lenses. (b) Custom 3D printed holder. (c) Polymer lens integrated into FLIR Lepton 3.5. (d) Photo and LWIR images using lens 6. (e) Photo and LWIR images using Lens 5. (f) Photo and LWIR images using lens 4.

Chapter 4 references

(1) Tonkin, S. J.; Pham, L. N.; Gascooke, J. R.; Johnston, M. R.; Coote, M. L.; Gibson, C. T.; Chalker, J. M. Thermal Imaging and Clandestine Surveillance using Low-Cost Polymers with Long-Wave Infrared Transparency. *Advanced Optical Materials* **2023**, *11* (16), 2300058. DOI: https://doi.org/10.1002/adom.202300058.
(2) Molineux, J.; Lee, T.; Kim, K. J.; Kang, K.-S.; Lyons, N. P.; Nishant, A.; Kleine, T. S.; Durfee, S. W.; Pyun, J.; Norwood, R. A. Fabrication of Plastic Optics from Chalcogenide Hybrid Inorganic/Organic Polymers for Infrared Thermal Imaging. *Advanced Optical Materials* **2024**, *12* (7), 2301971. DOI: https://doi.org/10.1002/adom.202301971.
(3) Griebel, J. J.; Nguyen, N. A.; Namnabat, S.; Anderson, L. E.; Glass, R. S.; Norwood, R. A.; Mackay, M. E.; Char, K.; Pyun, J. Dynamic Covalent Polymers via Inverse Vulcanization of Elemental Sulfur for Healable Infrared Optical Materials. *ACS Macro Letters* **2015**, *4* (9), 862-866. DOI: 10.1021/acsmacrolett.5b00502.
(4) Kleine, T. S.; Nguyen, N. A.; Anderson, L. E.; Namnabat, S.; LaVilla, E. A.; Showghi, S. A.; Dirlam, P. T.; Arrington, C. B.; Manchester, M. S.; Schwiegerling, J.; et al. High Refractive Index Copolymers with Improved Thermomechanical Properties via the Inverse Vulcanization of Sulfur and 1,3,5-Triisopropenylbenzene. *ACS Macro Letters* **2016**, *5* (10), 1152-1156. DOI: 10.1021/acsmacrolett.6b00602.
(5) Kleine, T. S.; Lee, T.; Carothers, K. J.; Hamilton, M. O.; Anderson, L. E.; Ruiz Diaz, L.; Lyons, N. P.; Coasey, K. R.; Parker Jr., W. O.; Borghi, L.; et al. Infrared Fingerprint Engineering: A Molecular-Design Approach to Long-Wave Infrared Transparency with Polymeric Materials. *Angewandte Chemie International Edition* **2019**, *58* (49), 17656-17660. DOI: https://doi.org/10.1002/anie.201910856.
(6) Boyd, D. A.; Nguyen, V. Q.; McClain, C. C.; Kung, F. H.; Baker, C. C.; Myers, J. D.; Hunt, M. P.; Kim, W.; Sanghera, J. S. Optical Properties of a Sulfur-Rich Organically Modified Chalcogenide Polymer Synthesized via Inverse Vulcanization and Containing an Organometallic Comonomer. *ACS Macro Letters* **2019**, *8* (2), 113-116. DOI: 10.1021/acsmacrolett.8b00923.
(7) Lee, M.; Oh, Y.; Yu, J.; Jang, S. G.; Yeo, H.; Park, J.-J.; You, N.-H. Long-wave infrared transparent sulfur polymers enabled by symmetric thiol cross-linker. *Nature Communications* **2023**, *14* (1), 2866. DOI: 10.1038/s41467-023-38398-5.
(8) Lee, M.; Jang, S. G.; Yeo, H.; Park, J.-J.; Moon, B.; You, N.-H. Structural Effect of Cyclic Olefin Cross-Linkers on Long-Wave Infrared-Transmitting Sulfur Polymers. *Macromolecules* **2024**, *57* (6), 2905-2914. DOI: 10.1021/acs.macromol.4c00018.
(9) Lee, J. M.; Noh, G. Y.; Kim, B. G.; Yoo, Y.; Choi, W. J.; Kim, D.-G.; Yoon, H. G.; Kim, Y. S. Synthesis of Poly(phenylene polysulfide) Networks from Elemental Sulfur and p-Diiodobenzene for Stretchable, Healable, and Reprocessable Infrared Optical Applications. *ACS Macro Letters* **2019**, *8* (8), 912-916. DOI: 10.1021/acsmacrolett.9b00306.
(10) Qiu, Y.; Li, J.; Li, T.; Ma, X.; Jiang, X. Photo-Curing Vis-IR Hybrid Fresnel Lenses with High Refractive Index. *Macromolecular Chemistry and Physics* **2021**, *222* (24), 2100311. DOI: https://doi.org/10.1002/macp.202100311.
(11) Cao, Y.; Tong, X.; Wang, F.; Yang, J.; Cao, Y.; Strat, S. T.; Tisse, C.-L. A deep thermal-guided approach for effective low-light visible image enhancement. *Neurocomputing* **2023**, *522*, 129-141. DOI: https://doi.org/10.1016/j.neucom.2022.12.007. Nguyen, T. X.; Rosser, K.; Chahl, J. A Review of Modern Thermal Imaging Sensor Technology and Applications for Autonomous Aerial Navigation. In *Journal of Imaging*, 2021; Vol. 7.
(12) Venkatesh, V. C. Precision manufacture of spherical and aspheric surfaces on plastics, glass, silicon and germanium. *Current Science* **2003**, *84* (9), 1211-1219. (acccessed 2024/08/24/).JSTOR. Gabriel, C. Chalcogenide and germanium hybrid optics. In *Proc.SPIE*, 2011; Vol. 8189, p 818911. DOI: 10.1117/12.897757.
(13) Higashihara, T.; Ueda, M. Recent Progress in High Refractive Index Polymers. *Macromolecules* **2015**, *48* (7), 1915-1929. DOI: 10.1021/ma502569r.
(14) Fischer, R. *Lens design for the infrared*; SPIE, 1991.
(15) Czepiel, M.; Bańkosz, M.; Sobczak-Kupiec, A. Advanced Injection Molding Methods: Review. *Materials (Basel)* **2023**, *16* (17). DOI: 10.3390/ma16175802 From NLM. Farotti, E.; Natalini, M. Injection molding. Influence of process parameters on mechanical properties of polypropylene polymer. A first study. *Procedia Structural Integrity* **2018**, *8*, 256-264. DOI: https://doi.org/10.1016/j.prostr.2017.12.027.
(16) Bennett, H. E.; Porteus, J. O. Relation Between Surface Roughness and Specular Reflectance at Normal Incidence. *J. Opt. Soc. Am.* **1961**, *51* (2), 123-129. DOI: 10.1364/JOSA.51.000123. Papatzacos, P.; Akram, M. N.; Bardalen, E.; Øhlckers, P. Simulated effects of wet-etched induced surface roughness on IR transmission and reflection. In *2020 IEEE 8th Electronics System-Integration Technology Conference (ESTC)*, 15-18 Sept. 2020, 2020; pp 1-4. DOI: 10.1109/ESTC48849.2020.9229821.
(17) Silva-Bermudez, P.; Ramirez, G.; Rodil, S. E. 11 - Corrosion resistant coatings for dental implants. In *Bio-Tribocorrosion in Biomaterials and Medical Implants*, Yan, Y. Ed.; Woodhead Publishing, 2013; pp 250-308.

Thomas, T. R. Characterization of surface roughness. *Precision Engineering* **1981**, *3* (2), 97-104. DOI: https://doi.org/10.1016/0141-6359(81)90043-X.
(18) Wheeler, C. U.S. Air Force Aerial Camera Resolution Tester. *Optical Engineering* **1975**, *14* (2), 142120.
(19) Goncalves, D.; Griffith, D. Estimating uncertainty in resolution tests. *Optical Engineering* **2006**, *45* (5), 053601.
(20) Fakhri, S. A.; Motayyeb, S.; Saadatseresht, M.; Zakeri, H.; Mousavi, V. COMPARISON OF UAV IMAGE SPATIAL RESOLUTION BASED ON THE SIEMENS STAR TARGET. *ISPRS Ann. Photogramm. Remote Sens. Spatial Inf. Sci.* **2023**, *X-4/W1-2022*, 143-150. DOI: 10.5194/isprs-annals-X-4-W1-2022-143-2023.
(21) Meem, M.; Majumder, A.; Banerji, S.; Garcia, J. C.; Kigner, O. B.; Hon, P. W. C.; Sensale-Rodriguez, B.; Menon, R. Imaging from the visible to the longwave infrared wavelengths via an inverse-designed flat lens. *Opt. Express* **2021**, *29* (13), 20715-20723. DOI: 10.1364/OE.423764.
(22) Lengwenus, A.; Erichsen, P. *MTF measurement of infrared optical systems*; SPIE, 2009.
(23) Chrzanowski, K. Testing thermal imagers. *Practical guide. Warsaw: Military University of Technology* **2010**.
(24) Williams, T. *An Instrument For Measuring The MTF Of Lenses Used In Thermal Imaging And Other Infrared Systems (2 TO 14 um)*; SPIE, 1974.
(25) Dobek, K. Optical aberrations and modulation transfer function of a thermal lens for use in imaging. *Appl. Opt.* **2021**, *60* (5), 1326-1335. DOI: 10.1364/AO.414274.
(26) Samir, M.; Andrew Robert, H. Wavefront coding for aberration compensation in thermal imaging systems. In *Proc.SPIE*, 2001; Vol. 4442, pp 34-42. DOI: 10.1117/12.449972.
(27) Jamieson, T. Refracting Afocal Systems In Thermal Imagers. *Optical Engineering* **1980**, *19* (6), 196888.
(28) Gaschet, C.; Jahn, W.; Hugot, E.; Chambion, B.; Nikitushkina, L.; Moulin, G.; Getin, S.; Vandeneynde, A.; Henry, D. Tunable curvature of visible CMOS image sensors: Innovative packaging approach for new optical functions. In *2016 6th Electronic System-Integration Technology Conference (ESTC)*, 13-15 Sept. 2016, 2016; pp 1-6. DOI: 10.1109/ESTC.2016.7764517.
(29) Gordiyenko, E. Y.; Glushchuk, N. I.; Pushkar', Y. Y.; Fomenko, Y. V.; Shustakova, G. V. A multi-element thermal imaging system based on an uncooled bolometric array. *Instruments and Experimental Techniques* **2012**, *55* (4), 494-497. DOI: 10.1134/S0020441212030050.
(30) Lewis, C.; Runalls, R.; Turner, G.; Davies, S. *Optical Requirements For Thermal Imaging Lenses*; SPIE, 1979.

Chapter 5 - Conclusions and future experiments

Chapter introduction

So far in this thesis, a range of synthesis methods have been explored to prepare different sulfur-based polymers. The application of these polymers in thermal imaging was discussed and many demonstrations of their use in different imaging systems was given. The purpose of this chapter is to give an overview of the new developments, applications and impact of the research covered in this thesis. Following this, a discussion of planned and future experiments will be discussed. The focus of these following experiments would be to continue the research and explore both commercial and academic applications.

To give some context to the conclusion chapter, the overall goals of this thesis will be reestablished. The main problem that was being investigated in this thesis was the development of polymer based thermal imaging optics. There is a need for thermal imaging optics, like windows or lenses to replace conventional materials like germanium of zinc selenide. These materials are expensive, both in raw material costs and in manufacturing methods.[1, 2] Germanium is typically obtained as a byproduct of zinc or other metals, however, for optical applications, a high purity is required.[1] The purification process is costly and complex, raising the price of germanium optical devices. Unlike plastics, germanium cannot be injection or compression moulded. Instead, it must be ground and polished into the desired lens geometry.[2] These processes often require costly equipment and does not benefit from the same economies of scale that are present in polymer manufacturing. Zinc selenide has many of the same difficulties as germanium but also has the added disadvantage that selenium is a toxic and reactive material, making the manufacturing hazardous and difficult.[3] The crystalline structure of zinc is also extremely important for thermal imaging optics. The crystalline purity affects the absorption, thermal stability, refractive index and durability of zinc selenide lenses.[4] To ensure the correct crystalline structure, a high temperature and energy intensive method must be used.[4] For these reasons, lenses made from germanium and zinc selenide are extremely expensive.

The main goals of this thesis were to develop sulfur-polymer alternatives which could be used in thermal imaging lenses. A polymer alternative would address many of the short comings of conventional infrared transparent optical materials. Polymer materials often benefit from highly scalable and cost-effective manufacturing methods like injection moulding, compression moulding or liquid casting methods. The materials used for sulfur-based polymers are also often very inexpensive relative to germanium or zinc selenide.

While sulfur-based polymers clearly show significant reduction in cost over conventional infrared optical materials, there are several other features that the material must have to be used as a lens in thermal imaging. The first is infrared transmission in the long wave infrared regions (7 μm – 14 μm), a high refractive index, thermal stability and manufacturability. The thesis so far has described the process for preparing polymers which possess each of these features, as well as the fabrication and testing of lenses and other optics which were tested in thermal camera systems. The key findings and experiments will be summarised in the following sections, followed by a discussion of future experiments and a thesis conclusion.

Chapter overviews

Overview of chapter 2

The main goals in chapter two were to develop a method to utilise volatile monomers in an inverse vulcanization reaction with sulfur. Following this, a reaction using molten sulfur and cyclopentadiene would be fully investigated and the resulting polymers would be characterised for use in thermal imaging.

The use of volatile monomers was a major goal for several reasons. The first is that inverse vulcanization reactions often occur at high temperatures (>140 °C).[5] At this temperature, most common monomers for polymer synthesis are gasses. Therefore, by necessity, most monomers used in inverse vulcanization reactions were large molecules with a high boiling point. By developing a method to utilise monomers in the gas phase, it would expand the range of polymers which could be prepared, potentially leading to new breakthroughs and high-performance materials.

The use of small volatile monomers is particularly useful in thermal imaging optics. Large, high boiling point monomers typically have many chemical environments and functional groups, leading to a range of absorbances in the long wave infrared region. In contrast, smaller molecules are often simple, with minimal absorbance at the critical wavelengths of light while also often possessing a greater degree of unsaturation. When a molecule with a greater degree of unsaturation is utilised in an inverse vulcanization reaction, the organic portion of the resulting polymer can be minimised. This is because there will often be more alkenes where sulfur can react relative to the mass of the organic portion of the polymer. As most of the absorption in the long wave infrared region is due to organic groups, minimising the organic content of the polymer is usually desirable. By maximising the unsaturation, the sulfur content can be increased, without leading to significant increases in the average sulfur chain length. This is important because greater sulfur chain lengths would likely increase the chances of the sulfur reforming stable S_8 crystals in a process known as sulfur blooming. With these factors in mind, cyclopentadiene presented as a potential high-performance material for thermal imaging as it had two alkenes but only five carbon atoms.

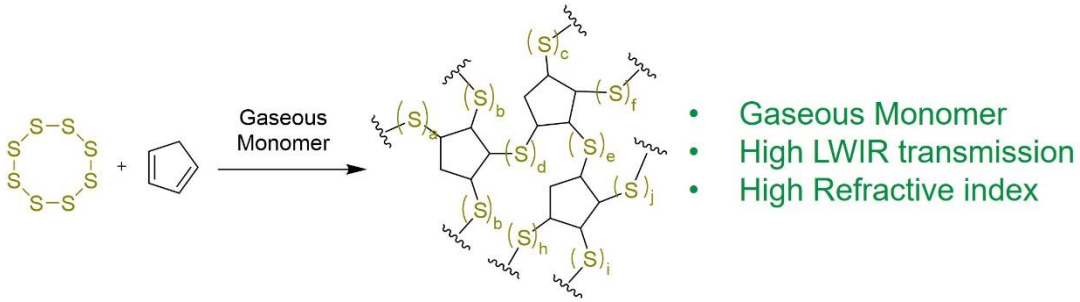

Figure 5.1: Reaction between sulfur and cyclopentadiene to form a polymer with high long wave infrared transmission and high refractive index.

A conventional inverse vulcanization reaction could not be utilised to react sulfur and cyclopentadiene due to its low boiling point (42.5 °C) To overcome this issue, two new reactors were developed. The first reactor utilised a simple reflux set up to react cyclopentadiene in the liquid phase as it is constantly recycled into the reaction. The second reactor would pump gaseous cyclopentadiene through molten sulfur. This reactor, called the gas phase method utilised a two vail set up. The first vial had cyclopentadiene and was attached to a condenser. This vial had a connection to a second vial which contained sulfur. Both vials were heated to 140 °C, causing the cyclopentadiene to evaporate and start condensing. This filled the atmosphere within the

reactor with gaseous cyclopentadiene. The sulfur vial had an attached gas pump which circulated the atmosphere through molten sulfur. Using this reactor set up, the cyclopentadiene could react with molten sulfur while in the gas phase.

Cyclopentadiene is known to readily undergo a Diels-Alder reaction to form dicyclopentadiene.[6] The rate of this conversion was studied, and it was found that over the course of the reaction, it was quite likely that some would form. When using the reflux method, the dicyclopentadiene would remain a liquid and react with the sulfur, likely becoming incorporated into the polymer. However, the advantage of the gas phase reaction was that it prevented any dicyclopentadiene from reacting. This is because the boiling point of dicyclopentadiene (170 °C) is higher than the temperature of the reaction. Due to the two-vial reactor, any dicyclopentadiene formed would remain as a liquid in the first vial. It would not volatilise and be pumped into the molten sulfur where it could react.

In a series of experiments, the effect of dicyclopentadiene content in the polymers was investigated. By intentionally dosing polymers with dicyclopentadiene during the synthesis, polymers with a range of dicyclopentadiene were formed. These polymers were investigated for infrared transmission and glass transition temperature. It was found that increased dicyclopentadiene content increased glass transition temperature significantly. However, this came at the cost of the mid and long wave infrared transmission which sharply decreased with increased dicyclopentadiene content. Therefore, it was determined that for applications in long wave infrared imaging, dicyclopentadiene should be isolated from the reaction.

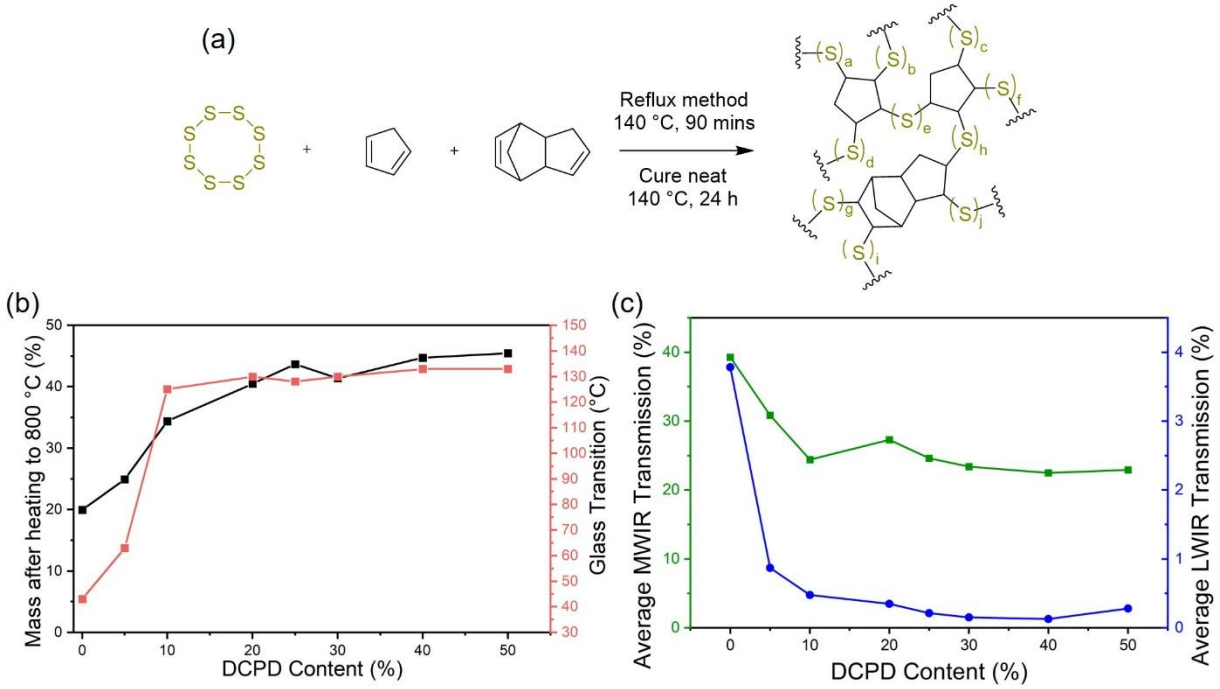

Figure 5.2: Terpolymer reactions with polymers made from varying compositions of sulfur, cyclopentadiene and dicyclopentadiene. (a) Reaction scheme from polymerisation reaction. (b) plot showing the glass transition temperature and the mass after heating the polymer to 800 °C under a flow of nitrogen for polymers with varying dicyclopentadiene compositions. All polymers had a sulfur content of 50 %. (c) Plot showing the average MWIR (3 µm – 5 µm) and LWIR (7 µm – 14 µm) for polymers with varying dicyclopentadiene compositions. All polymers had a sulfur content of 50 %.

The chemical, properties of the polymers prepared using both methods were fully characterised using solid state NMR, FTIR and Raman spectroscopy. To complement these techniques, the polymers were reduced with sodium borohydride and analysed by GC-MS. The chemical structure of the polymers was found to depend on the synthesis method. As a comparison, a polymer made with only dicyclopentadiene and sulfur was also reduced and analysed. It was found that the polymer made from dicyclopentadiene showed peaks that indicated that it had only reacted at one of the alkenes. The more strained alkene was found to be reacted, but the other alkene was left unchanged. There were some very small peaks where the dicyclopentadiene had reacted at the other alkene, indicating that crosslinking was possible, however, they were very minor. In the cyclopentadiene polymer prepared with the reflux method, peaks that corresponded to cyclopentadiene that had reacted with sulfur at both alkenes were present. This indicates that unlike dicyclopentadiene, it readily reacted at both alkenes. However, there were some peaks that corresponded to fully saturated dicyclopentadiene. This dicyclopentadiene had sulfur attached at both alkenes, indicating that not only the more strained alkene had reacted. This was contributed to cyclopentadiene that had reacted at one alkene then undergone a Diels-Alder reaction with another cyclopentadiene molecule to prepare dicyclopentadiene. When the reaction proceeded this way, the less strained alkene in dicyclopentadiene would already be reacted. This is likely why no alkenes were seen in the polymers made using the reflux method with cyclopentadiene. When the reaction was done using the gas phase method, only products from cyclopentadiene which had reacted at both alkenes were present. No dicyclopentadiene was observed at all. This indicated that the gas phase method was effective in isolated dicyclopentadiene from the reaction. These results were complemented with solid state NMR and FTIR which showed alkenes present in the polymers prepared using dicyclopentadiene but not in either of the methods using cyclopentadiene.

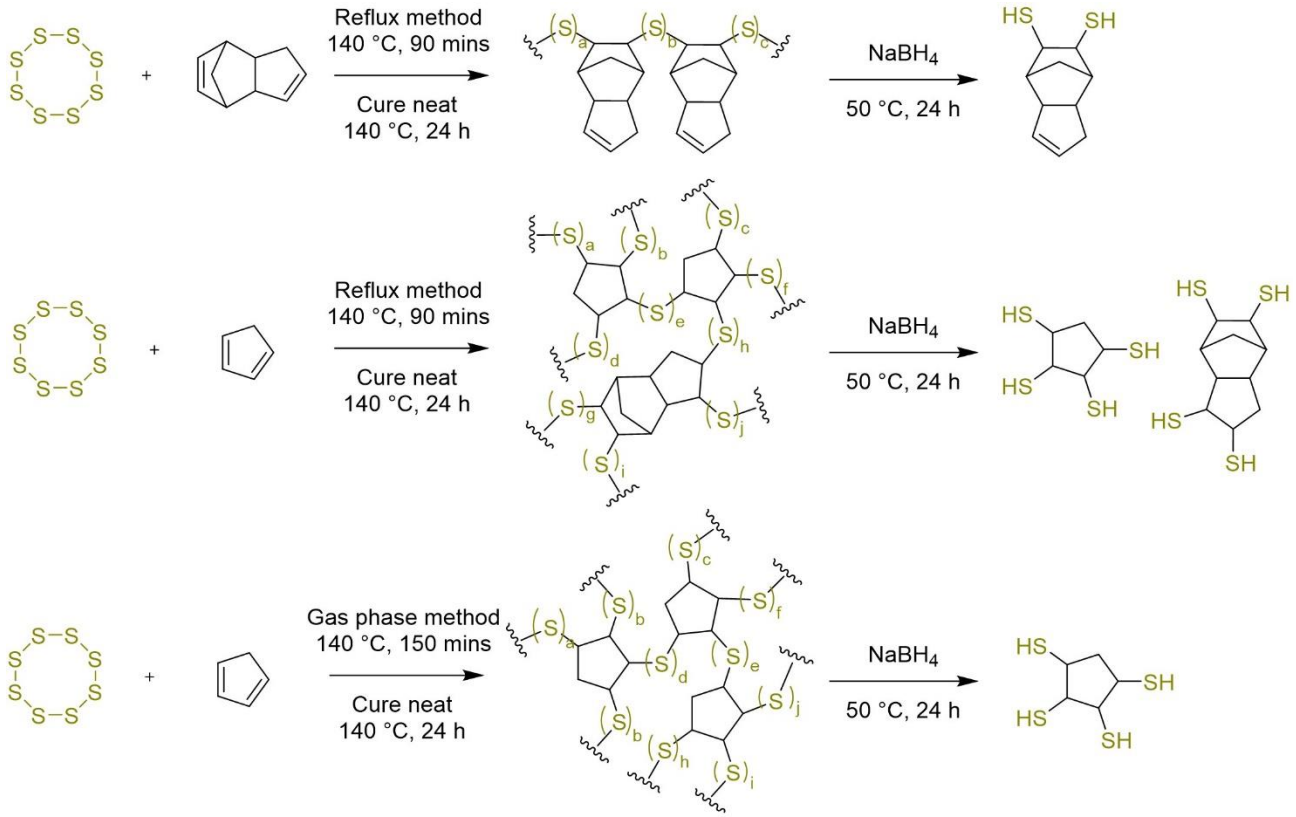

Figure 5.3: Reactions between sulfur and dicyclopentadiene or cyclopentadiene using the reflux method or the gas phase method. The proposed polymer structure as well as the major peaks observed in the GC-MS spectra of the polymers when reduced with sodium borohydride.

After characterising the polymers prepared through each of the method, the long wave infrared properties were investigated. A 1 mm thick window of polymers made with range of sulfur compositions were prepared. Both the reflux method and the gas phase method were tested. It was found that as the sulfur content of the polymer increased, the long wave infrared transmission (7 μm – 14 μm) also increased. This was expected as increasing the sulfur content of the polymer minimised the organic portion. Most of the absorption in the long wave infrared region was from the organic portion.

The long wave infrared transmission of the polymers prepared using the gas phase method was greater than the reflux method for every sulfur composition. This result can be explained by the findings of the terpolymer experiments. In those experiments, the presence of dicyclopentadiene in the polymer structure had a significant effect on the long wave infrared transmission. The reduction experiments showed that the polymer made with the gas phase method had no dicyclopentadiene while the reflux method did possess some. This dicyclopentadiene in the polymer structure was likely responsible for absorption of much of the long wave infrared radiation in the polymers made by the reflux method. However, both polymers made from cyclopentadiene had excellent transmission in the long wave infrared region. The reflux method had an average transmittance of 10.5 % and the gas phase method had a transmittance of 15.6 %. These were for sulfur compositions of 70 % and 67 % respectively. At the time that this research was performed, these were the best transmissions reported for a sulfur-based polymer with a thickness of 1 mm or greater. Unlike other polymers that were published at this time, the transmission was so high that thermal images of humans could be taken through the 1 mm thick windows. These results were extremely promising and allowed for demonstrations of thermal imaging applications to be explored in chapter 4.

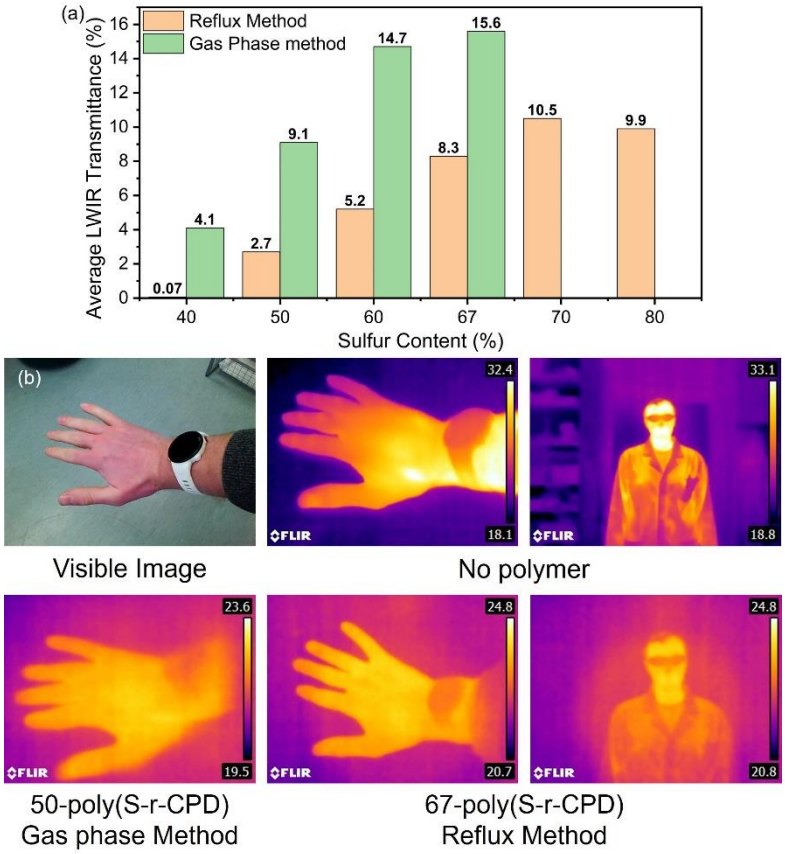

Figure 5.4: (a) Average long wave infrared transmission of polymers prepared from cyclopentadiene using the reflux and gas phase method. (b) Imaging through 1 mm thick polymer windows using a FLIR E6 thermal camera.

Overview of chapter 3

The third chapter focused on the development of a sulfur-based polymer with a norbornane core. This polymer had be identified from theoretical studies by the Pyun group as having potential for excellent long wave infrared transparency and thermal stability.[7] However, no group had been able to synthesise the polymer for several key reasons. The first is the volatility of the monomer. When attempting to prepare the polymer directly from norbornadiene, there was difficulty performing an inverse vulcanization due to it having a boiling point of only 90 °C. The other issue was side reactions and rearrangement of the norbornane core. Norbornadiene is known to undergo an intramolecular [2+2] cycloaddition.[8-10] If this occurred, a cyclopropane group would be formed, fundamentally changing the polymer structure. To successfully synthesise the desired polymer, both the issues of volatility and rearrangement would need to be solved.

The first approach used to attempt to prepare this polymer involved the use of a range of solvents. After a range of experiments, it was found that a solvent system of 50-50 DMF-xylenes could prepare stable polymers. The use of DMF was important as it was found to have an interesting effect on trisulfides. When two symmetric trisulfides with different end groups were added to DMF and analysed by GC-MS, the appearance of a new peak was observed. This peak belonged to an unsymmetric trisulfide with one of each of the end groups of the starting trisulfides. This indicated that DMF could aid in breaking sulfur-sulfur bonds, leading to a metathesis reaction. DMF was used in the solvent for the reaction to induce sulfur-sulfur bond metathesis and keep a low molecule weight of the polymer so that it would not vitrify prematurely, an issue that occurred when no solvent was used. The addition of xylenes in the solvent system was found to aid in dissolving the sulfur and improving the efficiency of the reaction.

After preparing a range of polymers with differing compositions, the polymers were characterised for a range of useful properties. It was found that the polymers possessed excellent thermal stability but had a very poor long wave infrared transparency. The chemical structure of the polymers was fully characterised by reduction with lithium aluminium hydride followed by GC-MS analysis. This showed that while the norbornadiene did react at both alkenes, there was a significant amount of rearrangement to form the cyclopropane group. The addition of many additional modes of vibration from the cyclopropane group likely caused the poor transmission in the long wave infrared region.

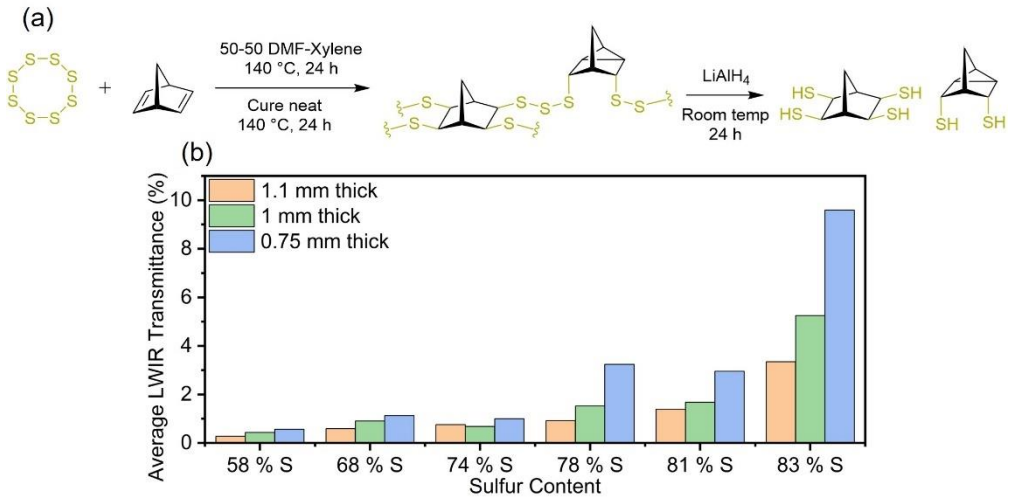

Figure 5.5: (a) Solution phase reaction between sulfur and NBD showing proposed polymer structure and products from lithium aluminium hydride reduction. (b) Average transmission of polymers with different sulfur content. Transmission was much poorer than expected.

After the solution phase reactions, the intermediates were isolated during the reaction by taking an aliquot of the reaction medium at different time points in the reaction. The aliquots were analysed by GC-MS. It was found that there were a range of cyclic sulfide intermediates in the reaction. Some of these showed molecules where one of the alkenes in norbornadiene had reacted with sulfur and formed an epi, tri or pentasulfide ring. Other molecules included molecules where rearrangement had occurred to form the cyclopropane group that was noticed in the polymer structure of the solution phase polymerisations. One molecule, molecule 6 is the figure below, showed a reaction at both alkenes of norbornadiene to form trisulfide rings.

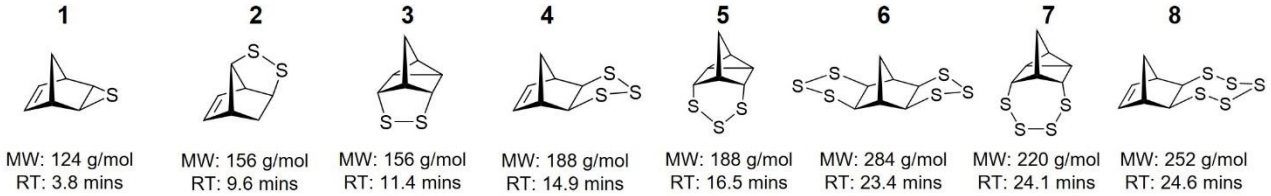

Figure 5.6: Intermediates isolated from solution phase reaction between sulfur and norbornadiene.

After identifying each of the intermediates from the reaction, work was started to modify the conditions to maximise their yield and isolate them. Using column chromatography, hot recrystallisations and liquid-liquid extractions, pure samples of **3**, **4**, **6** and **8** were collected and characterised unambiguously by NMR, GC-MS and X-ray crystallography. These molecules were then used as stating monomers to prepare polymers. Using either solution reaction or neat, each molecule was reacted with itself or with additional sulfur. Using the cyclic sulfides as monomers was very valuable as it allowed for the resulting polymers analysed to understand the effect of rearrangement on the properties of the polymers obtained. Molecule **6** was of particular importance as it showed reaction at both alkenes. Using this as a starting monomer presented a possible route to prepare the desired polymer without the possibility of rearrangement and with the stereochemistry of the molecule already in place.

The polymers prepared from the isolated cyclic sulfides were analysed with a range of techniques like FTIR and solid-state NMR. They were then compared to the polymer prepared directly from norbornadiene. It was found that the polymer made from **3** had several very large absorptions in the long wave infrared region. These absorptions were also present in the polymers made directly from norbornadiene and are likely responsible for the poor transmission of the polymers. In contrast, the polymers made from **4** or **6** did not show these absorbances. This indicated that they did not rearrange to form the cyclopropane group during polymerisation. Following this, each polymer was reduced with lithium aluminium hydride and analysed by GC-MS. It was found that polymers prepared from **4** or **6,** had the desired structure with four sulfur chains from each norbornane unit.

It was decided to focus on polymers prepared from molecule **6** as the stereochemistry was locked in place and there was no potential for alkenes in the polymer prepared from the reaction. The monomer synthesis was scaled up and optimised so that more of monomer 6 could be prepared. It was then polymerised in several different sulfur compositions. Following this, the polymer was comprehensively characterised. Solid state NMR indicated that the norbornane core did not change after the reaction with sulfur, confirming that no rearrangement occurred. Raman showed that the trisulfide ring opened and sulfur chains with varying lengths were formed. These results indicated that by utilising molecule **6** as the starting material, the issues of norbornadiene volatility and rearrangement could be avoided to form the desired polymer.

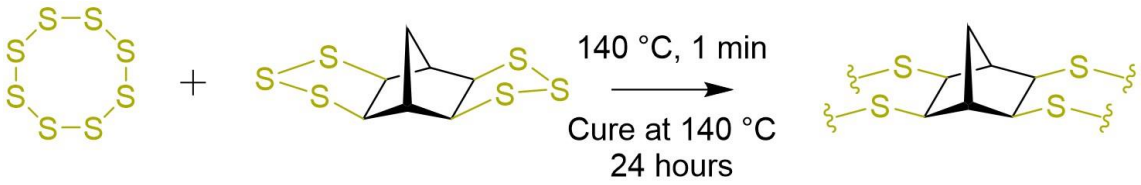

Figure 5.7: Reaction scheme showing the polymerisation of norbornane bistrisulfide.

The thermal and optical properties of the polymer was then tested. It was found to possess a glass transition temperature of 130 °C – 180 °C depending on sulfur composition. It was also found to possess a refractive index of 1.871 and an exceptional LWIR transmission. These properties made it very well suited to be used in thermal imaging applications.

To demonstrate the transmittance of the polymer to long wave infrared light. Windows of different thicknesses and sulfur compositions were prepared. These windows were placed in front of the lens of a FLIR E6 thermal camera. The transparency of the polymer was excellent, being able to clearly image a person even with thicknesses of 1 mm. With the 85 % sulfur composition, the average transmission over the entire long wave infrared region was over 20 %. With the exceptional thermal stability as well as long wave infrared transparency, it made the polymer well suited for thermal imaging applications which were demonstrated in chapter 4.

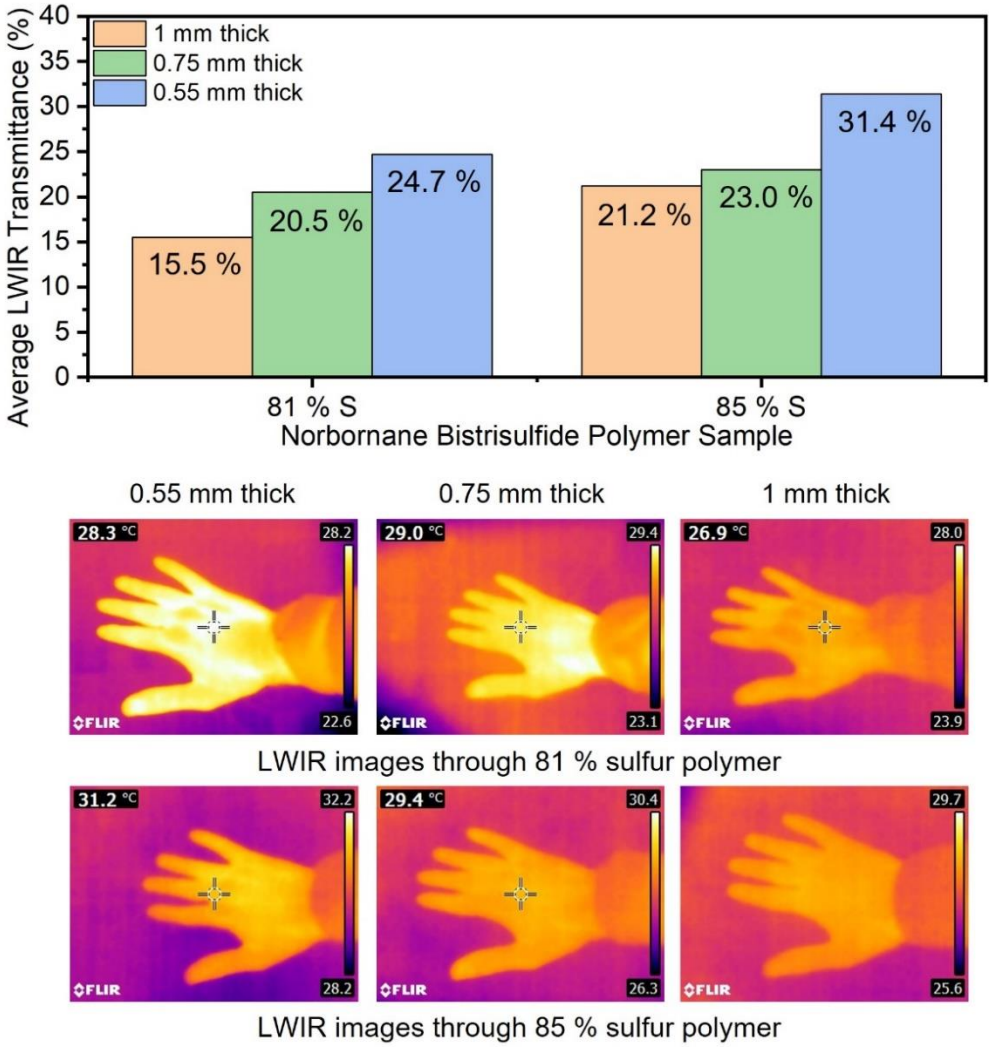

Figure 5.8: The average long wave infrared transmittance and thermal images through polymer windows prepared from norbornane bistrisulfide with different thicknesses and sulfur compositions.

Overview of chapter 4

In chapter 4, the most promising polymers and compositions from chapter 2 and 3 were utilised for applications in thermal imaging. The applications chosen for each polymer was selected based on their properties so that each polymer could find an application that was most suitable for it. The demonstrated applications will be described here as well as the industries that they could be used in.

The cyclopentadiene based polymer developed in chapter 2 has several unique features from the norbornane based polymer from chapter 3. The first is that is black and opaque to visible light. While for some applications, this may be considered a weakness, it does provide some unique advantages. Being opaque to visible light means that it could be used to conceal a thermal camera while not affecting its operation. When this feature is combined with the low cost of the polymer, many unique applications become apparent. Large sheets of the polymer could be prepared using scalable methods like compression moulding. These large sheets would be prohibitively expensive using other materials with long wave infrared transparency like germanium. Another advantage of the cyclopentadiene polymer was that its glass transition temperature could be modified by adjusting the sulfur content in the polymer. Using high sulfur compositions, the polymer was soft and flexible. There are very few materials which show transparency in the long wave infrared region without being rigid and brittle.[11] In the application of a long wave infrared transparent sheet, this property is of great value. A flexible sheet could be bent and formed around a supporting structure without breaking. Furthermore, as the polymer was not brittle it could absorb impacts without shattering. This would allow the polymer to act as a protective barrier for a thermal camera, particularly in applications where impacts are common. An example where this could be used would be in the agricultural industry. Thermal imaging finds use in a range of agricultural applications from irrigation scheduling, livestock monitoring and self-driving tractors.[12, 13] In many of these applications, the thermal camera can be prone to damage or harsh weather so a protective sheet made from low-cost materials that does not affect the operation of the camera would be invaluable. This is one of the key applications that the cyclopentadiene polymer could see use.

To demonstrate the application of a long wave infrared sheet, the cyclopentadiene polymer made from the reflux method was compressed using a heated die. This formed a large square sheet. An enclosure for the FLIR E6 thermal camera was designed and 3D printed which could incorporate the polymer sheet to allow the camera to be completely enclosed but still operational. The camera was then used to image a dog and some chickens demonstrating the use of the camera for wildlife or livestock monitoring.

To further demonstrate the use of the cyclopentadiene polymer, it was formed into a range of lenses. These lenses could be formed by casting the prepolymer or using a reactive injection moulding technique. The use of these rapid and scalable manufacturing methods gave this polymer a very large advantage over materials like germanium or silicon which usually require subtractive processes to form into powered optics.[2, 14] Combined with the low cost of the starting materials, this made the lenses extremely low cost. An application where low-cost lenses could be utilised would be in electronics. Thermal imaging is often used to identify damaged or malfunctioning components in electronics.[15] A set of low-cost polymer lenses could be used to provide a range of magnifications to work on small scale electronics. The construction industry[16] or autonomous vehicles[17, 18] could utilised lenses of different focal lengths to provide zoom and image distant objects that would not otherwise be possible. These polymer lenses could be used to enhance any thermal camera with improved magnification, providing value to many industries.

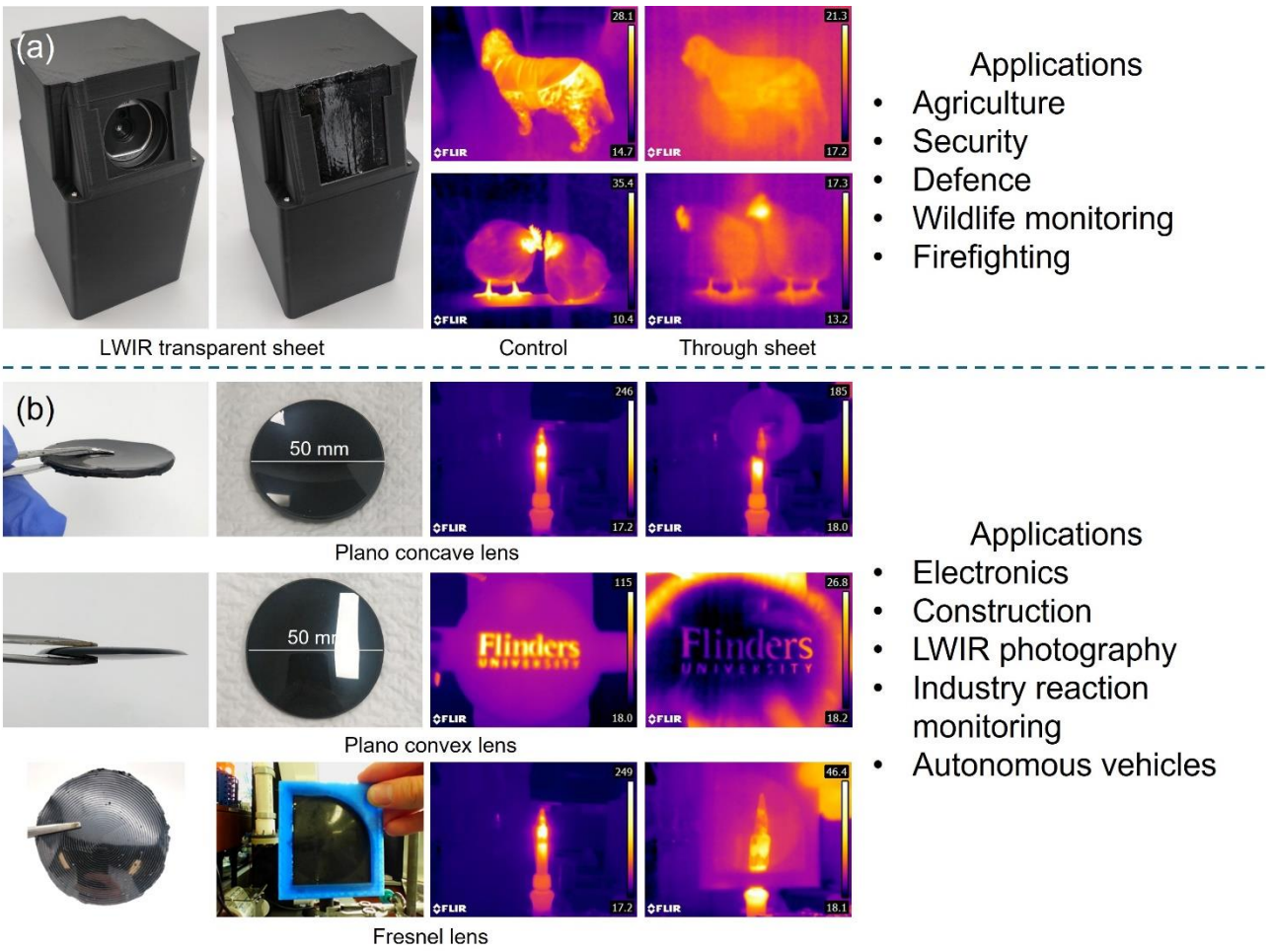

Figure 5.9: (a) LWIR transparent polymer sheet prepared from cyclopentadiene based sulfur polymer. The sheet was placed in a 3D printed enclosure and used to conceal and protect a FLIR E6 thermal camera while imaging a dog and chicken. (b) Plano concave, plano convex and Fresnel lenses prepared using cyclopentadiene based sulfur polymer. The lenses were used to magnify or reduce an image taken with a FLIR E6 thermal camera.

The polymer made in chapter 3 utilised a norbornane core. This polymer had several advantages over the cyclopentadiene based polymer from chapter 2. The first was an increased long wave infrared transparency. This meant that the polymer could likely be utilised to image lower temperature objects. The other major advantage was the thermal stability of the polymer. The norbornane based polymer had a glass transition temperature ranging from 130 °C to 200 °C based on sulfur composition. This meant that it could be utilised in applications which required a shape persistent and brittle material. The most obvious of these applications is as a lens. The high glass transition temperature means that the lens could be placed in a holder and would not deform or change shape with any pressure. It also so means that the lens could be used at high temperatures without significant or permanent deformation.

Like the cyclopentadiene based polymer, the norbornane polymer was prepared using scalable casting or compression moulding techniques, making them much lower cost than germanium or silicone alternatives. The applications for a low-cost thermal imaging lens are enormous. Applications like home security,[19] fire alarm systems[20] or automotives[18] would benefit greatly from low-cost thermal imaging. It would also open applications that are not currently possible due to the high cost and low production of thermal imaging cameras like commercial devices, the mobile phone industry or low weight and power drone technology.

To demonstrate the use of the norbornane based sulfur polymer from chapter 3, it was moulded into a range of plano convex lenses. It was possible to prepare these lenses by casting the prepolymer or with compression moulding but all the following images will be with cast lenses. By designing and 3D printing a range of holders, the lenses could be integrated into a FLIR Lepton 3.5 thermal imaging module. Unlike the cyclopentadiene polymer, these lenses completely replaced the stock silicon lens that was originally on the Lepton. This was a significant achievement as it completely replaced the expensive silicon lens which can account for a significant amount of the cost of a thermal imaging system. In these applications, the polymer was the only optic used to focus light onto the sensor of the camera. Despite a simple plano convex lens design, the polymer lenses performed excellently and demonstrated the potential for use as stand-alone lenses for infrared cameras.

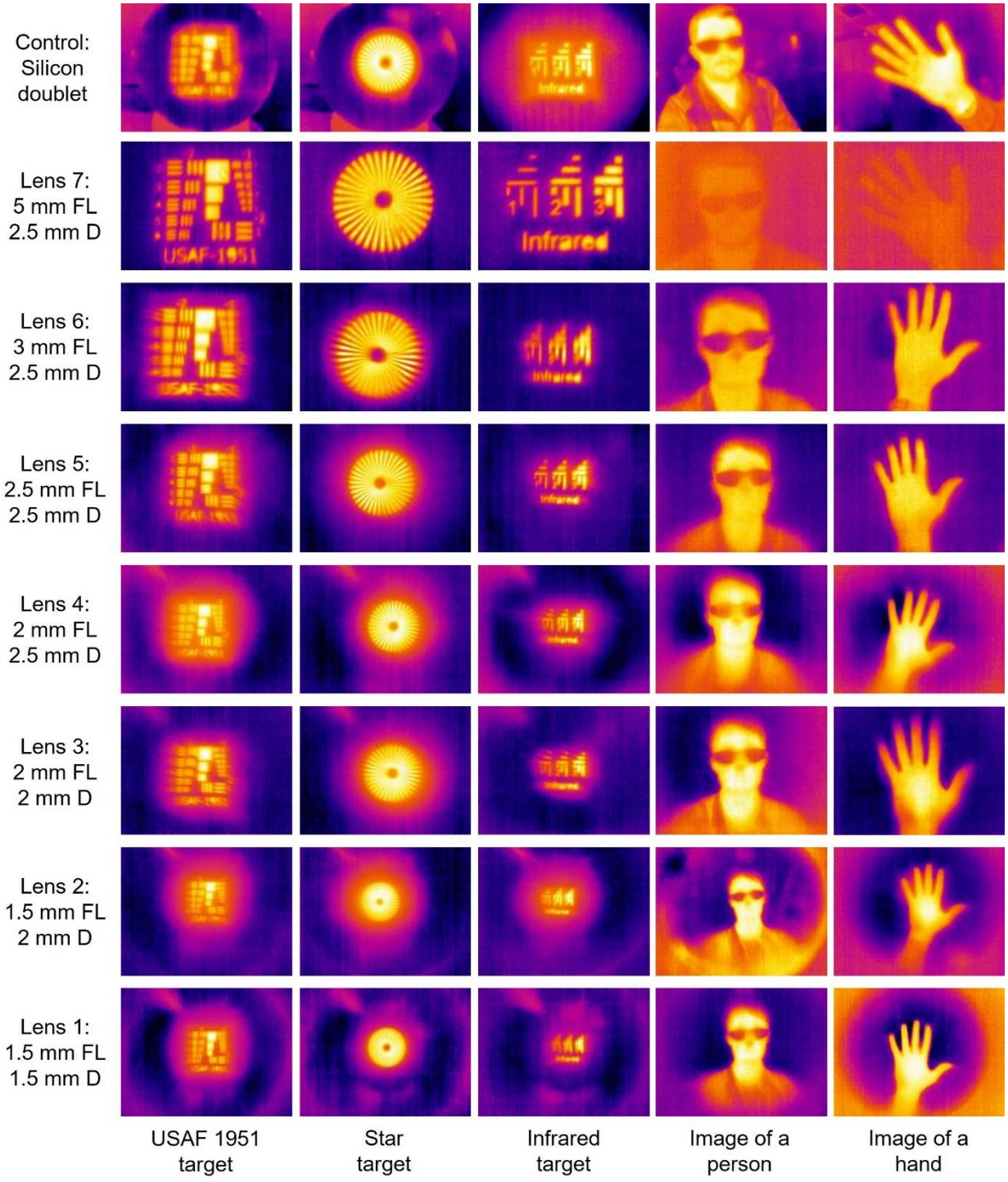

Figure 5.10: Thermal imaging using a FLIR Lepton 3.5 with a range of lenses made from a norbornane based sulfur polymer with a sulfur composition of 81 %.

Improvements and future experiments

Scale up of monomer synthesis

One of the main areas of this project that required improvement was the scale up the monomer synthesis. These experiments would be vital in demonstrating that the lenses or optics could be used in applications requiring high volumes. As the norbornane bistrisulfide polymer was higher performing, most of the following discussion will be based around it.

There are several challenges in the monomer synthesis of norbornane bistrisulfide monomer. The main ones are the formation of polymer during the monomer reaction and side reactions to form rearranged molecules with the cyclopropane functional group. Both issues need to be addressed to improve the yield and scale of the reaction. Many of the experiments that will be discussed here have already been done but the results will not be given here to protect the IP. Instead, this discussion will remain general in nature.

Polymer formation is a difficult issue to overcome. From NMR and GCMS experiments, it is known that the reaction to form norbornane bistrisulfide forms in two main steps. In the first step, one alkene on norbornadiene reacts to form either an epi, tri or pentasulfide. The first step is quite rapid, consuming most of the norbornadiene in the first hour. It is during this step that most of the rearrangement is also believed to occur. In the second step, the other alkene reacts, forming the norbornane bistrisulfide. This step is slower but after 24 hours, all alkenes are consumed. At both stages, it is likely that the monomer is in equilibrium with polymer products as the trisulfide rings could likely open and close at the temperature of the reaction (120 °C). In the first stage of the reaction, the polymer could only be linear as these would only one sulfide ring. However, in the second stage of the reaction, there would be two sulfide rings on each norbornadiene molecule. This means that the polymer would be crosslinked. The crosslinking would have two effects. The first is that for the monomer to be in solution, it would have to reform two sulfide rings. This would likely be more difficult to occur and would lead to more of the monomer becoming incorporated into the polymer. The other effect is that if the molecular weight of the crosslinked polymer reaches a certain level, it would be much more likely to precipitate out of solution. This was observed in the monomer reactions as a significant amount of polymer precipitate was formed over the reaction. Once the polymer had precipitated, it would be very unlikely that it would redissolve in the solution where it could potentially reform the monomer. This would likely create a driving force toward the polymer rather than the monomer, resulting in lower yields. Polymer precipitation was believed to be the leading reason why the yield of norbornane bistrisulfide was below 10 % using the methods described in this thesis so developing methods to prevent polymer formation and precipitation is vitally important.

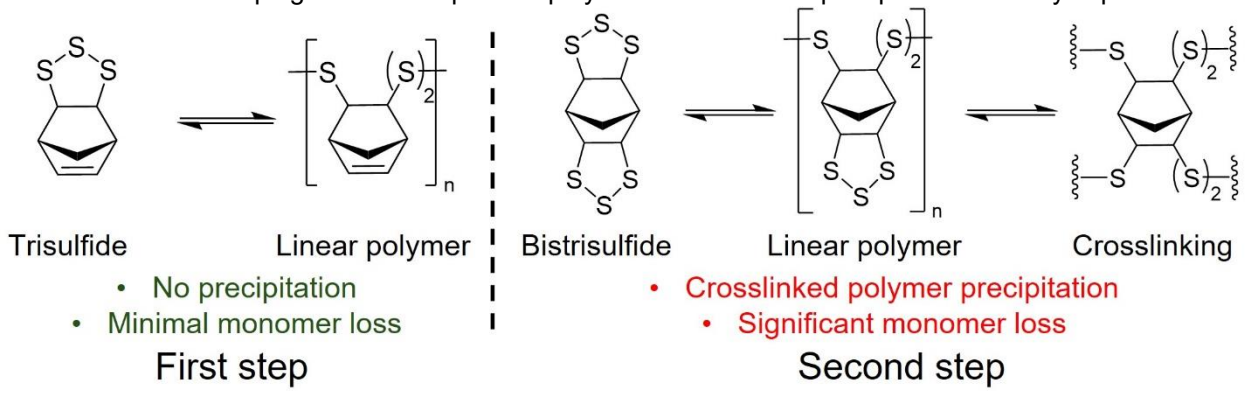

Figure 5.11: Formation of polymer during monomer synthesis reaction.

There are two main ways that the issue of polymer precipitation could be approached. The first is to utilise the norbornene trisulfide molecule as the target monomer. This would mean that the second step of the monomer reaction is eliminated entirely. However, utilised norbornene trisulfide as a monomer has its own issues which is discussed in the following section. The other way to approach the issue of polymer precipitation is to decrease the concentration of the reaction. By decreasing the concentration of the reaction, the chance of two monomer molecules coming in contact decreases. This would likely push the equilibrium toward the left in the reaction schemes above as it would be more likely that the monomer would reform their trisulfide ring than react with another monomer. The decreased concentration would also prevent the polymer from precipitating. At lower concentrations, it would likely take much longer for the polymer to reach a molecular weight that is high enough to precipitate from the solution. This would prevent it from precipitating out and pushing the equilibrium toward the polymer side.

While dilution of the reaction would result in less polymer and an increase in monomer, it would require more solvent to prepare the monomer. For this reason, the concentration should be tested thoroughly to determine the best compromise between polymer precipitation and solvent costs.

The other issue in the monomer synthesis was rearrangement to form cyclopropane impurities. These impurities were investigated in detail in chapter 3 and found to significantly reduce the long wave infrared transmission of the polymer. These molecules present an issue in the purification of the monomer as well as reduced overall yield. While exact mechanism for how this cyclopropane forms is not known, it has been shown to be more common in reactions at higher temperatures. The use of catalysts that induce an ionic mechanism also significantly reduce the relative concentration of rearranged impurities. These observations indicate that the monomer may be formed through an ionic mechanism while the rearranged molecules are formed through a radical one. This gives several approaches to reduce the rearranged impurities from forming.

The first is to reduce the temperature of the reaction. This would likely reduce radical mechanisms from occurring as they are likely induced by S-S bonds being broken thermally. There is a compromise when using lower temperatures that the reaction would likely occur slower, and the solubility of sulfur is greatly dependent on temperature. These factors would mean that the reaction would need to be made more dilute and ran for a longer time at lower temperatures.

The other way to reduce the formation of cyclopropane impurities would be to use catalysts which promote the formation of the monomer. In this thesis, a nickel ammine complex $[Ni(NH_3)]Cl_2$ was used. The ammines would help promote the desired reaction. There are many other catalysts which could be used to fill this role, but they will not be discussed in detail in this thesis. By utilising a catalyst and reducing the temperature of the reaction, the relative proportion of the cyclopropane impurities could be minimised.

Use of norbornene trisulfide as the monomer

One potential method to improve the monomer yield would be to utilise norbornene trisulfide rather than the bistrisulfide. This molecule has a trisulfide ring on one side and an alkene on the other. The advantage of using this molecule is that the monomer synthesis and purification may be simpler and higher yielding. In the synthesis of norbornane bistrisulfide, the reaction was left for 24 hours. The reason for this is that the reaction likely occurs at one alkene first before reacting at the other. This was seen in chapter 3 when extracting the intermediates from the reactions. Norbornene trisulfide formed quickly then reduced over time as it likely formed bistrisulfide or polymer. However, as the reaction time increased, the concentration of polymer also increased. The method for extracting the bistrisulfide molecule involved precipitation out of hexane. Before this step, the polymer had to be completely removed from the hexane with several washing steps. There were several issues that could occur during this process. The first is that norbornane bistrisulfide could precipitate early and become trapped by precipitated polymer. If this occurred, a loss in norbornane bistrisulfide yield was unavoidable as removing it from the polymer was very difficult. The other issue was that if the polymer was not fully removed from the hexane before precipitation of the norbornadiene, it would also precipitate and small amounts of it would become entangled in the monomer. When this occurred, the norbornane bistrisulfide could not be used and further purification was required. While the issue of polymer formation could be reduced using the methods described earlier, the issue is very difficult to completely remove if norbornane bistrisulfide was used.

Utilising norbornene trisulfide would significantly reduce the issue of polymer formation. As evidenced by NMR and GC-MS data, norbornene trisulfide forms quickly. This means that the monomer formation reaction could be shortened. In preliminary research, it was found that 90 minutes was optimal for norbornene trisulfide yield. The shorter reaction time resulted in significantly reduced polymer formation, making purification easier. The other advantage is that norbornene trisulfide is much more soluble in hexane that norbornane bistrisulfide. This feature could be utilised to more easily separate it from any formed polymer. During the workup to prepare norbornene trisulfide, there was no chance of it precipitating out of the hexane like norbornane bistrisulfide. Due to these advantages, the yield of norbornene trisulfide that could be isolated from the monomer synthesis reaction was as high as 40 %, a large improvement from the 9.48 % obtained for norbornane bistrisulfide.

While there are advantages to the use of norbornene trisulfide, there are also some significant disadvantages which were the reason they were not explored further in this thesis. The first was the potential for alkenes in the polymer structure. The FTIR data in chapter 3 indicated that alkenes could be present in the polymer even after the reaction. The alkenes gave a significant absorption at approximately 713 cm^{-1} which was just at the edge of the long wave infrared region. It was found that with higher sulfur loading, the alkene could completely react, however, this limited the range of compositions which could be made while avoiding alkenes. The other disadvantage was that the stereochemistry at the alkene was uncertain after it reacted with sulfur. The norbornane bistrisulfide monomer was confirmed by X-ray crystallography to be exo at both trisulfides. If there was variation after the norbornene trisulfide reacted with sulfur, this could introduce additional vibrations and reduce the long wave infrared transparency. With careful control over the polymer composition to prevent alkenes, norbornene trisulfide could be used as a potential replacement for norbornane bistrisulfide to increase the yield of the monomer

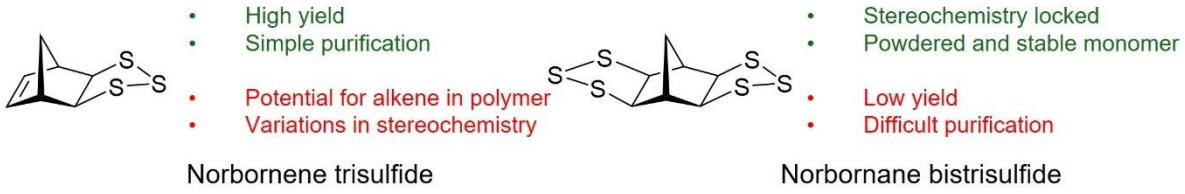

Figure 5.12: Comparison between norbornene trisulfide and norbornane bistrisulfide as monomers.

To confirm if norbornene trisulfide could be used as a monomer and if it had and change in the long wave infrared transparency, a window was prepared. To prepare this window, a silicone mould was cast using a 1 mm glass slide as a positive. The polymer was then prepared using the following method and cured into the shape of the window.

Norbornene trisulfide oil (100 mg) and sulfur (153 mg) were added to a vial with a magnetic stirrer. The ratio of sulfur to norbornene trisulfide was selected to give an average sulfur rank of 6. The vial was added to an oil bath that was preheated to 140 °C. The reaction was heated and stirred for a total of 5 minutes before being poured into a preheated silicone mould. The mould and prepolymer were then added to a 140 °C oven for 24 hours. This reaction was done solventless as it made the casting process easier. The reaction was very quick and if left for longer than seven minutes, it would vitrify and stop stirring.

After cure, the polymer window was analysed for long wave infrared transmission on a Perkin Elmer Frontier FTIR spectrometer and images were taken through the polymer window using a FLIR E6 thermal camera. It was found that the polymer had an average of over 18 % transmittance in the long wave infrared region. This was very similar to polymer samples made with norbornane bistrisulfide. The excellent transmittance also allowed for images of a person or a hand to be taken through the 1 mm thick window. Importantly, the FTIR spectrum was indistinguishable from that of polymers prepared with norbornane bistrisulfide and no alkene peaks were observed.

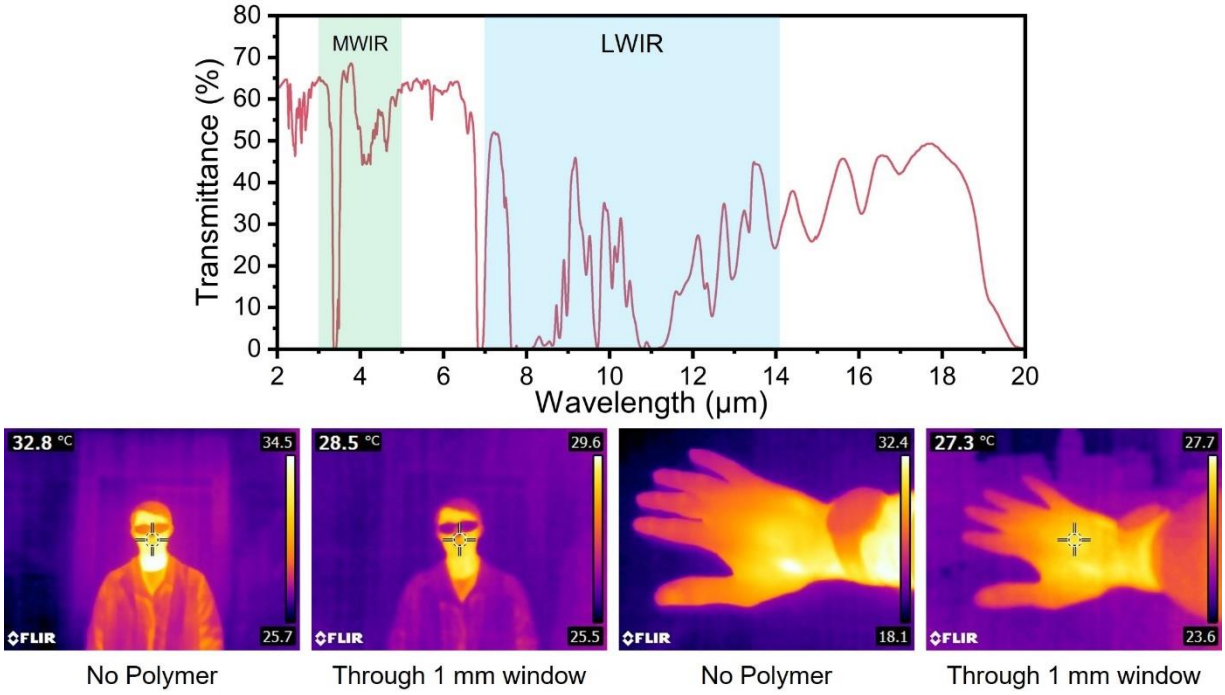

Figure 5.13: LWIR transmittance and thermal images taken through a 1 mm thick polymer window prepared with norbornene trisulfide. Sulfur content was 81 %.

Scale up of lens manufacturing

The next capability that would need to be explored to develop this research further would be the scale up of the lens manufacturing. One of the major advantages of polymer materials over germanium or silicon is the manufacturing methods that can be used. These methods allow for large volumes at extremely low cost. While the polymers made in this thesis have been prepared using low-cost materials and there is a path for scalable monomer synthesis, the manufacturing methods still need to be demonstrated. In this section, three potential methods will be discussed and a route toward scaled up manufacturing of lenses will be laid down. These methods are compression moulding, injection moulding and screw extrusion.

The first method that could be used for the scalable manufacture of lenses is compression moulding. This technique utilises high pressures and temperatures to form materials into the desired geometries. This technique was used on both the cyclopentadiene and norbornane based polymers with excellent results. Compression moulding could be used on the fully cured polymer to convert it from a powder to an array of lenses. This would increase the rate and consistency of lens manufacture over the casting method that is currently used. Another advantage of compression moulding is the minimal waste that would result. While it is likely that there would be some flashing or gating between lenses, this polymer would not be wasted. These pieces of polymer could be ground into a powder and resubjected to the compression mould to remove any waste from the process.

To demonstrate the use of compression moulding to prepare lenses, a simple 5 lens die was discussed in chapter 4. However, to reach the level of manufacturability required to meet many of the applications discussed in this thesis, a greater number of lenses would need to be prepared per compression. Some thought should also be given for the cycle time of the process. One of the major delays in the cycle time is the heating and cooling which should be addressed to increase production efficiency.

To meet the main considerations discussed above, a custom compression moulding system was designed. In this design, an array of 89 lenses was designed into a disk. This disk had a flash ring so that excess polymer would flow into a designated area in the die. The polymer would be placed on this piece before another disk is placed on top. These pieces would make up the die insert. The insert would be placed into a cylinder heating block and heated to the compression temperature. A push rod would be placed in the top and the entire die would be compressed. A figure showing the compression mould can be seen on the following page.

After compression, the polymer lenses would be in an array and could be separated by scoring and breaking along designed weak points. To address the issue of heating and cooling, the die inserts were kept thin. After compression, the inserts could be easily removed from the heating block using an ejector ring. The insert could be left to cool while a new insert is added. As the thermal mass of the inserts was kept low, they would not take long to heat or cool, decreasing the cycle time and improving the efficiency of the process.

This mould has been designed and manufactured. It is ready to be used and tested. Several things that would need to be optimised would be the mass of polymer used, the compression temperature and compression time. If these conditions could be optimised, it could significantly improve the rate of manufacture of lenses.

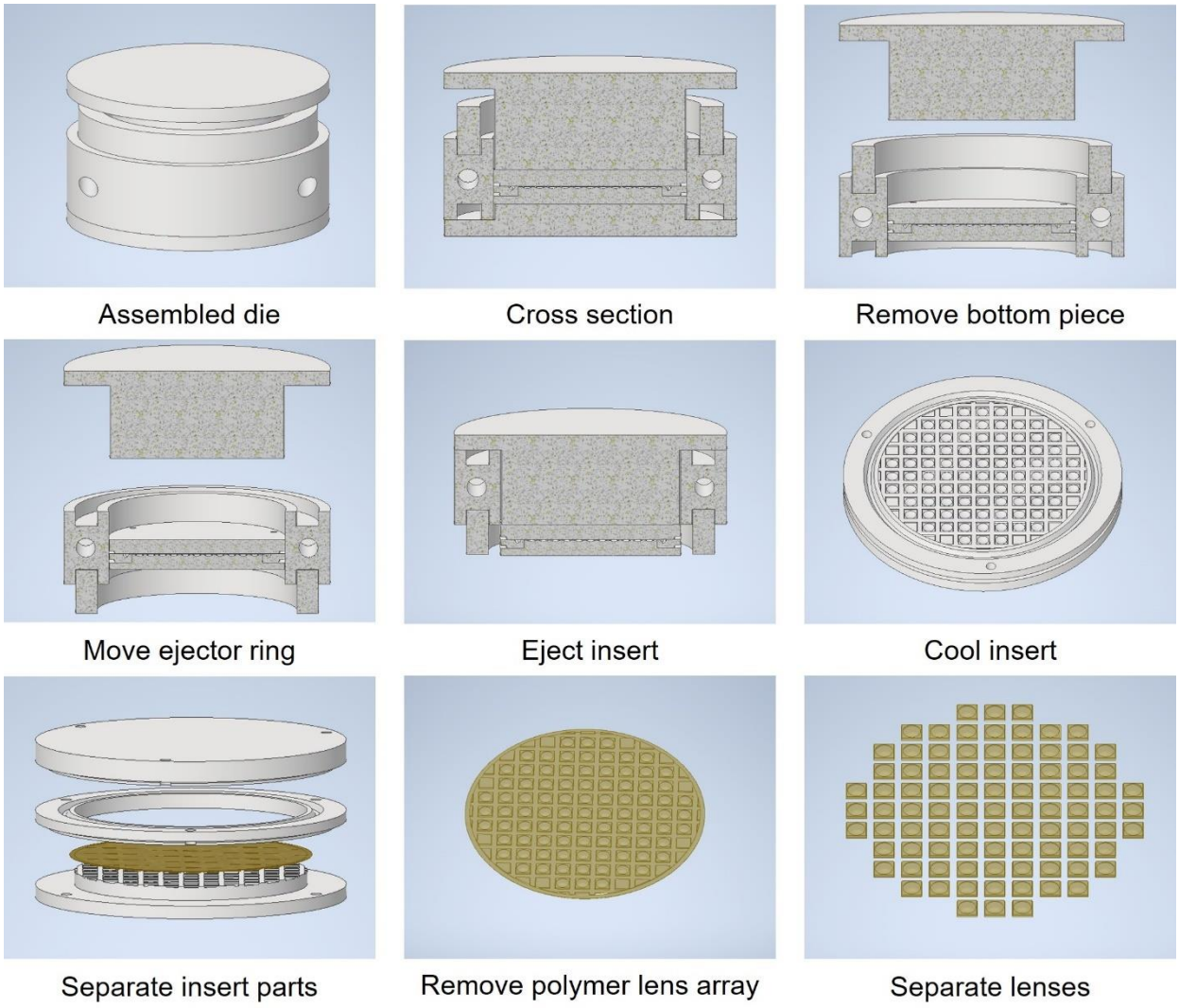

Figure 5.14: Compression mould with process of removing insert and separating lenses.

The next way that the lens manufacture could be scaled up would be to use injection moulding. Many of the plastic products produced and used around the world are made using injection moulding.[21] It is a scalable and efficient process. However, injection moulding is usually done with thermoplastic polymers.[21] These polymers are melted and injected into a mould. While the polymers described in this thesis are not thermoplastic due to high degrees of crosslinking, they do contain dynamic sulfur-sulfur bonds. At high temperatures, these bonds could be broken and reformed reversibly. This may allow it to be injection moulded like a thermoplastic.

To experiment with injection moulding, a Holipress desktop injection moulding system was purchased. By placing the norbornane bistrisulfide polymer in the press, it was determined that it could be extruded with high pressure. This gives confidence that the polymer may be able to be injected into a mould. Although they would likely require heated moulds and high pressure due to the viscosity of the material and the temperatures (>160 °C) required to break sulfur-sulfur bonds. So far, no lens moulds have been made but some design and simulations have been done.

The main advantage of injection moulding over the casting methods used in this thesis is that there is much greater force pushing the polymer into the mould. This force would allow for smaller gating sections and a greater number of lenses per injection. An example mould has been designed which could mould four lenses per injection. This mould was not designed to be a manufactured but instead used to test the injection

parameters required to inject the polymer. This mould would have a cavity on one side and be mostly flat on the other side of the mould. The polymer would be injected in the middle and fill four lenses through a gate at the bottom of each lens. To vent the air and prevent bubbles, each lens has an outlet. This mould is likely quite conservative and a more scalable mould with many lenses could likely be designed. The mould was designed to be made with silicone resin but due to the high pressures of injection moulding, it may need to be manufactured from aluminium or steel.

The final method that could be used to scale up lens manufacture would be screw extrusion. This method would be different from compression or injection moulding as it would use the monomer and do the reaction as it is moulded. In screw extrusion, the norbornane bistrisulfide monomer and the appropriate amount of sulfur would be mixed to form a powder. This powder could be placed in a hopper which feeds into a heated screw. The screw would serve several purposes. The first is to heat the powder, melting the sulfur and initiating the reaction. Following this, the high forces in the screw would force any air bubbles out of the polymer. Finally, the screw would provide a force to eject the polymer out of a nozzle. Screw extrusion reactors are quite common in industry and can be attached to a robotic arm or a gantry system so that the extruder can be controlled automatically.[22] While this could potentially allow for 3D printing of the polymer, it is still likely that moulds would be used for reliability and rapid moulding.[22]

The main advantage of screw injection is that is it very similar to the casting method used in this thesis but with some additional force to aid in filling the mould. Unlike injection moulding of the final polymer, the forces required to extrude the prepolymer would be much lower as it would still be liquid. This means that the moulds would not need to be as rigid and could be made from lower cost materials like silicone rather than aluminium or steel. Screw extrusion could be made continuous if the monomer powder was constantly added to the hopper. With many low-cost silicone moulds and a continuous extrusion of polymer, this process would likely cast lenses at a similar or faster rate than injection moulding. However, as the uncured prepolymer would be used, each mould would need to be added to an oven to cure before the lens could be removed. This would mean that many moulds would be required to match the output of other methods. Another disadvantage is that screw extruders are very prone to blockages.[22] As the polymer has a relatively short working time of several minutes, it is possible that it may vitrify in the screw. Careful control over the flow rate and temperature would be required to ensure that no premature vitrification occurs during extrusion.

It is possible that the final solution to manufacturing of the lenses may utilise several of the approaches discussed here. The many potential solutions are a significant advantage, and each could be used where appropriate for different part geometries and applications.

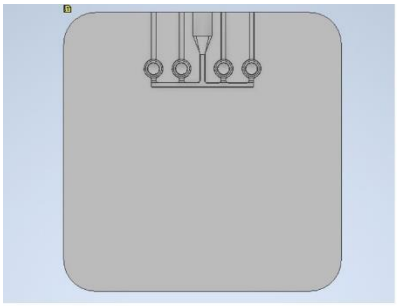

Injection mould cavity

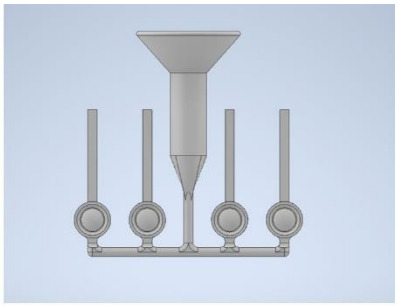

Injection moulding lenses

Figure 5.15: Design of injection mould.

Thesis conclusions

In this thesis, sulfur-based polymers were investigated for the application of thermal imaging optics. Using unique reactors and starting monomers, several of the highest performing polymers in literature were prepared. A range of novel methods were used to prevent side reactions, utilise volatile monomers and prevent vitrification in a range of polymerisation reactions.

The polymers were used to prepare optics with some of the best imaging in literature. Using the cyclopentadiene based polymer from chapter 2, long wave infrared transparent windows for protection or concealment of a thermal camera were produced. The cyclopentadiene polymer as well as the norbornane based polymer from chapter 3 were then utilised to prepared long wave infrared transparent lenses. By developing custom lens holders, the norbornane polymer windows were integrated into an infrared sensor, making a stand-alone thermal imaging camera with only polymer optics.

The research presented in this thesis would have many applications in a range of industries. The long wave infrared transparent sheet could fill a niche of a low-cost protective window which is not currently possible. This could be used in military,[23] agriculture,[12] wildlife surveillance[24] and manufacturing industries.[25] The norbornane based polymer lenses have incredible potential applications. As the cost of thermal imaging sensors decrease, there is a need for low-cost lenses to match. By incorporating the lenses developed in this thesis, the cost of thermal imaging could be significantly reduced, making it available to industries that it was previously inaccessible to. This would make it available to consumer markets like the mobile phone industry,[26] electronics,[15] self-driving vehicles,[27] fire detection and prevention[20] while also providing a cost saving to industries where thermal imaging is already used. The lenses have already displayed performance that would be appropriate for many of these industries at a fraction of the raw material cost of other optics. With further development on the scalability and manufacture of the lenses, they could find use in these industries in the coming years.

Chapter 5 references

(1) Depuydt, B.; Theuwis, A.; Romandic, I. Germanium: From the first application of Czochralski crystal growth to large diameter dislocation-free wafers. *Materials Science in Semiconductor Processing* **2006**, *9* (4), 437-443. DOI: https://doi.org/10.1016/j.mssp.2006.08.002.
(2) Venkatesh, V. C. Precision manufacture of spherical and aspheric surfaces on plastics, glass, silicon and germanium. *Current Science* **2003**, *84* (9), 1211-1219. (acccessed 2024/08/24/).JSTOR.
(3) Shabalina, L.; Spiridonova, V. Toxicity and character of the effect of some zinc compounds. *Journal of Hygiene, Epidemiology, Microbiology, and Immunology* **1988**, *32* (4), 397-405.
(4) Gavrishchuk, E. M.; Yashina, É. V. Zinc sulfide and zinc selenide optical elements for IR engineering. *J. Opt. Technol.* **2004**, *71* (12), 822-827. DOI: 10.1364/JOT.71.000822.
(5) Chung, W. J.; Griebel, J. J.; Kim, E. T.; Yoon, H.; Simmonds, A. G.; Ji, H. J.; Dirlam, P. T.; Glass, R. S.; Wie, J. J.; Nguyen, N. A.; et al. The use of elemental sulfur as an alternative feedstock for polymeric materials. *Nature Chemistry* **2013**, *5* (6), 518-524. DOI: 10.1038/nchem.1624.
(6) Huertas, D.; Florscher, M.; Dragojlovic, V. Solvent-free Diels–Alder reactions of in situ generated cyclopentadiene. *Green Chemistry* **2009**, *11* (1), 91-95.
(7) Kleine, T. S.; Lee, T.; Carothers, K. J.; Hamilton, M. O.; Anderson, L. E.; Ruiz Diaz, L.; Lyons, N. P.; Coasey, K. R.; Parker Jr., W. O.; Borghi, L.; et al. Infrared Fingerprint Engineering: A Molecular-Design Approach to Long-Wave Infrared Transparency with Polymeric Materials. *Angewandte Chemie International Edition* **2019**, *58* (49), 17656-17660. DOI: https://doi.org/10.1002/anie.201910856.
(8) Hemauer, F.; Steinrück, H.-P.; Papp, C. The Norbornadiene/Quadricyclane Pair as Molecular Solar Thermal Energy Storage System: Surface Science Investigations. *ChemPhysChem* **2024**, *25* (9), e202300806. DOI: https://doi.org/10.1002/cphc.202300806 (acccessed 2024/07/21).
(9) Jacovella, U.; Carrascosa, E.; Buntine, J. T.; Ree, N.; Mikkelsen, K. V.; Jevric, M.; Moth-Poulsen, K.; Bieske, E. J. Photo- and Collision-Induced Isomerization of a Charge-Tagged Norbornadiene–Quadricyclane System. *The Journal of Physical Chemistry Letters* **2020**, *11* (15), 6045-6050. DOI: 10.1021/acs.jpclett.0c01198.
(10) Orrego-Hernández, J.; Dreos, A.; Moth-Poulsen, K. Engineering of Norbornadiene/Quadricyclane Photoswitches for Molecular Solar Thermal Energy Storage Applications. *Accounts of Chemical Research* **2020**, *53* (8), 1478-1487. DOI: 10.1021/acs.accounts.0c00235.
(11) Marshall, C. M.; Molineux, J.; Kang, K.-S.; Kumirov, V.; Kim, K.-J.; Norwood, R. A.; Njardarson, J. T.; Pyun, J. Synthesis of Polycyclic Olefinic Monomers from Norbornadiene for Inverse Vulcanization: Structural and Mechanistic Consequences. *Journal of the American Chemical Society* **2024**, *146* (34), 24061-24074. DOI: 10.1021/jacs.4c08113.
(12) Zhou, Z.; Majeed, Y.; Naranjo, G. D.; Gambacorta, E. M. Assessment for crop water stress with infrared thermal imagery in precision agriculture: A review and future prospects for deep learning applications. *Computers and Electronics in Agriculture* **2021**, *182*, 106019.
(13) Ishimwe, R.; Abutaleb, K.; Ahmed, F. Applications of thermal imaging in agriculture—A review. *Advances in remote Sensing* **2014**, *3* (3), 128-140.
(14) Pawase, P.; Brahmankar, P. K.; Pawade, R. S.; Balasubramanium, R. Analysis of Machining Mechanism in Diamond Turning of Germanium Lenses. *Procedia Materials Science* **2014**, *5*, 2363-2368. DOI: https://doi.org/10.1016/j.mspro.2014.07.480.
(15) Laxmi; Mehra, R. Thermal imaging-based fault diagnosis of electronics circuit boards. In *Advances in Energy Technology: Select Proceedings of EMSME 2020*, 2022; Springer: pp 111-121.
(16) Glowacz, A. Fault diagnosis of electric impact drills using thermal imaging. *Measurement* **2021**, *171*, 108815. DOI: https://doi.org/10.1016/j.measurement.2020.108815.
(17) Awais, M.; Li, W.; Cheema, M. J. M.; Zaman, Q. U.; Shaheen, A.; Aslam, B.; Zhu, W.; Ajmal, M.; Faheem, M.; Hussain, S.; et al. UAV-based remote sensing in plant stress imagine using high-resolution thermal sensor for digital agriculture practices: a meta-review. *International Journal of Environmental Science and Technology* **2023**, *20* (1), 1135-1152. DOI: 10.1007/s13762-021-03801-5.
(18) Miethig, B.; Liu, A.; Habibi, S.; Mohrenschildt, M. v. Leveraging Thermal Imaging for Autonomous Driving. In *2019 IEEE Transportation Electrification Conference and Expo (ITEC)*, 19-21 June 2019, 2019; pp 1-5. DOI: 10.1109/ITEC.2019.8790493.
(19) Lee, T.-S.; Shie, J.-S. Feasibility study on low-resolution uncooled thermal imagers for home-security applications. *Optical Engineering* **2000**, *39* (6), 1431-1440.
(20) Kim, J.-H.; Lattimer, B. Y. Real-time probabilistic classification of fire and smoke using thermal imagery for intelligent firefighting robot. *Fire Safety Journal* **2015**, *72*, 40-49.
(21) Singh, G.; Verma, A. A Brief Review on injection moulding manufacturing process. *Materials Today: Proceedings* **2017**, *4* (2), 1423-1433.
(22) Valkenaers, H.; Vogeler, F.; Voet, A.; Kruth, J. P. Screw extrusion based 3D printing, a novel additive manufacturing technology. 2013.

(23) Akula, A.; Ghosh, R.; Sardana, H. Thermal imaging and its application in defence systems. In *AIP conference proceedings*, 2011; American Institute of Physics: Vol. 1391, pp 333-335.
(24) Havens, K. J.; Sharp, E. J. *Thermal imaging techniques to survey and monitor animals in the wild: a methodology*; Academic Press, 2015.
(25) Choudhary, A.; Mian, T.; Fatima, S. Convolutional neural network based bearing fault diagnosis of rotating machine using thermal images. *Measurement* **2021**, *176*, 109196.
(26) Yanai, O. Thermal imaging as a smartphone application: exploring and implementing a new concept. In *Infrared Technology and Applications XL*, 2014; SPIE: Vol. 9070, pp 189-194.
(27) Dai, X.; Yuan, X.; Wei, X. TIRNet: Object detection in thermal infrared images for autonomous driving. *Applied Intelligence* **2021**, *51* (3), 1244-1261.